LN's
Endless
Physics Notes

P6. MECHANICS, STRUCTURES AND MATERIALS

6.1. Kinematics, Forces and Dynamics

6.1.1. Constant Acceleration Kinematics

Linear Motion: for constant a (the SUVAT equations):

$$v = u + at \qquad s = ut + \tfrac{1}{2}at^2 \qquad s = vt - \tfrac{1}{2}at^2$$

$$v^2 = u^2 + 2as \qquad s = \tfrac{1}{2}t(u + v)$$

(s: relative displacement, u: initial velocity, v: final velocity, a: acceleration, t: time.)

These equations also apply in 2D and 3D, using coplanar vectors ($\mathbf{s}$, $\mathbf{u}$, $\mathbf{v}$, $\mathbf{a}$), except $v^2 = u^2 + 2as$ which must be evaluated component-wise. The equations $\mathbf{v} \cdot \mathbf{v} = \mathbf{u} \cdot \mathbf{u} + 2\mathbf{a} \cdot \mathbf{s}$ and $\mathbf{s} \times \mathbf{a} = \mathbf{v} \times \mathbf{u}$ also apply but provide incomplete additional information.

Rotational Motion: for constant α:
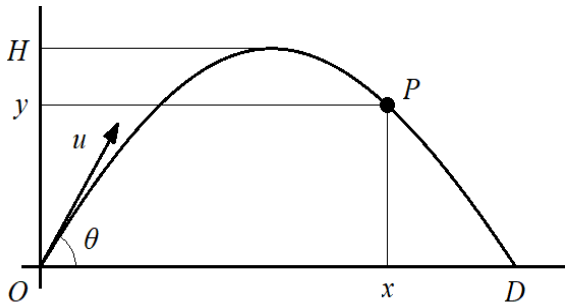
$$\omega = \omega_0 + \alpha t \qquad \theta = \omega_0 t + \tfrac{1}{2}\alpha t^2 \qquad \theta = \omega t - \tfrac{1}{2}\alpha t^2$$

$$\omega^2 = \omega_0^2 + 2\alpha\theta \qquad \theta = \tfrac{1}{2}t(\omega_0 + \omega)$$

(θ: angular displacement, ω_0: initial angular velocity, ω: final angular velocity, α: angular acceleration, t: time.)

6.1.2. Projectile Motion

Assumes a point particle in a uniform vertical gravitational field g ms^{-2} without resistive forces.

Flat Surface: trajectory is symmetric about the midpoint, where the maximum height occurs.

- Position: $x = (u\cos\theta)t$ and $y = (u\sin\theta)t - \frac{1}{2}gt^2$

- Range: $D = \frac{u^2\sin 2\theta}{g}$;

- Maximum height: $H = \frac{u^2\sin^2\theta}{2g} = \frac{D\tan\theta}{4}$;

- Flight time: $T = \frac{2u\sin\theta}{g} = \sqrt{\frac{2u^2 \pm 2\sqrt{u^4 - g^2 D^2}}{g^2}}$

- Equation of motion: $y = \tan\theta \times x\left(1 - \frac{x}{D}\right)$

- Total arc length: $s = \frac{u^2}{g}\left(\sin\theta + \cos^2\theta \tanh^{-1}(\sin\theta)\right)$

- Angle required to hit coordinate (x, y): $\theta = \tan^{-1}\frac{u^2 \pm \sqrt{u^4 - g^2 x^2 - 2gu^2 y}}{gx}$

  where u is minimised for $\theta^* = \frac{\pi}{4} + \frac{1}{2}\tan^{-1}\frac{y}{x}$.

Initial Elevation: initial displacement is $(0, y_0)$, where $y_0 > 0$.
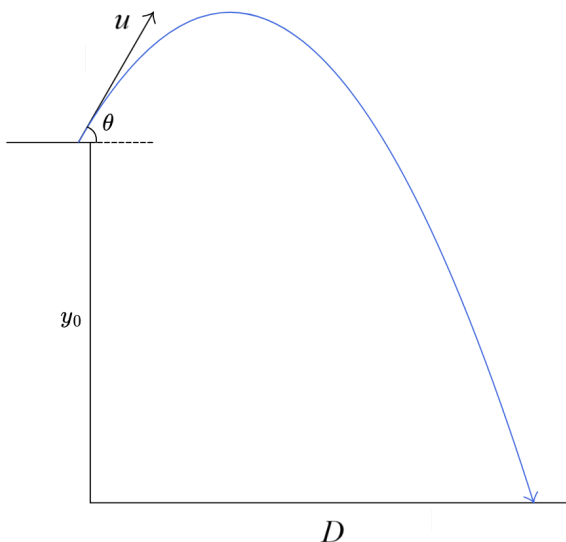
- Range: $D = \frac{u\cos\theta}{g}\left(u\sin\theta + \sqrt{u^2\sin^2\theta + 2gy_0}\right)$

- Angle for max range: $\theta^* = \cos^{-1}\sqrt{\frac{2gy_0 + u^2}{2gy_0 + 2u^2}}$

- Flight time: $T = \frac{u\sin\theta + \sqrt{u^2\sin^2\theta + 2gy_0}}{g}$

- Angle of impact: $\phi = \tan^{-1}\frac{\sqrt{u^2\sin^2\theta + 2gy_0}}{u\cos\theta}$

For realistic modelling of projectile motion, see Section 10.1.5 (ballistic kinematics).

6.1.3. Mechanical Forces

Resultant force:	$\mathbf{F} = \dot{\mathbf{p}} = m\mathbf{a} + \dot{m}\mathbf{v}$	Newton's Second Law: $\mathbf{F} = m\mathbf{a}$ if mass is constant
Weight:	$W = mg$	uniform gravitational field g
Upthrust:	$U = \rho_f V g$	buoyancy in fluids (W - U); Archimedes principle.
Pressure:	$F = pA$	distributed loading normal to a surface
Friction force:	$F \leq \mu_s N,\ F = \mu_k N$	angle of friction: $\tan \psi = \mu_s$
Spring force:	$\mathbf{F} = -k\mathbf{x}$	for linear elastic media (Hooke's law)
Dashpot force:	$\mathbf{F} = -\lambda \mathbf{v}$	for linear viscous media (Stokes' law)
Centripetal force:	$\mathbf{F} = -\dfrac{mv^2}{r}\,\mathbf{e}_r = -mr\omega^2\,\mathbf{e}_r$	radial force in uniform circular motion
Rolling resistance:	$F = C_{rr} N$	due to deformation of rolling bodies
Air resistance / lift:	$F = \tfrac{1}{2}\,C\,\rho_f A v^2$	distributed force due to fluid flow
Power and torque:	$P = Fv + \tau\omega,\ \boldsymbol{\tau} = \mathbf{r} \times \mathbf{F}$	torque is an unbalanced net moment
Work and impulse:	$E = \int \mathbf{F} \cdot d\mathbf{s},\ \ \mathbf{J} = \int \mathbf{F}\,dt$	E is change in energy, $\mathbf{J}$ is change in momentum

6.1.4 Friction
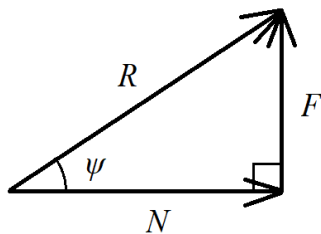
At a rough contact, there is a normal force N and a friction force F, forming a net reaction force R.

Stationary: $F \leq \mu_s N$ Moving: $F = \mu_k N$ where $\mu_s > \mu_k$

Angle of friction: $\tan \psi = \dfrac{F}{N} \leq \mu.$

Typical values of the coefficient of static friction, assuming all surfaces are clean and dry:

Surface 1	Surface 2	μ_s	Surface 1	Surface 2	μ_s
steel	steel	0.65	copper	copper	1.6
rubber	rubber	1.16	ice	steel	0.03
car tyre	asphalt	0.72	ice	wood	0.05
car tyre	grass	0.35	human skin	metals	0.9

Rolling resistance (e.g. in wheels) is **not** due to surface friction, but rather due to hysteresis losses in the wheel material. The harder the wheel and surface, the lower the coefficient of rolling resistance C_{rr}. Typical values of C_{rr} are:

car tyres (pneumatic, rubber)		train wheels (cast iron)	
concrete, asphalt	0.014	steel rail	0.0003
field, sand	0.2		

6.1.5. Mechanical Energy and Momentum

Mechanical Energy: internal (mechanical) energy $U =$ kinetic energy $T +$ potential energy V.

- Energy is the capacity of a system to do work. Mechanical energy is a form of energy.

- Mechanical work done by a force moving a body with displacement $\mathbf{r}$: $W = \int_1^2 \mathbf{F(r)} \cdot \mathrm{d}\mathbf{r}$.

- If the work done by a force is independent of the path taken, i.e. if there exists a scalar potential energy field V such that $\mathbf{F} = -\nabla V$, then $\mathbf{F}$ is a **conservative** force.

- **Conservation of Energy:** mechanical energy is constant when all forces acting on the system are conservative. Otherwise, total energy is conserved (always).

Linear Momentum: a vector $\mathbf{p} = m\mathbf{v}_\mathrm{G}$ (m: system mass, $\mathbf{v}_\mathrm{G}$: velocity of system COM)

- Newton's second law: $\mathbf{F} = \dfrac{d}{dt}\mathbf{p}$ ($\mathbf{F}$: resultant force on a system, $\mathbf{p}$: system momentum)
  For a system of constant mass m, Newton's second law is $\mathbf{F} = m\mathbf{a}$ ($\mathbf{a}$: acceleration of COM).

- Linear impulse: $\mathbf{J} = \Delta\mathbf{p} = \int_1^2 \mathbf{F}(t)\,\mathrm{d}t$. An 'ideal impulse' has $|\mathbf{F}| \to \infty$ and $\Delta t \to 0$, such that $\mathbf{J} = \mathbf{F}\,\Delta t$.

- **Conservation of Linear Momentum:** in a constant-mass system with no net external forces, the total linear momentum $\mathbf{p}$ is constant.

Angular Momentum: a vector $\mathbf{h} = \mathbf{r} \times \mathbf{p}$ ($\mathbf{r}$: displacement of COM, $\mathbf{p}$: momentum of system)
Rotational quantities can refer to an axis through the COM (spin) or any other arbitrary axis (orbital).

- Angular momentum: $\mathbf{h} = \mathbf{r}_\mathrm{G/O} \times \mathbf{p}$ (about a point) or $h = \mathbf{h}\cdot\mathbf{n} = m\,v_\theta r_\perp$ (about an axis)
- Moment of a force: $\mathbf{Q} = \mathbf{r} \times \mathbf{F}$ (about a point) or $Q = \mathbf{Q}\cdot\mathbf{n} = r_\perp F$ (about an axis)
- Net torque: $\mathbf{Q} = \dfrac{d}{dt}\mathbf{h}$ (about a point) or $Q = \dfrac{d}{dt}h$ (about an axis)

  (v_θ: tangential velocity of COM about axis, $r_\perp$: perpendicular distance of COM from axis)

- Angular velocity $\boldsymbol{\omega}$: a pseudovector defined by $\mathbf{v}_\perp = \boldsymbol{\omega} \times \mathbf{r}$ ($\mathbf{v}_\perp$: velocity perpendicular to axis)
  The direction of $\boldsymbol{\omega}$ is the axis of rotation, with a sign from the right-hand grip rule.

- For a rotating body (about COM) or orbiting particle (about axis), $\mathbf{h} = I\boldsymbol{\omega}$ (I: moment of inertia).

- Angular impulse: $\mathbf{r} \times \mathbf{J} = \Delta\mathbf{h} = \int_1^2 \mathbf{Q}(t)\,\mathrm{d}t$.

- **Conservation of Angular Momentum:** in a constant-inertia system with no net external torques about a point or axis, the angular momentum $\mathbf{h}$ (point) or h (axis) is constant.

6.1.6. Relative Velocity and Angular Momentum in a Rigid Body

Relative position, velocity and acceleration:

$$\mathbf{r}_{G/P} = -\mathbf{r}_{P/G} = \mathbf{r}_G - \mathbf{r}_P, \quad \dot{\mathbf{r}}_{G/P} = -\dot{\mathbf{r}}_{P/G} = \dot{\mathbf{r}}_G - \dot{\mathbf{r}}_P, \quad \ddot{\mathbf{r}}_{G/P} = -\ddot{\mathbf{r}}_{P/G} = \ddot{\mathbf{r}}_G - \ddot{\mathbf{r}}_P.$$

For planar (fixed-axis) rotation, angular momentum about a point P:

$$\mathbf{h}_P = \mathbf{h}_G + \mathbf{r}_{G/P} \times \mathbf{p} \qquad\qquad \text{(from parallel axis theorem)}$$

If P is a moving point then G must be the centre of mass (COM).

6.1.7. Variable Mass Problems

When a body B gains or loses mass in the form of particles P:

$$\mathbf{F} = m\mathbf{a} - \dot{m}\mathbf{v}_{P/B}$$

($\mathbf{F}$: force exerted on B, $\mathbf{a}$: acceleration of B, $\mathbf{v}_{P/B}$: velocity of P relative to B, m: mass of B, $\dot{m}$: rate of change of mass of B)

In general, mechanical energy is **not** conserved in a variable mass process. For example, lifting a coiled chain results in net energy loss due to inelastic collisions, and launching a rocket results in net energy gain due to conversion of chemical energy to mechanical energy.

6.1.8. Collisions, Impacts and the Coefficient of Restitution

For two objects moving at initial velocities $\mathbf{u}_A$ and $\mathbf{u}_B$, colliding to new velocities $\mathbf{v}_A$ and $\mathbf{v}_B$,

- Coefficient of restitution: $e = \dfrac{relative\ speed\ of\ separation}{relative\ speed\ of\ approach}$ (Galilean invariant)

  1D: $e = \dfrac{v_B - v_A}{u_A - u_B}$ 2D: $e = \dfrac{(\mathbf{v}_B - \mathbf{v}_A) \cdot \hat{\mathbf{n}}}{(\mathbf{u}_B - \mathbf{u}_A) \cdot \hat{\mathbf{n}}}$ ($\hat{\mathbf{n}}$: unit normal vector to plane of contact)

- Fraction of total kinetic energy retained in the system $= e^2$.

Perfectly elastic collision: $e = 1$, kinetic energy is conserved,
Perfectly inelastic collision: $e = 0$, kinetic energy is lost entirely (converted to heat)

Oblique Collision Between Smooth Inelastic Spheres

(m_1 and m_2: masses of spheres, $\mathbf{u}_1$ and $\mathbf{u}_2$: initial velocities of spheres, $\mathbf{v}_1$ and $\mathbf{v}_2$: final velocities of spheres after collision, e: coefficient of restitution between spheres, $\mathbf{r}_1$ and $\mathbf{r}_2$: position vectors of sphere COMs at moment of collision. Indices i, j are from {1, 2} as properties are symmetric.)

- Velocity of zero momentum frame of reference: $\mathbf{v}_{\text{ZM}} = \dfrac{1}{m_1 + m_2}(m_1\mathbf{u}_1 + m_2\mathbf{u}_2)$

- Final velocities: $\mathbf{v}_i = \mathbf{u}_i + \dfrac{m_j(1 + e)(\mathbf{u}_j - \mathbf{u}_i) \cdot \hat{\mathbf{n}}}{m_i + m_j}\hat{\mathbf{n}}$ where $\hat{\mathbf{n}} = \dfrac{\mathbf{r}_i - \mathbf{r}_j}{|\mathbf{r}_i - \mathbf{r}_j|}$

- Impulse: $\mathbf{J}_i = m_i(\mathbf{v}_i - \mathbf{u}_i) = \dfrac{m_i m_j}{m_i + m_j}(1 + e)((\mathbf{u}_j - \mathbf{u}_i) \cdot \hat{\mathbf{n}})\hat{\mathbf{n}}$

Viscoelastic Modelling of Inelastic Collisions: for 1D vertical motion with a rigid surface

Ball in contact with floor
for $0 < t < t_1$ (region shown shaded)
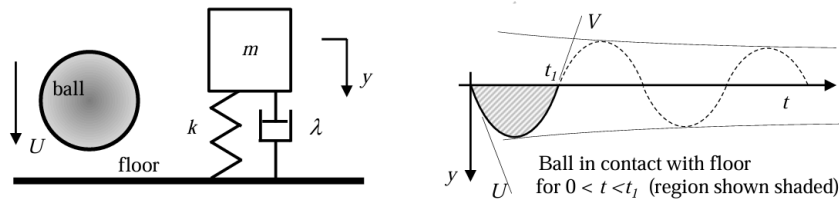
The contact period, $0 < t < t_1$, can be modelled as the first half-period of the impulse response of an underdamped ($\zeta < 1$) spring-mass-dashpot system (Section 6.2.4).

- Contact time: $t_1 = \dfrac{\pi}{\omega_d}$ where $\omega_d = \omega_n\sqrt{1 - \zeta^2}$, $\omega_n = \sqrt{\dfrac{k}{m}}$ and $\zeta = \dfrac{\lambda}{2\sqrt{km}}$.

- Coefficient of restitution: $e = \dfrac{V}{U} = exp\left(- \dfrac{\pi\zeta}{\sqrt{1 - \zeta^2}}\right)$ (perfectly inelastic: $e = 0 \leftrightarrow \zeta = 1$)

- Contact force: $F(t) = - my''$, where $y(t) = \dfrac{\omega_n N}{\sqrt{1 - \zeta^2}}exp\left(- \zeta\omega_n t\right)sin\ \omega_d t$ and $N = \dfrac{U}{\omega_n^2}$.

- Impulse: $J = \displaystyle\int_0^{t_1} F(t)\,dt = F_{avg}t_1 = m(V + U)$.

Impacts:

- To model an impact, sketch the three cases **1)** before, **2)** at impact, **3)** after contact.
- During the impact, assume all non-impulsive forces are negligible, and that the contact time is infinitesimal.
- To relate the three cases, use conservation of linear momentum ($\mathbf{J} = \Delta\mathbf{p}$) and angular momentum ($\mathbf{r} \times \mathbf{J} = \Delta\mathbf{h}$).

For rigid body impacts, consider momenta at the both COM and at the contact point. To apply angular momentum correctly, ensure that:

- Is the body rotating about a fixed axis? i.e. is the body attached to a pivot point?
  - **Yes:** can use either I_O (moment of inertia about the axis of rotation) or I_G
  - **No:** must use I_G (moment of inertia about an axis through the COM).

- Are we taking moments about a fixed or a moving axis? (must be fixed if using I_O above)
  - **Fixed:**   use $\mathbf{r}_{J/O} \times \mathbf{J} = \int \mathbf{Q}_O \, dt = \mathbf{h}_{OB} - \mathbf{h}_{OA}$ (where $\mathbf{h}_O = \mathbf{h}_G + \mathbf{r}_G \times m\mathbf{v}_G$)
  - **Moving:** use $\mathbf{r}_{J/G} \times \mathbf{J} = \int \mathbf{Q}_G \, dt = \mathbf{h}_{GB} - \mathbf{h}_{GA}$

Examples
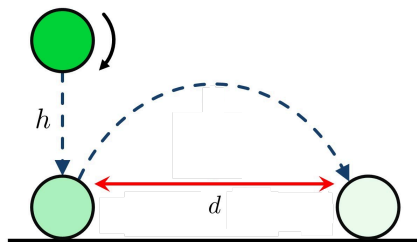
h: initial height, ω_0: initial angular velocity, e: coefficient of restitution, μ: coefficient of friction, d: landing distance

- Horizontal speed after impact: $u_x = \mu\sqrt{2gh}(1 + e)$
- Decrease in ω on impact: $|\Delta\omega| = \dfrac{mu_x r}{I_G}$
- Horizontal range: $d = 4\mu he(1 + e)$

6.1.9. Principles of Mechanical Systems (Simple Mechanical Machines)

- Mechanical advantage (force amplification factor) $= \dfrac{F_{load}}{F_{effort}} = \dfrac{F_{output}}{F_{input}}$
- Energy balance on static machines: $\sum \mathbf{F} \cdot \mathbf{x} + \sum \boldsymbol{\tau} \cdot \boldsymbol{\theta} = 0$
- Power balance on dynamic mechanisms: $\sum \mathbf{F} \cdot \mathbf{v} + \sum \boldsymbol{\tau} \cdot \boldsymbol{\omega} = 0$

Levers

Principle of moments: sum of moments $M = Fx$ of all forces on the beam about the fulcrum must be zero for rotational equilibrium. Force balance is also required, via a contact force at the fulcrum (which it must be able to support without failing). Using an 'effort' force (input), a load's moment is balanced.

- Class 1 lever: load and effort are on opposite sides of a fulcrum.
- Class 2 lever: load and effort are on one side of a fulcrum, with the effort further away.
- Class 3 lever: load and effort are on one side of a fulcrum, with the load further away.

Pulleys

The tension in a light flexible inextensible rope in contact with small, light, frictionless pulleys is constant. The sum of the forces acting on any static pulley must be zero. For a suspended pulley, the ratio of displacements, velocities and accelerations is equal to the ratio of the numbers of attached ropes.

If any of these assumptions about the system are broken, the tension forces either side of the pulley will be unequal, even at static equilibrium, due to inertial/frictional forces and torques.

Belts (Capstans/Winches, Conveyors)
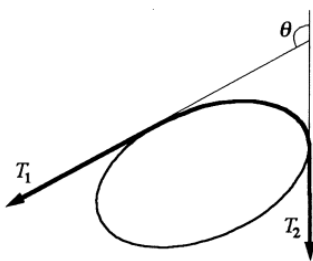
For a belt or cable passing over a rounded rough contact (subtending angle θ) of distributed coefficient of friction μ, sliding begins when

$$\frac{T_1}{T_2} \geq e^{\mu\theta} \quad \text{or} \quad \frac{T_1}{T_2} \leq e^{-\mu\theta} \qquad \text{(the capstan equation)}$$

For a motor powered conveyor belt, the input torque equals the moment of the friction force, μWr.

Pistons and Hydraulic Jacks

Pistons are often actuated by plane mechanisms (Section 6.1.10) to convert rotary motion into linear motion.

Hydraulic jacks are used to transmit forces over distance through a fluid: $p_{fluid} = \dfrac{F_{input}}{A_{input}} = \dfrac{F_{output}}{A_{output}}$

Cams and Wheels (Rolling Body Kinematics)

For pure rolling, the speed of the contact point of a wheel is zero. For pure sliding, the speed of the contact point of a wheel is equal to the translational speed of the wheel.

Equivalent rolling circles at instantaneous centres Q_1 and Q_2 are shown, with angular velocities related by $\dfrac{\omega_2}{\omega_1} = -\dfrac{|Q_1 N_1|}{|Q_2 N_2|} = -\dfrac{|Q_1 P|}{|Q_2 P|}$.

Sliding speed at C: $\quad (\omega_1 - \omega_2)\, PC$.
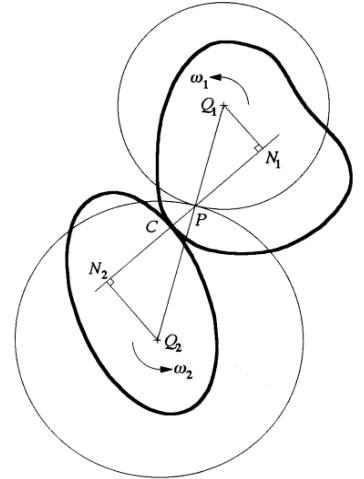
Gears

Gears roll on each other at constant angular velocity with slipping at the teeth.
For two coplanar circular gears in contact, they rotate in opposite directions.

- Gear tooth module, $m = \dfrac{pitch\ circle\ diameter,\, d}{number\ of\ teeth,\, n}$ (meshing gears must have same m)

- Rotation rate, $\omega = \dfrac{contact\ speed,\, v}{gear\ radius,\, r}$ (meshing gears must have same v)

- Gear ratio: $\dfrac{\omega_1}{\omega_2} = \dfrac{n_1}{n_2} = \dfrac{r_2}{r_1} = \dfrac{\tau_2}{\tau_1}$ (torque amplification factor)

- Compound gears: two concentric gears with the same ω in the same direction.

- Rack and pinion: straight track with one gear (either moving or fixed) so that $v = \omega r$.

Planetary gears (epicyclic gears): a central sun gear (s) meshing with N planetary gears (p) translating uniformly with a carrier frame (c), also meshing with an outer ring gear (r). For meshing, $n_s + n_r = kN$ (k: an integer). The four angular velocities satisfy $n_s \omega_s + n_p \omega_p = (n_s + n_p)\omega_c$ and $n_p \omega_p + (n_r - n_p)\omega_c = n_r \omega_r$ (two degrees of freedom).
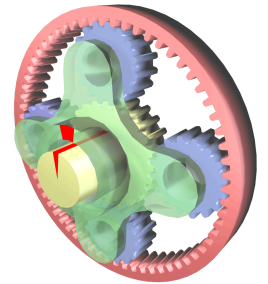
Arbitrary gear shape design: using kinematics to find target geometry

Let $f: \mathrm{R} \to \mathrm{C}$ be a parameterisation $f(s)$ of the first gear shape in the complex plane with its axle at the origin $\{x = \mathrm{Re}(f), y = \mathrm{Im}(f)\}$. During rotation with a second gear, the shape is

$$\gamma(s,\, t) = \left(f(s)\, e^{i\omega t} + R \right) e^{i\Omega t}$$

(ω: first gear angular velocity, Ω: second gear angular velocity, R: axle separation, t: time). The second gear shape is the envelope of this curve, given by $\gamma(s,\, t)$, where

$$t = \frac{-\phi(s) \pm \alpha(s)}{\omega}, \quad \phi(s) = \angle f'(s) \quad \text{and} \quad \alpha(s) = \cos^{-1}\left(-\frac{\omega + \Omega}{R\Omega}\, \mathrm{Re}\left(\frac{f'(s)^*}{|f'(s)|} f(s) \right) \right).$$

This method does not work if the resulting gear has retrograde motion or is self-intersecting.

**All Notes** 6.1. Kinematics, Forces and Dynamics

Crank Shafts and Rotors

A slender shaft is loaded with heavy rotors along its length which rotate about the shaft.
Imbalance of a rotor, U [kg mm] = Rotor mass, M [kg] × Rotor COM to shaft distance, e [mm]

- **Static balance:** COM of the system lies on shaft axis → resultant bearing force is zero.
- **Dynamic balance:** resultant moment of the bearing forces about any point on the shaft is zero.

An imbalanced rotor can be modelled as a uniform rotor plus an imbalance mass m at its outer radius r, for a net imbalance $U = mr$.
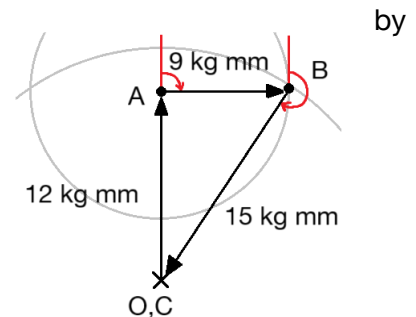

All dimensions in metres
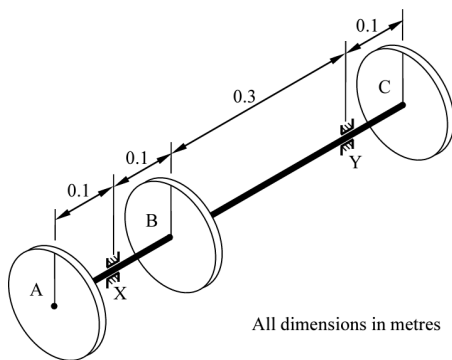
Example (left): bearings X and Y, rotors A, B, C (diameter: 0.2 m). Imbalances: A = 12 kg mm, B = 9 kg mm, C = 15 kg mm, along the lines on the rotors. Shaft rotation speed: 5000 rpm.

Diagram of imbalances: need to rotate B by 90° and C by 216.9° to achieve static balance (zero resultant).

Dynamic moment about X due to centrifugal loading: $M_A = \dfrac{U_A \omega_A^2 d_{AX}}{1000}$...

Bearing force at Y supplies out-of-balance (net) moment. Material of mass m can be cut from the outsides of A and C at angular positions in the direction of the bearing force to achieve dynamic balance ($mr\omega^2 d_{AC} = M_{net}$).

Clutches and Gearboxes
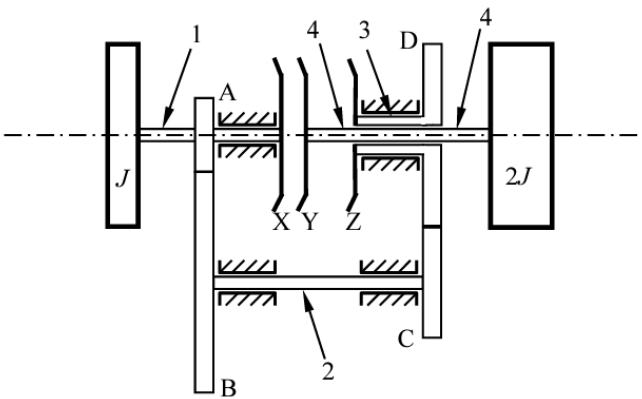
Example (left): two-speed gearbox. Shafts 1, 2 and 3 are mounted in rigid bearings and are axially constrained. Shaft 4 is mounted inside shaft 3 (can slide relative to shaft 3 and rotate at different speed). When shaft 4 slides to the left, clutch plates X and Y engage, so that shafts 1 and 4 rotate together; when it slides to the right, clutch plates Y and Z engage, so that shafts 3 and 4 rotate together. If shafts 1 and 4 carry rotors with polar moment of inertia of J and $2J$ respectively, while gear wheels A, B, C, and D have $N_A = 12$, $N_B = 36$, $N_C = 18$ and $N_D = 30$ teeth respectively, then:

Gear speeds: $\omega_1 N_A = \omega_2 N_B$ and $\omega_2 N_C = \omega_3 N_D$
Impulse between gears: $I_{AB} N_B = I_{CD} N_C$ (equilibrium of BC)

The total angular momentum of the system about the axis of the rotors is **not** conserved even when not slipping at the clutch since gear contact forces exert moments about the shafts.

After starting with Y at X, consider 'rotational impact' of clutch moving to engage Z:

Angular momenta before/after: on rotor J: $J\omega_1 + I_{AB} r_A = J\omega_1'$; on rotor $2J$: $2J\omega_1 - I_{CD} r_D = 2J\dfrac{N_A N_C}{N_B N_D}\omega_1'$

Kinetic energy before: $\frac{1}{2}(3J)\omega_1^2$; Kinetic energy after: $\frac{1}{2}J\omega_1'^2 + \frac{1}{2}(2J)\left(\dfrac{N_A N_C}{N_B N_D}\omega_1'\right)^2$; Efficiency $= \dfrac{KE_{after}}{KE_{before}}$

All Notes   6.1. Kinematics, Forces and Dynamics

6.1.10. Kinematics of Plane Mechanisms

A mechanistic assembly of rigid rods connected by pin joints can be actuated by applying a torque to one of the joints. Common types of 'four-bar mechanisms' with their **velocity diagrams** are shown:

Crank Rocker: torque applied at A, rocker CD oscillates about D

$$v_B = \omega L_{AB}, \; v_C = \omega_{CD} L_{CD}$$

$$\omega_{BC} = \frac{v_B}{d_{IB}} = \frac{v_C}{d_{IC}}$$

(I: instantaneous centre of BC)
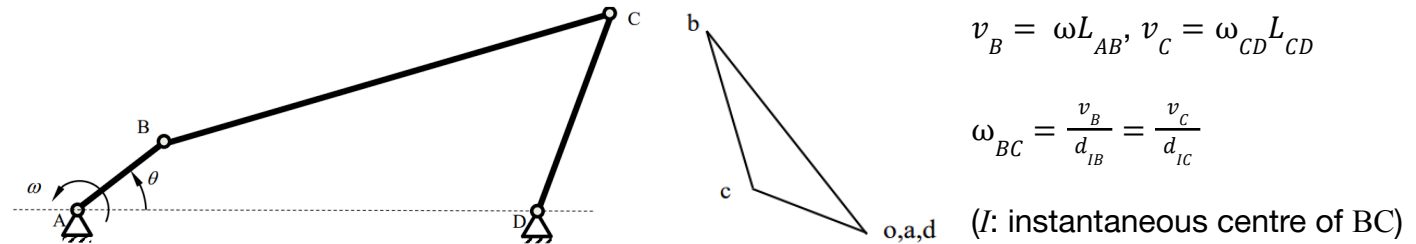
Slider Crank: torque applied at O, slider B oscillates in a line

$$v_A = \omega L_{OA}$$

$$\omega_{AB} = \frac{v_A}{d_{IA}} = \frac{v_B}{d_{IB}}$$

Sliding speed: $v_{B\backslash X}$

(X: point instantaneously at B but fixed to frame)
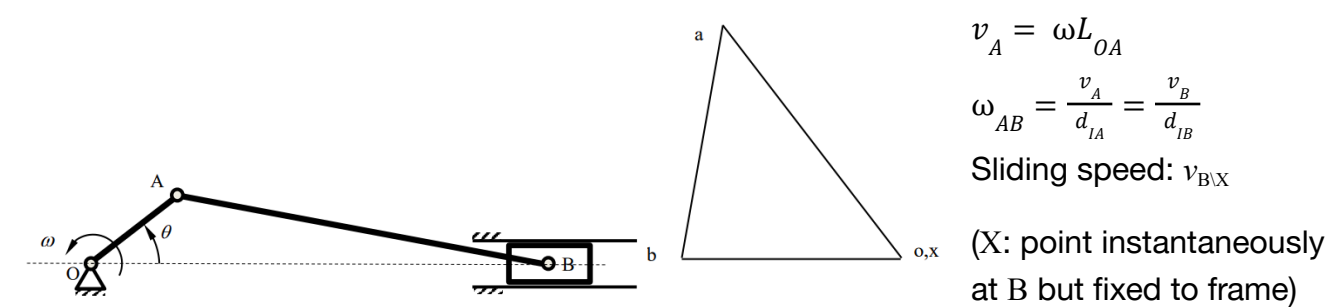
Quick Return: torque applied at A, rod BC oscillates

$$v_B = \omega L_{AB}$$

$$\omega_{slider} = \omega_{long\;rod} = \frac{v_B}{d_{IB}} = \frac{v_Y}{d_{IC}}$$

$v_Y \parallel r_{B\backslash C} \perp v_X$; Sliding speed: $v_{B\backslash X}$
(X: point instantaneously at B but fixed to long rod, Y: point instantaneously at C but fixed to an imaginary 'extended slider')
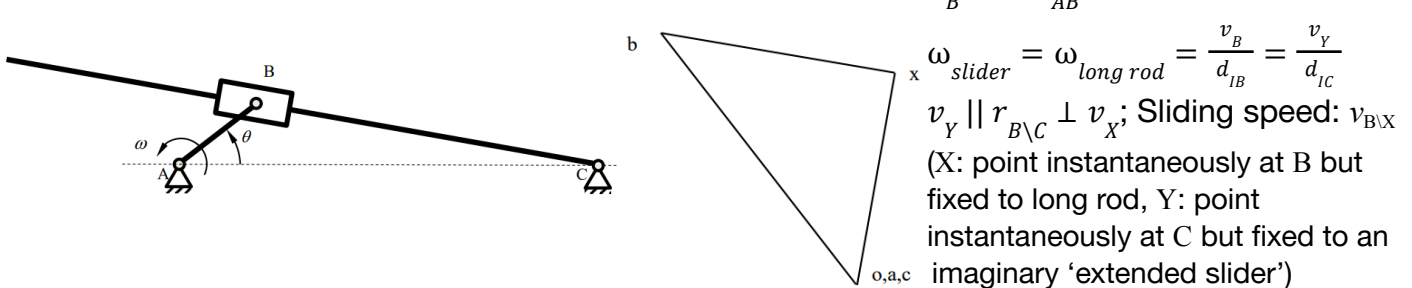
Velocity Image Theorem: for any rigid lamina ABC rotating at ω, the corresponding velocity diagram is obtained by rotating the lamina 90° in the direction of ω and scaling by factor ω.

Acceleration Diagrams: for rigid link AB (length L, angular speed ω, angular acceleration α):
$\mathbf{a}_{B\backslash A} = -L\omega^2 \mathbf{e}_r + L\alpha \mathbf{e}_\theta$ ($\mathbf{e}_r$: unit vector of $\mathbf{r}_{B\backslash A}$, $\mathbf{e}_\theta$: unit vector perpendicular to $\mathbf{e}_r$ in direction of ω).
The acceleration image is a rotation of the lamina by some angle (not necessarily 90°).

Virtual Work and Virtual Power: $\sum_i \mathbf{F}_i \cdot \mathbf{v}_i + \sum_i T_i \, \omega_i = 0$

Include both real and D'Alembert (inertial) forces/torques to balance member accelerations
($\mathbf{F}_{COM} = -m\mathbf{a}_{COM}$ and $T_{COM} = -I\alpha_{COM}$) if links are not light. Frictional torques T_{fr} acting at joints should use the relative angular velocity between the links. Power loss by frictional torque: $|P| = T_{fr}(\omega_1 - \omega_2)$.

6.1.11. Vector Kinematics in 2D Polar and Intrinsic Coordinates

(r: displacement, R: radius of curvature, ω: angular velocity, ($\mathbf{e}$, $\mathbf{e}^*$) orthonormal vectors.)

Polar Coordinates (r, θ): $\dot{\hat{e}}_r = \dot{\theta}\,\hat{e}_\theta$ $\dot{\hat{e}}_\theta = -\dot{\theta}\,\hat{e}_r$

$$\boldsymbol{r} = r\,\hat{e}_r \qquad \dot{\boldsymbol{r}} = \dot{r}\,\hat{e}_r + r\dot{\theta}\,\hat{e}_\theta \qquad \ddot{\boldsymbol{r}} = \left(\ddot{r} - r\dot{\theta}^2\right)\hat{e}_r + \left(r\ddot{\theta} + 2\dot{r}\dot{\theta}\right)\hat{e}_\theta$$
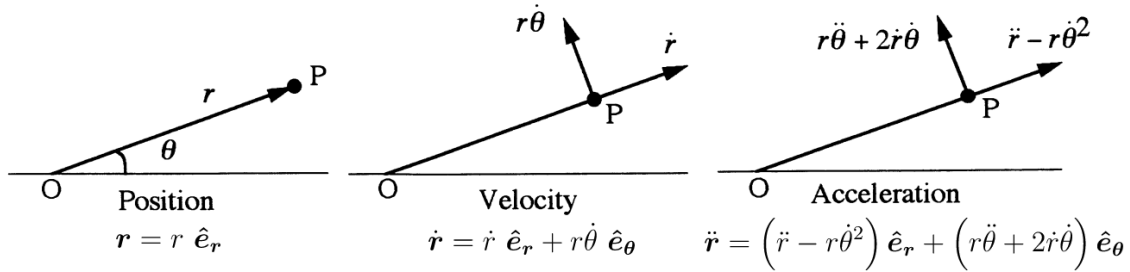
Acceleration components: $\{r\ddot{\theta}$: tangential; $2\dot{r}\dot{\theta}$: Coriolis; $\ddot{r}$: radial; $-r\dot{\theta}^2$: centripetal$\}$

Intrinsic Coordinates (s, ψ): $\dot{\hat{e}}_t = \dot{\psi}\,\hat{e}_n$ $\dot{\hat{e}}_n = -\dot{\psi}\,\hat{e}_t$

$$\dot{\boldsymbol{r}} = \dot{s}\,\hat{e}_t \qquad \qquad \ddot{\boldsymbol{r}} = \ddot{s}\,\hat{e}_t + \dot{s}\dot{\psi}\,\hat{e}_n$$
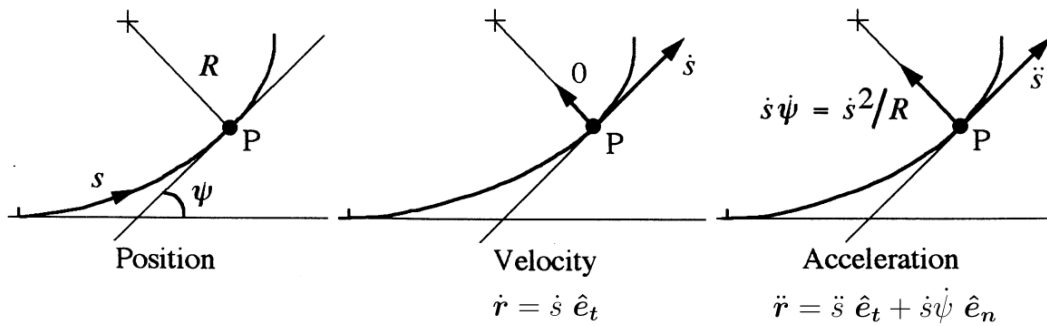
Differentiation of a rotating vector:

For any unit vector rotating at rate $\boldsymbol{\omega}$, $\dot{\hat{e}} = \boldsymbol{\omega} \times \hat{e}^*$

For vector kinematics in 3D spherical coordinates, see Section 3.5.13.

6.1.12. Vector Kinematics in Non-Inertial Reference Frames

A body R moves and rotates with angular velocity $\boldsymbol{\omega}$ with respect to a reference frame F. If point Q is fixed on the body, and another point P moves relative to the body with $\mathbf{r}$ as the position vector of P relative to Q, then the displacement $\mathbf{r}_P$, velocity $\mathbf{v}_P$ and acceleration $\mathbf{a}_P$ of P relative to frame F are given by:
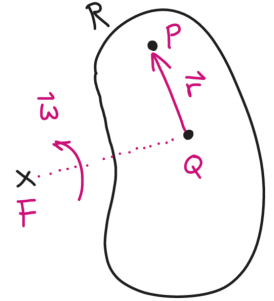
$$\mathbf{r}_P = \mathbf{r}_Q + \mathbf{r},$$

$$\mathbf{v}_P = \underbrace{\mathbf{v}_Q}_{\substack{\text{velocity of Q}\\\text{in frame F}}} + \left[\frac{d\mathbf{r}}{dt}\right]_F = \mathbf{v}_Q + \underbrace{\left[\frac{d\mathbf{r}}{dt}\right]_R}_{\substack{\text{apparent motion of P}\\\text{relative to body R}}} + \underbrace{\boldsymbol{\omega} \times \mathbf{r}}_{\substack{\text{contribution due to}\\\text{rotation of body R}}}$$

$$\mathbf{a}_P = \underbrace{\mathbf{a}_Q}_{\substack{\text{accelertion of}\\\text{Q in frame F}}} + \underbrace{\left[\frac{d^2\mathbf{r}}{dt^2}\right]_R}_{\substack{\text{apparent acceleration}\\\text{relative to body R}}} + \underbrace{\frac{d\boldsymbol{\omega}}{dt} \times \mathbf{r}}_{\substack{\text{Euler}\\\text{acceleration}}} + \underbrace{2\boldsymbol{\omega} \times \left[\frac{d\mathbf{r}}{dt}\right]_R}_{\substack{\text{Coriolis}\\\text{acceleration}}} + \underbrace{\boldsymbol{\omega} \times (\boldsymbol{\omega} \times \mathbf{r})}_{\substack{\text{centripetal}\\\text{acceleration}}}$$

Reference frame conversion: if the non-inertial 'body frame' R translating at velocity $\mathbf{U}$ and rotating at rate $\boldsymbol{\omega}$ relative to a reference frame F, then the rate of change of any vector $\mathbf{x}$ in the two frames are related by: ($(\mathbf{U}\cdot\nabla)\mathbf{x}$: advection operator)

$$\underbrace{\left[\frac{d\mathbf{x}}{dt}\right]_F}_{\substack{\text{rate of change}\\\text{in frame F}}} = \underbrace{\left[\frac{d\mathbf{x}}{dt}\right]_R}_{\substack{\text{rate of change}\\\text{in frame R}}} + \underbrace{\boldsymbol{\omega} \times \mathbf{x}}_{\substack{\text{contribution due}\\\text{to rotation of F}\\\text{relative to R}}} + \underbrace{(\mathbf{U} \cdot \boldsymbol{\nabla})\,\mathbf{x}}_{\substack{\text{contribution due}\\\text{to translation of F}\\\text{relative to R}}}$$
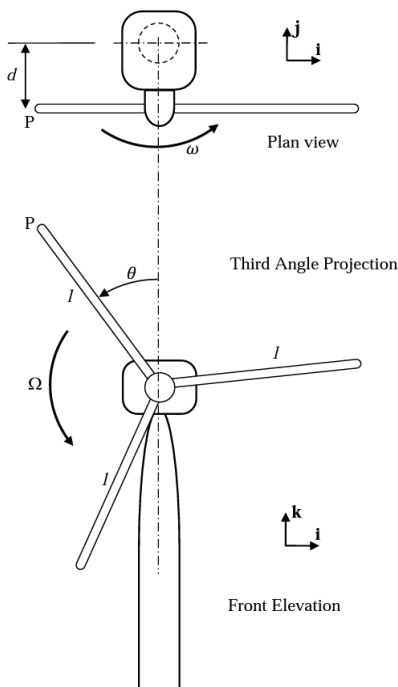
If frame F is inertial then it is in frame F that forces and torques can be computed via Newton's second law.

Example (left): kinematics of a horizontal-axis wind turbine with yaw control. Constant speeds: blade rotation rate is Ω, housing rotation rate is ω.

P: the tip of a turbine blade, at distance l from the housing ($\boldsymbol{\Omega} = -\Omega\mathbf{j}$ in frame R)
Q: the housing, at distance d from the tower
R: the frame rotating with the housing at angular velocity $\boldsymbol{\omega} = \omega\mathbf{k}$ relative to F
F: the frame fixed to the tower $\{\mathbf{i}, \mathbf{j}, \mathbf{k}\}$

$\mathbf{r}_P = (-l \sin\theta)\mathbf{i} + (-d)\mathbf{j} + (l \cos\theta)\mathbf{k}$ $\qquad\qquad$ ($\mathbf{r}_Q = -d\mathbf{j}$, $\mathbf{r} = -l \sin\theta\,\mathbf{i} + l \cos\theta\,\mathbf{k}$)

$\mathbf{v}_P = (\omega d - \Omega l \cos\theta)\mathbf{i} + (-\omega l \sin\theta)\mathbf{j} + (-\Omega l \sin\theta)\mathbf{k}$
$\qquad\qquad$ ($\mathbf{v}_Q = \omega d\mathbf{i}$, $[\mathbf{v}]_R = -\Omega l \cos\theta\,\mathbf{i} - \Omega l \sin\theta\,\mathbf{k}$, $\boldsymbol{\omega} \times \mathbf{r} = -\omega l \sin\theta\,\mathbf{j}$)

$\mathbf{a}_P = ((\Omega^2 + \omega^2)\,l \sin\theta)\mathbf{i} + (\omega^2 d - 2\omega\Omega l \cos\theta)\mathbf{j} + (-\Omega^2 l \cos\theta)\mathbf{k}$
$\qquad\qquad$ ($\mathbf{a}_Q = \omega^2 d\mathbf{j}$, $[\mathbf{a}]_R = \Omega^2 l \sin\theta\,\mathbf{i} - \Omega^2 l \cos\theta\,\mathbf{k}$,
$\qquad\qquad$ $\mathbf{a}_{\text{Euler}} = \mathbf{0}$, $\mathbf{a}_{\text{Coriolis}} = -2\omega\Omega l \cos\theta\,\mathbf{j}$, $\mathbf{a}_{\text{centripetal}} = \omega^2 l \sin\theta\,\mathbf{i}$)

The inertial force loading (per unit length along the blade) is $\mathbf{w}(x) = -\rho A\,\mathbf{a}(x)$. This loading gives rise to an internal shear force $\mathbf{S}(x)$ and bending moment $\mathbf{M}(x)$, which can be found by taking a free-body cut at x.

Plan view

Third Angle Projection

Front Elevation

6.1.13. Moments of Inertia

Moments of inertia:

$$I_{xx} = \int (y^2 + z^2)\, dm = mk_x^2, \qquad k_x\text{: radius of gyration about } x\text{-axis}$$

$$I_{yy} = \int (x^2 + z^2)\, dm = mk_y^2, \qquad k_y\text{: radius of gyration about } y\text{-axis}$$

$$I_{zz} = \int (x^2 + y^2)\, dm = mk_z^2, \qquad k_z\text{: radius of gyration about } z\text{-axis}$$

Products of inertia: $\qquad I_{xy} = \int xy\, dm, \; I_{yz} = \int yz\, dm, \; I_{xz} = \int xz\, dm$

Parallel Axis Theorem: $I_{x'x'} = I_{xx} + m((\Delta y)^2 + (\Delta z)^2)$ etc, and $I_{x'y'} = I_{xy} + m\,(\Delta x)(\Delta y)$ etc.

Perpendicular Axis Theorem: for a lamina in the xy plane only, $I_{z'z'} = I_{x'x'} + I_{y'y'}$.

Inertia matrix: $\qquad \mathbf{I} = \begin{bmatrix} I_{xx} & -I_{xy} & -I_{xz} \\ -I_{xy} & I_{yy} & -I_{yz} \\ -I_{xz} & -I_{yz} & I_{zz} \end{bmatrix}$

The eigenvalues of $\mathbf{I}$ are the principal moments of inertia, and the eigenvectors are the principal axes, about which $\mathbf{h} = I\boldsymbol{\omega}$ i.e. $\mathbf{h} \parallel \boldsymbol{\omega}$.
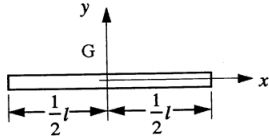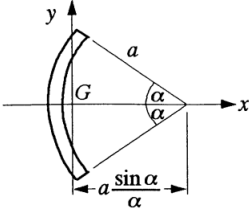
For a body with a plane of symmetry, two principal axes lie in the plane while the third is normal to the plane. An 'AAC' body is axisymmetric (e.g. prisms, all laminas). An 'AAA' body is symmetric in all three axes and has dynamic similarity.

Inertia matrix in the body frame of reference, with $\mathbf{R}$ as a rotation matrix from the inertial frame to the body frame: $\mathbf{I}_{\text{body}} = \mathbf{R}\mathbf{I}_{\text{principal}}\mathbf{R}^{\mathsf{T}}$, where all products of inertia are zero and the diagonal entries of $\mathbf{I}_{\text{principal}}$ are the principal moments of inertia (Sylvester's law of inertia).
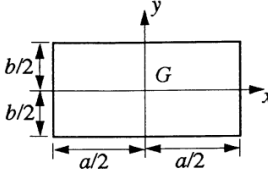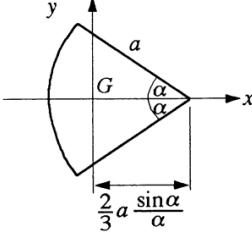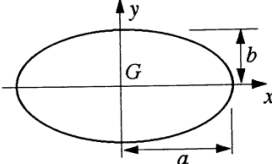
For formulas for moments of inertia of specific geometries, see Section 6.3.

6.1.14. Moments of Inertia and Centroids of 1D Bodies

Rods:

	k_x^2	k_y^2

Straight rod

0 $\dfrac{1}{12}l^2$

Curved rod

$\dfrac{1}{2}a^2\left(1-\dfrac{\sin 2\alpha}{2\alpha}\right)$ $\dfrac{1}{2}a^2\left\{1-2\left(\dfrac{\sin\alpha}{\alpha}\right)^2+\dfrac{\sin 2\alpha}{2\alpha}\right\}$

Laminas:

	A	k_x^2	k_y^2

Rectangular lamina

ab $\dfrac{1}{12}b^2$ $\dfrac{1}{12}a^2$

Sectorial lamina

αa^2 $\dfrac{a^2}{4}\left(1-\dfrac{\sin 2\alpha}{2\alpha}\right)$ $\dfrac{a^2}{4}\left\{1-\left(\dfrac{4\sin\alpha}{3\alpha}\right)^2+\dfrac{\sin 2\alpha}{2\alpha}\right\}$

Elliptic lamina

πab $\dfrac{b^2}{4}$ $\dfrac{a^2}{4}$

Laminas (continued):

	A	k_x^2	k_y^2

Triangular lamina

$$\frac{h}{2}(b_1 + b_2)$$

$$\frac{h^2}{18}$$

$$\frac{\left(b_1^2 + b_1 b_2 + b_2^2\right)}{18}$$

$$I_{xy} = m.\frac{h}{36}(b_1 - b_2)$$
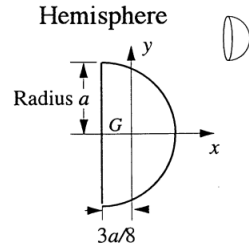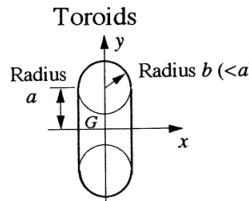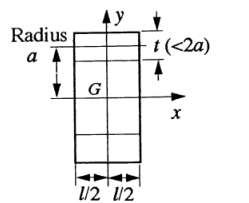
Regular polygonal lamina with N sides $(N > 2)$

$$\pi a^2 \left(\frac{\sin\frac{2\pi}{N}}{\frac{2\pi}{N}}\right)$$

$$\frac{a^2}{12}\left(2 + \cos\frac{2\pi}{N}\right)$$

$$\frac{a^2}{12}\left(2 + \cos\frac{2\pi}{N}\right)$$
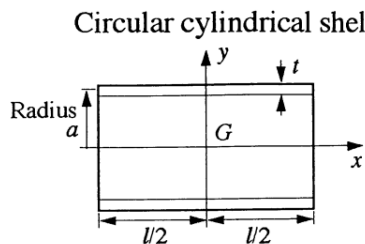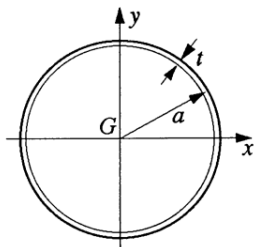
3D Solids of Revolution (Axisymmetric Bodies):

	V	k_x^2	$k_y^2 = k_z^2$

Cylinder

$$\pi a^2 l$$

$$\frac{a^2}{2}$$

$$\frac{a^2}{4} + \frac{l^2}{12}$$

Spheroid

$$\frac{4\pi ab^2}{3}$$

$$\frac{2b^2}{5}$$

$$\frac{\left(a^2 + b^2\right)}{5}$$

Cone

$$\frac{\pi a^2 h}{3}$$

$$\frac{3a^2}{10}$$

$$\frac{3\left(4a^2 + h^2\right)}{80}$$
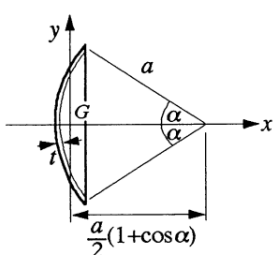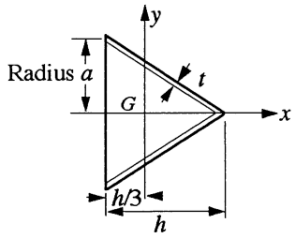
3D Solids of Revolution (Axisymmetric Bodies) (continued):

$$V \qquad\qquad k_x^{\,2} \qquad\qquad k_y^{\,2} = k_z^{\,2}$$

Hemisphere

$$\frac{2\pi a^3}{3} \qquad\qquad \frac{2a^2}{5} \qquad\qquad \frac{83a^2}{320}$$

Toroids

$$2\pi^2 ab^2 \qquad\qquad a^2 + \frac{3b^2}{4} \qquad\qquad \frac{a^2}{2} + \frac{5b^2}{8}$$

$$2\pi atl \qquad\qquad a^2 + \frac{t^2}{4} \qquad\qquad \frac{a^2}{2} + \frac{t^2}{8} + \frac{l^2}{12}$$

3D Shells of Revolution

$$V \qquad\qquad k_x^{\,2} \qquad\qquad k_y^{\,2} = k_z^{\,2}$$

Circular cylindrical shell

$$2\pi alt \qquad\qquad a^2 \qquad\qquad \frac{a^2}{2} + \frac{l^2}{12}$$

Spherical shell

$$4\pi a^2 t \qquad\qquad \frac{2a^2}{3} \qquad\qquad \frac{2a^2}{3}$$

3D Shells of Revolution (continued):

$$V \qquad\qquad k_x^2 \qquad\qquad k_y^2 = k_z^2$$

Spherical cap shell

$$2\pi a^2 t (1 - \cos\alpha) \qquad\qquad \frac{a^2}{12}(1 - \cos\alpha)(5 + \cos\alpha)$$

$$\frac{a^2}{3}(1 - \cos\alpha)(2 + \cos\alpha)$$

Conical shell

$$\pi a t \left(a^2 + h^2\right)^{\frac{1}{2}} \qquad \frac{a^2}{2} \qquad \frac{a^2}{4} + \frac{h^2}{18}$$

6.1.15. Second Moments of Area

The second moment of area of a plane cross-section about the x axis is denoted I_{xx}:

$$I_{xx} = \int y^2 \, dA$$

Warning: both moment of inertia and second moment of area use the symbol I. Moment of inertia has dimensions of $\mathbf{ML}^2$. Second moment of area has dimensions $\mathbf{L}^4$.

If the mass-per-unit-area σ is uniform across the cross-section, then

moment of inertia = $\sigma \times$ second moment of area

Second moments of area for common beam cross-sections:
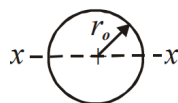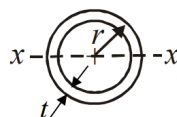
Solid circular section   Thin-walled circular section   Solid rectangle
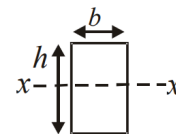
$$I_{xx} = \frac{\pi r_o^4}{4} \qquad\qquad I_{xx} \approx \pi r^3 t \qquad\qquad I_{xx} = \frac{bh^3}{12}$$

6.1.16. Polar Second Moments of Area

The polar second moment of area of a plane cross-section in the xy plane is denoted J:

$$I_{zz} = J = \int (x^2 + y^2)\, dA$$

If the mass-per-unit-area σ is uniform across the cross-section, then

polar moment of inertia $= \sigma \times$ polar second moment of area

For common cross-sections:
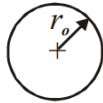
Solid circular section   Thick-walled circular section   Thin-walled circular section
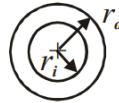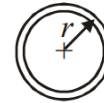
$$J = \frac{\pi\, r_o^{\,4}}{2} \qquad\qquad J = \frac{\pi\, (r_o^4 - r_i^4)}{2} \qquad\qquad J \approx 2\pi\, r^3 t$$

Main applications of I and J:

- Moment of inertia I is important for kinematics of rotating bodies.
- Second moment of area I is important for bending stresses in beams.
- Polar second moment of area J is important for torsional stresses in shafts.

6.1.17. Gyroscope Dynamics

For motion relative to axes aligned with the rotation of a rigid body (the body frame B, rotating at $\boldsymbol{\omega}$ relative to the rest frame):

Rate of change of a vector: $\dfrac{d}{dt}\mathbf{x} = \mathbf{x}_{\mathrm{B}} + \boldsymbol{\omega} \times \mathbf{x}_{\mathrm{B}}$

Euler's Equations: Torque-angular momentum in the body frame.

If A, B and C are the principal moments of inertia about P which is either at a fixed point or at the centre of mass, the angular velocity of the body is $\boldsymbol{\omega} = [\omega_1, \omega_2, \omega_3]^{\mathsf{T}}$ and the moment about P of external forces is $\mathbf{Q} = [Q_1, Q_2, Q_3]$, then

Body-fixed reference frame:	Non-body-fixed reference frame:
	(the AAC gyroscope equations)

$$A\dot{\omega}_1 - (B - C)\omega_2\omega_3 = Q_1$$
$$B\dot{\omega}_2 - (C - A)\omega_3\omega_1 = Q_2$$
$$C\dot{\omega}_3 - (A - B)\omega_1\omega_2 = Q_3$$

$$A\dot{\Omega}_1 - (A\Omega_3 - C\omega_3)\Omega_2 = Q_1$$
$$A\dot{\Omega}_2 + (A\Omega_3 - C\omega_3)\Omega_1 = Q_2$$
$$C\dot{\omega}_3 = Q_3$$

| using axes aligned with the principal axes of inertia of the body at P | using axes such that ω_3 and Q_3 are aligned with the symmetry axis of the body |

The reference frame when not fixed in the body rotates with angular velocity $\boldsymbol{\Omega} = [\Omega_1, \Omega_2, \Omega_3]^{\mathsf{T}}$ with $\Omega_1 = \omega_1$ and $\Omega_2 = \omega_2$.

For a simple gyroscope (J: polar moment of inertia parallel to $\boldsymbol{\omega}$):
$$\mathbf{Q} = \mathbf{r} \times m\mathbf{g} = J\,\boldsymbol{\Omega} \times \boldsymbol{\omega}$$

In general, resultant torque is $\mathbf{Q} = \mathbf{I}\boldsymbol{\alpha} + \boldsymbol{\omega} \times \mathbf{h}$,
where the additional $\boldsymbol{\omega} \times \mathbf{h}$ term is the Coriolis torque.
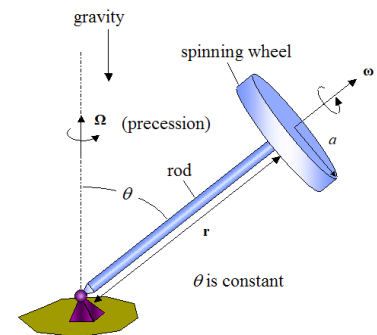
6.1.18. Representations of 3D Rigid Body Orientation

Three consecutive rotations applied starting from the rest frame to transform it into the body frame. The rotations may be 'intrinsic' (referring to the successively transformed body axes) or 'extrinsic' (always referring to the fixed rest frame axes). Two common schemes are:

Proper Euler Angles $\{\alpha, \beta, \gamma\}$: uses only two reference axes (first and last are the same)

Most common convention: z-x'-z'' (intrinsic). Rotate α about body z-axis, rotate β about new body x-axis (x'), rotate γ about new body z-axis (z''). If the body-frame unit vectors are measured in the rest frame as ($\hat{X} = X_1\mathbf{i} + X_2\mathbf{j} + X_3\mathbf{k}$, etc), then:

$$\alpha = \cos^{-1}\frac{-Z_2}{\sqrt{1-Z_3^2}} = \text{atan2}(Z_1, -Z_2), \quad \beta = \cos^{-1}Z_3, \quad \gamma = \cos^{-1}\frac{Y_3}{\sqrt{1-Z_3^2}} = \text{atan2}(X_3, Y_3)$$

Tait-Bryan / Nautical Angles $\{\varphi, \theta, \psi\}$: uses all three reference axes

Most common convention: z-y'-x'' (intrinsic). Rotate ψ about body z-axis, rotate θ about new body y axis (y'), rotate φ about new body x-axis (x''). If the body-frame unit vectors are measured in the rest frame as ($\hat{X} = X_1\mathbf{i} + X_2\mathbf{j} + X_3\mathbf{k}$, etc), then:

$$\varphi = \sin^{-1}\frac{X_2}{\sqrt{1-X_3^2}}, \quad \theta = \sin^{-1}(-X_3), \quad \psi = \sin^{-1}\frac{Y_3}{\sqrt{1-X_3^2}}$$

The Tait-Bryan angles are often used for vehicle navigation (e.g. aeroplanes, ships), in which the $\{X, Y, Z\}$ axes are specific to the vehicle. In the z-y'-x'' convention:

The 3 × 3 linear transformation matrix from fixed to body frames: $\mathbf{M} = \mathbf{R}_Z(\psi)\, \mathbf{R}_Y(\theta)\, \mathbf{R}_X(\varphi)$, where $\mathbf{R}$ are the rotation matrices (Section 4.2.1).

- ψ: yaw angle, giving the bearing about the Z-axis, aligned in the 'down' direction.
- θ: pitch angle, giving the elevation about the Y-axis, aligned in the 'right' direction.
- φ: roll angle, giving the bank about the X-axis, aligned in the 'forward' direction.

Axis-Angle and Quaternion Representation of Rotations

Any sequence of 3D rotations can be represented as a single rotation φ about an axis $\mathbf{X} = [X_1, X_2, X_3]$, due to the Rodriguez formula (Section 4.2.1).

Quaternions can be considered an extension of how complex numbers can represent 2D rotations. A quaternion $q = w + x\mathbf{i} + y\mathbf{j} + z\mathbf{k}$, such that $\{w, x, y, z\}$ are real and $\mathbf{i}^2 = \mathbf{j}^2 = \mathbf{k}^2 = \mathbf{ijk} = -1$.

Unit quaternion $q = \cos\frac{\varphi}{2} + X_1 \sin\frac{\varphi}{2}\mathbf{i} + X_2 \sin\frac{\varphi}{2}\mathbf{j} + X_3 \sin\frac{\varphi}{2}\mathbf{k}$ represents $\mathbf{R}_\mathbf{X}(\varphi)$ via $x' = qxq^{-1}$.

Working in terms of quaternions instead of matrices results in significant computational speedups, and also avoids the issue of 'gimbal lock' for degenerate rotations.

6.2. Linear Systems and Mechanical Vibrations

6.2.1. Equations for Natural Oscillations

Angular velocity, period and frequency: $\omega = 2\pi f = \dfrac{2\pi}{T}$ (*T*: time period)

Simple 1D SHM kinematics: $x = A\cos\omega t, \quad v = -A\omega\sin\omega t, \quad a = -A\omega^2\cos\omega t$

$$v = \pm\,\omega\sqrt{A^2 - x^2}, \qquad a = -\omega^2 x$$

Max speed $= A\omega$ Max acceleration $= A\omega^2$

Energy balance (no external forces): $T + V = constant \iff \dfrac{d}{dt}(T + V) = 0$

6.2.2. Common Undamped Oscillating Systems

For a linear spring-mass system: $\omega^2 = \dfrac{k}{m}, \qquad T = 2\pi\sqrt{\dfrac{m}{k}}, \qquad \dfrac{1}{2}mv^2 + \dfrac{1}{2}kx^2 = C$

For a plane pendulum: $\Omega^2 = \dfrac{g}{L}, \qquad T = 2\pi\sqrt{\dfrac{L}{g}}, \dfrac{1}{2}m\omega^2 L^2 - mgL\cos\theta = C$

For a rotational spring-flywheel: $\Omega^2 = \dfrac{\kappa}{J}, \qquad T = 2\pi\sqrt{\dfrac{J}{\kappa}}, \qquad \dfrac{1}{2}J\omega^2 + \dfrac{1}{2}\kappa\theta^2 = C$

For a standing wave on a string: $\omega^2 = \dfrac{\pi^2 P}{L^2\rho}, \qquad T = 2L\sqrt{\dfrac{\rho}{P}}$

(*k*: spring constant, *m*: mass, *g*: gravity, *L*: length, *κ*: rotational stiffness,
J: polar moment of inertia, *P*: string tension, *ρ*: string mass per unit length)

6.2.3. Step Response of a Linear Second Order System

For a model of the form $\dfrac{1}{\omega_n^2}y'' + \dfrac{2\zeta}{\omega_n}y' + y = x$ with $y(0) = y'(0) = 0$ and $x = K\,H(t)$,

$$\frac{y}{K} = 1 - \frac{1}{2\omega_n\sqrt{\zeta^2-1}}\left(\lambda^{(+)}e^{\lambda^{(-)}t} - \lambda^{(-)}e^{\lambda^{(+)}t}\right), \qquad \text{if overdamped } (\zeta > 1)$$

$$\frac{y}{K} = 1 - (1 + \omega_n t)\,e^{-\omega_n t}, \qquad \text{if critically damped } (\zeta = 1)$$

$$\frac{y}{K} = 1 - \frac{1}{\sqrt{1-\zeta^2}}\,e^{-\zeta\omega_n t}\cos\!\left(\omega_d t - \psi\right), \qquad \text{if underdamped } (\zeta < 1)$$

$$\frac{y}{K} \approx 1 - e^{-\zeta\omega_n t}\cos\omega_n t, \qquad \text{if lightly damped } (\zeta \ll 1)$$

where $\qquad \lambda^{(\pm)} = \left(-\,\zeta \pm \sqrt{\zeta^2 - 1}\right)\omega_n, \qquad\qquad \omega_d = \omega_n\sqrt{1 - \zeta^2}, \qquad \sin\psi = \zeta.$

Dimensionless plots of step response:
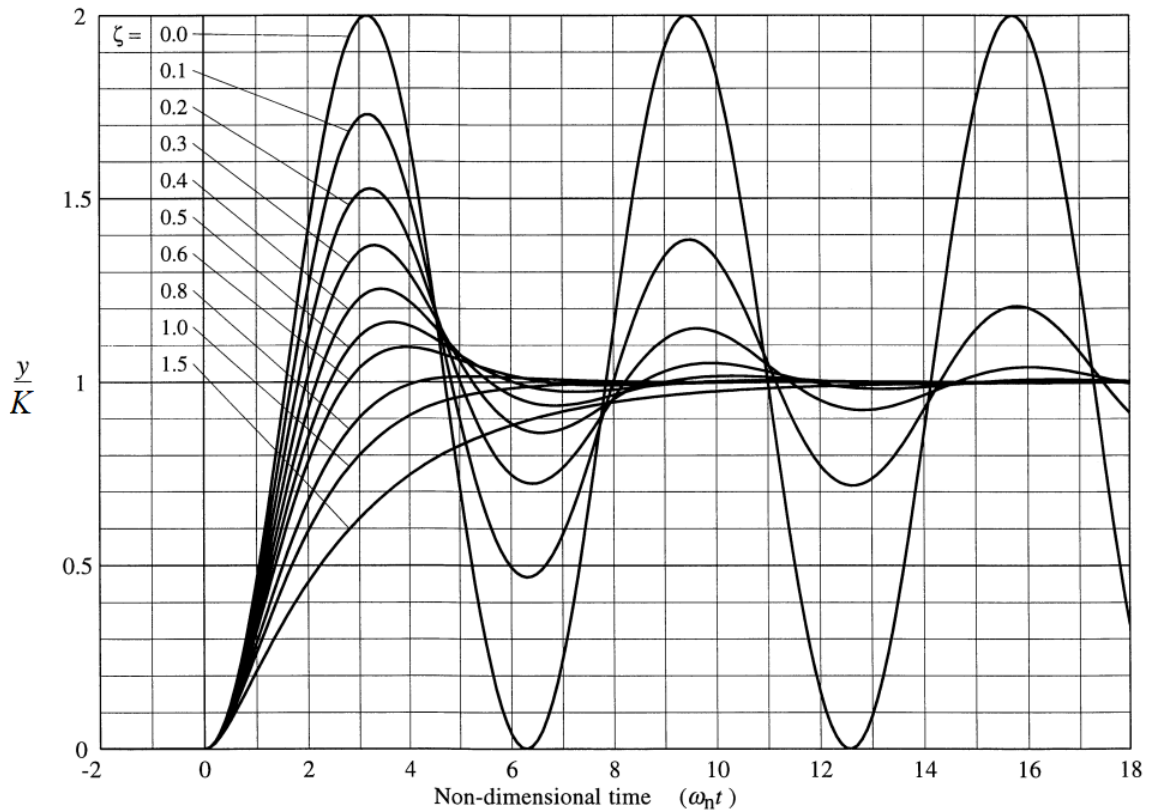
6.2.4. Impulse Response of a Linear Second Order System

For a model of the form $\dfrac{1}{\omega_n^2}\ddot{y} + \dfrac{2\zeta}{\omega_n}\dot{y} + y = x$ with $y(0) = \dot{y}(0) = 0,\ x(t) = N\delta(t)$,

$$\frac{y(t)}{\omega_n N} = \frac{1}{2\sqrt{\zeta^2 - 1}}\left(e^{\lambda_+ t} - e^{\lambda_- t}\right)$$

if overdamped ($\zeta > 1$)

$$\frac{y(t)}{\omega_n N} = \omega_n t\, e^{-\omega_n t}$$

if critically damped ($\zeta = 1$)

$$\frac{y(t)}{\omega_n N} = \frac{1}{\sqrt{1 - \zeta^2}}\, e^{-\zeta \omega_n t}\, \sin \omega_d t$$

if underdamped ($\zeta < 1$)

$$\frac{y(t)}{\omega_n N} \approx e^{-\zeta \omega_n t}\, \sin \omega_n t$$

if very lightly damped ($\zeta \ll 1$)

where $\lambda_{\pm} = (-\zeta \pm \sqrt{\zeta^2 - 1})\,\omega_n$ (system s-domain poles), $\omega_d = \omega_n\sqrt{1 - \zeta^2}$, and $\sin \psi = \zeta$.

Transfer function in s-domain: $\dfrac{\hat{y}(s)}{\hat{x}(s)} = \dfrac{N\omega_n^2}{s^2 + 2\omega_n\zeta s + \omega_n^2}$

Dimensionless plots of impulse response for a variety of damping rates ζ:
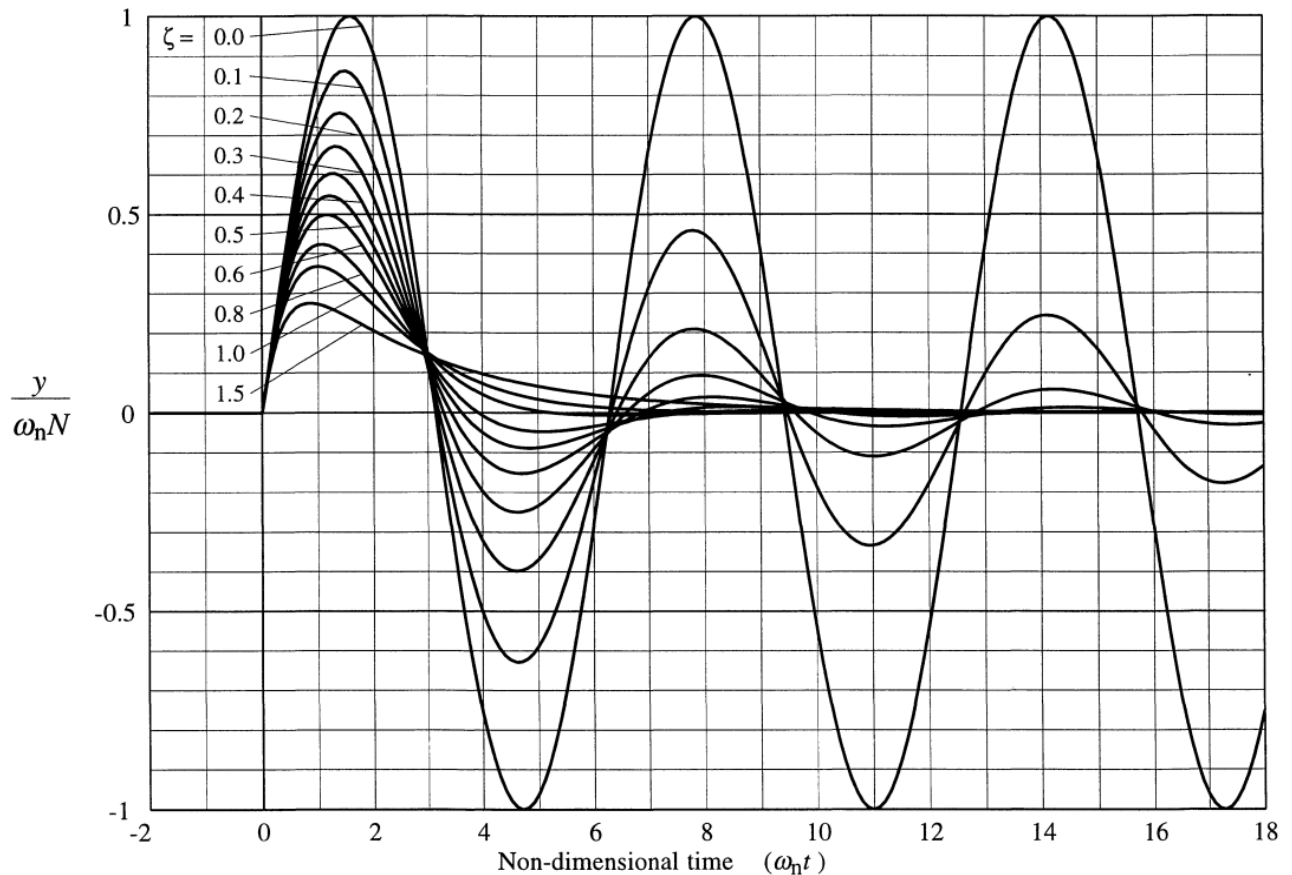
6.2.5. Harmonic Response of a Linear Second Order System (Forced Displacements)
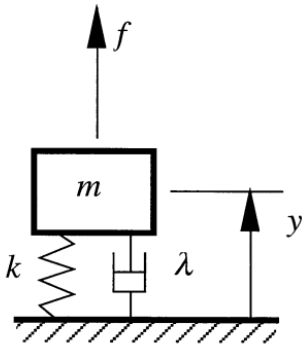
For a model of the form $\dfrac{1}{\omega_n^2}\ddot{y} + \dfrac{2\zeta}{\omega_n}\dot{y} + y = x$, the harmonic gain is

$$\frac{Y}{X} = \frac{1}{-\tilde{\omega}^2 + 2i\zeta\tilde{\omega} + 1}, \qquad \left|\frac{Y}{X}\right| = \frac{1}{\sqrt{(1-\tilde{\omega}^2)^2 + (2\zeta\tilde{\omega})^2}}$$

$(x = \mathrm{Re}(X\,\mathrm{e}^{i\omega t}) = X\cos\omega t, \ \ y = \mathrm{Re}(Y\,\mathrm{e}^{i\omega t}) = |Y|\cos(\omega t + \phi), \ \ \tan\phi = \dfrac{-2\tilde{\omega}}{1-\tilde{\omega}^2}, \ \ \tilde{\omega} = \dfrac{\omega}{\omega_n})$

For a mass-spring-damper system (Section 6.2.8), let $x = \dfrac{f}{k}, \ \omega_n = \sqrt{\dfrac{k}{m}}, \ \zeta = \dfrac{\lambda}{2\sqrt{km}}$.

Maximum response: $|Y_{\max}| = \dfrac{X}{2\zeta\sqrt{1-\zeta^2}}$ when $\dfrac{\omega}{\omega_n} = \sqrt{1 - 2\zeta^2}$, existing if $\zeta < \dfrac{1}{\sqrt{2}}$.

Dimensionless frequency response (Bode plot) at steady-state:
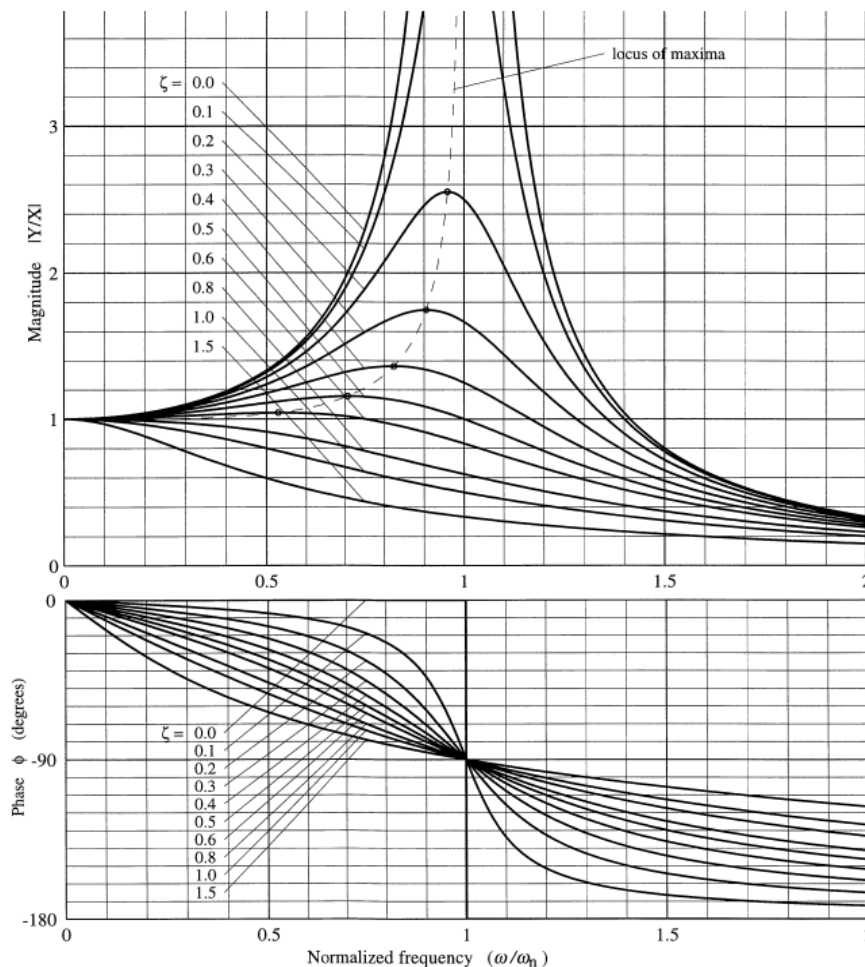
6.2.6. Harmonic Response of a Linear Second Order System (Base Displacements)

In cases where the input is a base displacement rather than a force, the RHS takes the form of a D'Alembert force. The two common cases (aside from that in Section 6.2.5) are shown.

If $x = \mathrm{Re}(X\,e^{i\omega t}) = X\cos\omega t,\ y = \mathrm{Re}(Y\,e^{i\omega t}) = |Y|\cos(\omega t + \phi)$ then: $\qquad (\omega_n = \sqrt{\dfrac{k}{m}},\ \zeta = \dfrac{\lambda}{2\sqrt{km}})$

Relative Response to Base Displacement: $\qquad$ **Absolute Response** to Base Displacement
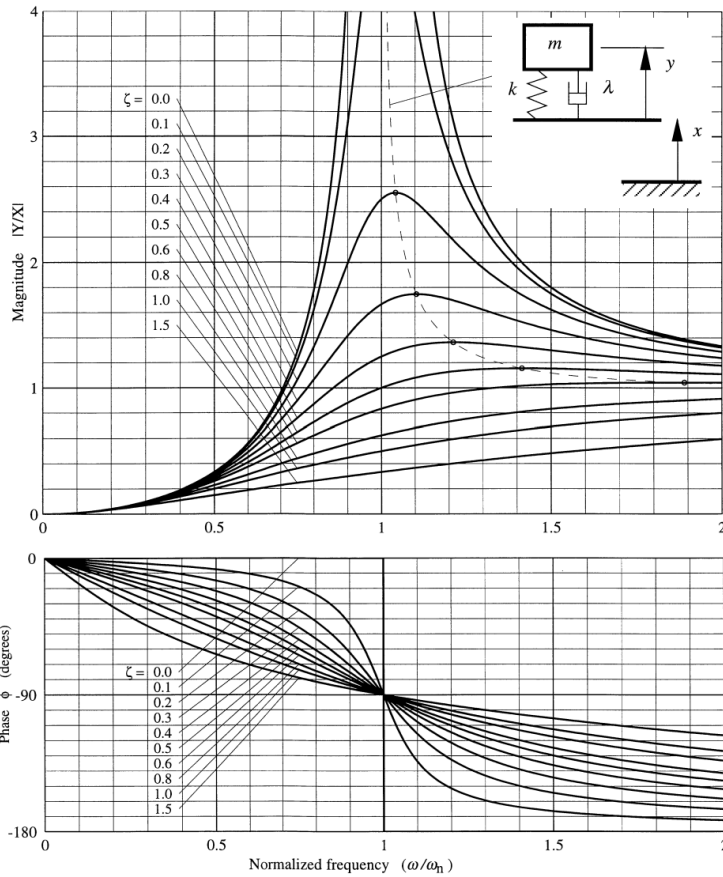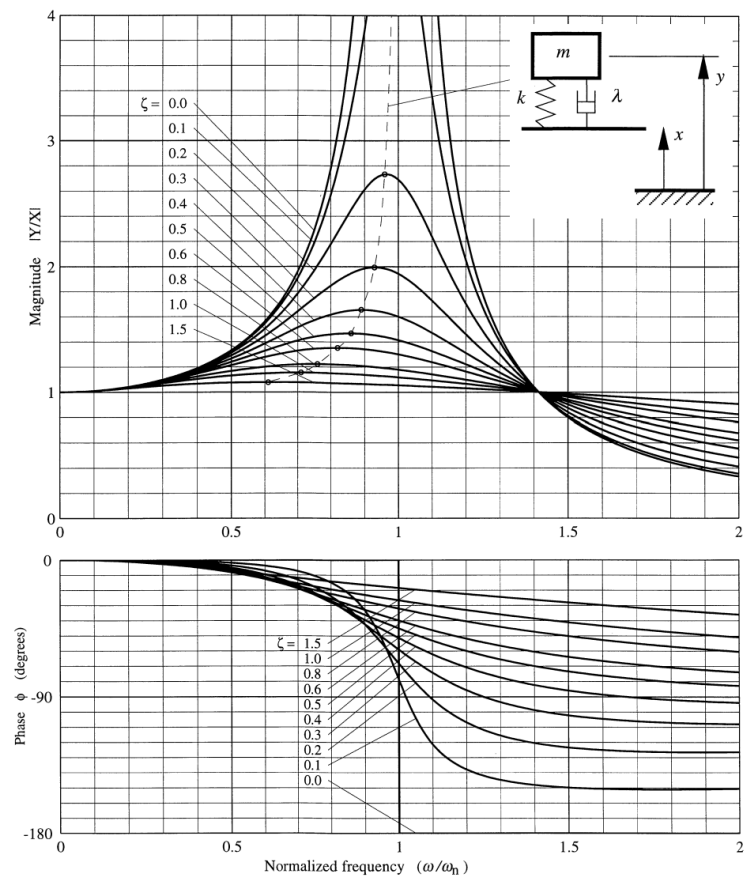
$$\frac{1}{\omega_n^2}y'' + \frac{2\zeta}{\omega_n}y' + y = -\frac{1}{\omega_n^2}x'' \qquad\qquad \left(\tilde{\omega} = \frac{\omega}{\omega_n}\right) \qquad\qquad \frac{1}{\omega_n^2}y'' + \frac{2\zeta}{\omega_n}y' + y = \frac{2\zeta}{\omega_n}x' + x$$

$$\frac{Y}{X} = \frac{\tilde{\omega}}{-\tilde{\omega}^2 + 2i\zeta\tilde{\omega} + 1} \qquad\qquad\qquad\qquad\qquad \frac{Y}{X} = \frac{2i\zeta\tilde{\omega} + 1}{-\tilde{\omega}^2 + 2i\zeta\tilde{\omega} + 1}$$

$$\left|\frac{Y}{X}\right| = \tilde{\omega}^2\left[\left(1 - \tilde{\omega}^2\right)^2 + 2\zeta\tilde{\omega}\right]^{-1/2}, \quad \tan\phi = \frac{-2\zeta\tilde{\omega}}{1 - \tilde{\omega}^2} \qquad \left|\frac{Y}{X}\right| = \left(\frac{1 + (2\zeta\tilde{\omega})^2}{(1 - \tilde{\omega}^2)^2 + (2\zeta\tilde{\omega})^2}\right)^{1/2}, \quad \tan\phi = \frac{-2\zeta\tilde{\omega}^3}{1 - (1 - 4\zeta^2)\tilde{\omega}^2}$$

$$|Y_{\max}| = \frac{X}{2\zeta\sqrt{1 - \zeta^2}} \quad \text{when} \quad \tilde{\omega} = \frac{1}{\sqrt{1 - 2\zeta^2}} \qquad\qquad |Y_{\max}| \approx \frac{X}{2\zeta}\left(1 + \frac{5}{2}\zeta^2\right) \quad \text{when} \quad \tilde{\omega} = 1 - \zeta^2$$

existing if $\zeta < 1/\sqrt{2}$ $\qquad\qquad\qquad\qquad\qquad\qquad\qquad\qquad\qquad$ existing always, but valid only if $\zeta \ll 1$

6.2.7. Measures of Damping and Stiffness for an Underdamped System

If y_0 and y_N are peaks of a step or impulse response separated by N periods, then the logarithmic decrement is

$$N\Delta = \ln\frac{y_0}{y_N} = \frac{2\pi N\,\zeta}{\sqrt{1-\zeta^2}}$$

Time constant τ and attenuation rate α of exponential envelope $e^{-t/\tau}$: $\qquad \tau = \frac{2Q}{\omega_n} = \frac{1}{\zeta\omega_n} = \frac{1}{\alpha}$.

Q-factor: $\qquad Q = 2\pi \times \dfrac{energy\ stored}{energy\ dissipated\ per\ cycle} = \dfrac{1}{2\zeta}$

Loss factor: η, often used to suppress frequency dependence of ζ for practical systems. At resonance, $\eta = 2\zeta$.

Proportion of energy lost per cycle $= 2\pi\eta$.

Complex stiffness: $k^* = k(1 + j\eta)$

Loss tangent: $\tan\delta$, equal to the tangent of the phase shift, $\tan\phi$ (δ: loss angle)

$\qquad\qquad\qquad\qquad \delta = \arg k^*$ (dissipative modulus / elastic modulus)

Sinusoidal Forced Loading: if $\varepsilon(t) = e^{j\omega t}$ and $\sigma(t) = G^*(\omega)\,e^{j\omega t}$, then:

Dynamic modulus: $\qquad G^*(\omega) = G'(\omega) + j\,G''(\omega)$ $\qquad\qquad$ (G': storage, G'': loss)

In the Laplace domain: $\qquad \overline{G'}(s)\,\overline{G''}(s) = s^{-2}$

For more on viscoelasticity and the electrical circuit analogy see Section 6.2.9.

(Note that this is the **opposite** of the analogous electrical system, in which real and imaginary parts of impedance are effectively swapped in terms of dissipation (resistance) vs exchange (reactance).)

For lightly damped systems ($\zeta \ll 1$):

Logarithmic decrement: $\quad N\Delta \approx 2\pi\,N\zeta$

Loss factor and loss tangent: $\qquad \eta \approx \frac{2\zeta\omega}{\omega_n}$ and $\tan\delta \approx \eta$ $\qquad$ (δ: loss angle)

Q factor: $\qquad Q = \dfrac{1}{2\zeta}$

Half-power bandwidth: $\qquad \Delta\omega = \dfrac{\omega_n}{Q} = 2\omega_n\zeta = \dfrac{2}{\tau}$ $\qquad$ for which $|Y| \geq \dfrac{1}{\sqrt{2}}\,|Y_{max}|$

$\qquad\qquad\qquad\qquad$ (valid for both forced displacements and base displacements)

6.2.8. Mass-Spring-Damper Systems
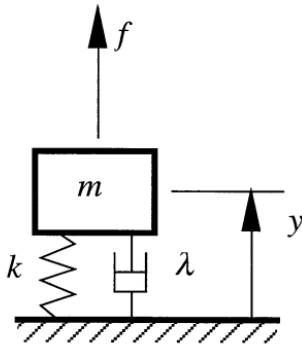
The spring and damper exert resistive forces of magnitude ky and $\lambda y'$ respectively. This system has dynamic model

$$my'' + \lambda y' + ky = f \quad \Leftrightarrow \quad \frac{1}{\omega_n^2}y'' + \frac{2\zeta}{\omega_n}y' + y = x, \text{ where}$$

$$x = \frac{f}{k} \qquad \omega_n = \sqrt{\frac{k}{m}} \qquad \zeta = \frac{\lambda}{2\sqrt{km}}$$

$$T = \frac{2\pi}{\omega_d} = \frac{2\pi}{\omega_n\sqrt{1-\zeta^2}} \qquad Q = \frac{\sqrt{mk}}{\lambda} \qquad \Delta\omega = \frac{\lambda}{m}$$

Mechanical power balance:

$$\frac{\mathrm{d}}{\mathrm{d}t}\left(\underbrace{\frac{1}{2}m\dot{y}^2}_{\substack{\text{kinetic}\\\text{energy}}} + \underbrace{mgy}_{\substack{\text{gravitational}\\\text{potential energy}}} + \underbrace{\frac{1}{2}ky^2}_{\substack{\text{elastic strain}\\\text{energy}}} \right) = \underbrace{f\dot{y}}_{\substack{\text{driving}\\\text{power}}} - \underbrace{\lambda\dot{y}^2}_{\substack{\text{damper}\\\text{dissipation}}}$$

Transfer function: $\quad \dfrac{\bar{y}}{\bar{f}} = \dfrac{1}{ms^2 + \lambda s + k}$

Combining in:	Series	Parallel
Springs k_1 and k_2	$\dfrac{1}{k'} = \dfrac{1}{k_1} + \dfrac{1}{k_2}$	$k' = k_1 + k_2$
Dampers λ_1 and λ_2	$\dfrac{1}{\lambda'} = \dfrac{1}{\lambda_1} + \dfrac{1}{\lambda_2}$	$\lambda' = \lambda_1 + \lambda_2$

6.2.9. Fundamental Models of Viscoelasticity and their Dynamic Responses

Viscoelastic materials can be modelled by 'springs' with Young's modulus E and 'dampers' with dynamic viscosity η, for which the stress σ, strain ε and strain rate $\dot{\varepsilon}$ are related by $\sigma = E\varepsilon$ and $\sigma = \eta\dot{\varepsilon}$. (For shear phenomena, τ, γ and G may be used instead.)

The Kelvin-Voigt, Maxwell, and Standard Linear Solid (SLS) models are shown below.

Kelvin-Voigt   Maxwell   Standard Linear Solid (SLS)

| Dynamic model (ODE) | $\tau_1\dot{\varepsilon} + \varepsilon = \sigma/E_1$ | $\tau_1\dot{\sigma} + \sigma = \eta_1\dot{\varepsilon}$ | $\tau_1\dot{\sigma} + \sigma = E_2(\varepsilon + \tau^*\dot{\varepsilon})$ |

$\sigma(t) = \sigma_0 H(t)$
Creep response
(stress step)

$\varepsilon(t) = \varepsilon_0 H(t)$
Relaxation response
(strain step)

$\varepsilon(t) = \varepsilon_0 e^{i\omega t}$
$\sigma(t) = \sigma_0 e^{i\omega t}$
Harmonic response

| | $\dfrac{\sigma}{\varepsilon} = E_1(1 + i\omega\tau_1)$ | $\dfrac{\sigma}{\varepsilon} = \dfrac{i\omega\eta_1}{1 + i\omega\tau_1}$ | $\dfrac{\sigma}{\varepsilon} = E_2 \cdot \dfrac{1 + i\omega\tau^*}{1 + i\omega\tau_1}$ |
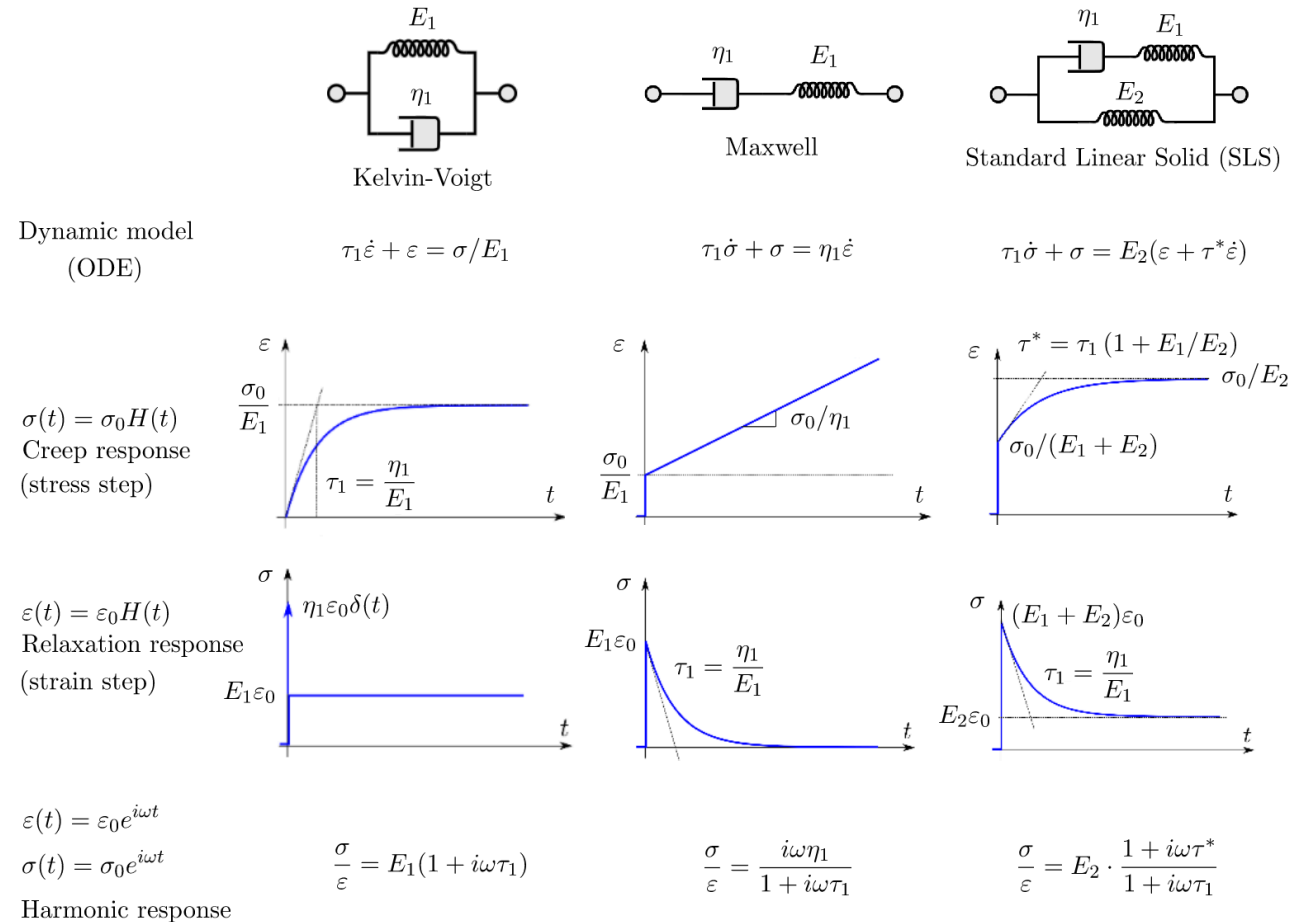
The SLS model may alternatively formulated in series, which are dynamically equivalent:

$$\sigma + \tau_a \frac{E_a}{E_a + E_b}\dot{\sigma} = \frac{E_a E_b}{E_a + E_b}\varepsilon + \tau_a\dot{\varepsilon}$$

$$\tau_a = \frac{\eta_a}{E_a}$$

$$\begin{cases} E_a = (E_1 + E_2)\frac{E_2}{E_1} \\ E_b = E_1 + E_2 \\ \eta_a = \eta_1\left(1 + \frac{E_2}{E_1}\right)^2 \end{cases} \Leftrightarrow \begin{cases} E_1 = \frac{E_b^2}{E_a + E_b} \\ E_2 = \frac{E_a E_b}{E_a + E_b} \\ \eta_1 = \frac{E_b^2}{(E_a + E_b)^2}\eta_a \end{cases}$$

Parallel SLS   Series SLS   Series SLS dynamic model   Transformations
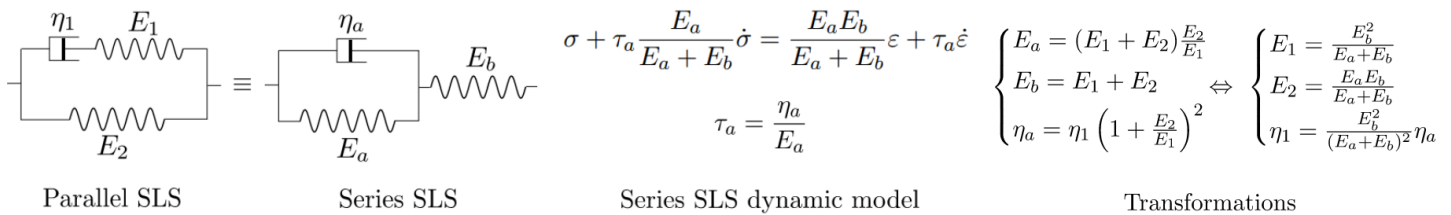
Combining models: Creep responses add in series. Relaxation responses add in parallel.

Electrical circuit analogy: $v \leftrightarrow \sigma$, $i \leftrightarrow \varepsilon$, $\sigma = \varepsilon Z$; $Z_{\text{spring}} = E$ ('resistor'), $Z_{\text{damper}} = j\omega\eta$ ('inductor')
(If formulated instead with $v \leftrightarrow \varepsilon$ and $i \leftrightarrow \sigma$ then use admittances instead.)

6.2.10. Applications of Viscoelasticity and Nonlinear Elasticity

Linear models work well for certain classes of substances as first-order approximations:

- The **Kelvin-Voigt model** best represents viscous gelatinous substances such as hydrogels. The stresses in the polymer chains approximately represent the spring while the stresses in the water approximately represent the dashpot.

- The **Maxwell model** best represents long chain mobile molecules which slide over each other, binding and unbinding.

- The **Standard Linear Solid model** best represents thermoplastic polymers below their glass transition temperature.
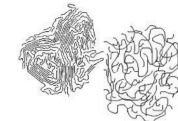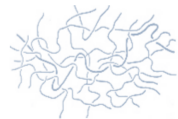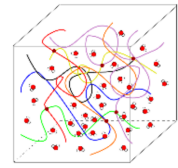
The Sequential Recruitment Model works for some materials where stiffness increases with strain e.g. biomaterials such as collagen (see Section 16.5.7).

This may occur when material fibres are reorienting themselves under strain to help carry the imposed stress, effectively 'recruiting' linear elastic elements in parallel.
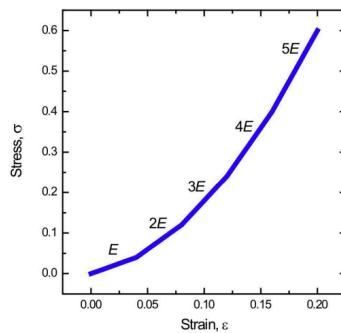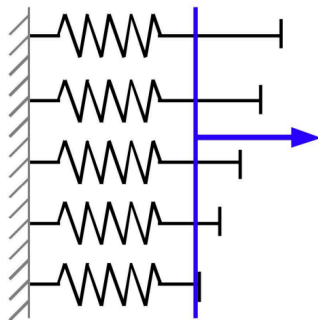
For a stress-strain response of the form

$$\sigma = a\varepsilon^2 + b\varepsilon,$$

this is modelled by an incremental stiffness of $\frac{dE}{d\varepsilon} = a$

and an initial stiffness of $E(0) = b$.

Mechanical properties of matter can be investigated experimentally using a universal mechanical tester (UMT), dynamic mechanical analyser (DMA), or rheometer.

6.2.11. Routh-Hurwitz Stability Criteria of Higher Order Systems

For a higher order system with **positive** coefficients of y and its derivatives i.e. all $a_i > 0$,

2nd-order: $a_2 y'' + a_1 y' + a_0 y = x$ is stable, always (provided $a_i > 0$)

3rd-order: $a_3 y''' + a_2 y'' + a_1 y' + a_0 y = x$ is stable if also $a_1 a_2 > a_0 a_3$

4th-order: $a_4 y'''' + a_3 y''' + a_2 y'' + a_1 y' + a_0 y = x$ is stable if also $a_1 a_2 a_3 > a_0 a_3^2 + a_4 a_1^2$

6.2.12. Vibration of a Conservative System with One Degree of Freedom

Potential energy: $V(q)$ Kinetic energy: $T = \dfrac{1}{2}M(q)\dot{q}^2$

At an equilibrium position $q = q_0$: $V'(q_0) = 0$ which is stable if $V''(q_0) > 0$.

Small oscillations about this equilibrium have natural frequency $\omega_n^{\,2} = \dfrac{V''(q_0)}{M(q_0)}$

6.2.13. Lagrangian Mechanics

For mechanical systems, the Lagrangian is defined as $\mathcal{L} = T - V$. The action is $S = \int L\,dt$. The path of a system in phase space (q, q') will minimise the action S, so the equations of motion are given by applying the Euler-Lagrange equation to S. Then, for a holonomic system with generalised coordinates q_i,

$$\frac{d}{dt}\left(\frac{\partial \mathcal{L}}{\partial \dot{q}_i}\right) = \frac{\partial \mathcal{L}}{\partial q_i} + Q_i \qquad \text{or expanding,} \qquad \frac{d}{dt}\left[\frac{\partial T}{\partial \dot{q}_i}\right] - \frac{\partial T}{\partial q_i} + \frac{\partial V}{\partial q_i} = Q_i$$

where T is the total kinetic energy, V is the total potential energy, and Q_i are the nonconservative generalised forces.

Noether's theorem: every differentiable symmetry of the action of a physical system with conservative forces has a corresponding conservation law.

Linearisation about an equilibrium $\mathbf{q}_0$: let $\mathbf{q} = \mathbf{q}_0 + \delta\mathbf{q}$, $\qquad \dot{\mathbf{q}} = \delta\dot{\mathbf{q}}$, $\qquad \ddot{\mathbf{q}} = \delta\ddot{\mathbf{q}}$.
Expand the Lagrangian to **second** order in $\delta\mathbf{q}$ and its derivatives.

In general, with $\mathbf{M}$ as the mass matrix and $\mathbf{K}$ as the stiffness matrix,

$$M_{ij} = \left.\frac{\partial^2 T}{\partial \dot{q}_i \partial \dot{q}_j}\right|_{\mathbf{q}=\mathbf{q}_0} \qquad K_{ij} = \left.\frac{\partial^2 V}{\partial q_i \partial q_j}\right|_{\mathbf{q}=\mathbf{q}_0}.$$

Then the Lagrangian linearised about $\mathbf{q}_0$ is

$$\mathcal{L}(\delta\mathbf{q}, \delta\dot{\mathbf{q}}) \approx V(\mathbf{q}_0) + \frac{1}{2}\delta\dot{\mathbf{q}}^T M \delta\dot{\mathbf{q}} - \frac{1}{2}\delta\mathbf{q}^T K \delta\mathbf{q}$$
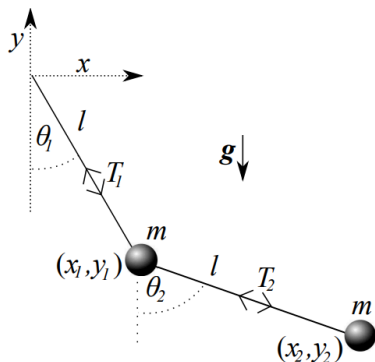
Typical Lagrangian of a double pendulum (polar coords):

$$\mathcal{L}(\theta_1, \theta_2, \dot{\theta}_1, \dot{\theta}_2) = \frac{1}{2}ml^2\left(2\dot{\theta}_1^2 + \dot{\theta}_2^2 + 2\dot{\theta}_1\dot{\theta}_2\cos(\theta_2 - \theta_1)\right)$$

$$+ mgl(2\cos\theta_1 + \cos\theta_2).$$

6.2.14. Parametric Resonance

When the mass, stiffness or damping factors are functions of time t, the governing
equation has the form $\ddot{q} + \omega_0^2 q = h\omega_0^2 \cos(\omega t)q$ for $h \ll 1$.   (Matthieu's equation)

For simple systems without coupling of modes, the resonant frequency of a parametrically
resonating system is **twice** the resonance frequency of the same nonparametric system.

Higher order terms in ω_0 lead to nonlinear vibrations.

6.2.15. Hamiltonian Mechanics

The generalised momentum p_i and the Hamiltonian $H(\mathbf{p}, \mathbf{q})$ are defined as

$$p_i = \frac{\partial T}{\partial \dot{q}_i}, \qquad H(\boldsymbol{p}, \boldsymbol{q}) = \sum_i p_i \dot{q}_i - T + V$$

Note that the velocities must be expressed as a function of the generalised momenta p
and the generalised displacements q.

Hamilton's equations are then $\dot{q}_i = \frac{\partial H}{\partial p_i}, \qquad \dot{p}_i = -\frac{\partial H}{\partial q_i} + Q_i.$

For the Hamiltonian as it applies to quantum mechanics, see Section 10.1.9.

6.2.16. Canonical Transformation of Hamilton's Equation

The total time derivative of some function $f(\mathbf{p}, \mathbf{q}, t)$ can be expressed in terms of the
Poisson bracket $\{f, H\}$ in the form

$$\frac{df}{dt} = \frac{\partial f}{\partial t} + \{f, H\}, \qquad \{f, H\} \equiv \sum_i \left[\frac{\partial f}{\partial q_i} \frac{\partial H}{\partial p_i} - \frac{\partial f}{\partial p_i} \frac{\partial H}{\partial q_i} \right].$$

Common forms of Canonical Transform for Hamilton's equations (to the "Kamiltonian" K) are:

Type	Generating function	1st eqn	2nd eqn	Kamiltonian
1	$G_1(\boldsymbol{q}, \boldsymbol{Q}, t)$	$\boldsymbol{p} = \dfrac{\partial G_1}{\partial \boldsymbol{q}}$	$\boldsymbol{P} = -\dfrac{\partial G_1}{\partial \boldsymbol{Q}}$	$K = H + \dfrac{\partial G_1}{\partial t}$
2	$G_2(\boldsymbol{q}, \boldsymbol{P}, t)$	$\boldsymbol{p} = \dfrac{\partial G_2}{\partial \boldsymbol{q}}$	$\boldsymbol{Q} = \dfrac{\partial G_2}{\partial \boldsymbol{P}}$	$K = H + \dfrac{\partial G_2}{\partial t}$
3	$G_3(\boldsymbol{p}, \boldsymbol{Q}, t)$	$\boldsymbol{q} = -\dfrac{\partial G_3}{\partial \boldsymbol{p}}$	$\boldsymbol{P} = -\dfrac{\partial G_3}{\partial \boldsymbol{Q}}$	$K = H + \dfrac{\partial G_3}{\partial t}$
4	$G_4(\boldsymbol{p}, \boldsymbol{P}, t)$	$\boldsymbol{q} = -\dfrac{\partial G_4}{\partial \boldsymbol{p}}$	$\boldsymbol{Q} = \dfrac{\partial G_4}{\partial \boldsymbol{P}}$	$K = H + \dfrac{\partial G_4}{\partial t}$

6.2.17. Undamped Vibration Modes and Response

The forced vibration of an N-degree-of-freedom system with mass matrix $\mathbf{M}$ and stiffness matrix $\mathbf{K}$ (both symmetric and positive definite) is governed by

$$\mathbf{M}\ddot{\mathbf{y}} + \mathbf{K}\mathbf{y} = \mathbf{f}$$

where $\mathbf{y}$ is the vector of displacements and $\mathbf{f}$ is the vector of forces.

Kinetic energy and potential energy: $T = \dfrac{1}{2}\dot{\mathbf{y}}^T\mathbf{M}\dot{\mathbf{y}}$ $V = \dfrac{1}{2}\mathbf{y}^T\mathbf{K}\mathbf{y}$

Natural frequencies ω_n and mode shapes $\mathbf{u}^{(n)}$: $\mathbf{K}\mathbf{u}^{(n)} = \omega_n^2\mathbf{M}\mathbf{u}^{(n)}$

Orthogonality and normalisation of modes: $\mathbf{u}^{(j)^T}\mathbf{M}\mathbf{u}^{(k)} = \begin{cases} 0 & j \neq k \\ 1 & j = k \end{cases}$

$$\int u_j(x)u_k(x)\mathrm{d}m = \begin{cases} 0 & j \neq k \\ 1 & j = k \end{cases}$$

$$\mathbf{u}^{(j)^T}\mathbf{K}\mathbf{u}^{(k)} = \begin{cases} 0 & j \neq k \\ \omega_j^2 & j = k \end{cases}$$

6.2.18. General Response in Modal Coordinates

The general response of the system can be written as a sum of modal responses:

$$\mathbf{y}(t) = \sum_{j=1}^{N} q_j(t)\mathbf{u}^{(j)} = \mathbf{U}\mathbf{q}(t)$$

where $\mathbf{U}$ is a matrix whose N columns are the normalised eigenvectors $\mathbf{u}^{(j)}$ and q_j can be thought of as the 'quantity' of the jth mode.

Modal coordinates satisfy $\quad \ddot{\mathbf{q}} + \left[\mathrm{diag}(\omega_j^2)\right]\mathbf{q} = \mathbf{Q} \qquad \mathbf{y} = \mathbf{U}\mathbf{q}, \;\; \text{modal force } \mathbf{Q} = \mathbf{U}^{\mathsf{T}}\mathbf{f}$

Transfer functions for the general responses are

Step Response:

$$h(j,k,t) = y_k(t) = \sum_{n=1}^{N} \frac{u_j^{(n)} u_k^{(n)}}{\omega_n^2}\left[1 - \cos\omega_n t\right]$$

for $t \geq 0$ (with no damping), or

$$h(j,k,t) \approx \sum_{n=1}^{N} \frac{u_j^{(n)} u_k^{(n)}}{\omega_n^2}\left[1 - e^{-\omega_n \zeta_n t}\cos\omega_n t\right]$$

for $t \geq 0$ (with small damping).

Impulse Response:

$$g(j,k,t) = y_k(t) = \sum_{n=1}^{N} \frac{u_j^{(n)} u_k^{(n)}}{\omega_n}\sin\omega_n t$$

for $t \geq 0$ (with no damping), or

$$g(j,k,t) \approx \sum_{n=1}^{N} \frac{u_j^{(n)} u_k^{(n)}}{\omega_n} e^{-\omega_n \zeta_n t}\sin\omega_n t$$

for $t \geq 0$ (with small damping).

Harmonic Response:

$$H(j,k,\omega) = \frac{y_k}{f_j} = \sum_{n=1}^{N} \frac{u_j^{(n)} u_k^{(n)}}{\omega_n^2 - \omega^2}$$

(with no damping), or

$$H(j,k,\omega) = \frac{y_k}{f_j} \approx \sum_{n=1}^{N} \frac{u_j^{(n)} u_k^{(n)}}{\omega_n^2 + 2i\omega\omega_n \zeta_n - \omega^2}$$

(with small damping)

Pattern of antiresonances: For a system with well-separated resonances (low modal overlap), if the factor $u^{(n)}{}_j u^{(n)}{}_k$ has the same sign for two adjacent resonances then the transfer function will have an anti resonance between the two peaks. If it has opposite signs, there will be no antiresonance.

6.2.19. Governing Equations for Continuous Systems

Transverse Vibration of a Stretched String:

Equation of motion	Potential energy	Kinetic energy

$$m\frac{\partial^2 y}{\partial t^2} - P\frac{\partial^2 y}{\partial x^2} = f(x,t) \qquad V = \frac{1}{2}P\int\left(\frac{\partial y}{\partial x}\right)^2 dx \qquad T = \frac{1}{2}m\int\left(\frac{\partial y}{\partial t}\right)^2 dx$$

(P: tension, m: mass per unit length, $y(x, t)$: transverse displacement, $f(x, t)$: applied lateral force per unit length.)

Torsional Vibration of a Circular Shaft:

Equation of motion	Potential energy	Kinetic energy

$$\rho J\frac{\partial^2 \theta}{\partial t^2} - GJ\frac{\partial^2 \theta}{\partial x^2} = \tau(x,t) \qquad V = \frac{1}{2}GJ\int\left(\frac{\partial \theta}{\partial x}\right)^2 dx \qquad T = \frac{1}{2}\rho J\int\left(\frac{\partial \theta}{\partial t}\right)^2 dx$$

(G: shear modulus, $J = \frac{\pi}{2}(a^4 - b^4)$: second polar moment of area, ρ: density,
$\theta(x, t)$: angular displacement, $\tau(x, t)$: applied torque per unit length.
a: external radius, b: internal radius ($b = 0$ if solid).

Axial Vibration of Rod or Column:

Equation of motion	Potential energy	Kinetic energy

$$\rho A\frac{\partial^2 y}{\partial t^2} - EA\frac{\partial^2 y}{\partial x^2} = f(x,t) \qquad V = \frac{1}{2}EA\int\left(\frac{\partial y}{\partial x}\right)^2 dx \qquad T = \frac{1}{2}\rho A\int\left(\frac{\partial y}{\partial t}\right)^2 dx$$

(E: Young's modulus, ρ: density, A: cross-sectional area, $y(x, t)$: transverse displacement,
$f(x, t)$: applied lateral force per unit length.)

Bending Vibration of an Euler Beam:

Equation of motion	Potential energy	Kinetic energy

$$\rho A\frac{\partial^2 y}{\partial t^2} + EI\frac{\partial^4 y}{\partial x^4} = f(x,t) \qquad V = \frac{1}{2}EI\int\left(\frac{\partial^2 y}{\partial x^2}\right)^2 dx \qquad T = \frac{1}{2}\rho A\int\left(\frac{\partial y}{\partial t}\right)^2 dx$$

(E: Young's modulus, ρ: density, A: cross-sectional area, I: second moment of area,
$y(x, t)$: transverse displacement, $f(x, t)$: applied lateral force per unit length.)

6.3. Solid Mechanics and Structural Mechanics

6.3.1. Uniaxial Stress and Strain

For a homogeneous isotropic specimen in a simple uniaxial tensile test (e.g. a metal rod):
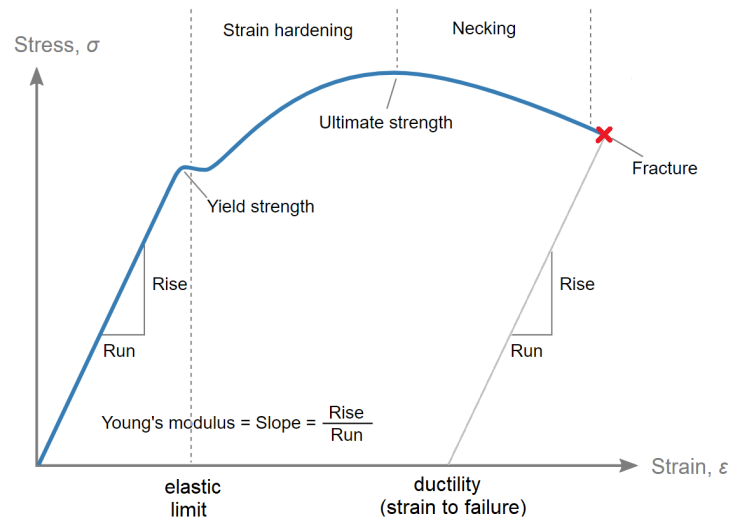
- Nominal stress: $\sigma_n = \dfrac{F}{A_0}$ (F: tensile force, A_0: initial cross-sectional area)

- Nominal strain: $\varepsilon_n = \dfrac{x}{l_0} = \dfrac{l - l_0}{l_0}$ (x: extension, l: length, l_0: initial length)

  ('nominal stress/strain' is also known as 'engineering stress/strain'.)

- True stress: $\sigma_t = \dfrac{F}{A} = \sigma_n(1 + \varepsilon_n)$ (A: cross-sectional area)

- True strain: $\varepsilon_t = \int_{l_0}^{l} \dfrac{dl}{l} = ln\left(\dfrac{l}{l_0}\right) = ln(1 + \varepsilon_n)$ (true strains are additive)

In the elastic region (from unloaded to yield stress σ_y; slope = E: Young's modulus)

- Hooke's law for linear elasticity: $F = kx = k(l - l_0)$ or $E = \dfrac{\sigma}{\varepsilon} = \dfrac{Fl_0}{Ax}$

- Elastic potential energy (strain energy): $U = \dfrac{1}{2}kx^2 = \dfrac{1}{2}Fx$ (area under F-x graph)

In the plastic region:

- Strain energy per unit volume: $U/V = \int_0^{\varepsilon} \sigma_n \, d\varepsilon_n$ (area under σ-ε graph)

- Plastic strains occur at constant volume. Strain hardening occurs up to the ultimate tensile strength (UTS). Necking decreases the cross-sectional area until the point of rupture if perfectly ductile. On failure, the specimen suddenly contracts by relaxing the elastic strain.

6.3.2. Stress-Strain Relationships for Homogeneous Isotropic Elastic Solids

Elastic moduli: material properties

- Young's modulus: $E = \frac{\sigma}{\varepsilon}$ (uniaxial only - effective E_{xx} is $\frac{\sigma_{xx}}{\varepsilon_{xx}}$ etc.)
- Poisson's ratio: $\nu = -\frac{lateral\ strain}{tensile\ strain}$ (lateral strain is **not** for volume conservation)
- Dilatation (volumetric strain): $\Delta = \frac{change\ in\ volume}{initial\ volume} = ln\left(\frac{\rho_{initial}}{\rho_{final}}\right) = \varepsilon_{xx} + \varepsilon_{yy} + \varepsilon_{zz}\ (+\ O(\varepsilon^2))$
- Shear modulus: $G = \frac{\tau}{\gamma} = \frac{E}{2(1+\nu)}$
- Bulk modulus: $K = \frac{hydrostatic\ stress}{volumetric\ strain} = \frac{p}{\Delta} = \frac{E}{3(1-2\nu)}$
- Compressibility: $1/K$;   Speed of sound in solid/liquid: $a = \sqrt{K/\rho}$

Stresses and strains induced by temperature changes:

- Thermal strain: $\varepsilon = \alpha\,\Delta T$ (α: linear coefficient of thermal expansion, equal in all directions)
- Axial material law: $\varepsilon_{xx} = \frac{1}{E}(\sigma_{xx} - \nu\sigma_{yy} - \nu\sigma_{zz}) + \alpha\,\Delta T$, similar for other directions
- Shear material law: $\gamma_{xy} = \frac{1}{G}\tau_{xy}$, similar for other directions (pure elastic strains)
- Complementary shear: $\tau_{xy} = \tau_{yx}$ and $\gamma_{xy} = \gamma_{yx}$.

The axial and shear elastic laws can be combined into a constitutive law with tensors.
In matrix form, the axial stress $\boldsymbol{\sigma} = [\sigma_{xx}\ \ \sigma_{yy}\ \ \sigma_{zz}]^\mathsf{T}$ and strain $\boldsymbol{\varepsilon} = [\varepsilon_{xx}\ \ \varepsilon_{yy}\ \ \varepsilon_{zz}]^\mathsf{T}$ vectors are related by:

$$\boldsymbol{\varepsilon} = \frac{1}{E}\begin{bmatrix} 1 & -\nu & -\nu \\ -\nu & 1 & -\nu \\ -\nu & -\nu & 1 \end{bmatrix}\boldsymbol{\sigma} + \begin{bmatrix} 1 \\ 1 \\ 1 \end{bmatrix}\alpha\Delta T \quad \Leftrightarrow \quad \boldsymbol{\sigma} = \frac{E}{(1+\nu)(1-2\nu)}\begin{bmatrix} 1-\nu & \nu & \nu \\ \nu & 1-\nu & \nu \\ \nu & \nu & 1-\nu \end{bmatrix}\left(\boldsymbol{\varepsilon} - \begin{bmatrix} 1 \\ 1 \\ 1 \end{bmatrix}\alpha\Delta T\right)$$

Constrained thermal displacements are resisted by tensile/compressive stresses.
Biaxial constraint: for plane stress with the z face unstressed and $\Delta T = 0$, the stresses are

$$\sigma_{xx} = \frac{E}{1-\nu^2}\left(\varepsilon_{xx} + \nu\,\varepsilon_{yy}\right) \text{ and } \sigma_{yy} = \frac{E}{1-\nu^2}\left(\nu\,\varepsilon_{xx} + \varepsilon_{yy}\right)$$

Common cases:

- Contraction of a constrained thin surface layer: biaxial surface stress $\sigma = \frac{E}{1-\nu}(\alpha_{surface} - \alpha_{bulk})\,\Delta T$.

- Freezing of water: $p = K_{ice}\,ln\left(\frac{\rho_{water}}{\rho_{ice}}\right)$, $\varepsilon_{cont} = \alpha\,\Delta T$, then pressure vessel formulas (Section 6.4.6).

Special cases:
Large strain bending in materials with high ν (e.g. rubber, $\nu = 0.5$) produces anticlastic
curvature, and these materials are incompressible under hydrostatic loading.
Auxetic metamaterials expand in both directions (i.e. negative ν) and can occur in
specially designed mesh geometries e.g. minimal surfaces.

6.3.3. Planar Transformations of Stress and Strain

Mohr's circle of stress. Shear stress is plotted as positive when acting clockwise.
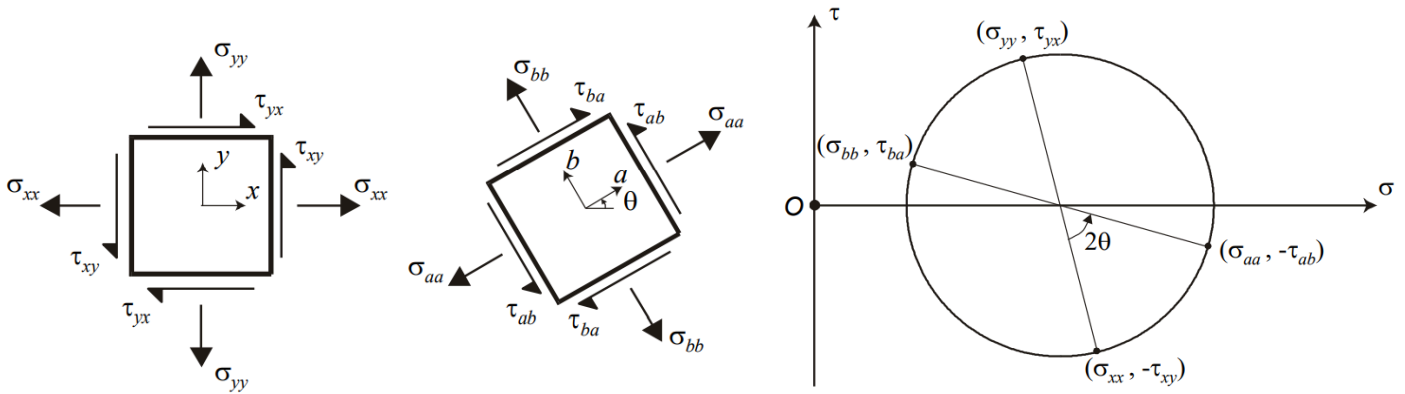
$$\sigma_{aa} = \sigma_{xx}\cos^2\theta + \sigma_{yy}\sin^2\theta + 2\tau_{xy}\sin\theta\cos\theta$$

$$\tau_{ab} = -\sigma_{xx}\sin\theta\cos\theta + \sigma_{yy}\sin\theta\cos\theta + \tau_{xy}\left(\cos^2\theta - \sin^2\theta\right)$$

Mohr's circle of strain. Shear strain is plotted as positive when acting clockwise.
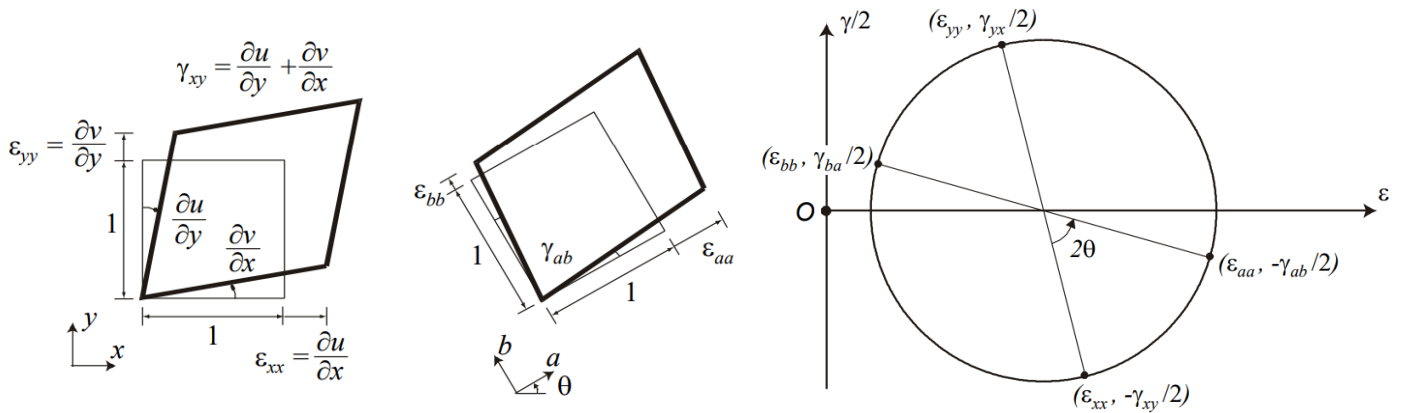
$$\varepsilon_{aa} = \varepsilon_{xx}\cos^2\theta + \varepsilon_{yy}\sin^2\theta + \gamma_{xy}\sin\theta\cos\theta$$

$$\gamma_{ab} = -2\varepsilon_{xx}\sin\theta\cos\theta + 2\varepsilon_{yy}\sin\theta\cos\theta + \gamma_{xy}\left(\cos^2\theta - \sin^2\theta\right)$$

6.3.4. Principal Stresses in 3D

The principal stresses can be calculated as the eigenvalues of the stress tensor $\boldsymbol{\sigma}$, and the orthogonal principal directions are the corresponding eigenvectors: $\boldsymbol{\sigma} = \mathbf{D\Sigma D}^{\mathsf{T}}$ (since $\boldsymbol{\sigma} = \boldsymbol{\sigma}^{\mathsf{T}}$).

$$\underline{\boldsymbol{\sigma}} = \begin{bmatrix} \sigma_{xx} & \tau_{xy} & \tau_{xz} \\ \tau_{yx} & \sigma_{yy} & \tau_{yz} \\ \tau_{zx} & \tau_{zy} & \sigma_{zz} \end{bmatrix}$$

3D Mohr's Circle:
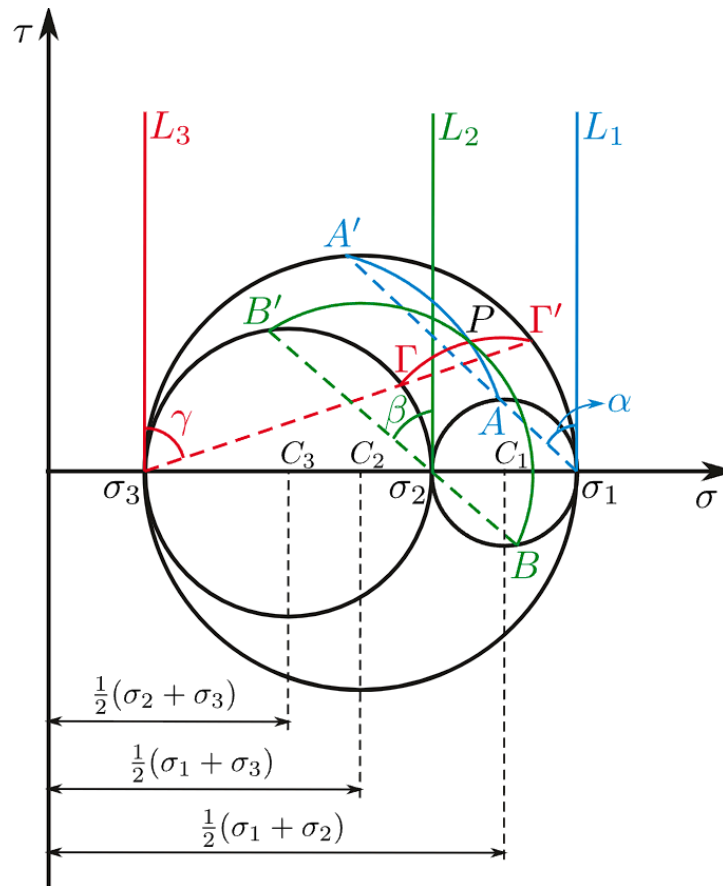
6.3.5. Yield Criteria for Isotropic Solids

If Y is the yield stress in simple uniaxial tension and (σ_1, σ_2, σ_3) are the principal stresses of a given stress state, then yielding is predicted to occur according to

- Hydrostatic component: $\sigma_h = (\sigma_1 + \sigma_2 + \sigma_3)/3$, which does **not** contribute to yielding
- Tresca's Criterion: $\max\{|\sigma_1 - \sigma_2|, |\sigma_2 - \sigma_3|, |\sigma_3 - \sigma_1|\} = Y$
- Von Mises' Criterion: $(\sigma_1 - \sigma_2)^2 + (\sigma_2 - \sigma_3)^2 + (\sigma_3 - \sigma_1)^2 = 2Y^2$

Failure surfaces according to each criterion:
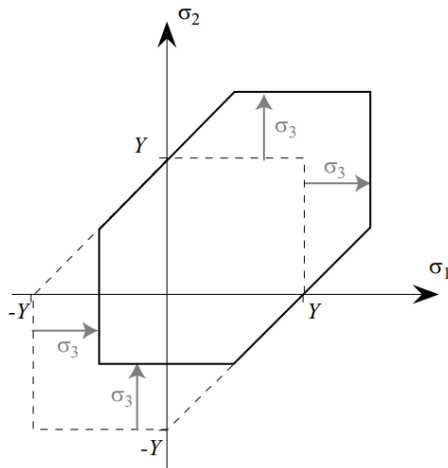
Tresca criterion failure surface   **Von Mises** criterion failure surface
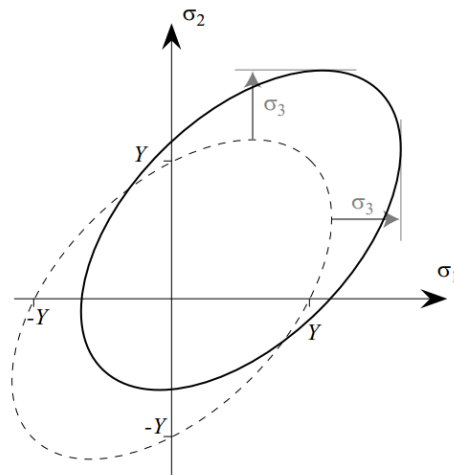
The Von Mises ellipse exactly circumscribes the Tresca hexagon. The maximum discrepancy is for pure shear ($\sigma_1 = -\sigma_2$) where the difference is about 15%.

When the failure surfaces are projected parallel to the hydrostatic axis ($\sigma_1 = \sigma_2 = \sigma_3$), both Tresca and Von Mises become a regular hexagon and a circle respectively. The components along the axes in this projection are the deviatoric stresses $\boldsymbol{\sigma}_{\text{dev}} = \boldsymbol{\sigma} - \sigma_h \mathbf{I}$.
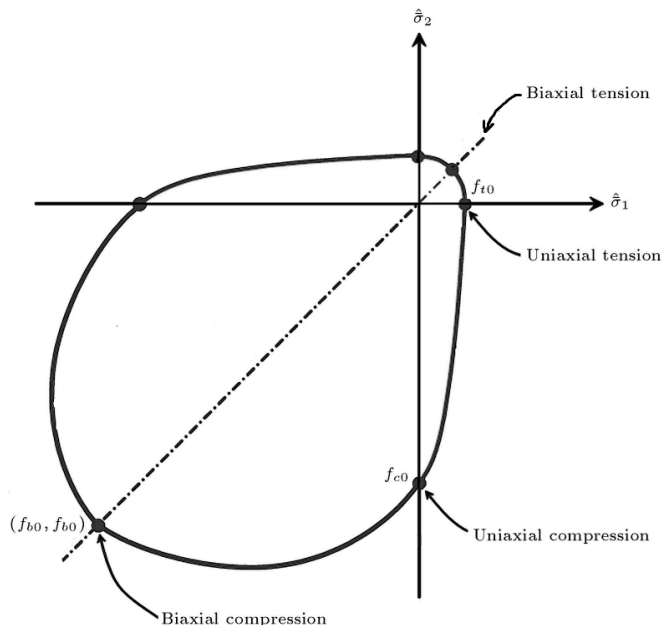
← **Failure Surface for Concrete:**

Concrete is weak in tension and strong in compression. The largest flaw governs tensile fracture, whereas compression leads initially to stable crack growth and material crushing.

The Coulomb-Mohr and modified Mohr failure theories approximate brittle failure.

42

6.3.6. Thin-Walled Cylinders Under Uniform Pressure (Hydrostatic Loading)

(σ_h: hoop stress (circumferential / azimuthal), σ_l: longitudinal (axial) stress, t: thickness, r: radius, p: gauge pressure $= p_{in} - p_{out}$. If $p > 0$ then stresses are tensile; else compressive.)

- Stresses: $\sigma_h = \dfrac{pr}{t}, \ \sigma_l = \dfrac{pr}{2t}, \ \sigma_t \approx 0$ (away from ends; $t \ll r$)

- Strains: $\varepsilon_h = \dfrac{pr}{2Et}(2 - v), \ \varepsilon_l = \dfrac{pr}{2Et}(1 - 2v), \ \varepsilon_t = \dfrac{-pr}{2Et}(3v)$

- Dimensional changes: $\dfrac{\Delta l}{l} = \varepsilon_l, \ \dfrac{\Delta r}{r} = \dfrac{\Delta C}{C} = \varepsilon_h, \ \dfrac{\Delta t}{t} = \varepsilon_t$

6.3.7. Forces, Moments and Displacements of Beams

Sign conventions:
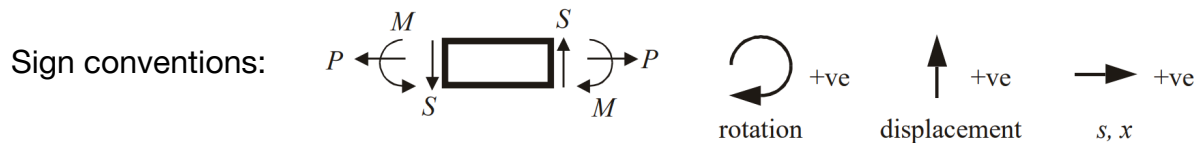
(x: distance parallel to beam, y: position on section from neutral axis, v: transverse deflection, ψ: beam rotation, κ: beam curvature, R: radius of curvature, ε: axial strain, s: arc length along beam, P: axial force, M: bending moment, S: shear force, w: shear force per unit length parallel to beam)

- Compatibility of rotations ψ and curvatures κ: $\kappa = \dfrac{1}{R} = \dfrac{d\psi}{ds}$

- Plane sections remain plane: $\varepsilon = \kappa y$

- Transverse deflections due to a load: $\psi = -\dfrac{dv}{dx}$ and $\kappa = -\dfrac{d^2 v}{dx^2}$

Equilibrium of transverse force per unit length w, shear force S and bending moment M:

$$w = \frac{dS}{dx}; \quad S = \frac{dM}{dx}$$
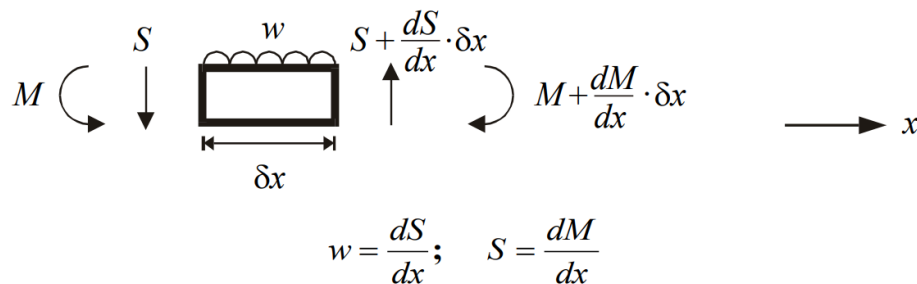
6.3.8. Elastic Bending of Beams

Neutral axis
(no bending stress)
is at the centoidal level
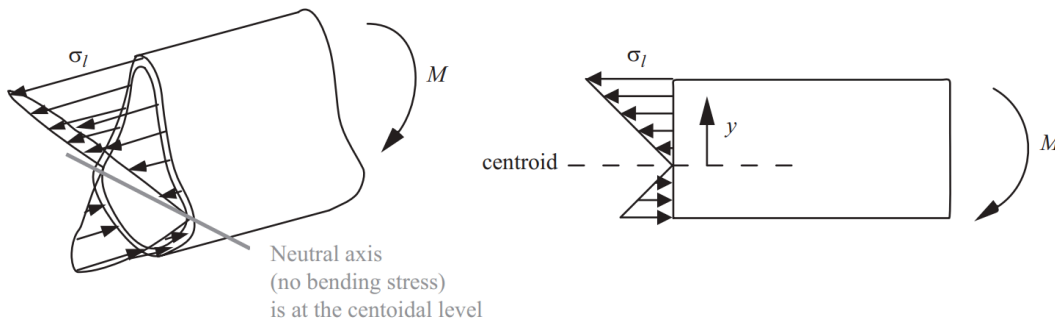
- Longitudinal stress due to a bending moment: $\dfrac{\sigma_l}{y} = \dfrac{M}{I} = E\,\Delta\kappa$

- Transverse displacement due to a bending moment: $M(x) = -EI\,\dfrac{d^2v}{dx^2}$.

(σ_l: longitudinal stress, y: distance from neutral axis, v: transverse displacement, M: bending moment, $\Delta\kappa$: change in curvature, I: second moment of area of section about the neutral axis, E: Young's modulus. The 'flexural rigidity' is denoted $B = EI$.)
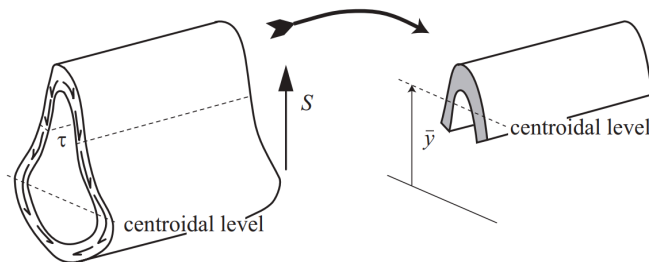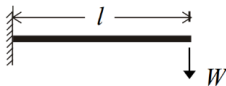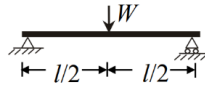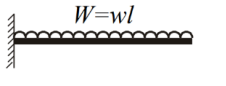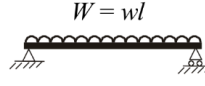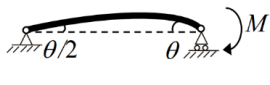
- Shear flow due to a shear force: $q = \dfrac{S}{I}\displaystyle\int_{A_c} y\,dA = \dfrac{S A_c \bar{y}}{I}$

- Shear stress (average over cut length): $\tau_{avg} = \dfrac{q}{a} = \dfrac{S A_c \bar{y}}{Ia}$ (Zhuravskii's formula)

(q: shear flow (total longitudinal shear force per unit longitudinal length of the beam), S: shear force, $A_c\bar{y}$: first moment of area of the cut-off portion (area × distance from centroid to neutral axis), I: second moment of area of the section about the neutral axis, a: total length of the cut through the beam in the plane of the cross-section)
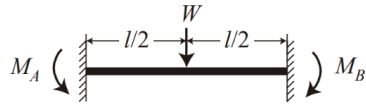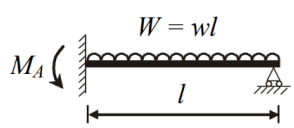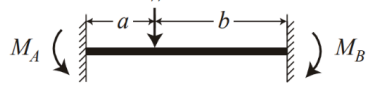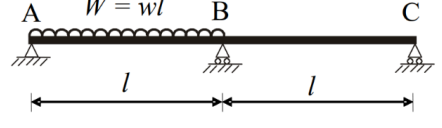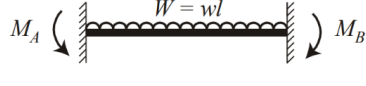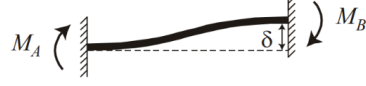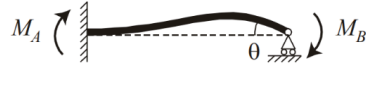
Analysis of sections with longitudinal stiffeners (e.g. semi-monocoque structures) can be simplified by 'smearing' the stiffener area into the beam, increasing its thickness slightly.

6.3.9. Standard Cases of Elastic Beam Bending

Bending of statically determinate beams:

Cantilever with end point load W:

	end rotation	end deflection
	$\dfrac{Wl^2}{2EI}$	$\dfrac{Wl^3}{3EI}$

Cantilever with UDL $W = wl$:

	end rotation	end deflection
	$\dfrac{Wl^2}{6EI} = \dfrac{wl^3}{6EI}$	$\dfrac{Wl^3}{8EI} = \dfrac{wl^4}{8EI}$

Cantilever with end moment M:

	$\dfrac{Ml}{EI}$	$\dfrac{Ml^2}{2EI}$

Simply supported with central point load W:

	end rotation	central deflection	M_{MID}
	$\dfrac{Wl^2}{16EI}$	$\dfrac{Wl^3}{48EI}$	$\dfrac{Wl}{4}$

Simply supported with UDL $W = wl$:

	end rotation	central deflection	M_{MID}
	$\dfrac{Wl^2}{24EI} = \dfrac{wl^3}{24EI}$	$\dfrac{5Wl^3}{384EI} = \dfrac{5wl^4}{384EI}$	$\dfrac{Wl}{8} = \dfrac{wl^2}{8}$

Simply supported with end moment M:

$$\theta = \frac{Ml}{3EI}$$

Clamping moments of statically indeterminate beams:

Fixed-fixed with central point load W (at $l/2$):

	M_A	M_B
	$\dfrac{Wl}{8}$	$\dfrac{Wl}{8}$

Fixed-fixed with point load W (at a, b):

	M_A	M_B
	$\dfrac{Wb^2a}{l^2}$	$\dfrac{Wa^2b}{l^2}$

Fixed-fixed with UDL $W = wl$:

	M_A	M_B
	$\dfrac{Wl}{12} = \dfrac{wl^2}{12}$	$\dfrac{Wl}{12} = \dfrac{wl^2}{12}$

Fixed-fixed with support settlement δ:

	M_A	M_B
	$\dfrac{6EI\delta}{l^2}$	$\dfrac{6EI\delta}{l^2}$

Fixed-pinned with end rotation θ:

	M_A	M_B
	$\dfrac{2EI\theta}{l}$	$\dfrac{4EI\theta}{l}$

Fixed-pinned (propped cantilever) with UDL $W = wl$:

$$M_A: \quad \frac{Wl}{8} = \frac{wl^2}{8}$$

Two-span continuous beam ABC with UDL $W = wl$ over each span l:

$$M_B: \quad \frac{Wl}{16} = \frac{wl^2}{16}$$

Saint-Venant's principle: the difference in the effects* induced by two different but statically equivalent loads is negligible in regions located very far from the loads.

* e.g. displacements, induced shear forces, bending moments, stress states etc.

6.3.10. Elastic Torsion of Beams

Hollow Circular Beams: (r: radius, J: polar second moment of inertia (aka torsion constant), T: torque, τ: shear stress, G: shear modulus)

- Torque-stress relationship: $\dfrac{\tau}{r} = \dfrac{T}{J}$

- Angular displacement

  per unit beam length: $\phi' = \dfrac{T}{GJ}$

  (GJ: torsional rigidity)
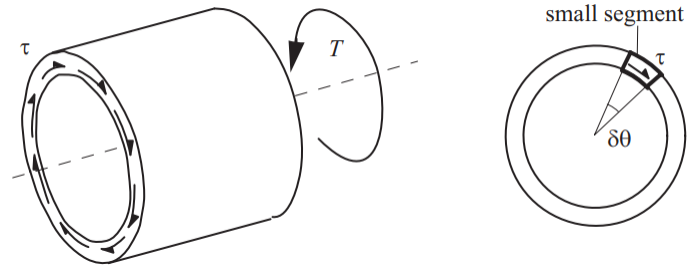
General Cross-Sections: (q: shear flow, $t = t(s)$: section thickness (may be non-uniform), γ: shear strain, s: arc length around section, A_e: area enclosed by section at mid-thickness)

- Circulating shear flow and shear stress: $q = \dfrac{T}{2\,A_e}, \quad \tau = \dfrac{q}{t}$

- Angular displacement **per unit beam length:** $\phi' = \dfrac{\oint \gamma\,ds}{2\,A_e}$ (Bredt-Batho equation)

- Torque: $T = GJ\phi'$ where $J = \dfrac{4\,A_e^{\,2}}{\oint \frac{ds}{t}}$

Warping: non-circular cross-sections warp out of plane under torsion.
(I, J: second moments for **minor** axis, Γ: cross-sectional constant for warping,
$E\Gamma$: warping rigidity, h: distance between flange centroids in a symmetric I-beam)

- End-moment for elastic lateral torsional buckling: $M_{LT} = \dfrac{\pi}{L}\sqrt{EIGJ\left(1 + \dfrac{\pi^2}{L^2}\dfrac{E\Gamma}{GJ}\right)}$

- For I-beams, $\Gamma \approx \dfrac{1}{4}Ih^2$ and the bimoment (warping moment) is $B = Th = -E\Gamma\dfrac{d^2\phi}{dx^2}$

6.3.11. Elastic Bending of Composite Beams

Composite beams are made of two or more materials.

Sandwich Beams: e.g. timber/honeycomb/foam interior with Al-alloy face sheets
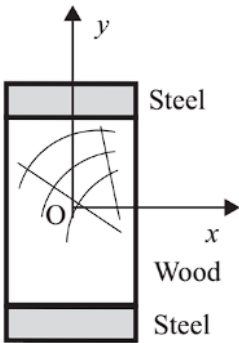
The wood section (width w) can be 'transformed' into an equivalent steel section of width $w \times (E_{\text{wood}} / E_{\text{steel}})$ (like the web of an I-beam).

Stress in steel: $\sigma_l = \dfrac{My}{I_{steel}}$,   Stress in wood: $\sigma_l = \dfrac{My}{I_{wood}}$ where

Shear stress in adhesive: $\tau = \dfrac{S(A\bar{y})_{steel}}{I_{transformed}\, w}$

Reinforced Concrete Beams: concrete with carbon steel rebar through the tensile side
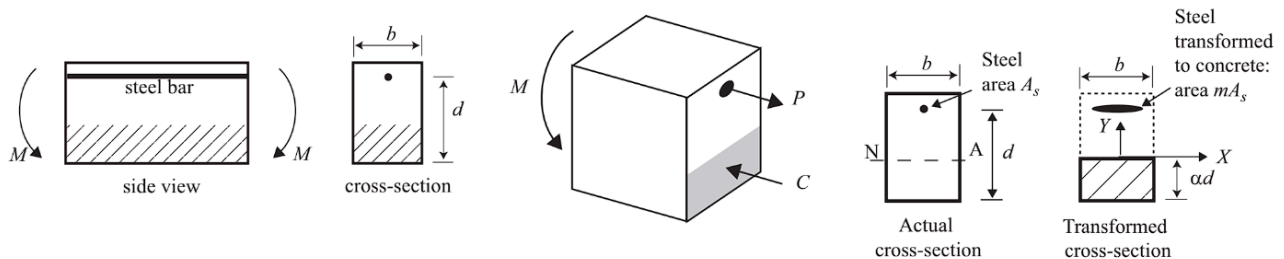
The 'transformed' beam is all concrete ($m = E_{\text{steel}} / E_{\text{concrete (compression)}}$), with all tensile concrete becoming imaginary. The neutral axis position α satisfies $\dfrac{bd}{2mA_s}\alpha^2 + \alpha - 1 = 0$.

The maximum stresses in the steel and concrete are $\left| \dfrac{\sigma_{steel}}{\sigma_{concrete}} \right|_{max} = \dfrac{m(1-\alpha)}{\alpha}$.

If $\left| \dfrac{\sigma_{steel}}{\sigma_{concrete}} \right|_{max} = \dfrac{\sigma_y^{(steel,\, tension)}}{\sigma_f^{(concrete,\, compression)}}$ then this is a 'balanced design' (neither part is limiting).

6.3.11. Cables, Ropes, Chains and Segmented Arches

Friction due to Cable or Belt Contact (The Capstan Equation)

A flexible inextensible cable in contact with a curved surface develops different tensions either side of the contact due to friction, such that

$$\frac{T_2}{T_1} \leq e^{\mu\theta} \qquad (\mu\text{: coefficient of friction, } \theta\text{: angle subtended by contact, } T\text{: tension})$$

with equality when on the limit of sliding in either direction.

Tension in a Hanging Cable, Rope or Chain (The Catenary Equation)

A freely hanging inextensible cable, rope or chain suspended between any two points forms a catenary curve under its own self-weight. In Cartesian coordinates, this curve has the general shape $y = a \cosh x/a$. If the mass per unit cable length is λ then:

$$y = a \cosh\left(\frac{x}{a}\right)$$
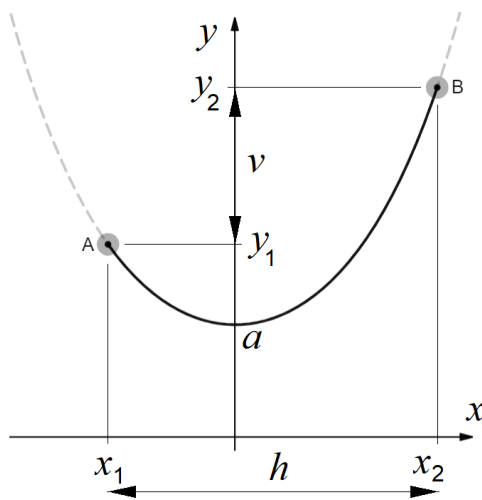
Different Elevations   **Same Elevation**

Arc length: $s = a\left(\sinh \frac{x_2}{a} - \sinh \frac{x_1}{a}\right)$ $s = 2a \sinh \frac{L}{a} \approx 2L + \frac{4d^2}{3L}$ for small $\frac{d}{L}$

Parameters: $\sqrt{s^2 - v^2} = 2a \sinh \frac{h}{2a}$ $a = \frac{s^2}{8d} - \frac{d}{2}$ and $L = a \cosh^{-1}\left(1 + \frac{d}{a}\right)$

Tension: $|T_x| = \lambda g a, \ T_y = \lambda g a \sinh \frac{|x|}{a} \ \Rightarrow \ |T| = \sqrt{T_x^2 + T_y^2} = \lambda g a \cosh \frac{x}{a} \quad (m = \lambda s)$

Compressive Forces in Arches

Arches carry loads, including their self-weight, via compression. They are typically made of brick or stone, which are cheap and strong in compression (masonry).

For a segmented arch, each segment (voussoir) exerts compressive contact forces on each neighbouring segment, with the end segments in contact with the base (buttress). For any arch, the locus of contact forces (**thrust line**) must be contained within the geometry of the arch itself in order to be stable. Friction between the segments is not required for stability, although friction can help improve resilience to varying loads.

A **hanging chain** illustrates the geometry of the thrust line in an unloaded arch (self-weight only, producing a catenary curve): the thrust line in the arch is simply the **reflection** of this. This also applies to rigid arches. By hanging weights from the chain of a desired design mass, the shape of the thrust line in the corresponding arch can be deduced, allowing architects to easily design arbitrarily shaped segmented arches (**funicular analysis for form finding**).
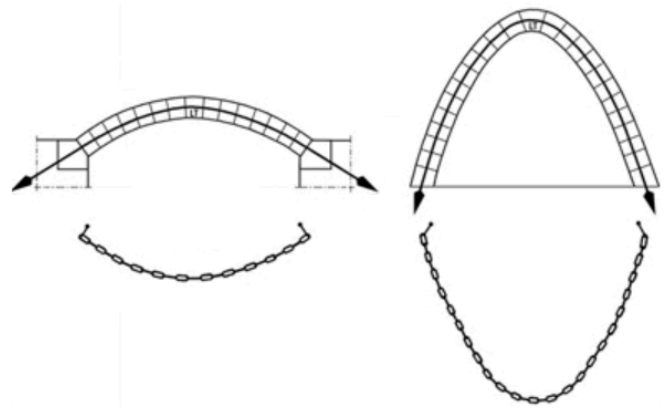
Both 'chain' and 'arch' models can be useful in construction: for example, an arch bridge and a suspension bridge are the inversions of each other. In these cases, the weight distribution is uniform in the horizontal direction, transforming the catenary into the parabola.

The bending moment at any point within an arch (or frame) is proportional to the distance between the point and the closest point on the thrust line. The tensile side of the arch is usually the outer edge (when loads are vertically downwards). The point of maximum bending moment is therefore the point furthest from this line. In a pinned arch, the thrust line must pass through the pins, since there can be no bending moment at a frictionless pin.

A 'tied arch' can be formed by connecting the two supports together with a rod, which will be placed into tension in order to carry the horizontal components of the reaction force. This allows for vertical, frictionless supports to be used for the arch instead.

6.3.12. Stress Distribution in a Rotating Axisymmetric Bodies

Rotating Thin Disk or Plate: The force balance on an infinitesimal sector element with zero axial stress rotating at angular speed ω about the axis gives

$$\sigma_r = A + \frac{B}{r^2} - \frac{3+\nu}{8}\rho\omega^2 r^2 \qquad\qquad \sigma_\theta = A - \frac{B}{r^2} - \frac{1+3\nu}{8}\rho\omega^2 r^2$$

(σ_r: radial stress, σ_θ: hoop stress, r: radial distance, v: Poisson's ratio, ρ: density)

- Solid disk, radius R: $\qquad\qquad\qquad A = \frac{1}{8}\rho R^2 \omega^2 \qquad$ and $\quad B = 0$

- Disk of radius R_2 with hole of radius R_1: $\quad A = \frac{(3+v)\left(R_1^{\,2} + R_2^{\,2}\right)\rho\omega^2}{8} \quad$ and $\quad B = -A$

Rotating Long Cylinder or Shaft: The force balance on an infinitesimal sector element rotating at angular speed ω about the axis gives

$$\sigma_r = A - \frac{B}{r^2} - \frac{3-2\nu}{8(1-\nu)}\rho\omega^2 r^2 \qquad\qquad \sigma_\theta = A + \frac{B}{r^2} - \frac{1+2\nu}{8(1-\nu)}\rho\omega^2 r^2$$

(σ_r: radial stress, σ_θ: hoop stress, r: radial distance, v: Poisson's ratio, ρ: density)

- Solid cylinder, radius R: $\qquad\qquad A = \frac{(3-2v)\rho R^2 \omega^2}{8(1-v)} \qquad$ and $B = 0$

- Cylinder R_2 with hollow radius R_1: $\quad A = \frac{(3-2v)\left(R_1^{\,2} + R_2^{\,2}\right)\rho\omega^2}{8(1-v)} \quad$ and $B = \frac{(3-2v)\rho R_1^{\,2} R_2^{\,2} \omega^2}{8(1-v)}$

6.3.13. Transverse Loading of a Circular Plate (2D Deflection)

For axisymmetric loading, the peak deflection and stress is at the centre (σ_r: radial stress, σ_t: hoop stress). For **small** (linear) deflections:
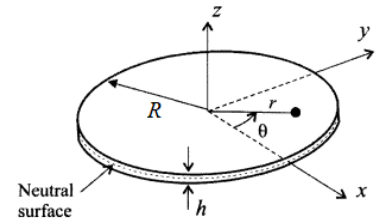
Conditions	Central deflection	Central stress	
		$\sigma_{r,\,max}$	$\sigma_{z,\,max}$
Uniform loading, clamped edges	$\dfrac{3pR^4}{16Eh^3}(1-v)$	$\dfrac{3pR^2}{4h^2}$	$\dfrac{3pR^2}{8h^2}(1+v)$
Uniform loading, simply supported circumference	$\dfrac{3pR^4}{16Eh^3}(5+v)(1-v)$	$\dfrac{3pR^2}{8h^2}(3+v)$	$\dfrac{3pR^2}{8h^2}(3+v)$
Central load, clamped edges	$\dfrac{3FR^2}{4\pi Eh^3}(1-v^2)$	$\dfrac{3F}{2\pi h^2}$	$\dfrac{3vF}{2\pi h^2}$
Central load, simply supported circumference	$\dfrac{3FR^2}{4\pi Eh^3}(3+v)(1-v)$	$\dfrac{3F}{2\pi h^2}(1+v)\ln\dfrac{R}{r}$	$\dfrac{3F}{2\pi h^2}[(1+v)\ln\dfrac{R}{r} + (1-v)]$

Large Deflections of Thin Elastic Membranes: numerical data given for $v = 0.3$

Boundary conditions		A	B	Centre		Edge			
				$\alpha_r = \alpha_t$	$\beta_r = \beta_t$	α_r	α_t	β_r	β_t
Clamped	Fixed	0.471	0.171	0.976	2.86	0.476	0.143	-4.40	-1.32
	Free to move	0.146	0.171	0.500	2.86	0	-0.333	-4.40	-1.32
Simply supported	Fixed	1.852	0.696	0.905	1.778	0.610	0.183	0	0.755
	Free to move	0.262	0.696	0.295	1.778	0	-0.427	0	0.755
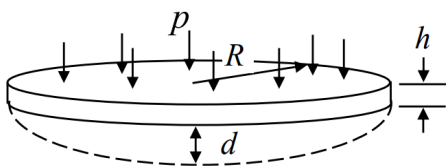
Central deflection: $\dfrac{d}{h} + A\left(\dfrac{d}{h}\right)^3 = B\,\dfrac{p}{E}\left(\dfrac{R}{h}\right)^4$

Middle plane stress: $\sigma_r = \alpha_r E\left(\dfrac{d}{R}\right)^2,\qquad \sigma_t = \alpha_t E\left(\dfrac{d}{R}\right)^2$

Extreme fibre stress: $\sigma_r{}' = \beta_r E\,\dfrac{dh}{R^2},\qquad \sigma_t{}' = \beta_t E\,\dfrac{dh}{R^2}$

6.3.14. Spherical Indentation into an Infinite Compressible Elastic Plate
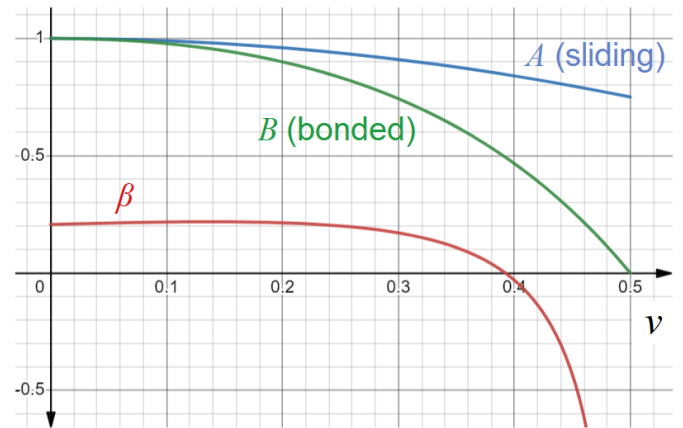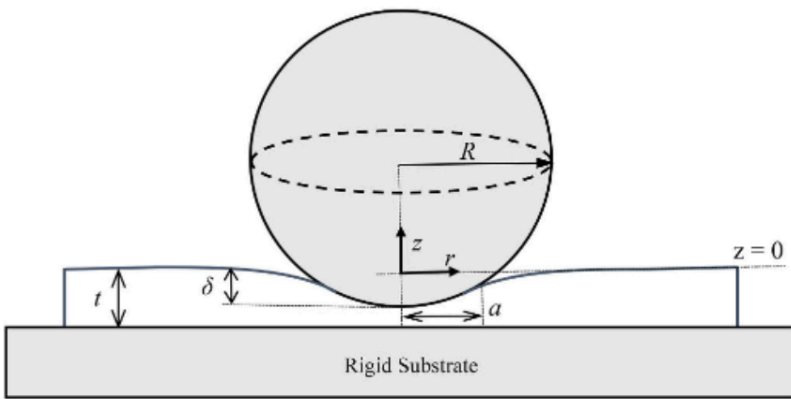
The deflection of the compressible elastic layer depends on whether it is bonded to the rigid substrate or allowed to slide. The values of constants β, A, B depend on v of the layer.

	a and δ	F and a	F and δ
Sliding	$\dfrac{\delta R}{a^2} = \dfrac{1}{2}$	$\dfrac{1}{8}\dfrac{a}{R}\left(\dfrac{a}{t}\right)^3 = \dfrac{FA}{2\pi E t^2}$	$\dfrac{R\delta^2}{t} = \dfrac{FA}{\pi E}$
Bonded	$\dfrac{\delta R}{a^2} = \dfrac{1}{2} + \beta\left(\dfrac{t}{a}\right)$	$\dfrac{a}{R}\left(\dfrac{1}{8} + \dfrac{\beta}{2}\dfrac{t}{a}\right)\left(\dfrac{a}{t}\right)^3 = \dfrac{FB}{2\pi E t^2}$	$\dfrac{R\delta^2}{t} = \dfrac{FB}{\pi E}$

6.3.15. Curvature of a Bimetallic Strip due to Differential Strains with Constraint

When two thin films (thickness t_1, t_2) are bound at a plane interface and subject to e.g. thermal strain by heating, there is an induced curvature κ and radius ρ given by
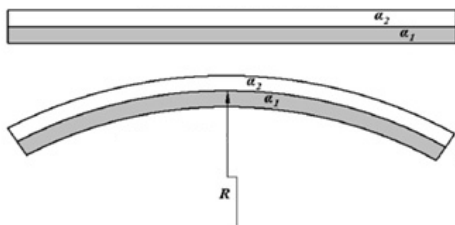
$$\kappa = \frac{1}{R} = \frac{6(1+m)^2}{h\left(3(1+m)^2 + (1+mn)\left(m^2 + \dfrac{1}{mn}\right)\right)} \cdot (\varepsilon_2 - \varepsilon_1)$$

$$= \frac{3(\varepsilon_2 - \varepsilon_1)}{2h} \quad \text{if } m = n = 1.$$

where $\quad \varepsilon = \alpha \Delta T, \qquad m = \dfrac{t_1}{t_2}, \qquad h = t_1 + t_2, \qquad n = \dfrac{E_1}{E_2}.$

(α [K^{-1}]: linear expansion coefficient, ΔT [K]: increase in temperature)

Other responsive stimuli to strain follow a similar pattern.

6.3.16. Euler Buckling of Elastic Columns

The axial compressive buckling load P of a **perfectly straight** elastic beam is given by

$$P = \frac{\pi^2 EI}{L_e^2}$$ (I: second moment of inertia, L_e: effective buckling length)
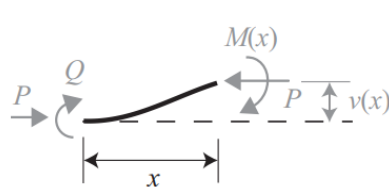
If $P = \alpha^2 EI$, the critical value of α can be found by solving

Equilibrium: $P\,v(x) = M(x) + Q$

Compatibility: $M(x) = -EI \dfrac{d^2 v(x)}{dx^2}$
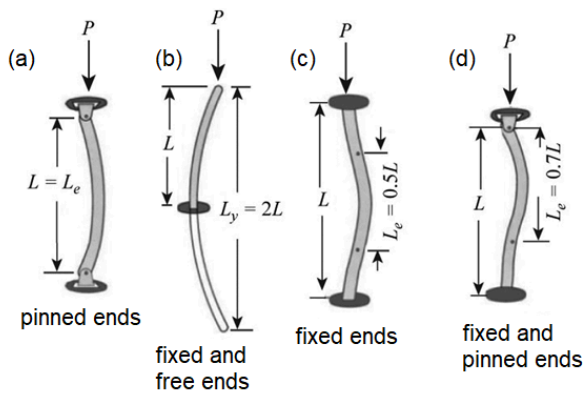
← Typical support cases:

For a beam of length L, the value of L_e can sometimes be inferred from symmetry as the distance between inflection points on the deformed beam. For simple supports, $L_e = L$.

An exact value for case (d) is $L_e = \frac{\pi L}{\beta}$, where $\beta \approx 4.49341\ldots$ is the smallest positive solution to the equation $\beta = \tan\beta$.

(a) pinned ends $L = L_e$
(b) fixed and free ends $L_y = 2L$
(c) fixed ends $L_e = 0.5L$
(d) fixed and pinned ends $L_e = 0.7L$

Buckling stress: for a beam with cross-sectional area A,

- Euler buckling stress: $\sigma_E = \dfrac{P}{A} = \dfrac{\pi^2 E}{(L_e/r)^2}$ ($\frac{L_e}{r}$: slenderness, $r = \sqrt{\frac{I}{A}}$: radius of gyration)

- If $\sigma_E > \sigma_y$ then the column will yield in compression (crushing) before buckling, which occurs for slenderness values of $\dfrac{L_e}{r} < \pi\sqrt{\dfrac{E}{\sigma_y}}$.

Imperfect Buckling of an Elastic Column: small initial deformations lower the buckling load
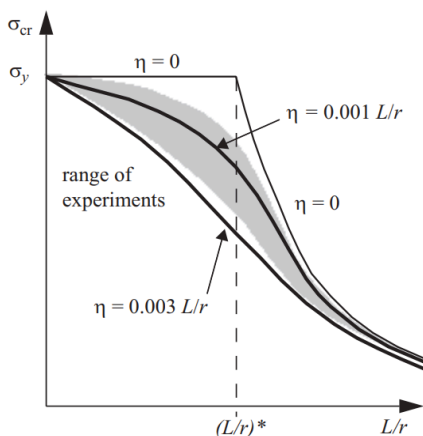
For an initial deformation with first mode shape $v(x) = \delta_0 \sin\frac{\pi x}{L}$, the buckling stress falls from $P/A = \sigma_E$ to σ_{cr}, where   (Perry's formula)

$$\left(\sigma_y - \sigma_{cr}\right)\left(\sigma_E - \sigma_{cr}\right) = \eta\,\sigma_{cr}\,\sigma_E \quad \text{where } \eta = \frac{\delta_0\, y_{max}}{r^2}.$$

(y_{max}: maximum section distance from neutral axis)

An experimental correlation is $\eta \approx 0.001 \times \frac{L}{r}$, with $\eta = 0.003 \times \frac{L}{r}$ as a safe lower bound.

(Robertson's correlation, incorporated into Eurocode 3 (EN 1993)).

6.3.18. Statically Determinate Trusses

A plane pin-jointed truss is a 2D assembly of light elastic bars, frictionless point joints and supports (pinned, roller or built-in/encastre), with loads applied at joints only, so that the bars carry only axial forces at equilibrium.

In 2D, the components of the truss satisfy $b - 2j + r = s - m$ (Maxwell-Calladine rule).

(b: number of bars, j: number of joints, r: number of reaction force components (restraints), s: number of states of self-stress, m: number of mechanistic degrees of freedom)

- If $s - m < 0$ then the assembly is a mechanism.
- If $s - m > 0$ then the assembly is redundant and rigid.
- The condition $s - m = 0$ is necessary (but not sufficient) for a non-redundant rigid assembly. It is possible for an assembly to have $s = m \neq 0$.
- If $s = 0$ then the assembly is **statically determinate** (bar forces independent of materials)
- If $m = 0$ then the assembly is kinematically determinate (displacements are fixed)

Force Methods in a Statically Determinate Truss: first-order linear elastic analysis

Denote the b bar forces T_i and the r reaction forces R_j. These can be found by either:

- **Method of joints:** take a free body cut through the bars around every joint and resolve the forces: solve the system ($2j$ equations in ($b + r$) unknowns) algebraically.
- **Method of sections:** choose free body cuts to expose a small number (typically 3-5) of forces; balance forces and take moments about where many lines of action of forces intersect to find their values. Continue until all unknowns are found.

Exploit symmetry and anti-symmetry and identify zero-force members to simplify analysis.

Displacement Methods in a Kinematically Determinate Truss: first-order small displacements

Once all internal forces T_i under a given load have been found, bar extensions can be found using $e_i = T_i L_i / AE$ (L: bar length, A: bar area, E: bar Young's modulus). Joint displacements $\boldsymbol{\delta}_i$ can be found by either:

- **Displacement diagram:** mark all known fixed joints at a common reference point $o...$. For each bar connected to a fixed joint, draw a solid line segment to a distance e_i in the direction of the endpoint, and if the bar is free to rotate, then draw a perpendicular dashed line from it. The endpoint displacement lies on this line. Repeat until intersections of the lines are found to identify the displacement vectors $\boldsymbol{\delta}_i$ of the joints, measured using scale drawings relative to o.

- **Virtual work (Castigliano's Theorem):** for **any** system of external forces $\mathbf{F}_i$ at the joints in equilibrium with bar tensions T_j (equilibrium set), and any system of joint displacements $\boldsymbol{\delta}_i$ compatible with member extensions e_j (compatibility set): the equation $\sum_i \mathbf{F}_i \cdot \boldsymbol{\delta}_i = \sum_j T_j e_j$, (external work = internal work) can be used by applying virtual load(s) $\mathbf{F}_i^* = 1$ at a joint where the displacement is desired, and finding the new virtual tensions T_j^* under this load. Solve for the desired real displacement(s) $\boldsymbol{\delta}_i$ using the real extensions e_j. If there is only one virtual load and it is parallel to the only real applied load F, then $\delta = \sum_j T_j^2 L_j / AEF$ (since $T_j = FT_j^*$).

6.3.19. Statically Indeterminate Trusses and Frames

A linear-elastic, pin-jointed (no bending moments), joint-loaded truss can be represented by:

- An equilibrium matrix, $\mathbf{A}$, such that $\mathbf{At} = \mathbf{f}$, formed by resolving in two orthogonal directions at each joint. Solutions to $\mathbf{At} = \mathbf{0}$ are states of self-stress.

- A compliance matrix, $\mathbf{C}$, such that $\mathbf{e} = \mathbf{Ct} + \mathbf{e}_0$, given by $\mathbf{C}_{ii} = \dfrac{L_i}{A_i E_i}$ and zero off-diagonal.

The compatibility constraint is represented as $\mathbf{e} = \mathbf{A}^\mathsf{T}\boldsymbol{\delta}$ ($\mathbf{A}^\mathsf{T}$: compatibility matrix).
Solutions to $\mathbf{A}^\mathsf{T}\boldsymbol{\delta} = \mathbf{0}$ are internal/rigid body mechanisms.

($\mathbf{t}$: unknown bar tensions, $\mathbf{f}$: external loads, $\mathbf{e}$: bar extensions, $\boldsymbol{\delta}$: bar displacements
$\mathbf{e}_0$: initial (misfit) bar extensions e.g. thermal expansion gives $(\mathbf{e}_0)_i = \alpha_i\, L_i\, \Delta T_i$

If the truss is statically indeterminate, then $\mathbf{At} = \mathbf{f}$ is an underconstrained system of equations, providing the 'particular solution' $\mathbf{t}_0$ and a set of 'states of self-stress' $\mathbf{s}_i$.

- To find $\mathbf{t}_0$, identify and remove (set force to zero) redundant bars to make the truss statically determinate, and solve for equilibrium with the applied load.

- To find each $\mathbf{s}_i$, remove all loads and remove (set force to zero) all but one redundant bars, which can be set to any arbitrary value e.g. 1, and solve again. Note that $\mathbf{s}_i$ are vectors spanning the null space of $\mathbf{A}$ since $\mathbf{As}_i = \mathbf{0}$ (Section 4.3.1).

- To find each x_i, invoke virtual work using $\mathbf{e} \cdot \mathbf{s}_i = 0$, for all i, solving for x_i.

- The equilibrium solutions are then $\mathbf{t} = \mathbf{t}_0 + \sum x_i\, \mathbf{s}_i$ and $\mathbf{e} = \mathbf{Ct} + \mathbf{e}_0$.

For frame structures which are statically indeterminate:

- Remove redundant supports and replace them with pins and reinstated unknown point bending moments.

- Find displacements and rotations of sections using compatibility or virtual work. The virtual work equations are $P^*\delta = \int_{frame} M\,\kappa^*\,ds$ and $Q^*\psi = \int_{frame} M\,\kappa^*\,ds$, or if bulk solid bodies are involved then $p^*V = \int_{solid} \sigma\,\varepsilon^*\,dV = \int_{solid} \tau\,\gamma^*\,dV$
  (P^*, Q^*: virtual loads and torques, $\kappa^* = M^*/EI$: virtual curvature, M: bending moment, ds: incremental distance along the frame, p^*: virtual pressure, V: volume change, σ: axial stress, ε^*: virtual axial strain, τ: shear stress, γ^*: virtual shear strain.)

- For each added pin, invoke continuity to set rotations either side equal.

- Solve for the required value(s) of the pin bending moments.

- Solve for reaction forces and plot shear forces/bending moments as required.

6.4.20. Periodic and Amorphous Rigid-Jointed Frameworks (Lattices and Foams)

In a rigid-jointed mechanistic assembly, bars parallel to applied forces do not develop a force, but other bars develop elastic bending moments (curvature) and the joints translate. For rigid-perfectly plastic modes, joints act as plastic hinges (Section 6.6.13).

Plane (2D) lattices will be stiff for $Z \geq 4$ and mechanistic for $Z < 4$.
Space (3D) lattices will be stiff for $Z \geq 6$ and mechanistic for $Z < 6$.

Example: Kagome plane lattice
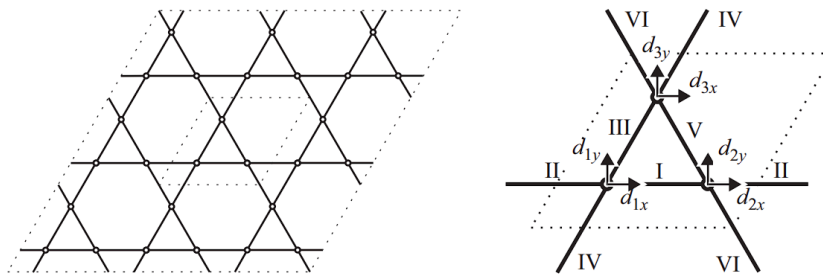
$$
\begin{bmatrix}
-1 & 0 & 1 & 0 & 0 & 0 \\
1 & 0 & -1 & 0 & 0 & 0 \\
-1/2 & -\sqrt{3}/2 & 0 & 0 & 1/2 & \sqrt{3}/2 \\
1/2 & \sqrt{3}/2 & 0 & 0 & -1/2 & -\sqrt{3}/2 \\
0 & 0 & 1/2 & -\sqrt{3}/2 & -1/2 & \sqrt{3}/2 \\
0 & 0 & -1/2 & \sqrt{3}/2 & 1/2 & -\sqrt{3}/2
\end{bmatrix}
\begin{bmatrix}
d_{1x} \\ d_{1y} \\ d_{2x} \\ d_{2y} \\ d_{3x} \\ d_{3y}
\end{bmatrix}
=
\begin{bmatrix}
e_{\mathrm{I}} \\ e_{\mathrm{II}} \\ e_{\mathrm{III}} \\ e_{\mathrm{IV}} \\ e_{\mathrm{V}} \\ e_{\mathrm{VI}}
\end{bmatrix}
$$

6.3.21. Plastic Theory

(For the prediction of failure in elastic deformation modes with Tresca and Von Mises theory), see Section 6.4.4.)

Plasticity theory is a failure-oriented design theory, assuming a flat stress-strain curve after yield (rigid-perfectly plastic: with ductility and neglects work hardening) and identical properties in tension and compression.

Elastic section modulus (Z_e) and Plastic section modulus (Z_p)

$$Z_e = \sum_{region\ i} A_i |\bar{y}_i| \qquad\qquad Z_p = \sum_{region\ i} A_i |\bar{y}_{i(EA)}|$$

($\bar{y}_i$: centroid of region i to **neutral axis**, $\bar{y}_{i(EA)}$: centroid of region i to **equal-area axis**)

The sum is over areas which are bending or yielding in either tension or compression. The equal-area axis is also known as the 'plastic neutral axis' (PNA).

The bending moment at which the extreme fibre of a beam yields plastically is the moment at first yield (elastic moment capacity), M_y.

The bending moment at which the entirety of a beam section yields plastically is the plastic moment capacity, M_p.

These are related to the material yield stress σ_y by $M_y = Z_e \sigma_y$ and $M_p = Z_p \sigma_y$.

Values of Z_e and Z_p for some cross-section are given.
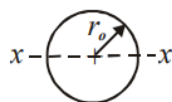
Solid circular section	Thin circular section	Rectangular section

$$Z_e = \frac{\pi r_o^3}{4} \qquad\qquad Z_e \approx \pi r^2 t \qquad\qquad Z_e = \frac{bh^2}{6}$$
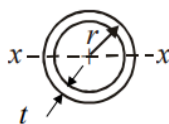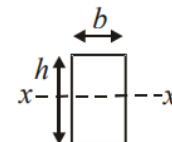
$$Z_p = \frac{4 r_o^3}{3} \qquad\qquad Z_p \approx 4 r^2 t \qquad\qquad Z_p = \frac{bh^2}{4}$$

6.3.22. Upper Bound Theorem for Plastic Failure of Structures

If an estimate of the plastic collapse load W_{mech} is calculated for any arbitrary compatible mechanism by equating the work done by the applied load, and the plastic energy dissipated, and the actual collapse load is W_c, then $W_{mech} \geq W_c$.

Typical application: plastic failure load of frame or beam due to **plastic hinge** formation.

External work = $W_c\,\delta$
Internal dissipation = $3\,M_p\,\theta$
Geometry: relates δ and θ:

(M_p: plastic moment capacity of beam: $M_p = Z_p\,\sigma_y$)
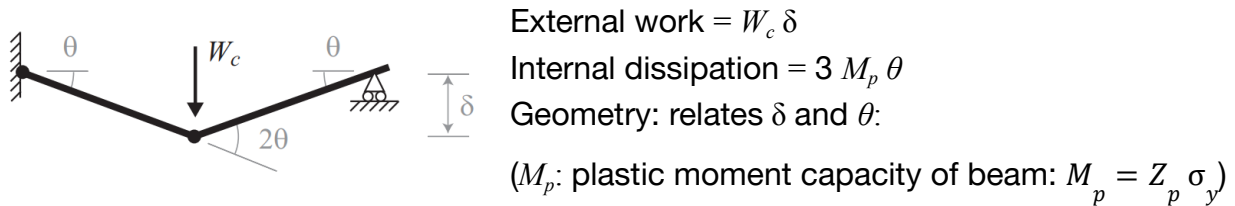
Statically determinate structures collapse with **one** plastic hinge. Statically indeterminate structures (e.g. multi-span beams, frames) collapse with **multiple** plastic hinges.

6.3.23. Plastic Failure Modes of Portal Frames (Plastic Hinge Mechanisms)

Beam mechanism   **Sway mechanism**   **Combined mechanism**
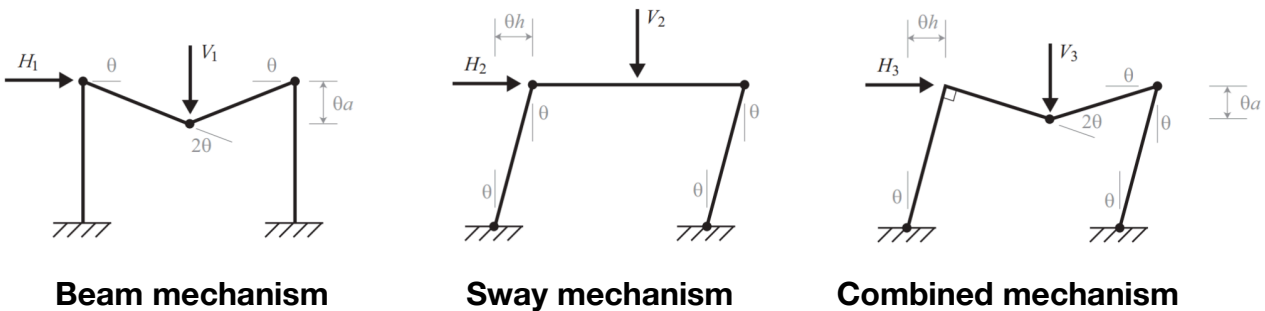
An 'interaction diagram' shows the regions of each mode as a function of H and V.

The geometry of combined mechanisms can be deduced using the method of instantaneous centres for each of the rigid regions between plastic hinges:
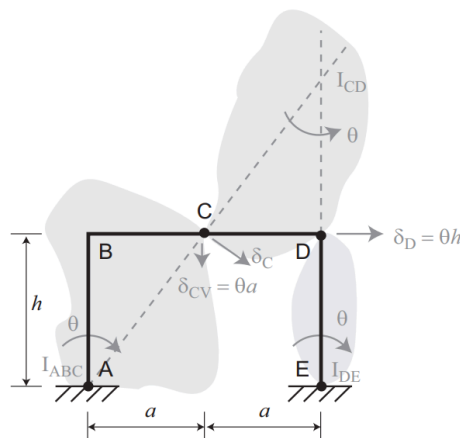
6.3.24. Yield Line and Slip Plane Analysis of Slabs, Plates and Continua
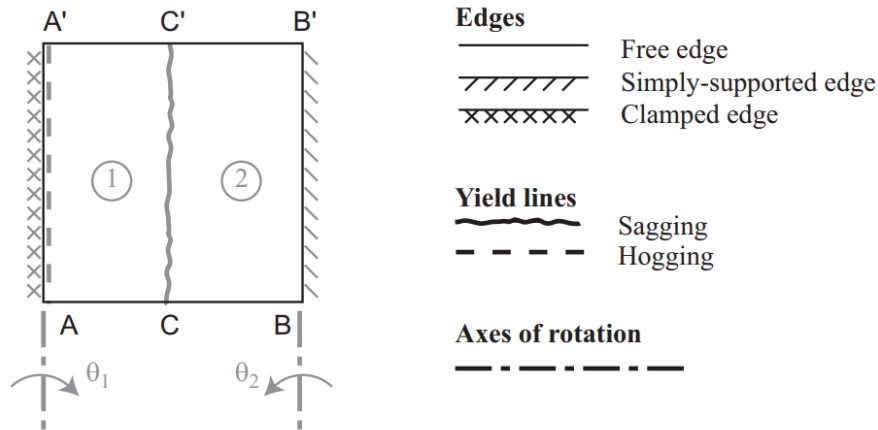
Plastic moment capacity per unit length of a yield line: $m = \dfrac{M_p}{b} = \dfrac{Z_p\, \sigma_y}{b} = \dfrac{1}{4}\, d^2 \sigma_y$

(d: thickness of rectangular plate cross section)

By the upper bound theorem, $\displaystyle\sum_{forces} F\, \delta + \sum_{pressures} p\, \Delta V = \sum_{yield\ lines} mL\, \Delta\theta.$

If the volume generated ΔV due to a pressure loading is difficult to calculate, an alternative way of writing this term is $pA\, \Delta z_g$, where A is the plane area of the region and Δz_g is the distance descended by the centroid of the region, which can be related to δ by similarity.

The $L\, \Delta\theta$ terms can be found using either a displacement diagram (yield line length × relative angle of rotation) or the projection method (resolve into component of yield line parallel to axis × rotation about axis).

Slabs made of reinforced concrete do fail by yield lines, but the energy absorbed is all in the steel reinforcement, and the above calculation for moment capacity is not valid. For calculations on reinforced concrete, see Section 6.5.7. Similar analyses can be done for soil slippage in shear (Section 6.5.4).

For continua (rigid plastic solids), the upper bound theorem is

$$\sum_{forces} F\, \delta + \sum_{pressures} p\, \Delta V = \sum_{shear\ zones} kA\, \Delta x$$

where k is the shear yield stress, A is the area of the slip plane and Δx is the relative displacement of each rigid block. For continuum mechanics analysis, see Section 6.2.27.

6.3.25. Lower Bound Theorem for Plastic Failure of Structures

If a set of internal stresses can be found in the structure that are in equilibrium with an applied load W_{equil}, and nowhere violate the yield condition, and the actual collapse load is W_c, then $W_c \geq W_{equil}$.

To perform a lower bound analysis:

- Make the structure statically determinate by adding unknown bending moments M_x at newly-positioned pins.

- Determine the generalised bending moment distribution in terms of M_x.

- Optimise the distribution so that the peaks and troughs are as close to M_p as possible with no larger value. Calculate the value of M_x at which this occurs.

For beam section optimisation, plastic moduli Z_p are given for common steel UBs in Section 6.5.9.

6.3.26. Continuum Mechanics Formulation of Deformation

For tensor notation, see Section 4.4.1.

Isotropic Linear Elasticity

(σ_{ij}: stress tensor, ε_{ij}: infinitesimal strain tensor, b_i: body force vector, t_i^e: external traction vector, u_i: displacement vector, U: strain energy density scalar)

- Equilibrium: $\qquad\qquad\quad \sigma_{ij,j} + b_i = 0 \quad\text{and}\quad \sigma_{ij} = \sigma_{ji}$
- Compatibility: $\qquad\qquad \varepsilon_{ij,kp} + \varepsilon_{kp,ij} - \varepsilon_{pj,ki} - \varepsilon_{ki,pj} = 0$
- Constitutive law: $\qquad\quad \sigma_{ij} = \frac{E}{1+v}\varepsilon_{ij} + \frac{vE}{(1+v)(1-2v)}\varepsilon_{kk}\delta_{ij}$
- Lame's constants: $\qquad\quad \mu = G = \frac{E}{2(1+v)}, \quad \lambda = \frac{vE}{(1+v)(1-2v)}$
- Strain energy density: $\quad \sigma_{ij} = \frac{\partial U}{\partial \varepsilon_{ij}}$

At equilibrium, the potential energy Π is minimised. Hence, for any small kinematically admissible perturbation δu_i,

$$\delta\Pi = \int_V \delta U\, dV - \int_S t_i^e \delta u_i\, dS - \int_V b_i \delta u_i\, dV = 0$$

Isotropic Linear Viscoelasticity

(E_r: relaxation modulus, J_c: creep compliance, $H(t)$: Heaviside step function)

- Relaxation response: $\qquad$ if $\varepsilon(t) = \varepsilon_0 H(t)$ then $\sigma(t) = \varepsilon_0 E_r(t)$
- Creep response: $\qquad\qquad$ if $\sigma(t) = \sigma_0 H(t)$ then $\varepsilon(t) = \sigma_0 J_c(t)$
- Laplace domain: $\qquad\qquad \overline{E}_r(s)\,\overline{J}_c(s) = s^{-2}$

Boltzmann superposition principle in 1D (convolution theorem for impulse responses):

$$\sigma(t) = \int_0^t \frac{\partial \varepsilon(\tau)}{\partial \tau} E_r(t-\tau)d\tau \qquad\qquad \varepsilon(t) = \int_0^t \frac{\partial \sigma(\tau)}{\partial \tau} J_c(t-\tau)d\tau$$

Correspondence principle: in the Laplace domain, the viscoelastic solution corresponds to the elastic solution, with the substitutions $E \to s\,\overline{E}_r(s)$ and $v \to s\,\overline{v}_r(s)$ (for any time-dependent moduli).

6.4. Geotechnical and Civil Engineering

6.4.1. Definitions in Soil Mechanics

The structure of soil can be divided into a solid phase, liquid phase and gas phase:

Soil structure   Volumes   Weights
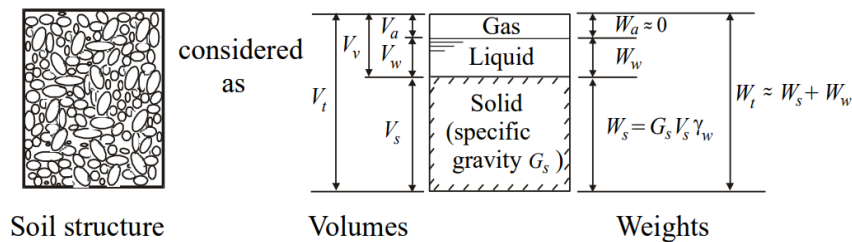
Quantities defining the composition are given by: (Unit weight of water: γ_w = 9.81 kN m^{-3})

- Specific gravity of soil solids: $G_s = \dfrac{\rho_s}{\rho_{water}}$

- Voids ratio: $e = \dfrac{V_v}{V_s}$

- Water content: $w = \dfrac{W_w}{W_s}$

- Degree of saturation: $S_r = \dfrac{V_w}{V_v} = w\dfrac{G_s}{e}$

- Bulk unit weight of soil: $\gamma = \dfrac{W_t}{V_t} = \dfrac{\gamma_w(G_s + S_r e)}{1 + e}$

- Dry unit weight of soil: $\gamma = \dfrac{W_s}{V_t} = \dfrac{\gamma_w G_s}{1 + e}$

- Buoyant unit weight of soil: $\gamma' = \gamma - \gamma_w = \dfrac{\gamma_w(G_s - 1)}{1 + e}$

- Relative density: $I_D = \dfrac{e_{max} - e}{e_{max} - e_{min}}$

    where e_{max} is the maximum voids ratio achievable in a quick tilt test, and e_{min} is the minimum voids ratio achievable by vibratory compaction.

6.4.2. Classification of Particle Sizes

Clay: smaller than 0.002 mm (two microns)   Gravel: between 2 and 60 mm

Silt: between 0.002 and 0.06 mm   Cobbles: between 60 and 200 mm

Sand: between 0.06 and 2 mm   Boulders: larger than 200 mm

D_x: particle size such that x% by weight of a soil sample is composed of finer grains.

6.4.3. Groundwater Seepage
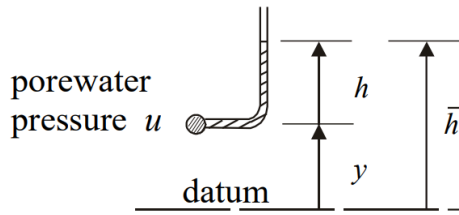
Head	$h = u / \gamma_w$
Potential	$\bar{h} = h + y$
Hydraulic gradient	$i = -\nabla \bar{h}$

Darcy's law for laminar flow:

$$v = ki \qquad (v: \text{superficial seepage velocity, } k: \text{coefficient of permeability})$$

Typical values:

Clays:	k between 10^{-11} ms^{-1} and 10^{-9} ms^{-1}
1 micron $< D_{10} < 10$ mm:	$k \approx 0.01 \times (D_{10}$ in mm$)^2$ ms^{-1}
$D_{10} > 10$ mm:	non-laminar flow.

6.4.4. Plane-Strain Soil Stresses

In this section only, compressive stresses are taken as positive.

The effective stress in saturated soil the difference between the total stress and the pore water pressure: $\sigma = \sigma' + u$ and $\tau = \tau' (+ 0)$.
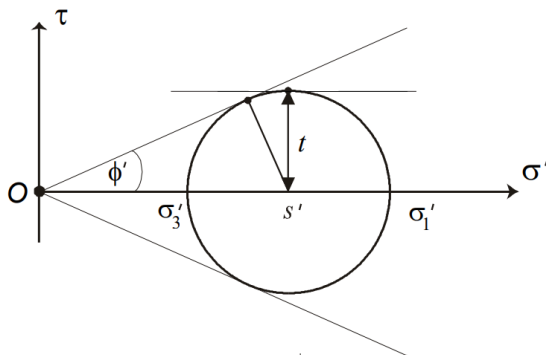
Mohr's circle:

Mobilised angle of shearing: ϕ'

Mean effective stress: $s' = \dfrac{\sigma_1' + \sigma_3'}{2}$

Mobilised shear strength: $t = \dfrac{\sigma_1' - \sigma_3'}{2} = \dfrac{\sigma_1 - \sigma_3}{2}$

$$\sin \phi' = \frac{t}{s'} = \frac{\sigma_1 - \sigma_3}{\sigma_1 + \sigma_3}$$

6.4.5. Undrained Strength of Soil: Tresca Cohesion Hypothesis

Undrained behaviour is exhibited by clays in the short term.

In constant-volume tests on clay, failure occurs when t reaches $t_{max} = c_u$ where c_u is the undrained shear strength, which depends primarily on the voids ratio e.

The active and passive total horizontal stresses (σ_a and σ_p) are related to the vertical total stress σ_v by

$$\sigma_a = \sigma_v - 2c_u \quad \text{and} \quad \sigma_p = \sigma_v + 2c_u$$

6.4.6. Drained Strength of Soil: Coulomb Friction hypothesis

Drained behaviour is exhibited by sands in the short term and all soils in the long term.

Earth pressure coefficient: K,   such that $\sigma_h' = K \sigma_v'$

Active pressure ($\sigma_v' > \sigma_h'$): $K_A = \dfrac{1 - sin\,\varphi'}{1 + sin\,\varphi'}$

Passive pressure ($\sigma_v' < \sigma_h'$): $K_P = \dfrac{1 + sin\,\varphi'}{1 - sin\,\varphi'}$

(Assuming principal stresses are vertical and horizontal.)

Angle of shearing resistance: φ'_{max} at peak strength, φ'_{crit} at large strain (critical state).

$$\varphi'_{max} = \varphi'_{crit} + \varphi'_{dilatancy}$$

where φ'_{crit} is the ultimate angle of shearing resistance of a random aggregate deforming at constant volume, and $\varphi'_{dilatancy} \to 0$ as $I_D \to 0$, or s' becomes large.

Typical properties for a quartz sand: $\varphi'_{crit} = 33^o$, $\varphi'_{max} = 53^o$ ($I_D = 1$, $s' < 150$ kN m^{-2})
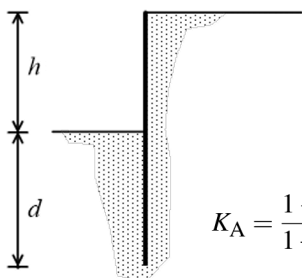
Geotechnical engineering of deep excavations with a cantilevered pile wall support: if passive side mobilised friction is δ, then the static solutions are (Lancellotta, 2002)

$$K_A = \frac{1 - \sin\varphi'}{1 + \sin\varphi'} \qquad K_P = \frac{\cos\delta}{1 - \sin\varphi'}\left[\cos\delta + \sqrt{\sin^2\varphi' - \sin^2\delta}\,\right]e^{2\Theta\tan\varphi'} \qquad 2\Theta = \sin^{-1}\left[\frac{\sin\delta}{\sin\varphi'}\right] + \delta$$

6.4.7. Design Standards of Reinforced Concrete
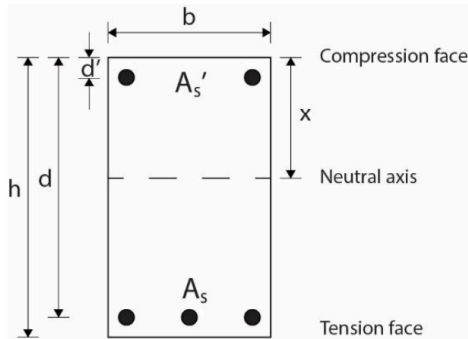
Design compressive strength of concrete is based on the characteristic cylinder or cube strength f_{ck} [MPa]:

$$f_{cd} = \frac{2}{3} \, \alpha_{cc} \, f_{ck}$$

$\alpha_{cc} = 0.85$ for compression in flexure and axial loading and $\alpha_{cc} = 1.0$ for other phenomena.

Design tensile strength of steel is based on the characteristic tensile yield stress of steel f_{yk}:

$$f_{yd} = \frac{f_{yk}}{1.15}$$

At failure in bending, the stress in the concrete is $0.6 \, f_{cd}$ over the whole area of concrete in compression and the stress in the steel is f_{yd}.

Moment capacity of singly reinforced beam:

$$M = f_{yd} A_s \left(d - \frac{x}{2} \right) \qquad x = \frac{5}{3} \frac{f_{yd}}{f_{cd}} \frac{A_s}{b} \quad (\leq 0.5d \text{ to avoid over-reinforcement})$$

Moment capacity of doubly reinforced beam (if compression reinforcement is yielding):

$$M = 0.6 \, f_{cd} \, bx \left(d - \frac{x}{2} \right) + A_s' \, f_{yd} (d - d')$$

Shear capacity of unreinforced webs:

$$V_{Rd,c} = \frac{0.18}{\gamma_c} \left(k \left(100 \, \rho_l \, f_{ck} \right)^{1/3} \right) b_w d \geq 0.035 \, k^{3/2} \, f_{ck}^{1/2} \, b_w d$$

where $k = 1 + \sqrt{\frac{200}{d}} \leq 2$ (with d in mm), b_w: width of the web,

ρ_l: reinforcement ratio of the anchored steel with $\rho_l = \frac{A_s}{b_w d} \leq 0.02$.

If this resistance is insufficient to carry the applied load, internal stirrups are required, designed (assuming a 45 degrees truss angle) according to:

$$V_s = \frac{A_{sw} f_{yd} (0.9 \, d)}{1.15 \, s} \quad (A_{sw}: \text{area of stirrup legs, } s: \text{stirrup spacing})$$

$$V_{max} = \frac{1}{2} f_{c,max} (0.9 \, bd) \quad \text{where } f_{c,max} = 0.4 \, f_{ck} \left(1 - \frac{f_{ck}}{250} \right)$$

The shear resistance is controlled by the smaller of V_s or V_{max}.

6.4.8. Standard Bar Sizes and Reinforcement Areas

Available steel types:

Deformed high yield steel: f_{yk} = 500 N mm^{-2}
Plain mild steel: f_{yk} = 250 N mm^{-2}

Reinforcement area (in mm^2) per metre width from bar diameter and bar spacing:

Bar Dia. (mm)	Spacing of bars (mm)									
	75	100	125	150	175	200	225	250	275	300
6	377	283	226	189	162	142	126	113	103	94.3
8	671	503	402	335	287	252	224	201	183	168
10	1050	785	628	523	449	393	349	314	285	262
12	1510	1130	905	754	646	566	503	452	411	377
16	2680	2010	1610	1340	1150	1010	894	804	731	670
20	4190	3140	2510	2090	1800	1570	1400	1260	1140	1050
25	6550	4910	3930	3270	2810	2450	2180	1960	1790	1640
32	10700	8040	6430	5360	4600	4020	3570	3220	2920	2680
40	16800	12600	10100	8380	7180	6280	5580	5030	4570	4190

6.4.9. Properties of Structural Steel Sections (Hot-Rolled)

Universal Beams: designation $a \times b \times c$ where $a \approx$ depth [mm], $b \approx$ width [mm], $c \approx$ mass/length [kg/m]

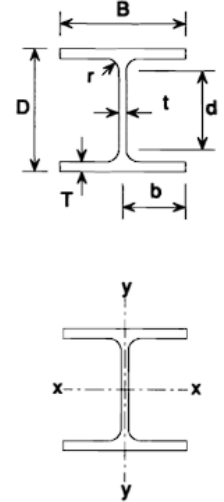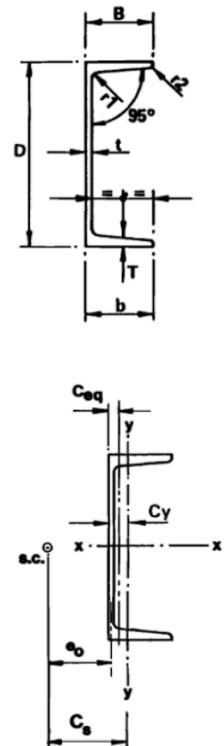| Section Designation	Mass Per Metre (kg/m)	Depth Of Section D (mm)	Width Of Section B (mm)	Thickness Web t (mm)	Thickness Flange T (mm)	Second Moment Of Area Axis x-x (cm⁴)	Second Moment Of Area Axis y-y (cm⁴)	Radius Of Gyration Axis x-x (cm)	Radius Of Gyration Axis y-y (cm)	Elastic Modulus Axis x-x (cm³)	Elastic Modulus Axis y-y (cm³)	Plastic Modulus Axis x-x (cm³)	Plastic Modulus Axis y-y (cm³)	Torsional Constant J (cm⁴)	Area Of Section A (cm²)
914x419x388	388.0	921.0	420.5	21.4	36.6	719600	45440	38.2	9.59	15630	2161	17670	3341	1734	494
914x419x343	343.3	911.8	418.5	19.4	32.0	625800	39160	37.8	9.46	13730	1871	15480	2890	1193	437
914x305x289	289.1	926.6	307.7	19.5	32.0	504200	15600	37.0	6.51	10880	1014	12570	1601	926	368
914x305x253	253.4	918.4	305.5	17.3	27.9	436300	13300	36.8	6.42	9501	871	10940	1371	626	323
914x305x224	224.2	910.4	304.1	15.9	23.9	376400	11240	36.3	6.27	8269	739	9535	1163	422	286
914x305x201	200.9	903.0	303.3	15.1	20.2	325300	9423	35.7	6.07	7204	621	8351	982	291	256
838x292x226	226.5	850.9	293.8	16.1	26.8	339700	11360	34.3	6.27	7985	773	9155	1212	514	289
838x292x194	193.8	840.7	292.4	14.7	21.7	279200	9066	33.6	6.06	6641	620	7640	974	306	247
838x292x176	175.9	834.9	291.7	14.0	18.8	246000	7799	33.1	5.90	5893	535	6808	842	221	224
762x267x197	196.8	769.8	268.0	15.6	25.4	240000	8175	30.9	5.71	6234	610	7167	959	404	251
762x267x173	173.0	762.2	266.7	14.3	21.6	205300	6850	30.5	5.58	5387	514	6198	807	267	220
762x267x147	146.9	754.0	265.2	12.8	17.5	168500	5455	30.0	5.40	4470	411	5156	647	159	187
762x267x134	133.9	750.0	264.4	12.0	15.5	150700	4788	29.7	5.30	4018	362	4644	570	119	171
686x254x170	170.2	692.9	255.8	14.5	23.7	170300	6630	28.0	5.53	4916	518	5631	811	308	217
686x254x152	152.4	687.5	254.5	13.2	21.0	150400	5784	27.8	5.46	4374	455	5000	710	220	194
686x254x140	140.1	683.5	253.7	12.4	19.0	136300	5183	27.6	5.39	3987	409	4558	638	169	178
686x254x125	125.2	677.9	253.0	11.7	16.2	118000	4383	27.2	5.24	3481	346	3994	542	116	159
610x305x238	238.1	635.8	311.4	18.4	31.4	209500	15840	26.3	7.23	6589	1017	7486	1574	785	303
610x305x179	179.0	620.2	307.1	14.1	23.6	153000	11410	25.9	7.07	4935	743	5547	1144	340	228
610x305x149	149.2	612.4	304.8	11.8	19.7	125900	9308	25.7	7.00	4111	611	4594	937	200	190
610x229x140	139.9	617.2	230.2	13.1	22.1	111800	4505	25.0	5.03	3622	391	4142	611	216	178
610x229x125	125.1	612.2	229.0	11.9	19.6	98610	3932	24.9	4.97	3221	343	3676	535	154	159
610x229x113	113.0	607.6	228.2	11.1	17.3	87320	3434	24.6	4.88	2874	301	3281	469	111	144
610x229x101	101.2	602.6	227.6	10.5	14.8	75780	2915	24.2	4.75	2515	256	2881	400	77.0	129
533x210x122	122.0	544.5	211.9	12.7	21.3	76040	3388	22.1	4.67	2793	320	3196	500	178	155
533x210x109	109.0	539.5	210.8	11.6	18.8	66820	2943	21.9	4.60	2477	279	2828	436	126	139
533x210x101	101.0	536.7	210.0	10.8	17.4	61520	2692	21.9	4.57	2292	256	2612	399	101	129
533x210x92	92.1	533.1	209.3	10.1	15.6	55230	2389	21.7	4.51	2072	228	2360	356	75.7	117
533x210x82	82.2	528.3	208.8	9.6	13.2	47540	2007	21.3	4.38	1800	192	2059	300	51.5	105
457x191x98	98.3	467.2	192.8	11.4	19.6	45730	2347	19.1	4.33	1957	243	2232	379	121	125
457x191x89	89.3	463.4	191.9	10.5	17.7	41020	2089	19.0	4.29	1770	218	2014	338	90.7	114
457x191x82	82.0	460.0	191.3	9.9	16.0	37050	1871	18.8	4.23	1611	196	1831	304	69.2	104
457x191x74	74.3	457.0	190.4	9.0	14.5	33320	1671	18.8	4.20	1458	176	1653	272	51.8	94.6
457x191x67	67.1	453.4	189.9	8.5	12.7	29380	1452	18.5	4.12	1296	153	1471	237	37.1	85.5
457x152x82	82.1	465.8	155.3	10.5	18.9	36590	1185	18.7	3.37	1571	153	1811	240	89.2	105
457x152x74	74.2	462.0	154.4	9.6	17.0	32670	1047	18.6	3.33	1414	136	1627	213	65.9	94.5
457x152x67	67.2	458.0	153.8	9.0	15.0	28930	913	18.4	3.27	1263	119	1453	187	47.7	85.6
457x152x60	59.8	454.6	152.9	8.1	13.3	25500	795	18.3	3.23	1122	104	1287	163	33.8	76.2
457x152x52	52.3	449.8	152.4	7.6	10.9	21370	645	17.9	3.11	950	84.6	1096	133	21.4	66.6
406x178x74	74.2	412.8	179.5	9.5	16.0	27310	1545	17.0	4.04	1323	172	1501	267	62.8	94.5
406x178x67	67.1	409.4	178.8	8.8	14.3	24330	1365	16.9	3.99	1189	153	1346	237	46.1	85.5
406x178x60	60.1	406.4	177.9	7.9	12.8	21600	1203	16.8	3.97	1063	135	1199	209	33.3	76.5
406x178x54	54.1	402.6	177.7	7.7	10.9	18720	1021	16.5	3.85	930	115	1055	178	23.1	69.0
406x140x46	46.0	403.2	142.2	6.8	11.2	15690	538	16.4	3.03	778	75.7	888	118	19.0	58.6
406x140x39	39.0	398.0	141.8	6.4	8.6	12510	410	15.9	2.87	629	57.8	724	90.8	10.7	49.7
356x171x67	67.1	363.4	173.2	9.1	15.7	19460	1362	15.1	3.99	1071	157	1211	243	55.7	85.5
356x171x57	57.0	358.0	172.2	8.1	13.0	16040	1108	14.9	3.91	896	129	1010	199	33.4	72.6
356x171x51	51.0	355.0	171.5	7.4	11.5	14140	968	14.8	3.86	796	113	896	174	23.8	64.9
356x171x45	45.0	351.4	171.1	7.0	9.7	12070	811	14.5	3.76	687	94.8	775	147	15.8	57.3
356x127x39	39.1	353.4	126.0	6.6	10.7	10170	358	14.3	2.68	576	56.8	659	89.1	15.1	49.8
356x127x33	33.1	349.0	125.4	6.0	8.5	8249	280	14.0	2.58	473	44.7	543	70.3	8.79	42.1
305x165x54	54.0	310.4	166.9	7.9	13.7	11700	1063	13.0	3.93	754	127	846	196	34.8	68.8
305x165x46	46.1	306.6	165.7	6.7	11.8	9899	896	13.0	3.90	646	108	720	166	22.2	58.7
305x165x40	40.3	303.4	165.0	6.0	10.2	8503	764	12.9	3.86	560	92.6	623	142	14.7	51.3
305x127x48	48.1	311.0	125.3	9.0	14.0	9575	461	12.5	2.74	616	73.6	711	116	31.8	61.2
305x127x42	41.9	307.2	124.3	8.0	12.1	8196	389	12.4	2.70	534	62.6	614	98.4	21.1	53.4
305x127x37	37.0	304.4	123.4	7.1	10.7	7171	336	12.3	2.67	471	54.5	539	85.4	14.8	47.2
305x102x33	32.8	312.7	102.4	6.6	10.8	6501	194	12.5	2.15	416	37.9	481	60.0	12.2	41.8
305x102x28	28.2	308.7	101.8	6.0	8.8	5366	155	12.2	2.08	348	30.5	403	48.5	7.40	35.9
305x102x25	24.8	305.1	101.6	5.8	7.0	4455	123	11.9	1.97	292	24.2	342	38.8	4.77	31.6
254x146x43	43.0	259.6	147.3	7.2	12.7	6544	677	10.9	3.52	504	92.0	566	141	23.9	54.8
254x146x37	37.0	256.0	146.4	6.3	10.9	5537	571	10.8	3.48	433	78.0	483	119	15.3	47.2
254x146x31	31.1	251.4	146.1	6.0	8.6	4413	448	10.5	3.36	351	61.3	393	94.1	8.55	39.7
254x102x28	28.3	260.4	102.2	6.3	10.0	4005	179	10.5	2.22	308	34.9	353	54.8	9.57	36.1
254x102x25	25.2	257.2	101.9	6.0	8.4	3415	149	10.3	2.15	266	29.2	306	46.0	6.42	32.0
254x102x22	22.0	254.0	101.6	5.7	6.8	2841	119	10.1	2.06	224	23.5	259	37.3	4.15	28.0
203x133x30	30.0	206.8	133.9	6.4	9.6	2896	385	8.71	3.17	280	57.5	314	88.2	10.3	38.2
203x133x25	25.1	203.2	133.2	5.7	7.8	2340	308	8.56	3.10	230	46.2	258	70.9	5.96	32.0
203x102x23	23.1	203.2	101.8	5.4	9.3	2105	164	8.46	2.36	207	32.2	234	49.8	7.02	29.4
178x102x19	19.0	177.8	101.2	4.8	7.9	1356	137	7.48	2.37	153	27.0	171	41.6	4.41	24.3
152x89x16	16.0	152.4	88.7	4.5	7.7	834	89.8	6.41	2.10	109	20.2	123	31.2	3.56	20.3
127x76x13	13.0	127.0	76.0	4.0	7.6	473	55.7	5.35	1.84	74.6	14.7	84.2	22.6	2.85	16.5
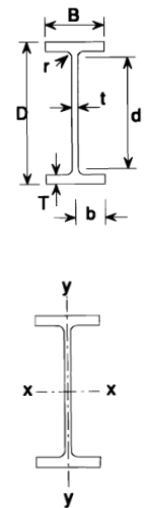
Universal Columns: designation $a \times b \times c$ where $a \approx$ depth [mm], $b \approx$ width [mm], $c \approx$ mass/length [kg/m]

Section Designation	Mass Per Metre (kg/m)	Depth Of Section D (mm)	Width Of Section B (mm)	Thickness Web t (mm)	Thickness Flange T (mm)	Second Moment Of Area Axis x-x (cm⁴)	Second Moment Of Area Axis y-y (cm⁴)	Radius Of Gyration Axis x-x (cm)	Radius Of Gyration Axis y-y (cm)	Elastic Modulus Axis x-x (cm³)	Elastic Modulus Axis y-y (cm³)	Plastic Modulus Axis x-x (cm³)	Plastic Modulus Axis y-y (cm³)	Torsional Constant J (cm⁴)	Area Of Section A (cm²)
356x406x634	633.9	474.6	424.0	47.6	77.0	274800	98130	18.4	11.0	11580	4629	14240	7108	13720	808
356x406x551	551.0	455.6	418.5	42.1	67.5	226900	82670	18.0	10.9	9962	3951	12080	6058	9240	702
356x406x467	467.0	436.6	412.2	35.8	58.0	183000	67830	17.5	10.7	8383	3291	10000	5034	5809	595
356x406x393	393.0	419.0	407.0	30.6	49.2	146600	55370	17.1	10.5	6998	2721	8222	4154	3545	501
356x406x340	339.9	406.4	403.0	26.6	42.9	122500	46850	16.8	10.4	6031	2325	6999	3544	2343	433
356x406x287	287.1	393.6	399.0	22.6	36.5	99880	38680	16.5	10.3	5075	1939	5812	2949	1441	366
356x406x235	235.1	381.0	394.8	18.4	30.2	79080	30990	16.3	10.2	4151	1570	4687	2383	812	299
356x368x202	201.9	374.6	374.7	16.5	27.0	66260	23690	16.1	9.60	3538	1264	3972	1920	558	257
356x368x177	177.0	368.2	372.6	14.4	23.8	57120	20530	15.9	9.54	3103	1102	3455	1671	381	226
356x368x153	152.9	362.0	370.5	12.3	20.7	48590	17550	15.8	9.49	2684	948	2965	1435	251	195
356x368x129	129.0	355.6	368.6	10.4	17.5	40250	14610	15.6	9.43	2264	793	2479	1199	153	164
305x305x283	282.9	365.3	322.2	26.8	44.1	78870	24630	14.8	8.27	4318	1529	5105	2342	2034	360
305x305x240	240.0	352.5	318.4	23.0	37.7	64200	20310	14.5	8.15	3643	1276	4247	1951	1271	306
305x305x198	198.1	339.9	314.5	19.1	31.4	50900	16300	14.2	8.04	2995	1037	3440	1581	734	252
305x305x158	158.1	327.1	311.2	15.8	25.0	38750	12570	13.9	7.90	2369	808	2680	1230	378	201
305x305x137	136.9	320.5	309.2	13.8	21.7	32810	10700	13.7	7.83	2048	692	2297	1053	249	174
305x305x118	117.9	314.5	307.4	12.0	18.7	27670	9059	13.6	7.77	1760	589	1958	895	161	150
305x305x97	96.9	307.9	305.3	9.9	15.4	22250	7308	13.4	7.69	1445	479	1592	726	91.2	123
254x254x167	167.1	289.1	265.2	19.2	31.7	30000	9870	11.9	6.81	2075	744	2424	1137	626	213
254x254x132	132.0	276.3	261.3	15.3	25.3	22530	7531	11.6	6.69	1631	576	1869	878	319	168
254x254x107	107.1	266.7	258.8	12.8	20.5	17510	5928	11.3	6.59	1313	458	1484	697	172	136
254x254x89	88.9	260.3	256.3	10.3	17.3	14270	4857	11.2	6.55	1096	379	1224	575	102	113
254x254x73	73.1	254.1	254.6	8.6	14.2	11410	3908	11.1	6.48	898	307	992	465	57.6	93.1
203x203x86	86.1	222.2	209.1	12.7	20.5	9449	3127	9.28	5.34	850	299	977	456	137	110
203x203x71	71.0	215.8	206.4	10.0	17.3	7618	2537	9.18	5.30	706	246	799	374	80.2	90.4
203x203x60	60.0	209.6	205.8	9.4	14.2	6125	2065	8.96	5.20	584	201	656	305	47.2	76.4
203x203x52	52.0	206.2	204.3	7.9	12.5	5259	1778	8.91	5.18	510	174	567	264	31.8	66.3
203x203x46	46.1	203.2	203.6	7.2	11.0	4568	1548	8.82	5.13	450	152	497	231	22.2	58.7
152x152x37	37.0	161.8	154.4	8.0	11.5	2210	706	6.85	3.87	273	91.5	309	140	19.2	47.1
152x152x30	30.0	157.6	152.9	6.5	9.4	1748	560	6.76	3.83	222	73.3	248	112	10.5	38.3
152x152x23	23.0	152.4	152.2	5.8	6.8	1250	400	6.54	3.70	164	52.6	182	80.2	4.63	29.2

Channels:

Nominal Size (mm)	Mass Per Metre (kg)	Depth Of Section D (mm)	Width Of Section B (mm)	Thickness Web t (mm)	Thickness Flange T (mm)	Second Moment Of Area Axis x-x (cm⁴)	Second Moment Of Area Axis y-y (cm⁴)	Radius Of Gyration Axis x-x (cm)	Radius Of Gyration Axis y-y (cm)	Elastic Modulus Axis x-x (cm³)	Elastic Modulus Axis y-y (cm³)	Plastic Modulus Axis x-x (cm³)	Plastic Modulus Axis y-y (cm³)	Torsional Constant J (cm⁴)	Area of Section A (cm²)
432x102	65.54	431.8	101.6	12.2	16.8	21370	627	16.0	2.74	990	79.9	1205	153	61.5	83.4
381x102	55.10	381.0	101.6	10.4	16.3	14870	579	14.6	2.87	781	75.7	931	144	46.4	70.1
305x102	46.18	304.8	101.6	10.2	14.8	8208	499	11.8	2.91	539	66.5	638	128	35.9	58.9
305x89	41.69	304.8	88.9	10.2	13.7	7078	326	11.5	2.47	464	48.6	559	92.9	28.1	53.3
254x89	35.74	254.0	88.9	9.1	13.6	4445	302	9.89	2.58	350	46.7	414	89.6	23.2	45.4
254x76	28.29	254.0	76.2	8.1	10.9	3355	162	9.67	2.12	264	28.1	316	53.9	12.3	35.9
229x89	32.76	228.6	88.9	8.6	13.3	3383	285	9.01	2.61	296	44.8	348	86.3	20.6	41.6
229x76	26.06	228.6	76.2	7.6	11.2	2615	159	8.87	2.19	229	28.3	271	54.5	11.6	33.2
203x89	29.78	203.2	88.9	8.1	12.9	2492	265	8.11	2.64	245	42.4	287	81.7	18.1	37.9
203x76	23.82	203.2	76.2	7.1	11.2	1955	152	8.02	2.24	192	27.7	226	53.5	10.6	30.4
178x89	26.81	177.8	88.9	7.6	12.3	1753	241	7.17	2.66	197	39.3	230	75.4	15.3	34.1
178x76	20.84	177.8	76.2	6.6	10.3	1338	134	7.10	2.25	151	24.8	176	48.1	8.26	26.6
152x89	23.84	152.4	88.9	7.1	11.6	1168	216	6.20	2.66	153	35.8	178	68.3	12.7	30.4
152x76	17.88	152.4	76.2	6.4	9.0	852	114	6.11	2.23	112	21.0	130	41.2	6.05	22.8
127x64	14.90	127.0	63.5	6.4	9.2	482	67.2	5.04	1.88	76.0	15.2	89.4	29.3	5.00	19.0
102x51	10.42◆	101.6	50.8	6.1	7.6	207	29.0	3.95	1.48	40.8	8.14	48.7	15.7	2.58	13.3
76x38	6.70◆	76.2	38.1	5.1	6.8	74.3	10.7	2.95	1.12	19.5	4.09	23.5	7.78	1.26	8.56

Equal Angles:

Designation		Mass Per Metre	Radius		Area Of Section	Distance Of Centre Of Gravity	Second Moment Of Area			Radius Of Gyration			Elastic Modulus
Size	Thickness		Root	Toe		cx and cy	Axis x-x, y-y	Axis u-u	Axis v-v	Axis x-x, y-y	Axis u-u	Axis v-v	Axis x-x, y-y
A A mm	t mm	kg	r1 mm	r2 mm	cm²	cm	cm⁴	cm⁴	cm⁴	cm	cm	cm	cm³
250x250	35	128	20.0	4.8	164	7.51	9305	14720	3886	7.54	9.49	4.88	532
	32	118	20.0	4.8	151	7.40	8650	13710	3592	7.58	9.54	4.89	491
	28	104	20.0	4.8	133	7.25	7741	12290	3194	7.63	9.61	4.90	436
	25	93.6	20.0	4.8	120	7.14	7030	11170	2890	7.67	9.67	4.92	394
200x200	24	71.1	18.0	4.8	90.8	5.85	3356	5322	1391	6.08	7.65	3.91	237
	20	59.9	18.0	4.8	76.6	5.70	2877	4569	1185	6.13	7.72	3.93	201
	18	54.2	18.0	4.8	69.4	5.62	2627	4174	1080	6.15	7.76	3.95	183
	16	48.5	18.0	4.8	62.0	5.54	2369	3765	973	6.18	7.79	3.96	164
150x150	18	40.1	16.0	4.8	51.2	4.38	1060	1680	440	4.55	5.73	2.93	99.8
	15	33.8	16.0	4.8	43.2	4.26	909	1442	375	4.59	5.78	2.95	84.6
	12	27.3	16.0	4.8	35.0	4.14	748	1187	308	4.62	5.82	2.97	68.9
	10	23.0	16.0	4.8	29.5	4.06	635	1008	262	4.64	5.85	2.99	58.0
120x120	15	26.6	13.0	4.8	34.0	3.52	448	710	186	3.63	4.57	2.34	52.8
	12	21.6	13.0	4.8	27.6	3.41	371	589	153	3.66	4.62	2.35	43.1
	10	18.2	13.0	4.8	23.3	3.32	316	502	130	3.69	4.65	2.37	36.4
	8	14.7	13.0	4.8	18.8	3.24	259	411	107	3.71	4.67	2.38	29.5
100x100	15	21.9	12.0	4.8	28.0	3.02	250	395	105	2.99	3.76	1.94	35.8
	12	17.8	12.0	4.8	22.8	2.91	208	330	86.5	3.02	3.81	1.95	29.4
	10+	15.0	12.0	4.8	19.2	2.83	178	283	73.7	3.05	3.84	1.96	24.8
	8	12.2	12.0	4.8	15.6	2.75	146	232	60.5	3.07	3.86	1.97	20.2
90x90	12	15.9	11.0	4.8	20.3	2.66	149	235	62.0	2.70	3.40	1.75	23.5
	10	13.4	11.0	4.8	17.2	2.58	128	202	52.9	2.73	3.43	1.76	19.9
	8	10.9	11.0	4.8	13.9	2.50	105	167	43.4	2.75	3.46	1.77	16.2
	7◆	9.61	11.0	4.8	12.3	2.46	93.2	148	38.6	2.76	3.47	1.77	14.3
	6	8.30	11.0	4.8	10.6	2.41	81.0	128	33.6	2.76	3.48	1.78	12.3
80x80	10	11.9	10.0	4.8	15.1	2.34	87.6	139	36.4	2.41	3.03	1.55	15.5
	8	9.63	10.0	4.8	12.3	2.26	72.4	115	29.9	2.43	3.06	1.56	12.6
	6	7.34	10.0	4.8	9.36	2.17	56.0	88.7	23.2	2.45	3.08	1.57	9.60
70x70	10	10.3	9.0	2.4	13.1	2.10	58.0	91.6	24.4	2.10	2.64	1.36	11.8
	8	8.36	9.0	2.4	10.7	2.02	48.3	76.5	20.1	2.12	2.67	1.37	9.70
	6	6.38	9.0	2.4	8.19	1.94	37.7	59.8	15.6	2.15	2.70	1.38	7.45
60x60	10	8.69	8.0	2.4	11.1	1.85	35.3	55.6	15.0	1.78	2.24	1.16	8.51
	8	7.09	8.0	2.4	9.07	1.78	29.6	46.7	12.4	1.80	2.27	1.17	7.00
	6	5.42	8.0	2.4	6.95	1.70	23.2	36.8	9.64	1.83	2.30	1.18	5.39
	5	4.57	8.0	2.4	5.86	1.65	19.8	31.4	8.23	1.84	2.31	1.18	4.56
50x50	8	5.82	7.0	2.4	7.44	1.53	16.5	25.9	6.96	1.49	1.87	0.968	4.74
	6	4.47	7.0	2.4	5.72	1.45	13.0	20.6	5.43	1.51	1.90	0.974	3.67
	5	3.77	7.0	2.4	4.83	1.41	11.1	17.7	4.63	1.52	1.91	0.979	3.11
	4	3.06	7.0	2.4	3.92	1.37	9.16	14.5	3.82	1.53	1.92	0.987	2.52
	3	2.33	7.0	2.4	2.99	1.32	7.06	11.1	2.97	1.54	1.93	0.996	1.92
45x45	6	4.00	7.0	2.4	5.12	1.33	9.30	14.7	3.90	1.35	1.69	0.872	2.93
	5	3.38	7.0	2.4	4.33	1.29	7.99	12.6	3.33	1.36	1.71	0.877	2.49
	4	2.74	7.0	2.4	3.52	1.24	6.58	10.4	2.75	1.37	1.72	0.883	2.02
	3	2.09	7.0	2.4	2.69	1.20	5.08	8.03	2.14	1.37	1.73	0.892	1.54
40x40	6	3.52	6.0	2.4	4.49	1.20	6.37	10.1	2.68	1.19	1.50	0.773	2.28
	5	2.97	6.0	2.4	3.80	1.17	5.48	8.68	2.29	1.20	1.51	0.776	1.93
	4	2.42	6.0	2.4	3.09	1.12	4.53	7.18	1.89	1.21	1.52	0.781	1.58
	3	1.84	6.0	2.4	2.36	1.08	3.51	5.55	1.47	1.22	1.53	0.788	1.20
30x30	5	2.18	5.0	2.4	2.78	0.919	2.17	3.42	0.919	0.883	1.11	0.575	1.04
	4	1.78	5.0	2.4	2.27	0.879	1.81	2.86	0.756	0.893	1.12	0.577	0.852
	3	1.36	5.0	2.4	1.74	0.836	1.41	2.23	0.588	0.900	1.13	0.581	0.652
25x25	5	1.77	3.5	2.4	2.25	0.796	1.19	1.87	0.515	0.728	0.912	0.478	0.701
	4	1.45	3.5	2.4	1.84	0.758	1.00	1.58	0.421	0.737	0.926	0.478	0.574
	3	1.11	3.5	2.4	1.41	0.718	0.784	1.24	0.325	0.745	0.939	0.480	0.440

Circular Hollow Sections:

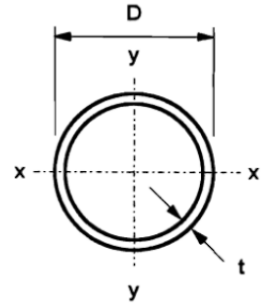| Designation		Mass per Metre	Area of Section	Ratio for Local Buckling	Second Moment of Area	Radius of Gyration	Elastic Modulus	Plastic Modulus	Torsional Constants		Surface Area per Metre
Outside Diameter D mm	Thickness t mm	kg	A cm^2	D / t	I cm^4	r cm	Z cm^3	S cm^3	J cm^4	C cm^3	m^2
21.3	3.2Δ	1.43	1.82	6.66	0.768	0.650	0.722	1.06	1.54	1.44	0.0669
26.9	3.2Δ	1.87	2.38	8.41	1.70	0.846	1.27	1.81	3.41	2.53	0.0845
33.7	2.6Δ	1.99	2.54	13.0	3.09	1.10	1.84	2.52	6.19	3.67	0.106
	3.2Δ	2.41	3.07	10.5	3.60	1.08	2.14	2.99	7.21	4.28	0.106
	4.0Δ	2.93	3.73	8.43	4.19	1.06	2.49	3.55	8.38	4.97	0.106
42.4	2.6Δ	2.55	3.25	16.3	6.46	1.41	3.05	4.12	12.9	6.10	0.133
	3.2Δ	3.09	3.94	13.3	7.62	1.39	3.59	4.93	15.2	7.19	0.133
	4.0Δ	3.79	4.83	10.6	8.99	1.36	4.24	5.92	18.0	8.48	0.133
48.3	3.2	3.56	4.53	15.1	11.6	1.60	4.80	6.52	23.2	9.59	0.152
	4.0	4.37	5.57	12.1	13.8	1.57	5.70	7.87	27.5	11.4	0.152
	5.0	5.34	6.80	9.66	16.2	1.54	6.69	9.42	32.3	13.4	0.152
60.3	3.2	4.51	5.74	18.8	23.5	2.02	7.78	10.4	46.9	15.6	0.189
	4.0	5.55	7.07	15.1	28.2	2.00	9.34	12.7	56.3	18.7	0.189
	5.0	6.82	8.69	12.1	33.5	1.96	11.1	15.3	67.0	22.2	0.189
76.1	3.2	5.75	7.33	23.8	48.8	2.58	12.8	17.0	97.6	25.6	0.239
	4.0	7.11	9.06	19.0	59.1	2.55	15.5	20.8	118	31.0	0.239
	5.0	8.77	11.2	15.2	70.9	2.52	18.6	25.3	142	37.3	0.239
88.9	3.2	6.76	8.62	27.8	79.2	3.03	17.8	23.5	158	35.6	0.279
	4.0	8.38	10.7	22.2	96.3	3.00	21.7	28.9	193	43.3	0.279
	5.0	10.3	13.2	17.8	116	2.97	26.2	35.2	233	52.4	0.279
114.3	3.6	9.83	12.5	31.8	192	3.92	33.6	44.1	384	67.2	0.359
	5.0	13.5	17.2	22.9	257	3.87	45.0	59.8	514	89.9	0.359
	6.3	16.8	21.4	18.1	313	3.82	54.7	73.6	625	109	0.359
139.7	5.0	16.6	21.2	27.9	481	4.77	68.8	90.8	961	138	0.439
	6.3	20.7	26.4	22.2	589	4.72	84.3	112	1177	169	0.439
	8.0	26.0	33.1	17.5	720	4.66	103	139	1441	206	0.439
	10.0	32.0	40.7	14.0	862	4.60	123	169	1724	247	0.439
168.3	5.0	20.1	25.7	33.7	856	5.78	102	133	1712	203	0.529
	6.3	25.2	32.1	26.7	1053	5.73	125	165	2107	250	0.529
	8.0	31.6	40.3	21.0	1297	5.67	154	206	2595	308	0.529
	10.0	39.0	49.7	16.8	1564	5.61	186	251	3128	372	0.529
	12.5	48.0	61.2	13.5	1868	5.53	222	304	3737	444	0.529
193.7	5.0	23.3	29.6	38.7	1320	6.67	136	178	2640	273	0.609
	6.3	29.1	37.1	30.7	1630	6.63	168	221	3260	337	0.609
	8.0	36.6	46.7	24.2	2016	6.57	208	276	4031	416	0.609
	10.0	45.3	57.7	19.4	2442	6.50	252	338	4883	504	0.609
	12.5	55.9	71.2	15.5	2934	6.42	303	411	5869	606	0.609
	16.0♦	70.1	89.3	12.1	3554	6.31	367	507	7109	734	0.609

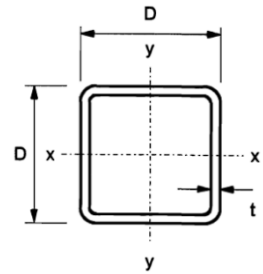## Square Hollow Sections:

Designation		Mass per Metre	Area of Section	Ratio for Local Buckling	Second Moment of Area	Radius of Gyration	Elastic Modulus	Plastic Modulus	Torsional Constants		Surface Area per Metre
Size	Thickness										
D D	t		A		I	r	Z	S	J	C	
mm	mm	kg	cm^2	d / t [(1)]	cm^4	cm	cm^3	cm^3	cm^4	cm^3	m^2
40x40	2.5	2.89	3.68	13.0	8.54	1.52	4.27	5.14	13.6	6.22	0.154
	3.0	3.41	4.34	10.3	9.78	1.50	4.89	5.97	15.7	7.10	0.152
	3.2	3.61	4.60	9.50	10.2	1.49	5.11	6.28	16.5	7.42	0.152
	4.0	4.39	5.59	7.00	11.8	1.45	5.91	7.44	19.5	8.54	0.150
	5.0	5.28	6.73	5.00	13.4	1.41	6.68	8.66	22.5	9.60	0.147
50x50	2.5	3.68	4.68	17.0	17.5	1.93	6.99	8.29	27.5	10.2	0.194
	3.0	4.35	5.54	13.7	20.2	1.91	8.08	9.70	32.1	11.8	0.192
	3.2	4.62	5.88	12.6	21.2	1.90	8.49	10.2	33.8	12.4	0.192
	4.0	5.64	7.19	9.50	25.0	1.86	9.99	12.3	40.4	14.5	0.190
	5.0	6.85	8.73	7.00	28.9	1.82	11.6	14.5	47.6	16.7	0.187
	6.3	8.31	10.6	4.94	32.8	1.76	13.1	17.0	55.2	18.8	0.184
60x60	3.0	5.29	6.74	17.0	36.2	2.32	12.1	14.3	56.9	17.7	0.232
	3.2	5.62	7.16	15.8	38.2	2.31	12.7	15.2	60.2	18.6	0.232
	4.0	6.90	8.79	12.0	45.4	2.27	15.1	18.3	72.5	22.0	0.230
	5.0	8.42	10.7	9.00	53.3	2.23	17.8	21.9	86.4	25.7	0.227
	6.3	10.3	13.1	6.52	61.6	2.17	20.5	26.0	102	29.6	0.224
	8.0	12.5	16.0	4.50	69.7	2.09	23.2	30.4	118	33.4	0.219
70x70	3.0	6.24	7.94	20.3	59.0	2.73	16.9	19.9	92.2	24.8	0.272
	3.6	7.40	9.42	16.4	68.6	2.70	19.6	23.3	108	28.7	0.271
	5.0	9.99	12.7	11.0	88.5	2.64	25.3	30.8	142	36.8	0.267
	6.3	12.3	15.6	8.11	104	2.58	29.7	36.9	169	42.9	0.264
	8.0	15.0	19.2	5.75	120	2.50	34.2	43.8	200	49.2	0.259
80x80	3.0	7.18	9.14	23.7	89.8	3.13	22.5	26.3	140	33.0	0.312
	3.6	8.53	10.9	19.2	105	3.11	26.2	31.0	164	38.5	0.311
	5.0	11.6	14.7	13.0	137	3.05	34.2	41.1	217	49.8	0.307
	6.3	14.2	18.1	9.70	162	2.99	40.5	49.7	262	58.7	0.304
	8.0	17.5	22.4	7.00	189	2.91	47.3	59.5	312	68.3	0.299
90x90	3.6	9.66	12.3	22.0	152	3.52	33.8	39.7	237	49.7	0.351
	5.0	13.1	16.7	15.0	200	3.45	44.4	53.0	316	64.8	0.347
	6.3	16.2	20.7	11.3	238	3.40	53.0	64.3	382	77.0	0.344
	8.0	20.1	25.6	8.25	281	3.32	62.6	77.6	459	90.5	0.339
100x100	4.0	11.9	15.2	22.0	232	3.91	46.4	54.4	361	68.2	0.390
	5.0	14.7	18.7	17.0	279	3.86	55.9	66.4	439	81.8	0.387
	6.3	18.2	23.2	12.9	336	3.80	67.1	80.9	534	97.8	0.384
	8.0	22.6	28.8	9.50	400	3.73	79.9	98.2	646	116	0.379
	10.0	27.4	34.9	7.00	462	3.64	92.4	116	761	133	0.374
120x120	4.0	14.4	18.4	27.0	410	4.72	68.4	79.7	635	101	0.470
	5.0	17.8	22.7	21.0	498	4.68	83.0	97.6	777	122	0.467
	6.3	22.2	28.2	16.0	603	4.62	100	120	950	147	0.464
	8.0	27.6	35.2	12.0	726	4.55	121	146	1160	176	0.459
	10.0	33.7	42.9	9.00	852	4.46	142	175	1382	206	0.454
	12.5	40.9	52.1	6.60	982	4.34	164	207	1623	236	0.448

Rectangular Hollow Sections:

Designation Size D B mm	Thickness t mm	Mass per Metre kg	Area of Section A cm²	Ratios for Local Buckling (1) d/t	Ratios for Local Buckling (1) b/t	Second Moment of Area Axis x-x cm⁴	Second Moment of Area Axis y-y cm⁴	Radius of Gyration Axis x-x cm	Radius of Gyration Axis y-y cm	Elastic Modulus Axis x-x cm³	Elastic Modulus Axis y-y cm³	Plastic Modulus Axis x-x cm³	Plastic Modulus Axis y-y cm³	Torsional Constants J cm⁴	Torsional Constants C cm³	Surface Area per Metre m²
50x30	2.5	2.89	3.68	17.0	9.00	11.8	5.22	1.79	1.19	4.73	3.48	5.92	4.11	11.7	5.73	0.154
	3.0	3.41	4.34	13.7	7.00	13.6	5.94	1.77	1.17	5.43	3.96	6.88	4.76	13.5	6.51	0.152
	3.2	3.61	4.60	12.6	6.38	14.2	6.20	1.76	1.16	5.68	4.13	7.25	5.00	14.2	6.80	0.152
	4.0	4.39	5.59	9.50	4.50	16.5	7.08	1.72	1.13	6.60	4.72	8.59	5.88	16.6	7.77	0.150
	5.0	5.28	6.73	7.00	3.00	18.7	7.89	1.67	1.08	7.49	5.26	10.0	6.80	19.0	8.67	0.147
60x40	2.5	3.68	4.68	21.0	13.0	22.8	12.1	2.21	1.60	7.61	6.03	9.32	7.02	25.1	9.73	0.194
	3.0	4.35	5.54	17.0	10.3	26.5	13.9	2.18	1.58	8.82	6.95	10.9	8.19	29.2	11.2	0.192
	3.2	4.62	5.88	15.8	9.50	27.8	14.6	2.18	1.57	9.27	7.29	11.5	8.64	30.8	11.7	0.192
	4.0	5.64	7.19	12.0	7.00	32.8	17.0	2.14	1.54	10.9	8.52	13.8	10.3	36.7	13.7	0.190
	5.0	6.85	8.73	9.00	5.00	38.1	19.5	2.09	1.50	12.7	9.77	16.4	12.2	43.0	15.7	0.187
	6.3	8.31	10.6	6.52	3.35	43.4	21.9	2.02	1.44	14.5	11.0	19.2	14.2	49.5	17.6	0.184
80x40	3.0	5.29	6.74	23.7	10.3	54.2	18.0	2.84	1.63	13.6	9.00	17.1	10.4	43.8	15.3	0.232
	3.2	5.62	7.16	22.0	9.50	57.2	18.9	2.83	1.63	14.3	9.46	18.0	11.0	46.2	16.1	0.232
	4.0	6.90	8.79	17.0	7.00	68.2	22.2	2.79	1.59	17.1	11.1	21.8	13.2	55.2	18.9	0.230
	5.0	8.42	10.7	13.0	5.00	80.3	25.7	2.74	1.55	20.1	12.9	26.1	15.7	65.1	21.9	0.227
	6.3	10.3	13.1	9.70	3.35	93.3	29.2	2.67	1.49	23.3	14.6	31.1	18.4	75.6	24.8	0.224
	8.0	12.5	16.0	7.00	2.00	106	32.1	2.58	1.42	26.5	16.1	36.5	21.2	85.8	27.4	0.219
90x50	3.0	6.24	7.94	27.0	13.7	84.4	33.5	3.26	2.05	18.8	13.4	23.2	15.3	76.5	22.4	0.272
	3.6	7.40	9.42	22.0	10.9	98.3	38.7	3.23	2.03	21.8	15.5	27.2	18.0	89.4	25.9	0.271
	5.0	9.99	12.7	15.0	7.00	127	49.2	3.16	1.97	28.3	19.7	36.0	23.5	116	32.9	0.267
	6.3	12.3	15.6	11.3	4.94	150	57.0	3.10	1.91	33.3	22.8	43.2	28.0	138	38.1	0.264
	8.0	15.0	19.2	8.25	3.25	174	64.6	3.01	1.84	38.6	25.8	51.4	32.9	160	43.2	0.259
100x50	3.0	6.71	8.54	30.3	13.7	110	36.8	3.58	2.08	21.9	14.7	27.3	16.8	88.4	25.0	0.292
	3.2	7.13	9.08	28.3	12.6	116	38.8	3.57	2.07	23.2	15.5	28.9	17.7	93.4	26.4	0.292
	4.0	8.78	11.2	22.0	9.50	140	46.2	3.53	2.03	27.9	18.5	35.2	21.5	113	31.4	0.290
	5.0	10.8	13.7	17.0	7.00	167	54.3	3.48	1.99	33.3	21.7	42.6	25.8	135	36.9	0.287
	6.3	13.3	16.9	12.9	4.94	197	63.0	3.42	1.93	39.4	25.2	51.3	30.8	160	42.9	0.284
	8.0	16.3	20.8	9.50	3.25	230	71.7	3.33	1.86	46.0	28.7	61.4	36.3	186	48.9	0.279
100x60	3.0	7.18	9.14	30.3	17.0	124	55.7	3.68	2.47	24.7	18.6	30.2	21.2	121	30.7	0.312
	3.6	8.53	10.9	24.8	13.7	145	64.8	3.65	2.44	28.9	21.6	35.6	24.9	142	35.6	0.311
	5.0	11.6	14.7	17.0	9.00	189	83.6	3.58	2.38	37.8	27.9	47.4	32.9	188	45.9	0.307
	6.3	14.2	18.1	12.9	6.52	225	98.1	3.52	2.33	45.0	32.7	57.3	39.5	224	53.8	0.304
	8.0	17.5	22.4	9.50	4.50	264	113	3.44	2.25	52.8	37.8	68.7	47.1	265	62.2	0.299
120x60	3.6	9.66	12.3	30.3	13.7	227	76.3	4.30	2.49	37.9	25.4	47.2	28.9	183	43.3	0.351
	5.0	13.1	16.7	21.0	9.00	299	98.8	4.23	2.43	49.9	32.9	63.1	38.4	242	56.0	0.347
	6.3	16.2	20.7	16.0	6.52	358	116	4.16	2.37	59.7	38.8	76.7	46.3	290	65.9	0.344
	8.0	20.1	25.6	12.0	4.50	425	135	4.08	2.30	70.8	45.0	92.7	55.4	344	76.6	0.339
120x80	5.0	14.7	18.7	21.0	13.0	365	193	4.42	3.21	60.9	48.2	74.6	56.1	401	77.9	0.387
	6.3	18.2	23.2	16.0	9.70	440	230	4.36	3.15	73.3	57.6	91.0	68.2	487	92.9	0.384
	8.0	22.6	28.8	12.0	7.00	525	273	4.27	3.08	87.5	68.1	111	82.6	587	110	0.379
	10.0	27.4	34.9	9.00	5.00	609	313	4.18	2.99	102	78.1	131	97.3	688	126	0.374
150x100	4.0	15.1	19.2	34.5	22.0	607	324	5.63	4.11	81.0	64.8	97.4	73.6	660	105	0.490
	5.0	18.6	23.7	27.0	17.0	739	392	5.58	4.07	98.5	78.5	119	90.1	807	127	0.487
	6.3	23.1	29.5	20.8	12.9	898	474	5.52	4.01	120	94.8	147	110	986	153	0.484
	8.0	28.9	36.8	15.8	9.50	1087	569	5.44	3.94	145	114	180	135	1203	183	0.479
	10.0	35.3	44.9	12.0	7.00	1282	665	5.34	3.85	171	133	216	161	1432	214	0.474
	12.5	42.8	54.6	9.00	5.00	1488	763	5.22	3.74	198	153	256	190	1679	246	0.468
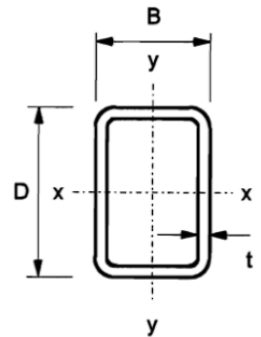
### 6.4.10. Properties of Aluminium Sections (Extrusions)

When designing with aluminium there is limited use of standard sections since the extrusion process is very versatile and it is possible to achieve a wide variety of section shapes. Standard profiles are covered by British Standard BS1161.
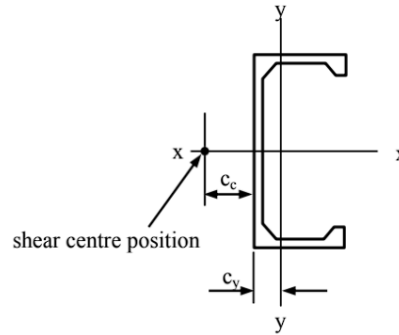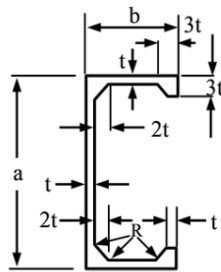
I-Beams:

$R = 1.5t_1$

Size (mm)	Thickness (mm)		Mass/unit length (kg/m)	Area of section (mm² × 10²)	Centroid (mm)	Second moments of area (mm⁴ × 10⁴)		Radii of gyration (mm)		Moduli of section (mm³ × 10³)		Torsion constant (mm⁴ × 10⁴)
$a \times b$	web t_1	flange t_2	W	A	c_x and c_y	I_x	I_y	r_x	r_y	Z_x	Z_y	J
60 × 30	4	6	1.59	5.83	0	31.6	2.76	23.3	6.89	10.5	1.84	0.753
80 × 40	5	7	2.54	9.38	0	91.6	7.63	31.2	9.02	22.9	3.82	1.69
100 × 50	6	8	3.72	13.7	0	210	17.0	39.2	11.1	42.1	6.80	3.30
120 × 60	6	9	4.77	17.6	0	403	32.8	47.8	13.6	67.2	10.9	4.76
140 × 70	7	10	6.33	23.4	0	725	57.9	55.7	15.7	104	16.5	8.00
160 × 80	7	11	7.64	28.2	0	1170	94.6	64.5	18.3	147	23.7	10.8

Channel Sections:
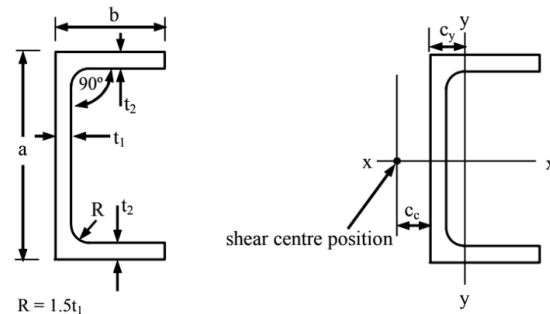
$R = 1.5t_1$

Size (mm)	Thickness (mm)		Mass/ unit length (kg/m)	Area of section (mm² × 10²)	Centroid (mm)		Second moments of area (mm⁴ × 10⁴)		Radii of gyration (mm)		Moduli of section (mm³ × 10³)		Torsion constant (mm⁴ × 10⁴)	Shear centre from back of section (mm)
$a \times b$	web t_1	flange t_2	W	A	c_x	c_y	I_x	I_y	r_x	r_y	Z_x	Z_y	J	c_c
60 × 30	5	6	1.69	6.24	0	9.87	32.2	5.03	22.7	8.98	10.7	2.50	0.690	11.7
80 × 35	5	7	2.29	8.44	0	11.3	79.8	9.57	30.8	10.6	20.0	4.04	1.12	13.8
100 × 40	6	8	3.20	11.8	0	12.4	171	16.9	38.1	11.9	34.2	6.12	2.07	15.2
120 × 50	6	9	4.19	15.5	0	15.9	339	36.8	46.8	15.4	56.5	10.8	3.22	19.7
140 × 60	7	10	5.66	20.9	0	18.9	625	71.5	54.7	18.5	89.2	17.4	5.51	23.6
160 × 70	7	10	6.58	24.3	0	21.8	970	116	63.2	21.8	121	24.0	6.41	27.6
180 × 75	8	11	8.06	29.8	0	22.7	1480	159	70.5	23.1	164	30.5	9.63	29.0
200 × 80	8	12	9.19	33.9	0	24.5	2110	210	78.8	24.9	211	37.8	12.4	31.3
240 × 100	9	13	12.5	46.0	0	30.3	4170	450	95.2	31.2	345	64.6	20.2	39.2

Lipped Channel Sections:

$$
\begin{aligned}
*A &= 74.00t^2 \\
R &= 2t \\
a &= 32t \\
b &= 16t \\
c_x &= 0 \\
c_y &= 5.36t \\
c_c &= 6.91t \\
I_x &= 12371t^4 \\
I_y &= 2407t^4 \\
r_x &= 12.93t \\
r_y &= 5.70t \\
Z_x &= 773t^3 \\
Z_y &= 226t^3 \\
J &= 41.29t^4
\end{aligned}
$$

*Excludes small areas present at internal radii $(4\times\ldots\ldots^2)$

Size (mm)	Thickness (mm)	Mass/ unit length (kg/m)	Area of section (mm² × 10²)	Centroid (mm)		Second moments of area (mm⁴ × 10⁴)		Radii of gyration (mm)		Moduli of section (mm³ × 10³)		Torsion constant (mm⁴ × 10³)	Shear centre from back of section (mm)
$a \times b$	t	W	A	c_x	c_y	I_x	I_y	r_x	r_y	Z_x	Z_y	J	c_c
80 × 40	2.5	1.25	4.62	0	13.4	48.3	9.40	32.3	14.2	12.1	3.53	1.61	17.3
100 × 50	3.13	1.96	7.23	0	16.8	118	23.0	40.4	17.8	23.6	6.90	3.94	21.6
120 × 60	3.75	2.82	10.4	0	20.1	245	47.6	48.5	21.4	40.8	11.9	8.16	25.9
140 × 70	4.38	3.84	14.2	0	23.5	453	88.2	56.6	24.9	64.8	18.9	15.1	30.2

Equal Bulb Angle Sections:

u-u and v-v are principal axes

$$
\begin{aligned}
*A &= 54.92t^2 & c_x &= 6.07t & r_x &= 6.89t & Z_u &= 285t^3 \\
R &= 2t & c_y &= 6.07t & r_y &= 6.89t & Z_v &= 138t^3 \\
a &= b = 20t & I_x &= 2605t^4 & r_u &= 8.57t & \alpha &= 45° \\
& & I_y &= 2605t^4 & r_v &= 4.64t & \tan\alpha &= 1 \\
& & I_u &= 4030t^4 & Z_x &= 187t^3 & J &= 51.32t^4 \\
& & I_v &= 1180t^4 & Z_y &= 187t^3 & &
\end{aligned}
$$
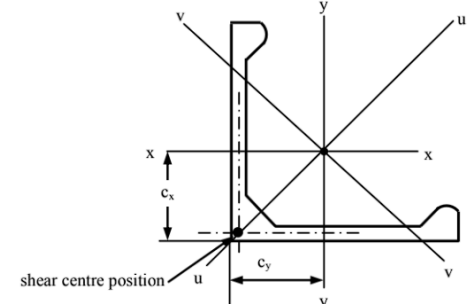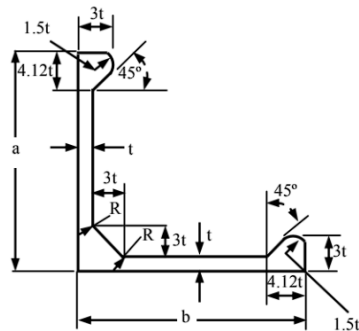
*Excludes small areas present at internal radii $(4\times0.086t^2)$

Size (mm)	Thick-ness (mm)	Mass/ unit length (kg/m)	Area of section (mm² × 10²)	Centroid (mm)	Second moments of area (mm⁴ × 10⁴)			Radii of gyration (mm)			Moduli of section (mm³ × 10³)			Torsion constant (mm⁴ × 10⁴)
$a \times b$	t	W	A	c_x and c_y	I_x and I_y	I_u	I_v	r_x and r_y	r_u	r_v	Z_x and Z_y	Z_u	Z_v	J
50 × 50	2.5	0.930	3.43	15.2	10.2	15.7	4.61	17.2	21.4	11.6	2.92	4.45	2.16	0.200
60 × 60	3	1.34	4.94	18.2	21.1	32.6	9.56	20.7	25.7	13.9	5.05	7.70	3.73	0.416
80 × 80	4	2.38	8.79	24.3	66.7	103	30.2	27.6	34.3	18.6	12.0	18.2	8.82	1.31
100 × 100	5	3.72	13.7	30.3	163	252	73.8	34.4	42.8	23.2	23.4	35.6	17.2	3.21
120 × 120	6	5.36	19.8	36.4	338	522	153	41.3	51.4	27.8	40.4	61.6	29.8	6.65

6.4.11. Properties of Glass Fibre Reinforced Plastic (GFRP) Sections (Pultrusions)

A wide variety of shapes is also possible with the pultrusion process and each GFRP manufacturer will produce a different standard product range. Typical examples:

I- Beams   Channels   Square Hollow Sections
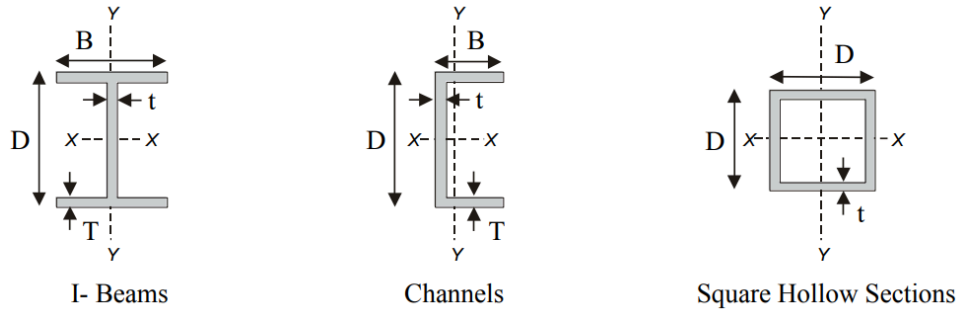
I-beams:

Section Designation	Depth D (mm)	Width B (mm)	Web t (mm)	Flange T (mm)	I_{xx} (cm⁴)	I_{yy} (cm⁴)	Area A (cm²)
53 × 50	53	50	7	7	40.8	14.7	9.73
102 × 51	102	51	6.35	6.35	186	14.2	12.1
150 × 150	150	150	10	10	1660	564	43.0
200 × 200	200	200	10	10	4100	1330	58.0

Channels:

Section Designation	Depth D (mm)	Width B (mm)	Web t (mm)	Flange T (mm)	I_{xx} (cm⁴)	I_{yy} (cm⁴)	Area A (cm²)
50.8 × 25.4	50.8	25.4	3.2	3.2	11.6	1.82	3.05
73 × 25	73	25	5.0	5.0	39.4	2.76	5.65
100 × 40	100	40	5.0	5.0	121	11.9	8.50
200 × 50	200	50	10	10	1390	48.0	28.0
200 × 60	200	60	8.0	8.0	1300	68.9	24.3
500 × 60	500	60	7.0	7.0	11800	73.9	42.4

Square Hollow Sections:

Designation		Area A (cm²)	$I_{xx} = I_{yy}$ (cm⁴)
Size D D (mm)	Thickness t (mm)		
31.8 × 31.8	3.0	3.46	4.83
44.0 × 44.0	6.0	9.12	22.5
51.0 × 51.0	3.2	6.12	23.4
100 × 100	4.0	15.3	236

6.4.12. Building Codes for Structural Design

Building codes are sets of practical experimentally-determined guidelines for safe and reliable structural design. Their adoption and legislature varies by region and sector.

Eurocodes: collection of ten standards (EN 1990 - EN 1999). Used in the EU and UK.

0. Basis of structural design
1. Actions on structures (loading conditions)
2. Concrete structures
3. Steel structures
4. Composite steel-concrete structures
5. Timber structures
6. Masonry structures
7. Geotechnical design
8. Earthquake resistant design
9. Aluminium structures

Other sources of design information, often extending beyond structural design, include:

- ISO: wide range of standards e.g. production, performance, management; used worldwide
- ASME: standards for mechanical devices requiring structural integrity; used in USA

6.5. Fracture Mechanics and Failure Analysis

6.5.1. Dislocations, Plastic Flow and Hardness

Dislocations are line defects in crystalline solids which can glide along the lattice and are important for many plasticity and failure mechanisms in materials.

- Burger's vector, $\mathbf{b}$:   additional lattice spacing created around a dislocation core
- Force on dislocation due to applied shear stress: $F = \tau\, b$
  (F: force per unit length of dislocation, τ: remote shear stress, $b = |\mathbf{b}|$)

- Line tension in dislocation: $T \approx \frac{1}{2} G b^2$ (G: shear modulus)

- Shear stress for dislocation movement on a single slip plane: $\tau_y = \dfrac{cT}{bL}$

  (L: inter-obstacle distance, c: constant. For strong obstacles, $c \approx 2$, and for weaker obstacles, $c < 2$.)

- Shear yield stress of a polycrystalline solid: $k \approx \frac{3}{2}\tau_y$
- Uniaxial yield stress of a polycrystalline solid: $\sigma_y \approx 2k$.
- Hardness: $H \approx 3\sigma_y$, expressed in MPa.
- Vickers Hardness: $HV = H/g$, expressed in kgf mm^{-2} (g: acceleration due to gravity).

For a microscopic analysis of dislocations and their stress fields, see Section 13.2.4.

6.5.2. Fast Fracture

Material defects cause stress concentrations, forming plastic zones and contributing to crack growth, which can lead to fast fracture if a critical size is reached under stress.

- Stress intensity factor: $K = Y\sigma\sqrt{\pi a}$. Fast fracture occurs for $K \geq K_{IC}$, a material property. (Y: dimensionless constant dependent on geometry - typically $Y \approx 1$, σ: remote tensile stress, $2a$: total closed crack length)

- *J*-integral for strain energy release rate:

$$J = G = -\frac{\partial U}{\partial A} = \oint_{\Gamma}\left(W dy - \mathbf{T} \cdot \frac{\partial \mathbf{u}}{\partial x}\, ds\right)$$
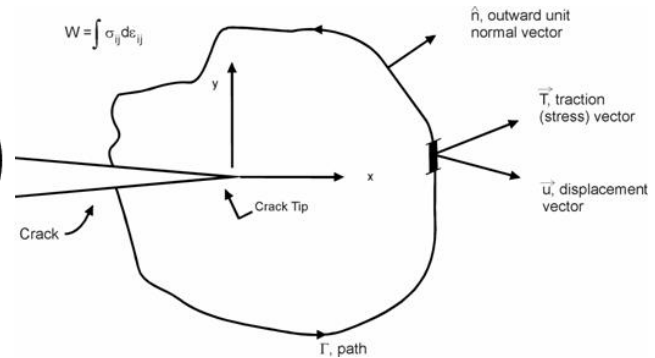
- Strain energy release rate and compliance:

$$G = \frac{P^2}{2}\frac{dC}{da}$$

	Plane stress	Plane strain
Stress-energy relations	$K_I = \sqrt{EG_I},\ K_{II} = \sqrt{EG_{II}}$ $K_{III} = \sqrt{2\mu G_{III}}$	$K_I = \sqrt{\frac{EG_I}{1-v^2}},\ K_{II} = \sqrt{\frac{EG_{II}}{1-v^2}}$ $K_{III} = \sqrt{\frac{2\mu G_{III}}{1-v^2}}$
Crack tip plastic zone size (mode I)	$d_p = \frac{1}{\pi}\left(\frac{K_I}{\sigma_y}\right)^2$	$d_p = \frac{1}{3\pi}\left(\frac{K_I}{\sigma_y}\right)^2$
Crack opening displacement	$\delta = \frac{K_I^2}{\sigma_y E}$	$\delta = \frac{K_I^2}{2\sigma_y E}$

(σ_y: remote yield stress, K_{IC}: plane strain fracture toughness, G_{IC}: critical strain energy release rate, E: Young's modulus, v: Poisson's ratio, $C = E^{-1}$: compliance, P: applied force)

K_{IC} and G_{IC} are only valid when conditions for linear elastic fracture mechanics apply. Typically the crack length and specimen dimensions must be at least 50 times the process zone size.

Micromechanisms of fracture

- Metals: plastic zone formation at crack tips → void nucleation → void linkage
- Ceramics: fast fracture of 'worst' flaw (tension); mode II shear failure (compression)
- Polymers: crazing (opening of cracks bridged by fibres), shear yielding, cold drawing
- Composites: fibres pulled out from sockets in matrix, impeding crack advance

Statistics of Fracture

1D 'weakest link' theory implies a **Weibull distribution**:

$$P_S(V) = \exp\left[-\int_V \left(\frac{\sigma}{\sigma_0}\right)^m \frac{dV}{V_0} \right]$$

(P_s: survival probability of component, V: volume of component σ: tensile stress on component, V_0: volume of test sample σ_0: reference failure stress for volume V_0 which gives $P_S = 1/e \approx 0.37$, m: Weibull modulus (measure of variability: high $m \to$ small spread).)

6.5.4. Asymptotic Crack Tip Stress Fields in a Linear Elastic Solid

Mode I (opening)
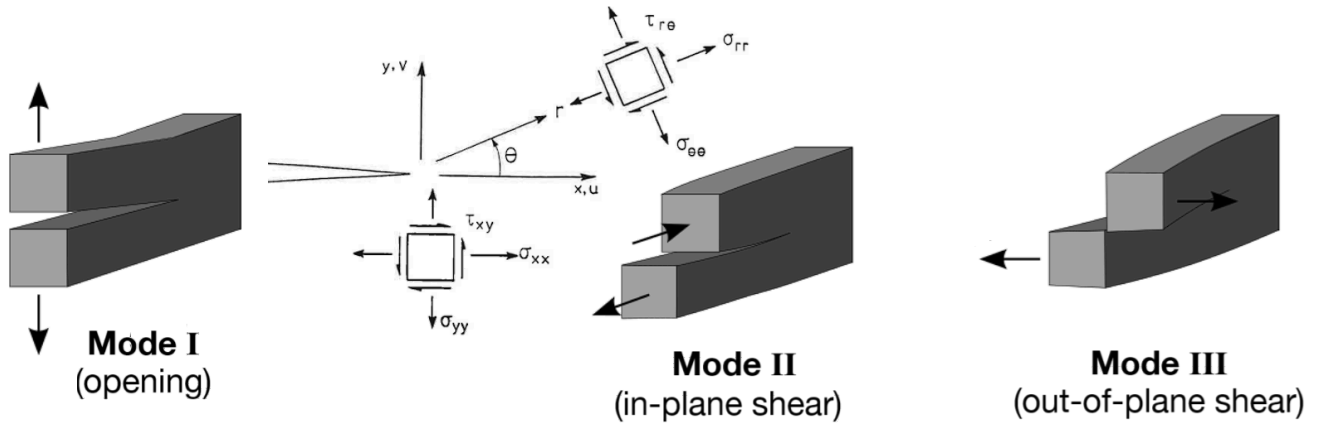
$$\sigma_{yy} = \frac{K_I}{\sqrt{2\pi r}} \cos\frac{\theta}{2}\left(1 + \sin\frac{\theta}{2}\sin\frac{3\theta}{2}\right)$$

$$\sigma_{xx} = \frac{K_I}{\sqrt{2\pi r}} \cos\frac{\theta}{2}\left(1 - \sin\frac{\theta}{2}\sin\frac{3\theta}{2}\right)$$

$$\tau_{xy} = \frac{K_I}{\sqrt{2\pi r}} \cos\frac{\theta}{2}\sin\frac{\theta}{2}\cos\frac{3\theta}{2}$$

$$\sigma_{rr} = \frac{K_I}{\sqrt{2\pi r}}\left(\frac{5}{4}\cos\frac{\theta}{2} - \frac{1}{4}\cos\frac{3\theta}{2}\right)$$

$$\sigma_{\theta\theta} = \frac{K_I}{\sqrt{2\pi r}}\left(\frac{3}{4}\cos\frac{\theta}{2} + \frac{1}{4}\cos\frac{3\theta}{2}\right)$$

$$\tau_{r\theta} = \frac{K_I}{\sqrt{2\pi r}}\left(\frac{1}{4}\sin\frac{\theta}{2} + \frac{1}{4}\sin\frac{3\theta}{2}\right)$$

$$u = \begin{cases} \frac{K_I}{G}\sqrt{\frac{r}{2\pi}}\left(\frac{1-v}{1+v} + \sin^2\frac{\theta}{2}\right)\cos\frac{\theta}{2} & \text{Plane stress} \\ \frac{K_I}{G}\sqrt{\frac{r}{2\pi}}\left(1 - 2v + \sin^2\frac{\theta}{2}\right)\cos\frac{\theta}{2} & \text{Plane strain} \end{cases}$$

$$v = \begin{cases} \frac{K_I}{G}\sqrt{\frac{r}{2\pi}}\left(\frac{2}{1+v} - \cos^2\frac{\theta}{2}\right)\sin\frac{\theta}{2} & \text{Plane stress} \\ \frac{K_I}{G}\sqrt{\frac{r}{2\pi}}\left(2 - 2v - \cos^2\frac{\theta}{2}\right)\sin\frac{\theta}{2} & \text{Plane strain} \end{cases}$$
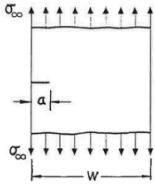
$$w = 0$$

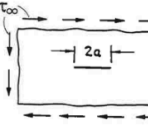**Mode II** (in-plane shear)
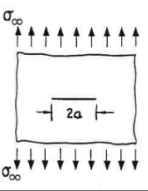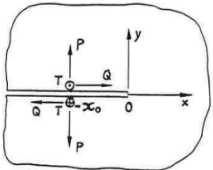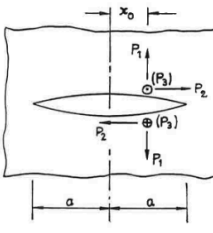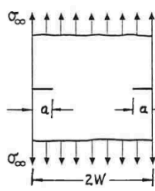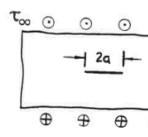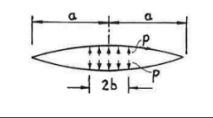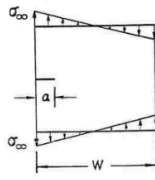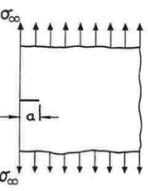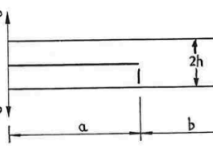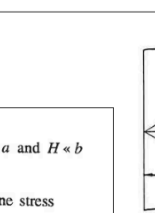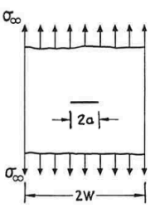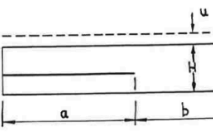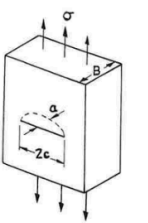
$$\sigma_{yy} = \frac{K_{II}}{\sqrt{2\pi r}} \cos\frac{\theta}{2}\sin\frac{\theta}{2}\cos\frac{3\theta}{2}$$

$$\sigma_{xx} = -\frac{K_{II}}{\sqrt{2\pi r}} \sin\frac{\theta}{2}\left(2 + \cos\frac{\theta}{2}\cos\frac{3\theta}{2}\right)$$

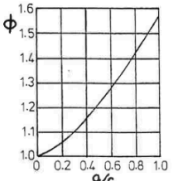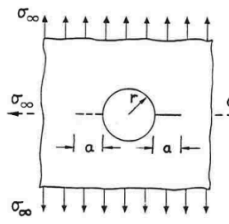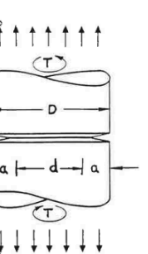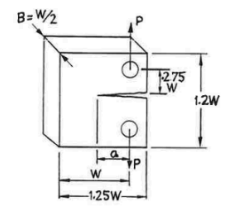$$\tau_{xy} = \frac{K_{II}}{\sqrt{2\pi r}} \cos\frac{\theta}{2}\left(1 - \sin\frac{\theta}{2}\sin\frac{3\theta}{2}\right)$$

$$\sigma_{rr} = \frac{K_{II}}{\sqrt{2\pi r}}\left(-\frac{5}{4}\sin\frac{\theta}{2} + \frac{3}{4}\sin\frac{3\theta}{2}\right)$$

$$\sigma_{\theta\theta} = -\frac{K_{II}}{\sqrt{2\pi r}}\left(\frac{3}{4}\sin\frac{\theta}{2} + \frac{3}{4}\sin\frac{3\theta}{2}\right)$$

$$\tau_{r\theta} = \frac{K_{II}}{\sqrt{2\pi r}}\left(\frac{1}{4}\cos\frac{\theta}{2} + \frac{3}{4}\cos\frac{3\theta}{2}\right)$$

$$u = \begin{cases} \frac{K_{II}}{G}\sqrt{\frac{r}{2\pi}}\left(\frac{2}{1+v} + \cos^2\frac{\theta}{2}\right)\sin\frac{\theta}{2} & \text{Plane stress} \\ \frac{K_{II}}{G}\sqrt{\frac{r}{2\pi}}\left(2 - 2v + \cos^2\frac{\theta}{2}\right)\sin\frac{\theta}{2} & \text{Plane strain} \end{cases}$$

$$v = \begin{cases} \frac{K_{II}}{G}\sqrt{\frac{r}{2\pi}}\left(\frac{v-1}{1+v} + \sin^2\frac{\theta}{2}\right)\cos\frac{\theta}{2} & \text{Plane stress} \\ \frac{K_{II}}{G}\sqrt{\frac{r}{2\pi}}\left(-1 + 2v + \sin^2\frac{\theta}{2}\right)\cos\frac{\theta}{2} & \text{Plane strain} \end{cases}$$

$$w = 0$$

Mode III (out-of-plane shear)

$$\tau_{zx} = -\frac{K_{III}}{\sqrt{2\pi r}} \sin\frac{\theta}{2}$$

$$\tau_{yz} = \frac{K_{III}}{\sqrt{2\pi r}} \cos\frac{\theta}{2}$$

$$\sigma_{xx} = \sigma_{yy} = \sigma_{zz} = \tau_{xy} = 0$$

$$w = \frac{K_{III}}{G}\sqrt{\frac{2r}{\pi}} \sin\frac{\theta}{2}$$

$$u = v = 0$$

6.5.5. Stress Intensity Factors Correlations (*J*-Integral Solutions) by Geometry and Mode

$$K_I = \sigma_\infty \sqrt{\pi a}$$

$$K_{II} = \tau_\infty \sqrt{\pi a}$$

$$K_{III} = \tau_\infty \sqrt{\pi a}$$

$$K_I = 1.12\,\sigma_\infty \sqrt{\pi a}$$

$$K_I = \sigma_\infty \sqrt{\pi a}\left(\frac{1 - a/2W + 0.326a^2/W^2}{\sqrt{1 - a/W}}\right)$$

$$K_I = \frac{2P}{\sqrt{2\pi x_0}}$$

$$K_{II} = \frac{2Q}{\sqrt{2\pi x_0}}$$

$$K_{III} = \frac{2T}{\sqrt{2\pi x_0}}$$

$$K_I = \frac{P_1}{\sqrt{\pi a}}\sqrt{\frac{a + x_0}{a - x_0}}$$

$$K_{II} = \frac{P_2}{\sqrt{\pi a}}\sqrt{\frac{a + x_0}{a - x_0}}$$

$$K_{III} = \frac{P_3}{\sqrt{\pi a}}\sqrt{\frac{a + x_0}{a - x_0}}$$

$$K_I = \frac{2pb}{\sqrt{\pi a}\,b}\frac{a}{b}\arcsin\frac{b}{a}$$

$$K_I = \frac{2\sqrt{3}}{h\sqrt{h}}\frac{Pa}{B} \qquad h \ll a \text{ and } h \ll b$$

$$K_I = \sqrt{\frac{1}{2\alpha H}}\,Eu \qquad H \ll a \text{ and } H \ll b$$

$$\alpha = \begin{cases} 1 - v^2 & \text{Plane stress} \\ 1 - 3v^2 - 2v^3 & \text{Plane strain} \end{cases}$$

$$K_I = \sigma_\infty \sqrt{\pi a}\left(1.12 - 0.23\frac{a}{W} + 10.6\frac{a^2}{W^2} - 21.7\frac{a^3}{W^3} + 30.4\frac{a^4}{W^4}\right) \qquad a/W < 0.7$$

$$K_I = \sigma_\infty \sqrt{\pi a}\left(\frac{1.12 - 0.61a/W + 0.13a^3/W^3}{\sqrt{1 - a/W}}\right)$$

$$K_I = \sigma_\infty \sqrt{\pi a}\left(1.12 - 1.39\frac{a}{W} + 7.3\frac{a^2}{W^2} - 13\frac{a^3}{W^3} + 14\frac{a^4}{W^4}\right) \qquad a/W < 0.7$$

$$K_I = 0.683\,\sigma_{max}\sqrt{\pi a}$$

$$K_I = \frac{1.12}{\Phi}\sigma\sqrt{\pi a}$$

$$\Phi = \int_0^{\pi/2}\left(1 - \frac{c^2 - a^2}{c^2}\sin^2\theta\right)^{\frac{1}{2}}d\theta$$

$$K_I = \sigma_\infty \sqrt{\pi a}\left(\frac{D}{d} + \frac{1}{2} + \frac{3}{8}\frac{d}{D} - 0.36\frac{d^2}{D^2} + 0.73\frac{d^3}{D^3}\right)\frac{1}{2}\sqrt{\frac{D}{d}}$$

$$K_{III} = \frac{16T}{\pi D^3}\sqrt{\pi a}\left(\frac{D^2}{d^2} + \frac{1}{2}\frac{D}{d} + \frac{3}{8} + \frac{5}{16}\frac{d}{D} + \frac{35}{128}\frac{d^2}{D^2} + 0.21\frac{d^3}{D^3}\right)\frac{3}{8}\sqrt{\frac{D}{d}}$$

$$K_I = \sigma_\infty \sqrt{\pi a}\,F\!\left(\frac{a}{r}\right)$$

$\frac{a}{r}$	One crack U	One crack B	Two cracks U	Two cracks B
0.00	3.36	2.24	3.36	2.24
0.10	2.73	1.98	2.73	1.98
0.20	2.30	1.82	2.41	1.83
0.30	2.04	1.67	2.15	1.70
0.40	1.86	1.58	1.96	1.61
0.50	1.73	1.49	1.83	1.57
0.60	1.64	1.42	1.71	1.52
0.80	1.47	1.32	1.58	1.43
1.0	1.37	1.22	1.45	1.38
1.5	1.18	1.06	1.29	1.26
2.0	1.06	1.01	1.21	1.20
3.0	0.94	0.93	1.14	1.13
5.0	0.81	0.81	1.07	1.06
10.0	0.75	0.75	1.03	1.03
∞	0.707	0.707	1.00	1.00

value of $F(a/r)$[†]

†U = uniaxial σ_∞ B = biaxial σ_∞.

$$K_I = \frac{4P}{B}\sqrt{\frac{\pi}{W}}\left\{1.6\left(\frac{a}{W}\right)^{1/2} - 2.6\left(\frac{a}{W}\right)^{3/2} + 12.3\left(\frac{a}{W}\right)^{5/2} - 21.2\left(\frac{a}{W}\right)^{7/2} + 21.8\left(\frac{a}{W}\right)^{9/2}\right\}$$

$$K_I = \frac{P}{B}\sqrt{\frac{\pi}{W}}\left\{16.7\left(\frac{a}{W}\right)^{1/2} - 104.7\left(\frac{a}{W}\right)^{3/2} + 369.9\left(\frac{a}{W}\right)^{5/2} - 573.8\left(\frac{a}{W}\right)^{7/2} + 360.5\left(\frac{a}{W}\right)^{9/2}\right\}$$

6.5.6. Fatigue

Cyclic loading of a material can eventually lead to fatigue failure even if the applied stresses are below the yield stress due to crack propagation and fast fracture.

S-N **curve** for a given material specimen:

- **Basquin's law** of **high cycle fatigue**: $\Delta\sigma \, N_f^{\,\alpha} = C_1$
- **Coffin-Manson law** of **low cycle fatigue**: $\Delta\varepsilon^{pl} \, N_f^{\,\beta} = C_2$
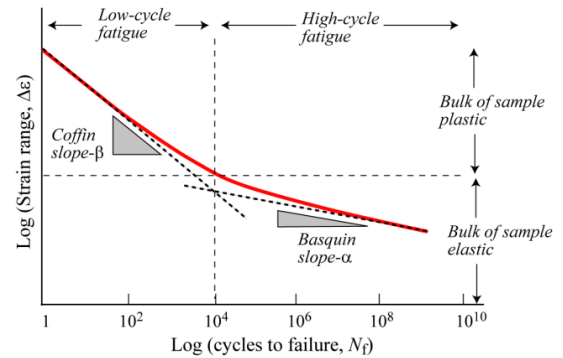
Fatigue limit: the (practically) horizontal asymptote to the *S-N* curve, occuring in some materials. It is typically around ~0.4-$0.5\sigma_y$, if it exists. Some research suggests the fatigue limit may never truly exist in metals (i.e. N_f remains finite but very large for all nonzero $\Delta\sigma$).

($\Delta\sigma$: stress range, $\Delta\varepsilon^{pl}$: plastic strain range, N: number of cycles, N_f: cycles to failure, $\{\alpha, \beta, C_1, C_2\}$: constants, σ_{ts}: tensile strength.)

- **Goodman's rule**: for the same fatigue life, a stress range $\Delta\sigma$ operating with a mean stress σ_m is equivalent to a larger stress range $\Delta\sigma_0$ and zero mean stress, according to the relationship:

$$\Delta\sigma_0 = \frac{\Delta\sigma}{1 - (\sigma_m/\sigma_{ts})}$$ (other correlations exist: see Gerber parabola, Goodman-Haigh diagrams)

- **Miner's Rule** for cumulative damage (for i loading blocks, each of constant stress amplitude and duration N_i cycles):

$$\sum_i \frac{N_i}{N_{fi}} = 1$$ (accuracy is variable)

- **Paris' law** for crack growth / propagation:

  In the linear regime (phase II): $\dfrac{da}{dN} = A\,(\Delta K)^n$

(a: crack length, $\{A, n\}$: constants, ΔK: tensile stress intensity factor range)
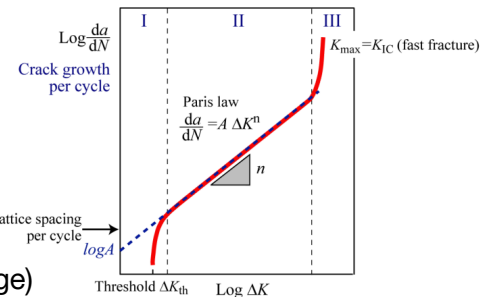
Pressure Vessel Design: flaws in the shell are hazards for fast fracture (risk of explosion).

- For cylindrical vessels (Section 6.4.6), the dominant (hoop) stress is $\sigma_h = pr/t$.
- Proof test: pressurise a vessel to a level above its working pressure. If it survives, then we have an upper bound on the crack length present in the shell by $K_{IC} = Y\sigma_h\sqrt{\pi a}$.

- Critical crack length: $a_c = \dfrac{1}{\pi}\left(\dfrac{K_{IC}}{Y\sigma_h}\right)^2$ (need $a_c > t$ for leak before break criterion).

If $a_c \ll t \to$ break first. If $a_c \gg t \to$ leak first. Once a vessel has been proof tested, integrated Paris' law can find the remaining lifetime by solving for N. As the crack approaches the outside of the wall, the effective geometric factor Y may change (Section 6.5.5).

6.5.7. Tribology: Friction, Wear and Lubrication

Amontons-Coulomb's laws of friction:

1. Friction is directly proportional to the applied load: $F = \mu N$
2. Friction is independent of the apparent area of contact.
3. Kinetic friction is independent of sliding velocity.

The **static friction** μ_s is typically higher than the **kinetic friction** μ_k due increased adhesion, as well as due to the breakdown of asperities in the kinetic regime.

For **ductile** materials, the true contact area A_t due to a load W is related to the **hardness** H of the bulk material by $W = HA_t$.

This assumes linear elasticity. The friction F between two objects in contact is made up of shear stresses τ acting at microscopic asperities over a true contact area A_t, so that $F = \tau A_t$ with $\tau \leq \tau_y$. Sliding occurs when $\tau = \tau_y$, the shear yield stress of the surface material. In the case of non-noble metals, this is the oxide of the bulk metal and is much smaller.

The **wear rate** Q is defined by the volume worn away per unit sliding distance: $Q = -\Delta V / s$. The wear coefficient K is defined by $Q = KA_t = K(W/H)$ (for ductile materials), which varies by wear mechanism (abrasion or adhesion).

Lubrication of an interface by inserting a fluid significantly reduces the wear rate.

Triboelectric charging (static electric charge accumulation) can occur at sliding interfaces, causing discharge when brought in contact with grounded conductors. For the triboelectric series, see Section 6.6.24.

6.5.8. Creep Deformation

Creep is a slow plastic deformation due to a sustained tensile or shear stress. In metals and polymers, this occurs typically for $T / T_m > 0.4$. The strain follows a similar curve to Paris' law (Section 6.6.6) with a (1) fast startup stage, (2) steady linear stage, (3) runaway to failure stage.

In metals, stage 2 creep occurs due to atom diffusion along **grain boundaries** or **dislocation cores** (Coble creep) or through the **lattice** (Nabarro-Herring creep), and **gliding dislocations** climbing obstacles (power-law creep). Stage 3 creep can occur due to increasing true stress (necking), near-yield plastic deformation or microstructural cavitation (void nucleation on grain boundaries), in which failure by yielding will follow quickly if the external stress continues.

Creep is an important failure mechanism in metals working at high temperatures. Creep lifetimes can be mitigated by using high melting point metals (e.g. Ni, Cr, Ti, W), lower operating temperatures (e.g. air cooling or a thermal barrier coating), casting with an elongated grain microstructure (or pure oriented single crystal), and forming crystals with coherent interfaces between ordered crystal structures to impede dislocation glide by creating a lattice strain (e.g. γ/γ' precipitate phase boundary).

Diffusion coefficient at temperature: $D = D_0 \, exp\left(- \frac{Q}{RT}\right)$ (Section 6.6.6)

Stage 2 (diffusional creep): $\dot{\varepsilon}_{ss} = A \, \sigma^n \, \exp\left(-\frac{Q}{RT}\right)$ or equivalently $\frac{\dot{\varepsilon}_{ss}}{\dot{\varepsilon}_0} = \exp\left(-\frac{Q}{RT}\right)\left(\frac{\sigma}{\sigma_0}\right)^n$

Stages 1 and 2 (Miller-Norton law): $\varepsilon = \frac{C\sigma^n t^{m+1}}{m+1}\exp\left(-\frac{Q}{RT}\right)$ or equivalently $\dot{\varepsilon} = C\sigma^n t^m \exp\left(-\frac{Q}{RT}\right)$

Estimated creep lifetime (Monkman-Grant relation): $t_f \times \dot{\varepsilon}_{ss} = \text{constant}$

($\dot{\varepsilon}_{ss}$: true plastic strain rate, $(A, n, C, m, \varepsilon_0')$: power-law constants, σ: deviatoric Von Mises tensile stress, Q: creep activation energy, approximately equal to the diffusional energy (Section 6.6.10), ε_{cr}: true creep strain. For Coble creep, $n = 1$. For dislocation (power-law) creep, $3 < n < 8$.)

In high-temperature, high-stress applications (e.g. centrifugal loading on turbine blades), preventing creep is the primary design constraint. Single-crystal (SX) nickel superalloys (e.g. MAR-M200) have been developed which eliminate grain boundaries entirely which act as diffusional short-circuits.

6.5.9. Creep Mechanism Maps

Deformation mechanism maps with contours of strain rate in s^{-1} are shown below for

- nickel superalloy MAR-M200 (12.5% W, 10% Co, 9% Cr, 5% Al), grain size 100 μm
- pure nickel, grain size 1 μm
- pure tungsten, grain size 100 μm
- pure ice, grain size 10 mm   (data from Ashby, 1983)

On the vertical axis, the shear stress is normalised by the shear modulus $\mu = G$.
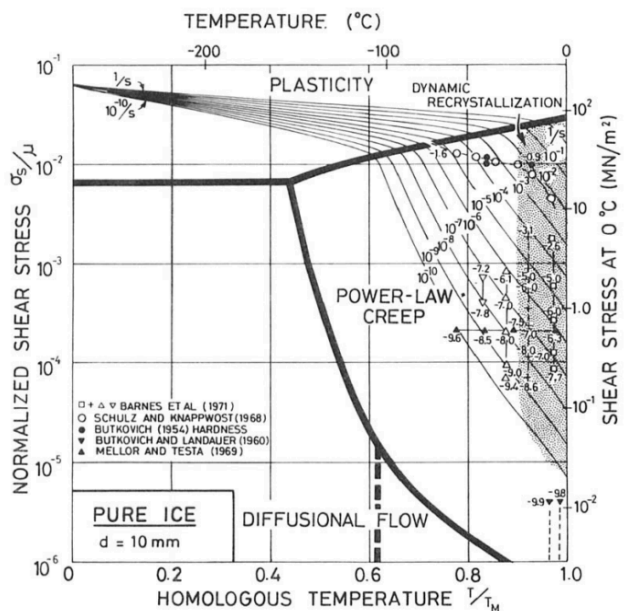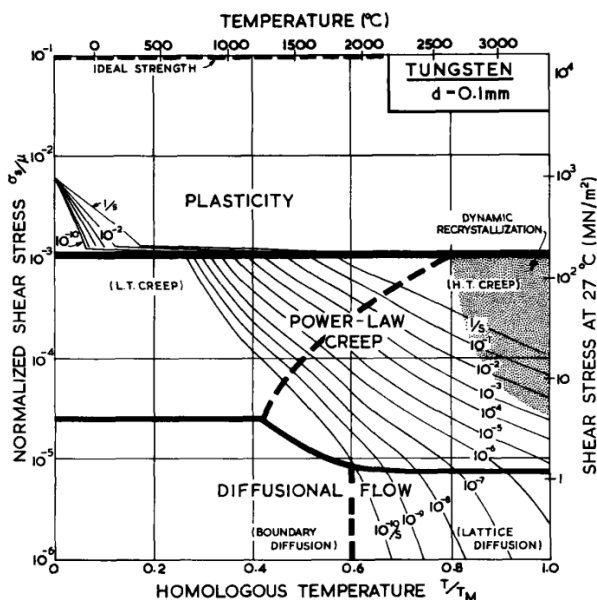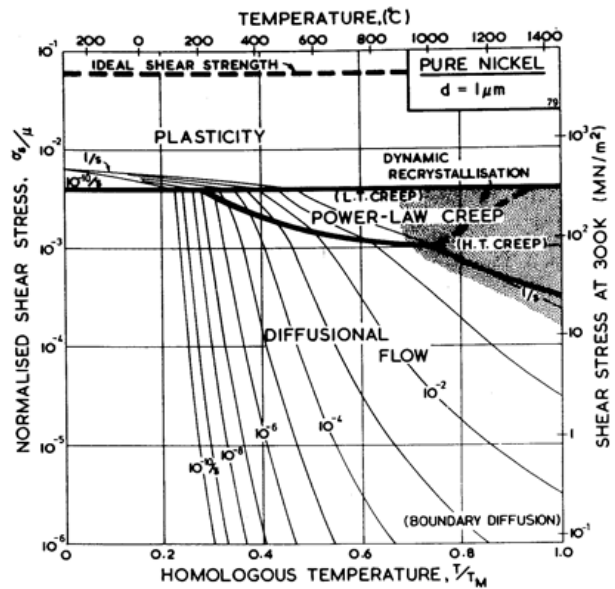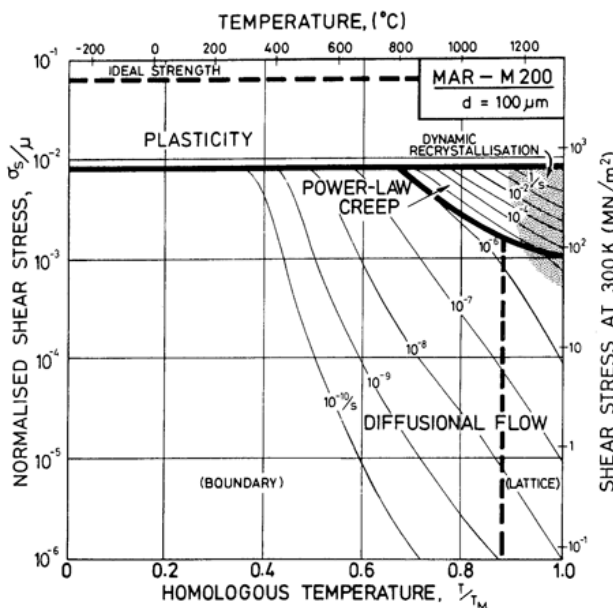
6.5.10. Oxidation and Corrosion of Metals

For electrochemistry, see Section 13.5.

Metals of differing electrode potentials in contact with each other and an electrolyte (e.g. seawater) will progressively corrode due to electrochemical reactions, leading to the metals dissolving or oxidising.

Iron corrosion in acidic environment: $Fe \rightarrow Fe^{2+} + 2\ e^-$; $2\ H^+ + 2\ e^- \rightarrow H_2$
Iron corrosion in a neutral environment: $Fe \rightarrow Fe^{2+} + 2\ e^-$; $O_2 + 2\ H_2O + 4\ e^- \rightarrow 4\ OH^-$
Rust formation: $Fe^{2+} + 2\ OH^- \rightarrow Fe(OH)_2$; $2\ Fe(OH)_2 + (x-1)\ H_2O \rightarrow Fe_2O_3 \cdot x\ H_2O + 2\ H^+ + 2\ e^-$
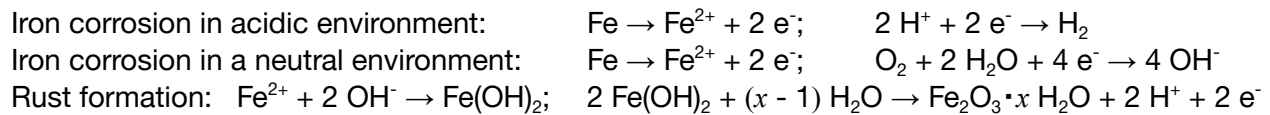
Corrosion Kinetics

Metal components can gain or lose mass due to corrosion. The rate of change of mass can be:

- Linear decrease: for an oxide layer that falls off or is volatile
- Linear increase: for an oxide layer forming a porous or cracked structure allowing oxygen access
- Parabolic increase ($\sim t^{1/2}$): for an adhering oxide layer that provides a diffusion barrier to oxygen

Thickness of oxide layer: $\hat{h}(t) = \sqrt{1 + \hat{t}} - 1$ where $\hat{h} = \dfrac{k_{ox}}{D_{ox}}h,\ \ \hat{t} = \dfrac{2\ M_{ox}\ c_g\ k_{ox}^{\ 2}}{\rho D_{ox}}t$ (Deal-Grove model)

(k_{ox}: oxidation rate constant, D_{ox}: diffusion coefficient of O_2 in metal oxide layer,
M_{ox}: molar mass of oxide, c_g: O_2 concentration at oxide-gas interface, ρ: oxide density, h: thickness, t: time)
At higher temperatures, D_{ox} is increased, increasing the rate of oxide formation (corrosion rate).
For some metals (e.g. Al, Cr, Ti), the oxide layer is impermeable to oxygen, protecting the bulk metal.

Localised corrosion occurs when the materials promote the anodic reaction, due to:

- defects in a protective coating (paint, natural oxide layer, etc). This leads to pitting.
- electrolyte present in crevices (e.g. under nuts and bolts). Low oxygen favours the anodic reaction.
- cracks. Corrosion can directly promote crack growth under cyclic stresses (corrosion fatigue).

Stress corrosion cracking occurs under tensile stress, where cracks grow faster due to corrosion.

Hydrogen embrittlement (hydrogen-induced cracking): the cathodic reaction produces H_2 which can diffuse interstitially through most metals, initiating and propagating crack growth, worse at lower temperatures. Stainless steels and Al-alloys are less susceptible to this. At very high temperatures, hot hydrogen can dissociate into $H^{\bullet}$ atoms which de-carburise carbon steels to form trapped pressurised methane at grain boundaries and microcavities, which weakens the steel, presents a fire hazard, and accelerates crack growth ('high-temperature hydrogen attack').

Corrosion engineering: techniques to mitigate large-scale corrosion include:

- Galvanic (cathodic) protection: use of sacrificial anodes (e.g. zinc on iron) for preferential discharge.
- Impressed current: external voltage applied to decrease the potential of the structure.
- Coating: painting the surface with epoxy to create a physical barrier with the environment.
- Passivation in alkaline environments: e.g. hot bluing, concrete. Promotes insoluble oxide formation.
- Alloying steel: e.g. chromium. Cr forms a self-healing chromium oxide layer spontaneously. On heating, the Cr can deplete from the grains to form carbides on grain boundaries, risking intergranular corrosion. This is mitigated by adding stabilising elements in the alloy (e.g. Ti, Nb).

Corrosion Thermodynamics

Oxidation reactions of metals are exothermic ($\Delta H < 0$) and entropy-reducing ($\Delta S < 0$), and are spontaneous (thermodynamically favoured, exergonic, $\Delta G < 0$) for most metals at room temperature.

The **Ellingham diagram** (Section 15.1.3) shows the variation of ΔG for oxidation with temperature T, which becomes less exergonic with increasing T. However, the increased corrosion rate takes precedent for moderately high temperatures as oxidation remains spontaneous.

Some noble metals (e.g. Au) cannot be corroded at room temperature due to their high stability. Pure silver resists corrosion due to the activation energy barrier, but can tarnish in the presence of sulfur.

Standard Gibbs free energy of oxidation

ΔG° in kJ **per mole of oxygen:** $x\,\text{M} + \text{O}_2 \rightarrow \text{M}_x\text{O}_2$ at $T = 298$ K.
Corrosion is feasible for exergonic reactions ($\Delta G < 0$).

Material	Oxide	Free energy (kJ/mol O_2)
Beryllium	BeO	− 1182
Magnesium	MgO	− 1162
Aluminium	Al_2O_3	− 1045
Zirconium	ZrO_2	−1028
Titanium	TiO	− 848
Silicon	SiO_2	− 836
Niobium	Nb_2O_5	− 757
Chromium	Cr_2O_3	− 701
Zinc	ZnO	− 636
Silicon nitride	$3SiO_2 + 2N_2$	− 629
Silicon carbide	$SiO_2 + CO_2$	− 580
Molybdenum	MoO_2	− 534
Tungsten	WO_3	− 510
Iron	Fe_3O_4	− 508
Nickel	NiO	− 439
Most polymers	–	− 400
Diamond, graphite	CO_2	− 389
Lead	Pb_3O_4	− 309
Copper	CuO	− 254
Silver	Ag_2O	− 5
Gold	Au_2O_3	+ 80

Galvanic series in seawater

Metals of different E in direct contact are at risk of corrosion. Seawater contains chloride ions which penetrate oxide layers and accelerate electrochemical reactions.

E in V vs. S.C.E.
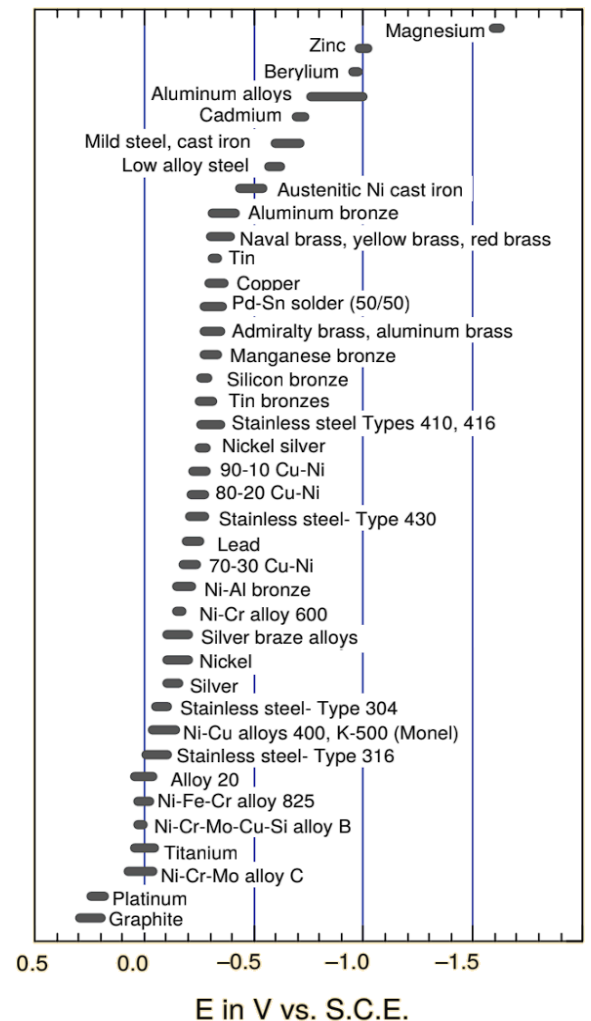
6.6. Materials Processing, Design and Datasets

6.6.1. Materials Selection

Process of material selection, single objective:

1. Identify **objective** (what is to be maximised or minimised? e.g. mass, cost, embodied CO_2)
2. Identify **functional constraints** (what is prescribed? e.g. stiffness-limited, strength-limited?)
3. Identify **geometrical constraints** (which dimensions are fixed, and which can vary?)
4. Eliminate free variables, and identify performance index of properties by proportionality.
5. Use material property charts (Section 6.6.14) or material selector software (e.g. Ansys Granta) to short-list the best materials.
6. Refine the selection using relevant secondary criteria: property limits (e.g. toughness), qualitative suitability (e.g. corrosion), manufacturing limits.

Performance indices for common optimisation problems

Function	Objective	Constraint	Index
Tie (tensile forces)	min mass	stiffness prescribed	E/ρ
Beam (bending moments)	min mass	stiffness prescribed	$E^{1/2}/\rho$
	min mass	strength prescribed	$\sigma_y^{2/3}/\rho$
Column (compressive forces)	min mass	buckling load prescribed	$E^{1/2}/\rho$
Shaft (torsion)	min mass	stiffness prescribed	$G^{1/2}/\rho$
Spring	min mass	strain energy prescribed	$\sigma_y^2/(\rho E)$
Thermal insulation	min mass	heat flux prescribed	$1/(\lambda c_p \rho)$
Electromagnet	max magnetic field	temperature rise prescribed	$c_p \rho/\rho_e$

(E: Young's modulus, σ_y: yield strength, ρ: density, C_m: material cost per unit mass, λ: thermal conductivity, c_p: specific heat capacity, ρ_e: electrical resistivity)

To design for minimum cost (or minimum embodied energy/CO_2…), replace ρ with ρC_m.

For material datasets including environmental resistance, see Section 6.6.2-3.
For the material property charts, see Section 6.6.4.
For process compatibility charts, see Section 6.6.5.

Shape Effects: designing axisymmetric components

If shape and/or area (of a cross-section) are free variables, shape factors can be used to measure geometric efficiency, and act as secondary constraints.

- Shape factor, stiffness-limited, in bending: $\Phi_E = \dfrac{I}{I_{square}} = \dfrac{12\,I}{A^2}$ (I: second moment of area)

- Shape factor, strength-limited, in bending: $\Phi_\sigma = \dfrac{Z_e}{Z_{e,square}} = \dfrac{6\,Z_e}{A^{3/2}}$ (Z_e: elastic section modulus)

Larger values of Φ correspond to more intricate shapes e.g. thin-flanged I-beam compared to a square or circle. Materials can be processed to a maximum Φ:

Material	Max Φ_E	Max Φ_σ	Material	Max Φ_E	Max Φ_σ
Steels	64	13	Fibre composites	36	9
Aluminium alloys	49	10	Wood	9	3

To incorporate shape factor into performance indices, replace E with $E\Phi_E$ (stiffness-limited) or replace σ_y with $\sigma_y\Phi_\sigma$ (strength-limited).

Multiple Constraints

If the design is simultaneously stiffness and strength limited (specified deflection and must not fail), compute the objective function for each functional constraint and evaluate both for each material. Rank the materials based on the worse of the two metrics.

Alternatively, plot a property chart with the two performance indices against each other and choose materials to maximise their product (above straight line $x + y$ on log-log axes).

Example: For a cantilever of fixed length L, it must carry a load F with maximum displacement δ, without failing. Identify materials to minimise materials cost C.

- Functional constraints: $\dfrac{F}{\delta} = \dfrac{3EI}{L^3} = \dfrac{E\Phi_E A^2}{4L^3}$ and $FL = Z_e \sigma_y = \dfrac{\Phi_\sigma A^{3/2}\sigma_y}{6}$.

- Eliminate free variable: $A = \left(\dfrac{4FL^3}{\delta E\Phi_E}\right)^{1/2}$ and $A = \left(\dfrac{6FL}{\Phi_\sigma \sigma_y}\right)^{2/3}$. $\{L, F, \delta\}$ are constants.

- Objective: $min\ C = max\ \dfrac{1}{C_m \rho A} = max\ \dfrac{E^{1/2}\Phi_E^{1/2}}{C_m \rho}$ and $max\ \dfrac{\sigma_y^{2/3}\Phi_\sigma^{2/3}}{C_m \rho}$ (performance indices).

$min\ m \rightarrow$ CFRP; $min\ C$, ignoring shape $\rightarrow$ wood; $min\ C$, considering shape $\rightarrow$ aluminium alloy.

Use e.g. Section 6.4.10 to find the aluminium extruded I-beam with the highest $\Phi_E^{1/2}\,\Phi_\sigma^{2/3} = \dfrac{I^{1/2}Z_e^{2/3}}{A^2}$.

6.6.3. Process Selection

Once a raw material has been selected (Section 6.6.1), a process needs to be selected, to achieve both the 1) desired shape and 2) desired properties (by manipulating microstructure).

Primary shaping: raw material → component

- **Casting:** pour liquid metal into mould, solidify and cool, remove mould.
- **Moulding:** viscous flow of molten polymer or glass to fill a mould.
- **Forming:** plastically deform solid metal to shape (hot or cold).
- **Powder:** fill die with powder (metal/ceramic), hot press to shape

Consider suitability for the geometry e.g. prismatic → rolling/extrusion, sheet → metal forming.

Machining involves using e.g. lathe, mill to cut and remove material with high precision. **Heat treatment** exploits microstructural changes to achieve a particular range of physical properties.

To select a process, eliminate processes that cannot achieve the required product tolerances (Section 6.6.10). The feasible processes are then typically ranked on total cost, using a cost model:

$$C = C_m + \frac{C_c}{n} + \frac{\dot{C_L}}{\dot{n}}$$

(C_m: material cost per unit (including consumables), C_c: tooling cost per unit (dedicated machinery), C_L': overhead cost per unit rate (labour, energy, share of capital), n: batch size, n': production rate.)

The **'economic batch size'** of a process represents the range of n for which $\dfrac{C_c / n}{C_m}$ is small.

Technical evaluation is needed to determine process operating conditions (pressure, temperature, time etc) to form a target defect-free microstructure and associated properties.

6.6.4. Theory of Phase Diagrams

For any horizontal line (isotherm), each two-phase field is adjacent to a one-phase field.

Vertical line or thin field at w_B wt% B: chemical compound A_xB_y where $\dfrac{x}{y} = \dfrac{(100 - w_B) / M_{r,A}}{w_B / M_{r,B}}$

Single phase regions are labelled as their crystal polymorphs $\alpha, \beta, \gamma \ldots$

Proportions of a two-phase mixture between α and β: $\dfrac{wt\% \, \alpha}{wt\% \, \beta} = \dfrac{(w_\beta - w) / (w_\beta - w_\alpha)}{(w - w_\alpha) / (w_\beta - w_\alpha)} = \dfrac{w_\beta - w}{w - w_\alpha}$ (lever rule)

Nucleation of solids (solidification/freezing) begins on cooling below the **liquidus** line. Melting of solids begins at the grain boundaries above the solidus line.

Special phase transformations during cooling of a melt at a particular mixture composition:

Eutectic reaction: L (l) $\rightarrow$ α (s) + β (s)   Peritectic reaction: α (s) + L (l) $\rightarrow$ β (s)

Eutectoid reaction: α (s) $\rightarrow$ β (s) + γ (s)   Peritectoid reaction: α (s) + β (s) $\rightarrow$ γ (s)

Total Gibbs Free Energy of Non-Eutectic (Non-Azeotropic) Binary Mixtures: at any given temperature, an equilibrium phase minimises its total Gibbs free energy. In a two-phase region (T_3 and T_4 below), the composition is at the common tangent intersection to the solid phase and liquid phase curves.

Free energy functions
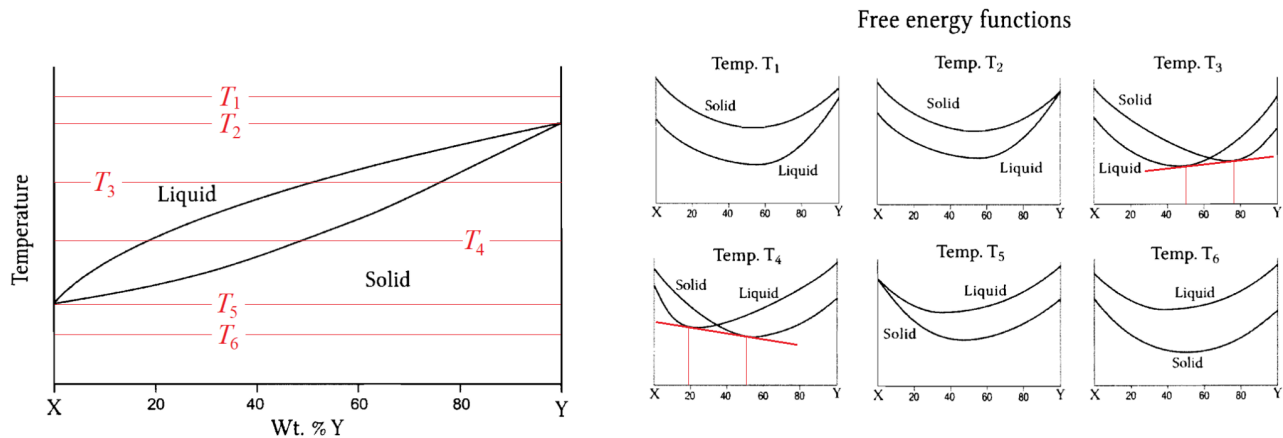
Phase Separation Thermodynamics
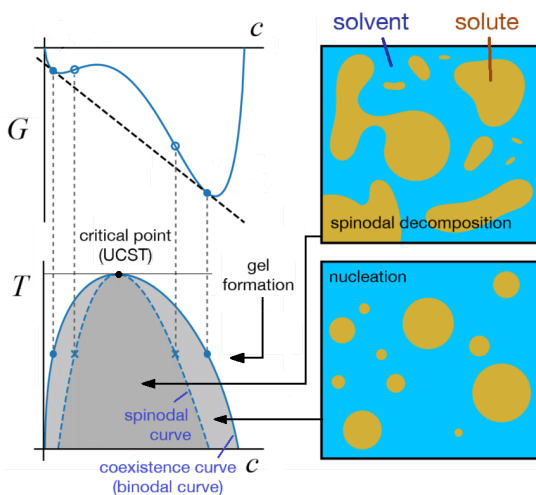
- **Spinodal curve:** limit of single phase stability, at free energy inflection points $d^2G/dx^2 = 0$. Phase separation occurs within the spinodal (unstable).

- **Binodal curve (coexistence curve):** limit of two-phase stability, at the common tangent to the free energy curve. The coexistence curve bounds the miscibility gap.

- Between the binodal and spinodal points, nucleation occurs with a metastable precipitate phase.

6.6.5. Microstructure from Phase Diagrams

While the phase diagram gives the thermodynamically favoured equilibrium phase proportions, it does not directly show their microscopic arrangement, dominated by diffusion kinetics. Common phase transformations and their resulting microstructures are:

- **Liquid to Concentrated Solid Solution:** under the liquidus line (upper melting point), grains of solid phase nucleate in the liquid and grow as cooling continues.
- **Single to Two-Phase Solid Solutions:** in solid grains, phase separation occurs by formation of nanoscopic precipitate clusters within the matrix. Atoms diffuse between matrix and precipitate.
- **Eutectic Solidification:** liquid phase spontaneously forms intricate microstructure of two solid phases. Grains are not observed.
- **Off-Eutectic Solidification:** solid phase nucleates first, liquid phase moves closer to eutectic composition. At the eutectic point, the remaining liquid undergoes eutectic solidification, and the other phase can develop precipitates within its grains.
- **Eutectoid Reaction:** in solid phase grains, new grains nucleate on the boundaries, consisting of lamellar (nanoscopic alternating plates, stacked normal to grain growth) microstructure of the two resulting solid phases. Atoms diffuse between the layers of the lamellar structure.
- **Off-Eutectoid Reaction:** one of the two solid phase grains undergoes the eutectoid reaction, developing the lamellar structure, and the other phase can develop precipitates within its grains. Commonly used in hypo-eutectoid steels, where lamellar structure (pearlite) is effective in obstructing dislocation motion, providing strength in addition to ferrite's intrinsic toughness.

6.6.6. Kinetics of Microstructural Evolution

Nucleation and Grain Growth

- Free energy of a nucleated solid in a fluid for $T < T_m$: $G(r) = \frac{4}{3}\pi r^3 \Delta G_V + 4\pi r^2 \gamma$

- Critical radius r for nucleation: $\frac{dG}{dr} = 0$ at $r = r^*$, where $r^* = \frac{2\gamma}{|\Delta G_V|} = \frac{2\gamma T_m}{|\Delta H_V| (T_m - T)}$

(ΔG_V: Gibbs free energy of fusion (per unit volume), ΔH_V: specific latent heat of fusion (per unit volume), T_m: liquid melting point (liquidus line), γ: solid-liquid surface energy)

Some undercooling (supercooling) $T_m - T$ is required to begin solidification. The latent heat of fusion ΔH_V is released, heating the melt back up to T_m, where the remainder of solidification occurs. When T_m is taken from the liquidus line of the phase diagram, freezing point depression by solute is accounted for.

Since r can be much larger for the same V in a spherical cap than a sphere, heterogeneous nucleation will always dominate over homogeneous nucleation.

- Solid growth rate v: $v = \frac{\Delta H_V}{k_B T} \frac{T_m - T}{T_m} e^{-Q/(k_B T)}$; max v and w occur at some undercooling $T_m - T > 0$.

- Rate of nucleation w: $w \propto e^{-\Delta G^*/(k_B T)} e^{-Q/(k_B T)}$, where $\Delta G^* = \Delta G_V(r^*) = \frac{16\pi\gamma^3 T_m^2}{3(\Delta H_V)^2(T_m - T)^2}$.

Mass and Heat Transfer in Solids (Diffusion and Heat Conduction)

In 1D, mass and heat transfer are governed by analogous differential equations:

- 1D diffusional flow (Fick's law, steady state): $J = -D\dfrac{\partial C}{\partial x} \Rightarrow \dfrac{\partial C}{\partial t} = D\dfrac{\partial^2 C}{\partial x^2}$

- 1D heat flow (Fourier's law, steady state): $q' = -\lambda\dfrac{dT}{dx} \Rightarrow \dfrac{\partial T}{\partial t} = \alpha\dfrac{\partial^2 T}{\partial x^2}$

For the 2D or 3D forms of these PDEs, see Section 3.7.3.

- Diffusion coefficient D [m^2 s^{-1}]: $D = D_0 \exp\left(-\dfrac{Q_a}{RT}\right)$

- Thermal diffusivity α [m^2 s^{-1}]: $\alpha = \dfrac{\lambda}{\rho c_p}$

(J: diffusive flux per unit area [mol s^{-1} m^{-2}], C: concentration [mol m^{-3}], q': heat flux per unit area [W m^{-2}], T: temperature [K], x: 1D position [m], t: time [s], Q_a: diffusional activation energy [J], λ: thermal conductivity [W m^{-1} K^{-1}], ρ: density [kg m^{-3}], c_p: specific heat capacity [J K^{-1} kg^{-1}].)

For many 1D problems of diffusion and heat flow, the solution for concentration or temperature depends on the error function distribution, erf (Section 1.7.3.):

$$C(x, t) = f\left[\mathrm{erf}\left(\frac{x}{2\sqrt{Dt}}\right)\right] \quad \text{and} \quad T(x, t) = f\left[\mathrm{erf}\left(\frac{x}{2\sqrt{\alpha t}}\right)\right]$$

A characteristic diffusion distance in all problems is given by $x \sim \sqrt{Dt}$, with the corresponding characteristic heat flow distance in thermal problems being $x \sim \sqrt{\alpha t}$.

Impulse Response: if $C(x, 0) = n_0\, \delta(x)$,   ($n_0$ is the initial amount (mol m^{-2})

$\Rightarrow \quad C(x, t) = \dfrac{n_0}{2\sqrt{\pi Dt}}\, \exp\left(-\dfrac{x^2}{4Dt}\right)$ (bell curve, increasing width with t)

Step Response: if $C(x, 0) = C_0 + (C_1 - C_0)\, H(x)$,   ($C_0$: external conc, C_1: internal conc)

$\Rightarrow \quad C(x, t) = C_0 + (C_1 - C_0)\, \mathrm{erf}\left(\dfrac{x}{2\sqrt{Dt}}\right)$

(slope from $C(0) = C_0$, $C(\infty) = C_1$, increasing width with t)

Harmonic Response: if $C(x, 0) = C_0 + (C_1 - C_0)\, \sin\left(\dfrac{2\pi x}{w}\right)$,   ($w$: length period of variation)

$\Rightarrow \quad C(x, t) = C_0 + (C_1 - C_0)\, \sin\left(\dfrac{2\pi x}{w}\right) \exp\left(-\dfrac{4\pi^2 Dt}{w^2}\right)$

The harmonic response can be used to find responses to arbitrary initial conditions using Fourier series.

6.6.7. Heat Treatment of Steel

Heat treatment is used to form strong, tough microstructures, mainly by precipitation hardening (pinning of dislocations by hard second phase microparticles). This helps to alleviate the usual trade-off between strength and toughness. Heat treatment is primarily applied as a secondary process, but can also occur due to similar thermal histories in e.g. welding, hot rolling.

Heat treatable alloys require heating to a single solid phase and cooling to form a two-phase mixture of solids. All steels satisfy this requirement: austenitisation involves the initial heating stage to convert the steel to single solid phase austenite (γ). On cooling, microstructural hardness is dependent on the temperature-time curve (thermal history). The steel phase diagram is shown in Section 6.6.33.

Slow Cooling of Hypoeutectoid Steels: left of the eutectoid (0.8 wt% C) point on phase diagram

A: Between ~800 °C and 723 °C (eutectoid line), ferrite (α) grains nucleate on austenite (γ) grain boundaries
B: remaining austenite undergoes the eutectoid reaction to form lamellar pearlite (hard phase of $\alpha + Fe_3C$).
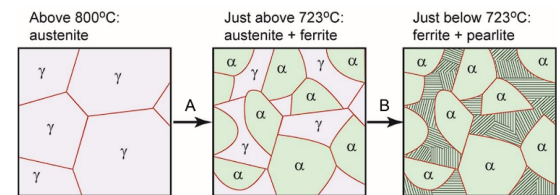
Slow-cooled steels are known as **'normalised'** steels, often occurring after hot rolling. The carbon content determines their properties: low carbon steel has $\sigma_y \sim 200$ MPa and high ductility, while normalised eutectoid steel (100% pearlite) has $\sigma_y \sim 450$ MPa with lower ductility.

Fast Cooling of Hypoeutectoid Steels: non-equilibrium states

The TTT diagram for hypoeutectoid steels (Section 6.6.34) implies four possible routes:

* Above the C-curves and above the eutectoid line (AC$_1$):   forms ferrite + austenite.
* Above the C-curves and below the eutectoid line: forms ferrite + pearlite (lamellar $\alpha + Fe_3C$)
* Below the C-curves and above the martensite line (M$_1$):forms bainite (fine Fe_3C needles in α)
* Below the C-curves and below the martensite line: forms martensite (metastable α')

Martensite is the metastable SSSS state, formed by diffusionless transformation of γ. Martensite is initially in the FCC unit cell, but since the equilibrium state is BCC, it can undergo a sudden 'shock wave' lattice shear to a distorted BCC unit cell (Bain strain), forming long thin needles of martensite through the remaining unstable γ grains. The lower the final temperature, the more martensite formed. With higher carbon content, pearlite predominates at higher T, the times to transformations increase and the martensite lines move to lower temperatures. Bainite has $\sigma_y \sim 600$ MPa while martensite has $\sigma_y \sim 2$ GPa, but is impractically brittle as-quenched ($K_{IC} < 5$ MPa m$^{1/2}$), and must undergo tempering.

Quenching and Tempering of High Carbon Steels

Heating martensite to 450-600 °C reduces its yield stress to $\sigma_y = 450$-800 MPa while providing it with essential toughness similar to normalised steels. A fine-scale dispersion of Fe_3C forms and the Fe lattice relaxes back to undistorted BCC. The tempering temperature also influences the softening rate and the volume fraction of precipitates formed.

Hardenability: ease of forming martensite on cooling, allowing larger bar diameters for through-hardening.

High hardenability is desired for cutting tools, requiring quenching and tempering.
Low hardenability is desired in welds, where weld fracture could occur in the heat-affected zone.

Surface Hardening of Steels

Many steel components used in machinery (e.g. gears, bearings, tool edges) are subjected to high surface stresses, due to friction and sliding contact. Surface engineering is used to harden the surface of the component ('case hardening') to increase its hardness and wear resistance without damaging the strength and toughness of the underlying steel.

Carburising: the steel is immersed in a carbon-rich atmosphere at high temperature e.g. gaseous CO or molten NaCN (older). Carbon diffuses into the surface of the component. The higher local C content increases both the hardness and hardenability, facilitating surface martensite formation which can then be tempered.

Thermal modelling (Section 6.6.1) can be used to estimate the carburisation time required for a given case depth: $erf\left(\frac{x_{case}}{2\sqrt{Dt_{case}}}\right) = 1 - \frac{C_{min} - C_0}{C_S - C_0}$.

(C_{min}: minimum C concentration at depth x_{case}, t_{case}: time required, C_0: initial bulk C concentration, C_S: maximum solubility of austenite at the carburising temperature, D: diffusion coefficient of C in steel at the carburising temperature)

Transformation Hardening: a heat source is applied to the surface, austenitising a thin layer, then cooling it quickly to form a layer of martensite. Surface heating may use a traversing flame, laser, electron gun or high frequency induction coils (induces surface eddy currents). Air cooling may be sufficient to form martensite, or a water-quench can be used.

Joining of Steels

Two metallic components can be joined at an interface using welding. Lower carbon-steels are suitable for welding, while high-carbon and high-alloy steels are less suitable, requiring preheating.

Metal-Inert Gas (MIG) Welding: a consumable (continuously fed) metal electrode at high voltage generates an electrical arc which melts the metal. When the components are melted together along an interface, they will re-solidify together, joining them. An inert gas stream is blown over the molten weld pool to prevent atmospheric contaminants entering the weld.

Tungsten-Inert Gas (TIG) Welding: an inert (fixed) tungsten electrode at high voltage arcs to a manually held metal welding rod, triple-melting the workpieces-rod interface. The TIG torch may be water-cooled to prevent overheating.

The **'heat affected zone' (HAZ)** is the region around the weld which did not melt but whose microstructure may still be affected by the process. The HAZ may undergo grain recrystallisation and growth (lower strength), over-ageing of precipitates, stress concentrations (thermal expansion, warping of thin sections), brittle martensite formation in steels on cooling (requiring post-weld tempering), or sensitisation of non-stabilised Cr-alloy steels (Cr is removed from grains to the boundaries, increasing susceptibility to intergranular corrosion).

6.6.8. Heat Treatment of Aluminium Alloys

Aluminium alloys are 'light alloys' (like titanium and magnesium). The strength of pure Al is very low (σ_y = 40 MPa) but can be increased ~10x using Al alloys and heat treatment. Al-Si is a casting alloy. Al-Cu is a heat treatable alloy. Al-Mg is light and non-heat treatable.

Slow Cooling of Aluminium Alloys: equilibrium processes only

In slow cooling, temperature changes are slow enough to maintain equilibrium compositions throughout. After heating to the Al-rich solid field of the phase diagram (~550 ℃), on cooling below the solvus line (~450 ℃), the secondary phase is rejected from the solid solution. This forms a precipitate (usually of an intermetallic compound e.g. $CuAl_2$), first by heterogeneous nucleation on grain boundaries and slowly by homogeneous nucleation in grains. The hard phase precipitates are coarse (well spaced), giving low yield strength and high ductility due to weak dislocation pinning.

Fast Cooling of Aluminium Alloys: controllable non-equilibrium process

The rates of phase transformations due to nucleation thermodynamics (Section 6.6.6) result in a 'C-curve' distribution, with rapid phase transformation occuring at some optimal undercooling below T_E. This is displayed for a given alloy in a 'TTT diagram' (time-temperature transformation). Quenching (rapid cooling) to some $T < T_E$ followed by isothermal holding for a given time results in a certain fraction of transformation, before removing to room temperature. This provides solid solution hardening, but the solute atoms provide weak pinning, so the yield strength is low.

If the cooling rate is fast enough to miss the C-curves (critical cooling rate), no precipitate will form at all, and the resulting room-temperature composition will be a metastable 'supersaturated solid solution' (SSSS). Continuous cooling transformations are illustrated on a 'CCT diagram'.

Age Hardening of Aluminium Alloys: increase the strength after fast cooling

A more complete thermal history to achieve hardness and strength in Al alloys is 1) solid solution heat treatment (dissolve alloy elements, forming single phase), 2) quenching (forms SSSS), 3) age hardening (reheating for precipitation). There are two methods of age hardening:

- Artificial ageing: reheat for a few hours at ~200 ℃ (two phase).
- Natural ageing: leave for several days at room temperature.

The precipitate lattice structure is coherent with the Al, reducing the interface energy penalty to nucleation, but loses coherence when they coarsen too much (grow and spread out). Age hardening therefore has a 'peak aged' state, where shear resistance to dislocation glide is maximised. Over-aged Al-alloys are soft. Natural ageing avoids this issue, though at slightly reduced strengths.
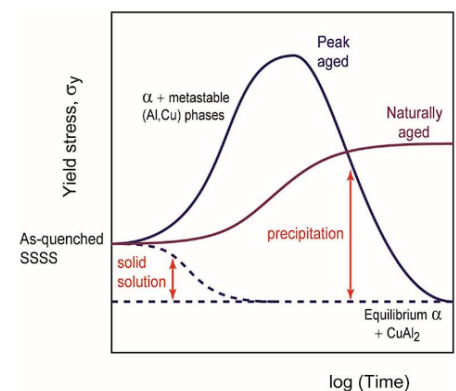
Non-Heat Treatable Aluminium Alloys

Al-Mg ('5000 series') and Al-Mg-Mn ('3000 series') cannot be age hardened, due to the difficult nucleation of Mg_5Al_8 intermetallic solute, so the precipitates do not form. These alloys remain metastable in operation and are hardened by solid solution and work hardening.

6.6.10. Casting of Metals (Cast Alloys)

A mould is filled with a molten metal or metal alloy, and it is allowed to cool and solidify. The resulting crystal grain structure (grain size and anisotropy) depends on the rates of internal heat conduction and so is highly shape-dependent.

Casting is often the first shaping step, forming large bulk metals (continuous casting, forming ingots, slabs, billets) and can be followed by deformation processing. Alloys can also be cast into 'near net shape', requiring only minimal secondary shaping processes to form the final product (e.g. die casting, sand casting, investment casting).

Grain Structure due to Cooling

1. **Chill zone:** rapid undercooling and large heterogeneous nucleation sites lead to numerous nuclei forming very small grains.
2. **Columnar zone:** grains oriented towards the centre can only grow in that direction.
3. **Equiaxed zone:** once the core liquid has undercooled, nucleation can begin slowly, forming larger grains in the centre.
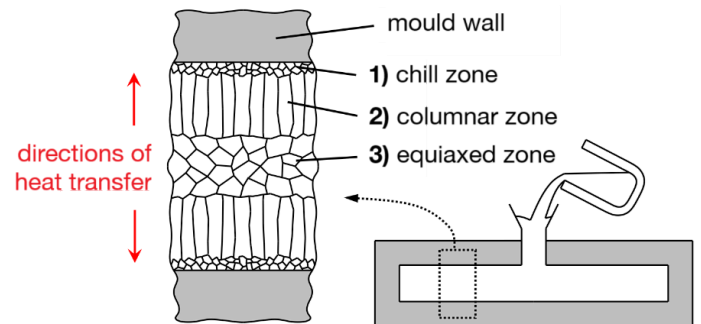
Controlling Grain Structure

When casting with metal alloys, smaller grain size provides a more uniform distribution of alloying elements and impurities due to segregation. This can be achieved by adding 'inoculants' (e.g. TiB_2 microparticles for Al casting alloys) to the molten cast, promoting rapid heterogeneous nucleation.

Eutectic compositions are optimal for casting alloys (low melting point, uniform melting temperature → can fill mould completely before solidifying). Al-11.3 wt% Si is a eutectic casting alloy with high strength, but the brittle Si needles require further alloying. In cast iron (Fe-4.3 wt% C), a small addition of Mg improves toughness by causing the graphite phase to form as spheres instead of flakes ('poisoning').

Chvorinov's rule: solidification time is proportional to volume-to-surface area ratio squared.
The microstructural length scale (e.g. lamella plate spacing) is inversely proportional to solidification rate.

Segregation: alloy/impurity concentrations are typically anisotropic in casting

The first solid to form (centre of grains) is always purer than the average alloy composition due to the diverging solidus and liquidus lines away from the eutectic point. The same is true for the material in the chill zone, producing both macroscopic and microscopic variation. Diffusion occurs too slowly to homogenise these fluctuations. Impurities concentrate on grain boundaries, possibly forming brittle precipitates or gas-filled cavities, leading to variable strength and reduced toughness.

Segregation can be reduced using inoculants for a finer grain size, or by adding small alloying additions that react with impurities. This forms a fine dispersion of solid particles during solidification, trapping the impurity in a harmless state (e.g. Mn and Al in carbon steels, trapping impurity S and O as MnS and Al_2O_3). The casting can also be homogenised by reheating, redistributing the solute by faster diffusion.

6.6.11. Deformation of Metals (Wrought Alloys)

Ductile alloys can be shaped by inducing compressive plastic strains without failure (deformation processing), in processes such as forging, rolling, extrusion and sheet metal forming.

Cold Working: deformation processes at room temperature. Microstructural changes include:

1. The grains change shape, following the overall imposed strain ('pancaked grains').
2. Work hardening occurs due to increase in dislocation density, increasing yield strength.

Deformation to large plastic strains risks failure by fracture due to reduced ductility.

Annealing: heating to $\sim 0.5\ T_m$ reverses the effects of work hardening

The thermal energy provided in annealing causes microstructural changes:

1. Recovery: at lower $\sim 0.1\ T_m$, dislocations of opposite orientation can annihilate each other on collision, or many dislocations of similar orientation can migrate and align into 'sub-grains', reducing the overall strain energy in the lattice. There is a small reduction in yield stress.

2. Recrystallisation: at higher $\sim 0.3\ T_m$, new defect-free grains are nucleated within the deformed work-hardened grains, significantly reducing dislocation density and dropping the yield strength.

In cold-rolling, the yield stress increases and thickness decreases slightly with each pass. An annealing schedule is used to 'reset' the yield stress when it rises too high, before continuing passes.

Hot Working: combined deformation and annealing, around $\sim 0.7\ T_m$

In hot working, strain hardening does not occur, reducing tooling forces and allowing larger strains.

Open-Die Hot Forging Analysis: workpiece struck with compressive plastic deformation by a die

Slab material flows away from the centre, resisted by friction stress at the lubricated die interface.
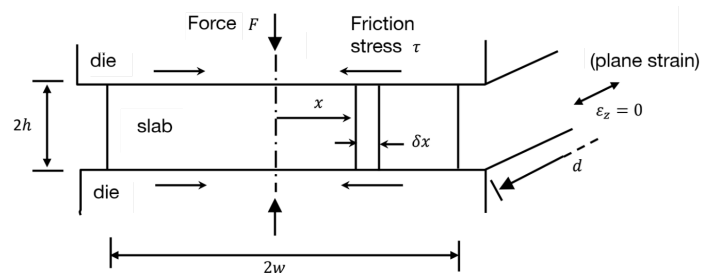
Equilibrium: $\dfrac{d\sigma_x}{dx} = \dfrac{-\tau}{h}$; Tresca yield criterion:

$p - \sigma_x = Y \;\Rightarrow\; \dfrac{dp}{dx} = \dfrac{-\tau}{h}$

Friction law: either Coulomb or Tresca

Coulomb friction: $\tau = \mu p$; Tresca friction: $\tau = mk = m\dfrac{Y}{2}$ ($m = 1$ represents 'sticking friction')

Applying Tresca friction, $\displaystyle\int_{p(x)}^{Y} dp = \dfrac{-mY}{2h}\int_{x}^{w} dx \;\Rightarrow\; p(x) = Y\left(1 + \dfrac{m}{2h}(w - x\,sgn\,x)\right)$ ('friction hill')

Total forging load per unit depth, $F = \displaystyle\int_{-w}^{w} p(x)\,dx = 2wY\left(1 + \dfrac{mw}{4h}\right)$.

Hot Rolling Analysis: pressure maximum at the 'neutral plane' ($V = \omega R$)

Rolling torque, $T = F\alpha R$ ($\alpha \sim 0.3$)
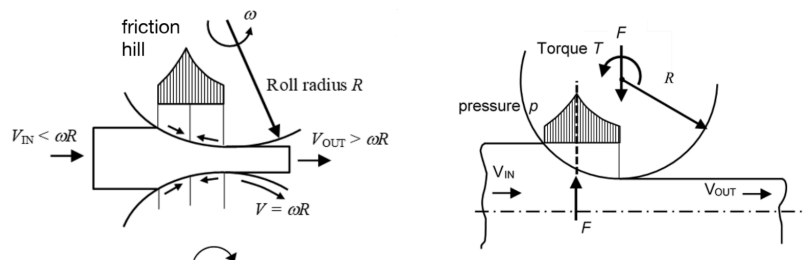
6.6.12. Processing of Thermoplastic Polymers

Solidification of Thermoplastic Polymers

Thermoplastics can solidify into a semi-crystalline structure, with regions of aligned (spherulites) and amorphous polymer chains. Higher crystallinity gives higher stiffness, higher density, higher glass transition temperature, lower ductility, lower toughness (more brittle) and lower optical transparency (scattering, birefringence and opacity).

Polymers are strong (high elastic modulus E) and brittle below a glass transition temperature T_g, and rapidly degrade into viscous liquids above this point.

- Thermoset: high degree of cross-linking $\rightarrow$ high T_g and E
- Elastomer: low degree of cross-linking $\rightarrow$ medium T_g and E
- Thermoplastic: no cross-linking $\rightarrow$ low T_g and E

Cross-linking can be induced by heat, pressure, acid catalysis, irradiation, or chemical agents (cross-linkers). In the vulcanisation process of rubber, elastomers are cured with sulfur or metal oxides to form stronger rubbers.

A complex monomer (large side groups, branching) will be slow to rearrange by diffusion and will therefore typically be difficult to crystallise. Low crystallinity (amorphous structure) is obtained when a polymer is formed by rapid cooling from a melt (e.g. film blowing). Crystallisation rate is maximum at some $T_g < T < T_m$, similar to C-curves on a TTT diagram (Section 6.6.7). Fast cooling rates, such as in producing thin sections of polymeric material, can avoid crystallinity.

Tacticity Control: relative stereochemistry of adjacent chiral centres between monomers

Isotactic (meso diads; homochiral)   Syndiotactic (racemo diads)   Atactic (random)
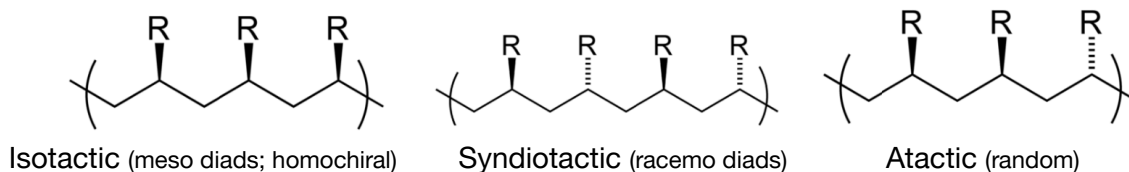
Tacticity cannot be changed after polymer formation as it is set by polymerisation conditions e.g. catalyst.

- Isotactic polymers are semi-crystalline. Most biopolymers are homochiral in this way.
- Syndiotactic polymers are highly crystalline.
- Atactic polymers are amorphous and are sometimes viscous liquids at room temperature.

Deformation Processing of Thermoplastics: variety of methods

- Fibre drawing: pressure screw extrudes thin polymer filament onto coiling drum.
- Stretch blow moulding: polymer preform ('parison') inflated to fill a mould. Anisotropic alignment.
- Film blowing: extruded polymer inflated, cooled and wound onto drum.

6.6.13. Powder Processing (Technical Ceramics)

Powder methods are suitable for near-net shape forming processes for ceramics and cemented carbides. It can provide good tolerances and surface finish with little final machining needed. It is easy to make complex shapes cost-effectively, and material wastage is very low.

Powder Manufacture

Metal powders are produced by atomisation (high pressure jets of water or gas directed at molten metal). Ceramic powders are typically made by crushing or grinding followed by sieving, producing very irregular particles.

Processing of Powders

- **Powder blending:** metal or ceramic powder is blended with various additives. Can be used for alloy steels. For ceramics, the additives are sintering aids (low melting phase to bind particles together), grain growth inhibitors (second-phase particles that pin grain boundaries) and a lubricant binder (e.g. zinc stearate, improves powder flow/mould filling, reduces die friction).

- **Compaction (cold isostatic pressing):** powder is pressed into a shaped mould/die at very high pressure to form a weak 'green compact', which can be 'green machined' to add holes/slots. On sintering, the ceramics shrink in dimensions due to loss in porosity, while metals do not shrink. Inhomogeneous porosity (due to non-uniform die friction) leads to undesirable internal stresses on contraction. Cold isostatic pressing is suitable for complex-shaped ceramics.

- **Pressureless sintering:** continuous conveying of powder through a furnace. The furnace atmosphere is controlled to prevent oxidation or decarburisation (e.g. of steels). Particles bond together, forming the grains in the bulk material. Sintering rate: $\frac{\partial \rho}{\partial t} = \frac{\gamma D}{a^3}$ (ρ: density, γ: surface energy, D: self-diffusion coefficient, a: particle diameter). Porosity goes from being interconnected to being discrete and then shrinking. Mechanical properties improve with decreased porosity.

- **Liquid phase sintering:** sintering is faster if a liquid phase is present, drawn by capillary action into the spaces between the particles e.g. sintering of alumina + 1% MgO which reacts to form a low melting-point glass which bonds the alumina grains together (e.g. for spark-plug insulator).

- **Hot isostatic pressing (hiping):** like cold isostatic pressing, but powder is canned in a metal container to provide shape and subjected simultaneously to high temperature. Hiping allows very low final porosity with short process time.

- **Metal Injection Moulding (MIM) and ceramic Powder Injection Moulding (PIM):** used for producing small, high-precision, low porosity components. Uses conventional polymer injection moulding technology with a blended polymer-metal or polymer-ceramic feedstock to make initial compacts which are then carefully treated to remove the polymer binder. Restricted to thin sections (limited by de-binding process).

- **Slip casting:** the 'traditional' manually handled process, often used for pottery and tiles. Clay slip (clay-water slurry) poured into mould, then the solid discs are pressed into a rotating tool, then transferred to racks for drying, followed by glazing and firing in a kiln.

6.6.14. Composite Processing (Composites)

6.6.15. Design Against In-Service Failures

6.6.16. Designing with Hybrid Materials

Hybrid materials (composites, sandwich structures, lattices and segmented structures) can be used when no single material is suitable: hybrid materials fill in the empty spaces of the material property charts. The two materials, configuration and volume fractions are chosen to optimise the goal at hand.

Properties of Hybrid Materials by Topology

	Composite		Sandwich		Lattice		Segment		
Function	Particulate	Fibrous	1-sided	2-sided	Bending	Stretching	1-D	2-D	3-D
Mechanical properties									
Axial stiffness / wt	●	●				●			
Axial strength / wt	●	●				●			
Flexural stiffness / wt	●	●	●	●		●			
Flexural strength / wt	●	●	●	●		●			
Axial compliance					●				
Flexural compliance					●		●	●	
Toughness		●							
Damage tolerance							●	●	●
Energy absorption		●			●				
Thermal management									
Insulation	●	●		●	●				
Conduction							●	●	
Electrical management									
Insulation									
Conduction							●	●	
Low dielectric loss				●	●	●			
Corrosion protection									
Oxidation			●	●					
Aqueous corrosion			●	●					

Types of Composites
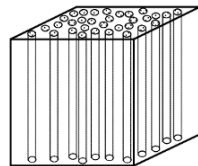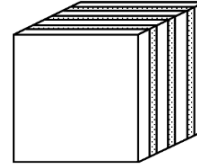
Particulate	Fibre	Laminate

Theoretical Ranges on Physical Properties (Voigt-Reuss equations)

Composite property	Lower bound	Upper bound
Young's modulus, E	$\left(\dfrac{V_f}{E_f} + \dfrac{1-V_f}{E_m}\right)^{-1}$	$V_f E_f + (1 - V_f)E_m$
Tensile strength, σ_{ts}	$\sigma_y^{(m)}\left(1 + \dfrac{\sqrt{f}}{16(1-\sqrt{f})}\right)$	$V_f \sigma_f^{(f)} + (1 - V_f)\sigma_y^{(m)}$
Thermal expansion coefficient, α	$\dfrac{E_f \alpha_f V_f + E_m \alpha_m (1 - V_f)}{E_f V_f + E_m(1 - V_f)}$	$\alpha_f V_f(1 + \nu_f) + \alpha_m(1 - V_f)(1 + \nu_m)$ $- \alpha_{min}(V_f \nu_f + (1 - V_f)\nu_m)$
Thermal conductivity, λ	$\lambda_m\left(\dfrac{\lambda_f + 2\lambda_m - 2V_f(\lambda_m - \lambda_f)}{\lambda_f + 2\lambda_m + 2V_f(\lambda_m - \lambda_f)}\right)$	$V_f \lambda_f + (1 - V_f)\lambda_m$

Quantities independent of configuration:

- Density, ρ: $\qquad\qquad\qquad\quad \rho = V_f \rho_f + (1 - V_f)\rho_m$
- Specific heat capacity, c_p: $\quad c_p \approx c_v = \dfrac{1}{\rho}(V_f \rho_f c_p^{(f)} + (1 - V_f)\rho_m c_p^{(m)})$
- Dielectric constant, ε: $\qquad\quad \varepsilon = V_f \varepsilon_f + (1 - V_f)\varepsilon_m$
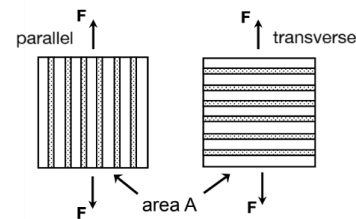
({m: matrix, f: fibre}, V_f: volume fraction of fibres.) Anisotropy ratio $= \dfrac{upper\ bound}{lower\ bound}$.

For Young's modulus, tensile strength and conductivity, maximum is achieved for parallel fibres, minimum for transverse fibres.

For tensile strength, maximum assumes a continuous ductile matrix with strong reinforcing particles. Other correlations are known for specific configurations.

For conductivity, good interface properties are assumed. Debonding, interfacial layers and large differences in moduli can result in conductivity below the lower bound (reflects phonons, creating an interface impedance, on a structural scale which is shorter than the phonon wavelengths).

For electrical conductivity, correlations are the same as thermal conductivity if **percolation** is absent. For random packing of spheres, the percolation threshold is $p_c = 0.20$. For $V_f \gg p_c$, electrical conductivity is much closer to the maximum. For a random network of fibres of aspect ratio $\beta = L/d$, the percolation threshold falls to $\beta^{-1/2} p_c$.

6.6.17. Designing with Steel

UK Steel designations

There is no internationally agreed system for classifying steels - the current UK system is detailed in British Standard BS970, using 6 digit codes (e.g. 080M40, 304S12).

The first 3 numbers relate to the class of steel:

- 000-199: C steels, C-Mn steels (the figures give the mean Mn content, from 0-1.99%)
- 200-240: Free machining steels (2nd & 3rd figures indicate sulphur content, from 0-0.4%)
- 250: Spring steels (Si-Mn steels)
- 300-499: Stainless, Heat-resisting and Valve steels
- 500-999 Alloy steels (subdivided by main alloy types, e.g. Ni-Cr, Ni-Cr-Mo etc)

The character refers to the supply conditions, or indicates stainless steel: A = chemical composition only, H = hardenability requirements given, M = mechanical requirements given, S = stainless steel. The last 2 numbers give the mean carbon content, for A, H and M steels (from 0-0.99%).

Example: 080M40 = 0.8% Mn, 0.4% carbon steel with specified composition and properties

Many product forms are also covered by British Standards, e.g. steel sheet, forgings, reinforcing bar etc. The national steel trade association, UK Steel, maintains a data handbook for all steels available in the UK (over 1000 specifications).

6.6.17. Designing with Concrete (Reinforced Concrete and Prestressed Concrete)

For standard codes of concrete construction in civil engineering, see Section 6.4.6.

Concrete is a cheap, durable and versatile material used for static structures, composed of water, sand (fine aggregate), gravel (coarse aggregate) and cement. A typical mix (by mass) is cement : sand : gravel = 1 : 2 : 3. For concrete beams, 1 : 1.5 : 3 is often used. It is very strong in compression but weak in tension (fails by fracture).

Portland cement is made by crushing and roasting a mixture of limestone ($CaCO_3$), clay or shale (provides SiO_2 and Al_2O_3) and iron ore (Fe_2O_3). The limestone decomposes to lime (CaO, releasing CO_2), which then reacts to form a variety of silicates and aluminosilicates in the clinker.

For large outdoor concrete structures e.g. patios, supports, the ground must be suitably prepared, by removing grass and organic matter (topsoil), flattening and compacting the soil (subgrade). A base layer of stone/gravel provides support, and a wooden formwork around the perimeter helps maintain the shape. After pouring the concrete mix, spread and level with a screed, and leave to cure with plenty of moisture (e.g. wet burlap) for 28 days for maximum strength. When choosing location, consider rainwater runoff and drainage, as concrete is impermeable. For industrial-scale concrete pile production, autoclaving (high pressure steam curing) is common to accelerate cement hydration.

Concrete is non-flammable and fire-resistant but degrades at very high temperatures (not fireproof), as heat can reverse the curing reactions in the binder (cement), losing mass from water evaporation, dropping the compressive strength. In RC, the steel may also debond, fail or melt, losing tensile strength entirely, as well as concrete cracking from differential thermal expansion. At lower temperatures (~300 °C), spalling can occur as water-filled pores evaporate. Refractory cement, using crushed firebrick (grog) and corundum aggregates, can be used for better fire resistance.

Reinforced Concrete (RC): steel rebar is used to provide tensile strength, especially at one edge of a beam in bending. The steel is coated for corrosion protection against salt and water. The rebars are long and thin hot-rolled carbon steel cylinders. Glass fibre reinforced plastic (GFRP, fibreglass) can alternatively be used as the rebar material to make GFRC which is more lightweight than steel RC.

Prestressed Concrete (PC): to reduce crack formation in the tensile side of RC, the concrete can be put into compression on its formation. There are two methods:

- Pre-tensioning: rebars (tendons) placed in tension in hydraulic jacks, and the concrete is poured around the rebars. Once cured, the tension is released, compressing the concrete.

- Post-tensioning: rebars pulled in tension and cured concrete compressed simultaneously.

Reinforced Autoclaved Aerated Concrete (RAAC): during the mixing step, a foaming agent (aluminium powder) is added to the alkaline slurry which releases hydrogen gas bubbles, forming a porous structure. RAAC is lightweight and a good thermal insulator, though has reduced strength relative to standard RC and has a shorter service life (faster crack propagation, faster corrosion).

6.6.18. Designing with Wood (Lumber, Timber, Glulam, Plywood, Veneer)

Classifications of Wood

Hardwood comes from the logging of angiosperm trees (fruit-bearing plants). Softwood comes from the logging of gymnosperm trees (cone-bearing plants).

Lumber is unprocessed wood fibre, typically in beam, plank or board form. Engineered woods are physical or material composites of wood.

Processing of Wood Logs

Logs from trees can be converted into lumber by sawing (cutting with a ripsaw), hewing (cutting with an axe) or splitting (cutting with a wedge, knife or froe).

Lumber is often cut to standard dimensions (e.g. 2×4 is a beam with section 50×100 mm).

6.6.19. Prototypical Manufacturing Methods

3D Printing: produces complex shapes by extrusion, typically ~1-20 cm dimensions

Compatible materials: many polymers (e.g. PLA, ABS, nylon, PC, PMMA), polymer composites (e.g. with wood, magnetic powder), carbon fibre, sandstone.

- Design a model of the part using computer aided design software (CAD).
- Save the part as an STL file (`.stl`), which saves the part as a triangulated mesh.
- Use 3D printing software to import the model. Check the filament material and automatically add supports if necessary. Slice the model to obtain the G-code instruction file (`.gcode`) for printing.
- Insert a USB thumb drive containing the `.gcode` file into the 3D printer.
- Check that the nozzle and stage temperatures are set correctly for the material.
- Start the print job; collect from the stage once finished.

Laser Cutting: produces flat shapes from thin soft materials (e.g. up to 5 mm plywood)

Compatible materials: wood, some polymers, cardboard, foam, fabric, thin metal sheets. Glass can be engraved but not be cut. Always check whether a specific polymer can be laser cut: some release toxic fumes (e.g. chlorine, hydrogen cyanide) due to photochemical breakdown of the polymer.

- Design a drawing of the part and save as a DXF file (`.dxf`).

Plasma Cutting: produces flat shapes from thicker metal pieces (e.g. up to 15 mm steel)

Welding

Mills and Lathes (Manual and CNC-Operated):

Printed Circuit Board (PCB) Fabrication

6.7.20. Mechanics of Materials Data

Metals, Alloys and Ceramics:

		Melting or softening temperature, T_m (°C)		Density, ρ (Mg m^{-3})		Young's modulus, E (GPa)		Yield stress, σ_y (MPa)		Tensile strength, σ_{ts} (MPa)		Fracture toughness (plane strain), K_{IC} (MPa m$^{1/2}$)	
Metals		Lower	Upper	Lower	Upper	Lower	Upper	Lower	Upper	Lower	Upper	Lower	Upper
	Cast irons	1130	1250	7.05	7.25	165	180	215	790	350	1000	22	54
	High carbon steels	1289	1478	7.8	7.9	200	215	400	1155	550	1640	27	92
	Med carbon steels	1380	1514	7.8	7.9	200	216	305	900	410	1200	12	92
Ferrous	Low carbon steels	1480	1526	7.8	7.9	200	215	250	395	345	580	41	82
	Low alloy steels	1382	1529	7.8	7.9	201	217	400	1100	460	1200	14	200
	Stainless steels	1375	1450	7.6	8.1	189	210	170	1000	480	2240	62	280
	Aluminium alloys	475	677	2.5	2.9	68	82	30	500	58	550	22	35
	Copper alloys	982	1082	8.93	8.94	112	148	30	500	100	550	30	90
	Lead alloys	322	328	10	11.4	12.5	15	8	14	12	20	5	15
Non-ferrous	Magnesium alloys	447	649	1.74	1.95	42	47	70	400	185	475	12	18
	Nickel alloys	1435	1466	8.83	8.95	190	220	70	1100	345	1200	80	110
	Titanium alloys	1477	1682	4.4	4.8	90	120	250	1245	300	1625	14	120
	Zinc alloys	375	492	4.95	7	68	95	80	450	135	520	10	100
Ceramics													
	Borosilicate glass	450	602	2.2	2.3	61	64	264	384	22	32	0.5	0.7
	Glass ceramic	563	1647	2.2	2.8	64	110	750	2129	62	177	1.4	1.7
Glasses	Silica glass	957	1557	2.17	2.22	68	74	110	1600	45	155	0.6	0.8
	Soda-lime glass	442	592	2.44	2.49	68	72	360	420	31	35	0.55	0.7
	Brick	927	1227	1.9	2.1	15	30	50	140	7	14	1	2
Porous	Concrete, typical	927	1227	2.2	2.6	15	25	32	60	2	6	0.35	0.45
	Stone	1227	1427	2.5	3	20	60	34	248	5	17	0.7	1.5
	Alumina	2004	2096	3.5	3.98	215	413	690	5500	350	665	3.3	4.8
	Aluminium nitride	2397	2507	3.26	3.33	302	348	1970	2700	197	270	2.5	3.4
	Boron carbide	2372	2507	2.35	2.55	400	472	2583	5687	350	560	2.5	3.5
Technical	Silicon	1407	1412	2.3	2.35	140	155	3200	3460	160	180	0.83	0.94
	Silicon carbide	2152	2500	3	3.21	300	460	1000	5250	370	680	2.5	5
	Silicon nitride	2388	2496	3	3.29	280	310	524	5500	690	800	4	6
	Tungsten carbide	2827	2920	15.3	15.9	600	720	3347	6833	370	550	2	3.8

Notes:

- For glasses, T_m is given as the glass transition temperature, above which the material properties degrade rapidly.
- For ceramics, σ_y is given as the compression strength (about ~10 times yield in tension).

Composites, Natural Materials and Polymers:

		Melting or softening temperature, T_m (°C)		Density, ρ (Mg m^{-3})		Young's modulus, E (GPa)		Yield stress, σ_y (MPa)		Tensile strength, σ_{ts} (MPa)		Fracture toughness (plane strain), K_{IC} (MPa m$^{1/2}$)	
Composites		Lower	Upper	Lower	Upper	Lower	Upper	Lower	Upper	Lower	Upper	Lower	Upper
Metal	Al/SiC	525	627	2.66	2.9	81	100	280	324	290	365	15	24
Polymer	CFRP	(decomposes)		1.5	1.6	69	150	550	1050	550	1050	6.1	88
	GFRP	(decomposes)		1.75	1.97	15	28	110	192	138	241	7	23
Natural													
	Bamboo	77	102	0.6	0.8	15	20	35	44	36	45	5	7
	Cork	77	102	0.12	0.24	0.013	0.05	0.3	1.5	0.5	2.5	0.05	0.1
	Leather	107	127	0.81	1.05	0.1	0.5	5	10	20	26	3	5
	Wood, longitudinal	77	102	0.6	0.8	6	20	30	70	60	100	5	9
	Wood, transverse)	77	102	0.6	0.8	0.5	3	2	6	4	9	0.5	0.8
Polymers													
	Butyl rubber	-73	-63	0.9	0.92	0.001	0.002	2	3	5	10	0.07	0.1
	EVA	-73	-23	0.945	0.955	0.01	0.04	12	18	16	20	0.5	0.7
	Isoprene	-83	-78	0.93	0.94	0.0014	0.004	20	25	20	25	0.07	0.1
Elastomer	Natural rubber	-78	-63	0.92	0.93	0.0015	0.0025	20	30	22	32	0.15	0.25
	Neoprene	-48	-43	1.23	1.25	0.0007	0.002	3.4	24	3.4	24	0.1	0.3
	Polyurethane (elPU)	-73	-23	1.02	1.25	0.002	0.003	25	51	25	51	0.2	0.4
	Silicones	-123	-73	1.3	1.8	0.005	0.02	2.4	5.5	2.4	5.5	0.03	0.5
	ABS	88	128	1.02	1.21	1.1	2.9	18.5	51	27.6	55.2	1.19	4.3
	Cellulose polymers	-9	107	0.98	1.3	1.6	2	25	45	25	50	1	2.5
	Ionomer (I)	27	77	0.93	0.96	0.2	0.424	8.3	15.9	17.2	37.2	1.14	3.43
	Nylons (PA)	44	56	1.12	1.14	2.62	3.2	50	94.8	90	165	2.22	5.62
	Polycarbonate (PC)	142	205	1.14	1.21	2	2.44	59	70	60	72.4	2.1	4.6
	PEEK	143	199	1.3	1.32	3.5	4.2	65	95	70	103	2.73	4.3
Thermo-plastic	Polyethylene (PE)	-25	-15	0.939	0.96	0.621	0.896	17.9	29	20.7	44.8	1.44	1.72
	PET	68	80	1.29	1.4	2.76	4.14	56.5	62.3	48.3	72.4	4.5	5.5
	Acrylic (PMMA)	85	165	1.16	1.22	2.24	3.8	53.8	72.4	48.3	79.6	0.7	1.6
	Acetal (POM)	-18	-8	1.39	1.43	2.5	5	48.6	72.4	60	89.6	1.71	4.2
	Polypropylene (PP)	-25	-15	0.89	0.91	0.896	1.55	20.7	37.2	27.6	41.4	3	4.5
	Polystyrene (PS)	74	110	1.04	1.05	2.28	3.34	28.7	56.2	35.9	56.5	0.7	1.1
	Polyurethane (tpPU)	120	160	1.12	1.24	1.31	2.07	40	53.8	31	62	1.84	4.97
	PVC	75	105	1.3	1.58	2.14	4.14	35.4	52.1	40.7	65.1	1.46	5.12
	Teflon (PTFE)	107	123	2.14	2.2	0.4	0.552	15	25	20	30	1.32	1.8
	Epoxies	(decomposes)		1.11	1.4	2.35	3.075	36	71.7	45	89.6	0.4	2.22
Thermosets	Phenolics	(decomposes)		1.24	1.32	2.76	4.83	27.6	49.7	34.5	62.1	0.79	1.21
	Polyester	(decomposes)		1.04	1.4	2.07	4.41	33	40	41.4	89.6	1.09	1.70

Notes:

- For polymers, T_m is given as the glass transition temperature. Material properties degrade rapidly above this.
- Thermosets, CFRP (carbon fibre reinforced composite) and GFRP (glass fibre reinforced composite) decompose when heated rather than melt.
- For applications and full names/abbreviations of polymers, see Section 16.5.1.

Polymer Foams: properties are dependent mainly on the mesh/scaffold geometry.

Foams		Melting or softening temperature, T_m (°C)		Density, ρ (Mg m⁻³)		Young's modulus, E (GPa)		Yield stress, σ_y (MPa)		Tensile strength, σ_{ts} (MPa)		Fracture toughness (plane strain), K_{IC} (MPa m$^{1/2}$)	
		Lower	Upper	Lower	Upper	Lower	Upper	Lower	Upper	Lower	Upper	Lower	Upper
Flexible	Very low density (VLD)	112	177	0.016	0.035	0.0003	0.001	0.01	0.12	0.24	0.85	0.005	0.02
	Low density (LD)	112	177	0.038	0.07	0.001	0.003	0.02	0.3	0.24	2.35	0.015	0.05
	Medium density (MD)	112	177	0.07	0.115	0.004	0.012	0.05	0.7	0.43	2.95	0.03	0.09
Rigid	Low density (LD)	67	171	0.036	0.07	0.023	0.08	0.3	1.7	0.45	2.25	0.002	0.02
	Medium density (MD)	67	157	0.078	0.165	0.08	0.2	0.4	3.5	0.65	5.1	0.007	0.049
	High density (HD)	67	171	0.17	0.47	0.2	0.48	0.8	12	1.2	12.4	0.024	0.091

## 6.6.21. Environmental Resistance and Durability

Qualitative assessment of material resilience in **fire, fresh water, salt water, sunlight (UV)** and **wearing** environments. **A** = very good; **B** = good; **C** = average; **D** = poor; **E** = very poor.

			Flammability	Fresh water	Salt water	Sunlight (UV)	Wear resistance
Metals							
Ferrous		Cast Irons	A	B	C	A	A
		High Carbon Steels	A	B	C	A	A
		Medium Carbon Steels	A	B	C	A	A
		Low Carbon Steels	A	B	C	A	A
		Low Alloy Steels	A	B	C	A	A
		Stainless Steels	A	A	A	A	B
Non-ferrous		Aluminium Alloys	B	A	B	A	C
		Copper Alloys	A	A	A	A	A
		Lead Alloys	A	A	A	A	C
		Magnesium Alloys	A	A	D	A	C
		Nickel Alloys	A	A	A	A	B
		Titanium Alloys	A	A	A	A	C
		Zinc Alloys	A	A	C	A	E
Ceramics							
Glasses		Borosilicate Glass	A	B	B	A	A
		Glass Ceramic	A	A	A	A	A
		Silica Glass	A	A	A	A	B
		Soda-Lime Glass	A	A	A	A	A
Porous		Brick, Concrete, Stone	A	A	A	A	C
Technical		Alumina	A	A	A	A	A
		Aluminium Nitride	A	A	A	A	A
		Boron Carbide	A	A	A	A	A
		Silicon	A	A	B	A	B
		Silicon Carbide	A	A	A	A	A
		Silicon Nitride	A	A	A	A	A
		Tungsten Carbide	A	A	A	A	A
Composites							
Metal		Aluminium/Silicon Carbide	A	A	B	A	B
Polymer		CFRP	B	A	A	B	C
		GFRP	B	A	A	B	C
Natural							
		Bamboo	D	C	C	B	D
		Cork	D	B	B	A	B
		Leather	D	B	B	B	B
		Wood	D	C	C	B	D

			Flammability	Fresh water	Salt water	Sunlight (UV)	Wear resistance
Polymers [1]							
Elastomer		Butyl Rubber	E	A	A	B	B
		EVA	E	A	A	B	B
		Isoprene (IR)	E	A	A	B	B
		Natural Rubber (NR)	E	A	A	B	B
		Neoprene (CR)	E	A	A	B	B
		Polyurethane Elastomers (elPU)	E	A	A	B	B
		Silicone Elastomers	B	A	A	B	B
Thermoplastic		ABS	D	A	A	C	D
		Cellulose Polymers (CA)	D	A	A	B	C
		Ionomer (I)	D	A	A	B	C
		Nylons (PA)	C	A	A	C	C
		Polycarbonate (PC)	B	A	A	B	C
		PEEK	B	A	A	A	C
		Polyethylene (PE)	D	A	A	D	C
		PET	D	A	A	B	C
		Acrylic (PMMA)	D	A	A	A	C
		Acetal (POM)	D	A	A	C	B
		Polypropylene (PP)	D	A	A	D	C
		Polystyrene (PS)	D	A	A	C	D
		Polyurethane Thermoplastics (tpPU)	C	A	A	B	C
		PVC	A	A	A	A	C
		Teflon (PTFE)	A	A	A	B	B
Thermoset		Epoxies	B	A	A	B	C
		Phenolics	B	A	A	A	C
		Polyester	D	A	A	A	C
Polymer Foams							
		Flexible Polymer Foams	E	A	A	C	D
		Rigid Polymer Foams	C	A	A	B	E

6.6.22. Maximum Service Temperature

The shaded bars extend to the maximum service temperature – materials may be used safely for all temperatures up to this value, without significant property degradation. Note the logarithmic axis.
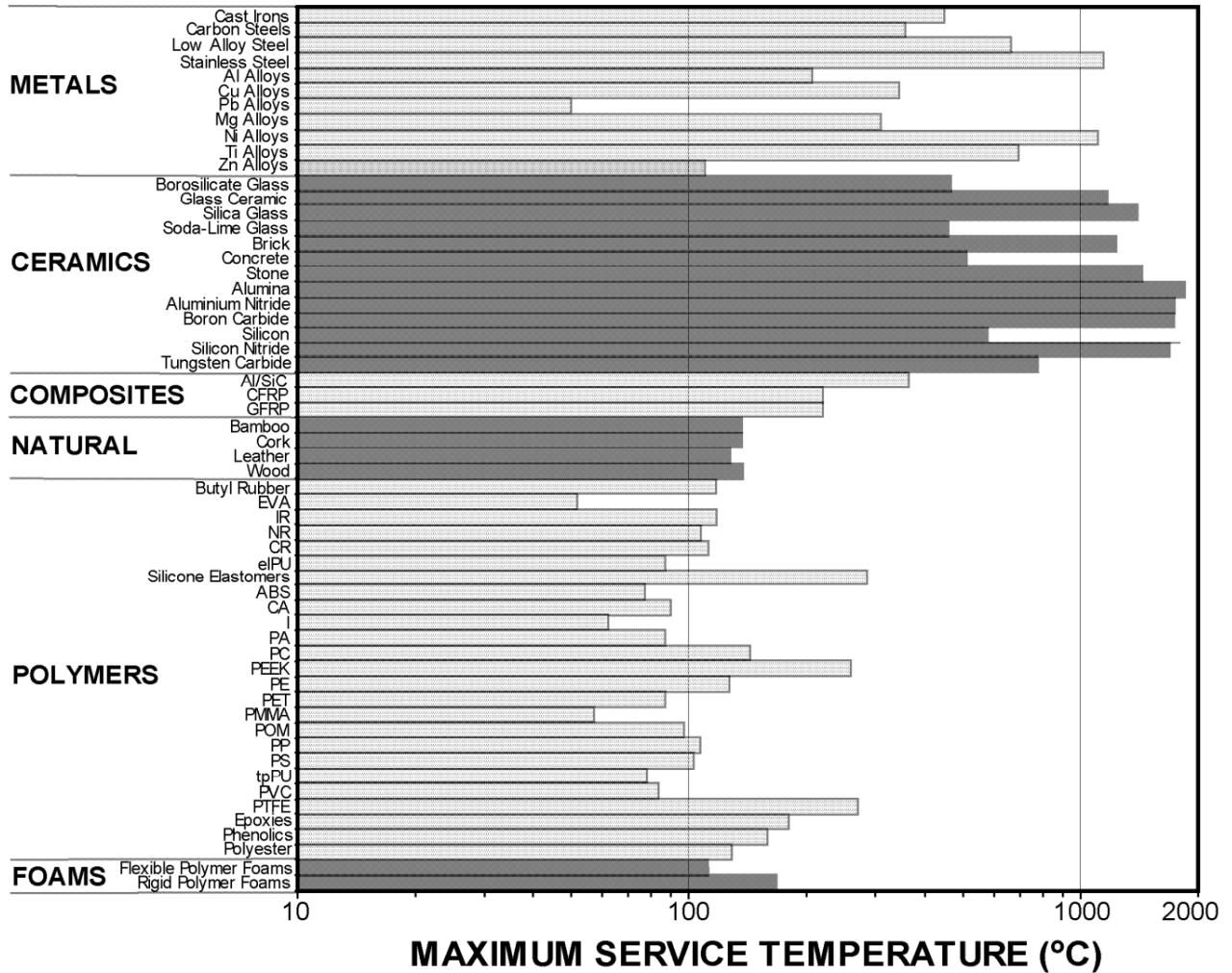
There is a modest range of maximum service temperature in a given material class – not all variants within a class may be used up to the temperature shown, so caution should be exercised if a material appears close to its limit.

6.6.23. Material Price

Material price per kg, C_m in £ (GBP). C_m represents raw material price/kg, and does not include manufacturing or end-of-life costs.
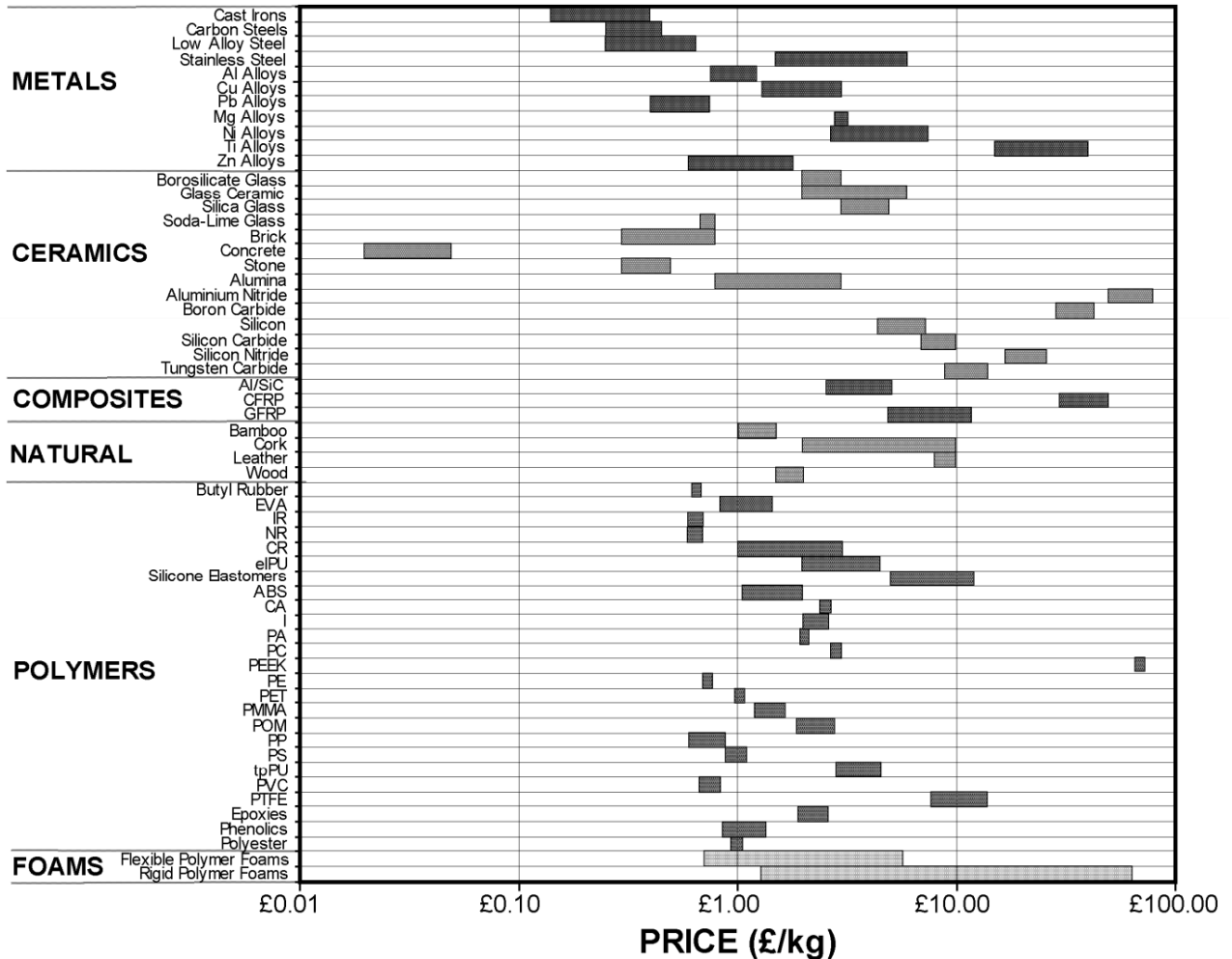
Note that this data is from 2003 and can vary over time due to inflation, currency exchange rates and supply/demand. For these reasons it should be used only for rough comparison between materials and not the raw numerical data.

Note the logarithmic axis.

6.6.24. Triboelectric Effect (Anti-Static Design)

Electrical insulators (ceramics, polymers, natural materials, foams) develop static electric charges on mechanical rubbing. The triboelectric series, quantified by surface charge density (in $\mu C\ m^{-2}$), is given.
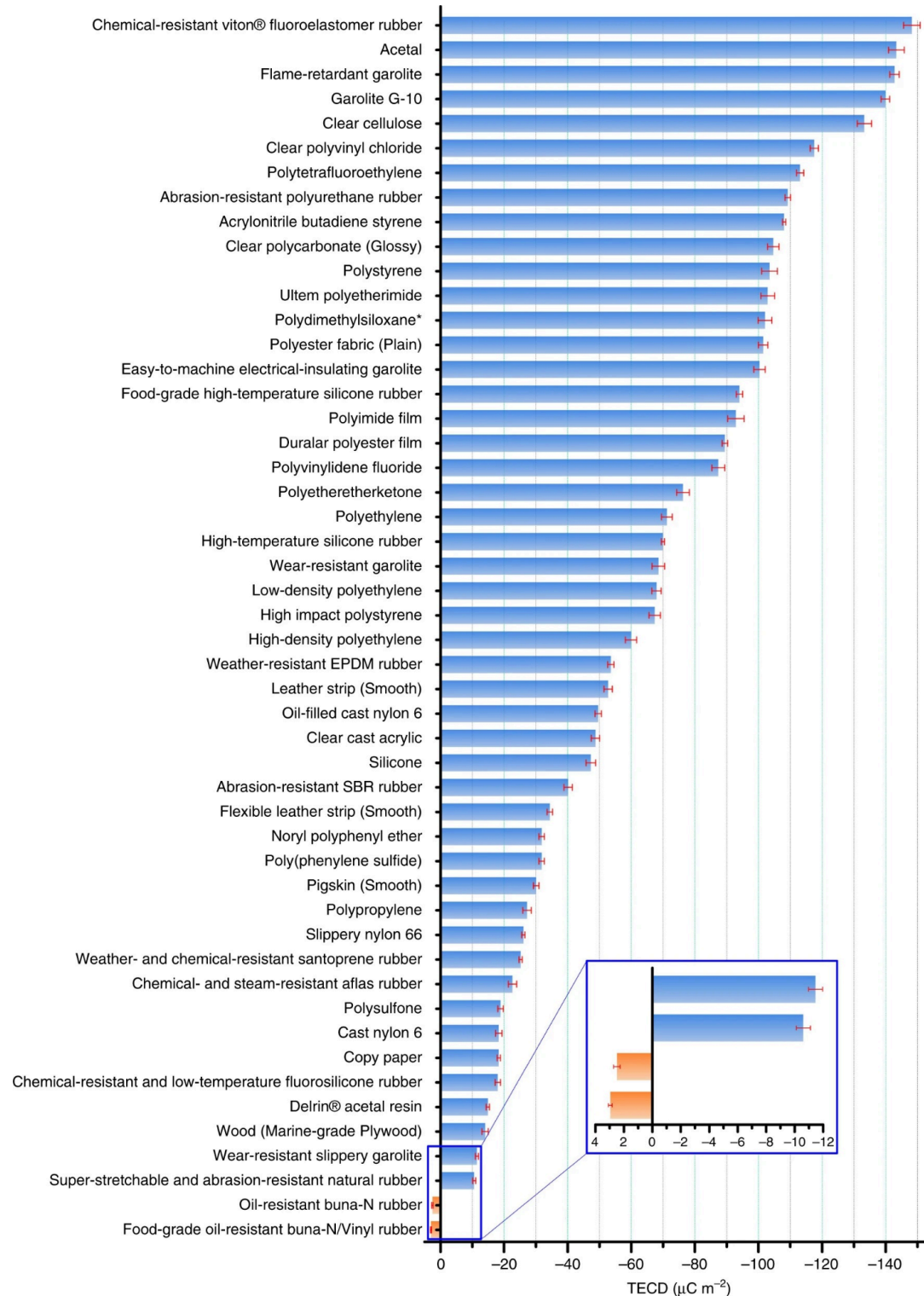
6.6.25. Main Applications of Materials

Metals:

Metal class	Metal	Applications
Ferrous	Cast irons	Automotive parts, engine blocks, machine tool structural parts, lathe beds
	High carbon steels	Cutting tools, springs, bearings, cranks, shafts, railway track
	Medium carbon steels	General mechanical engineering (tools, bearings, gears, shafts)
	Low carbon steels	Steel structures ("mild steel") — bridges, oil rigs, ships; rebar for reinforced concrete; automotive parts, car body panels; galvanised sheet; packaging (cans, drums)
	Low alloy steels	Springs, tools, ball bearings, automotive parts (gears connecting rods, etc.)
	Stainless steels	Transport, chemical and food processing plant, nuclear plant, domestic ware (cutlery, washing machines, stoves), surgical implements, pipes, pressure vessels, liquid gas containers
Non-ferrous	Casting aluminium alloys	Automotive parts (cylinder blocks), domestic appliances (irons)
	Non-heat-treatable aluminium alloys	Electrical conductors, heat exchangers, foil, tubes, saucepans, beverage cans, lightweight ships, architectural panels
	Heat-treatable aluminium alloys	Aerospace engineering, automotive bodies and panels, lightweight structures and ships
	Copper alloys	Electrical conductors and wire (oxygen-free copper, OFHC), electronic circuit boards, heat exchangers, boilers, cookware, coinage, sculptures
	Lead alloys	Roof and wall cladding, solder, X-ray shielding, battery electrodes
	Magnesium alloys	Automotive castings, wheels, general lightweight castings for transport, nuclear fuel containers; principal alloying addition to aluminium alloys
	Nickel alloys	Gas turbines and jet engines, thermocouples, coinage; alloying addition to austenitic stainless steels
	Titanium alloys	Aircraft turbine blades; general structural aerospace applications; biomedical implants.
	Zinc alloys	Die castings (automotive, domestic appliances, toys, handles); coating on galvanised steel

Ceramics, Natural Materials and Composites:

Ceramic class	Ceramic	Applications
Glasses	Borosilicate glass	Ovenware, laboratory ware, headlights
	Glass ceramic	Cookware, lasers, telescope mirrors
	Silica glass	High performance windows, crucibles, high temperature applications
	Soda-lime glass	Windows, bottles, tubing, light bulbs, pottery glazes
Porous	Brick	Buildings
	Concrete	General civil engineering construction
	Stone	Buildings, architecture, sculpture
Technical	Alumina	Cutting tools, spark plugs, microcircuit substrates, valves
	Aluminium nitride	Microcircuit substrates and heat sinks
	Boron carbide	Lightweight armour, nozzles, dies, precision tool parts
	Silicon	Microcircuits, semiconductors, precision instruments, IR windows, MEMS
	Silicon carbide	High temperature equipment, abrasive polishing grits, bearings, armour
	Silicon nitride	Bearings, cutting tools, dies, engine parts
	Tungsten carbide	Cutting tools, drills, abrasives

Natural Material	Applications
Bamboo	Building, scaffolding, paper, ropes, baskets, furniture
Cork	Corks and bungs, seals, floats, packaging, flooring
Leather	Shoes, clothing, bags, drive-belts
Wood	Construction, flooring, doors, furniture, packaging, sports goods

| Composite class	Composite	Applications
Metal	AlSiC	Automotive parts, sports goods
Polymer	CFRP	Lightweight structural parts (aerospace, bike frames, sports goods, boat hulls and oars, springs)
	GFRP	Boat hulls, automotive parts, chemical plants, glass fibre reinforced concrete

Polymers and Foams

Polymer Class	Polymer	Abbr.	Applications
Elastomers	Butyl rubber		Tyres, seals, anti-vibration mountings, electrical insulation, tubing
	Ethylene-vinyl-acetate	EVA	Bags, films, packaging, gloves, insulation, running shoes
	Isoprene	IR	Tyres, inner tubes, insulation, tubing, shoes
	Natural rubber	NR	Gloves, tyres, electrical insulation, tubing
	Neoprene	CR	Wetsuits, O-rings and seals, footwear
	Polyurethane	el-PU	Packaging, hoses, adhesives, fabric coating
	Silicone		Electrical insulation, electronic encapsulation, medical implants
Thermo-plastics	Acrylonitrile butadiene styrene	ABS	Communication appliances, automotive interiors, luggage, toys, boats
	Cellulose polymers	CA	Tool and cutlery handles, decorative trim, pens
	Ionomers	I	Packaging, golf balls, blister packs, bottles
	Polyamides (nylons)	PA	Gears, bearings, plumbing, packaging, bottles, fabrics, textiles, ropes
	Polycarbonates	PC	Safety goggles, shields, helmets, light fittings, medical components
	Polyetheretherketone	PEEK	Electrical connectors, racing car parts, fibre composites
	Polyethylene	PE	Packaging, bags, squeeze tubes, toys, artificial joints
	Polyethylene terephthalate	PET	Blow moulded bags, film, audio/video tape, sails
	Polymethyl methacrylate (acrylic)	PMMA	Aircraft windows, 3D printer ink, lenses, reflectors, lights, CDs
	Polyoxymethylene (acetal)	POM	Zips, domestic and appliance parts, handles
	Polypropylene	PP	Ropes, garden furniture, pipes, kettles, electrical insulation, astroturf
	Polystyrene	PS	Toys, packaging, cutlery, audio cassette/CD cases
	Polyurethane	tp-PU	Cushioning, seating, shoe soles, hoses, car bumpers, insulation
	Polyvinylchloride	PVC	Pipes, gutters, window frames, packaging
	Polytetrafluoroethylene (Teflon)	PTFE	Non-stick coatings, bearings, skis, electrical insulation, tape
Thermo-sets	Epoxies	EP	Adhesives, fibre composites, electronic encapsulation
	Phenolics	PHEN	Electrical plugs, sockets, cookware, handles, adhesives
	Polyester	PEST	Furniture, boats, sports goods

Polymer Foam	Applications
Flexible polymer foam	Packaging, buoyancy, cushioning, sponges, sleeping mats
Rigid polymer foam	Thermal insulation, sandwich panels, packaging, buoyancy

6.6.25. Uniaxial Tensile Response (Stress-Strain) Curves
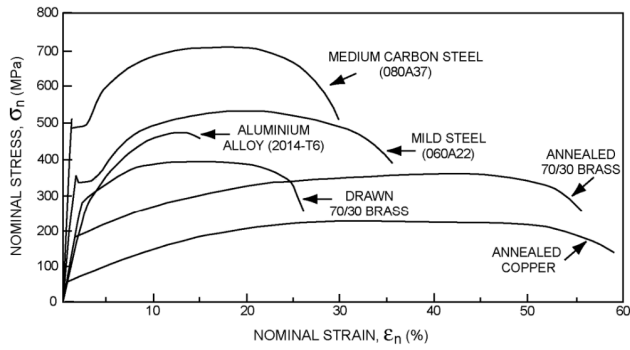
Metals and Alloys
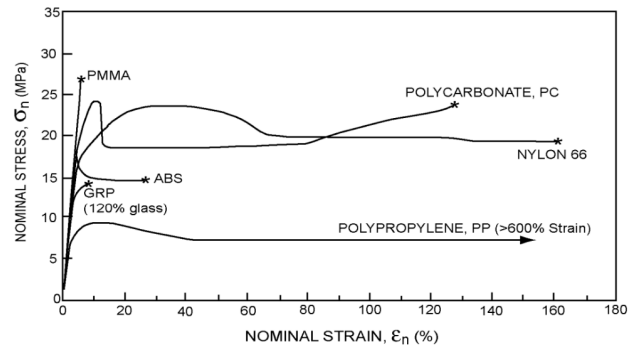
Polymers
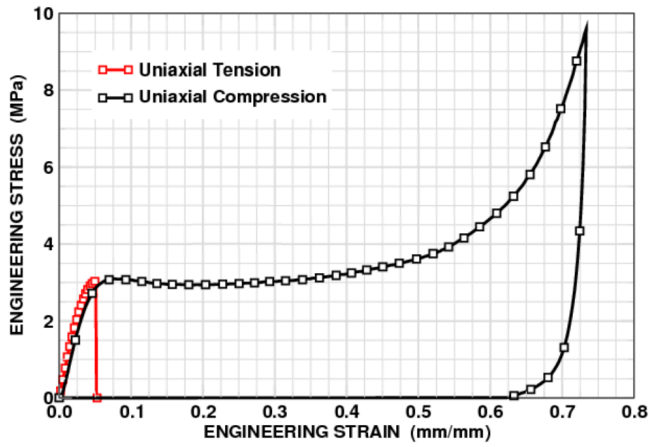
Polyurethane Foam, ρ = 176 kg m^{-3}

6.6.26. Viscoelastic Stress-Strain Responses of Polymeric Materials

Data recorded at 25 °C.
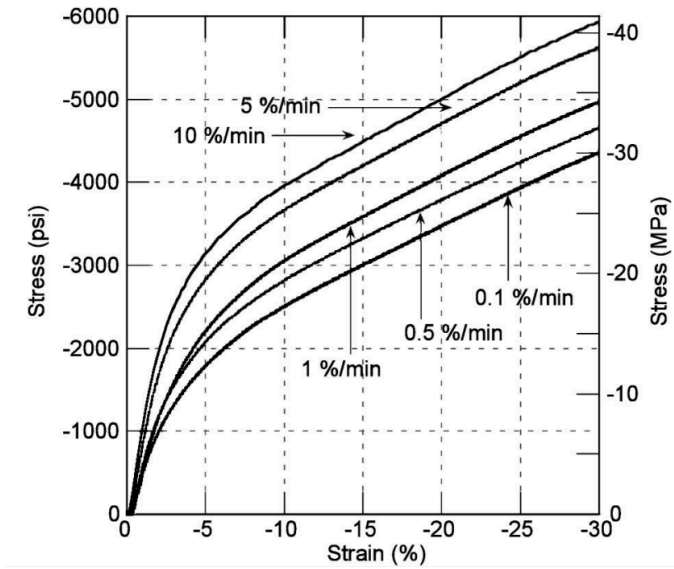
HDPE (high-density polyethylene)   PVC (polyvinyl chloride)
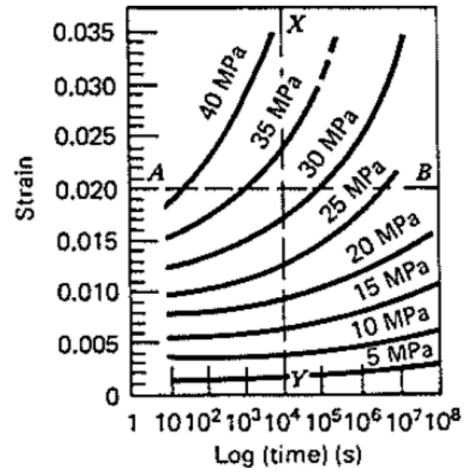
For the high-temperature creep response of materials, see Section 6.6.6.

6.6.27. Material Property Charts for Performance-Limited Design

Materials can be ranked using various performance indices based on the charts below.
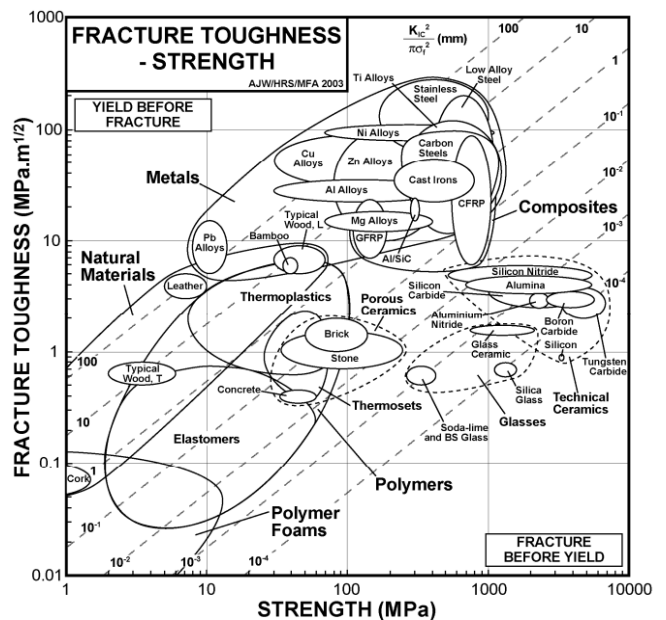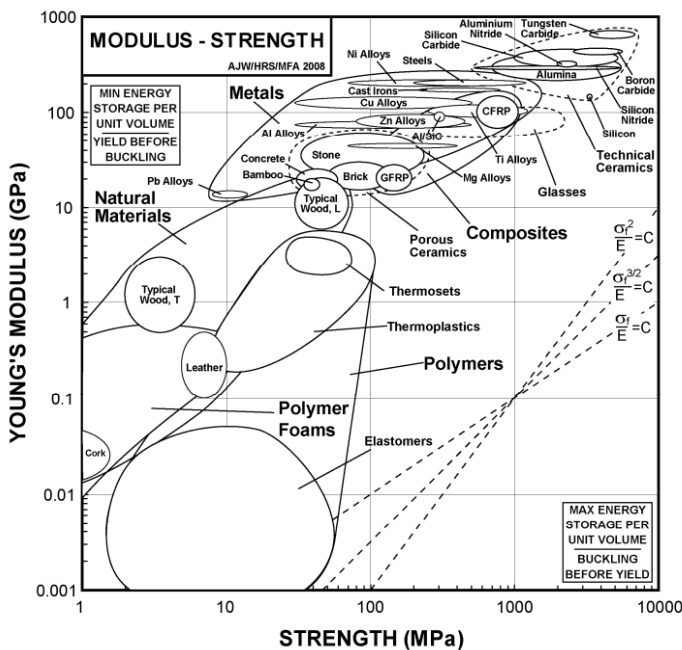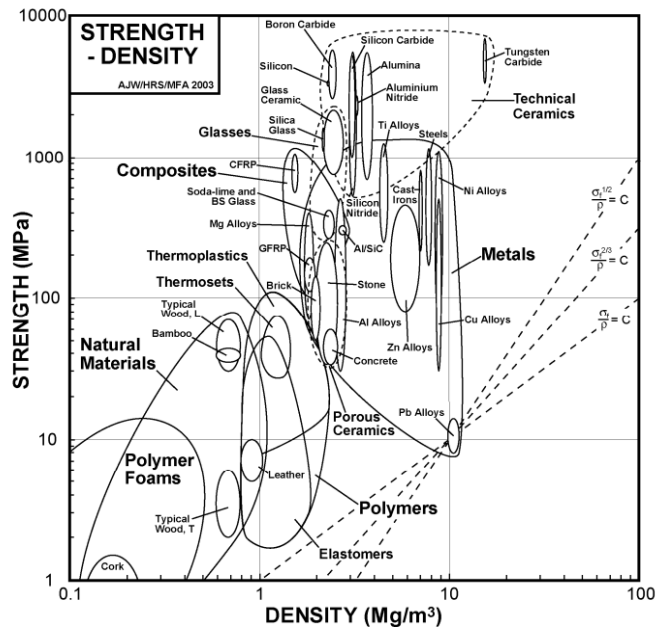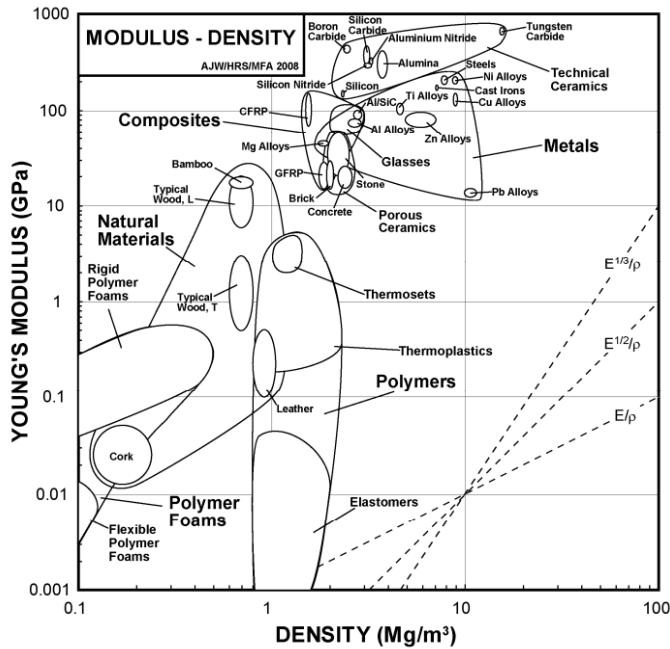
Failure strength is defined as the tensile elastic limit (usually yield stress) for all materials other than ceramics, for which it is the compressive strength.

The contours on the fracture toughness-strength graph represent process zone size, as per the definition in Section 6.6.2 (plane stress).

6.6.28. Material Property Charts for Energy-Limited Design

H_m: embodied energy per unit **mass**; ρH_m: embodied energy per unit **volume**.
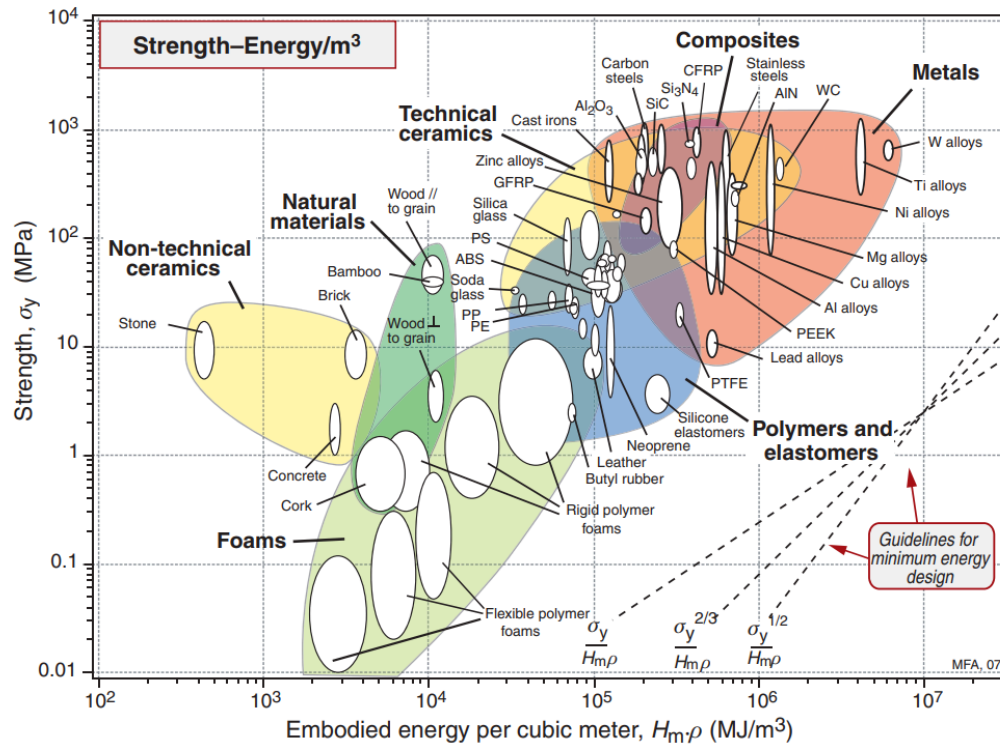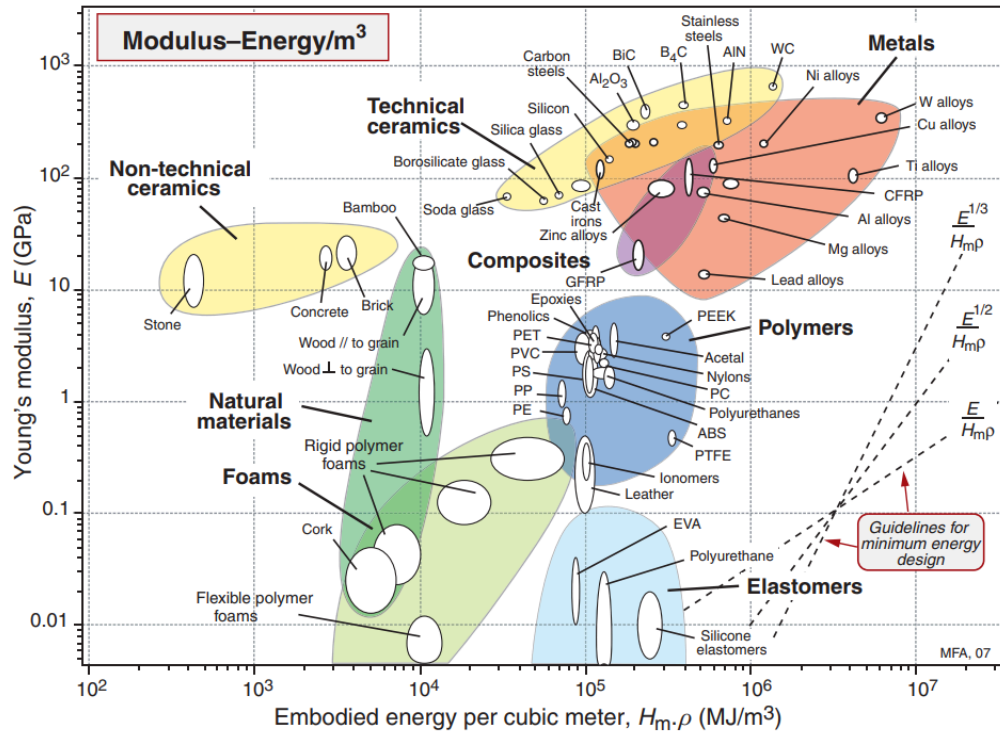
6.6.29. Material Process Compatibility

Material processing techniques compatible with various materials are shown with • .

For metals:

Metals		Sand Casting	Die Casting	Investment Casting	Rolling/ Forging	Extrusion	Sheet Forming	Powder Methods	Machining
Ferrous	Cast Irons	•	•	•					
	Medium/High Carbon Steels	•		•	•			•	•
	Low Carbon Steels	•		•	•		•	•	•
	Low Alloy/Stainless Steels	•	•	•	•		•	•	•
Non-ferrous	Aluminium, Copper, Lead, Magnesium, Zinc Alloys	•	•	•	•	•	•	•	•
	Nickel Alloys	•	•	•	•		•	•	•
	Titanium Alloys		•		•	•	•	•	•

For polymers:

Polymers	Machining	Injection Moulding	Blow Moulding	Compression Moulding	Rotational Moulding	Polymer Casting	Composite Forming
Elastomers	•			•	•		
Thermoplastics	•	•	•	•	•		
Thermosets				•	•	•	•
Polymer Foams	•	•			•		

For other materials:

- Ceramics are all processed by powder compaction methods, and Glasses are also moulded. Both are difficult to machine.

- Polymer Composites are shaped by dedicated forming techniques, and are difficult to machine.

- Natural Materials can only be machined, though some woods are also hot formed.

6.6.30. Attribute Charts for Shaping Processes

Typical attainable ranges are specified.

MASS

SECTION THICKNESS

SURFACE ROUGHNESS

DIMENSIONAL TOLERANCE

ECONOMIC BATCH SIZE
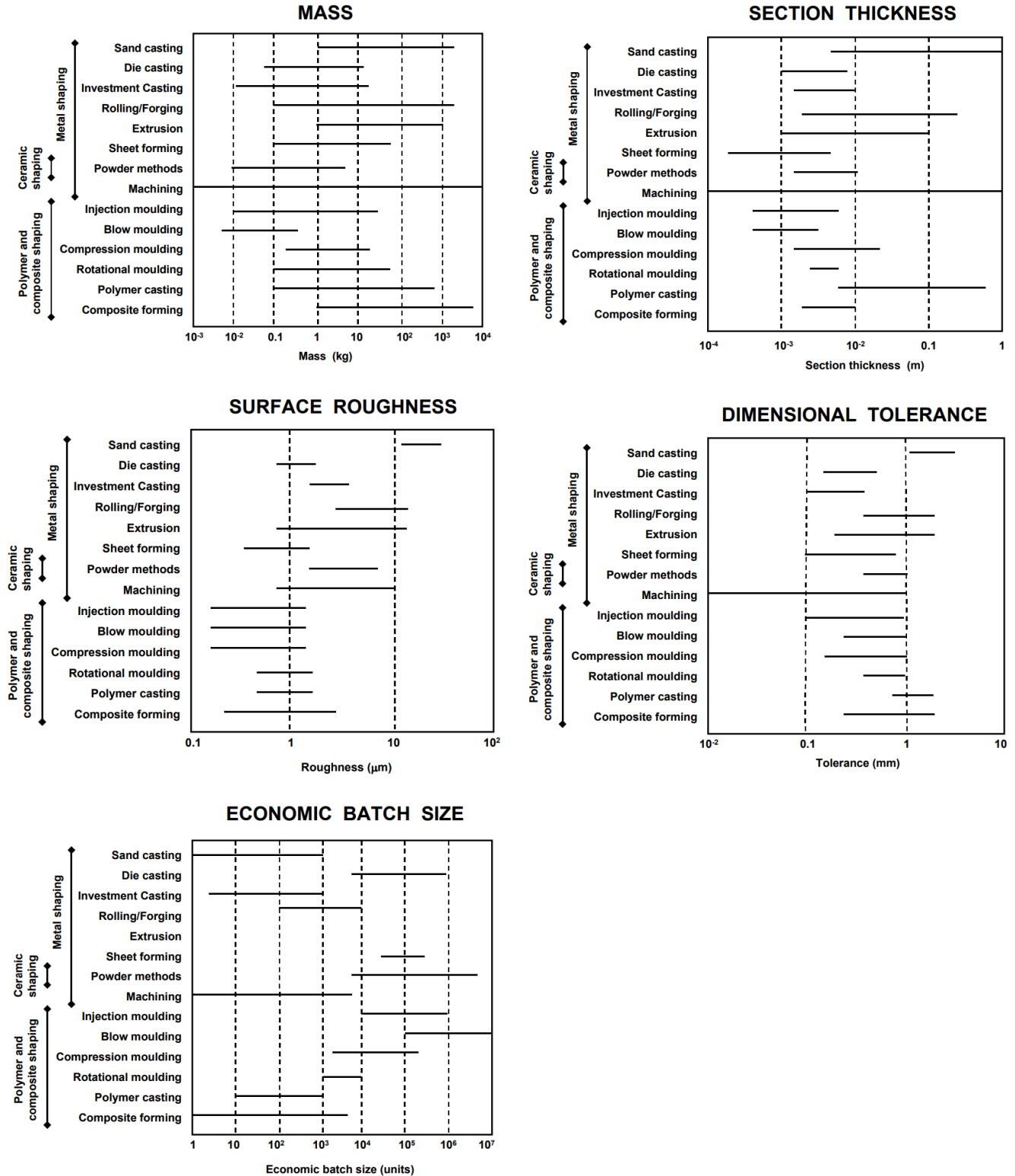
6.6.31. Binary Phase Diagrams Involving Metals

Copper-Nickel (Cu-Ni)
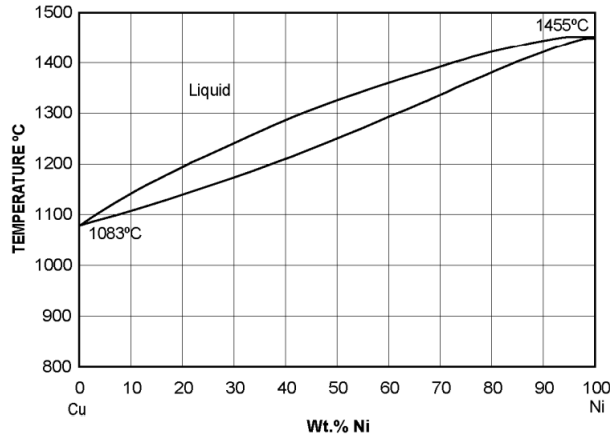
Lead-Tin (Pb-Sn)
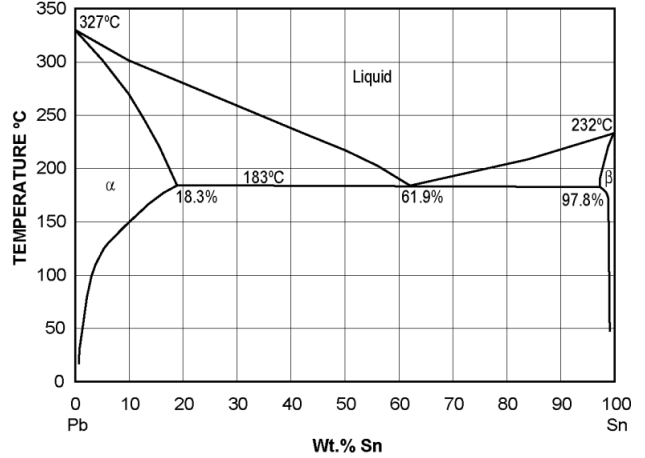
Aluminium-Copper (Al-Cu)
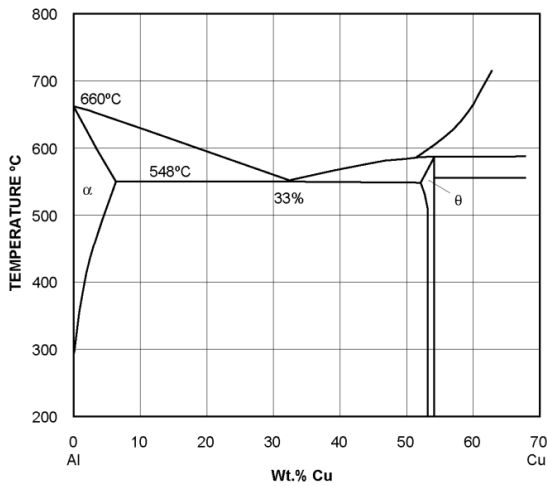
Titanium-Aluminium (Ti-Al)
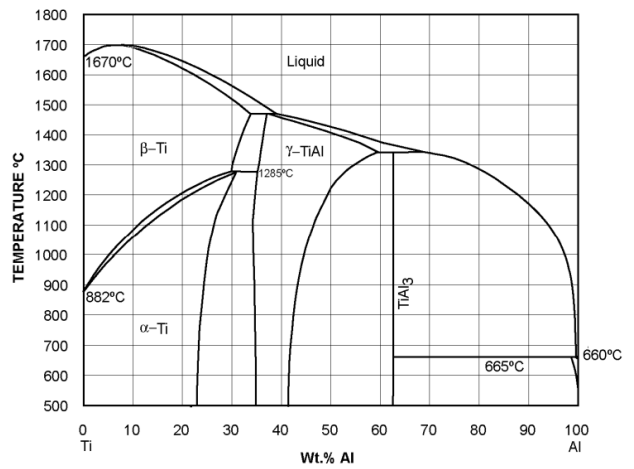
Copper-Tin (Cu-Sn)

Copper-Zinc (Cu-Zn)

23
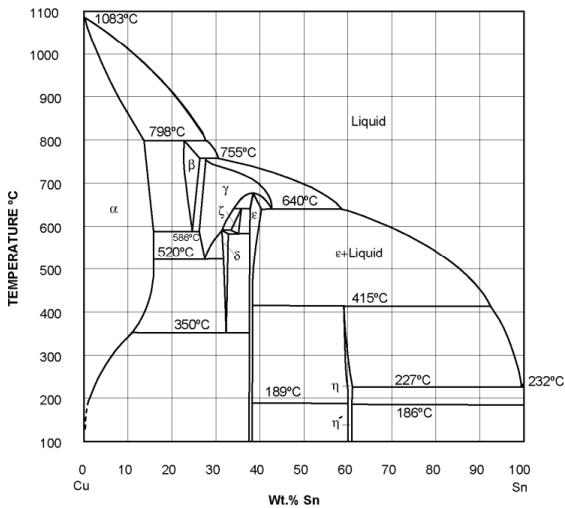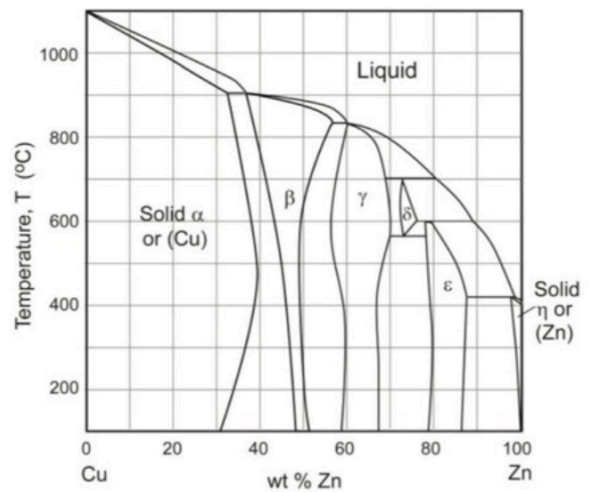
Manganese-Iron (Mn-Fe)
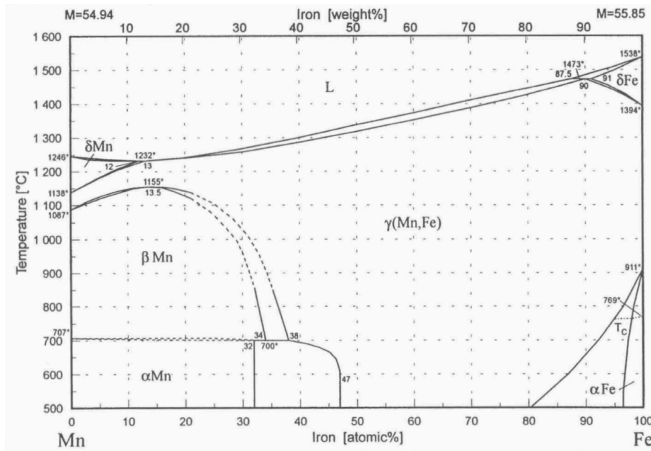
Silver-Strontium (Ag-Sr)
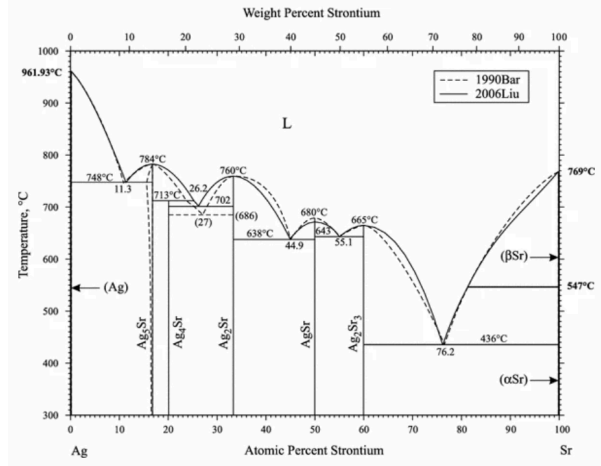
6.6.32. Binary Phase Diagrams Involving Non-Metals

* For a more detailed phase diagram for the iron-carbon system, see Section 6.6.15.

Iron-Carbon (Fe-C)*
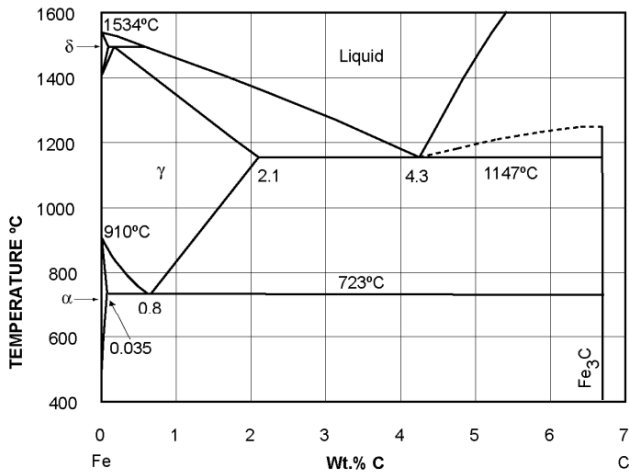
Aluminium-Silicon (Al-Si)
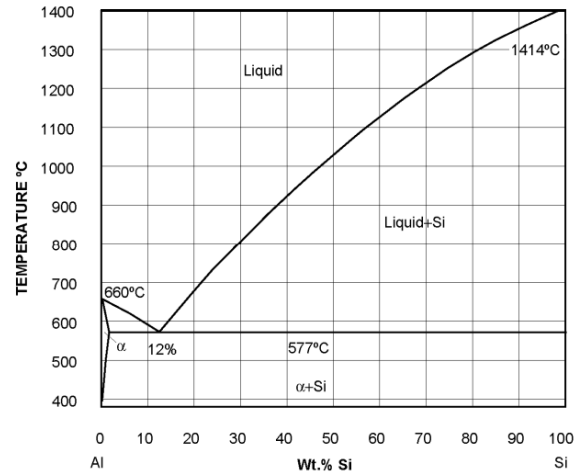
Silica-Alumina (SiO$_2$-Al$_2$O$_3$)
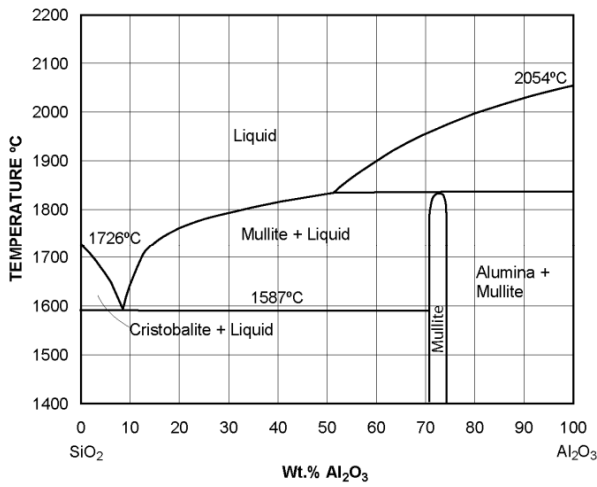
Copper-Antimony (Cu-Sb)
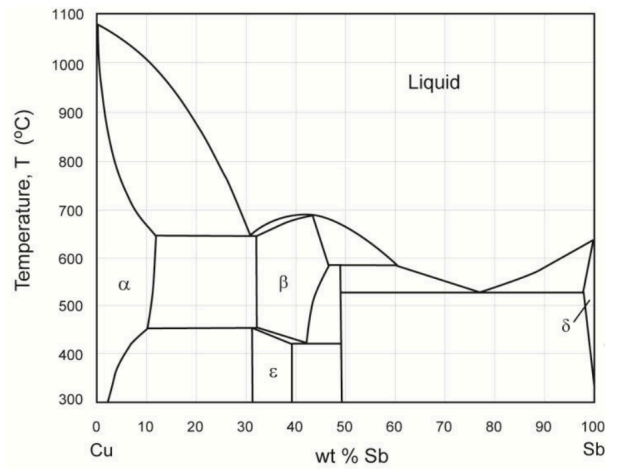
Iron-Silicon (Fe-Si)
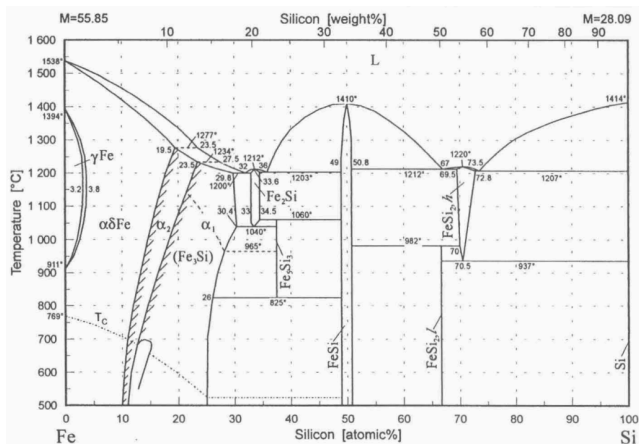
Manganese-Carbon (Mn-C)
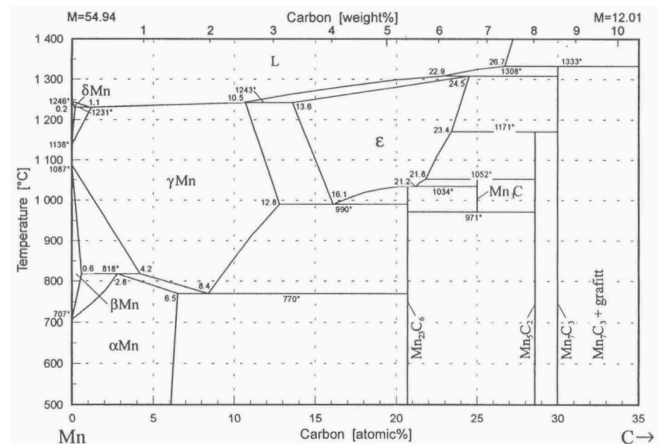
Manganese-Silicon (Mn-Si)
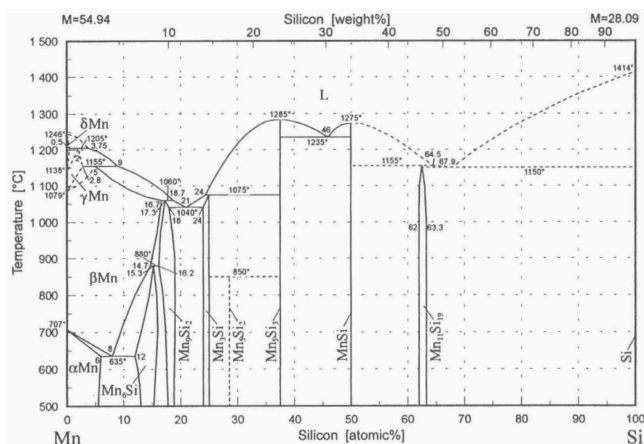
Silicon-Carbon (Si-C)
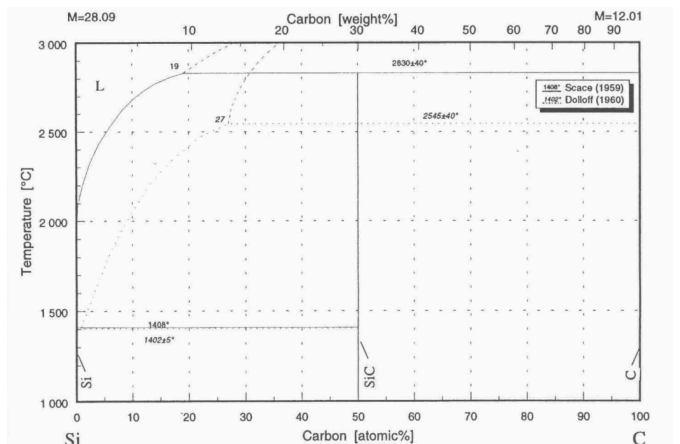
6.6.33. Equilibrium Microstructural Classification of Steels by Phase Composition

Phase diagram showing equilibrium microstructure, including the phases of pure Fe (ferrite (α, BCC), austenite (γ, FCC) and δ-iron (δ, BCC)), as well as ledeburite (fibrous α + Fe_3C), pearlite (lamellar α + Fe_3C) and cementite (Fe_3C). Compositions beyond cementite will form graphite (pure C), which are not shown.
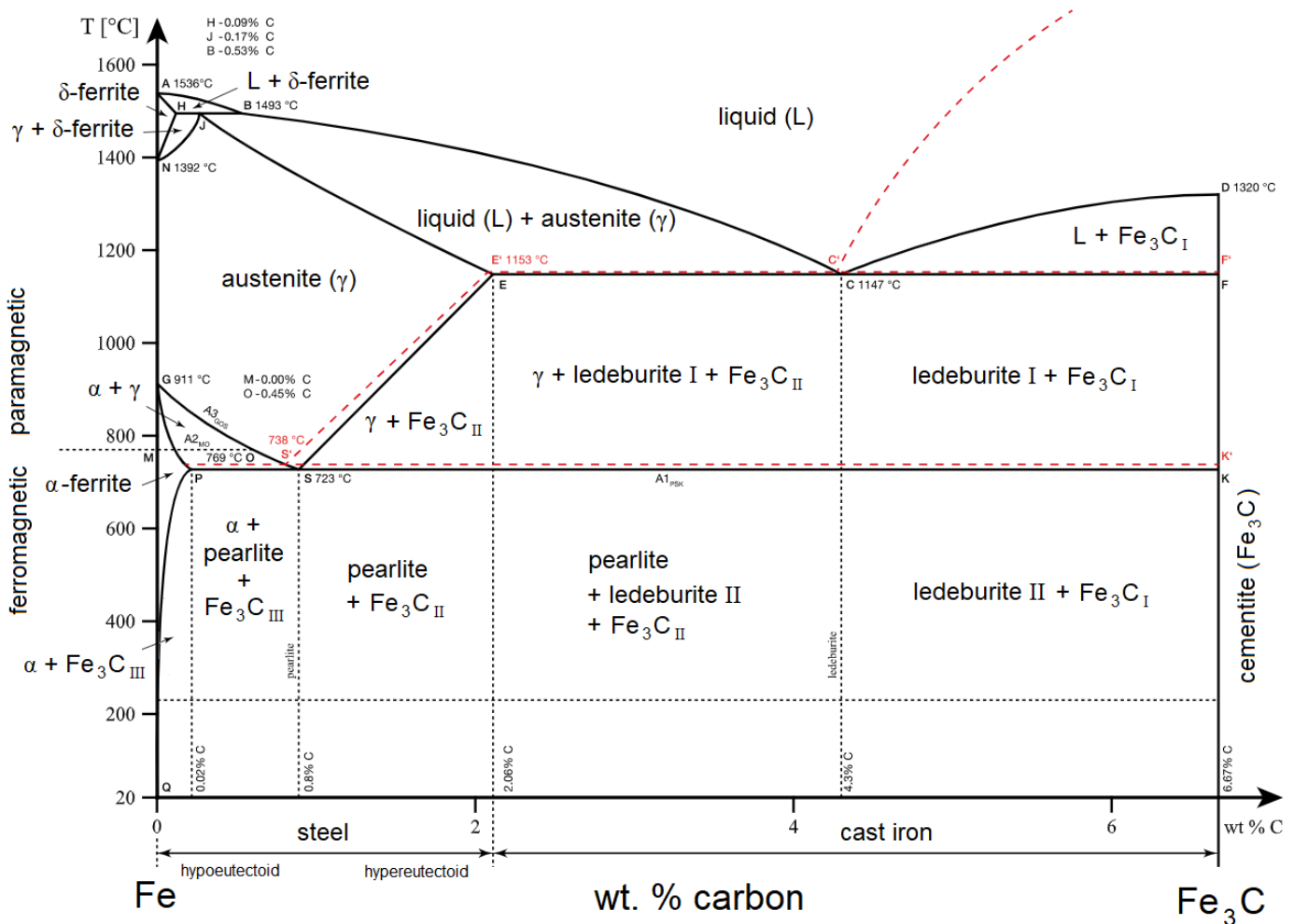
The key labelled points and lines on the above phase diagram are:

A: melting point of pure Fe   ABCD: liquidus line   AHJECF: solidus line
C: eutectic point (4.3%, 1147 °C)   J: peritectic point   M: Curie point of pure Fe
S: eutectoid point (0.8%, 723 °C)   An: arrest line   X': metastable equivalent

An equilibrium microstructure will be attained when the cooling rate from the melt is less than the critical cooling rate (CCR), which can be determined from a TTT diagram (Section 6.7.13.). Otherwise, a certain fraction of metastable bainite or martensite (quench to low temperature) will form, for which the transformations are shown by the red dashed lines.

6.6.34. Heat Treatment Data for Steels

1% nickel steel, BS 503M40 (En12):

TTT Diagram
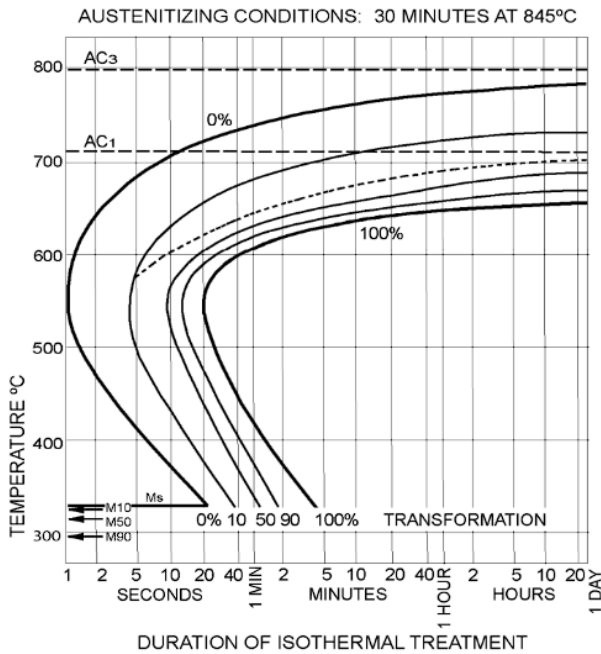
CCT Diagram
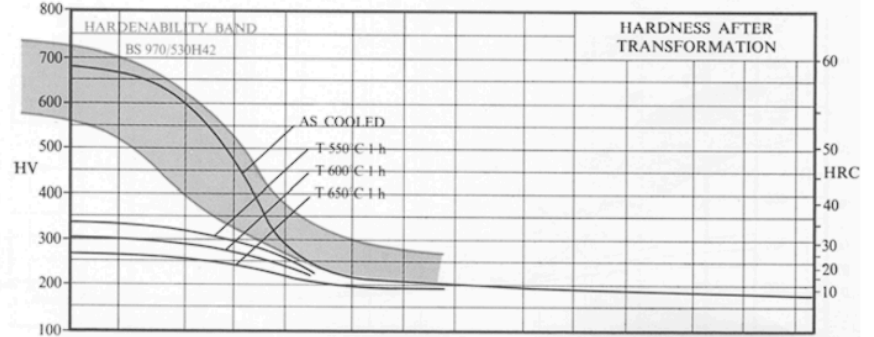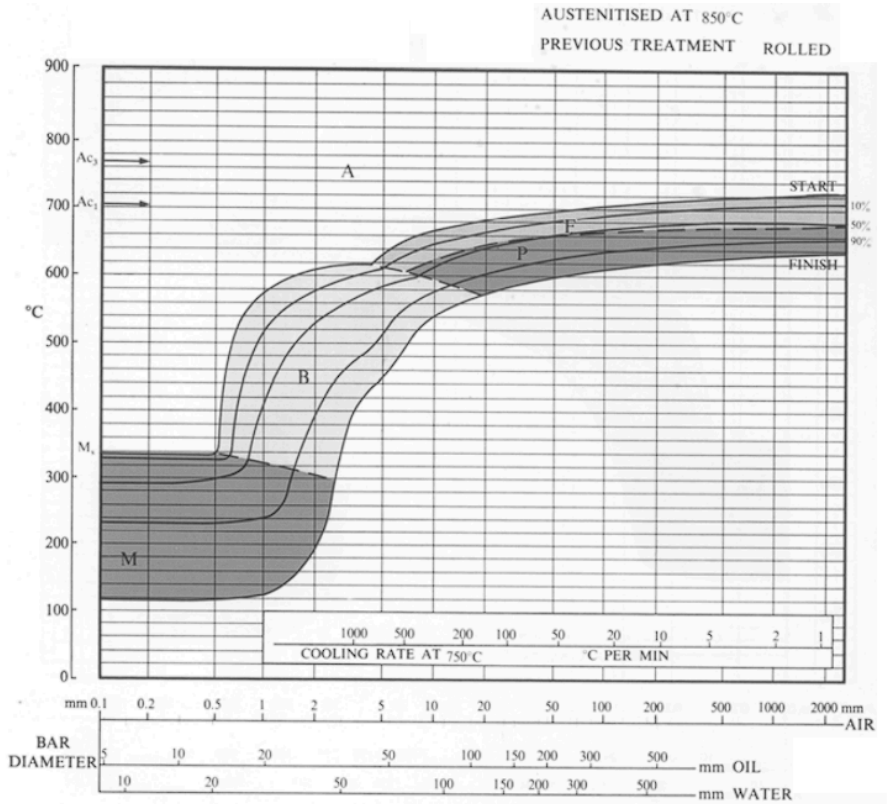
Jominy End-Quench Distance to Effective Diameter

Jominy End-Quench Hardenability Curves

- TTT diagram: AC_1 = eutectoid line, dotted curve = carbide line (where ferrite growth stops and pearlite growth begins).
- CCT diagram, zones A = austenite, F = ferrite, P = pearlite, B = bainite, M = martensite.
- Conversion: correlation between bar diameter (oil-quenched) and distance along Jominy bar which have equivalent cooling rates. Independent of steel type (i.e. also applies for En24 below).

1.5% Ni-Cr-Mo steel, BS 817M40 (En24):

TTT Diagram   ### CCT Diagram
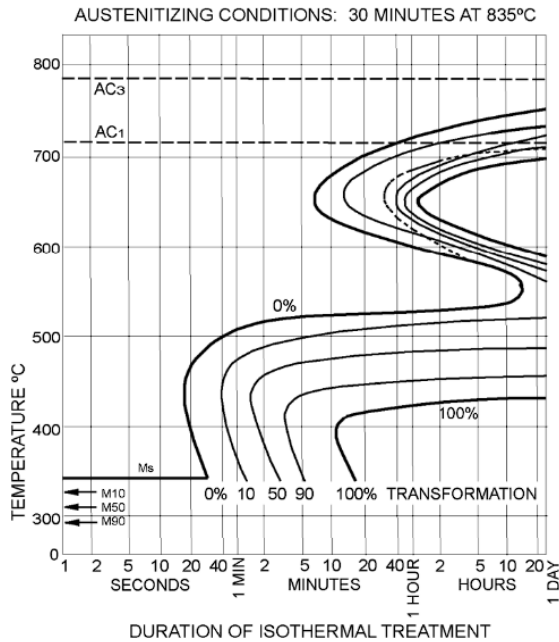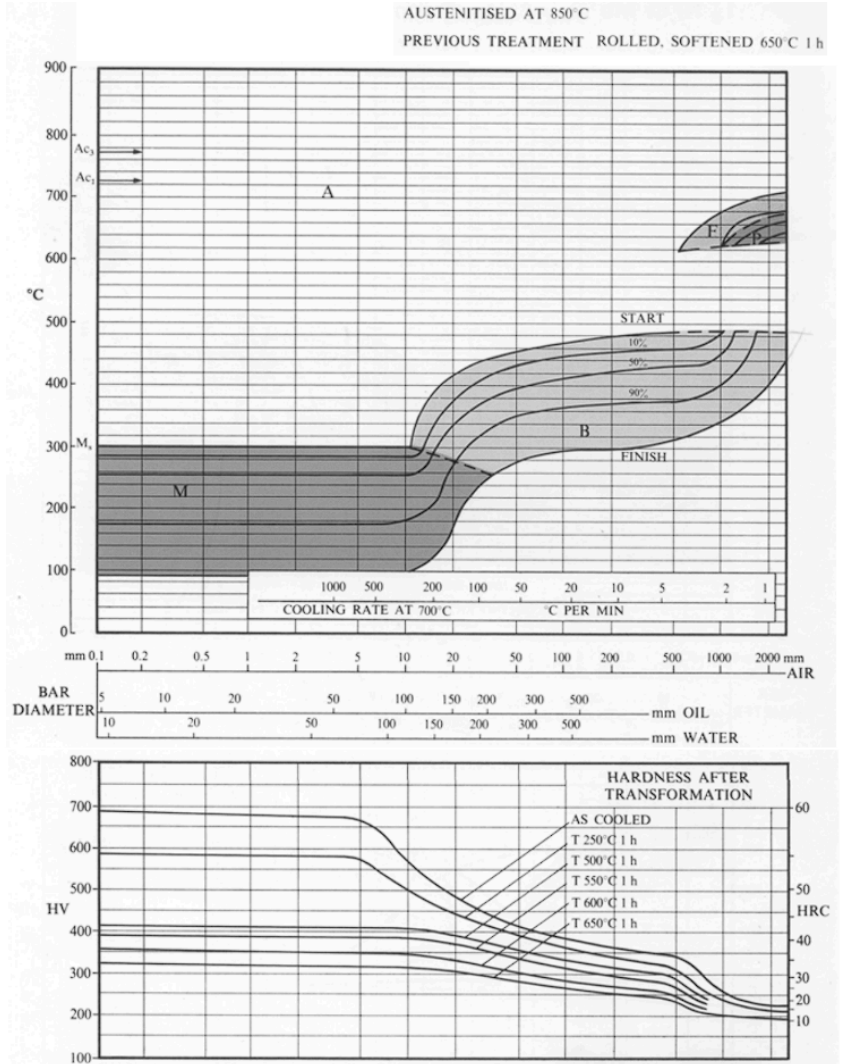
Jominy End-Quench Hardenability Curves

- TTT diagram: the lower set of C-curves correspond to precipitation of compounds with the alloyed metals rather than with carbon. AC_1 = eutectoid line, dotted curve = carbide line (where ferrite growth stops and pearlite growth begins).
- CCT diagram, zones A = austenite, F = ferrite, P = pearlite, B = bainite, M = martensite.

Equivalent Diameters for Standard Component Shapes
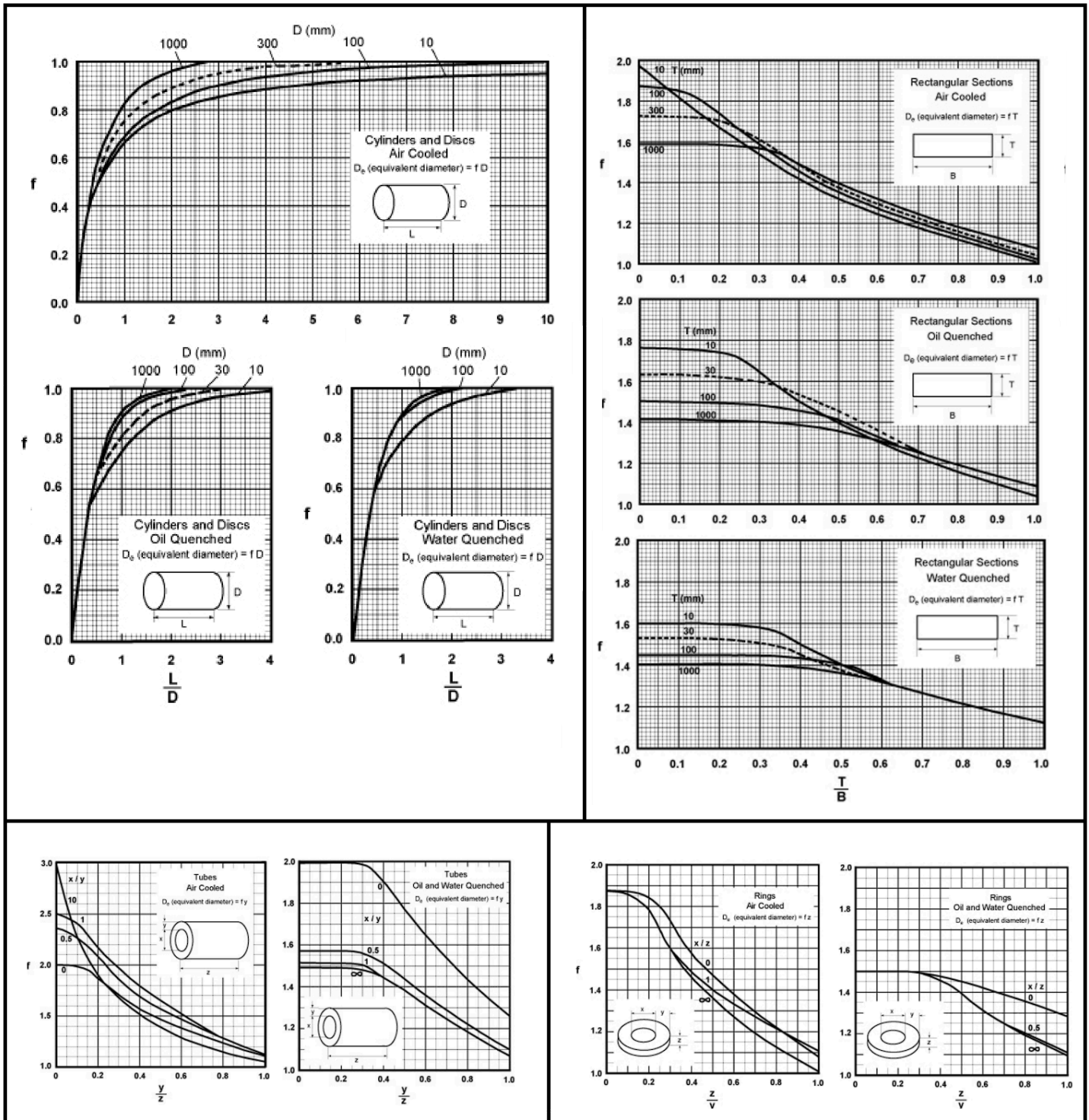
6.7. Sustainability and Energy Engineering

6.7.1. Quantification of Emissions and Economics of Power Systems

Metrics for Emissions: most energy systems release greenhouse gases to some extent

Global Warming Potential of a gas, $\text{GWP} = \dfrac{\int_0^{T_h} a_x\,[x]\,dt}{\int_0^{T_h} a_{CO_2}\,[CO_2]\,dt}$, for a specified time horizon T_h

(Normalised relative to CO_2. a_x: radiative efficiency of the gas, $[x]$: time-dependent abundance of the gas in the atmosphere.)

The CO_2 mass equivalent of a gas is its GWP at $T_h = 100$ years e.g. 1 kg CH_4 = 28 kg CO_2e.
Mass equivalent can also be written in tonnes e.g. 1 ton R-134a = 1.43 ktCO_2e.

Gas	Atmospheric lifetime (years)	GWP (T_h = 20 yrs)	GWP (T_h = 100 yrs) defines the CO_2 mass equivalent (CO_2e)
CO_2	>100	1	1
CH_4	12.4	84	28
N_2O	121	264	265
R-134a (CF_3CH_2F)	14	3830	1430

Economic Metrics for Energy Systems: important for making investment decisions

Capital expenditure costs (CapEx): pre-development costs (adjusted for research over time), construction costs, infrastructure costs

Operating expenditure costs (OpEx): fixed + variable operating costs, connections, carbon transport/storage, decommissioning, insurance, heat revenues, fuel prices, carbon costs

Expected generation: plant capacity, expected availability and efficiency, load factor

Net Present Value (NPV) of total costs [\$] $= \displaystyle\sum_{n=1}^{N_{periods}} \frac{CapEx_n + OpEx_n}{(1+r)^n}$ 　　　　(n: period e.g. year)

Net Present Value (NPV) of electricity generation [MWh] $= \displaystyle\sum_{n=1}^{N_{periods}} \frac{net\ electricity\ generated\ in\ period\ n}{(1+r)^n}$

(r: rate of discount e.g. real rate of inflation)

Levelised Cost of Electricity (life-cycle cost, LCOE) [\$ MWh^{-1}] $= \dfrac{NPV\ of\ total\ costs}{NPV\ of\ electricity\ generation}$,
the discounted lifetime cost of building, operating and decommissioning an energy generation system.

6.7.2. Climate Modelling

Simple 'one-tank' model: $\frac{dC}{dt} = k\left(E(t) - \frac{1}{\tau}\left(C(t) - C_{pre}(t)\right)\right)$

($C(t)$: carbon (**not** CO_2) content of the atmosphere, $E(t)$: carbon emissions from burning fossil fuels and cement production, $k \sim 0.5$: airborne fraction due to absorption into biosphere and ocean surface, $\tau \sim 200$ yrs: relaxation timescale due to mixing into deep ocean, $C_{pre} = 600$ GtC: pre-industrial level.)

6.7.3. Ashby Methodology for Sustainable Product Assessment

1. **Define and articulate** the objective, scale, and timing.
   (SMART goals: specific, measurable, achievable, relevant, time-bound.)

2. **Stakeholder analysis:** consider influence vs interest, and interactions between groups (Government, the public, local communities, owners, manufacturers, suppliers, trade unions, customers, lobbyists, investors, National press, managers, colleagues, team.)

3. **Fact-finding:** consider materials, environment, society, economics, legislation, energy.

4. **Synthesis:** the corporate 'triple bottom line' (natural, human & financial capital).

5. **Reflection:** is this a sustainable development?

6.7.4. Life-Cycle Assessment (LCA, Eco-Audit)

An LCA assesses the environmental impact of a product, considering e.g. CO_2 emissions, water consumption, energy consumption, at every stage, from mining the raw materials to disposing of the product after its useful lifetime.
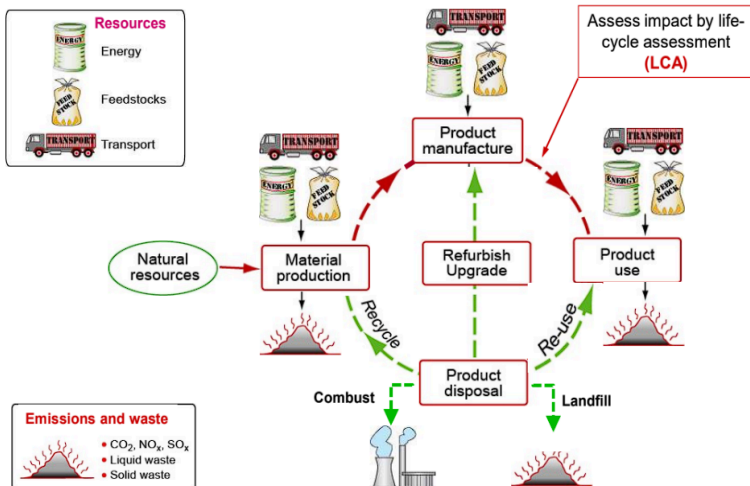
The metrics for environmental impact can be broken down into the stages of its lifecycle:

- **Materials:** minimise by materials selection, optimising for mass / embodied CO_2 / energy.
- **Manufacture:** minimise by choosing less energy-intensive materials processing
- **Transport:** minimise distance moved / lower energy modes of transport
- **Use:** minimise mass / thermal losses / electrical losses (max energy efficiency)
- **Disposal:** select non-toxic, recyclable materials

6.7.5. Improving the Sustainability of Existing Fossil-Fuel Power

Combined-cycle gas turbines (CCGTs) are the modern standard power station for burning natural gas, the least-polluting form of fossil fuel (other than hydrogen), achieving an efficiency of around ~60%. For the thermodynamics of CCGTs, see Section 7.2.8.
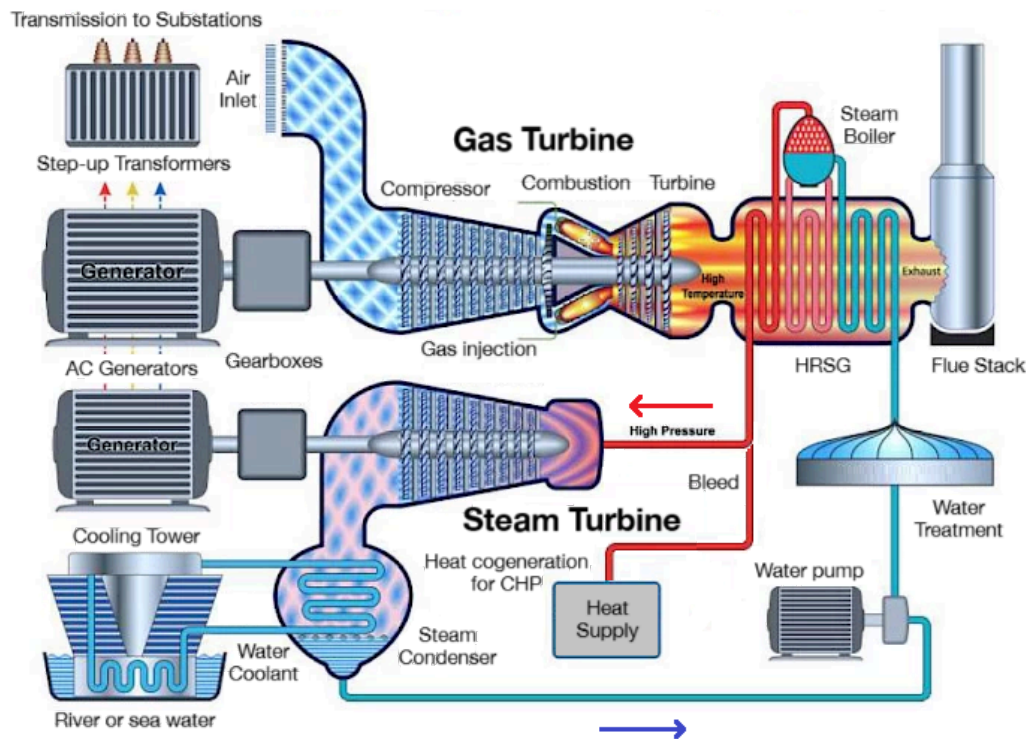
- **Superheating and reheating stages:** the steam cycle turbine can reach higher temperatures to increase turbine output power.

- **Combined heat and power (CHP):** heat can be extracted from any of the high-temperature points (e.g. HRSG outlet for hot steam, or pump outlet/coolant outlet for hot water) that can be sent directly to customers or used in thermal storage.

- **Carbon capture and storage (CCS)** from the flue output, removing some CO_2 at the expense of requiring some energy input.

- **Solid oxide fuel cells (SOFCs):** operate efficiently at high temperatures. They can generate extra electricity from supplied H_2 (waste heat utilisation) or from the gas supply (pre-combustion). Methane-fired plants can use steam-methane reforming (SMR) to convert CH_4 into H_2 for a SOFC.

- **Bioenergy with CCS (BECCS):** near-carbon-neutral biogas (~75% methane) as a natural gas source, with CCS for net-negative generation, with the possibility of SMR and SOFC cogeneration.

- **Further advances in turbomachinery (blade cooling, anti-creep ceramics):** can push turbine inlet temperatures higher, although there is only marginal room left for gains.

6.7.5. Solar Power Technologies (Solar PV, CSP)

Photovoltaic Cells (PV): conversion of sunlight to DC electricity using semiconductors

Electrical Circuit Analysis: solar cell modelled as a current source and diode with resistances
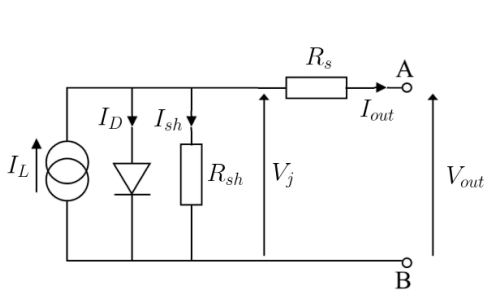
(I_L: luminous current, I_D: diode current, I_{sh}: leakage current, R_{sh}: shunt resistance, V_j: junction voltage, R_s: series resistance)

- Nodal analysis: $I_{out} = I_L - I_D - I_{sh}$; $V_j = V_{out} + I_{out} R_s$; $V_j = I_{sh} R_{sh}$
- Shockley diode equation: $I_D = I_0 \left[exp\left(\frac{eV_j}{nkT}\right) - 1 \right]$
- Open-circuit: $I_{out} = 0 \Rightarrow V_{out} = V_{OC} \approx \frac{nkT}{e} \, ln\left(\frac{I_L}{I_0} + 1\right)$ if $\frac{V_{out}}{R_{sh}} << I_L$
- Short-circuit: $V_{out} = 0 \Rightarrow I_{out} = I_{SC} \approx I_L$

Overall efficiency $= \frac{electrical\ power\ output}{light\ power\ input} = \frac{I\,[A] \times V\,[V]}{J\,[W\ m^{-2}] \times A\,[m^2]}$ (J: surface irradiance, A: normal absorbing area)

Fill factor $= \frac{P_{max}}{I_{SC} \times V_{OC}} = \frac{I_{max} \times V_{max}}{I_{SC} \times V_{OC}}$ (ideal operating point: load impedance $R = \frac{V_{max}}{I_{max}}$, for max power)

Factors affecting the light energy input include latitude, month of year, time of day, panel orientation relative to the Sun, cloud cover, reflections from environment, shading losses, dust accumulation. Maximum power point tracking (MPPT) is an online algorithm used to adjust the operating point by varying the duty ratio in a DC-to-DC converter, achieving maximum power in varying conditions.

Power production during the day follows a 'duck curve', with solar power meeting the bulk of daytime demand but not in the evening, where consumption is highest.

Solar water heating is a household alternative to gas-fired boilers using solar panels installed on a roof.

Traditional solar panels use the semiconductor silicon, in either polycrystalline or monocrystalline. Advances in functional materials (Section 8.6.10) has allowed for the use of thin-film materials (e.g. CdTe, CIGS), including use of multiple layers.

Shockley-Queisser limit: maximum single p-n junction solar-cell efficiency is ~33.16%.

Perovskite solar panels have shown to be highly efficient ($CsSnI_3$, ~31%) while being easy to manufacture. Organic hybrid perovskites (e.g. $CH_3NH_3PbX_3$) for PV cells are under research, especially lead-free organic perovskites. Control over the photonic properties (e.g. anti-reflection, scattering) can further improve efficiency.

Concentrated Solar Power (CSP): mirrors reflect sunlight to produce heat.

The sunlight over a large area is focussed by parabolic mirrors and/or Fresnel lenses to generate heat, which can be used as the heat input to a steam turbine (Section 7.2.12) or to a reverse heat engine (refrigerator e.g. space cooling). It can also complement high-temperature energy processes such as molten salt battery storage with e.g. calcium potassium nitrate for night-time power generation (Section 13.5.13) or cogeneration schemes (CHP).

6.7.5. Wind Power Technologies (HAWT, VAWT, Offshore)

Good sites for large land-based wind turbines are at the top of gentle hills, where turbulent downstream eddy formation is minimised. The tops or bottoms of sharp cliffs are unsuitable, and the turbine should be a distance at least $10h$ away from any obstacles of height h, and taller than h.

Simple Model of Wind Turbine Aerodynamics
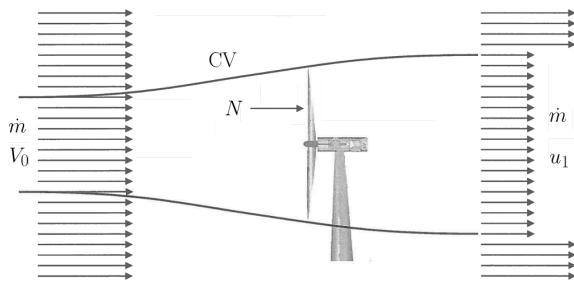
(CV: axisymmetric control volume following stream lines, $\dot{m}$: air mass flow rate, V_0: upstream velocity, u_1: downstream wake velocity, N: force on rotors, u: velocity at rotors, A: rotor area)

- Pressure drop across turbine: $\Delta p = \frac{1}{2}\rho(V_0^2 - u_1^2)$ (Bernoulli)
- Rotor force: $N = \Delta p\, A = \rho A u(V_0 - u_1)$ (SFME)
- Axial induction factor: a, where $u_1 = (1 - 2a)V_0$ ($0 < a < \frac{1}{2}$)
- Power developed: $P = Nu = 2\rho V_0^3 a(1 - a)^2 A$

- Available power in flow: $P_{max} = \frac{1}{2}\dot{m}V_0^2 = \frac{1}{2}\rho A V_0^3$.

- Power coefficient: $C_P = \frac{P}{P_{max}} = 4a(1 - a^2)$, maximised at $a = \frac{1}{3}$, $C_P = 59\%$ (Betz efficiency limit)

- Capacity factor: $\dfrac{total\ energy\ generated\ in\ reality}{maximum\ possible\ energy\ generated} = \dfrac{\sum_i min\left\{2\rho a(1 - a)^2 A(V_{0i})^3, P_{gen}\right\} \times t_i}{P_{gen}}$

(P_{gen}: generator power rating, t_i: fraction of total time where wind speed is V_{0i} (sum over buckets))

Additional loads are due to centrifugal force and self-weight. These are cyclic (periodic) with frequency $f = \frac{\omega B}{2\pi}$ (fatigue inducing: Section 6.6.6). Storm loading should also be considered. Wind loading is often modelled using the Wisper spectrum and generalisations to Miner's rule for fatigue modelling.

Wind Turbine Blade Design

For an aerodynamic analysis of wind turbines, see Section 7.2.17.

Wind turbines exploit electromagnetic induction, using AC generators (Section 8.4.11). The prime mover achieves high rpm by coupling with a gearbox in the housing.

The magnets used in wind turbines use rare-earth elements (Dy, Nd, Pr) which are critical materials, threatening the supply chains for their large-scale manufacture.

Horizontal axis wind turbines (HAWTs) can be fitted with anemometers and yaw controllers to face the oncoming wind at all times, improving the capacity. This requires some additional power to overcome the dynamic inertial forces (Coriolis force/gyroscopic torque) acting on the blades.

Offshore Wind Farms

Offshore wind farms experience higher wind speeds and therefore greater efficiencies than those on land. They also have less impact on the landscape view and land usage, helping to reduce opposition due to NIMBYism.

Vertical axis wind turbines (VAWTs) are a more convenient construction, but with lower efficiency.

(V_0: upstream speed, A: turbine swept area, ρ: fluid density, θ: local twist angle of blade, ω: blade angular speed, $\sigma = \frac{cB}{2\pi r}$: rotor solidity, B: number of blades, c: chord length, $a = 1 - \frac{U}{V_0}$: axial induction factor, r: radial position)

Flow angle: $\tan \phi = \frac{(1-a)\,V_0}{(1+a')\,\omega R}$ Local angle of attack: $\alpha = \phi - \theta$

Lift and drag coefficient (below stall): $C_L \approx 2\pi\alpha$ $C_D \approx$ const. (for $\alpha < 15°$; using radians)

Relative velocity: $V_{rel}^2 = V_0^2(1-a)^2 + r^2\omega^2(1+a')^2$

Force coefficients: $C_N = \frac{F_N}{\frac{1}{2}\rho V_{rel}^2 c} = C_L \cos\phi + C_D \sin\phi$ $C_T = \frac{F_T}{\frac{1}{2}\rho V_{rel}^2 c} = C_L \sin\phi - C_D \cos\phi$

Induction factors: axial: $a = \dfrac{1}{1 + \frac{4\sin^2\phi}{\sigma C_N}}$ angular: $a' = \dfrac{1}{1 + \frac{4\sin\phi\cos\phi}{\sigma C_N}}$

Tip speed ratio: $\lambda = \frac{\omega R}{V_0}$

Aerodynamic loads: blade element forces/torques (BEM):
$$\delta N = 4\pi r\rho V_0^2 a(1-a)\,\delta r, \quad \delta T = 4\pi r^3 \rho V_0(1-a)\omega a'\,\delta r$$

Total power: $P = \omega T = \omega \int_{r_0}^{R} \delta T = \omega B \int_{r_0}^{R} r\,F_T\,dr$

Available power: $P_{av} = \frac{1}{2}\rho A V_0^3$

Power coefficient: $C_P = \frac{P}{P_{av}} = \frac{P}{\frac{1}{2}\rho A U^3} = 4a(1-a^2)$ ($a = 1 - \frac{U}{V_0}$: axial induction factor)

Betz limit: $C_{P,max} = \frac{16}{27} \approx 59\%$ when $a = \frac{1}{3}$.

Capacity factor: $\dfrac{energy\ generated\ over\ a\ long\ time}{rated\ power \times time}$, a measure of installation effectiveness.

6.7.6. Nuclear Fission Technologies

6.7.7. Nuclear Fusion Technologies

6.7.8. Geothermal Energy Technologies

6.7.9. Bioenergy Technologies

Plants and other biomass remove CO_2 from the atmosphere during their life due to photosynthesis, making plants a carbon sink by storing the carbon as carbohydrates.

When the biomass is burned, they release the CO_2 again, producing bioheat which can be used to produce electricity. This process is approximately carbon neutral, with some net operational emissions. Biomass can also be used to form biogas (by methanisation, Section 14.3.2), biofuel (by fermentation into bioethanol, Section 17.3.2) and biochar (by phytomining/pyrolysis, Section 15.1.5). When combined with carbon capture and storage (BECCS), the system becomes carbon negative.

Biofuel cells use enzymes or immobilised bacteria to carry out redox reactions that generate electricity. Glucose biofuel cells (Section 13.5.12) can act on the carbohydrates in plants. Nitrogenase bioelectrocatalysis cells are under research to cogenerate ammonia and hydrogen from atmospheric nitrogen gas: $N_2 + 8\ H^+ + 8\ e^- + 16\ ATP \rightarrow 2\ NH_3 + H_2 + 16\ ADP + 16\ P_i$. Genetic engineering can be used to optimise the enzymes and microorganisms operating in these processes e.g. directed evolution (Section 17.4.5) of the RuBisCo enzyme for photosynthesis.

6.7.9. Hydropower Technologies (Hydroelectric, Tidal Barrage, Wave Power)

6.7.10. Energy Storage

Pumped-Storage Hydroelectricity

Compressed Air Energy Storage

An improvement under research is adiabatic CAES.

Batteries and Supercapacitors

Molten salt batteries (Section 13.5.13) and redox flow batteries (Section 13.5.14).

These are dispatchable and fast-responding to varying grid demands.

These technologies are typically installed at grid-scale in battery energy storage systems (BESS). Currently, BESS primarily uses lithium-ion batteries.

Superconducting Magnetic Energy Storage (SMES)

Carbon Capture and Storage

Removal of CO_2 from gas supplies or exhausts is typically done by chemisorption. CO_2 dissolves in an alkaline solution to form carbonate precipitates which can be removed as solids. CCS requires energy input for compression and liquefaction which reduces the energy output of an attached power plant.

6.7.11. Renewable Heat Technologies

Heat Pumps:

Air-source heat pumps

Passive Daytime Radiative Cooling (PDRC): zero-input alternative to refrigeration/air-con.

PDRCs use thermally emissive materials to form a radiator with high performance. It is considered a type of geoengineering as it increases the thermal radiation emitted from the Earth, by emitting in the longwave IR range (through the infrared window). It can help to combat the urban heat island effect in dense cities.

PDRC systems can be coupled with thermoelectric generators that exploit the resulting temperature gradient to produce electricity.

Passive Solar Building Design:

Buildings can use Trombe walls which act as thermal capacitors, storing heat in the day and radiating it inside at night. The insulation material for the Trombe wall must have low thermal conductivity, such as nanoporous silica aerogel.

P7. THERMOFLUID MECHANICS

7.1. Fluid Mechanics

7.1.1. Hydrostatic Pressure

Pressure difference due to a column of liquid: $\Delta p = \rho g\, \Delta h$.

The equivalent resultant force per unit width on the wall of the container due to this triangular pressure distribution is

$$F = \int_0^h \rho g x\, dx = \frac{1}{2}\rho g h^2 \text{ acting at a depth } h^* = \frac{2}{3}h \text{ below the free surface.}$$

7.1.2. Buoyancy

For a body of volume V completely submerged in a fluid of density ρ_f, the buoyant (upthrust) force is given by $F = \rho_f V g$. This is equal to the weight of the displaced fluid. For a body partially submerged to a depth $h(x, y)$ which varies over an area of fluid, the distributed buoyancy pressure $p(x, y)$ is given by $p = \rho_f h g$, normal to the body surface.

7.1.3. Radial Pressure Gradient on Curved Streamlines

An infinitesimal fluid parcel at a point on a curved streamline experiences radial pressure gradients due to centrifugal force.

The pressure gradient **normal** to a streamline with a radius of

curvature R is given by $\quad \dfrac{dp}{dn} = \dfrac{\rho V^2}{R} = \kappa \rho V^2 \quad$ (κ: curvature)

There is low pressure at the centre of the bend, increasing outwards.
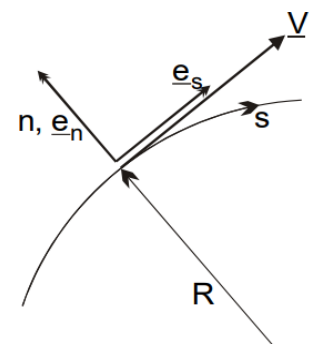
7.1.4. Surface Tension, Excess Pressure and Capillary Action

Surface Tension: force per unit length in the plane of the liquid surface.

- Surface energy (excess potential energy per liquid surface area): $\Delta E = \gamma \, \Delta A$
  (γ [N/m or J/m²]: surface tension.

- For a liquid-solid interface, a meniscus forms with contact angle θ and interfacial pressure p_i:
  - Adhesion > cohesion (wettable): $0° < \theta < 90°$, convex meniscus, pressure $p_l = p_\infty - \frac{2\gamma}{x}$.
  - Adhesion < cohesion (hydrophobic): $90° < \theta < 180°$, concave meniscus, pressure $p_l = p_\infty + \frac{2\gamma}{x}$.
  - Adhesion = cohesion: $\theta = 90°$, flat meniscus, pressure $p_l = p_\infty$.

- Surface tension for liquids drops to zero at the critical temperature, decreasing linearly at other T.

Internal Excess Pressure: pressure change across interface

- Excess pressure in a liquid drop or bubble of radius r: $p_{in} - p_\infty = \frac{2\gamma}{r}$ (Young-Laplace equation)

- Excess pressure a film bubble (e.g. soap bubble): $p_{in} - p_\infty = \frac{4\gamma}{r}$ (two free surfaces)

Capillary action: excess pressure can do work against gravity

- Height ascended in capillary tube: $\Delta h = \frac{2\gamma \cos\theta}{x\rho g} = \frac{2\gamma}{r\rho g}$
  (ρ: density, x: tube radius, r: radius of curvature of meniscus)

- Net vertical reaction force on tube: $F = 2\pi x\gamma$

- Tube of insufficient length to accommodate ascent: meniscus reshapes to curvature $r' = \frac{\Delta h \, r}{L}$. The tube will not overflow.

convex meniscus   concave meniscus
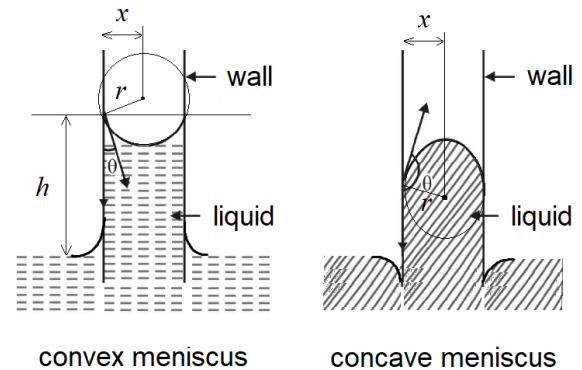
Floating Bodies with Surface Tension

Partially submerged bodies experience surface tension at their wetted perimeter. If $\theta > 90°$ (hydrophobic) then the effective buoyancy increases (more weight can be supported without sinking). If $\theta < 90°$ (wettable) then buoyancy is weakened.

For a **spherical** body in a fluid, force balance gives:

$$\underbrace{\frac{4}{3}\rho_s\pi R^3 g}_{\text{sphere weight}} = (\underbrace{\frac{2}{3}\pi R^3}_{\text{submerged volume}} + \underbrace{\pi R^2(R+h)}_{\text{displaced volume}})\rho_f g - \underbrace{2\pi R\gamma\cos\theta}_{\text{surface tension}}$$
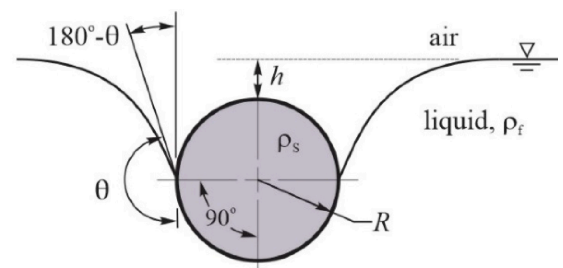
For a **long horizontal cylindrical** body in a fluid, force balance (per unit length) gives:

$$\underbrace{\rho_s\pi R^2 g}_{\substack{\text{cylinder} \\ \text{weight}}} = (\underbrace{\frac{1}{2}\pi R^2}_{\substack{\text{submerged} \\ \text{volume}}} + \underbrace{2R(R+h)}_{\substack{\text{displaced} \\ \text{volume}}})\rho_f g - \underbrace{2\gamma\cos\theta}_{\substack{\text{surface} \\ \text{tension}}}$$

143

7.1.5. Conservation of Energy along Streamlines

Bernoulli's Equation for incompressible inviscid steady flow along a streamline (irrotational flows):

$$p + \frac{1}{2}\rho V^2 + \rho g z = C = \text{constant} \quad \text{(fluid mechanical energy per unit volume)}$$

static pressure + dynamic pressure + hydrostatic pressure = total pressure (total)

The 'head' is related to the pressure by $H = \frac{p}{\rho g}$ and has units of length ('effective height').

Head gain/loss due to external work (e.g. pump: $W_x > 0$, turbine: $W_x < 0$) $= \dfrac{\dot{W}_x}{Q}$.
(W_x': external power input to flow, Q: volumetric flow rate).

Bernoulli's equation is not Gallileian invariant, since flow steadiness may depend on the reference frame.

Application of Bernoulli's equation: pipe flow with sources and resistances.

Conservation of energy:
$$C_{out} - C_{in} = p_{input} - p_{loss}$$
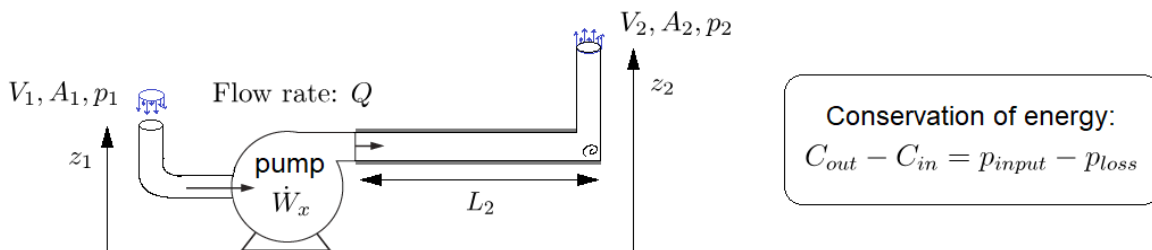
$$\underbrace{p_1 + \frac{1}{2}\rho\left(\frac{Q}{A_1}\right)^2 + \rho g z_1}_{\text{total pressure in, } C_{in}} + \underbrace{\frac{\dot{W}_x}{Q}}_{\text{pump}} = \underbrace{p_2 + \frac{1}{2}\rho\left(\frac{Q}{A_2}\right)^2 + \rho g z_2}_{\text{total pressure out, } C_{out}} + \underbrace{4c_f \frac{L_2}{d_2}\frac{1}{2}\rho\left(\frac{Q}{A_2}\right)^2}_{\text{pipe friction loss}} + \underbrace{\frac{\mu L_2 Q}{2\pi d_2^4}}_{\text{viscous loss}} + \underbrace{\frac{1}{2\rho}\left(\frac{Q}{C_d A_2}\right)^2}_{\text{corner loss}}$$

7.1.6. Viscosity and Reynolds Number

- Interfacial shear stress: $\tau = \mu \dfrac{dV}{dy}$ (μ: dynamic viscosity, $\dfrac{dV}{dy}$: transverse velocity gradient
- Newtonian fluid: μ is independent of shear rate.
- Kinematic viscosity: $\nu = \dfrac{\mu}{\rho}$ (ρ: fluid density)
- Reynolds number: $Re_d = \dfrac{\rho V d}{\mu}$ (d: characteristic length dimension)
- Laminar flow for Re < 2000; turbulent flow for Re > 4000; transitional flow for 2000 < Re < 4000

- Stokes' law (drag on sphere; x: diameter, V: relative speed; in creeping flow ($Re_x < 0.3$)):
- Non-dimensional form (C_D: drag coefficient, Re_x: Reynolds number): $C_D = \dfrac{24}{Re_x}$ ($F_{drag} = \frac{1}{2} C_D \rho_f A V^2$)

  (ρ_f: fluid density, ρ_p: particle density, A: projected cross-sectional area normal to flow)
- Viscous torque on a rotating sphere: $Q_{drag} = \pi x^3 \mu \omega$ (in the direction $-\omega$)

- Terminal velocity accounting for viscosity and buoyancy: $U_T = \dfrac{x^2(\rho_p - \rho_f)g}{18\mu}$

7.1.7. Fluid Dynamics of Control Volumes

A control volume is that region of space that is enclosed by a rigid control surface. For steady-flow, conditions within the control volume are not changing (on average) so that the mass, momentum, energy and entropy within the control volume remain constant.

- Volumetric flow rate: $\quad Q = \displaystyle\oiint_{cs} \mathbf{v} \cdot d\mathbf{A} \quad$ (volume of fluid crossing CS per unit time)

- Mass flow rate: $\quad\quad \dot{m} = \rho Q \quad\quad\quad$ (mass of fluid crossing CS per unit time)

For an incompressible flow, both m' and Q are conserved across a CV.

Conservation of Mass (the Continuity Equation):

$$\underbrace{\frac{\mathrm{d}}{\mathrm{d}t} \iiint_{cv} \rho\, dV}_{\text{internal change}} + \underbrace{\oiint_{cs} \rho\mathbf{v} \cdot d\mathbf{A}}_{\text{mass flow}} = 0 \quad\Leftrightarrow\quad \frac{\mathrm{d}m_{cv}}{\mathrm{d}t} + \sum_{\text{out}} \dot{m} - \sum_{\text{in}} \dot{m} = 0$$

For steady flow, $\mathrm{d}m_{cv}/\mathrm{d}t = 0$, so that the sum of mass flows in and out are equal.

Conservation of Momentum (the Steady Flow Momentum Equation, SFME):

$$\underbrace{\frac{\mathrm{d}}{\mathrm{d}t} \iiint_{cv} \rho\mathbf{v}\, dV}_{\text{internal change}} + \underbrace{\oiint_{cs} \rho\mathbf{v}\,\mathbf{v} \cdot d\mathbf{A}}_{\text{momentum flow}} = \underbrace{\mathbf{F}}_{\substack{\text{external} \\ \text{forces}}} - \underbrace{\oiint_{cs} p\, d\mathbf{A}}_{\text{pressures}}$$

(d$\mathbf{A}$: area normal element, oriented positive out of the CV, $\mathbf{F}$: non-pressure forces on flow)

For steady flow, the 'internal change' term is zero. $\quad \sum \dot{m}_{out} V_{x,out} - \sum \dot{m}_{in} V_{x,in} = \sum F_x + \left(\sum pA\right)_x$

In scalar component form in Cartesian coordinates: $\quad \sum \dot{m}_{out} V_{y,out} - \sum \dot{m}_{in} V_{y,in} = \sum F_y + \left(\sum pA\right)_y$

7.1.8. Navier-Stokes Equations and Euler Equations

For viscous unsteady flow of an incompressible fluid, the velocity profile $\mathbf{V}$ satisfies

$$\nabla \cdot \underline{V} = 0 \qquad\qquad \rho\left(\frac{\partial \underline{V}}{\partial t} + \underline{V} \cdot \nabla \underline{V}\right) = -\nabla p + \rho \underline{g} + \mu \nabla^2 \underline{V}$$

(p: static pressure scalar field, $\mathbf{g}$: gravity vector field, $\mathbf{V} \cdot \nabla$: advection operator, ∇^2: vector (component-wise) Laplacian operator.)

If gravity and viscosity are neglected (inviscid flow) from the Navier-Stokes equation, this simplifies to the Euler equations: $\qquad \nabla \cdot \mathbf{V} = 0 \quad$ and $\quad \rho\dfrac{\partial V}{\partial t} + \rho\mathbf{V} \cdot \nabla \mathbf{V} = -\nabla p$

7.1.9. Drag Coefficient for Rough Spheres and Non-Spherical Bodies

Sphericity of an irregular particle: $\psi = \dfrac{A_s}{A_p} = \dfrac{6V_p}{x_p A_p} = (36\pi)^{1/3}\dfrac{V_p^{2/3}}{A_p}.$

(A_s: surface area of a sphere with the same volume as the particle,
A_p: surface area of the particle, $x_p = x_{SV}$: equivalent diameter of the particle.)

Sphere: $\psi = 1$; Ellipsoid (2:1:1): $\psi = 0.929$; Cube: $\psi = 0.806$; Torus (2:1): $\psi = 0.710$, Tetrahedron: $\psi = 0.671$.

Sphere relative surface roughness: $\dfrac{\varepsilon}{D}$ (ε: rms surface roughness amplitude, D: diameter)
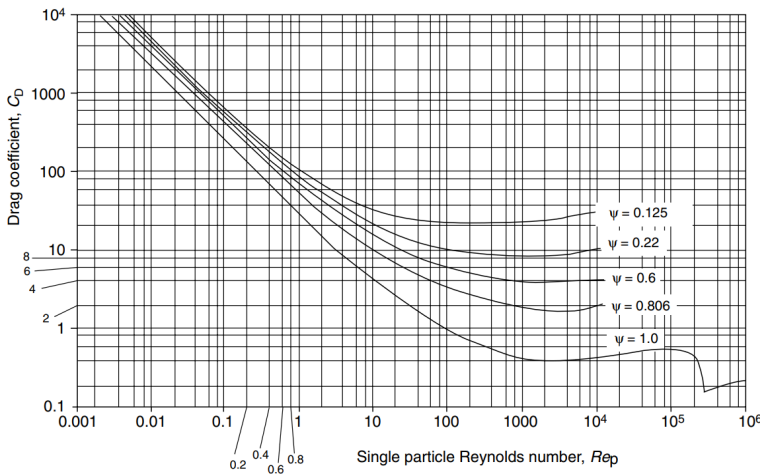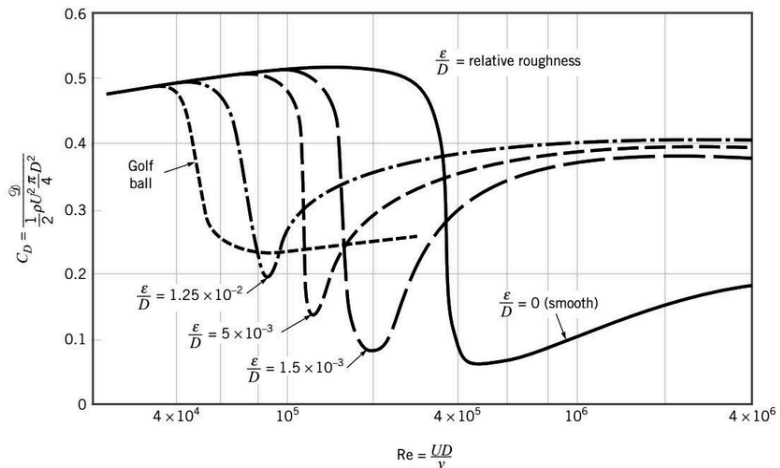
Non-Spherical Bodies: $C_D = f(\mathrm{Re}, \psi)$ **Rough Spherical Bodies:** $C_D = f(\mathrm{Re}, \dfrac{\varepsilon}{D})$

To determine terminal velocity U_T for a given particle size x,

$$C_D\, Re_p^2 = \frac{4x^3 \rho_f(\rho_p - \rho_f)g}{3\mu^2}$$ (straight line of gradient -2 on log-log plot)

To determine particle size x for a given terminal velocity U_T,

$$\frac{C_D}{Re_p} = \frac{4\mu(\rho_p - \rho_f)g}{3 U_T^3 \rho_f^2}$$ (straight line of gradient +1 on log-log plot)

where $Re_p = \dfrac{\rho_f U_T x}{\mu}$ and ρ_p is the density of the particle.

146

7.1.10. Frictional Losses in Pipes

The pressure drop along a pipe of constant diameter d and length L, with viscous flow is

$$\Delta p = 4c_f \frac{L}{d}\frac{1}{2}\rho V^2 = f \frac{L}{d}\frac{1}{2}\rho V^2$$

where c_f is the (Fanning) 'friction coefficient' and f is the (Darcy) 'friction factor'.

If the rms surface roughness of the pipe is ε then f is found from the Moody diagram:
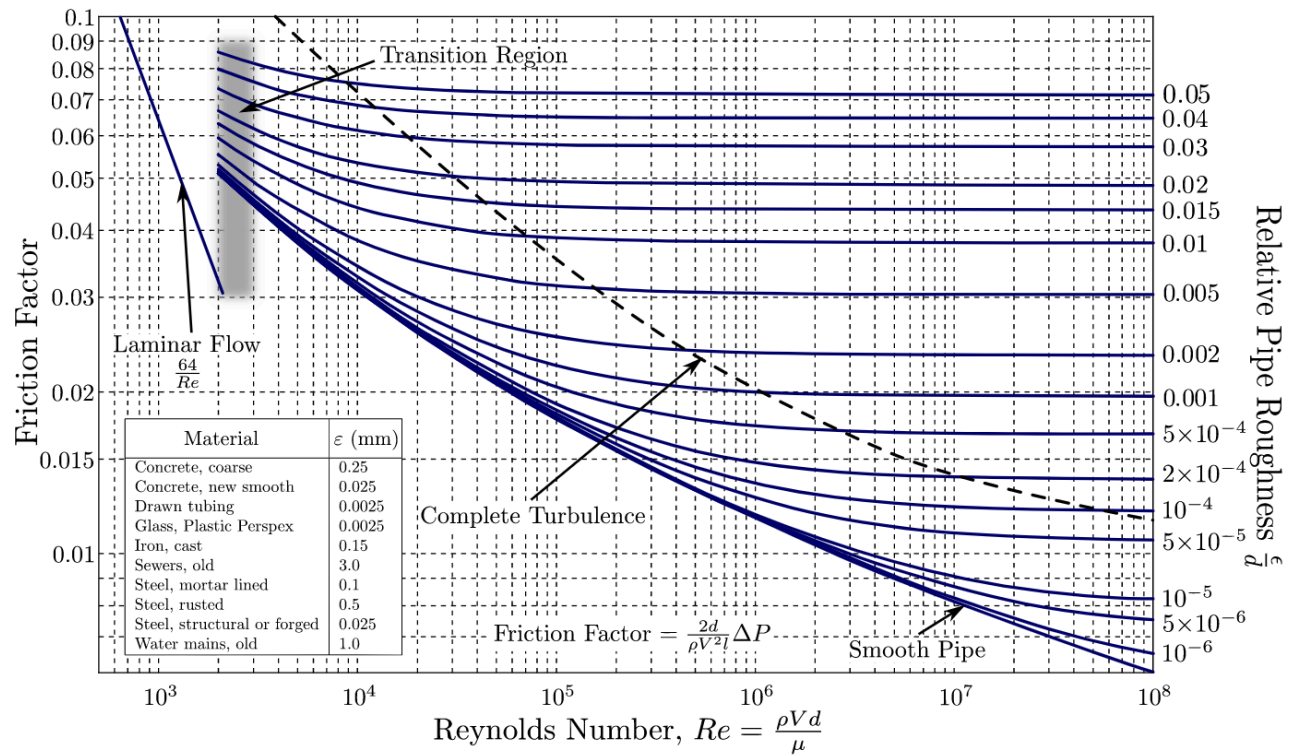
Laminar regime: $f = \dfrac{64}{Re}$ \qquad (Poiseuille's law, dimensionless form)

Turbulent regime: $f^{-1/2} = -2\log_{10}\left(\dfrac{\varepsilon/d}{3.7} + \dfrac{2.51}{Re \times f^{1/2}}\right)$ \qquad (Colebrook equation, implicit)

7.1.11. Flow Through Orifices, Weirs and Open Channels

Orifice Flow: a plate with a small hole placed into the flow to reduce the pressure.

For flow through an orifice plate, $Q = \dfrac{C_d}{\sqrt{1 - \beta^4}} \cdot \epsilon A \cdot \sqrt{2\rho\,\Delta p}$

(Q: volumetric flow rate, C_d: discharge coefficient, $\beta = \dfrac{d_{orifice}}{d_{pipe}}$: diameter ratio, A: orifice area, ε: expansibility factor, ρ: fluid density, Δp: pressure drop across plate)

Values of the discharge coefficient C_d for various plate geometries are given.

Sharp Edge $C_d = 0.60$, Round Edge 0.97, Short Pipe 0.82, Reentrant 0.72, Converging depends on angle. See curve at right.

Orifices and Nozzles Discharging from Plenum. Coefficient of Discharge (C_d) vs Angle of Convergence in Degrees θ. NOTE: The loss is least at 13°
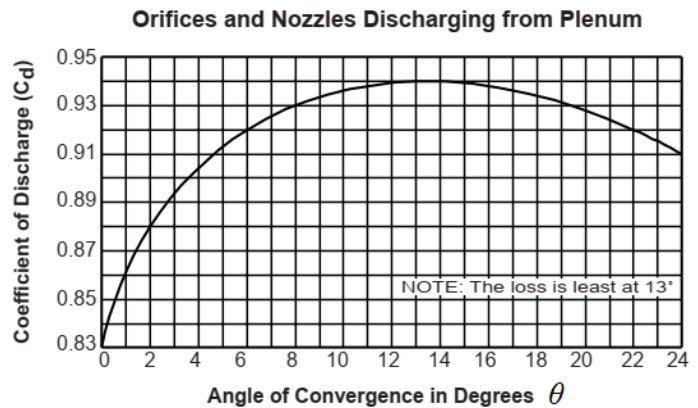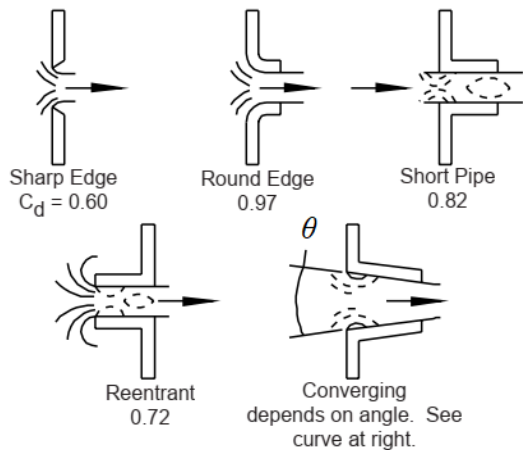
Experimental expansibility factor correlation: $\epsilon = 1 - \left(0.351 + 0.256\beta^4 + 0.93\beta^8\right)\left[1 - \left(\dfrac{p_2}{p_1}\right)^{1/\gamma}\right]$

For incompressible fluids e.g. water, $\gamma \to \infty$ so $\varepsilon \to 1$.
(γ: adiabatic index of fluid, p_1: static pressure upstream, p_2: static pressure in plate)

Different correlations are appropriate for nozzles and Venturi tubes.

Weir Flow: flow from one upstream source to a downstream outlet, like a waterfall.

For a common man-made weir, the V-notch weir: $Q = \dfrac{8}{15}\sqrt{2g}\,C_e \tan\dfrac{\theta}{2}\,(h + k)^{5/2}$

(g: acceleration due to gravity, C_e: flow correction factor, θ: opening angle of V-notch, h: height of inlet fluid above bottom of V-notch, k: head correction.)

Open Channel / Conduit Flow: flow is driven by gravity rather than pressure gradient

- Hydraulic radius: $R_h = \frac{A}{P}$ (A: flow cross-sectional area, P: wetted perimeter)

For an open channel, correlations for the cross-sectional average velocity u are:

- Chezy's formula: $u = C \times R_h^{1/2} S^{1/2}$ (C: Chezy coefficient, S: slope)
- Manning's formula: $u = \frac{1}{n} \times R_h^{2/3} S^{1/2}$ (n: Manning roughness coefficient, S: slope)
  For a clean smooth channel, $n \sim 0.01$ s m$^{-1/3}$. For a channel with stones/debris, $n \sim 0.06$ s m$^{-1/3}$.
- Hazen-Williams formula: $u = 0.849 \times C_{HW} \times R_h^{0.63} S^{0.54}$ (C_{HW}: material dependent)

The volumetric flow rate (discharge, capacity) is then $Q = Au$.

7.1.12. Pump Selection

Pumps (as well as fans and compressors) are turbomachinery components for providing flow and mechanical energy (as pressure) to a hydraulic fluid.

- Volumetric flow rate Q is typically given in m³/hr, L/min or gpm (gallons per minute).

- Pressure head H is typically given in m or ft. The pump head rise is the value of $\frac{\Delta p_{pump}}{\rho g}$.
  (Δp_{pump}: change in total pressure across the pump.)

Centrifugal Pumps: motor-powered rotating impeller (rotor) pushes fluid around a volute channel

- **Characteristic curve:** plot of pump head rise H for a given flow rate Q. Often shows curves for different impeller diameters d and rotational speeds ω, as well as the efficiency η at Q. The 1st stage minimum input pressure required to avoid cavitation (NPSH$_R$, net positive suction head required) can also be shown as a function of Q. The absolute pressure minus the vapour pressure of the fluid at the inlet must be at least $\rho g \times$ NPSH$_R$.
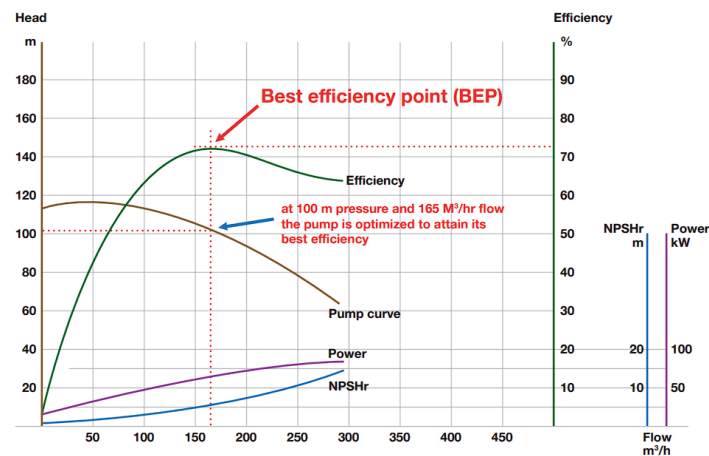
- Pump affinity laws (scaling laws for dynamically similar pumps): $Q \propto \omega d$, $H \propto \omega^2 d^2$, $P_s \propto \omega^3 d^3$.

- Shut-off head: pump head rise H when $Q = 0$.
- Free delivery flow rate: pump flow rate Q when $H = 0$ (often beyond optimal operation region).
- BEP (best efficiency point): point where η is maximum.

- Resistance coefficient, K_m: for a component or system with a head loss, $H = K_m Q^2$ (in SI units).

- Isentropic mechanical power input to flow from pump, $P_s = Q\,\Delta p_{pump} = \rho g Q H$ ('water horsepower', whp).

- Electrical power input to pump: $P_e = P_s / \eta = \rho g Q H / \eta$ (η: machine efficiency) ('brake horsepower', bhp. The rated power of the motor should be equal to the end-of-curve (maximum, not operating point) power for safety, to protect against overloading the motor.

- Variable speed/frequency drives (VSDs/VFDs): allows adjusting of the frequency of the AC motor input supply to set ω which allows the pump characteristic curve to move.

Positive Displacement Pumps: traps fluid within chamber and does work to move it out

- PD pumps have constant flow rate Q (dependent on speed only) i.e. their characteristic H vs Q curve is a straight vertical line at Q.

7.1.12. Laminar Viscous Flow in Pipes and Between Plates

Typical solutions for a viscous fluid moving in one direction between two plates:

$$u(r) = u_{max}(1 - r^2/R^2)$$
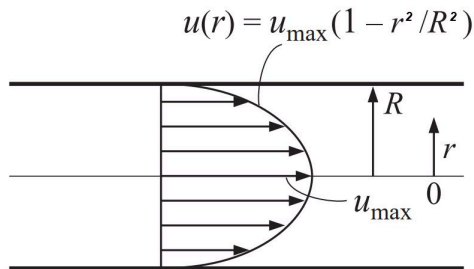
Poiseuille Flow
Uniform pressure gradient
Parabolic velocity profile ($u_{max} = 2Q/\pi R^2$)
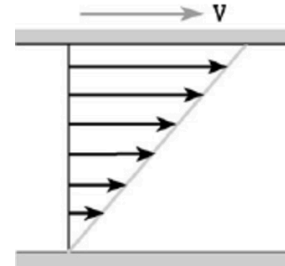
Couette Flow
Moving boundary condition
Linear velocity profile

The profiles of these two cases can be superimposed to find solutions with both streamwise pressure gradients and moving boundary conditions.

An adverse streamwise pressure gradient on a Couette flow can induce flow reversal at the stationary plate edge.

Laminar Viscous Cylindrical Pipe Flow (Hagen-Poiseuille formula):

(Δp: pressure drop across pipe, Q: volumetric flow rate, r: pipe radius, $x = 2r$: pipe diameter, L: pipe length, Q' [W]: heat transfer rate)

- Hydraulic-electrical circuit analogy: Q ~ current, p ~ voltage, R_{hyd} ~ resistance

- Flow rate: $Q = \dfrac{\Delta p}{R_{hyd}}$ where hydraulic resistance $R_{hyd} = \dfrac{8\mu L}{\pi r^4} = \dfrac{\mu L}{2\pi x^4}$

- Heat dissipation due to viscosity (thermal power): $Q' = Q\,\Delta p = \dfrac{(\Delta p)^2}{R_{hyd}} = Q^2 R_{hyd}$

In **turbulent** Poiseuille flow, the u_{max} region is broadened as momentum is transferred by eddies, giving steeper velocity profiles at the walls and increasing heat transfer.

Viscous heat dissipation: $\dot{Q} = \displaystyle\int \tau \, \frac{\partial v_x}{\partial y} \, \mathrm{d}V$

($\tau = \mu \dfrac{dV}{dy}$: interfacial shear stress, x: streamwise coordinate, y or r: transverse coordinate)

7.1.13. Boundary Layers and Aerodynamics of External Flows

Laminar Boundary Layers: thin boundary layer, gradual velocity gradient to free stream

Near a wall, viscosity cannot be neglected as the no-slip condition is always satisfied. A flowing fluid imposes a necessary velocity gradient, and the region where this gradient occurs is the boundary layer. Momentum diffuses away from the wall in the boundary layer.

Boundary layer Reynolds: $Re_\delta = \dfrac{\rho_\infty V_\infty \delta}{\mu_\infty}$ Streamwise Reynolds: $Re_x = \dfrac{\rho_\infty V_\infty x}{\mu_\infty}$

Boundary layer thickness along an infinite flat body (plate): $\delta \sim \sqrt{\dfrac{\mu_\infty x}{\rho_\infty V_\infty}}$ $\Rightarrow$ $\dfrac{\delta}{x} = 4.64\, Re_x^{-1/2}$

(x: distance along wall from stagnation)

Bernoulli's equation is **not** valid in a boundary layer due to viscous forces, which give rise to viscous drag on the body. Dimensionless viscous drag $C_D = 24\,/\,Re_D$ (Stokes flow).

When an adverse pressure gradient acts on the flow, flow reversal can occur in the boundary layer, in a similar manner to Couette flow (Section 7.1.10). Regions of high curvature on a body (e.g. high angle of attack on an airfoil) result in large streamwise pressure drops as the fluid is unable to follow the surface, which can lead to boundary layer separation and transition to turbulence.

Turbulent Boundary Layers: wide boundary layer, steep velocity gradient, filled-out velocity profile

Turbulent boundary layers grow faster than laminar boundary layers, retaining the steep velocity gradient at the wall. The surrounding pressure field exerts forces on the body (form drag and lift), which dominate as turbulence increases. For Re > 1000, viscous drag (skin friction) is negligible.

If a turbulent boundary layer is about to experience flow reversal, the high-viscosity eddies can facilitate the diffusion of momentum flux from the full velocity profile region into the reversing region, providing it with momentum needed to prevent reversal, delaying boundary layer separation from bodies. For bluff bodies, this decreases the low pressure wake region, reducing form drag significantly.

Laminar boundary layers can be 'tripped' into turbulence by surface irregularities, where the sudden high curvature of the body forces subsequent boundary layer separation. If a laminar boundary layer becomes separated and transitions to turbulence, it may be able to re-attach to the body downstream, forming a 'separation bubble'. Aerofoil shapes are often designed to ensure that, once separated, the flow transitions to turbulence quickly, so that the separation bubble is short. If the transition occurs too far downstream, the bubble will cover a large area of the wing, or the flow may not even be able to re-attach at all (stall: sudden loss of lift and increase in drag).

The sudden reduction of drag for slightly larger velocities due to laminar/turbulent transition in the boundary layer, and the corresponding separation delay, can give rise to a resonance phenomenon. This can sometimes be observed in poles, chimneys and other slender objects, and needs to be addressed to avoid structural failure. When boundary layers separate, they create a shear layer. Shear layers are inherently unstable as their velocity profile has an inflection point. They develop waves that roll up into Kelvin-Helmholtz vortices (vortex shedding). Positive feedback produces a downstream Von Kármán vortex street at a constant frequency, which can resonate structures (aeroelastic flutter).

7.1.14. Properties of Velocity Fields (Flow Fields)

If $\mathbf{u}$ is a velocity vector field for a flow, then a particle's position $\mathbf{r}$ in the field obeys $\frac{d}{dt}\mathbf{r} = \mathbf{u}$. The streamlines of $\mathbf{u}$ illustrate trajectories of the particle over time, $\mathbf{r}(t)$.

- Vorticity: $\boldsymbol{\omega} = \nabla \times \mathbf{u}$ (local angular velocity is equal to $\frac{1}{2}\boldsymbol{\omega}$)

- Material derivative: $\frac{Df}{Dt} = \frac{df}{dt} + \mathbf{u}\cdot\nabla f$ (derivative of quantity f moving with the fluid)

- Potential flow: if there exists φ such that $\mathbf{u} = \nabla\varphi$, then $\boldsymbol{\omega} = \mathbf{0}$ (irrotational flow)

- Incompressible fluid: $\nabla\cdot\mathbf{u} = 0$ (isochoric flow)

- Mass continuity equation: $\nabla\cdot(\rho\mathbf{u}) + \frac{\partial\rho}{\partial t} = 0$ (if $\frac{\partial\rho}{\partial t} = 0$, ρ constant along streamlines of $\mathbf{u}$)

- Kutta-Joukowski theorem: lift force per unit depth on a body in a 2D flow is $L' = \rho_\infty V_\infty \Gamma$
  ($\mathbf{L} \perp \mathbf{V}_\infty$; ρ_∞: free stream density, V_∞: free stream velocity relative to body)

  The circulation of $\mathbf{u}$ around the body is given by $\Gamma = \oint_C \mathbf{u}\cdot d\mathbf{l}$ (Section 3.5.15).

  (C: anticlockwise path around the body, away from the boundary layer, in potential flow region)

- For a rotating object in a flow, the lift force is responsible for the **Magnus effect**, with $\mathbf{L} \parallel (\mathbf{V}_\infty \times \boldsymbol{\omega})$. For a cylinder, $\Gamma = 2\pi\omega r^2 \to$ total lift force $L = 2\pi\rho_\infty V_\infty \omega r^2 l$.
  For a sphere, $\Gamma = 2\pi r^2\omega \to$ total lift force $L = \frac{8}{3}\pi r^3 \rho_\infty V_\infty \omega$.

- Kelvin's circulation theorem: $\frac{D\Gamma}{Dt} = 0$ for barotropic fluids in conservative forces.

- Coandă effect: fluid jet streamlines tend to follow convex surfaces, if the curvature is not too sharp. The curved streamlines generate a normal pressure gradient that can result in a net body force on the surface.

7.1.15. Taylor-Couette Flow

A viscous fluid between two concentric solid cylinders (radii r_1, r_2) driven to rotate at different relative rates (angular velocities ω_1, ω_2) exhibits Taylor-Couette flow.

Let $\eta = \dfrac{r_i}{r_o}$ and $\mu = \dfrac{\omega_o}{\omega_i}$. The Taylor number is $Ta = \dfrac{4\omega_i^2 r_i^4}{\nu^2} \dfrac{(1-\mu)(1-\frac{\mu}{\eta^2})}{(1-\eta^2)^2}$.

Azimuthal velocity profile for circular pure Couette flow (no axial throughput):

$$v_\theta(r) = Ar + Br^{-1} \text{ where } A = \omega_i \frac{\mu - \eta^2}{1 - \eta^2} \text{ and } B = \omega_i r_i^2 \frac{1-\mu}{1-\eta^2}$$

For thin-gap applications ($\eta \approx 1$), $Ta = -\dfrac{2A\,\omega_i r_o^4}{\nu^2}(1-\eta)^4(1+\mu)$.

Taylor-Couette flow is exploited in some industrial chemical reactors (the Taylor-Couette reactor, TCR) using an axial input flow velocity u_{ax}. A TCR ($u_{ax} \approx \omega r$) can be considered intermediate between a PFR ($u_{ax} \gg \omega r$) (Section 14.2.7) and a CSTR ($\omega r \gg u_{ax}$) (Section 14.2.6).

Axial Reynolds number: $Re_{ax} = \dfrac{u_{ax} d}{\nu}$.

For low Re (laminar), the flow is analogous to Couette flow (Section 7.1.12).

- For Ta < Ta$_{c1}$, flow is steady, where the lower critical Taylor number is
  $Ta_{c1} \approx 41.3 \times \dfrac{(1+\eta)^2}{2\eta\sqrt{(1-\eta)(3+\eta)}}$.

- For Ta$_{c1}$ < Ta < Ta$_{c2}$, flow forms laminar toroidal vortices (shown right), where Ta$_{c2}$ is an upper critical Taylor number.

  Vortex aspect ratio, $\Gamma = \dfrac{L_{vortex}}{r_o - r_i}$. Typical range: $0.8 < \Gamma < 2.0$.

  Using rotors with protruding ribs at regular axial intervals helps to stabilise the vortices within them.

- For Ta > Ta$_{c2}$, oscillating wavy vortices form, which become more turbulent for larger Ta.
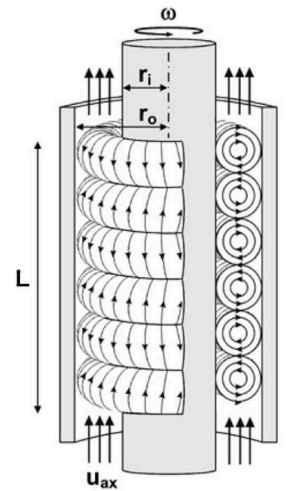
Specialist applications of TCRs include continuous filtration/desalination (inner cylinder is a semi-permeable membrane), reactors for homogeneous catalysis (high mixing, high throughput, narrow residence time distribution), low-shear heterogeneous transport (cells, enzyme colloids), and selective crystallisation of pharmaceutical compound polymorphs.

7.2. Thermofluid Dynamics

7.2.1. Dimensionless Numbers in Thermofluid Dynamics

- Reynolds number: $Re = \dfrac{\rho_f V d}{\mu} = \dfrac{V d}{\nu}$ (fluid flow: flow is laminar for Re < 2000)

- Mach number: $M = \dfrac{V}{a}$ (flow is incompressible for M < 0.3)

- Froude number: $Fr = \dfrac{V}{\sqrt{gz}}$ (flow is supercritical for Fr > 1)

- Prandtl number: $Pr = \dfrac{\mu\, c_p}{\lambda} = \dfrac{\nu}{\alpha}$ (momentum diffusivity for Pr > 1, thermal diffusivity for Pr < 1)

- Biot number: $Bi = \dfrac{hs}{\lambda}$ (lumped heat transfer model valid for Bi < 0.1)

- Fourier number: $Fo = \dfrac{\alpha\tau}{s^2}$ (temperature reaches steady state for Fo > 1)

- Grashof number: $Gr = \dfrac{gd^3\,\beta\,\Delta T}{\nu^2} = \dfrac{-gd^3\rho\,\Delta\rho}{\mu^2}$ (natural convection: boundary layer is laminar for Gr < 10^6)

- Eötvös number: $Eo = \dfrac{\Delta\rho\, gd^2}{\gamma}$ (porous flow: capillary action dominant for Eo < 1)

- Nusselt number: $Nu = \dfrac{hd}{\lambda}$ (heat transfer: slug/laminar flow for Nu < 10)

- Rayleigh number: $Ra = Gr\,Pr = \dfrac{gd^3\,\beta\,\Delta T}{\nu\alpha} = \dfrac{-gd^3\,\Delta\rho}{\mu\alpha}$

- Stanton number: $St = \dfrac{Nu}{Re\,Pr} = \dfrac{h}{\rho_f V c_p}$

- Rossby number: $Ro = \dfrac{V}{2\,\Omega L\,\sin\phi}$ (Coriolis forces dominate for Ro < 1)

- Taylor number: $Ta = \dfrac{4\Omega^2 R^4}{\nu^2}$

- Strouhal number: $Sr = \dfrac{fL}{V}$

- Drag coefficient: $C_D = \dfrac{F_{drag}}{\frac{1}{2}\rho_f A V^2}$

- Lift coefficient: $C_L = \dfrac{F_{lift}}{\frac{1}{2}\rho_f A V^2}$

- Friction coefficient: $c_f = \dfrac{\tau_{wall}}{\frac{1}{2}\rho_f V^2}$ (Fanning skin friction coefficient)

- Friction factor: $f = 4\,c_f$ (Darcy friction factor)

- Discharge coefficient: $C_d = \dfrac{m'_{actual}}{m'_{ideal}}$

(ρ_f: fluid density, V: fluid velocity relative to reference, d or L: body length (e.g. pipe diameter, plate length), μ: dynamic viscosity, ν: kinematic viscosity, a: speed of sound in fluid, g: acceleration due to gravity, z: fluid vertical elevation, c_p: isobaric specific heat capacity of fluid, λ: thermal conductivity of fluid, α: thermal diffusivity of fluid, h: heat transfer coefficient from body to fluid, s: volume-to-surface area ratio, τ: elapsed time, β: coefficient of volume expansion, ΔT: bulk-surface temperature difference, $\Delta\rho$: density difference between fluids, γ: surface tension, Ω: body angular velocity, φ: fluid latitude on spherical body, f: frequency of oscillation, A: body cross-sectional area, F: forces, τ_{wall}: shear stress at wall, m': mass flow rate.)

7.2.2. Laws of Thermodynamics and Systems

Thermodynamic Systems:

A system is a quantity of matter occupying a control volume, enclosed by a control surface. The surroundings to a system is everything not contained within the control surface.

	Energy transfer allowed	Energy transfer not allowed
Mass transfer allowed	Open system	Insulated system
Mass transfer not allowed	Closed system	Isolated system

A system containing a constant mass is necessary but **not** sufficient to define a closed system: if mass enters and leaves the system at the same rate, this remains an open system.

A 'simple compressible system' is a system in which changes in bulk kinetic energy and gravitational potential energy are negligible (also the effects of surface tension, stress in deformed solids, and externally applied electromagnetic fields). The only contribution to the energy of a simple compressible system is the internal energy U.

Laws of Thermodynamics: in terms of energy and entropy,

- **First Law:** the energy in an isolated system is constant.
- **Second Law:** the entropy in an isolated system never decreases.
- **Third Law:** the entropy in a closed system at equilibrium is minimum at zero temperature.

- **'Zeroth Law':** if two thermodynamic systems are both in thermal equilibrium with a third system, then the two systems are in thermal equilibrium with each other.
- **'Fourth Law':** a system not at equilibrium evolves in time in such a way as to maximise its entropy production, constrained by the forces and fluxes that the system is subject to.

Thermodynamic Properties:

- **Extensive:** proportional to the system mass e.g. V, U, H, S
- **Intensive:** independent of the system mass e.g. p, T
- **Specific:** extensive property per unit mass e.g. v, u, h, s
- **Molar:** extensive property per mole e.g. $\bar{v}, \bar{u}, \bar{h}, \bar{s}$ (note: **kilo**moles used in this section)

Specific and molar properties are intensive, related by $\bar{x}\,[X/kmol] = x\,[X/kg] \times M_r\,[kg/kmol]$

Phases and Components: A phase is a quantity of homogeneous matter. A system may consist of a single phase or a number of co-existing phases.

- The three-phase state of H_2O (ice, water, steam) only exists in equilibrium along the triple-point line. The components of a phase are the minimum set of chemical substances which make up the phase. A single-component system is a pure substance.
- Air could be treated as a two-component mixture of N_2 and O_2. However, if liquefaction does not occur the composition remains constant and it is usually more convenient to treat it as a pure substance. The single component is a mixture of 79% N_2 and 21% O_2 by volume.

7.2.2. Thermodynamic State Variables

For a closed system (m: mass, H: enthalpy, U: internal energy, G: Gibbs free energy, A: Helmholtz free energy, p: pressure, T: temperature, V: volume, S: entropy). Thermodynamics potentials are $\{H, U, G, A\}$. Conjugate variables are $\{p, T, V, S\}$. Without external work/heat, the system obeys:

$$H = U + pV, \qquad\qquad G = H - TS, \qquad A = U - TS$$
$$dU = T\,dS - p\,dV, \qquad dH = T\,dS + V\,dp, \qquad dG = V\,dp - S\,dT, \qquad dA = -p\,dV - S\,dT$$

To account for chemical reactions, add $\mu\,dN$ to each differential (e.g. $dU = T\,dS - p\,dV + \mu\,dN$).
(μ: chemical potential, N: particle or mole count, summed over each chemical species.)
All the above equations are also valid when replaced with their specific or molar intensive properties.

G: the maximum reversible work a system can do in an isothermal, **isobaric** process.
A: the maximum reversible work a system can do in an isothermal, **isochoric** process.

Most commonly useful: $\qquad T\,dS = dU + p\,dV = dH - V\,dp$

Specific heat capacities: $\qquad$ isochoric: $c_v = \left(\dfrac{\partial u}{\partial T}\right)_v$, isobaric: $c_p = \left(\dfrac{\partial h}{\partial T}\right)_p$, adiabatic index: $\gamma = \dfrac{c_p}{c_v}$

Coefficients of expansion: $\quad$ volume expansion: $\beta = \dfrac{1}{v}\left(\dfrac{\partial v}{\partial T}\right)_p$, compressibility: $\kappa = -\dfrac{1}{v}\left(\dfrac{\partial v}{\partial p}\right)_T$

First law: $\qquad dU = \delta Q - \delta W;$ $\qquad\qquad$ Second law: $\quad \delta Q = T\,dS$

Contributions to work W and heat Q can be expressed as products of an intensive variable and its conjugate infinitesimal extrinsic variable, e.g. mechanical work $\delta W = p\,dV$, elastic strain energy $\delta W = \sigma\,d\varepsilon$, heat transfer $\delta Q = T\,dS$.

7.2.3. Ideal Gas Relationships

An ideal gas is a collection of particles with negligible size moving randomly, making elastic collisions with the container and making no inter-particle interactions. For microscopic properties of ideal gases, see Section 14.1.1-7.

(p: pressure, V: volume, n: moles, m: mass, T: temperature, ρ: density, M_r: molar mass, v: specific volume, $\overline{R} = 8.314$ J K^{-1} mol^{-1}: gas constant, γ: adiabatic index, f: molecular degrees of freedom)

- Ideal gas law: $\qquad\qquad\quad pV = n\overline{R}T = mRT \qquad\qquad$ where $R = \dfrac{\overline{R}}{M_r\,[kg\,mol^{-1}]}$ so $mR = n\overline{R}$

- Specific ideal gas law: $\qquad pv = RT \qquad\qquad\qquad$ where $v = \dfrac{V}{m} = \dfrac{1}{\rho}$

- Density gas law: $\qquad\qquad\; p = \rho RT$

- Density change: $\qquad\qquad$ isobaric: $\left(\dfrac{\partial \rho}{\partial T}\right)_p = -\rho\beta,$ $\quad$ isothermal: $\left(\dfrac{\partial \rho}{\partial p}\right)_T = \rho\kappa$

- Specific heat capacities: $\quad c_v = \dfrac{R}{\gamma - 1}, \quad c_p = \dfrac{\gamma R}{\gamma - 1}, \quad c_p - c_v = R \qquad$ where $\gamma = \dfrac{c_p}{c_v} = 1 + \dfrac{2}{f}$

  Monatomic gas e.g. He, Ar: $f = 3$; diatomic gas e.g. H_2, N_2, O_2: $f = 5$. For dry air at 20 °C, $\gamma = 1.400$.

- Speed of sound: $\qquad\qquad a = \sqrt{\gamma RT}$

7.2.4. Perfect Gas Relationships for Non-Flow Processes

A perfect gas has specific heat capacities which are independent of T.
A semi-perfect gas has specific heat capacities which are dependent on T only.
An ideal gas has specific heat capacities which may vary with state.

- Change in specific internal energy: $\Delta u = u_2 - u_1 = c_v\left(T_2 - T_1\right)$
- Change in specific enthalpy: $\Delta h = h_2 - h_1 = c_p\left(T_2 - T_1\right)$
- Change in specific entropy: $\Delta s = s_2 - s_1 = c_v\, ln\, \frac{T_2}{T_1} + R\, ln\, \frac{v_2}{v_1} = c_p\, ln\, \frac{T_2}{T_1} - R\, ln\, \frac{p_2}{p_1}$

$$= c_v\, ln\, \frac{p_2}{p_1} + c_p\, ln\, \frac{v_2}{v_1}$$

For a perfect gas, types of processes are:

Isobaric Processes: constant pressure p from state 1 → state 2

- Charles' law: $v_1 / T_1 = v_2 / T_2$ (vT^{-1} is constant)
- Work done: $W = p\, \Delta V = -mR\, \Delta T$
- Heat transferred: $Q = \Delta H = m\, c_p\, \Delta T$

Isochoric Processes: constant volume v from state 1 → state 2

- Gay-Lussac's law: $p_1 / T_1 = p_2 / T_2$ (pT^{-1} is constant)
- Work done: $W = 0$
- Heat transferred: $Q = \Delta U = m\, c_v\, \Delta T = \frac{mc_v}{R}\, v\, \Delta p$

Isothermal Processes: constant temperature T from state 1 → state 2

- Boyle's law: $p_1 v_1 = p_2 v_2$ (pv is constant)
- Work done: $W = -mRT\, ln\, \frac{v_2}{v_1} = -mRT\, ln\, \frac{p_1}{p_2}$
- Heat transferred: $Q = mRT\, ln\, \frac{v_2}{v_1} = mRT\, ln\, \frac{p_1}{p_2}$

Adiabatic Processes: no heat transfer from state 1 → state 2

- Adiabatic gas law: $p_1 v_1^{\gamma} = p_2 v_2^{\gamma}$ (pv^{γ}, $Tv^{\gamma-1}$, $Tp^{\frac{1-\gamma}{\gamma}}$ constant)
- Work done: $W = \frac{p_2 v_2 - p_1 v_1}{1 - \gamma} = -\frac{1}{\gamma - 1}mRT_1\left(\left(\frac{p_2}{p_1}\right)^{\frac{\gamma-1}{\gamma}} - 1\right)$
- Heat transferred: $Q = 0$

Any two of {adiabatic, reversible, isentropic} implies the third is also true.

Polytropic Processes: generalised power-law equation from state 1 → state 2 (n: polytropic index)

- Polytropic gas law: $p_1 v_1^{n} = p_2 v_2^{n}$ (pv^{n}, Tv^{n-1}, $Tp^{\frac{1-n}{n}}$ are constant)
- Polytropic coefficient: $n = (1 - \gamma)\frac{\partial Q}{\partial W} + \gamma$ ($\frac{\partial Q}{\partial W}$: instantaneous heat to work transfer ratio)
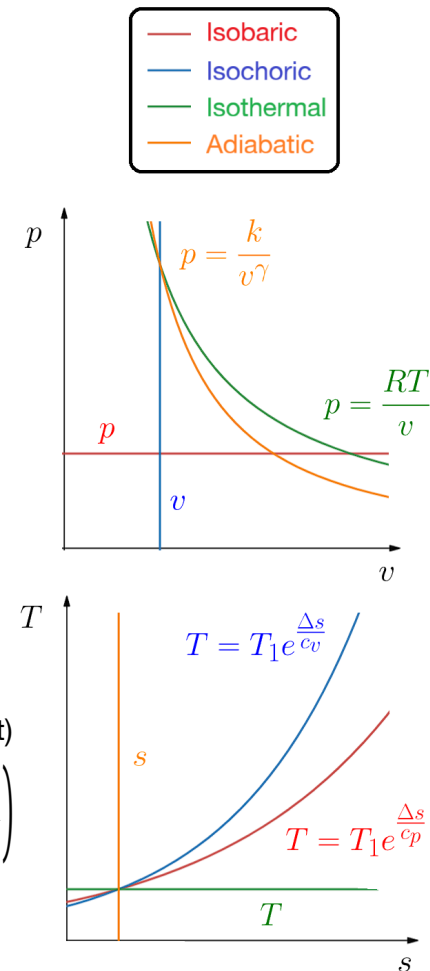
7.2.5. Thermodynamics of Non-Flow Processes

For a closed system of mass m undergoing a process between state 1 and state 2 are defined as positive and in the absence of capillarity, electric and magnetic fields:

First Law of Thermodynamics: conservation of energy

$$Q - W = m\left(u_2 + \frac{1}{2}V_2^2 + gz_2\right) - m\left(u_1 + \frac{1}{2}V_1^2 + gz_1\right)$$

(Q: heat transferred to system, W: work done by system, m: system mass, u: specific internal energy, V: bulk translational velocity, g: gravitational field, z: elevation)

For a cyclic process: $\oint dQ = \oint dW$ Displacement work by pressure p: $W = \int_1^2 p\,dV$

Second Law of Thermodynamics: entropy and heat transfer

$$m(s_2 - s_1) = \int_1^2 \frac{dQ}{T} + \Delta S_{irrev}$$

(m: system mass, s: specific entropy, dQ: infinitesimal heat transfer to system, T: system temperature (on boundary), $\Delta S_{\text{irrev}} \geq 0$: entropy created by irreversibilities in the system)

For a fully reversible process: $m\,ds_{\text{irrev}} = \sigma = \Delta S_{\text{irrev}} = 0$.

For a cyclic process: $\oint \frac{dQ}{T} \leq 0$ (the Clausius inequality)

7.2.6. Sources of Irreversible Entropy Creation in Flow Processes

| Viscous dissipation in boundary layers | Viscous mixing of flows of different velocity | Heat transfer across a finite ΔT |
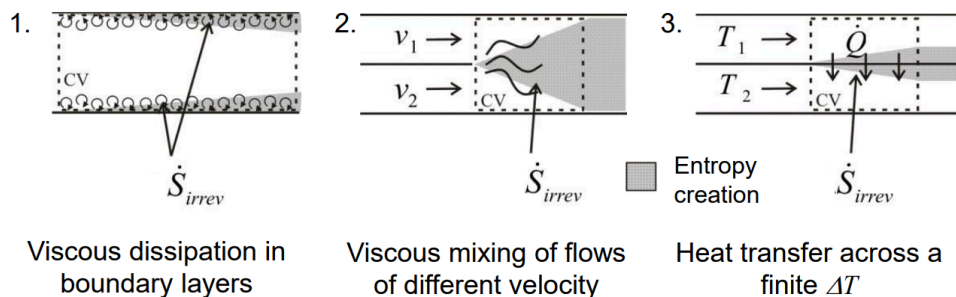
7.2.7. Thermodynamics of Control Volumes (Flow Processes and Open Systems)

A control volume is that region of space that is enclosed by a rigid control surface. For steady-flow, conditions within the control volume are not, on average, changing so that the mass, momentum, energy and entropy within the control volume remain constant.

Steady Flow Energy Equation (SFEE) (First Law of Thermodynamics): conservation of energy

$$\underbrace{\frac{dE_{cv}}{dt}}_{\substack{\text{internal} \\ \text{change}}} + \underbrace{\sum_{\text{out}} \dot{m}\left(h + \frac{1}{2}V^2 + gz\right)}_{\text{energy flow out of CV}} - \underbrace{\sum_{\text{in}} \dot{m}\left(h + \frac{1}{2}V^2 + gz\right)}_{\text{energy flow into CV}} = \underbrace{\dot{Q} - \dot{W}}_{\substack{\text{heat and work} \\ \text{transferred to} \\ \text{and from CV}}}$$

(E_{cv}: total system energy, $\dot{m}$: mass flow rate, h: specific enthalpy at inlet/outlet, V: flow speed, g: gravitational field, z: elevation, $\dot{Q}$: heat transfer rate to CV, $\dot{W}$: shaft power output)

For steady flow, the 'internal change' term is zero.

Steady Flow Entropy Equation (SFSE) (Second Law of Thermodynamics): entropy accounting

$$\underbrace{\frac{\mathrm{d}S_{cv}}{\mathrm{d}t}}_{\substack{\text{internal} \\ \text{change}}} + \underbrace{\sum_{\text{out}} \dot{m}s}_{\substack{\text{entropy} \\ \text{flow out}}} - \underbrace{\sum_{\text{in}} \dot{m}s}_{\substack{\text{entropy} \\ \text{flow in}}} = \underbrace{\oiint_{cs} \frac{d\dot{Q}}{T}}_{\substack{\text{isothermal} \\ \text{heat transfer}}} + \underbrace{\dot{S}_{\text{irrev}}}_{\substack{\text{irreversible} \\ \text{processes}}}$$

(S_{cv}: total system entropy, $\dot{m}$: mass flow rate, s: specific entropy at inlet/outlet, $d\dot{Q}$: infinitesimal heat transfer rate to CV, T: system temperature (on boundary), $\dot{S}_{\text{irrev}} \geq 0$: rate of entropy creation within the CV due to irreversibilities)

For steady flow, the 'internal change' term is zero.

7.2.8. Exergy and Available Power in Control Volumes

Heat is not as 'valuable' as work, as a heat engine can only extract work from heat up to the Carnot efficiency factor.
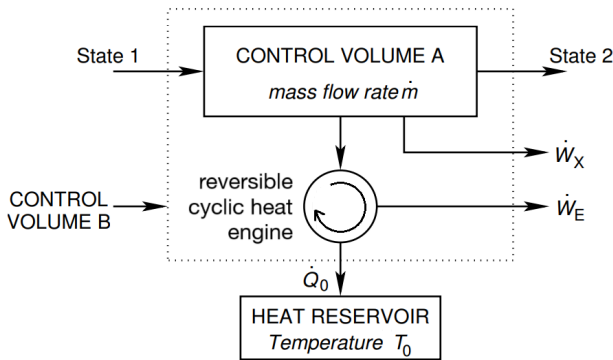
Availability: the maximum useful work $\dot{W}_X$ that can be obtained from CVA as it comes into equilibrium with its environment (i.e. using a hypothetical Carnot engine). Applying the SFEE (1st law) and SFSE (2nd law) to CVB:

$$[\dot{W}_X]_{\mathrm{MAX}} = \dot{m}(b_1 - b_2) \quad \text{or} \quad [-\dot{W}_X]_{\mathrm{MIN}} = \dot{m}(b_2 - b_1)$$

when work is the output   when work is the input

($b = h - T_0 s$: specific steady flow availability function)

- Dead state: $p_D = 1$ atm, $T_D = 298$ K
- Specific exergy: $e = b - b_D$ so $\Delta e = \Delta b$ (dead state availability: $b_D = h_D - T_0 s_D$)

Steady Flow Exergy Equation (SFXE): combination of first and second laws

$$\underbrace{\sum_{\mathrm{out}} \dot{m}\left(e + \frac{1}{2}V^2 + gz\right) - \underbrace{\sum_{\mathrm{in}} \dot{m}\left(e + \frac{1}{2}V^2 + gz\right)}_{\text{exergy flow rate}}}_{} = \underbrace{-\dot{W}_X}_{\substack{\text{shaft}\\\text{power}\\\text{output}}} + \underbrace{\oiint_{CS}\left(1 - \frac{T_0}{T_S}\right)d\dot{Q}_S}_{\substack{\dot{E}_Q:\text{ power potential}\\\text{of heat addition}\\\text{to system at }T_S}} - \underbrace{\oiint_{CS}\left(1 - \frac{T_0}{T_L}\right)d\dot{Q}_L}_{\substack{\dot{W}_{L,Q}:\text{ power potential}\\\text{of heat rejection}\\\text{to environment at }T_0}} - \underbrace{T_0\dot{S}_{irrev}}_{\substack{\dot{W}_{L,CR}:\text{ loss of}\\\text{available}\\\text{power due to}\\\text{irreversibilities}}}$$

(T_0: dead state, T_S: system temperature of heat addition, T_L: system temperature of heat rejection.
p-V (boundary expansion) work is **not** counted as useful output work ($W_X' = W' - p\, dV/dt$).
The fourth term on the RHS represents the irreversible exergy destruction rate (Gouy-Stodola theorem).)

An 'exergy analysis' of a component or system typically involves:

1) calculate the state properties of the working fluid around the system ($h_1, s_1, h_2, s_2, \ldots$)
2) calculate the exergy of the fluid at each state ($e_1 = b_1 = h_1 - T_D s_1 \ldots$)   (take datum $b_D = 0$)
3) calculate $\dot{Q}, \dot{E}_Q, \dot{W}_X, \dot{W}_{L,Q}, \dot{W}_{L,CR}$ for each component or process
4) apply the a) SFEE and b) SFXE to each component in turn
5) draw up overall a) energy and b) exergy balances showing how the heat supply rate is utilised
6) calculate the a) thermal efficiency (energy) and b) rational efficiency (exergy).

Components with the greatest contributions to exergy destruction can then be identified for targeting of potential improvements. For individual components, exergy efficiency is defined as:

7.2.8. Thermal Efficiency of Thermodynamic Cycles

$\dot{Q}_B$
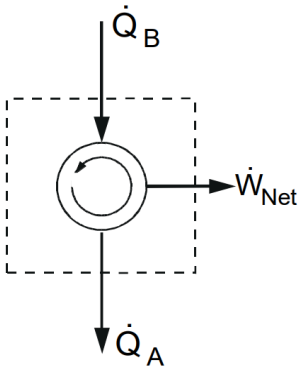
First-Law (overall, thermal) Efficiency: how much of the *total* energy was used?

$$\eta_{1st} = \frac{\dot{W}_{net}}{\dot{Q}_B} = 1 - \frac{\dot{Q}_A}{\dot{Q}_B} \qquad \text{where} \qquad \dot{W}_{net} = \dot{Q}_B - \dot{Q}_A$$

$\dot{W}_{Net}$ **Second-Law (rational, exergy) Efficiency:** how much of the *available* energy was used?

$$\eta_{2nd} = \frac{\dot{W}_{net}}{\dot{m}\Delta b} = \frac{\eta_{1st}}{\eta_{Carnot}} \qquad \text{where} \qquad \eta_{Carnot} = 1 - \frac{T_A}{T_B}$$

$\dot{Q}_A$

T_A as the dead state and T_B as the system state.

The 2nd law efficiency is always higher than the 1st law efficiency, accounting for the fact that heat is not as 'valuable' as work ($\eta_{Carnot} < 1$ for finite T_B and nonzero T_A).

Carnot cycle: the only cycle with 100% second-law efficiency (fully reversible: maximum possible first-law efficiency). It consists of alternating isothermal and adiabatic processes, making a rectangle on a *T-s* indicator diagram. It cannot be achieved in reality.

Practical consequences of the second law of thermodynamics can be stated as:

- **Kelvin-Planck Statement** of the Second Law: no cyclic device can generate only work from only heat from a single thermal reservoir (work is more 'valuable' than heat).

- **Clausius Statement** of the Second Law: no cyclic device can transfer heat from a cold reservoir to a hot reservoir without work input (heat naturally flows from hot to cold spaces).

7.2.9. The Otto Cycle and Diesel Cycle (Fossil Fuel Powered Automobiles)

Indicator (P-v and T-s) diagrams for ideal air-standard Otto and Diesel cycles:
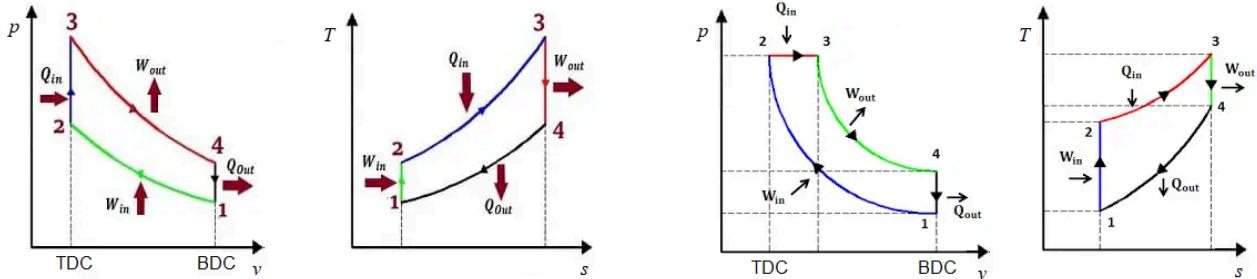
Otto Cycle (petrol/gasoline engines)	Diesel Cycle
1 → 2: adiabatic compression	1 → 2: adiabatic compression
2 → 3: isochoric ignition from spark plug	2 → 3: isobaric ignition from glow plug
3 → 4: adiabatic power stroke	3 → 4: adiabatic power stroke
4 → 1 → STP → 1: exhaust and intake	4 → 1 → STP → 1: exhaust and intake

TDC: top dead centre (piston before intake), BDC: bottom dead centre (piston after intake)
Real indicator diagrams have rounded corners since the crankshaft does not stop.

Engine Operation in Vehicles

- To initiate fuel combustion, a **spark plug** ignites the fuel-air mixture using electrical energy.
- In diesel engines, ignition occurs spontaneously (high T and p), but is assisted by a **glow plug**.
- The power stroke moves the piston down, turning the crankshaft, delivering torque to the drivetrain.
- A flywheel smooths the delivery of torque between cycles, providing maximum torque at a uniform engine speed, which is delivered to the drivetrain (wheels) by a gear system (by operating the clutch in a manual transmission vehicle).
- Four-stroke cycles require two revolutions of the crankshaft per cycle. Two-stroke cycles only require one, but are not used in automobiles due to fuel efficiency and emissions.
- Vehicles may have 3, 4, 6, 8 or more cylinders working together to supply torque to the crankshaft, in either e.g. V6 or I6 (inline) configurations.
- Some hybrid EVs and fuel-efficient cars use the Atkinson cycle (Otto-like, with 4 → 1 isobaric).

Power Development from Engines

- **Input power** from fuel combustion (as heat): $P_{input} = CV \times m'$
- **Shaft power:** $P_{indicated} = WfN_{cyl} = P_{brake} + P_{lost} = \eta_{th} P_{input}$
- **Brake power** (useful output power): $P_{brake} = T\omega = \eta_{mech} P_{indicated} = \eta_{th} \eta_{mech} P_{input} = \eta_{overall} P_{input}$

(CV: fuel calorific value, m' : mass flow rate, T: engine torque, ω: crankshaft angular velocity, W: work done per cycle, f: engine cycles per second, N_{cyl}: number of cylinders)

Additional devices used to enhance performance in automobiles include:

- **Supercharger:** compressor at inlet, powered by engine crankshaft via a belt drive
- **Turbocharger:** compressor at inlet, powered by hot exhaust flow
- **Intercooler:** a high-throughput heat exchanger used to prevent pre-ignition due to compression
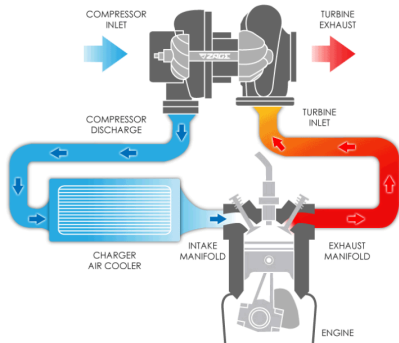
Turbocharger (top) and **intercooler** (left) fitted to an engine (bottom)
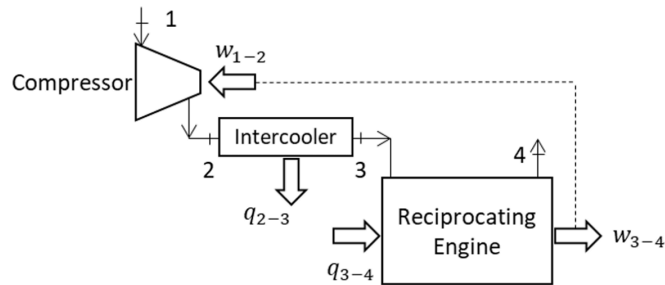
The **supercharger** supplies w_{1-2} from the engine shaft power w_{3-4}

7.2.10. The Stirling Cycle and Ericsson Cycle

Uses two cylinders separated by a regenerator. Useful for some high-efficiency applications e.g. space vehicles (heat supplied by radioisotope thermoelectric generators (RTGs)), submarine power and micro-scale CHP schemes.

Stirling Cycle:
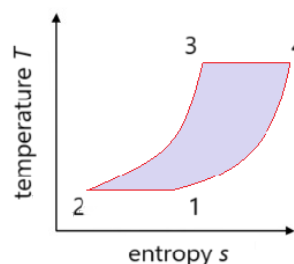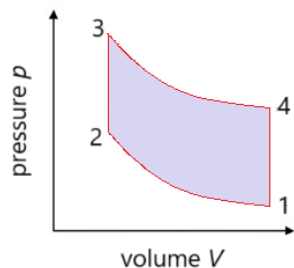
1 → 2: isothermal heat rejection
2 → 3: isochoric heating
3 → 4: isothermal heat addition
4 → 1: isochoric cooling

Ericsson Cycle:
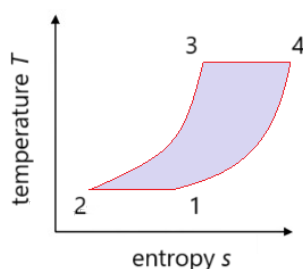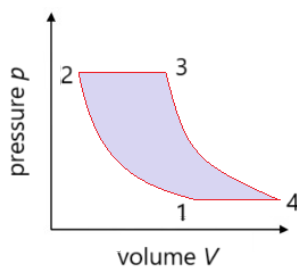
1 → 2: isothermal heat rejection
2 → 3: isobaric heating
3 → 4: isothermal heat addition
4 → 1: isobaric cooling

7.2.11. The Brayton Cycle / Joule Cycle (Gas Turbines and Jet Engines)

Gas Turbine (imperfect cycle in red):
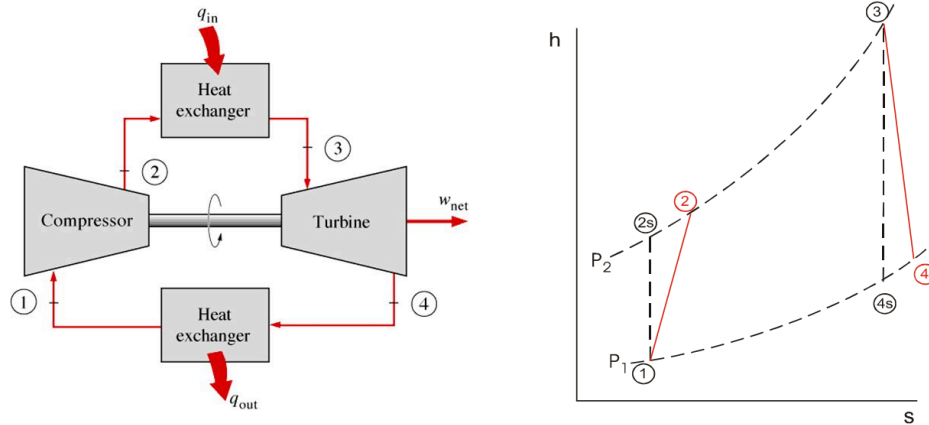
Isentropic efficiency of a non-ideal compressor η_c and turbine η_t:

$$\eta_c \equiv \frac{\text{Ideal Work Input}}{\text{Actual Work Input}} = \frac{h_{2s} - h_1}{h_2 - h_1} \qquad \eta_t \equiv \frac{\text{Actual Work Output}}{\text{Ideal Work Output}} = \frac{h_3 - h_4}{h_3 - h_{4s}}$$

The non-ideal ending state lies on the same isobar as the ideal ending state (pressure losses are neglected), but at a higher entropy and temperature.

Gas turbines are traditionally powered with fossil fuels, such as methane (natural gas), light crude oil, naphtha, syngas, kerosene etc. Cleaner options include non-fossil-fuel sources such as ethanol (biofuel), ammonia and hydrogen. The supply must be filtered to ensure it is particulate-free i.e. no charcoal, soot or tar, to avoid clogging and eroding the turbomachinery.

In an integrated gasification combined cycle (IGCC), solid fuels can be used by first converting to gaseous fuels (e.g. coal → syngas) in a gasifier, which is then used in the gas turbine. This allows for easier desulfurisation and CO_2 capture than coal-fired steam turbines, but burning coal (including 'clean coal') remains highly polluting and is being phased out.

Jet Engines
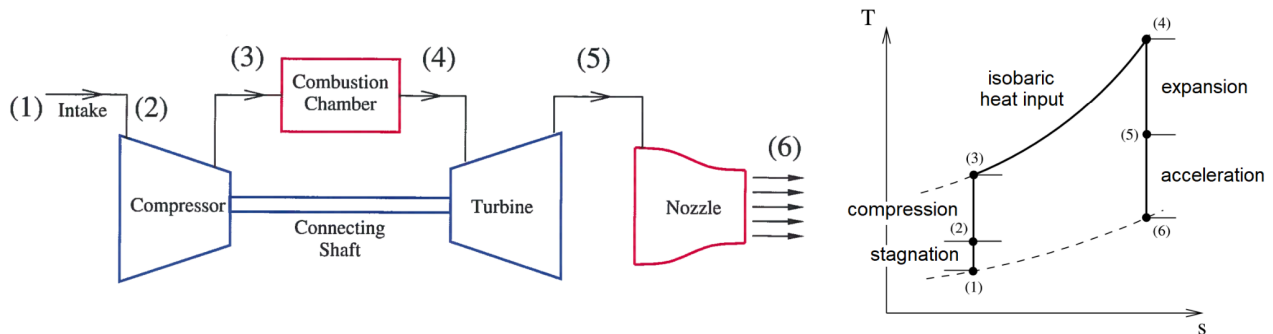
The main types of jet engines are:

| **Turbojet** | **Turboprop** | **Turbofan** | **Turboshaft** |
| | Propeller planes | Subsonic planes and jets | Helicopters |
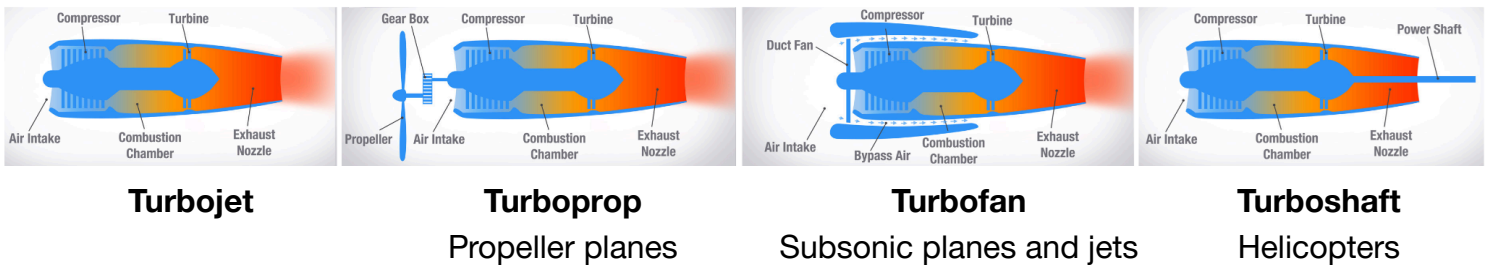
Modifications to the basic Joule cycle-based jet engine include:

- **Afterburner (Reheater):** reheat the exhaust stream with a bypassed fuel injection, increasing the exhaust enthalpy (temperature, velocity and engine thrust). Used in supersonic fighter jets.

- **Intercooler:** split the compressor into multiple stages with cooling inbetween, reducing the compressor input work, increasing the net power output.

- **Regenerator (Recuperator):** a heat exchanger between the hot exhaust gases to the compressor inlet, raising engine inlet temperature.

- **Ramjet:** remove the compressor and turbine, instead using only stagnation at the inlet in flight. Combustion occurs in shock cones. Used in supersonic jets. Flame holders are required downstream of the fuel injector to prevent the

7.2.12. Staged Combustion Cycle (Rocket Engines)

Rocket Engines: use a chemical other than atmospheric oxygen to react with the fuel
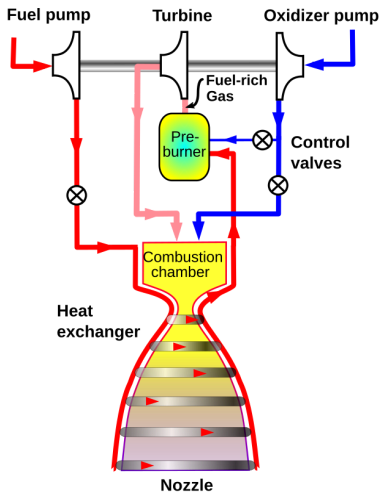
While jet engines contain on-board fuel and source their oxidiser (atmospheric oxygen) from the inlet, rocket engines carry both the fuel and oxidiser on-board, which are mixed in a combustor to generate exhaust gases and thrust. Rocket engines therefore have no inlet and can work in the vacuum of space.

Common **fuels** include H_2 (liquid), CH_4 (LNG), kerosene and lithium.

Common **oxidisers** include O_2 (liquid: LOX or gas: GOX), N_2F_4, ClF_5, F_2, OF_2, N_2O_4 and H_2O_2.

Rocket engines can be classified as:

- **Bipropellant:** heat generated from a fuel-oxidiser reaction (shown in above image). The fuel-oxidiser mixture can be described as:
  - **Hypergolic:** reaction is spontaneous at supplied temperature e.g. $N_2H_4 + N_2O_4$.
  - **Cryogenic:** reactants liquefied to low temperature, spark required to initiate combustion e.g. LH_2 + LOX.
- **Monopropellant:** heat generated from catalytic decomposition of a single fuel. Common monopropellants include N_2H_4, H_2O_2 and N_2O.

7.2.13. The Superheated Rankine Cycle (Steam Turbine)

An ideal Rankine cycle is shown, using mixtures of steam and condensate. It is often used in power plants to generate electricity, where the heat addition $q_{2\to3}$ comes from e.g. burning coal (highly polluting), oil, natural gas, biofuels, nuclear, geothermal or solar thermal power. In a combined heat and power (CHP, cogeneration) scheme, both output heat $q_{4\to1}$ and work $w_{3\to4}$ are distributed to consumers.
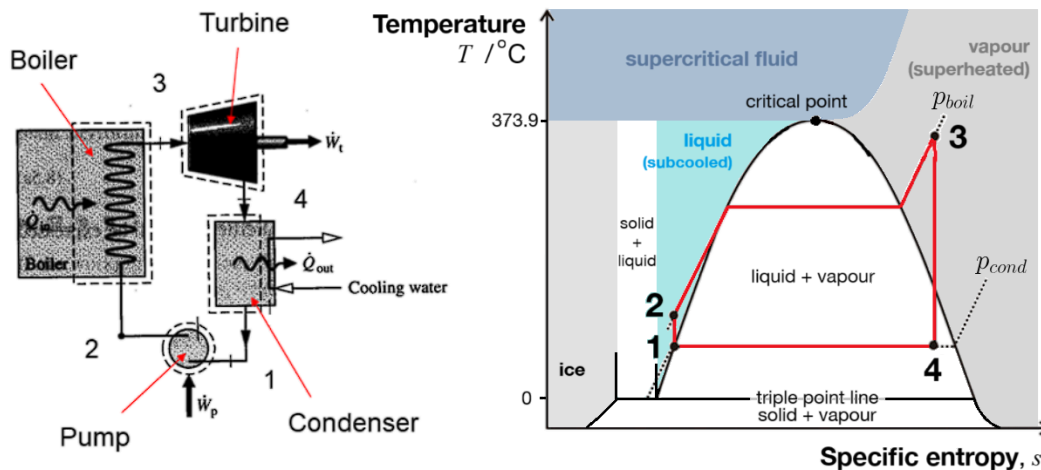
The turbine stage $w_{3\to4}$ may be split into **reheat stages** to increase the efficiency, up to a limit. Typically no more than two reheats are done due to practicalities and diminishing returns.

The steam quality (dryness fraction) at the turbine outlet (4) must be >90% to avoid water droplet condensation which leads to erosion of the turbine blades. The condenser pressure must be high enough to avoid ice crystal formation. The pump inlet total pressure must supply the required suction pressure at the pump inlet to avoid cavitation, achieved by physically positioning the pump at a lower elevation to gain hydrostatic pressure at the inlet.

A lower operating temperature alternative is to use an organic working fluid e.g. isopentane (organic Rankine cycle, ORC), useful for waste heat recovery. A recent development is the supercritical CO_2 Rankine cycle.

Combined-Cycle Gas Turbine (CCGT) and Heat Recovery Steam Generator (HRSG)

A CCGT uses the exhaust heat of a gas turbine to heat a steam turbine, improving efficiency.
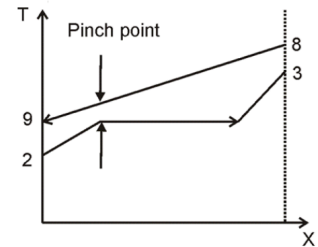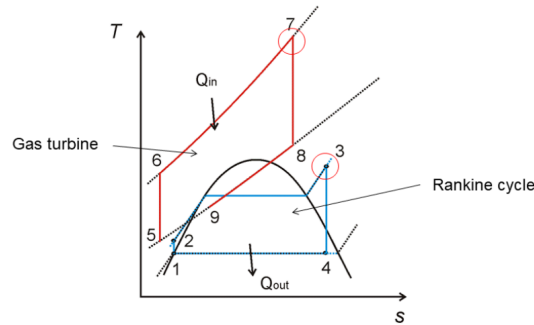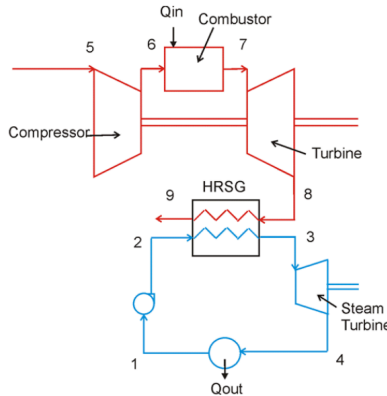
Combined Cycle Gas Turbine   **Indicator Diagrams**   **Thermal Gradient in HRSG**
gas turbine feeds Rankine cycle   (X: fraction of heat transferred)

In the HRSG: $\dfrac{\dot{m}_{gas}}{\dot{m}_{H_2O}} = \dfrac{h_3 - h_2}{c_{p,gas}\left(T_8 - T_9\right)}$ (find h_2, h_3, s_2, s_3 for water from Section 7.4.4.)

Entropy in HRSG: $\Delta \dot{S}_{irrev} = \dot{m}_{H_2O}\left(s_3 - s_2\right) + \dot{m}_{gas}\left(s_9 - s_8\right)$ $\left(s_9 - s_8 = c_p \, ln \dfrac{T_9}{T_8} - R \, ln \dfrac{p_9}{p_8}\right)$

The HRSG steam side consists of the economiser (2 → wet sat), evaporator (wet sat → dry sat) and superheater (dry sat → 3). The pinch point is typically at the economiser outlet.

7.2.14. The Refrigeration Cycle (Refrigerators and Heat Pumps)

Representative indicator T-s and p-h diagrams are shown, with an ideal compressor.
A typical working fluid is R-134a (a refrigerant / freon).
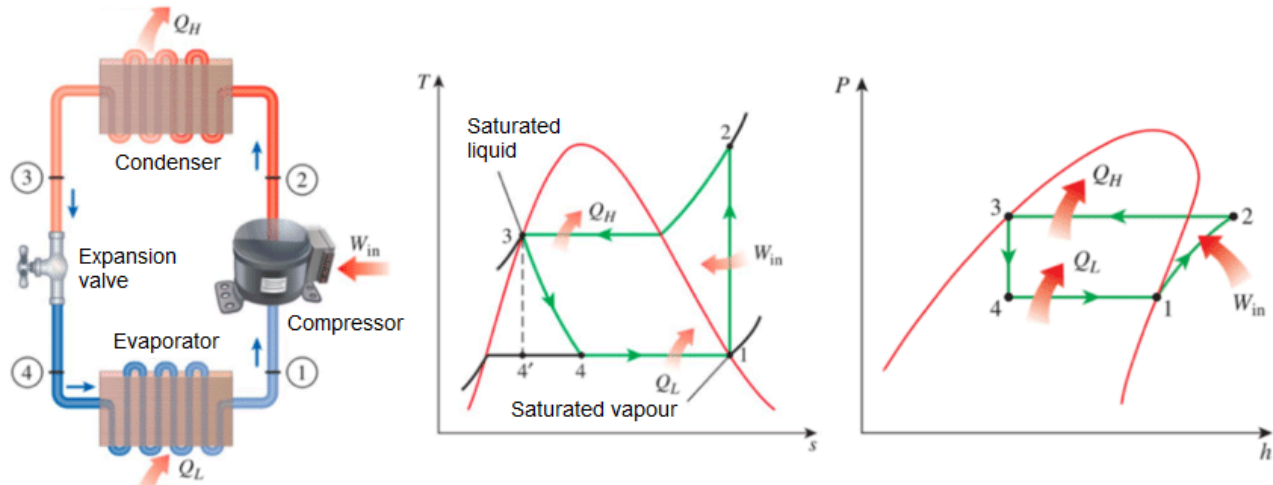
Coefficient of Performance: measures useful heat transfer per unit work input

$$\text{COP}_{\text{hp}} = \frac{\dot{Q}_H}{\dot{W}_{in}} \leq \frac{T_{hot}}{T_{hot} - T_{cold}} \qquad \text{COP}_{\text{ref}} = \frac{\dot{Q}_L}{\dot{W}_{in}} \leq \frac{T_{cold}}{T_{hot} - T_{cold}} \qquad \text{COP}_{\text{hp}} = 1 + \text{COP}_{\text{ref}}$$

COP can be considered the reciprocal of efficiency, since heat transfer is the desired output.

Heat removal ability: Q_L is often stated in any units of 1 TON = 3.516 kW = 12,000 BTU hr^{-1}.
A rate of 1 TON is equivalent to freezing 1 ton of liquid water into ice at 0 °C in 24 hours.

Refrigeration cycles are used in household refrigerators, dehumidifiers, air conditioning units and heat pumps as an energy efficient alternative to air conditioning.

Specialised applications involve cryogenic cooling for superconductors using liquid helium or nitrogen, using dedicated cycles e.g. Stirling cryocooler, Brayton magnetocaloric cycle, Gifford-McMahon cycle.

7.2.15. Humidity and Psychrometry

If liquid water is added to dry air then the liquid layer will evaporate until the vapour pressure of steam in the gas mixture is attained (can be found in Section 7.4.4. as $p(T)$). At this point the air is said to be saturated. If a steam-air mixture is cooled below the dew point temperature, condensation to liquid water will occur similarly.

Specific humidity (humidity ratio): $\omega = \dfrac{m_{steam}}{m_{air}} = \dfrac{M_{r(H_2O)}}{M_{r(air)}} \times \dfrac{p_{steam}}{p_{air}} = 0.622 \ \dfrac{p_{steam}}{P_{tot} - p_{steam}}$

Relative humidity: $\phi = \dfrac{p_{steam}}{p_{steam,sat}}$ (fraction of saturation pressure)

Psychrometric correlations or charts (e.g. flipped version of the Mollier diagram, Section 7.4.11, where $\phi = x$, dryness fraction) can be used to find the relative humidity and other state variables (e.g. specific enthalpy) from the dry bulb ($\phi = \phi_{mix}$) and wet bulb ($\phi = 1$) temperatures.

Dehumidifiers: condense water out of the air by dropping the temperature

A refrigeration cycle (Section 7.2.14) sets up a cold 'evaporator' coil and a hot 'condenser' coil. An external open air flow containing moisture is blown over the coils. The air meets the cold coil first, condensing out liquid water from the air, dropping the temperature and specific humidity. The cool, dry air is then warmed back up as it leaves over the hot coil.

An alternative refrigerant-free design is to use a desiccant to simply absorb water from the air without a temperature change.

Air conditioners operating in moist air will provide cooling as well as a dehumidification effect as their hot condenser coil rejects heat to the outside through a vent. Refrigerators can act as dehumidifiers for the food inside, reducing moisture content.

Humidifiers: add water vapour to the air directly

Water vapour is added to the air stream via simple evaporation. Liquid water is provided by the user in a reservoir, which can be dispersed as vapour by e.g. wick filter, mist formation by ultrasonic vibrator, or boiling of the water.

7.2.16. Thermochemistry of Combustion

Stoichiometry of Combustion Reactions

- **Stoichiometric combustion** of hydrocarbon fuels in atmospheric nitrogen-oxygen:

$$C_x H_y + \left(x + \frac{y}{4}\right)\left(O_2 + \frac{79}{21} N_2^*\right) \rightarrow x\, CO_2 + \frac{y}{2}\, H_2O + \frac{79}{21}\left(x + \frac{y}{4}\right) N_2^*$$
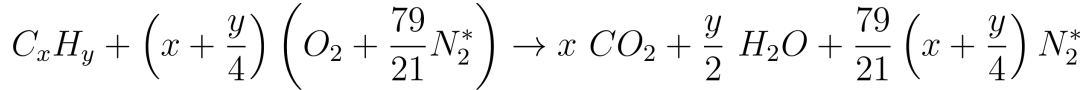
(Neglects small amounts of nitrogen oxidation to NO_x)

- **Air-to-fuel mass ratio (AFR):** $AFR = \dfrac{\dot{m}_{N_2^*,O_2}}{\dot{m}_{C_xH_y}}$ and $AFR_{stoichiometric} = \dfrac{28x + 7y}{12x + y}$

(M_r of atmospheric nitrogen, N_2* (diatomic nitrogen plus Ar, CO_2, etc.) = 28 g mol^{-1}.)

- **Lambda number:** $\lambda = \dfrac{AFR}{AFR_{stoichiometric}}$ and **equivalence ratio:** $\phi = \dfrac{1}{\lambda}$

($\lambda > 1 \rightarrow$ lean, oxygen-rich, complete combustion; $\lambda < 1 \rightarrow$ (fuel)-rich, incomplete combustion. Optimal combustion typically requires some $\lambda > 1$: the value of $\lambda - 1$ is the 'excess air'.)

- **Reaction in lean conditions:**

$$C_x H_y + \lambda\left(x + \frac{y}{4}\right)\left(O_2 + \frac{79}{21} N_2^*\right) \rightarrow \; x\, CO_2 + \frac{y}{2}\, H_2O + (\lambda - 1)\left(x + \frac{y}{4}\right) O_2 + \frac{79}{21}\lambda\left(x + \frac{y}{4}\right) N_2^*$$
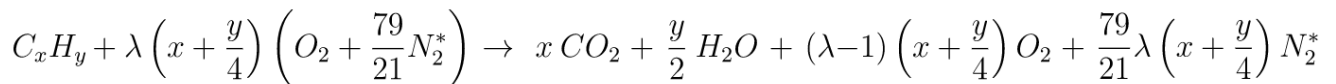
(Dry basis: water product is liquid (absent in gaseous mixture).
Wet basis: water product is gas (present in gaseous mixture), assumed when $T > 100$ °C.)

If $\lambda < 1$ (oxygen-deficient) then combustion is incomplete and products are C / CO / CO_2 / H_2. Hydrogen is always fully oxidised first to H_2O. For reactions see Section 14.3.4.

Energetics of Combustion (1st law analysis). For useful data see Section 7.4.1-3.

II: combustion at STP

Q_{10} Q_0 $Q_{02} = -(Q_0+Q_{10})$

ΔH₀ Combustion

R1   R0   P0   P2

I: heat removed to bring reactants to STP

III: heat added to bring products to final temperature

NB if the fuel is liquid, this term will include the latent heat of vaporisation.

$$\dot{Q} - \dot{W}_x = \dot{m}(h_{P2} - h_{R1}) = \dot{m}\left[(h_{P2} - h_{P0}) + (h_{P0} - h_{R0}) + (h_{R0} - h_{R1})\right]$$

III   II   I
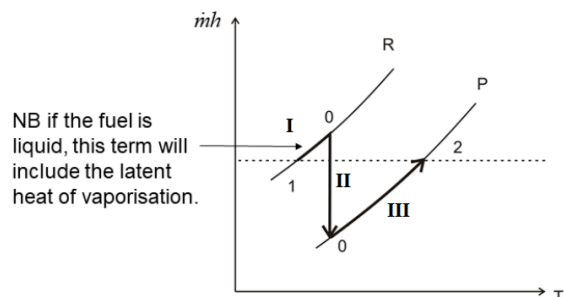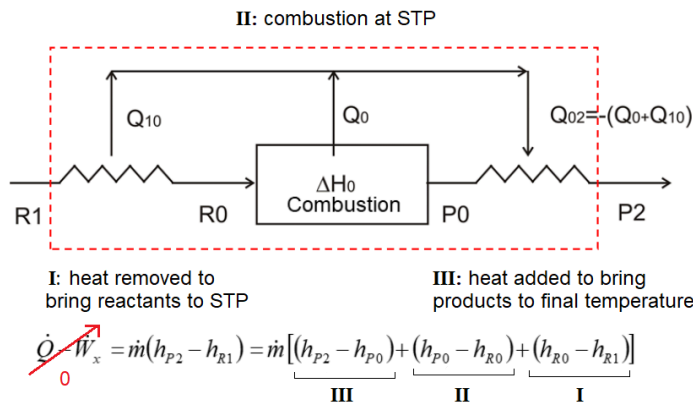
7.2.17. Aerodynamic Analysis of Turbines

(V_0: upstream speed, A: turbine swept area, ρ: fluid density, θ: local twist angle of blade, ω: blade angular speed, $\sigma = \frac{cB}{2\pi r}$: rotor solidity, B: number of blades, c: chord length, $a = 1 - \frac{U}{V_0}$: axial induction factor, r: radial position)

Flow angle: $\tan \phi = \frac{(1-a)\,V_0}{(1+a')\,\omega R}$ Local angle of attack: $\alpha = \phi - \theta$

Lift and drag coefficient (below stall): $C_L \approx 2\pi\alpha$ $C_D \approx$ const.   (for $\alpha < 15°$; using radians)

Relative velocity: $V^2_{rel} = V_0^2(1 - a)^2 + r^2\omega^2(1 + a')^2$

Force coefficients: $C_N = \frac{F_N}{\frac{1}{2}\rho V^2_{rel} c} = C_L \cos\phi + C_D \sin\phi$ $C_T = \frac{F_T}{\frac{1}{2}\rho V^2_{rel} c} = C_L \sin\phi - C_D \cos\phi$

Induction factors: axial: $a = \dfrac{1}{1 + \frac{4\sin^2\phi}{\sigma C_N}}$ angular: $a' = \dfrac{1}{1 + \frac{4\sin\phi\cos\phi}{\sigma C_N}}$

Tip speed ratio: $\lambda = \frac{\omega R}{V_0}$

Aerodynamic loads: blade element forces/torques (BEM):

$$\delta N = 4\pi r\rho V_0^2 a(1 - a)\,\delta r, \quad \delta T = 4\pi r^3 \rho V_0(1 - a)\omega a'\,\delta r$$

Total power: $P = \omega T = \omega \int_{r_0}^{R} \delta T = \omega B \int_{r_0}^{R} r\,F_T\,dr$

Available power: $P_{av} = \frac{1}{2}\rho A V_0^3$

Power coefficient: $C_P = \frac{P}{P_{av}} = \frac{P}{\frac{1}{2}\rho A U^3} = 4a(1 - a^2)$ $(a = 1 - \frac{U}{V_0}$: axial induction factor)

Betz limit: $C_{P,max} = \frac{16}{27} \approx 59\%$ when $a = \frac{1}{3}$.

Capacity factor: $\dfrac{energy\ generated\ over\ a\ long\ time}{rated\ power \times time}$, a measure of installation effectiveness.

Additional loads are due to centrifugal force and self-weight. These are cyclic (periodic) with frequency $f = \frac{\omega B}{2\pi}$ (fatigue inducing: Section 6.6.6). Storm loading should also be considered. Wind loading is often modelled using the Wisper spectrum and generalisations to Miner's rule for fatigue modelling.

7.3. Heat Transfer

7.3.1. Steady Heat Transfer by Conduction, Convection and Radiation

The rate of thermal energy transfer, $\dot{Q}$ (units: W) is related to a temperature change ΔT by a thermal resistance R_{th} (units: K W^{-1}) such that $\Delta T = \dot{Q} R_{th}$. The mechanisms include:

- **Convection:** $\dot{Q} = hA\left(T_{body} - T_{surroundings}\right)$, thermal resistance $R_{th} = \dfrac{1}{hA}$
  (h: heat transfer coefficient, A: area of heat transfer)

- **Conduction:** 1D axial $\dot{Q} = -\lambda A \dfrac{dT}{dx}$, thermal resistance $R_{th} = \dfrac{L}{\lambda A}$
  (λ: rod thermal conductivity, A: rod cross-sectional area, dT/dx: temp gradient along rod)

- **Conduction:** 2D radial $\dot{Q} = -2\pi r \lambda L \dfrac{dT}{dr}$, thermal resistance $R_{th} = \dfrac{\ln\left(\frac{r_2}{r_1}\right)}{2\pi \lambda L}$
  (r: radial coordinate in cylindrical rod, L: rod length, dT/dr: radial temp gradient)

- **Conduction:** 3D spherical $\dot{Q} = -4\pi r^2 \lambda \dfrac{dT}{dr}$, thermal resistance $R_{th} = \dfrac{r_2 - r_1}{4\pi \lambda r_1 r_2}$

- **Radiation:** $\dot{Q} = \varepsilon \dot{Q}_{black} = \varepsilon \sigma A T^4$, circuit equivalent in Section 7.3.7.
  (ε: grey body surface emissivity, A: surface area, $\sigma = 5.67 \times 10^{-8}$ W m^{-2} K^{-4}: Stefan-Boltzmann constant. Note that the net rate of heat transfer will be less due to incident radiation.)

Lumped model (Newton's law of cooling): for a body whose Biot number is very small (assumes no internal heat generation, environment thermal bath temp T_∞):

$$\frac{dT}{dt} = k\left(T_\infty - T\right) \quad \text{with solution} \quad \frac{T(t) - T_\infty}{T_0 - T_\infty} = \exp\left(-\frac{hA}{mc}t\right).$$

where $k = \dfrac{UA}{mc}$ and U is the overall heat transfer coefficient (primarily convection, so $U \approx h$).

Combined Conduction and Convection Models: insulated hot cylindrical pipe example
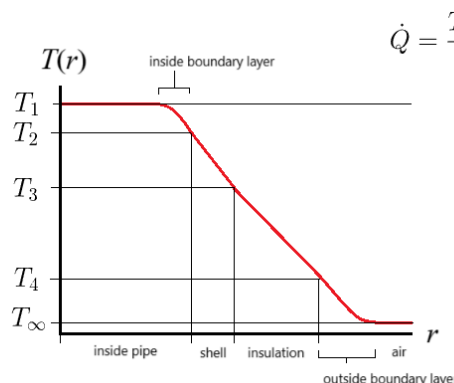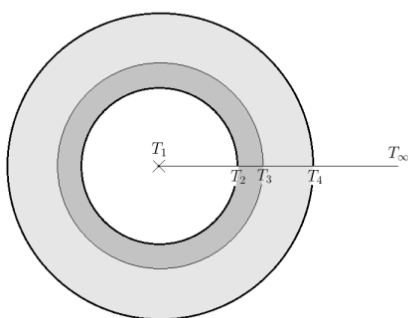
$$\dot{Q} = \frac{T_1 - T_\infty}{R_{total}},$$

$$R_{total} = \frac{1}{h_{in}A_{in}} + \frac{\ln(r_3/r_{in})}{2\pi \lambda_{shell}L} + \frac{\ln(r_{out}/r_3)}{2\pi \lambda_{insulation}L} + \frac{1}{h_{out}A_{out}}$$

7.3.2. Coflow and Counterflow Heat Exchangers

In a co-flow or counter-flow heat exchanger, the log-mean temperature difference (LMTD, ΔT_{LM}) and arithmetic-mean temperature difference (AMTD, ΔT_{AM}) are given by

$$\Delta T_{LM} = \frac{\Delta T_1 - \Delta T_2}{ln\left(\frac{\Delta T_1}{\Delta T_2}\right)} \quad \text{such that} \quad Q' = UA\,\Delta T_{LM} \quad \text{and} \quad \Delta T_{AM} = \tfrac{1}{2}\Big(\Delta T_1 - \Delta T_2\Big).$$

where $\Delta T_1 = T_{h1} - T_{c1}$ and $\Delta T_2 = T_{h2} - T_{c2}$ are temperature differences between the **same ends** of the exchanger (**not** across each tube).

Effectiveness:

$$\varepsilon = \frac{actual\ heat\ exchange}{maximum\ heat\ exchanged\ (counter\ flow)} = \frac{Q'}{Q'_{max}}$$

Efficiency:

$$\eta = \frac{actual\ heat\ exchange}{optimum\ heat\ exchanged} = \frac{Q'}{Q'_{opt}}$$

Maximum heat exchanged:

$$\dot{Q}_{max} = (\dot{m}c_p)_{min} \times (\Delta T)_{max},$$

the product of the smallest heat capacity flow with the largest temperature difference between **any** two ends in the heat exchanger.

Optimum heat exchanged:

$$\dot{Q}_{opt} = UA\,\Delta T_{AM}$$

During a phase change:

$$\dot{Q} = \dot{m}h_{fg}$$

the product of the rate of evaporation or condensation with the enthalpy of the phase change.

7.3.3. Cross-Flow and Shell-Tube Heat Exchangers

For more complex geometry heat exchangers, an empirical correction factor (the F factor) is introduced, such that $\dot{Q} = F \times UA\,\Delta T_m$, ($\Delta T_m$: LMTD of the equivalent counterflow HX.

Cross-flow,
Single-pass,

Both flows
unmixed:
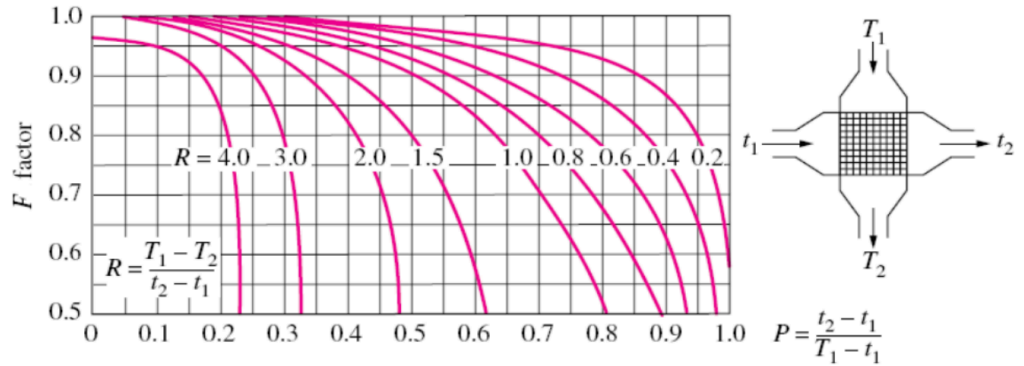
Cross-flow,
Single-pass,

One flow (T) mixed
and the other (t)
unmixed:
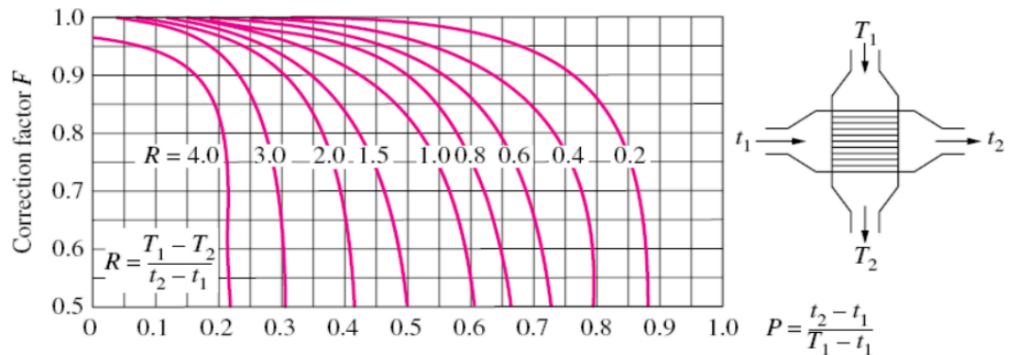
Shell-and-tube,

One shell pass and
2, 4, 6, etc. tube
passes.
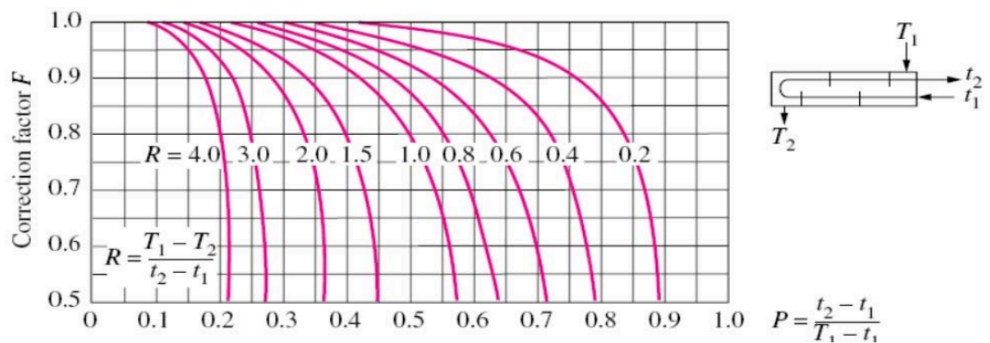
Shell-and-tube,

Two shell passes
and 4, 8, 12, etc.
tube passes.

176
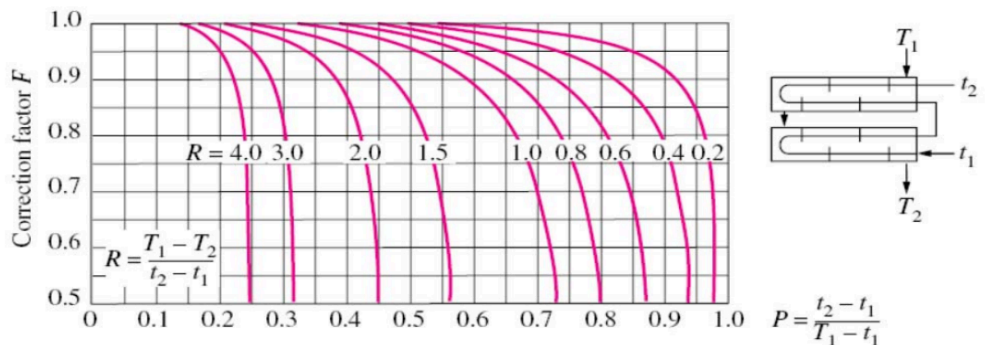
7.3.4. Correlations for Heat Transfer by Natural Convection

For linear models, heat transfer coefficient $h = \dfrac{q'}{A(T_s - T_\infty)}$ and Nusselt number $Nu_L = \dfrac{hL}{\lambda}$.

General approximate ranges for h [W m^{-2} K^{-1}] for different phase interfaces:

	Solid-Liquid	Solid-Gas	Liquid-Gas
Forced	500 - 20,000	20 - 300	20 - 3000
Natural	50 - 1,000	2 - 25	5 - 100

Natural (Free) Convection: heat is supplied or removed by buoyancy of surrounding fluid.

Correlations allow estimation of heat transfer coefficients h from the Nusselt number for a convection process.

Correlations for the Nusselt number, $Nu = f(Re,\ Pr)$ or $Nu = f(Ra,\ Pr)$ are:

Vertical isothermal plate T_s: plate temperature T_∞: free stream temperature ($T_s > T_\infty$) x: position along plate from bottom of plate ($0 < x < L$). For a plate inclined at an angle of θ to the vertical, where $\theta < 60°$, these correlations remain valid if $g \to g \cos \theta$ is used to calculate Ra$_L$.	All regimes: $\overline{Nu}_L = \left[0.825 + \dfrac{0.387\,Ra_L^{1/6}}{\left[1 + \left(\frac{0.492}{Pr} \right)^{9/16} \right]^{8/27}} \right]^2$ Ra$_L < 10^9$ (laminar): $\overline{Nu}_L = 0.68 + \dfrac{0.387\,Ra_L^{1/4}}{\left[1 + \left(\frac{0.492}{Pr} \right)^{9/16} \right]^{4/9}}$
Horizontal isothermal plate T_s: plate temperature T_∞: free stream temperature x: position along plate from bottom of plate ($0 < x < L$, $T_s > T_\infty$) $L = \dfrac{plate\ surface\ area}{plate\ face\ perimeter}$	Upper surface of hot plate or lower surface of cold plate; $10^4 < Ra_L < 10^7$: $\overline{Nu}_L = 0.54\,Ra_L^{1/4}$ $10^7 < Ra_L < 10^{11}$: $\overline{Nu}_L = 0.15\,Ra_L^{1/3}$ Lower surface of hot plate or upper surface of cold plate; $10^5 < Ra_L < 10^{10}$: $\overline{Nu}_L = 0.27\,Ra_L^{1/4}$
Horizontal isothermal cylinder T_s: cylinder temperature T_∞: free stream temperature D: cylinder diameter	Ra$_L < 10^{12}$: $\overline{Nu}_D = \left[0.60 + \dfrac{0.387\,Ra_D^{1/6}}{\left[1 + \left(\frac{0.559}{Pr} \right)^{9/16} \right]^{8/27}} \right]^2$
Isothermal sphere T_s: sphere temperature T_∞: free stream temperature D: sphere diameter	Ra$_D < 10^{11}$, Pr > 0.7: $\overline{Nu}_D = 2 + \dfrac{0.589\,Ra_D^{1/4}}{\left[1 + \left(\frac{0.469}{Pr} \right)^{9/16} \right]^{4/9}}$

7.3.5. Correlations for Heat Transfer by Forced Convection

Forced Convection: heat is supplied or removed by constantly flowing surrounding fluid.

For forced convection into gases, the HTC is on the order of 10-100 W m^{-2} K^{-1}.

The Reynolds analogy between heat and momentum transfer: $St = \frac{1}{2} c_f$

The film temperature between a temperature T and a flow at T_∞: $T_{film} = \frac{1}{2}(T + T_\infty)$

Flat isothermal plate oriented parallel to flow T_s: plate temperature U_∞: free stream velocity T_∞: free stream temperature x: position along plate from inlet edge of plate ($0 < x < L$, $T_s > T_\infty$)	Pr > 0.6 (laminar): $Nu_x = 0.332\, Re_x^{1/2}\, Pr^{1/3}$ Pr > 0.6 (laminar): $\overline{Nu_x} = 2\, Nu_x = 0.664\, Re_x^{1/2}\, Pr^{1/3}$ 0.6 < Pr < 60 (turbulent): $Nu_x = 0.0296\, Re_x^{4/5}\, Pr^{1/3}$ 0.6 < Pr < 60 (turbulent): $\overline{Nu_x} = 0.037\, Re_x^{4/5}\, Pr^{1/3}$
Flat plate with uniform heat flux oriented parallel to flow U_∞: free stream velocity T_∞: free stream temperature x: position along plate from inlet edge of plate ($0 < x < L$, $T_s > T_\infty$)	Pr > 0.6 (laminar): $Nu_x = 0.453\, Re_x^{1/2}\, Pr^{1/3}$ All regimes: $\overline{Nu_x} = 0.68\, Re_x^{1/2}\, Pr^{1/3}$ 0.6 < Pr < 60 (turbulent): $Nu_x = 0.0308\, Re_x^{4/5}\, Pr^{1/3}$
Isothermal cylinder in cross flow T_s: plate temperature U_∞: free stream velocity T_∞: free stream temperature D: diameter of cylinder	$Re_D\, Pr > 0.2$: $\overline{Nu_D} = 0.3 + \dfrac{0.62\, Re_D^{1/2}\, Pr^{1/3}\left[1 + \left(\frac{Re_D}{282000}\right)^{5/8}\right]^{4/5}}{\left[1 + \left(\frac{0.4}{Pr}\right)^{2/3}\right]^{1/4}}$ $0.4 < Re_D < 4$: $\overline{Nu_D} = 0.989\, Re_D^{0.33}\, Pr^{1/3}$ $4 < Re_D < 40$: $\overline{Nu_D} = 0.911\, Re_D^{0.385}\, Pr^{1/3}$ $40 < Re_D < 4000$: $\overline{Nu_D} = 0.683\, Re_D^{0.466}\, Pr^{1/3}$ $4000 < Re_D < 4 \times 10^4$: $\overline{Nu_D} = 0.193\, Re_D^{0.618}\, Pr^{1/3}$ $4 \times 10^4 < Re_D < 4 \times 10^5$: $\overline{Nu_D} = 0.027\, Re_D^{0.805}\, Pr^{1/3}$
Sphere in cross flow D: diameter of sphere	Re < 5×10^5: $Nu_D = 2 + \left(0.4\, Re_D^{1/2} + 0.06\, Re_D^{2/3}\right) Pr^{0.4}$

Forced Convection in Pipe Flow: fluid-wall convection due to internal pipe flow

For pipe flow, fluid properties are taken at the local mean temperature $T_m = \dfrac{2}{u_m r_{max}^2} \int\limits_0^{r_{max}} uTr\, dr,$

where u_m is the mean velocity, $u_m = \dfrac{2}{r_{max}^2} \int\limits_0^{r_{max}} u(r,\, x)\, r\, dr.$ (r_{max}: pipe internal radius)

a) $T_s = constant$ b) $q_s'' = constant$

Entrance region   Fully developed region

Laminar Pipe Flow	Case a): Isothermal, laminar: $\qquad Nu_D = 3.66$
T_s: pipe surface temperature U_∞: free stream velocity T_∞: free stream temperature D: diameter of cylinder	Case b): Constant heat flux, laminar: $\quad Nu_D = 4.36$ Full region including entrance effects: $\overline{Nu}_D = 1.86 \left(\dfrac{Re_D\, Pr}{L/D}\right)^{1/3} \left(\dfrac{\mu}{\mu_s}\right)^{0.14}$
Turbulent Pipe Flow	Small temperature differences: $\quad Nu_D = 0.023\, Re_D^{4/5}\, Pr^{0.3}$
T_s: pipe surface temperature U_∞: free stream velocity T_∞: free stream temperature D: diameter of cylinder	Large temperature differences: $\quad Nu_D = 0.027\, Re_D^{4/5}\, Pr^{1/3} \left(\dfrac{\mu}{\mu_s}\right)^{0.14}$ For non-circular pipes, use the hydraulic diameter, $D_h = \dfrac{4 A_c}{P}$ (A_c: area, P: perimeter)

Two-phase external flow boiling: evaporation and convection, hot vertical cylinders (Chen's correlation)

$$h = S \cdot \underbrace{\frac{\lambda^{0.79} c_p^{0.45} \rho_l^{0.49} g^{0.25} \Delta T^{0.24} \Delta p^{0.75}}{\sigma^{0.5} \mu^{0.29} h_{fg}^{0.24} \rho_v^{0.24}}}_{h_{pool}:\ \text{nucleate pool boiling (Forster-Zuber corr.)}} + F \cdot \underbrace{\frac{\mathrm{Re}^{0.8} \mathrm{Pr}^{0.4} \lambda}{d_{eq}}}_{\substack{h_{conv}:\ \text{forced convection} \\ \text{(Dittus-Boelter corr.)}}}$$

(λ: thermal conductivity, c_p: specific heat capacity, ρ: density, g: gravitational acceleration,
$\Delta T = T_{wall} - T_{sat}$, Δp_{sat}: bubble pressure drop, σ: surface tension, μ: dynamic viscosity,
h_{fg}: specific latent heat of vaporisation, d_{eq}: hydraulic diameter, Re_{tp}: two-phase Reynolds,

χ_{tt}: Lockhart-Martinelli parameter, $S = \dfrac{1}{1 + 2.53 \times 10^{-6} \times Re_{tp}^{1.17}}$, $F = \left(\dfrac{Re_{tp}}{Re}\right)^{0.8} = 2.35 \times \left(\dfrac{1}{\chi_{tt}} + 0.213\right)^{0.736}$.)
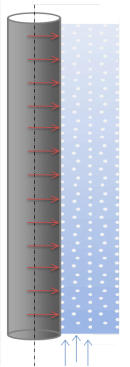
Simpler alternative correlations include McAdams' correlation and Thom's correlation, as well as accounting for the **Leidenfrost effect** (protective vapour layer forming at the surface).

7.3.6. Thermal Radiation

A 'black body' is an idealised object, which will completely absorb all radiation incident upon it, and emit the largest amount of power per unit area possible for a given temperature: ($\sigma = 5.67 \times 10^{-8}$ W m^{-2} K^{-4}: Stefan-Boltzmann constant)

Total energy flux, E_b [W m^{-2}] $= \sigma T^4$;   **Total entropy flux**, S_b [W K^{-1} m^{-2}] $= \frac{4}{3}\sigma T^3$

Spectra, such that $E_b = \int_0^\infty E_{b\lambda}\, d\lambda$ and $S_b = \int_0^\infty S_{b\lambda}\, d\lambda$, are

Energy spectrum, $E_{b\lambda} = \dfrac{2hc^2}{\lambda^5\left(exp\left(\frac{hc}{k\lambda T}\right)\right)}$ (λ: wavelength)

Entropy spectrum, $S_{b\lambda} = \dfrac{2n_0 kc}{\lambda^4}\left[\left(1 + \dfrac{\lambda^5 E_{b\lambda}}{2n_0 hc^2}\right) ln\left(1 + \dfrac{\lambda^5 E_{b\lambda}}{2n_0 hc^2}\right) - \dfrac{\lambda^5 E_{b\lambda}}{2n_0 hc^2}\, ln\,\dfrac{\lambda^5 E_{b\lambda}}{2n_0 hc^2}\right]$ (λ: wavelength)

Exergy spectrum, $e_{b\lambda}(T) = [E_{b\lambda}(T) - E_{b\lambda}(T_0)] - T_0[S_{b\lambda}(T) - S_{b\lambda}(T_0)]$ (same expression for total).

(monochromatic emissive black body spectra i.e. between wavelengths λ and $\lambda + d\lambda$; $\sigma = 5.67 \times 10^{-8}$ W m^{-2} K^{-4}: Stefan-Boltzmann constant, $c_1 = 2\pi hc^2 = 3.743 \times 10^{-16}$ W m^{-2}, $c_2 = hc / k_B = 1.4387 \times 10^4$ µm K, with wavelength λ in numerical units of µm, v []: frequency of radiation, $n_0 = \{1$ if polarised rays; 2 if unpolarised rays$\}$, T: emitter temperature, T_0: dead state / receiver temperature)

Grey Body: has an emissive power proportional to a black body at the same temperature for all wavelengths, with an emissivity ε such that $E_\lambda = \varepsilon E_{b\lambda}$ and $S_\lambda = \varepsilon S_{b\lambda}$.

For **matte black** materials, $\varepsilon \approx 1$, $\rho \approx 0$. For **shiny white** or mirror-like materials, $\varepsilon \approx 0$, $\rho \approx 1$.

Irradiation, G [W m^{-2}]: the total radiation incident on a surface
Luminosity, J [W m^{-2}]: the total radiation leaving a surface
Absorptivity α, Emissivity ε, Reflectivity ρ, and Transmissivity τ:

$$J = \varepsilon E_b + \rho G \qquad \text{where } \alpha + \rho + \tau = 1 \text{ and } \alpha = \varepsilon.$$

For most solids in the infrared range, $\tau = 0$.
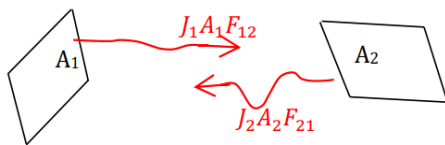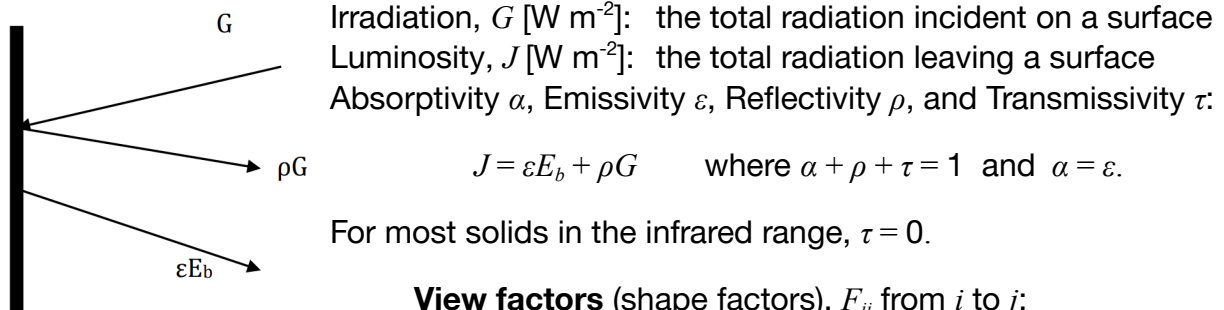
View factors (shape factors), F_{ij} from i to j:

$$A_i F_{ij} = A_j F_{ji}, \quad \sum_j F_{ij} = 1, \quad i \text{ is convex} \Leftrightarrow F_{ii} = 0$$

If the medium does not interact with infrared radiation

(i.e. $\tau_{medium} = 1$) then $Q = \dfrac{J_1 - J_2}{1/(A_1 F_{12})}$.

7.3.7. Electrical Analogy for Radiative Exchange Between Surfaces

- Electrical-radiative circuit analogy: $\quad I = \dfrac{\Delta V}{R_{elec}} \Leftrightarrow \dot{Q} = \dfrac{\Delta E}{R_{th}}$ (Ohm's law)

  (ΔE: radiation intensity difference, $\dot{Q}$: radiative heat transfer rate, R_{th}: thermal resistance)

- Grey body emission: $\quad R_{th} = \dfrac{1 - \varepsilon}{\varepsilon A}$ such that $E_b - J = \dot{Q} R_{th}$

  ($E_b = \sigma T^4$: black body intensity, J: luminosity, ε: emissivity, A: surface area)

- Radiative exchange: $\quad R_{th} = \dfrac{1}{AF}$ such that $J_1 - J_2 = \dot{Q}' R_{th}$

  (A: area of this body, F: view factor from this body to another, $\dot{Q}'$: heat transfer rate between bodies when the system is loses no radiation to the environment)

A typical two-body setup (with the environment as a third 'body') can be represented as

Star-Delta transformation

$$R_1' = \frac{F_{23}}{A_2 F_{23} F_{13} + A_2 F_{12} F_{23} + A_1 F_{12} F_{13}}$$

$$R_2' = \frac{F_{13}}{A_2 F_{23} F_{13} + A_2 F_{12} F_{23} + A_1 F_{12} F_{13}}$$

$$R_3' = \frac{F_{12}}{A_2 F_{23} F_{13} + A_2 F_{12} F_{23} + A_1 F_{12} F_{13}}$$
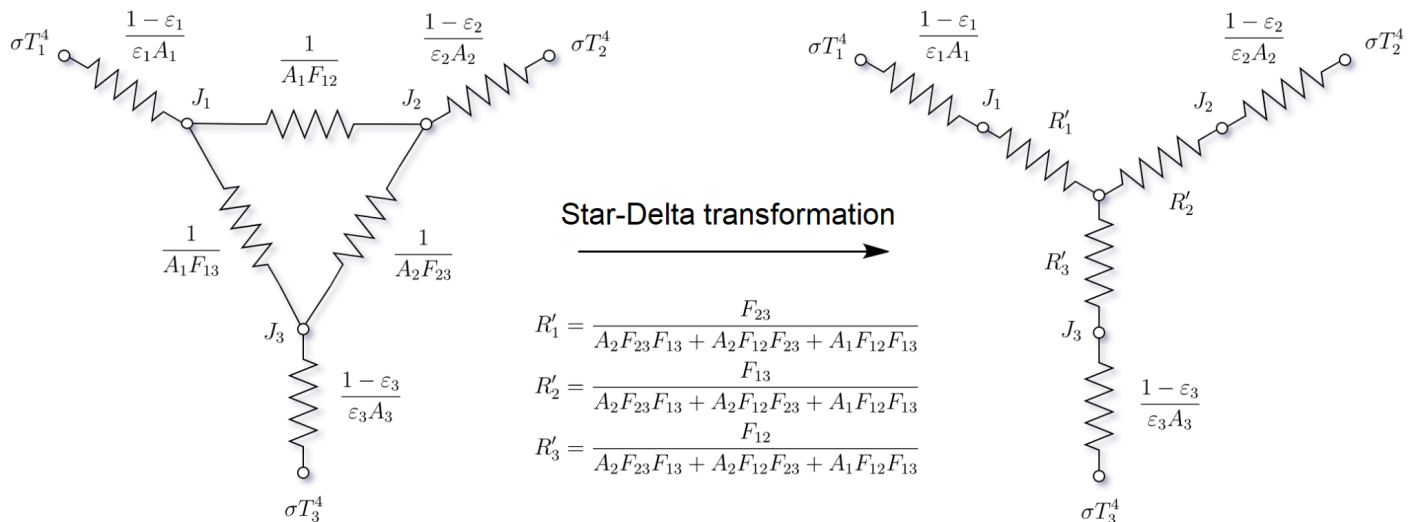
For the details of the Star-Delta transformation, see Section 8.2.2. Other simplifications:

- If a surface is insulated, there is no net current flow into it, so it can be simplified to be considered a black body (i.e. short / remove its $\sigma T^4 - J$ resistor).

- For the environment, since $A \to \infty$, it can be simplified to a black body (i.e. short / remove its $\sigma T^4 - J$ resistor).

7.4. Thermodynamic Data of Fluids

7.4.1. Combustion and Calorific Values of Hydrocarbon-Based Fuels

When heat transfer to a control volume is defined as positive and in the absence of shaft work, changes in KE and PE, capillarity, electric and magnetic fields, the rate of heat transfer and the calorific value (CV) are related by

$$\dot{Q} = \dot{m}_{fuel}\left(-CV\right) = \dot{n}_{fuel}\Delta\overline{h} \qquad \dot{m}_{fuel} = M\dot{n}_{fuel}$$

The calorific value is equal and opposite to the enthalpy of reaction when the reactants and products are at 25 °C and 1.01325 bar. In the evaluation of the lower calorific value and lower enthalpy of reaction, the steam is assumed to be dry saturated.

Stoichiometric Equation	Molar Mass M of Fuel $\dfrac{kg}{kmol}$	Phase	Calorific Value MJ/kg	
$C + \frac{1}{2}O_2 \rightarrow CO$	12	solid	9.190	
$C + O_2 \rightarrow CO_2$	12	solid	32.760	
$CO + \frac{1}{2}O_2 \rightarrow CO_2$	28	gas	10.100	
			Higher: H_2O to water	Lower: H_2O to steam
$H_2 + \frac{1}{2}O_2 \rightarrow H_2O$	2.016	gas	142.000	120.000
$CH_4 + 2O_2 \rightarrow CO_2 + 2H_2O$	16	gas	55.500	50.010
$C_2H_6 + 3.5O_2 \rightarrow 2CO_2 + 3H_2O$	30	gas	51.870	47.470
$C_3H_8 + 5O_2 \rightarrow 3CO_2 + 4H_2O$	44	gas	50.360	46.360
$C_4H_{10} + 6.5O_2 \rightarrow 4CO_2 + 5H_2O$	58	gas	49.520	45.730
$C_8H_{18} + 12.5O_2 \rightarrow 8CO_2 + 9H_2O$	114	gas	48.270	44.800
$C_8H_{18} + 12.5O_2 \rightarrow 8CO_2 + 9H_2O$	114	liquid	47.900	44.430

A dry basis uses the higher CV, a wet basis uses the lower CV.

7.4.2. Properties of Perfect Gases

At normal atmospheric conditions, and over a limited range of temperature and pressure, the gases listed below may be assumed to behave as perfect gases. That is, they may be assumed to have the equation of state $p\overline{v} = \overline{R}T$, and to have constant specific heat capacities.

Gas	Molar mass M kg/kmol	Gas constant R kJ/kg K	c_p kJ/kg K	c_v kJ/kg K	$\gamma \equiv \dfrac{c_p}{c_v}$
Air[#]	29.0	0.287	1.005	0.718	1.40
Atmospheric nitrogen[†]	28.15	0.295	1.033	0.738	1.40
N_2	28	0.297	1.04	0.74	1.40
O_2	32	0.260	0.92	0.66	1.40
Ar	40	0.208	0.52	0.31	1.67
H_2	2[*]	4.120	14.20	10.08	1.41
He	4	2.080	5.19	3.11	1.67
CO	28	0.297	1.04	0.74	1.40
CO_2	44	0.189	0.83	0.63	1.31
SO_2	64	0.130	0.61	0.48	1.26
CH_4	16	0.520	2.23	1.71	1.31
C_2H_6	30	0.277	1.75	1.47	1.19
C_3H_6	42	0.198	1.52	1.32	1.15

- Air contains 0.93 % of argon (Ar) and traces of other gases; these and the nitrogen together are called atmospheric nitrogen (atm N_2).

- Air contains 21.0% O_2 and 79.0% atm N_2 by **volume** (Volumetric / Molar Analysis).

- Air contains 23.2% O_2 and 76.8% atm N_2 by **weight** (Gravimetric Analysis).

- Molar volume: 1 kmol of any perfect gas occupies a volume of approximately 22.7 m³ at s.t.p. (0 °C and 1 bar) and contains 6.022×10^{26} particles.

7.4.3. Molar Enthalpies of Gases at High Temperature and Low Pressure

At low pressures, and over the temperature range quoted, the gases listed below behave as **semi-perfect** gases. That is, while having the molar equation of state $p\bar{v} = \bar{R}T$, their specific heat capacities c_p and c_v are not constant but are functions only of temperature.

Gas	Air	N_2	O_2	H_2	CO	CO_2	H_2O	Gas
Molar Mass kg/kmol	29	28	32	$2^\dagger$	28	44	18	Molar Mass kg/kmol
Temperature K				Molar enthalpy MJ/kmol				Temperature K
200	5.79	5.81	5.79	5.69	5.81	5.96	6.62	200
298.15=25°C	8.64	8.67	8.66	8.46	8.67	9.37	9.90	25°C=298.15
300	8.70	8.72	8.71	8.52	8.72	9.44	9.96	300
400	11.62	11.64	11.68	11.42	11.64	13.37	13.35	400
500	14.57	14.58	14.74	14.34	14.60	17.67	16.82	500
600	17.59	17.56	17.90	17.27	17.61	22.27	20.39	600
700	20.66	20.61	21.16	20.21	20.69	27.12	24.09	700
800	23.81	23.72	24.50	23.16	23.85	32.18	27.90	800
900	27.03	26.89	27.90	26.13	27.07	37.41	31.83	900
1000	30.30	30.14	31.37	29.14	30.36	42.78	35.90	1000
1100	33.64	33.44	34.88	32.18	33.71	48.27	40.09	1100
1200	37.02	36.79	38.43	35.26	37.11	53.87	44.41	1200
1300	40.44	40.19	42.01	38.38	40.54	59.55	48.84	1300
1400	43.90	43.62	45.63	41.54	44.02	65.31	53.39	1400
1500	47.39	47.09	49.27	44.75	47.53	71.13	58.05	1500
1600	50.92	50.59	52.94	48.00	51.07	77.01	62.81	1600
1700	54.47	54.12	56.63	51.29	54.63	82.94	67.65	1700
1800	58.04	57.67	60.35	54.62	58.21	88.92	72.58	1800
1900	61.63	61.25	64.09	58.00	61.81	94.93	77.59	1900
2000	65.24	64.84	67.86	61.40	65.42	100.97	82.67	2000
2100	68.87	68.44	71.65	64.84	69.06	107.05	87.81	2100
2200	72.52	72.06	75.46	68.31	72.70	113.15	93.01	2200
2300	76.18	75.70	79.29	71.82	76.36	119.28	98.27	2300
2400	79.86	79.35	83.14	75.35	80.03	125.43	103.58	2400
2500	83.55	83.01	87.02	78.90	83.71	131.61	108.94	2500
2600	87.25	86.68	90.92	82.48	87.40	137.80	114.34	2600
2700	90.96	90.36	94.83	86.09	91.10	144.02	119.78	2700
2800	94.69	94.05	98.77	89.72	94.80	150.25	125.26	2800
2900	98.42	97.74	102.72	93.37	98.51	156.50	130.77	2900
3000	102.16	101.44	106.70	97.04	102.23	162.76	136.31	3000

- The molar enthalpies listed are those in the ideal gas state at zero pressure, but the values given are also valid at and around atmospheric pressure.

- In this table, the arbitrary datum state for zero enthalpy is that of the substance in the ideal gas state at zero pressure and zero absolute temperature.

- The values for atmospheric nitrogen, N_2*, may be taken to be the same as those for N_2.

7.4.4. Saturated Water and Steam (Steam Tables)

Temperatures from the triple point to the critical point (showing $0.01\ °C \le T \le 100\ °C$):

Temp. °C	Pressure bar	Specific volume m³/kg		Spec. int. energy kJ/kg		Specific enthalpy kJ/kg			Specific entropy kJ/kg K		Temp. °C
T	p	v_f	v_g	u_f	u_g	h_f	h_{fg}	h_g	s_f	s_g	T
0.01	**0.00611**	**0.001000**	**206.005**	**0.0**	**2375.0**	**0.0**	**2500.9**	**2500.9**	**0.000**	**9.156**	**0.01**
2	0.00706	0.001000	179.776	8.4	2377.6	8.4	2496.2	2504.6	0.031	9.103	2
4	0.00814	0.001000	157.135	16.8	2380.4	16.8	2491.4	2508.2	0.061	9.051	4
6	0.00935	0.001000	137.652	25.2	2383.1	25.2	2486.7	2511.9	0.091	8.999	6
8	0.01073	0.001000	120.846	33.6	2385.9	33.6	2481.9	2515.6	0.121	8.949	8
10	0.01228	0.001000	106.319	42.0	2388.6	42.0	2477.2	2519.2	0.151	8.900	10
12	0.01403	0.001001	93.732	50.4	2391.4	50.4	2472.5	2522.9	0.181	8.851	12
14	0.01599	0.001001	82.804	58.8	2394.1	58.8	2467.7	2526.5	0.210	8.804	14
16	0.01819	0.001001	73.295	67.2	2396.9	67.2	2463.0	2530.2	0.239	8.757	16
18	0.02065	0.001001	65.005	75.5	2399.6	75.5	2458.3	2533.8	0.268	8.711	18
20	0.02339	0.001002	57.762	83.9	2402.3	83.9	2453.5	2537.4	0.296	8.666	20
22	0.02645	0.001002	51.422	92.3	2405.0	92.3	2448.8	2541.1	0.325	8.622	22
24	0.02986	0.001003	45.861	100.6	2407.8	100.6	2444.1	2544.7	0.353	8.578	24
25	**0.03170**	**0.001003**	**43.340**	**104.8**	**2409.1**	**104.8**	**2441.7**	**2546.5**	**0.367**	**8.557**	**25**
26	0.03364	0.001003	40.975	109.0	2410.5	109.0	2439.3	2548.3	0.381	8.535	26
28	0.03783	0.001004	36.673	117.4	2413.2	117.4	2434.6	2551.9	0.409	8.493	28
30	0.04247	0.001004	32.879	125.7	2415.9	125.7	2429.8	2555.5	0.437	8.452	30
32	0.04760	0.001005	29.527	134.1	2418.6	134.1	2425.1	2559.2	0.464	8.411	32
34	0.05325	0.001006	26.560	142.4	2421.3	142.4	2420.3	2562.8	0.492	8.371	34
36	0.05948	0.001006	23.929	150.8	2424.0	150.8	2415.5	2566.3	0.519	8.332	36
38	0.06633	0.001007	21.593	159.2	2426.7	159.2	2410.8	2569.9	0.546	8.294	38
40	0.07385	0.001008	19.515	167.5	2429.4	167.5	2406.0	2573.5	0.572	8.256	40
42	0.08210	0.001009	17.663	175.9	2432.1	175.9	2401.2	2577.1	0.599	8.218	42
44	0.09113	0.001010	16.010	184.2	2434.7	184.2	2396.4	2580.6	0.625	8.181	44
46	0.10100	0.001010	14.534	192.6	2437.4	192.6	2391.6	2584.2	0.652	8.145	46
48	0.11178	0.001011	13.212	201.0	2440.1	201.0	2386.8	2587.8	0.678	8.110	48
50	0.12352	0.001012	12.026	209.3	2442.7	209.3	2382.0	2591.3	0.704	8.075	50
52	0.13632	0.001013	10.962	217.7	2445.4	217.7	2377.1	2594.8	0.730	8.040	52
54	0.15023	0.001014	10.006	226.0	2448.0	226.1	2372.3	2598.3	0.755	8.007	54
56	0.16534	0.001015	9.145	234.4	2450.7	234.4	2367.4	2601.8	0.781	7.973	56
58	0.18172	0.001016	8.368	242.8	2453.3	242.8	2362.5	2605.3	0.806	7.940	58
60	0.19947	0.001017	7.667	251.1	2455.9	251.2	2357.7	2608.8	0.831	7.908	60
62	0.21868	0.001018	7.033	259.5	2458.5	259.5	2352.8	2612.3	0.856	7.876	62
64	0.23944	0.001019	6.460	267.9	2461.1	267.9	2347.9	2615.8	0.881	7.845	64
66	0.26184	0.001020	5.940	276.3	2463.7	276.3	2342.9	2619.2	0.906	7.814	66
68	0.28600	0.001022	5.468	284.6	2466.3	284.7	2338.0	2622.7	0.931	7.784	68
70	0.31202	0.001023	5.040	293.0	2468.8	293.1	2333.0	2626.1	0.955	7.754	70
72	0.34002	0.001024	4.650	301.4	2471.4	301.4	2328.1	2629.5	0.979	7.725	72
74	0.37010	0.001025	4.295	309.8	2474.0	309.8	2323.1	2632.9	1.004	7.696	74
76	0.40240	0.001026	3.971	318.2	2476.5	318.2	2318.1	2636.3	1.028	7.667	76
78	0.43704	0.001028	3.675	326.6	2479.0	326.6	2313.1	2639.7	1.052	7.639	78
80	0.47416	0.001029	3.405	335.0	2481.5	335.0	2308.0	2643.0	1.076	7.611	80
82	0.51388	0.001030	3.158	343.3	2484.1	343.4	2303.0	2646.4	1.099	7.584	82
84	0.55636	0.001032	2.932	351.7	2486.5	351.8	2297.9	2649.7	1.123	7.557	84
86	0.60174	0.001033	2.725	360.1	2489.0	360.2	2292.8	2653.0	1.146	7.530	86
88	0.65018	0.001035	2.534	368.6	2491.5	368.6	2287.6	2656.3	1.170	7.504	88
90	0.70183	0.001036	2.359	377.0	2494.0	377.0	2282.5	2659.5	1.193	7.478	90
92	0.75685	0.001037	2.198	385.4	2496.4	385.4	2277.3	2662.8	1.216	7.453	92
94	0.81542	0.001039	2.050	393.8	2498.8	393.9	2272.1	2666.0	1.239	7.428	94
96	0.87771	0.001040	1.914	402.2	2501.2	402.3	2266.9	2669.2	1.262	7.403	96
98	0.94390	0.001042	1.788	410.6	2503.6	410.7	2261.7	2672.4	1.285	7.378	98
100	1.01418	0.001043	1.672	419.1	2506.0	419.2	2256.4	2675.6	1.307	7.354	100
T	p	v_f	v_g	u_f	u_g	h_f	h_{fg}	h_g	s_f	s_g	T

Temperatures from the triple point to the critical point (showing 100 °C $\leq T \leq$ 373.95 °C):

Temp. °C	Pressure bar	Specific volume m³/kg		Spec. int. energy kJ/kg		Specific enthalpy kJ/kg			Specific entropy kJ/kg K		Temp. °C
T	p	v_f	v_g	u_f	u_g	h_f	h_{fg}	h_g	s_f	s_g	T
100	1.014	0.001043	1.67196	419.1	2506.0	419.2	2256.4	2675.6	1.307	7.354	100
105	1.209	0.001047	1.41856	440.1	2511.9	440.3	2243.1	2683.4	1.363	7.295	105
110	1.434	0.001052	1.20945	461.3	2517.7	461.4	2229.6	2691.1	1.419	7.238	110
115	1.692	0.001056	1.03598	482.4	2523.3	482.6	2216.0	2698.6	1.474	7.183	115
120	1.987	0.001060	0.89133	503.6	2528.8	503.8	2202.1	2705.9	1.528	7.129	120
125	2.322	0.001065	0.77012	524.8	2534.3	525.1	2188.0	2713.1	1.582	7.077	125
130	2.703	0.001070	0.66808	546.1	2539.5	546.4	2173.7	2720.1	1.635	7.026	130
135	3.132	0.001075	0.58179	567.4	2544.6	567.7	2159.1	2726.9	1.687	6.977	135
140	3.615	0.001080	0.50850	588.8	2549.6	589.2	2144.3	2733.4	1.739	6.929	140
145	4.157	0.001085	0.44600	610.2	2554.4	610.6	2129.2	2739.8	1.791	6.883	145
150	4.762	0.001091	0.39248	631.7	2559.0	632.2	2113.7	2745.9	1.842	6.837	150
155	5.435	0.001096	0.34648	653.2	2563.5	653.8	2098.0	2751.8	1.892	6.793	155
160	6.182	0.001102	0.30680	674.8	2567.8	675.5	2082.0	2757.4	1.943	6.749	160
165	7.009	0.001108	0.27244	696.5	2571.8	697.2	2065.6	2762.8	1.992	6.707	165
170	7.922	0.001114	0.24260	718.2	2575.7	719.1	2048.8	2767.9	2.042	6.665	170
175	8.926	0.001121	0.21659	740.0	2579.4	741.0	2031.7	2772.7	2.091	6.624	175
180	10.028	0.001127	0.19384	761.9	2582.8	763.1	2014.2	2777.2	2.139	6.584	180
185	11.235	0.001134	0.17390	783.9	2586.0	785.2	1996.2	2781.4	2.188	6.545	185
190	12.552	0.001141	0.15636	806.0	2589.0	807.4	1977.8	2785.3	2.235	6.506	190
195	13.988	0.001149	0.14089	828.2	2591.7	829.8	1959.0	2788.8	2.283	6.468	195
200	15.549	0.001157	0.12721	850.5	2594.2	852.3	1939.7	2792.0	2.331	6.430	200
205	17.243	0.001164	0.11508	872.9	2596.4	874.9	1919.9	2794.8	2.378	6.393	205
210	19.077	0.001173	0.10429	895.4	2598.3	897.6	1899.6	2797.3	2.424	6.356	210
215	21.059	0.001181	0.09468	918.0	2599.9	920.5	1878.8	2799.3	2.471	6.320	215
220	23.196	0.001190	0.08609	940.8	2601.2	943.6	1857.4	2800.9	2.518	6.284	220
225	25.497	0.001199	0.07841	963.7	2602.2	966.8	1835.3	2802.2	2.564	6.248	225
230	27.971	0.001209	0.07151	986.8	2602.9	990.2	1812.7	2802.9	2.610	6.213	230
235	30.626	0.001219	0.06530	1010.0	2603.2	1013.8	1789.4	2803.2	2.656	6.178	235
240	33.470	0.001229	0.05971	1033.4	2603.1	1037.6	1765.4	2803.0	2.702	6.142	240
245	36.512	0.001240	0.05466	1057.0	2602.7	1061.5	1740.7	2802.2	2.748	6.107	245
250	39.762	0.001252	0.05009	1080.8	2601.8	1085.8	1715.2	2800.9	2.793	6.072	250
255	43.229	0.001263	0.04594	1104.8	2600.5	1110.2	1688.9	2799.1	2.839	6.037	255
260	46.923	0.001276	0.04218	1129.0	2598.7	1134.9	1661.7	2796.6	2.885	6.002	260
265	50.853	0.001289	0.03875	1153.4	2596.5	1159.9	1633.6	2793.5	2.930	5.966	265
270	55.030	0.001303	0.03562	1178.1	2593.7	1185.2	1604.5	2789.7	2.976	5.930	270
275	59.464	0.001317	0.03277	1203.0	2590.3	1210.9	1574.3	2785.2	3.022	5.894	275
280	64.166	0.001333	0.03015	1228.3	2586.4	1236.8	1543.0	2779.9	3.068	5.858	280
285	69.146	0.001349	0.02776	1253.9	2581.8	1263.2	1510.5	2773.7	3.114	5.821	285
290	74.418	0.001366	0.02555	1279.8	2576.5	1290.0	1476.7	2766.7	3.161	5.783	290
295	79.991	0.001384	0.02353	1306.1	2570.5	1317.2	1441.5	2758.7	3.208	5.745	295
300	85.879	0.001404	0.02166	1332.8	2563.6	1344.9	1404.7	2749.6	3.255	5.706	300
305	92.094	0.001425	0.01993	1360.1	2555.8	1373.2	1366.2	2739.4	3.302	5.666	305
310	98.650	0.001447	0.01833	1387.8	2547.1	1402.1	1325.8	2727.9	3.351	5.624	310
315	105.561	0.001472	0.01685	1416.2	2537.2	1431.7	1283.3	2715.0	3.399	5.582	315
320	112.843	0.001499	0.01547	1445.2	2526.0	1462.1	1238.5	2700.6	3.449	5.537	320
325	120.510	0.001528	0.01418	1475.0	2513.4	1493.4	1190.9	2684.3	3.500	5.491	325
330	128.581	0.001560	0.01298	1505.7	2499.2	1525.8	1140.2	2666.0	3.552	5.442	330
335	137.073	0.001597	0.01185	1537.5	2483.0	1559.4	1086.0	2645.4	3.605	5.391	335
340	146.007	0.001638	0.01078	1570.7	2464.5	1594.6	1027.4	2621.9	3.660	5.336	340
345	155.406	0.001685	0.00977	1605.4	2443.2	1631.6	963.4	2595.1	3.718	5.276	345
350	165.293	0.001741	0.00881	1642.3	2418.3	1671.1	892.7	2563.8	3.779	5.211	350
355	175.700	0.001808	0.00787	1682.1	2388.6	1713.9	812.9	2526.9	3.844	5.138	355
360	186.660	0.001895	0.00695	1726.2	2351.8	1761.5	720.0	2481.6	3.916	5.054	360
365	198.218	0.002015	0.00601	1777.2	2303.6	1817.2	605.5	2422.7	4.000	4.949	365
370	210.438	0.002217	0.00495	1844.5	2230.1	1891.2	443.1	2334.3	4.112	4.801	370
373.95	220.640	0.003106	0.00311	2018.1	2018.1	2086.6	0.0	2086.6	4.410	4.410	373.95
T	p	v_f	v_g	u_f	u_g	h_f	h_{fg}	h_g	s_f	s_g	T

Pressures from the triple point to the critical point (showing $0.00611 \text{ bar} \leq p \leq 1.00 \text{ bar}$):

Pressure bar	Temp. °C	Specific volume m³/kg		Spec. int. energy kJ/kg		Specific enthalpy kJ/kg			Specific entropy kJ/kg K		Pressure bar
p	T	v_f	v_g	u_f	u_g	h_f	h_{fg}	h_g	s_f	s_g	p
0.00611	0.01	0.001000	206.0005	0.0	2375.0	0.0	2500.9	2500.9	0.000	9.156	0.00611
0.02	17.50	0.001001	66.990	73.4	2398.9	73.4	2459.5	2532.9	0.261	8.723	0.02
0.04	28.96	0.001004	34.791	121.4	2414.5	121.4	2432.3	2553.7	0.422	8.473	0.04
0.06	36.16	0.001006	23.733	151.5	2424.2	151.5	2415.2	2566.6	0.521	8.329	0.06
0.08	41.51	0.001008	18.099	173.8	2431.4	173.8	2402.4	2576.2	0.592	8.227	0.08
0.10	45.81	0.001010	14.670	191.8	2437.2	191.8	2392.1	2583.9	0.649	8.149	0.10
0.12	49.42	0.001012	12.358	206.9	2442.0	206.9	2383.4	2590.3	0.696	8.085	0.12
0.14	52.55	0.001013	10.691	220.0	2446.1	220.0	2375.8	2595.8	0.737	8.031	0.14
0.16	55.31	0.001015	9.431	231.5	2449.8	231.6	2369.1	2600.6	0.772	7.985	0.16
0.18	57.80	0.001016	8.443	241.9	2453.0	241.9	2363.0	2605.0	0.804	7.944	0.18
0.20	60.06	0.001017	7.648	251.4	2456.0	251.4	2357.5	2608.9	0.832	7.907	0.20
0.22	62.13	0.001018	6.994	260.1	2458.7	260.1	2352.4	2612.5	0.858	7.874	0.22
0.24	64.05	0.001019	6.446	268.1	2461.2	268.1	2347.7	2615.9	0.882	7.844	0.24
0.26	65.84	0.001020	5.979	275.6	2463.5	275.6	2343.3	2619.0	0.904	7.817	0.26
0.28	67.52	0.001021	5.578	282.6	2465.7	282.6	2339.2	2621.8	0.925	7.791	0.28
0.30	69.09	0.001022	5.229	289.2	2467.7	289.3	2335.3	2624.5	0.944	7.767	0.30
0.32	70.58	0.001023	4.922	295.5	2469.6	295.5	2331.6	2627.1	0.962	7.745	0.32
0.34	72.00	0.001024	4.650	301.4	2471.4	301.4	2328.1	2629.5	0.979	7.725	0.34
0.36	73.34	0.001025	4.407	307.0	2473.1	307.1	2324.7	2631.8	0.996	7.705	0.36
0.38	74.63	0.001026	4.190	312.4	2474.8	312.5	2321.5	2634.0	1.011	7.687	0.38
0.40	75.86	0.001026	3.993	317.6	2476.3	317.6	2318.4	2636.1	1.026	7.669	0.40
0.42	77.03	0.001027	3.815	322.5	2477.8	322.6	2315.5	2638.0	1.040	7.652	0.42
0.44	78.16	0.001028	3.652	327.3	2479.2	327.3	2312.6	2639.9	1.054	7.637	0.44
0.46	79.25	0.001029	3.503	331.8	2480.6	331.9	2309.9	2641.8	1.067	7.621	0.46
0.48	80.30	0.001029	3.367	336.2	2481.9	336.3	2307.2	2643.5	1.079	7.607	0.48
0.50	81.32	0.001030	3.240	340.5	2483.2	340.5	2304.7	2645.2	1.091	7.593	0.50
0.52	82.30	0.001031	3.123	344.6	2484.4	344.6	2302.2	2646.8	1.103	7.580	0.52
0.54	83.25	0.001031	3.015	348.6	2485.6	348.6	2299.8	2648.4	1.114	7.567	0.54
0.56	84.17	0.001032	2.914	352.4	2486.8	352.5	2297.4	2649.9	1.125	7.555	0.56
0.58	85.06	0.001032	2.820	356.2	2487.9	356.3	2295.2	2651.4	1.135	7.543	0.58
0.60	85.93	0.001033	2.732	359.8	2488.9	359.9	2293.0	2652.9	1.145	7.531	0.60
0.62	86.77	0.001034	2.649	363.4	2490.0	363.4	2290.8	2654.2	1.155	7.520	0.62
0.64	87.59	0.001034	2.572	366.8	2491.0	366.9	2288.7	2655.6	1.165	7.509	0.64
0.66	88.39	0.001035	2.499	370.2	2492.0	370.3	2286.6	2656.9	1.174	7.499	0.66
0.68	89.17	0.001035	2.430	373.5	2492.9	373.5	2284.6	2658.2	1.183	7.489	0.68
0.70	89.93	0.001036	2.365	376.7	2493.9	376.7	2282.7	2659.4	1.192	7.479	0.70
0.72	90.67	0.001036	2.304	379.8	2494.8	379.9	2280.8	2660.6	1.201	7.470	0.72
0.74	91.40	0.001037	2.245	382.9	2495.7	382.9	2278.9	2661.8	1.209	7.460	0.74
0.76	92.11	0.001037	2.190	385.8	2496.5	385.9	2277.0	2663.0	1.217	7.451	0.76
0.78	92.81	0.001038	2.137	388.8	2497.4	388.8	2275.2	2664.1	1.225	7.443	0.78
0.80	93.49	0.001039	2.087	391.6	2498.2	391.7	2273.5	2665.2	1.233	7.434	0.80
0.82	94.15	0.001039	2.040	394.4	2499.0	394.5	2271.7	2666.3	1.241	7.426	0.82
0.84	94.80	0.001039	1.994	397.2	2499.8	397.3	2270.0	2667.3	1.248	7.418	0.84
0.86	95.44	0.001040	1.951	399.9	2500.6	400.0	2268.4	2668.3	1.255	7.410	0.86
0.88	96.07	0.001040	1.909	402.5	2501.3	402.6	2266.7	2669.3	1.263	7.402	0.88
0.90	96.69	0.001041	1.870	405.1	2502.1	405.2	2265.1	2670.3	1.270	7.394	0.90
0.92	97.29	0.001041	1.832	407.6	2502.8	407.7	2263.5	2671.3	1.277	7.387	0.92
0.94	97.89	0.001042	1.795	410.1	2503.5	410.2	2262.0	2672.2	1.283	7.380	0.94
0.96	98.47	0.001042	1.760	412.6	2504.2	412.7	2260.4	2673.1	1.290	7.373	0.96
0.98	99.04	0.001043	1.726	415.0	2504.9	415.1	2258.9	2674.1	1.296	7.366	0.98
1.00	99.61	0.001043	1.694	417.4	2505.5	417.5	2257.4	2674.9	1.303	7.359	1.00
p	T	v_f	v_g	u_f	u_g	h_f	h_{fg}	h_g	s_f	s_g	p

Pressures from the triple point to the critical point (1.0 bar $\leq p \leq$ 25.5 bar):

Pressure bar	Temp. °C	Specific volume m³/kg		Spec. int. energy kJ/kg		Specific enthalpy kJ/kg			Specific entropy kJ/kg K		Pressure bar
p	T	v_f	v_g	u_f	u_g	h_f	h_{fg}	h_g	s_f	s_g	p
1.0	99.61	0.001043	1.6941	417.4	2505.5	417.5	2257.4	2674.9	1.303	7.359	1.0
1.5	111.35	0.001053	1.1594	467.0	2519.2	467.1	2226.0	2693.1	1.434	7.223	1.5
2.0	120.21	0.001061	0.8858	504.5	2529.1	504.7	2201.5	2706.2	1.530	7.127	2.0
2.5	127.41	0.001067	0.7187	535.1	2536.8	535.3	2181.1	2716.5	1.607	7.053	2.5
3.0	133.52	0.001073	0.6058	561.1	2543.1	561.4	2163.5	2724.9	1.672	6.992	3.0
3.5	138.86	0.001079	0.5242	583.9	2548.5	584.3	2147.7	2732.0	1.727	6.940	3.5
4.0	143.61	0.001084	0.4624	604.2	2553.1	604.7	2133.4	2738.1	1.776	6.896	4.0
4.5	147.90	0.001088	0.4139	622.7	2557.1	623.1	2120.2	2743.4	1.820	6.856	4.5
5.0	151.83	0.001093	0.3748	639.5	2560.7	640.1	2108.0	2748.1	1.860	6.821	5.0
5.5	155.46	0.001097	0.3426	655.2	2563.9	655.8	2096.6	2752.3	1.897	6.789	5.5
6.0	158.83	0.001101	0.3156	669.7	2566.8	670.4	2085.8	2756.1	1.931	6.759	6.0
6.5	161.98	0.001104	0.2926	683.4	2569.4	684.1	2075.5	2759.6	1.962	6.732	6.5
7.0	164.95	0.001108	0.2728	696.2	2571.8	697.0	2065.8	2762.8	1.992	6.707	7.0
7.5	167.75	0.001111	0.2555	708.4	2574.0	709.2	2056.4	2765.6	2.019	6.684	7.5
8.0	170.41	0.001115	0.2403	720.0	2576.0	720.9	2047.4	2768.3	2.046	6.662	8.0
8.5	172.94	0.001118	0.2269	731.0	2577.9	732.0	2038.8	2770.8	2.070	6.641	8.5
9.0	175.35	0.001121	0.2149	741.6	2579.6	742.6	2030.5	2773.0	2.094	6.621	9.0
9.5	177.66	0.001124	0.2041	751.7	2581.2	752.7	2022.4	2775.1	2.117	6.603	9.5
10.0	179.88	0.001127	0.1944	761.4	2582.7	762.5	2014.6	2777.1	2.138	6.585	10.0
10.5	182.01	0.001130	0.1855	770.8	2584.1	771.9	2007.0	2778.9	2.159	6.568	10.5
11.0	184.06	0.001133	0.1775	779.8	2585.5	781.0	1999.6	2780.6	2.178	6.552	11.0
11.5	186.04	0.001136	0.1701	788.5	2586.7	789.8	1992.4	2782.2	2.198	6.537	11.5
12.0	187.96	0.001138	0.1633	797.0	2587.8	798.3	1985.4	2783.7	2.216	6.522	12.0
12.5	189.81	0.001141	0.1570	805.2	2588.9	806.6	1978.6	2785.1	2.234	6.507	12.5
13.0	191.60	0.001144	0.1512	813.1	2589.9	814.6	1971.9	2786.5	2.251	6.494	13.0
13.5	193.35	0.001146	0.1458	820.8	2590.9	822.4	1965.3	2787.7	2.267	6.480	13.5
14.0	195.04	0.001149	0.1408	828.4	2591.8	830.0	1958.9	2788.8	2.284	6.467	14.0
14.5	196.68	0.001151	0.1361	835.7	2592.6	837.4	1952.6	2789.9	2.299	6.455	14.5
15.0	198.29	0.001154	0.1317	842.8	2593.4	844.6	1946.4	2791.0	2.314	6.443	15.0
15.5	199.85	0.001156	0.1276	849.8	2594.1	851.6	1940.3	2791.9	2.329	6.431	15.5
16.0	201.37	0.001159	0.1237	856.6	2594.8	858.5	1934.4	2792.8	2.343	6.420	16.0
16.5	202.86	0.001161	0.1201	863.3	2595.5	865.2	1928.5	2793.7	2.357	6.409	16.5
17.0	204.31	0.001163	0.1167	869.8	2596.1	871.7	1922.7	2794.5	2.371	6.398	17.0
17.5	205.72	0.001166	0.1134	876.1	2596.7	878.2	1917.0	2795.2	2.384	6.388	17.5
18.0	207.11	0.001168	0.1104	882.4	2597.2	884.5	1911.4	2795.9	2.397	6.377	18.0
18.5	208.47	0.001170	0.1075	888.5	2597.8	890.7	1905.9	2796.6	2.410	6.368	18.5
19.0	209.80	0.001172	0.1047	894.5	2598.2	896.7	1900.5	2797.2	2.423	6.358	19.0
19.5	211.10	0.001175	0.1021	900.4	2598.7	902.7	1895.1	2797.8	2.435	6.348	19.5
20.0	212.38	0.001177	0.0996	906.2	2599.1	908.5	1889.8	2798.3	2.447	6.339	20.0
20.5	213.63	0.001179	0.0972	911.8	2599.5	914.2	1884.6	2798.8	2.458	6.330	20.5
21.0	214.86	0.001181	0.0949	917.4	2599.9	919.9	1879.4	2799.3	2.470	6.321	21.0
21.5	216.06	0.001183	0.0928	922.9	2600.2	925.4	1874.3	2799.7	2.481	6.312	21.5
22.0	217.25	0.001185	0.0907	928.3	2600.6	930.9	1869.2	2800.1	2.492	6.304	22.0
22.5	218.41	0.001187	0.0887	933.6	2600.9	936.3	1864.2	2800.5	2.503	6.295	22.5
23.0	219.56	0.001189	0.0868	938.8	2601.1	941.5	1859.3	2800.8	2.513	6.287	23.0
23.5	220.68	0.001191	0.0850	943.9	2601.4	946.7	1854.4	2801.1	2.524	6.279	23.5
24.0	221.79	0.001193	0.0832	949.0	2601.6	951.9	1849.6	2801.4	2.534	6.271	24.0
24.5	222.88	0.001195	0.0816	954.0	2601.9	956.9	1844.8	2801.7	2.544	6.263	24.5
25.0	223.95	0.001197	0.0800	958.9	2602.1	961.9	1840.0	2801.9	2.554	6.256	25.0
25.5	225.01	0.001199	0.0784	963.8	2602.2	966.8	1835.3	2802.2	2.564	6.248	25.5
p	T	v_f	v_g	u_f	u_g	h_f	h_{fg}	h_g	s_f	s_g	p

Pressures from the triple point to the critical point (26.0 bar $\leq T \leq$ 145 bar):

Pressure bar	Temp. °C	Specific volume m³/kg		Spec. int. energy kJ/kg		Specific enthalpy kJ/kg			Specific entropy kJ/kg K		Pressure bar
p	T	v_f	v_g	u_f	u_g	h_f	h_{fg}	h_g	s_f	s_g	p
26.0	226.05	0.001201	0.0769	968.6	2602.4	971.7	1830.7	2802.3	2.574	6.241	26.0
26.5	227.07	0.001203	0.0755	973.3	2602.5	976.5	1826.1	2802.5	2.583	6.234	26.5
27.0	228.08	0.001205	0.0741	977.9	2602.7	981.2	1821.5	2802.7	2.592	6.226	27.0
27.5	229.07	0.001207	0.0727	982.5	2602.8	985.9	1816.9	2802.8	2.601	6.219	27.5
28.0	230.06	0.001209	0.0714	987.1	2602.9	990.5	1812.4	2802.9	2.611	6.212	28.0
28.5	231.02	0.001211	0.0702	991.6	2603.0	995.0	1808.0	2803.0	2.619	6.206	28.5
29.0	231.98	0.001213	0.0690	996.0	2603.1	999.5	1803.6	2803.1	2.628	6.199	29.0
29.5	232.92	0.001215	0.0678	1000.4	2603.1	1004.0	1799.2	2803.1	2.637	6.192	29.5
30	233.85	0.001217	0.06667	1004.7	2603.2	1008.4	1794.8	2803.2	2.645	6.186	30
32	237.46	0.001224	0.06248	1021.5	2603.2	1025.4	1777.7	2803.1	2.679	6.160	32
34	240.90	0.001231	0.05876	1037.7	2603.1	1041.8	1761.0	2802.9	2.710	6.136	34
36	244.18	0.001238	0.05545	1053.1	2602.8	1057.6	1744.8	2802.4	2.740	6.113	36
38	247.33	0.001245	0.05247	1068.1	2602.3	1072.8	1728.9	2801.7	2.769	6.091	38
40	250.35	0.001252	0.04978	1082.5	2601.7	1087.5	1713.3	2800.8	2.797	6.070	40
42	253.26	0.001259	0.04733	1096.4	2601.0	1101.7	1698.1	2799.8	2.823	6.049	42
44	256.07	0.001266	0.04510	1109.9	2600.1	1115.5	1683.1	2798.6	2.849	6.029	44
46	258.78	0.001273	0.04306	1123.0	2599.2	1128.9	1668.4	2797.3	2.874	6.010	46
48	261.40	0.001280	0.04118	1135.8	2598.1	1141.9	1653.9	2795.8	2.898	5.992	48
50	263.94	0.001286	0.03945	1148.2	2597.0	1154.6	1639.6	2794.2	2.921	5.974	50
52	266.40	0.001293	0.03784	1160.3	2595.7	1167.0	1625.5	2792.5	2.943	5.956	52
54	268.79	0.001299	0.03635	1172.1	2594.4	1179.1	1611.6	2790.7	2.965	5.939	54
56	271.12	0.001306	0.03496	1183.6	2593.0	1190.9	1597.8	2788.8	2.986	5.922	56
58	273.38	0.001312	0.03366	1194.9	2591.5	1202.5	1584.2	2786.7	3.007	5.906	58
60	275.58	0.001319	0.03245	1206.0	2589.9	1213.9	1570.7	2784.6	3.027	5.890	60
62	277.73	0.001326	0.03131	1216.8	2588.3	1225.0	1557.4	2782.4	3.047	5.875	62
64	279.83	0.001332	0.03024	1227.4	2586.5	1235.9	1544.1	2780.1	3.067	5.859	64
66	281.87	0.001339	0.02923	1237.8	2584.8	1246.7	1531.0	2777.7	3.085	5.844	66
68	283.87	0.001345	0.02828	1248.1	2582.9	1257.2	1518.0	2775.2	3.104	5.829	68
70	285.83	0.001352	0.02738	1258.1	2581.0	1267.6	1505.0	2772.6	3.122	5.815	70
72	287.74	0.001358	0.02653	1268.0	2579.0	1277.8	1492.2	2770.0	3.140	5.800	72
74	289.61	0.001365	0.02572	1277.8	2577.0	1287.9	1479.4	2767.3	3.157	5.786	74
76	291.45	0.001371	0.02495	1287.4	2574.9	1297.8	1466.7	2764.5	3.174	5.772	76
78	293.25	0.001378	0.02422	1296.8	2572.7	1307.6	1454.0	2761.6	3.191	5.759	78
80	295.01	0.001384	0.02352	1306.1	2570.5	1317.2	1441.4	2758.7	3.208	5.745	80
82	296.74	0.001391	0.02286	1315.3	2568.2	1326.7	1428.9	2755.7	3.224	5.732	82
84	298.43	0.001398	0.02223	1324.4	2565.9	1336.2	1416.4	2752.6	3.240	5.718	84
86	300.10	0.001404	0.02162	1333.4	2563.5	1345.5	1404.0	2749.4	3.256	5.705	86
88	301.74	0.001411	0.02104	1342.2	2561.0	1354.7	1391.5	2746.2	3.271	5.692	88
90	303.35	0.001418	0.02049	1351.0	2558.5	1363.8	1379.2	2742.9	3.287	5.679	90
92	304.93	0.001425	0.01996	1359.7	2556.0	1372.8	1366.8	2739.6	3.302	5.666	92
94	306.48	0.001431	0.01945	1368.2	2553.3	1381.7	1354.5	2736.1	3.317	5.654	94
96	308.01	0.001438	0.01895	1376.7	2550.7	1390.5	1342.1	2732.6	3.331	5.641	96
98	309.52	0.001445	0.01848	1385.1	2548.0	1399.3	1329.8	2729.1	3.346	5.628	98
100	311.00	0.001452	0.01803	1393.4	2545.2	1407.9	1317.5	2725.5	3.360	5.616	100
105	314.60	0.001470	0.01696	1413.9	2538.0	1429.3	1286.8	2716.1	3.396	5.585	105
110	318.08	0.001488	0.01599	1433.9	2530.4	1450.3	1256.0	2706.3	3.430	5.554	110
115	321.43	0.001507	0.01509	1453.6	2522.5	1471.0	1225.1	2696.1	3.464	5.524	115
120	324.68	0.001526	0.01426	1473.0	2514.3	1491.3	1194.1	2685.4	3.496	5.494	120
125	327.81	0.001546	0.01350	1492.2	2505.6	1511.5	1162.8	2674.3	3.529	5.464	125
130	330.85	0.001566	0.01278	1511.1	2496.5	1531.4	1131.3	2662.7	3.561	5.434	130
135	333.80	0.001588	0.01211	1529.8	2487.0	1551.2	1099.3	2650.6	3.592	5.403	135
140	336.67	0.001610	0.01149	1548.4	2477.1	1571.0	1067.0	2637.9	3.623	5.373	140
145	339.45	0.001633	0.01090	1566.9	2466.7	1590.6	1034.1	2624.7	3.654	5.342	145
p	T	v_f	v_g	u_f	u_g	h_f	h_{fg}	h_g	s_f	s_g	p

Pressures from the triple point to the critical point (150 bar $\leq T \leq$ 220.64 bar):

Pressure bar p	Temp. °C T	Specific volume m³/kg v_f	v_g	Spec. int. energy kJ/kg u_f	u_g	Specific enthalpy kJ/kg h_f	h_{fg}	h_g	Specific entropy kJ/kg K s_f	s_g	Pressure bar p
150	342.16	0.001657	0.01034	1585.4	2455.7	1610.3	1000.5	2610.8	3.685	5.311	150
155	344.79	0.001683	0.00981	1603.9	2444.2	1630.0	966.2	2596.3	3.715	5.279	155
160	347.35	0.001710	0.00931	1622.5	2432.0	1649.9	931.1	2581.0	3.746	5.247	160
165	349.86	0.001739	0.00883	1641.2	2419.1	1669.9	894.9	2564.8	3.777	5.213	165
170	352.29	0.001770	0.00837	1660.2	2405.4	1690.3	857.4	2547.7	3.808	5.179	170
175	354.67	0.001804	0.00793	1679.4	2390.7	1711.0	818.5	2529.5	3.840	5.143	175
180	356.99	0.001840	0.00750	1699.1	2374.9	1732.2	777.8	2510.0	3.872	5.106	180
185	359.26	0.001881	0.00709	1719.3	2357.9	1754.1	734.9	2489.0	3.905	5.067	185
190	361.47	0.001926	0.00668	1740.3	2339.1	1776.9	689.2	2466.0	3.940	5.026	190
195	363.63	0.001977	0.00627	1762.3	2318.4	1800.9	639.8	2440.7	3.976	4.981	195
200	365.75	0.002038	0.00586	1785.9	2294.8	1826.6	585.4	2412.1	4.015	4.931	200
205	367.81	0.002111	0.00544	1811.7	2267.3	1855.0	523.8	2378.9	4.057	4.875	205
210	369.83	0.002207	0.00499	1841.6	2233.5	1888.0	450.4	2338.4	4.107	4.808	210
215	371.79	0.002349	0.00448	1879.5	2187.4	1930.0	353.6	2283.6	4.171	4.719	215
220	373.71	0.002703	0.00364	1951.6	2092.4	2011.1	161.5	2172.6	4.294	4.544	220
220.64	373.95	0.003106	0.00311	2018.1	2018.1	2086.6	0.0	2086.6	4.410	4.410	220.64
p	T	v_f	v_g	u_f	u_g	h_f	h_{fg}	h_g	s_f	s_g	p

Above the critical temperature and pressure ($p \geq$ 220.64 bar, $T \geq$ 373.95 K), water enters the **supercritical** state, in which all properties of the liquid and vapour states become equal, so the two phases become fully miscible. The supercritical fluid properties can vary continuously between those of the liquid and vapour states depending on the values of p and T.

7.4.5. Thermodynamic Properties of Water and Steam (Steam Tables)

Specific Enthalpies (h: kJ kg^{-1}):

Pressure (bar) Temp (°C)	0.1	0.5	1	5	10	20	40	60	80	100	150	200	220.64 Critical Isobar	250	300	400	500	1000
0.01	0	0.1	0.1	0.5	1	2	4.1	6.1	8.1	10.1	15.1	20.1	22.1	25	29.9	39.6	49.2	95.4
25	104.8	104.9	104.9	105.3	105.8	106.7	108.5	110.4	112.2	114.1	118.6	123.2	125.1	127.8	132.3	141.3	150.2	194.1
50	2592.0	209.4	209.4	209.8	210.2	211.1	212.8	214.5	216.2	217.9	222.2	226.5	228.3	230.8	235.1	243.6	252.0	293.9
75	2639.8	314.0	314.1	314.4	314.8	315.6	317.2	318.8	320.5	322.1	326.1	330.1	331.8	334.2	338.2	346.2	354.3	394.3
100	2687.5	2682.4	2675.8	419.5	419.8	420.6	422.1	423.6	425.1	426.6	430.4	434.2	435.7	438.0	441.7	449.3	456.9	495.1
125	2735.2	2731.5	2726.7	525.3	525.6	526.3	527.7	529.1	530.5	531.8	535.3	538.8	540.3	542.4	545.9	553.0	560.1	596.3
150	2783.0	2780.2	2776.6	632.2	632.5	633.1	634.4	635.6	636.9	638.1	641.3	644.4	645.8	647.7	650.9	657.4	664.0	697.9
175	2831.2	2828.9	2826.1	2801.4	741.1	741.6	742.7	743.7	744.8	745.9	748.6	751.4	752.6	754.2	757.1	763.0	768.9	800.2
200	2879.6	2877.8	2875.5	2855.8	2828.3	852.5	853.3	854.1	854.9	855.8	858.0	860.3	861.2	862.6	865.0	870.0	875.2	903.4
225	2928.4	2926.8	2924.9	2908.8	2887.0	2836.1	967.1	967.6	968.1	968.7	970.1	971.7	972.4	973.4	975.2	979.0	983.2	1007.6
250	2977.4	2976.1	2974.5	2961.0	2943.1	2903.2	1085.8	1085.7	1085.7	1085.8	1086.1	1086.7	1087.0	1087.4	1088.4	1090.7	1093.5	1113.1
275	3026.9	3025.8	3024.4	3012.9	2997.8	2965.2	2887.3	1210.9	1210.0	1209.3	1207.8	1206.7	1206.4	1206.0	1205.7	1205.8	1206.8	1220.2
300	3076.7	3075.8	3074.5	3064.6	3051.6	3024.2	2961.7	2885.5	2786.5	1343.3	1338.3	1334.4	1333.0	1331.3	1328.9	1325.6	1324.0	1329.1
325	3126.9	3126.1	3125.0	3116.3	3105.0	3081.5	3029.5	2969.5	2898.4	2810.3	1485.6	1475.2	1471.7	1467.3	1461.1	1452.2	1446.4	1440.3
350	3177.5	3176.8	3175.8	3168.1	3158.2	3137.7	3093.3	3043.9	2988.1	2924.0	2693.1	1646.0	1635.6	1623.9	1608.8	1588.8	1576.1	1554.0
375	3228.5	3227.9	3227.0	3220.1	3211.3	3193.2	3154.7	3112.8	3066.9	3016.3	2858.9	2602.6	2337.7	1849.4	1791.8	1742.6	1716.6	1670.8
400	3279.9	3279.3	3278.6	3272.3	3264.5	3248.3	3214.5	3178.2	3139.4	3097.4	2975.7	2816.9	2732.9	2578.6	2152.8	1931.4	1874.4	1791.1
425	3331.8	3331.2	3330.5	3324.9	3317.8	3303.3	3273.2	3241.4	3207.7	3172.0	3072.3	2953.0	2896.1	2805.0	2611.8	2199.0	2060.7	1915.7
450	3384.0	3383.5	3382.8	3377.7	3371.3	3358.2	3331.2	3302.9	3273.3	3242.3	3157.9	3061.7	3017.8	2950.6	2821.0	2511.8	2284.7	2044.7
475	3436.6	3436.2	3435.6	3430.9	3425.1	3413.2	3388.7	3363.4	3337.1	3309.7	3236.6	3155.8	3120.0	3066.2	2966.8	2740.2	2520.0	2178.5
500	3489.7	3489.3	3488.7	3484.5	3479.1	3468.2	3446.0	3423.1	3399.5	3375.1	3310.8	3241.2	3210.8	3165.9	3084.7	2906.5	2722.6	2316.2
550	3597.1	3596.8	3596.3	3592.7	3588.1	3579.0	3560.3	3541.3	3521.8	3502.0	3450.4	3396.1	3373.0	3339.2	3279.7	3154.4	3025.3	2595.9
600	3706.3	3706.0	3705.6	3702.5	3698.6	3690.7	3674.9	3658.7	3642.4	3625.8	3583.1	3539.0	3520.4	3493.5	3446.7	3350.4	3252.5	2865.1
650	3817.2	3816.9	3816.6	3813.9	3810.5	3803.8	3790.1	3776.2	3762.3	3748.1	3712.1	3675.3	3659.8	3637.7	3599.4	3521.6	3443.4	3110.5
700	3929.9	3929.7	3929.4	3927.0	3924.1	3918.2	3906.3	3894.3	3882.2	3870.0	3839.1	3807.8	3794.7	3776.0	3743.9	3679.1	3614.6	3330.7
750	4044.4	4044.2	4043.9	4041.8	4039.3	4034.1	4023.6	4013.2	4002.6	3992.0	3965.2	3938.1	3926.9	3910.9	3883.4	3828.4	3773.9	3530.5
800	4160.6	4160.4	4160.2	4158.4	4156.1	4151.5	4142.3	4133.1	4123.8	4114.5	4091.1	4067.5	4057.7	4043.8	4020.0	3972.6	3925.8	3715.3

Specific Entropies (s: kJ kg^{-1} K^{-1}):

Pressure (bar) Temp (°C)	0.1	0.5	1	5	10	20	40	60	80	100	150	200	220.64 Critical Isobar	250	300	400	500	1000
0.01	0.0000	0.0000	0.0000	0.0000	0.0001	0.0001	0.0002	0.0003	0.0004	0.0005	0.0006	0.0006	0.0006	0.0006	0.0004	-0.0001	-0.0009	-0.0084
25	0.3672	0.3672	0.3672	0.3671	0.3670	0.3667	0.3662	0.3657	0.3651	0.3646	0.3632	0.3619	0.3613	0.3605	0.3591	0.3561	0.3532	0.3371
50	8.1741	0.7038	0.7038	0.7036	0.7034	0.7029	0.7020	0.7010	0.7001	0.6992	0.6969	0.6946	0.6937	0.6923	0.6901	0.6855	0.6810	0.6587
75	8.3167	1.0158	1.0157	1.0155	1.0152	1.0145	1.0133	1.0120	1.0108	1.0096	1.0065	1.0035	1.0022	1.0004	0.9975	0.9916	0.9858	0.9579
100	8.4489	7.6953	7.3610	1.3069	1.3065	1.3057	1.3042	1.3026	1.3011	1.2996	1.2958	1.2920	1.2905	1.2883	1.2847	1.2775	1.2705	1.2375
125	8.5726	7.8225	7.4932	1.5813	1.5808	1.5799	1.5780	1.5762	1.5743	1.5725	1.5680	1.5635	1.5617	1.5591	1.5548	1.5464	1.5381	1.4999
150	8.6892	7.9413	7.6148	1.8418	1.8412	1.8401	1.8379	1.8357	1.8335	1.8313	1.8260	1.8208	1.8186	1.8156	1.8106	1.8008	1.7912	1.7475
175	8.7997	8.0531	7.7284	6.9427	2.0905	2.0892	2.0865	2.0839	2.0813	2.0788	2.0725	2.0664	2.0639	2.0604	2.0545	2.0431	2.0321	1.9824
200	8.9049	8.1592	7.8356	7.0610	6.6955	2.3298	2.3267	2.3235	2.3205	2.3174	2.3100	2.3027	2.2998	2.2956	2.2888	2.2755	2.2628	2.2064
225	9.0053	8.2602	7.9374	7.1702	6.8165	6.4160	2.5612	2.5573	2.5536	2.5499	2.5409	2.5322	2.5287	2.5237	2.5156	2.5000	2.4853	2.4210
250	9.1015	8.3568	8.0346	7.2724	6.9265	6.5475	2.7935	2.7886	2.7839	2.7792	2.7680	2.7573	2.7530	2.7471	2.7373	2.7187	2.7013	2.6277
275	9.1938	8.4495	8.1277	7.3692	7.0286	6.6631	6.2312	3.0222	3.0159	3.0097	2.9951	2.9814	2.9760	2.9685	2.9563	2.9336	2.9128	2.8276
300	9.2827	8.5386	8.2172	7.4614	7.1246	6.7684	6.3639	6.0703	5.7937	3.2488	3.2279	3.2091	3.2018	3.1919	3.1760	3.1473	3.1218	3.0219
325	9.3684	8.6246	8.3034	7.5497	7.2158	6.8662	6.4797	6.2137	5.9851	5.7596	3.4793	3.4495	3.4385	3.4241	3.4017	3.3634	3.3308	3.2117
350	9.4513	8.7076	8.3866	7.6346	7.3029	6.9583	6.5843	6.3357	6.1321	5.9459	5.4437	3.7290	3.7069	3.6804	3.6436	3.5871	3.5431	3.3979
375	9.5315	8.7880	8.4671	7.7164	7.3864	7.0457	6.6809	6.4441	6.2561	6.0911	5.7050	5.2275	4.7985	4.0344	3.9313	3.8290	3.7642	3.5816
400	9.6094	8.8659	8.5452	7.7955	7.4669	7.1292	6.7714	6.5432	6.3658	6.2141	5.8819	5.5525	5.4001	5.1400	4.4757	4.1145	4.0029	3.7639
425	9.6849	8.9416	8.6209	7.8722	7.5447	7.2093	6.8570	6.6352	6.4655	6.3229	6.0229	5.7514	5.6384	5.4707	5.1473	4.5044	4.2746	3.9455
450	9.7584	9.0151	8.6946	7.9465	7.6200	7.2866	6.9386	6.7219	6.5579	6.4219	6.1434	5.9043	5.8098	5.6759	5.4421	4.9448	4.5896	4.1271
475	9.8300	9.0867	8.7663	8.0188	7.6931	7.3613	7.0169	6.8041	6.6445	6.5135	6.2505	6.0324	5.9487	5.8331	5.6404	5.2556	4.9097	4.3089
500	9.8998	9.1566	8.8361	8.0892	7.7641	7.4337	7.0922	6.8826	6.7266	6.5995	6.3480	6.1446	6.0682	5.9642	5.7956	5.4744	5.1762	4.4900
550	10.0344	9.2913	8.9709	8.2249	7.9008	7.5725	7.2355	7.0307	6.8799	6.7585	6.5230	6.3389	6.2715	6.1816	6.0402	5.7857	5.5563	4.8405
600	10.1631	9.4201	9.0998	8.3543	8.0310	7.7043	7.3705	7.1693	7.0221	6.9045	6.6796	6.5075	6.4455	6.3637	6.2373	6.0170	5.8245	5.1581
650	10.2866	9.5436	9.2234	8.4784	8.1557	7.8302	7.4988	7.3001	7.1556	7.0408	6.8233	6.6593	6.6008	6.5242	6.4074	6.2078	6.0373	5.4315
700	10.4055	9.6625	9.3424	8.5977	8.2755	7.9509	7.6214	7.4246	7.2821	7.1693	6.9572	6.7990	6.7431	6.6702	6.5598	6.3740	6.2178	5.6639
750	10.5202	9.7773	9.4572	8.7128	8.3909	8.0670	7.7390	7.5438	7.4028	7.2916	7.0836	6.9297	6.8756	6.8054	6.6997	6.5236	6.3775	5.8642
800	10.6311	9.8882	9.5681	8.8240	8.5024	8.1790	7.8523	7.6582	7.5184	7.4085	7.2037	7.0531	7.0004	6.9322	6.8300	6.6612	6.5225	6.0406

Specific Internal Energies (u: kJ kg^{-1}):

Pressure (bar) Temp (°C)	0.1	0.5	1	5	10	20	40	60	80	100	150	200	220.64 Critical Isobar	250	300	400	500	1000
0.01	0.0	0.0	0.0	0.0	0.0	0.0	0.1	0.1	0.1	0.2	0.2	0.3	0.3	0.3	0.3	0.3	0.3	-0.2
25	104.8	104.8	104.8	104.8	104.7	104.7	104.5	104.4	104.2	104.1	103.7	103.3	103.2	102.9	102.6	101.9	101.1	97.7
50	2443.3	209.3	209.3	209.3	209.2	209.0	208.7	208.4	208.2	207.9	207.1	206.4	206.2	205.8	205.1	203.7	202.5	196.6
75	2479.5	314.0	314.0	313.9	313.8	313.6	313.1	312.7	312.3	311.9	310.8	309.8	309.4	308.8	307.8	305.9	304.1	295.8
100	2515.5	2511.5	2506.2	418.9	418.8	418.5	417.9	417.4	416.8	416.2	414.8	413.5	412.9	412.2	410.9	408.4	405.9	395.1
125	2551.6	2548.7	2545.0	524.7	524.5	524.2	523.4	522.7	522.0	521.2	519.5	517.8	517.1	516.1	514.4	511.2	508.2	494.6
150	2587.9	2585.7	2582.9	631.6	631.4	630.9	630.0	629.1	628.2	627.3	625.1	622.9	622.0	620.8	618.7	614.8	611.0	594.3
175	2624.5	2622.8	2620.6	2601.6	740.0	739.4	738.2	737.0	735.9	734.8	732.0	729.3	728.2	726.7	724.1	719.3	714.6	694.4
200	2661.3	2660.0	2658.2	2643.3	2622.2	850.1	848.6	847.2	845.7	844.3	840.8	837.5	836.1	834.2	831.1	825.1	819.4	795.1
225	2698.5	2697.4	2695.9	2683.9	2667.3	2628.5	962.3	960.5	958.6	956.8	952.4	948.1	946.4	944.1	940.2	932.7	925.8	896.6
250	2736.1	2735.1	2733.9	2723.8	2710.4	2680.2	1080.8	1078.2	1075.8	1073.4	1067.6	1062.2	1060.0	1057.0	1052.0	1042.7	1034.2	999.1
275	2774.0	2773.2	2772.1	2763.6	2752.3	2727.8	2668.9	1203.0	1199.5	1196.2	1188.3	1181.0	1178.1	1174.2	1167.7	1155.9	1145.2	1102.7
300	2812.3	2811.6	2810.6	2803.2	2793.6	2773.2	2726.2	2668.4	2592.3	1329.4	1317.6	1307.1	1303.1	1297.6	1288.9	1273.3	1259.6	1207.6
325	2850.9	2850.3	2849.5	2843.0	2834.7	2817.2	2778.3	2733.1	2679.2	2611.6	1463.0	1445.8	1439.5	1431.2	1418.4	1396.7	1378.6	1314.3
350	2890.0	2889.4	2888.7	2883.0	2875.7	2860.5	2827.4	2790.4	2748.3	2699.6	2520.9	1612.7	1599.6	1583.9	1562.2	1529.3	1503.9	1422.8
375	2929.5	2929.0	2928.3	2923.2	2916.7	2903.3	2874.7	2843.4	2808.9	2770.7	2650.4	2449.1	2232.6	1799.9	1738.1	1677.0	1638.6	1533.6
400	2969.3	2968.9	2968.3	2963.7	2957.9	2945.9	2920.7	2893.7	2864.6	2833.1	2740.6	2617.9	2551.9	2428.5	2068.9	1854.9	1787.8	1646.8
425	3009.6	3009.2	3008.7	3004.5	2999.2	2988.5	2966.1	2942.4	2917.2	2890.4	2815.0	2723.5	2679.3	2607.8	2452.8	2097.5	1960.2	1762.9
450	3050.3	3049.9	3049.4	3045.6	3040.9	3031.1	3011.0	2989.9	2967.8	2944.5	2880.7	2807.2	2773.4	2721.2	2618.9	2364.2	2160.3	1881.9
475	3091.4	3091.0	3090.6	3087.1	3082.8	3073.9	3055.7	3036.7	3017.0	2996.5	2941.3	2879.7	2852.1	2810.5	2732.7	2549.7	2361.4	2003.6
500	3132.9	3132.6	3132.2	3129.0	3125.0	3116.9	3100.3	3083.1	3065.4	3047.0	2998.4	2945.3	2922.0	2887.3	2824.0	2681.6	2528.1	2126.9
550	3217.2	3217.0	3216.6	3213.9	3210.5	3203.6	3189.5	3175.2	3160.5	3145.4	3106.2	3064.7	3046.9	3020.8	2974.5	2875.0	2769.5	2371.0
600	3303.3	3303.1	3302.8	3300.4	3297.5	3291.5	3279.4	3267.2	3254.7	3242.0	3209.3	3175.3	3160.9	3140.0	3103.4	3026.8	2947.1	2597.9
650	3391.2	3391.0	3390.7	3388.6	3386.0	3380.8	3370.3	3359.6	3348.9	3337.9	3310.1	3281.4	3269.3	3251.9	3221.7	3159.5	3095.6	2798.9
700	3480.8	3480.6	3480.4	3478.5	3476.2	3471.6	3462.4	3453.0	3443.6	3434.0	3409.8	3385.1	3374.7	3359.9	3334.3	3282.0	3228.7	2976.1
750	3572.2	3572.0	3571.8	3570.2	3568.1	3564.0	3555.8	3547.5	3539.1	3530.7	3509.4	3487.7	3478.7	3465.8	3443.6	3398.6	3353.1	3135.2
800	3665.3	3665.2	3665.0	3663.6	3661.7	3658.0	3650.6	3643.2	3635.7	3628.2	3609.2	3590.1	3582.1	3570.7	3551.2	3511.8	3472.2	3281.7

Densities (ρ: kg m^{-3}):

Pressure (bar) Temp (°C)	0.1	0.5	1	5	10	20	40	60	80	100	150	200	220.64 Critical Isobar	250	300	400	500	1000
0.01	999.8	999.8	999.8	1000.0	1000.3	1000.8	1001.8	1002.8	1003.8	1004.8	1007.3	1009.7	1010.7	1012.2	1014.5	1019.2	1023.8	1045.3
25	997.0	997.0	997.0	997.2	997.5	997.9	998.8	999.7	1000.6	1001.5	1003.7	1005.8	1006.7	1008.0	1010.1	1014.3	1018.4	1037.9
50	0.0673	988.0	988.0	988.2	988.4	988.9	989.7	990.6	991.5	992.3	994.4	996.5	997.4	998.6	1000.7	1004.7	1008.7	1027.4
75	0.0624	974.8	974.8	975.0	975.2	975.7	976.6	977.5	978.3	979.2	981.3	983.5	984.4	985.6	987.7	991.8	995.8	1014.6
100	0.0582	0.293	0.590	958.5	958.8	959.2	960.2	961.1	962.0	962.9	965.2	967.4	968.4	969.6	971.8	976.1	980.3	999.8
125	0.0545	0.274	0.550	939.2	939.4	939.9	940.9	941.9	942.9	943.9	946.4	948.8	949.8	951.2	953.5	958.1	962.5	983.1
150	0.0512	0.257	0.516	917.0	917.3	917.9	919.0	920.1	921.2	922.3	925.0	927.7	928.8	930.3	932.9	937.9	942.7	964.8
175	0.0484	0.243	0.487	2.503	892.4	893.0	894.3	895.6	896.8	898.1	901.1	904.1	905.4	907.1	909.9	915.5	920.9	945.0
200	0.0458	0.230	0.460	2.353	4.850	865.0	866.5	868.0	869.5	870.9	874.5	878.0	879.4	881.3	884.6	890.9	897.0	923.7
225	0.0435	0.218	0.437	2.223	4.550	9.63	835.1	836.9	838.7	840.4	844.7	848.8	850.5	852.8	856.6	864.0	870.9	901.0
250	0.0414	0.207	0.416	2.108	4.300	8.97	798.9	801.2	803.5	805.7	811.0	816.1	818.1	820.9	825.6	834.3	842.4	876.7
275	0.0395	0.198	0.396	2.006	4.070	8.43	18.31	759.1	762.2	765.1	772.2	778.7	781.3	784.8	790.6	801.4	811.1	850.8
300	0.0378	0.189	0.379	1.913	3.880	7.97	16.99	27.63	41.2	715.3	725.6	734.7	738.2	743.0	750.7	764.4	776.5	823.2
325	0.0362	0.181	0.363	1.830	3.700	7.57	15.93	25.39	36.5	50.3	664.9	679.8	685.3	692.4	703.4	722.0	737.6	793.7
350	0.0348	0.174	0.348	1.754	3.540	7.21	15.04	23.67	33.4	44.6	87.1	600.6	612.0	625.5	643.9	671.9	693.2	762.3
375	0.0334	0.167	0.335	1.684	3.390	6.90	14.28	22.27	31.0	40.7	71.9	130.3	210.0	505.5	558.2	609.3	641.2	728.8
400	0.0322	0.161	0.322	1.620	3.260	6.61	13.62	21.09	29.1	37.8	63.8	100.5	121.9	166.5	357.4	523.3	577.8	692.9
425	0.0310	0.155	0.311	1.561	3.140	6.35	13.03	20.07	27.5	35.5	58.3	87.1	101.8	126.8	188.7	394.1	497.7	654.7
450	0.0300	0.150	0.300	1.506	3.030	6.11	12.49	19.17	26.2	33.6	54.1	78.6	90.3	109.0	148.4	270.9	402.0	614.2
475	0.0290	0.145	0.290	1.454	2.920	5.90	12.01	18.37	25.0	31.9	50.8	72.4	82.4	97.8	128.1	210.0	315.2	571.7
500	0.0280	0.140	0.280	1.407	2.820	5.69	11.57	17.65	23.9	30.5	48.0	67.6	76.4	89.7	115.1	177.8	257.1	528.3
550	0.0263	0.132	0.263	1.320	2.650	5.33	10.79	16.39	22.1	28.0	43.6	60.3	67.7	78.5	98.3	143.2	195.4	444.6
600	0.0248	0.124	0.248	1.244	2.490	5.01	10.12	15.32	20.6	26.1	40.1	55.0	61.4	70.7	87.4	123.6	163.7	374.2
650	0.0235	0.117	0.235	1.176	2.360	4.73	9.53	14.40	19.4	24.4	37.3	50.8	56.5	64.8	79.4	110.5	143.7	321.0
700	0.0223	0.111	0.223	1.115	2.230	4.48	9.01	13.60	18.2	22.9	34.9	47.3	52.5	60.1	73.2	100.7	129.6	282.0
750	0.0212	0.106	0.212	1.060	2.120	4.25	8.55	12.88	17.3	21.7	32.9	44.4	49.2	56.2	68.2	93.1	118.8	253.0
800	0.020	0.101	0.202	1.010	2.020	4.05	8.14	12.25	16.4	20.6	31.1	41.9	46.4	52.8	64.0	86.8	110.2	230.6

7.4.6. Transport Properties of Gases

The below values are correct for a pressure of 1 atm but may often be used with sufficient accuracy at other pressures. For air, $d\lambda_{air}/dp \sim 0.05$ W K^{-1} atm^{-1}.

Water and Steam Mixtures (H_2O (l) + H_2O (g))

Temp. °C	Specific volume m³/kg		Isobaric specific heat capacity kJ/kg K		Thermal conductivity W/m K		Dynamic viscosity kg/s m		Prandtl number $= \mu c_p / \lambda$		Temp. °C
	v_f	v_g	c_{p_f}	c_{p_g}	λ_f	λ_g	$\mu_f/10^{-3}$	$\mu_g/10^{-6}$	Pr_f	Pr_g	
0.01	0.00100	206.2	4.217	1.854	0.569	0.0173	1.755	8.8	13.02	0.942	0.01
10	0.00100	106.4	4.193	1.860	0.587	0.0185	1.301	9.1	9.29	0.915	10
20	0.00100	57.8	4.182	1.866	0.603	0.0191	1.002	9.4	6.95	0.918	20
30	0.00100	32.9	4.179	1.885	0.618	0.0198	0.797	9.7	5.39	0.923	30
40	0.00101	19.5	4.179	1.885	0.632	0.0204	0.651	10.1	4.31	0.930	40
50	0.00101	12.05	4.181	1.899	0.643	0.0210	0.544	10.4	3.53	0.939	50
60	0.00102	7.68	4.185	1.915	0.653	0.0217	0.462	10.7	2.96	0.947	60
70	0.00102	5.05	4.190	1.936	0.662	0.0224	0.400	11.1	2.53	0.956	70
80	0.00103	3.41	4.197	1.962	0.670	0.0231	0.350	11.4	2.19	0.966	80
90	0.00104	2.36	4.205	1.992	0.676	0.0240	0.311	11.7	1.93	0.976	90
100	0.00104	1.673	4.216	2.028	0.681	0.0249	0.278	12.1	1.723	0.986	100
125	0.00107	0.770	4.254	2.147	0.687	0.0272	0.219	13.3	1.358	1.047	125
150	0.00109	0.392	4.310	2.314	0.687	0.0300	0.180	14.4	1.133	1.110	150
175	0.00112	0.217	4.389	2.542	0.679	0.0334	0.153	15.6	0.990	1.185	175
200	0.00116	0.127	4.497	2.843	0.665	0.0375	0.133	16.7	0.902	1.270	200
225	0.00120	0.0783	4.648	3.238	0.644	0.0427	0.1182	17.9	0.853	1.36	225
250	0.00125	0.0500	4.867	3.772	0.616	0.0495	0.1065	19.1	0.841	1.45	250
275	0.00132	0.0327	5.202	4.561	0.582	0.0587	0.0972	20.2	0.869	1.56	275
300	0.00140	0.0216	5.762	5.863	0.541	0.0719	0.0897	21.4	0.955	1.74	300
325	0.00153	0.0142	6.861	8.440	0.493	0.0929	0.0790	23.0	1.100	2.09	325
350	0.00174	0.00880	10.10	17.15	0.437	0.1343	0.0648	25.8	1.50	3.29	350
360	0.00190	0.00694	14.6	25.1	0.400	0.168	0.0582	27.5	2.11	3.89	360
374.15	**0.00317**	**0.00317**	∞	∞	**0.24**	**0.24**	**0.045**	**45.0**	∞	∞	**374.15**

Superheated Steam (H_2O (g))

Temp. °C	Isobaric sp. heat capacity kJ/kg K	Thermal conductivity W/m K	Dynamic viscosity kg/s m	Prandtl number
	c_p	λ	$\mu/10^{-6}$	$Pr = \mu c_p / \lambda$
100	2.028	0.0245	12.1	0.986
200	1.979	0.0331	16.2	0.968
300	2.010	0.0434	20.4	0.946
400	2.067	0.0548	24.6	0.928
500	2.132	0.0673	28.8	0.912
600	2.201	0.0805	32.9	0.898
700	2.268	0.0942	36.8	0.887
800	2.332	0.1080	40.6	0.876

Air (79% N_2* (g) + 21% O_2 (g))

Temp. °C	Isobaric sp. heat capacity kJ/kg K	Thermal conductivity W/m K	Dynamic viscosity kg/s m	Prandtl number
	c_p	λ	$\mu/10^{-6}$	$Pr = \mu c_p / \lambda$
-100	1.01	0.016	12	0.75
0	1.01	0.024	17	0.72
100	1.02	0.032	22	0.70
200	1.03	0.039	26	0.69
300	1.05	0.045	30	0.69
400	1.07	0.051	33	0.70
500	1.10	0.056	36	0.70
600	1.12	0.061	39	0.71
700	1.14	0.066	42	0.72
800	1.16	0.071	44	0.73

Carbon Dioxide (CO_2 (g))

Temp. °C	Isobaric sp. heat capacity kJ/kg K	Thermal conductivity W/m K	Dynamic viscosity kg/s m	Prandtl number
	c_p	λ	$\mu/10^{-6}$	$Pr = \mu c_p / \lambda$
-50	0.79	0.011	11	0.79
0	0.83	0.015	14	0.78
100	0.92	0.022	18	0.75
200	1.00	0.030	22	0.73
300	1.06	0.038	26	0.72
400	1.11	0.046	29	0.71
500	1.16	0.053	32	0.70
600	1.20	0.061	35	0.69
700	1.23	0.069	38	0.68
800	1.25	0.078	41	0.67

Hydrogen (H_2 (g))

Temp. °C	Isobaric sp. heat capacity kJ/kg K	Thermal conductivity W/m K	Dynamic viscosity kg/s m	Prandtl number
	c_p	λ	$\mu/10^{-6}$	$Pr = \mu c_p / \lambda$
-200	10.6	0.050	3.3	0.71
-100	13.1	0.112	6.2	0.72
0	14.2	0.172	8.4	0.69
100	14.5	0.220	10.3	0.68
200	14.5	0.307	12.1	0.67
300	14.5	0.307	13.8	0.66
400	14.6	0.348	15.4	0.65
500	14.7	0.387	16.9	0.64
600	14.8	0.427	18.3	0.63
700	14.9	0.476	19.9	0.62
800	15.1	0.528	21.1	0.61

7.4.9. Properties of Refrigerant (Freon) R-134a
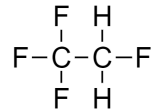
R-134a is a hydrofluorocarbon (HFC) with chemical formula $C_2H_2F_4$.
It is non-toxic, non-flammable, non-corrosive and non-ozone depleting.

1,1,1,2-tetrafluoroethane
(R-134a)

Saturation Temp. °C	Saturation Pressure bar	Saturated						Superheated by				Saturation Temp.
		Specific volume m³/kg		Specific enthalpy kJ/kg		Specific entropy kJ/kg K		20K		40K		°C
								kJ/kg	kJ/kg K	kJ/kg	kJ/kg K	
T_{sat}	P_{sat}	v_f	v_g	h_f	h_g	s_f	s_g	h	s	h	s	T_{sat}
-45	0.39	0.00070	0.46458	141.9	370.8	0.7687	1.7722	385.8	1.8348	401.3	1.8949	-45
-40	0.51	0.00071	0.36094	148.1	374.0	0.7956	1.7643	389.2	1.8270	405.0	1.8869	-40
-35	0.66	0.00071	0.28390	154.4	377.2	0.8221	1.7574	392.7	1.8201	408.6	1.8797	-35
-30	0.84	0.00072	0.22585	160.8	380.3	0.8483	1.7512	396.1	1.8139	412.3	1.8734	-30
-25	1.06	0.00073	0.18155	167.2	383.4	0.8743	1.7458	399.5	1.8085	416.0	1.8678	-25
-20	1.33	0.00074	0.14735	173.6	386.5	0.8999	1.7410	402.9	1.8037	419.7	1.8629	-20
-15	1.64	0.00074	0.12065	180.1	389.6	0.9253	1.7368	406.3	1.7995	423.4	1.8587	-15
-10	2.01	0.00075	0.09959	186.7	392.7	0.9505	1.7331	409.7	1.7959	427.0	1.8550	-10
-5	2.43	0.00076	0.08281	193.3	395.6	0.9753	1.7299	413.1	1.7927	430.7	1.8518	-5
0	2.93	0.00077	0.06933	**200.0**	398.6	**1.0000**	1.7270	416.4	1.7900	434.3	1.8491	0
5	3.50	0.00078	0.05840	206.8	401.5	1.0244	1.7245	419.7	1.7877	437.9	1.8469	5
10	4.15	0.00079	0.04947	213.6	404.3	1.0486	1.7222	422.9	1.7857	441.5	1.8450	10
15	4.88	0.00080	0.04212	220.5	407.1	1.0726	1.7202	426.1	1.7840	445.0	1.8434	15
20	5.72	0.00082	0.03602	227.5	409.8	1.0965	1.7183	429.3	1.7825	448.5	1.8422	20
25	6.65	0.00083	0.03093	234.6	412.3	1.1202	1.7165	432.3	1.7813	452.0	1.8412	25
30	7.70	0.00084	0.02666	241.7	414.8	1.1438	1.7148	435.4	1.7803	455.4	1.8405	30
35	8.87	0.00086	0.02305	249.0	417.2	1.1672	1.7130	438.3	1.7794	458.8	1.8399	35
40	10.17	0.00087	0.01999	256.4	419.4	1.1906	1.7112	441.2	1.7786	462.1	1.8395	40
45	11.60	0.00089	0.01736	263.9	421.5	1.2140	1.7093	444.0	1.7779	465.4	1.8393	45
50	13.18	0.00091	0.01511	271.6	423.4	1.2374	1.7073	446.7	1.7772	468.6	1.8392	50
60	16.82	0.00095	0.01148	287.5	426.6	1.2846	1.7022	451.8	1.7759	474.8	1.8392	60
70	21.16	0.00101	0.00871	304.3	428.6	1.3329	1.6953	456.4	1.7743	480.7	1.8394	70
80	26.33	0.00108	0.00654	322.4	428.8	1.3834	1.6848	460.4	1.7722	486.2	1.8395	80
90	32.45	0.00119	0.00481	342.9	425.4	1.4393	1.6665	463.8	1.7692	491.3	1.8392	90
100	39.73	0.00148	0.00345	373.3	407.7	1.5183	1.6105	466.4	1.7650	495.9	1.8384	100

Boiling point: -26.1 °C (at $p = 1$ bar)   Autoignition temperature: 770 °C
Solubility in water: 0.11 wt% (at 25 °C)   Critical temperature: 122 °C
Ozone depletion level (ODL): 0   Global warming potential (GWP): 1430

Alternative Refrigerants: R-134a is being phased out as a refrigerant due to its high GWP

Refrigerant	Composition	GWP	ODL
R-515b	azeotrope of 91.1% R-1234ze: (E)-1,3,3,3-tetrafluoropropene + 8.9% R-227ea: 1,1,1,2,3,3,3-heptafluoropropane	299	0
HFO-1233zd	(Z)-1-chloro-3,3,3-trifluoropropene	6	0
R-12a	propane + isobutane	3	0
HFO-1234yf	2,3,3,3-tetrafluoroprop-1-ene	1	0

For reliable data on these and various other fluids used in refrigeration and power, the
CoolProp library can be used, with interfaces in C++, Python, MATLAB, Excel, R, etc.

7.4.10. Pressure-Enthalpy (*p-h*) Phase Diagram of Refrigerant R-134a
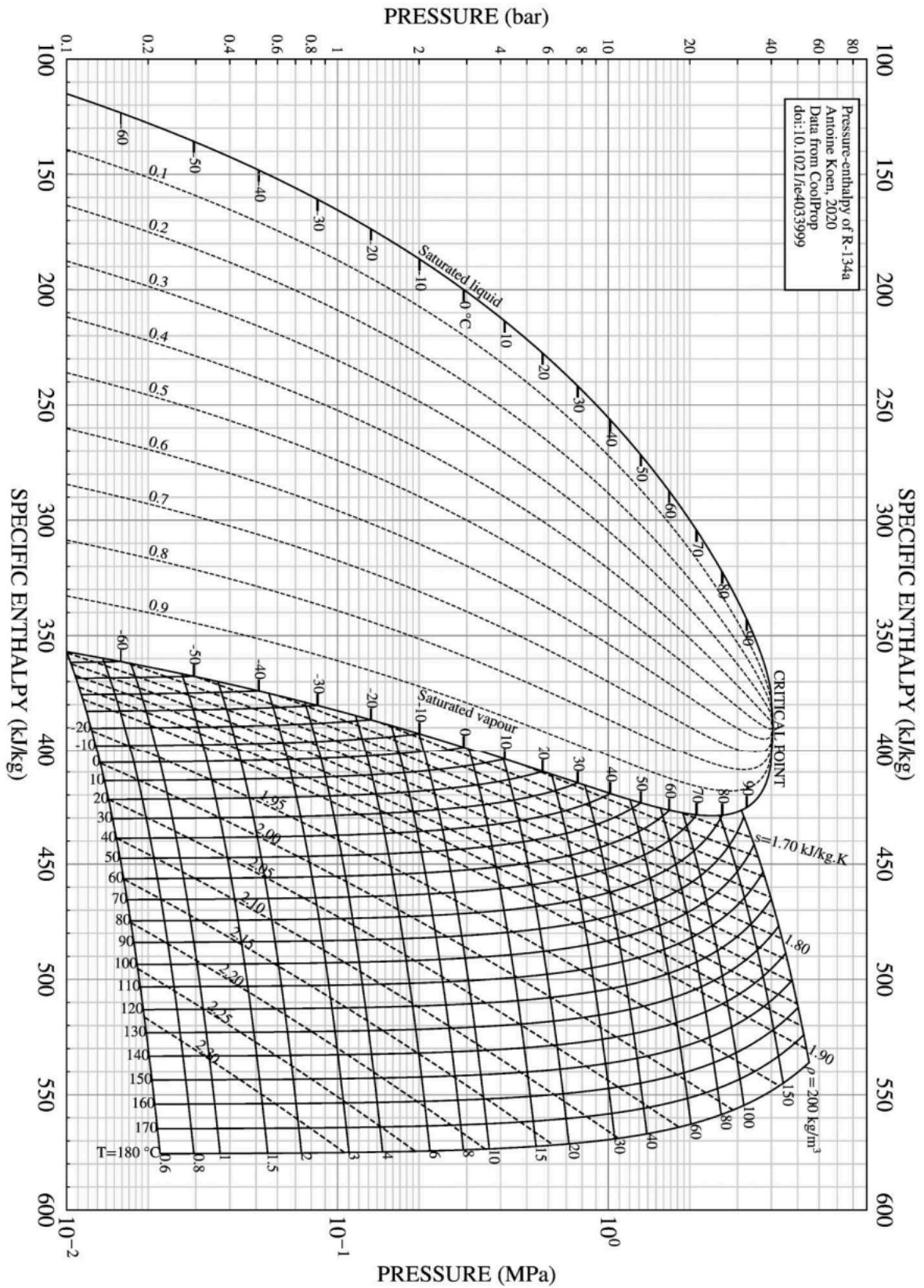
7.4.11. Enthalpy-Entropy (*h-s*) Phase Diagram of Steam (Mollier Diagram)
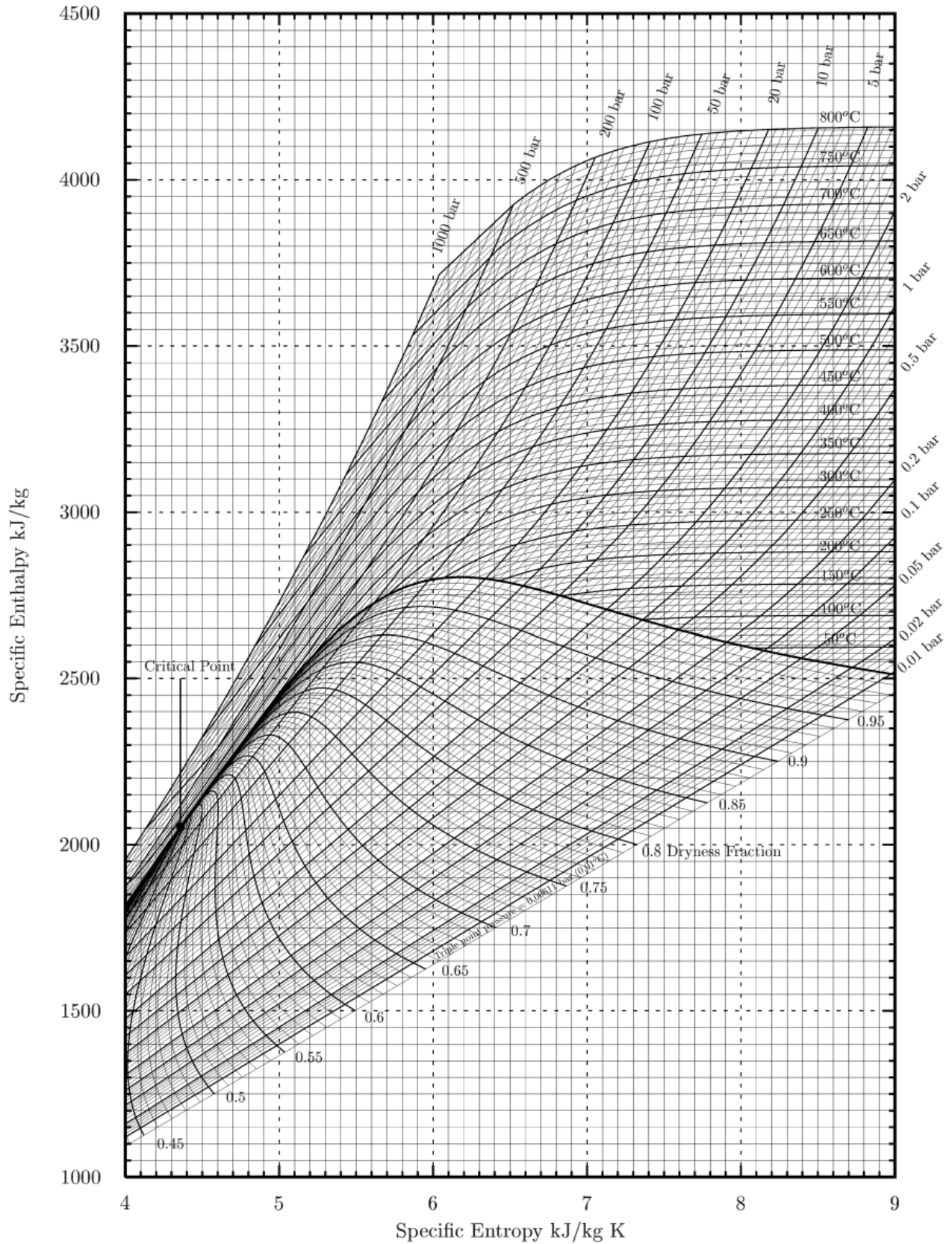
7.4.12. Enthalpy-Humidity (h-ω) Data for Water and Steam (Psychrometric Chart)

PSYCHROMETRIC CHART
Atmospheric pressure: 1 atm (101.325 kPa)
Altitude: 0 (sea level)

UNIVERSIDAD POLITÉCNICA DE MADRID
ETSI Agronómica, Alimentaria y de Biosistemas
Thermodynamics course
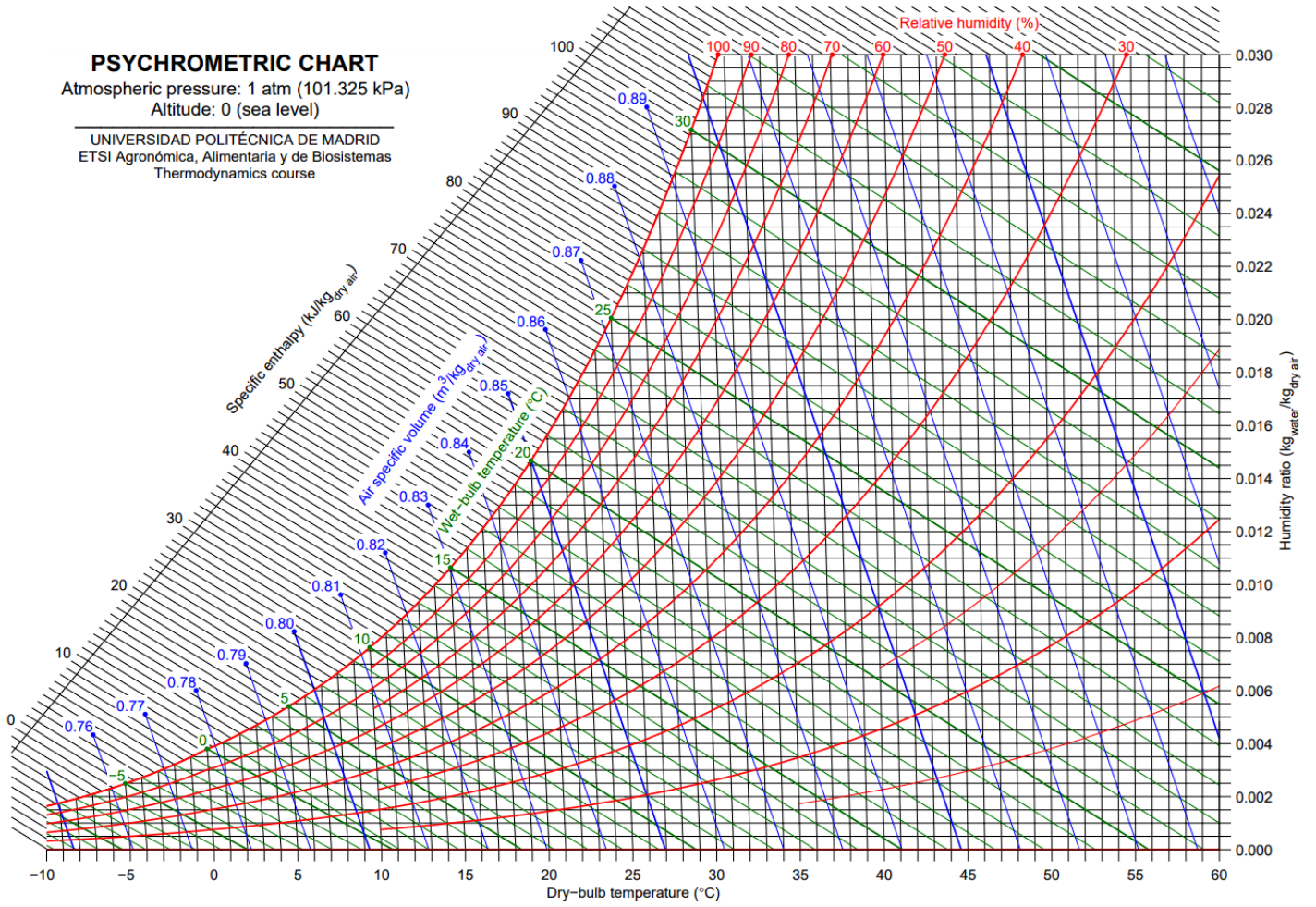
7.4.13. Perfect Gas Relations For Compressible Supersonic Flow

Nondimensional temperature, pressure, density and mass flow rate are plotted for $\gamma = 1.4$.

$$\frac{\dot{m}\sqrt{c_p T_0}}{A p_0} = \frac{\gamma}{\sqrt{\gamma-1}} M \left(1 + \frac{\gamma-1}{2} M^2\right)^{-\frac{1}{2}\left(\frac{\gamma+1}{\gamma-1}\right)}$$

$$\frac{T}{T_0} = \left(1 + \frac{\gamma-1}{2} M^2\right)^{-1}$$

$$\frac{\rho}{\rho_0} = \left(1 + \frac{\gamma-1}{2} M^2\right)^{-\frac{1}{\gamma-1}}$$

$$\frac{p}{p_0} = \left(1 + \frac{\gamma-1}{2} M^2\right)^{-\frac{\gamma}{\gamma-1}}$$

Mach Number
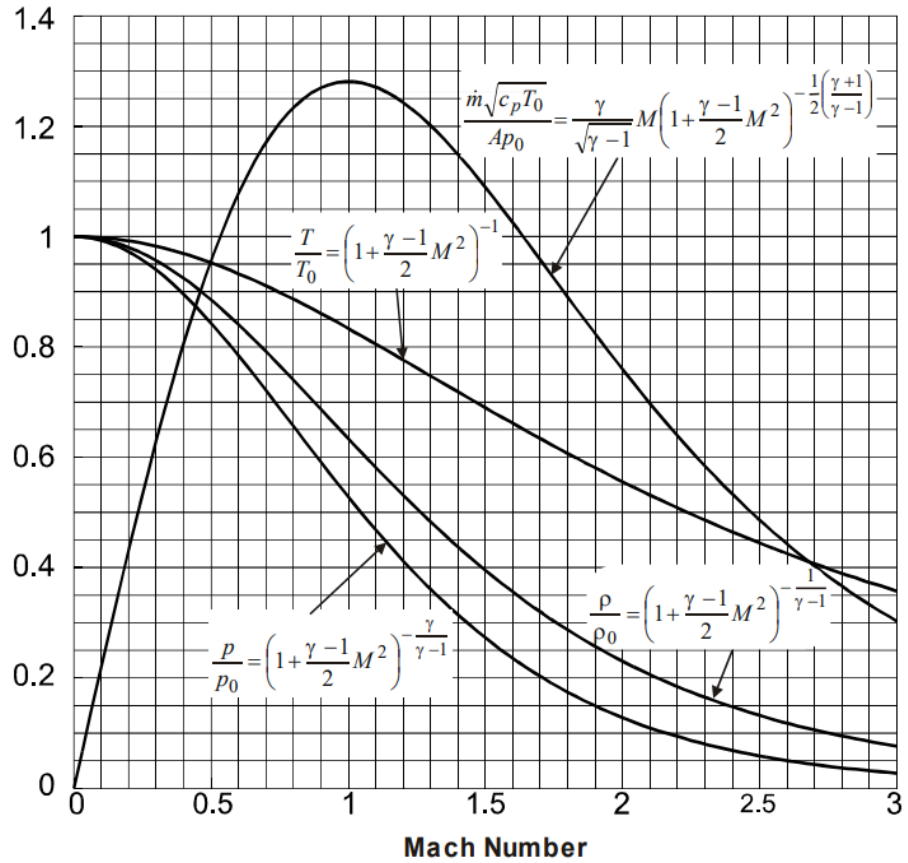
- $T_0 =$ const in adiabatic flow with no shaft work.

- If flow is isentropic, $p_0 =$ const and $\rho_0 =$ const when $T =$ const.

- At Mach 1 and when $\gamma = 1.4$, $\quad \dfrac{\dot{m}\sqrt{c_p T_0}}{A p_0} = 1.281$.

P8. ELECTRICITY AND ELECTROMAGNETISM

8.1. Electrostatics and Magnetostatics

8.1.1. Electric Fields

The electric field intensity $\mathbf{E}$ [V m^{-1}], electric flux density $\mathbf{D}$ [C m^{-2}] and electric polarisation $\mathbf{P}$ [C m^{-2}] vector fields are related by the constitutive relation $\mathbf{D} = \varepsilon_0 \mathbf{E} + \mathbf{P}$ ($\varepsilon_0 = 8.854 \times 10^{-12}$ F m^{-1}: vacuum permittivity). Only the $\mathbf{E}$-field is physically meaningful.

- Electric field is irrotational: $\nabla \times \mathbf{E} = \mathbf{0}$ (with an unchanging magnetic field)
- Electrostatic potential V: $\mathbf{E} = -\nabla V$

- Electromotive force (EMF, electrostatic potential difference): $\varepsilon = V_2 - V_1 = \int_1^2 \mathbf{E} \cdot \mathrm{d}\boldsymbol{l}$

- Electrostatic force on a point charge: $\mathbf{F} = q\mathbf{E}$
- Electrostatic potential energy: $E_e = qV$

- Capacitance: $C = \dfrac{q_{free}}{V}$ (V_2 on surface, $V_1 = 0$ taken at infinity)

Gauss's Law: flux of electric field is proportional to the enclosed charge

$$\Phi_E = \oiint_S \mathbf{E} \cdot d\mathbf{S} = \frac{q}{\varepsilon_0} \qquad \Leftrightarrow \qquad \nabla \cdot \mathbf{E} = \frac{\rho}{\varepsilon_0}$$

$$\Phi_D = \oiint_S \mathbf{D} \cdot d\mathbf{S} = q_{\text{free}} \qquad \Leftrightarrow \qquad \nabla \cdot \mathbf{D} = \rho_{\text{free}}$$

$$\Phi_P = \oiint_S \mathbf{P} \cdot d\mathbf{S} = -q_{\text{bound}} \qquad \Leftrightarrow \qquad -\nabla \cdot \mathbf{P} = \rho_{\text{bound}}$$

Charges: $\rho = \rho_{\text{free}} + \rho_{\text{bound}}$. Fluxes: $\varepsilon_0 \Phi_E = \Phi_D - \Phi_P$.
The bound charges represent immobilised dipoles within a material.

Poisson's equation: $\nabla^2 V = \dfrac{\rho}{\varepsilon_0}$ (if no charge, reduces to Laplace's equation: $\nabla^2 V = 0$)

In linear, homogeneous, isotropic media, the material dipoles respond to external electric fields such that $\mathbf{P} = \varepsilon_0 \chi_e \mathbf{E}$, therefore $\mathbf{D} = \varepsilon_0 \varepsilon_r \mathbf{E} = \varepsilon_0 (1 + \chi_e) \mathbf{E}$ ($\chi_e = \varepsilon_r$ - 1: electric susceptibility, $\varepsilon_r > 1$: relative permittivity).

There are alternative systems of units for electrostatic quantities, based on the CGS (centimetre gram second) system, e.g. ESU/stat, EMU/ab, Gaussian. These systems are not widely used for computations, and instead are only occasionally used to simplify some equations. They are not used here (metric SI units only).

8.1.2. Magnetic Fields

The magnetic flux density **B** [T], magnetic field intensity **H** [A m^{-1}] and magnetisation **M** [A m^{-1}] vector fields are related by the constitutive relation $\mathbf{B} = \mu_0(\mathbf{H} + \mathbf{M})$ ($\mu_0 = 4\pi \times 10^{-7}$ H m^{-1}: vacuum permeability).

- Magnetic field is irrotational: $\nabla \times \mathbf{H} = \mathbf{0}$ (with no current **and** an unchanging electric field)
- Magnetic flux is solenoidal: $\nabla \cdot \mathbf{B} = 0$ (Gauss's law for magnetism: no magnetic monopoles)
- Magnetostatic scalar potential Φ_M: $\mathbf{H} = -\nabla\Phi_M$
- Laplace's equation: $\nabla^2\Phi_M = 0$

- Magnetomotive force (MMF, magnetostatic potential difference): $\Phi_{M2} - \Phi_{M1} = \int_1^2 \mathbf{H}\cdot\mathrm{d}\boldsymbol{l}$

- Magnetostatic vector potential **A**: $\mathbf{B} = \nabla \times \mathbf{A}$

- Magnetic flux as circulation of **A**: $\oint_\Gamma \mathbf{A} \cdot d\boldsymbol{\Gamma} = \iint_S \nabla \times \mathbf{A} \cdot d\mathbf{S} = \Phi_\mathbf{B}.$

In linear, homogeneous, isotropic media, the material dipoles respond to external magnetic fields such that $\mathbf{M} = \chi_m\mathbf{H}$, therefore $\mathbf{B} = \mu_0\mu_r\mathbf{H}$ ($\chi_m = \mu_r$ - 1: magnetic permeability, μ_r: relative permeability).

8.1.3. Fields due to Electric Currents

- Electric current density: $\nabla \cdot \mathbf{J} = -\dot{\rho}$ (total electric current: $I = \dot{Q} = \mathbf{J} \cdot A\hat{\mathbf{n}}$)
- Other conceptual currents include:
    - Electric dipole current: $\mathbf{J}_P = \dot{\mathbf{P}}$
    - Magnetisation current: $\mathbf{J}_M = \nabla \times \mathbf{M}$ ($\mathbf{J}_M + \mathbf{J}_P$ = bound current)
    - Displacement current: $\mathbf{J}_D = \dot{\mathbf{D}}$

- Ohm's law (electric field due to current-carrying wire): $\mathbf{J} = \sigma\mathbf{E}$, $V = IR$ (σ: conductivity, R: resistance)

- Ampere's law (magnetic field due to a current loop): $\oint_C \mathbf{H} \cdot \mathbf{dl} = NI$ (MMF: circulation of **H**)

- Maxwell-Ampere circuital law: $\oint_C \mathbf{H} \cdot \mathbf{dl} = \int_S \left(\mathbf{J} + \dot{\mathbf{D}}\right) \, \mathbf{dS}$

- Biot-Savart law (magnetic field due to a current-carrying wire): $\mathbf{dH} = \dfrac{I}{4\pi r^2} \, \mathbf{dl} \times \hat{\mathbf{r}}$

  ($\mathbf{r} = r\hat{\mathbf{r}}$: displacement of a point on the wire relative to the fixed point of the field)

  By the Biot-Savart law, an infinitesimal current produces a circular field around it.

- Power per unit area in electromagnetic field (Poynting vector): $\mathbf{S} = \frac{1}{\mu_0}\mathbf{E} \times \mathbf{B}$

- Momentum density in electromagnetic field: $\mathbf{g} = \mu_0\varepsilon_0\mathbf{S} = \varepsilon_0\mathbf{E} \times \mathbf{B}$

8.1.4. Alternating Magnetic Fields

Electromagnetic Induction

- Induced EMF in a conductor due to changing flux: $\oint_C \mathbf{E} \cdot \mathbf{dl} = -\int_S \dot{\mathbf{B}} \, \mathbf{dS}$

- Induced EMF, scalar form (Faraday's law): $\varepsilon = -\dot{\Phi}_B$ ($\Phi_B = BAN \cos\theta$: magnetic flux linkage)

The electric field $\mathbf{E}$ resulting from electromagnetic induction is non-conservative, so the resulting voltage between two points is path-dependent: $\nabla \times \mathbf{E} = -\partial\mathbf{B}/\partial t \neq \mathbf{0}$.

In conductors, this EMF generates a current flow with a magnetic field to oppose the change in flux that produced it (Lenz's law).

8.1.5. Forces due to Electric and Magnetic Fields

- Net force on a charge (electric + Lorentz): $\mathbf{F} = q\mathbf{E} + q\mathbf{v} \times \mathbf{B}$ (v: velocity vector)
- Charge carrier drift velocity: $\mathbf{J} = \rho\mathbf{v}$ (scalar form: $I = nevA$)
- Force on a straight current-carrying wire: $\mathbf{F} = l\,\mathbf{I} \times \mathbf{B}$ (scalar form: $F = BIl$)

Current Loop Model of Magnetisation: magnetic dipole moment is $\boldsymbol{\mu} = NI\mathbf{A}$

- Atomic dipole moment: $\boldsymbol{\mu} = i\,\delta\mathbf{A}$ (for electron-counting calculation of $|\delta\mathbf{m}|$, see Section 15.5.10)

- Magnetisation due to aligned dipoles: $\mathbf{M} = \frac{N}{V}\boldsymbol{\mu}$ (N/V: number of dipoles per unit volume)

- Magnetostatic force on a dipole: $\mathbf{F} = \nabla(\boldsymbol{\mu} \cdot \mathbf{B})$ ($\boldsymbol{\mu}$: magnetic dipole moment)
- Magnetostatic torque on a dipole: $\boldsymbol{\tau} = \boldsymbol{\mu} \times \mathbf{B}$

8.1.6. Electric and Magnetic Fields for Common Geometries

Point: non-accelerating point charge or sphere, total charge Q, distance (centre to centre) r:

- Electric field E, electrostatic potential V and electrostatic potential energy U:

$$E = \frac{Q}{4\pi\varepsilon r^2} \qquad\qquad V = \frac{Q}{4\pi\varepsilon r} \qquad\qquad U = qV = \frac{Qq}{4\pi\varepsilon r}$$

- Inside a conductive sphere, $E = 0$ as all charges distribute evenly on the surface.

Between two point charges: cylindrical coordinates, $+q$ at $+a$ and $-q$ at $-a$ on z-axis:
(By the method of images, this also applies to a conducting plane and an image charge.)

- Potential: $\quad V(r, \theta, z) = \dfrac{1}{4\pi\varepsilon}\left(\dfrac{Q}{\sqrt{r^2 + (z-a)^2}} - \dfrac{Q}{\sqrt{r^2 + (z+a)^2}}\right)$

- Electric field: $\mathbf{E} = -\nabla V$ $\qquad$ (for ∇ in cylindrical coordinates, see Section 3.5.9.)

Line: static linear charge density λ or straight wire carrying current I:

$$\text{Static line charge: } E = \frac{\lambda}{2\pi\varepsilon r} \qquad\qquad \text{Current-carrying wire: } B = \frac{\mu I}{2\pi r}$$

Circle: static loop of linear charge density λ or current loop I of radius R:

$$\text{Along central axis: } E = \frac{\lambda R z}{2\varepsilon\left(z^2 + R^2\right)^{3/2}} \qquad\qquad B = \frac{\mu R^2 I}{2\left(z^2 + R^2\right)^{3/2}}$$

Plane: static planar charge density σ on two sides of a flat plane: $\qquad E = \dfrac{\sigma}{2\varepsilon}$

Solenoid: current-carrying, N' turns per unit length, **inside**: $\qquad B = \mu N' I$

Toroid: current-carrying, N turns of centre-to-ring radius R, inside: $\qquad B = \mu N' I \qquad (N' = \dfrac{N}{2\pi R})$

Magnetic Dipole: dipole moment $\mathbf{m} = \mathbf{M}V = I\mathbf{A}$:

$$\mathbf{B} = \frac{\mu}{4\pi r^3}[3(\mathbf{m}\cdot\mathbf{r})\mathbf{r} - \mathbf{m}] \left(+ \frac{2\mu}{3}\mathbf{m}\,\delta^3(\mathbf{r})\right) \qquad (\mathbf{r} \text{ is the } \textbf{unit} \text{ displacement vector: } \mathbf{x} = r\,\mathbf{r})$$

In polar coordinates (r, θ) relative to $\mathbf{m}$, $\qquad B_x = \dfrac{\mu}{4\pi}m\,\dfrac{3\cos^2\theta - 1}{r^3}, \quad B_y = \dfrac{\mu}{4\pi}m\,\dfrac{3\cos\theta\sin\theta}{r^3}$

Cuboidal Ferromagnet: side lengths ($2x_b$, $2y_b$, $2z_b$), constant axial magnetisation $\mathbf{M} = M_0\,\mathbf{j}$, magnet occupies region in Cartesian coordinates $\{(x, y, z): -x_b \leq x \leq x_b, -y_b \leq y \leq y_b, -z_b \leq z \leq z_b\}$.

$$H_x(x, y, z) = \frac{M_0}{4\pi} \sum_{k,l,m=1}^{2} (-1)^{k+l+m} \ln\{z + (-1)^m z_b + \alpha_{klm}(x, y, z)\}$$

$$H_y(x, y, z) = -\frac{M_0}{4\pi} \sum_{k,l,m=1}^{2} (-1)^{k+l+m} \, \text{sgn}\{y + (-1)^l y_b\} \, \text{sgn}\{x + (-1)^k x_b\} \, \tan^{-1}\left\{ \frac{|x + (-1)^k x_b| \, |z + (-1)^m z_b|}{|y + (-1)^l y_b| \, \alpha_{klm}(x, y, z)} \right\}$$

$$(x, y, z) = \frac{M_0}{4\pi} \sum_{k,l,m=1}^{2} (-1)^{k+l+m} \ln\{x + (-1)^k x_b + \alpha_{klm}(x, y, z)\}$$

(where $\alpha_{klm}(x, y, z) = \sqrt{\left(x + (-1)^k x_b\right)^2 + \left(y + (-1)^l y_b\right)^2 + \left(z + (-1)^m z_b\right)^2}$, $sgn(x) = \frac{x}{|x|}$)

Cylindrical Ferromagnet: length $2L$, radius R, constant axial magnetisation $\mathbf{M} = M_0\mathbf{z}$, magnet occupies region in cylindrical coordinates $\{(r, \theta, z): 0 \leq r \leq R, 0 \leq \theta < 2\pi, -L \leq z \leq L\}$

$$B_r(r, \theta, z) = \frac{\mu_0 M_0 R}{\pi}(\alpha_+ P_1(k_+) - \alpha_- P_1(k_-)); \qquad B_\theta(r, \theta, z) = 0; \qquad B_z(r, \theta, z) = \frac{\mu_0 M_0 R}{\pi(r+R)}(\beta_+ P_2(k_+) - \beta_- P_2(k_-))$$

(where $\alpha_\pm = \dfrac{1}{\sqrt{(z \pm L)^2 + (r + R)^2}}$, $\beta_\pm = (z \pm L)\alpha_\pm$, $\gamma = \dfrac{r - R}{r + R}$, $k_\pm^2 = \dfrac{(z \pm L)^2 + (r - R)^2}{(z \pm L)^2 + (r + R)^2}$,

$$P_1(k_\pm) = \frac{2E(\sqrt{1 - k_\pm^2}) - (1 + k_\pm^2) K(\sqrt{1 - k_\pm^2})}{1 - k_\pm^2}, \quad P_2(k_\pm) = \frac{(\gamma + 1)K(\sqrt{1 - k_\pm^2}) - \gamma(\gamma + 1) \Pi(1 - \gamma^2, \sqrt{1 - k_\pm^2})}{1 - \gamma^2},$$

K, E and Π are the first, second and third complete elliptic functions, Section 1.6.5)

Solenoid electromagnets have equivalent fields to cylindrical ferromagnets with $M_0 = N'I$
(N': turns per unit length, I: solenoid current)

8.1.7. Forces and Torques for Common Geometries

- **Two separated point charges or spheres:** $F = \dfrac{Q_1 Q_2}{4\pi\varepsilon r^2}$ (Coulomb force)

- **Current-carrying wire:** $F = BIL \sin\theta$ or $\mathbf{F} = L\mathbf{I} \times \mathbf{B}$ (Lorentz force)
  Moving charges: $F = Bqv \sin\theta$ or $\mathbf{F} = q\mathbf{v} \times \mathbf{B}$

- **Two parallel current-carrying wires:** $F = \dfrac{\mu I_1 I_2}{2\pi R}$

  (I_1 and I_2 parallel $\to F$ attractive; I_1 and I_2 anti-parallel $\to F$ repulsive)

- **Loop or solenoid** in uniform magnetic field, N turns:

$$\tau = NIAB \sin\theta \quad \text{or} \quad \boldsymbol{\tau} = \mathbf{m} \times \mathbf{B} \qquad (\mathbf{m}\text{: dipole moment of } I, \ \mathbf{m} = IN\mathbf{A})$$

- **Two magnetic dipoles:** force exerted on dipole 2 due to dipole 1 ($\mathbf{r}_{2/1} = \mathbf{r}_2 - \mathbf{r}_1$):

$$\mathbf{F}_2 = \frac{3\mu}{4\pi r^5}\left[(\mathbf{m}_1\cdot\mathbf{r}_{2/1})\mathbf{m}_2 + (\mathbf{m}_2\cdot\mathbf{r}_{2/1})\mathbf{m}_1 + (\mathbf{m}_1\cdot\mathbf{m}_1)\mathbf{r}_{2/1} - \frac{5}{r^2}(\mathbf{m}_1\cdot\mathbf{r}_{2/1})(\mathbf{m}_2\cdot\mathbf{r}_{2/1})\mathbf{r}_{2/1}\right]$$

  If $\mathbf{m}_1$ and $\mathbf{m}_2$ are aligned parallel, then $F = -\dfrac{3\mu m_1 m_2}{2\pi r^4}$ and $F = U_1 m_2$.

  Dipoles can approximate magnets ($\mathbf{m} \approx \mathbf{M}_0 V$) and solenoids ($\mathbf{m} \approx IN\mathbf{A}$), especially at longer distances.

8.1.8. Energy and Forces in an Electromagnet
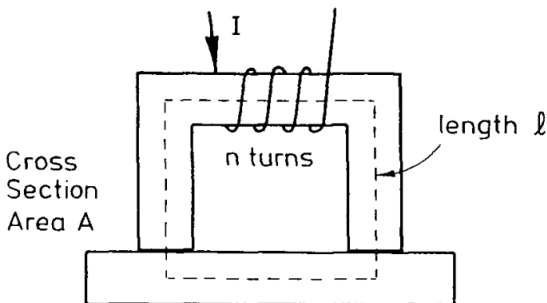
Magnetostatic energy U per unit volume V:

$$\frac{U}{V} = \int_0^B H\, dB \qquad = \frac{B^2}{2\mu} \text{ if linear } (\mu_r \text{ constant})$$

Field strength due to electromagnet:

$$H_m = \frac{nI}{l}$$

Attractive force on the pickup bar: $F = 2A \displaystyle\int_0^B H\, dB$ (virtual work)

Volume of air gap created by a finite vertical bar displacement δx is $2A\,\delta x$ i.e. $U = F\,\delta x = \dfrac{U}{V}\,\delta V$.

For a permanent magnet, the relationship between B and H is non-linear: for $\displaystyle\int_0^B H\, dB$, the

area under the B-H magnetisation curve will be required (see Section 8.6.2.)

8.1.9. Capacitances and Inductances for Common Geometries

Parallel plate capacitor:

- Single dielectric ε, shared area A, plate separation d:

$$C = \frac{\varepsilon A}{d}$$

- Partially filled dielectric (thickness t_1, vacuum/air thickness t_2):

$$C = \frac{\varepsilon_0 A}{\frac{t_1}{\varepsilon_r} + t_2}$$

Spheres:

- Single isolated sphere of radius R:

$$C = 4\pi\varepsilon R$$

- Concentric spheres of radius r_1 and r_2:

$$C = \frac{4\pi\varepsilon}{\frac{1}{r_1} - \frac{1}{r_2}}$$

Cylinders or coaxial cables:

- Static concentric cylinders of length l and radii r_1, r_2:

$$C = \frac{2\pi\varepsilon l}{\ln \frac{r_2}{r_1}}$$

- Coaxial cables with current I, length l, radii r_1, r_2:

$$L = \frac{\mu l}{2\pi} \ln \frac{r_2}{r_1}$$

Parallel wires (parasitics):

- Straight parallel wires of length l, separated by (centre-centre) distance s, with outer diameters d_1 and d_2:

$$C = \frac{2\pi\varepsilon l}{\cosh^{-1}\left(\frac{4s^2 - d_1^2 - d_2^2}{2d_1 d_2}\right)}; \quad \text{if } d_1 = d_2 = d \text{ then } C = \frac{\pi\varepsilon l}{\cosh^{-1}\left(\frac{s}{d}\right)}$$

$$L = \frac{\mu l}{2\pi} \cosh^{-1}\left(\frac{4s^2 - d_1^2 - d_2^2}{2d_1 d_2}\right); \quad \text{if } d_1 = d_2 = d \text{ then } L = \frac{\mu}{\pi} \cosh^{-1} \frac{s}{d}$$

Solenoids and toroids:

- Solenoid with N turns, area $A = \pi r^2$, current I, length l:

$$L = \frac{\mu N^2 A}{l}$$

- Toroid with N turns, loop area $A = \pi r^2$, current I, centre-ring radius R:

$$L = \frac{\mu N^2 A}{2\pi R}$$

8.2. DC Circuits

8.2.1. Circuit Resistance and the Norton/Thévenin Theorems

- Kirchoff's first law: sum of currents into a node is zero (conservation of charge)
- Kirchoff's second law: sum of voltages around a loop is zero (conservation of energy)
- For resistors in series: $R_{eq} = R_1 + R_2 + \ ... \ + R_n$

- For resistors in parallel: $R_{eq} = R_1 \ || \ R_2 \ || \ ... \ || \ R_n = \left(\dfrac{1}{R_1} + \dfrac{1}{R_2} + \ ... \ + \dfrac{1}{R_n} \right)^{-1}$

- For a cell with emf ε and internal resistance r, $\varepsilon - Ir = V = IR$ (Ohm's law)
  drawing current I into network resistance R: (V: terminal p.d.)
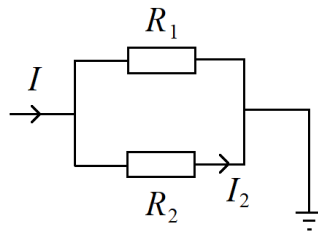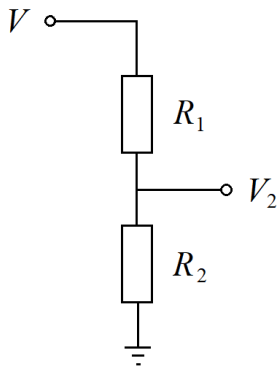
- Potential Divider: $V_2 = \dfrac{R_2}{R_1 + R_2} V$

- Current Divider: $I_2 = \dfrac{R_1}{R_1 + R_2} I$

Norton's Theorem and Thévenin's Theorem: any linear two-terminal network can be replaced at its terminals by:

Thévenin equivalent   **Norton equivalent**

$$RTH = R_N$$
$$V_{TH} = I_N R_N$$

$$I_N = \dfrac{V_{TH}}{R_{TH}}$$
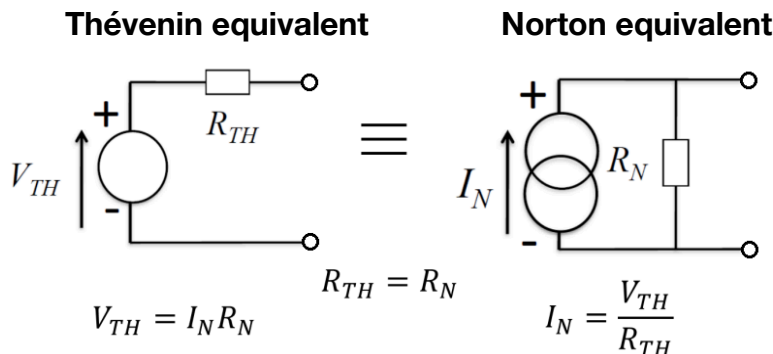
Norton: a current source I_N in parallel with a resistance R_N.

Thévenin: a voltage source V_{TH} in series with a resistance R_{TH}.

The Thévenin equivalent of a potential divider has $V_{TH} = \dfrac{R_2}{R_1 + R_2} V$ and $R_{TH} = R_1 \ || \ R_2$.

(In general, the Thévenin / Norton 'resistances' may be complex impedances (Section 8.3).)

8.2.2. Three-Terminal Star-Delta Transformation of Impedances

The Star-Delta (also known as Y/wye-mesh or T-π) Transformation converts equivalent circuit topologies between three terminals A, B and C.

| STAR (Y) | T | DELTA (MESH) | π |
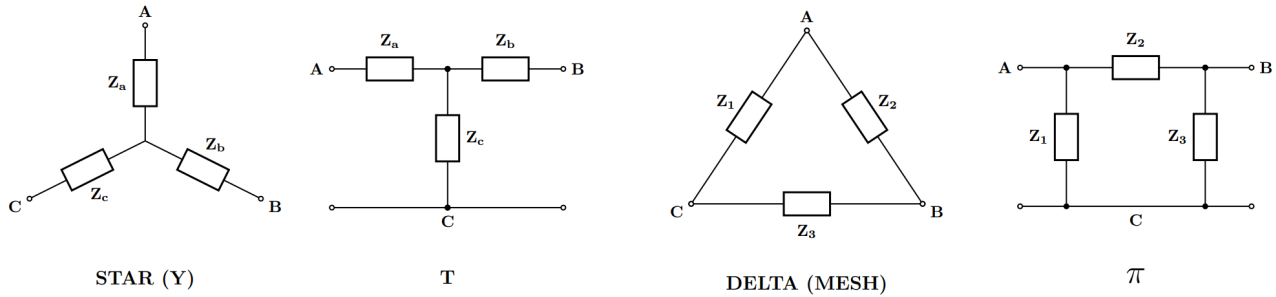
Star impedances:

$$Z_a = \frac{Z_1 Z_2}{Z_1 + Z_2 + Z_3}$$

$$Z_b = \frac{Z_2 Z_3}{Z_1 + Z_2 + Z_3}$$

$$Z_c = \frac{Z_3 Z_1}{Z_1 + Z_2 + Z_3}$$

Delta impedances:

$$Z_1 = Z_c + Z_a + \frac{Z_c Z_a}{Z_b}$$

$$Z_2 = Z_a + Z_b + \frac{Z_a Z_b}{Z_c}$$

$$Z_3 = Z_b + Z_c + \frac{Z_b Z_c}{Z_a}$$

If all three impedance branches are equal, then $Z_{\text{Delta}} = 3\, Z_{\text{Star}}$.

8.2.3. Wheatstone Bridge Circuit
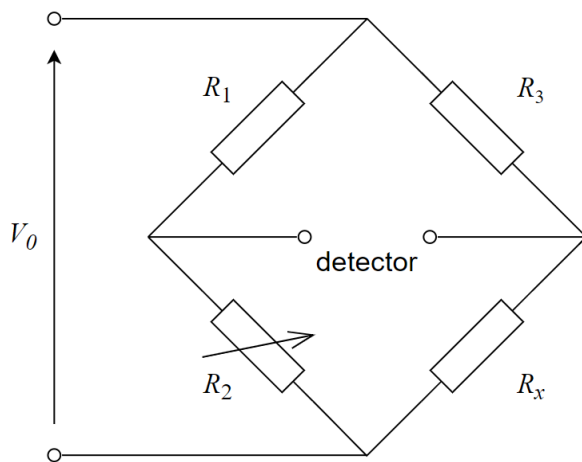
The bridge is balanced (no current and voltage at the detector) when

$$R_1 R_x = R_2 R_3$$

R_x is a fixed unknown resistance. R_2 is a known variable resistor (rheostat).

The detector may be a voltmeter, ammeter or galvanometer, which deflects when the bridge is unbalanced.

For other bridge circuits, see Section 8.3.5.

8.2.4. Three-Terminal Tee Transformation of Coupled Inductances

For inductances L_1 and L_2 connected with matching polarity as shown, with mutual inductance M, they can be replaced by the following network of three inductances:
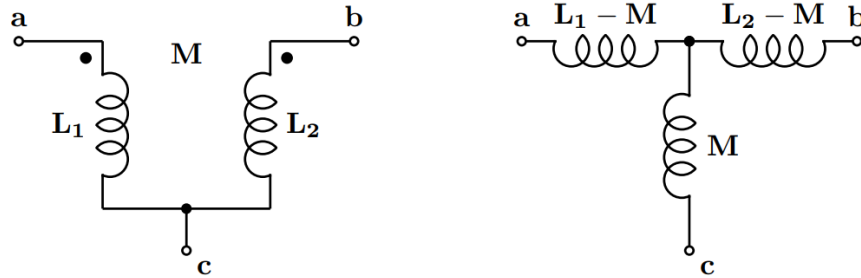
(The dot on the inductor indicates the positive terminal. The convention is that when positive current flows into the positive terminal, the current flows anticlockwise when viewed inwards from the positive end.)

8.2.5. Combining Capacitances and Inductances in Series and Parallel

In series: $\quad C_{eq} = \left(\dfrac{1}{C_1} + \dfrac{1}{C_2} + \ ... \ + \dfrac{1}{C_n} \right)^{-1} \qquad L_{eq} = L_1 + L_2 + \ ... \ + L_n$

In parallel: $\quad C_{eq} = C_1 + C_2 + \ ... \ + C_n \qquad\qquad L_{eq} = \left(\dfrac{1}{L_1} + \dfrac{1}{L_2} + \ ... \ + \dfrac{1}{L_n} \right)^{-1}$

8.2.6. Resistance, Capacitance and Inductance

For DC voltages and currents,

$$\text{Resistance:} \ \ R = \frac{V}{I} \qquad \text{Capacitance:} \ \ C = \frac{Q}{V} \qquad \text{Inductance:} \ \ L = \frac{\phi'}{I}$$

$$\text{Resistivity:} \ \ \rho = \frac{RA}{L} \qquad \text{Conductance:} \ G = \frac{1}{R} \qquad \text{Conductivity:} \ \sigma = \frac{GL}{A} = \frac{1}{\rho}$$

(V: voltage, I: current, Q: charge, ϕ': magnetic flux linkage, A: cross-sectional area, L: length)

Thermal power dissipated in a resistance: $\qquad P = I^2 R = \dfrac{V^2}{R} = IV$

Maximum Power Transfer Theorem: if a fixed voltage V is divided across R_1 and R_2, then maximum power is delivered to either resistor when $R_1 = R_2$.

8.2.7. Energy Transfer and Virtual Work for Capacitors and Inductors

Energy stored in a capacitor or inductor: $W = \frac{1}{2}CV^2$; $W = \frac{1}{2}LI^2$ (L: self-inductance)

Energy stored in coupled inductances: (+ if same polarity; - if opposite polarity)

$$W = \frac{1}{2}L_1 I_1^2 + \frac{1}{2}L_2 I_2^2 \pm MI_1 I_2 \qquad (M\text{: mutual inductance})$$

Coupling coefficient for inductors: $k = \dfrac{M}{\sqrt{L_1 L_2}}$;   full coupling when k = 1 i.e. $M \leq \sqrt{L_1 L_2}$.

Force between capacitive or inductive conductors separated by distance x (virtual work):

$$F = \frac{1}{2}V^2 \frac{\partial C}{\partial x} \qquad \text{and} \qquad F = \frac{1}{2}I^2 \frac{\partial M}{\partial x}$$

8.2.8. Kinetics of Electrical Conductance

Charge-carrier density: $n = \dfrac{N_A \rho\, n_C}{A_r}$ (number density, per unit volume)

(N_A: Avogadro's number, A_r: relative atomic mass of metal, ρ: mass density, n_C: number of delocalised electrons per atom)

Drift velocity v, mobility μ and relaxation time τ : $\mu = \dfrac{v}{E} = \dfrac{e\tau}{m}$ and $I = nevA = \dfrac{Ane^2\tau E}{m}$

Resistivity: $\rho = \dfrac{m}{ne^2\tau}$

8.2.9. Resistor, Capacitor and Inductor Codes

Resistor colour codes: 4-colour code: $ab\,c\,d \;\rightarrow\; R = (ab) \times 10^{c} \;\pm\; d\% \;\Omega$

5-colour code: $abc\,d\,e \;\rightarrow\; R = (abc) \times 10^{d} \;\pm\; e\% \;\Omega$

4-Band Code

560 kΩ   ±5%

Color		1ˢᵗ Band	2ⁿᵈ Band	3ʳᵈ Band	Multiplier	Tolerance
Black		0	0	0	10^{0}	
Brown		1	1	1	10^{1}	±1% (F)
Red		2	2	2	10^{2}	±2% (G)
Orange		3	3	3	10^{3}	
Yellow		4	4	4	10^{4}	
Green		5	5	5	10^{5}	±0.5% (D)
Blue		6	6	6	10^{6}	±0.25% (C)
Violet		7	7	7	10^{7}	±0.10% (B)
Grey		8	8	8		±0.05%
White		9	9	9		
Gold					10^{-1}	±5% (J)
Silver					10^{-2}	±10% (K)

231 Ω   ±0.1%

5-Band Code

Capacitor and inductor codes: code $xyz \;\rightarrow\; C = (xy) \times 10^{z}$ pF or $L = (xy) \times 10^{z}$ µH

Number	1	100	101	102	103	104	105
C	1 pF	10 pF	100 pF	1 nF	10 nF	100 nF	1 µF
L	1 µH	10 µH	100 µH	1 mH	10 mH	100 mH	1 H

Letter	B	C	D	E	F	G	J	K	M	Z
Tolerance	± 0.1 pF	± 0.25 pF	± 0.5 pF	± 0.5 %	± 1 %	± 2 %	± 5 %	± 10 %	± 20 %	-20%, +80%

For electrolytic (polarised) capacitors, the longer leg is positive. For SMD (surface mounted) capacitors, the side with the coloured/black tab mark is negative.

8.3. AC Circuits

8.3.1. Differential Equation Formulation of AC Capacitor and Inductor Circuits

AC voltage input: $v(t) = V \cos \omega t = \mathrm{Re}\{V\,\mathrm{e}^{j\omega t}\} = \mathrm{Re}\{\overline{v}(t)\}$

Device	Voltage and current	Impedance $\dfrac{\overline{v}(t)}{\overline{i}(t)}$	Reactance	Transfer function $\dfrac{\widehat{v}(s)}{\widehat{i}(s)}$
Resistor	$v(t) = R\,i(t)$ $i(t) = \dfrac{1}{R}\,v(t)$	$Z_R = R$	$X_R = 0$	R
Capacitor	$v(t) = \dfrac{1}{C}\displaystyle\int_0^t i(t)\,dt$ $i(t) = C\dfrac{dv(t)}{dt}$	$Z_C = \dfrac{1}{j\omega C}$	$X_C = \dfrac{-1}{\omega C}$	$\dfrac{1}{Cs}$
Inductor	$v(t) = L\dfrac{di(t)}{dt}$ $i(t) = \dfrac{1}{L}\displaystyle\int_0^t v(t)\,dt$	$Z_L = j\omega L$	$X_L = \omega L$	Ls

AC Ohm's law: $v = iZ$ ($Z = \dfrac{v}{i}$; 'complex resistance' accounting for phase difference)

In general, $Z = R + jX$ and $Y = G + jB$ where $Y = \dfrac{1}{Z} = \dfrac{i}{v}$ and $Z = \dfrac{1}{Y}$.

(Z: impedance, R: resistance, X: reactance, Y: admittance, G: conductance, B: susceptance)

Conversions: $Y = \dfrac{R - jX}{R^2 + X^2} = \dfrac{R - jX}{|Z|^2}, Z = \dfrac{G - jB}{G^2 + B^2} = \dfrac{G - jB}{|Y|^2}$

8.3.2. RMS Voltage and Single-Phase Mains Supply Standards

The root-mean-square value (rms value) of a signal is $V_{rms} = \dfrac{V_{peak}}{\sqrt{2}}$ and $I_{rms} = \dfrac{I_{peak}}{\sqrt{2}}$.

Unless otherwise specified, all a.c. voltages and currents are defined by their r.m.s. value. Mains supplies: 220-240 V @ 50 in the UK, EU and Asia; 110-120 V @ 60 in the USA.

8.3.3. Capacitive Coupling Circuit
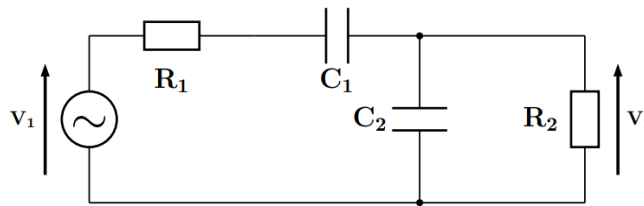
At midband, when the effects of C_1 and C_2 can be ignored, $v_2 = \dfrac{R_2}{R_1 + R_2} v_1$.

The -3 dB points (half-power, turnover) of the coupling circuit are:

- At high frequencies, v_2 drops to 70% of the midband value when $\dfrac{1}{\omega_2 C_2} = \dfrac{R_1 R_2}{R_1 + R_2}$.

- At low frequencies, v_2 drops to 70% of the midband value when $\dfrac{1}{\omega_1 C_1} = R_1 + R_2$.

ω_1 and ω_2 are known as the lower and upper half power angular frequencies. At these frequencies, there is a 45° phase shift between v_2 and v_1.

8.3.4. LC Resonant Circuit

Undamped resonant angular frequency, ω_0, is given when $\omega_0^2 LC = 1 \Rightarrow \omega_0 = \dfrac{1}{\sqrt{LC}}$.

Quality factor: $Q = \dfrac{\omega U}{P}$ (U: total stored energy in the system, P: mean power dissipation)

Half power bandwidth $= \omega_2 - \omega_1 = \dfrac{1}{Q} \times$ resonant frequency ω_0.
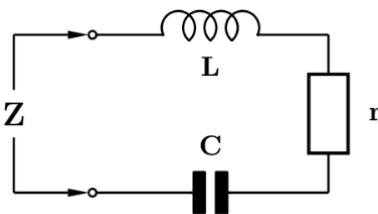
Series Resonant Circuit:

$$Q_0 = \frac{\omega_0 L}{r} = \frac{1}{r \omega_0 C},$$

$Z \approx r\left(1 + 2jQ_0 \dfrac{\delta\omega}{\omega_0}\right)$, at frequencies close to resonance

$Z = r(1 \pm j)$ when $\dfrac{\delta\omega}{\omega_0} = \pm \dfrac{1}{2Q_0}$.
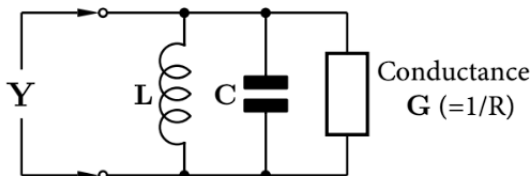
Parallel Resonant Circuit:

$$Q_0 = \frac{1}{\omega_0 LG} = \frac{\omega_0 C}{G} = \omega_0 RC,$$

$Y \approx G\left(1 + 2jQ_0 \dfrac{\delta\omega}{\omega_0}\right)$, at frequencies close to resonance

($Y = 1/Z$: admittance)

8.3.5. Balance Conditions for AC Bridge Circuits
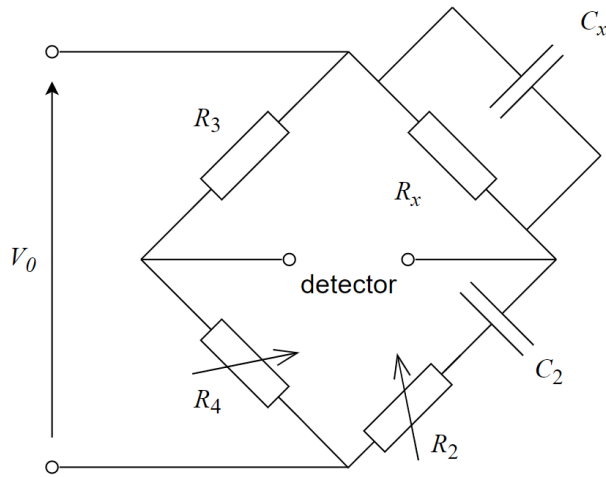
Wien Bridge: unknown $R_x \parallel C_x$

$$\omega^2 = \frac{1}{R_x R_2 C_x C_2} \quad \text{and} \quad \frac{C_x}{C_2} = \frac{R_4}{R_3} - \frac{R_2}{R_x}$$
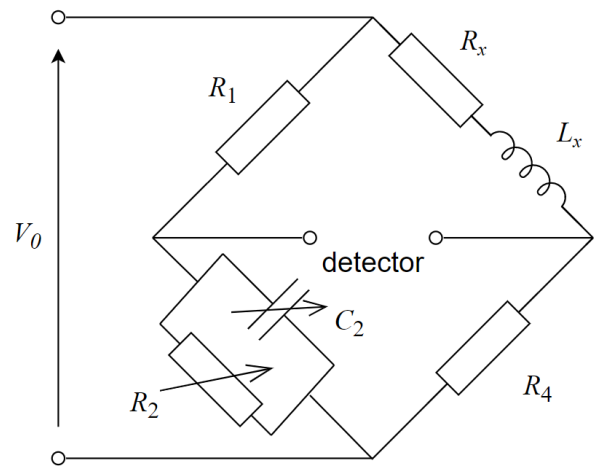
Maxwell Bridge: unknown $R_x + L_x$

$$R_2 R_x = R_1 R_4 \quad \text{and} \quad L_x = R_1 R_4 C_2$$
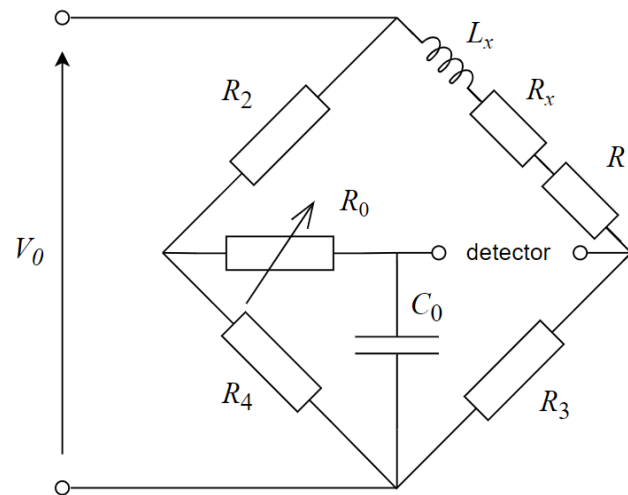
Anderson Bridge: unknown $R_x + L_x$

$$R_4 (R_x + R_1) = R_2 R_3 \quad \text{and} \quad L_x = \frac{R_3 C_0}{R_4} \left(R_2 R_4 + R_0 (R_2 + R_4) \right)$$

8.3.6. Full Wave Rectifier Bridge
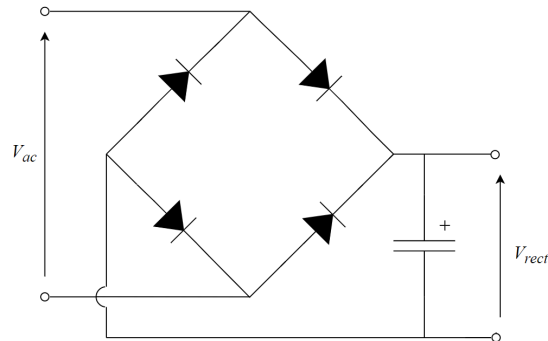
The diode bridge effectively produces $|V_{ac}|$ (decreased by two small potential drops due to the diodes) at the output. The smoothing capacitor ensures that the voltage does not drop significantly between cycles. The resulting waveform V_{rect} is approximately d.c. with a small ripple voltage.

8.3.8. Microwave and Radio Frequency (RF) Circuits

Cavity Magnetron: produces microwaves, used in radar and microwave ovens
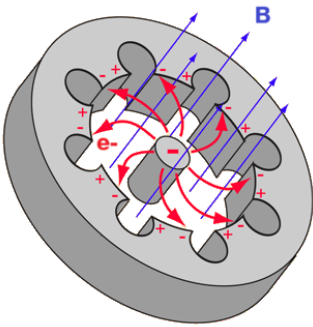
- A copper cathode is heated by a thoriated-tungsten filament, boiling off electrons (thermionic emission) into an evacuated space, attracted towards the copper anode.
- A permanent magnet produces a strong static axial magnetic field **B**.
- The electron trajectories in the space are curved into spiral-shaped paths by the Lorentz force of the **B**-field.
- The cavities in the anode act as LC resonators. As the electrons pass by the cavity ducts, AC current is induced around the cavities and radiation is generated inside.
- An antenna directs the microwaves into a waveguide for emission.

In a household microwave, the microwave radiation excites hydrogen bonds between water molecules in food creating phonons and thermal excitation (dielectric heating).

8.3.9. Switch-Mode Electronics

8.4. Electrical Power Engineering

8.4.1. Magnetic Circuits

A 'magnetic circuit' is a way to conceptualise the flow of magnetic flux.
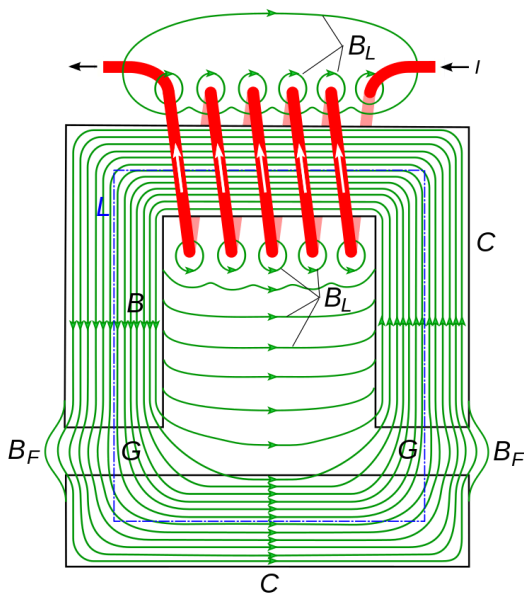
- **Magnetomotive force (mmf):** the ampere-turns NI (for electromagnets), analogous to voltage/electromotive force

- **Magnetic flux**, ϕ: the magnetic flux through a material, analogous to electric current

- **Reluctance,** $R = \dfrac{L}{\mu A}$: analogous to resistance (magnetic Ohm's law: $NI = \phi R$)

- **Magnetic flux density, B:** analogous to current density **J**

- **Permeance,** $P = \dfrac{1}{R}$: analogous to conductance G

- **Permeability,** μ: analogous to conductivity κ, with $B = \mu H$.

(C: iron core, G: air gap, I: current, B: magnetic flux density, H: magnetic field intensity, B_F: fringing fields, B_L: leakage flux, L: magnetic circuit mean path length)

The mean path length L can be used in Ampere's circuital law: $\oint_L H \, dL = NI$ (Section 8.1.3).

Magnetic flux $\phi = BA$ is conserved across boundaries. In the above example:

- Ampere's law: $H_m(L - 2L_g) + H_g(2L_g) = NI$, neglecting leakage
- Flux conservation: $B_m = B_g = B$, neglecting air gap/corner fringing
- Constitutive law: $B = \mu_0\mu_r H_m = \mu_0 H_g$, if core is a linear magnetic material

A good conductor of electric current (e.g. copper) has a low resistance (high conductivity). A good conductor of magnetic flux (e.g. iron) has low reluctance (high permeability).

Good magnetic flux conductors will channel more of the flux, minimising flux leakage.

A permanent ferromagnet in a magnetic circuit has $NI = 0$ but drives a magnetic flux around the circuit. The operating point can be found by intersection of its $B\text{-}H$ demagnetisation curve (Section 8.6.15) with the load line enforced by Ampere's law. Low-coercivity permanent magnets require a soft magnetic 'keeper' (armature) to prevent spontaneous loss of magnetisation over time due to e.g. stray magnetic interference.

8.4.2. AC Power

Electrical circuits may contain reactive components (complex impedance Z), causing AC voltages v and currents i to be out of phase. The phase difference is φ, defined as positive when i leads v i.e. if the phasors are $\widehat{v} = V_{rms}e^{j\alpha}$ and $\widehat{i} = I_{rms}e^{j\beta}$ then $\varphi = \beta - \alpha$.

Power triangle:
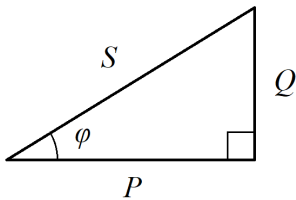
Apparent power: $S = VI$ (units: volt-amps, VA)
Power factor: $\cos \varphi$ ($\varphi > 0$: i leads v. $\varphi < 0$: i lags v)

Real power: $P = S \cos \varphi$ (units: watts, W)
Reactive power: $Q = S \sin \varphi$ (units: volt-amps reactive, VAR)

Reactive power indicates energy being exchanged between the source and reactive (inductive / capacitive) components and therefore not dissipated in any component.

Conventionally, reactive power is said to be 'consumed' if $Q > 0$ (inductive load e.g. heating element) and 'generated' if $Q < 0$ (capacitive load e.g. fluorescent light (CFLs)).

Ratings are based on apparent power S (volt-amps), so larger reactive power Q is effectively a waste of power since real power delivered P must be lower.

Power factor correction: determine the reactive power which must be generated (per phase if three-phase) to make the desired power factor (typically 1: unity $\rightarrow Q_{\text{required}} = -Q_{\text{actual}}$ so $Q_{\text{total}} = 0$). Find the corresponding capacitor ($Q_C = -\omega CV^2$) or inductor ($Q_L = V^2 / \omega L$) value. Assume that the voltage across the load remains the same. The line current and its power losses will decrease.

Most consumers of electricity are net inductive (due to the use of e.g. induction motors) requiring capacitor-based power factor correction. Industrial-scale consumers (e.g. factories, refineries) usually have low power factors and are charged for reactive power, requiring power factor correction. Household consumers are not charged and usually have near-unity power factors.

8.4.3. Single-Phase Transformer Equivalent Circuit

True circuit: $\overline{I}_1 N_1 = \overline{I}_2 N_2$ and $\overline{E}_1/N_1 = \overline{E}_2/N_2$.
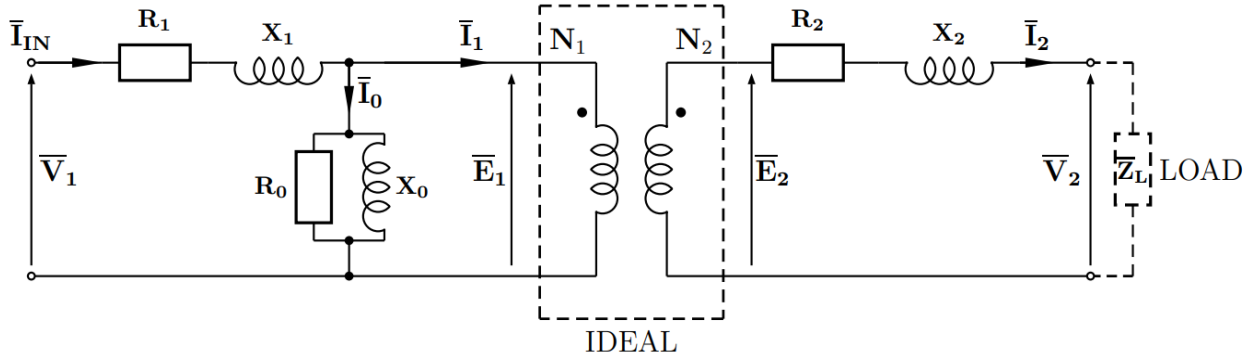
Simplified circuit (all referred to the primary coil: $R_{t1} = R_1 + \left(\dfrac{N_1}{N_2}\right)^2 R_2$ and $X_{t1} = X_1 + \left(\dfrac{N_1}{N_2}\right)^2 X_2$):
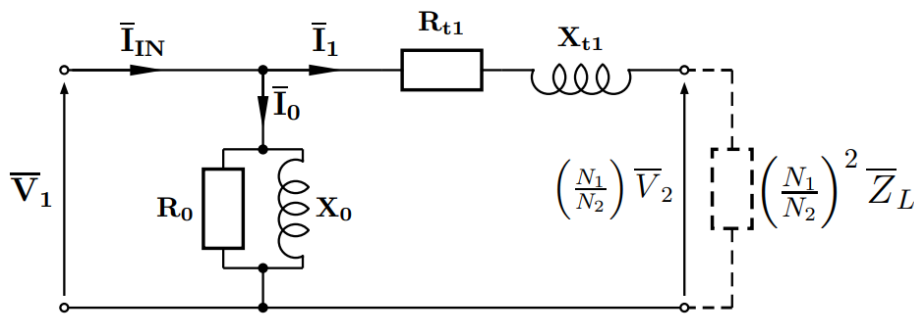
Physical significances of each component:

- R_{t1} represents the winding resistance (variable copper losses) of the coils
- X_{t1} represents the winding reactance of the coils (acting as inductors).
- R_0 represents the fixed iron losses (conduction through the transformer metal core)
- X_0 represents the leakage reactance (loss of flux escaping the metal core)

R_0 can be maximised by laminating the core which minimises eddy currents. X_0 can be maximised by using a soft iron core to ensure high permeability and low hysteresis losses.

Transformer tests: experimental analysis of a transformer to determine circuit parameters

- Open-circuit test: excite primary coil, secondary is open. $I_1 = I_2 = 0 \rightarrow N_1/N_2 = E_1/E_2 = V_1/V_2$. The series branch can be eliminated, leaving only $R_0 \parallel X_0$. Power: $V_1^2 = PR_0$ and $V_1^2 = QX_0$.

- Short-circuit test: excite primary coil, secondary is shorted. $V_2 = E_2 = E_1 = 0$. The parallel branch can be eliminated, leaving only $R_{t1} + jX_{t1}$. Power: $P = I_1R_{t1}^2$ and $Q = I_1X_{t1}$.

Efficiency: $\eta = \dfrac{P_{out}}{P_{in}} = 1 - \dfrac{P_{losses}}{P_{in}} = 1 - \dfrac{V_1^2/R_0 + I_1^2 R_{t1}}{P_{in}}$,   Regulation: $\dfrac{V_{2,OC} - V_2}{V_{2,OC}} = \dfrac{E_2 - V_2}{E_2}$ ($\times 100\%$)

8.4.4. Three-Phase Power

In a three-phase power system, generators (sources) provide three separate voltages with (ideally) identical magnitude and frequency but separated by phases of 120°.
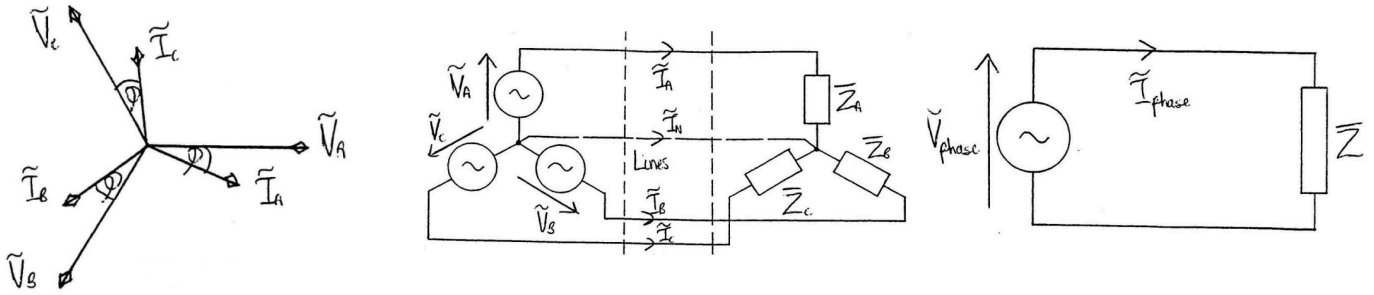
Phasor diagram   Star-connected three-phase system   Single-phase representation

If the star-connected source is perfectly balanced then the neutral wire has $I_N = 0$.

The line voltage V_L is the voltage between any two transmission lines (at the source).
The phase voltage V_{ph} is the voltage between any line and the nodal point.

- For a **star-connected source**: $V_L = \sqrt{3}\, V_{ph}$ and $I_L = I_{ph}$.
- For a **delta-connected source**: $V_L = V_{ph}$ and $I_L = \sqrt{3}\, I_{ph}$.

Star and Delta connected loads can be interconverted using the star-delta transformations (see Section 8.2.2). When balanced, $Z_* = \frac{1}{3} Z_\triangle$.

With multiple loads in parallel, use conservation of real power P and reactive power Q on a per-phase basis:

- For a **star-connected load**: $\frac{1}{3} P = Re\left(\frac{V_{ph}^2}{Z_*}\right)$ and $-\frac{1}{3} Q = Im\left(\frac{V_{ph}^2}{Z_*}\right)$

- For a **delta-connected load**: $\frac{1}{3} P = Re\left(\frac{V_L^2}{Z_*}\right)$ and $-\frac{1}{3} Q = Im\left(\frac{V_L^2}{Z_*}\right)$

Power factors can be corrected by adding a set of star or delta connected capacitors or inductors in parallel with the load (at each three-phase terminal).

8.4.5. Three-Phase Synchronous Machine (Generator) Equivalent Circuit

A prime mover is driven and rotates the rotor coils in the presence of a static magnetic field (induced by dc field current on the stator coils). AC current is induced in the rotor.

Equivalent circuit (generator convention):   Construction: (stator omitted)   Phasor diagram:
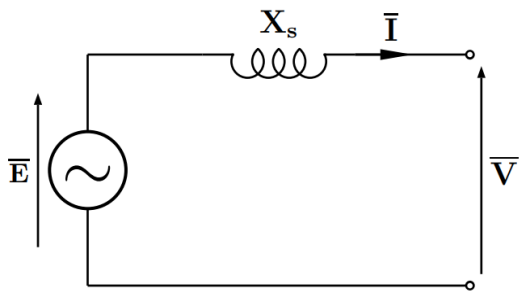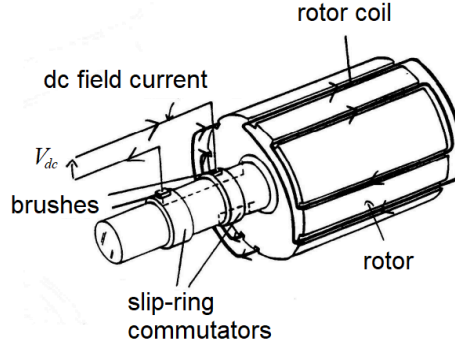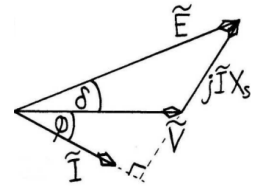
(E: phase excitation, X_S: synchronous reactance, I: input phase current, V: terminal phase pd, φ: phase difference, $\delta = \arg E - \arg V$: load angle, jIX_S: back-emf in stator)

$$\overline{E} = \overline{V} + jIX_S \qquad \text{or as phasors,} \qquad \overline{E} = \overline{V} + (IX_S) \angle \sin^{-1}(\cos\varphi)$$

$\delta > 0$: **generator (alternator)**. $\delta < 0$: **motor**. If $|\delta| \geq \pi/2$ then the machine is prone to instability.

Conditions for synchronous power generation: $\omega_S = \dfrac{\omega}{p_S}$ and $p_S = p_R$.

(ω_S: synchronous rotation speed of prime mover, ω: generated electricity frequency, p_S: pole **pairs** on stator, p_R: pole **pairs** on rotor).

A **dynamo** is a DC generator, using split-ring commutators instead of slip rings.

Three-phase generators are optimal: increasing the number of phases has diminishing returns on efficiency while costing more for wiring. Most generators are connected to public supplies, so stator voltage output has fixed magnitude and frequency (infinite bus assumption: no single generator variation affects the grid).
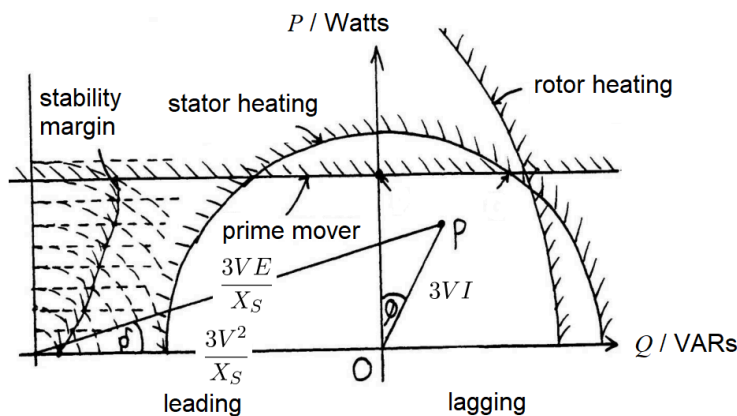
Operating chart: scale lengths by $\dfrac{3V}{X_S}$

Maximum EM torque: $T_{max} = \dfrac{3VE}{\omega_S X_S}$

EM torque: $T = T_{max} \sin\delta$

Power: $P_{in} = P_{out} + T\omega_S$

Stator heating limit based on rated S_{max}:
$S = 3\,V_{ph}\,I_{ph}$.

8.4.6. Three-Phase Induction Motor (AC) Equivalent Circuit (Asynchronous Motor)

Conditions for steady torque production: $\omega_S = \omega_R = \frac{\omega}{p}$ and $p_S = p_R$.

Slip: $s = 1 - \frac{\omega_R}{\omega_S}$. If $s = 0$ then $\omega_R = \omega_S$. If $s = 1$ then $\omega_R = 0$.

At the synchronous speed, the relative magnetic field rotation rate is zero (stationary), so there is no induced emf or rotor current so no torque is produced.

Equivalent circuit: side 1 is the stator; side 2 is the rotor (referred).
Assume $R_0 \gg R_1$ and $X_m \gg X_1$. Physical significance is similar to the transformer (per phase).

$$\overline{E} = \overline{V}_1 - (R_1 + jX_1)\,\overline{I}_1$$

(motoring convention)
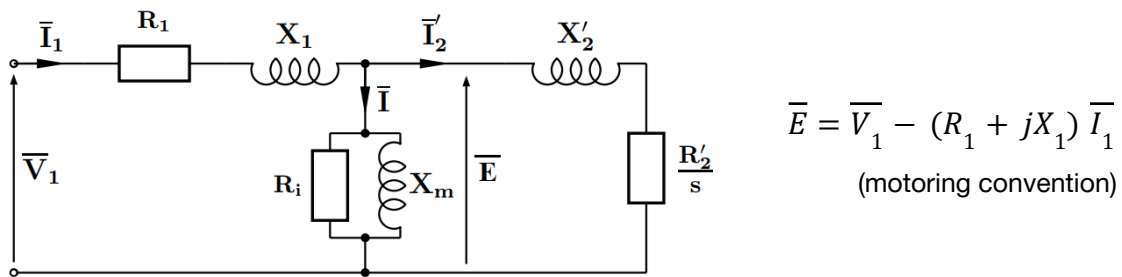
Motor tests:

- No-load test: let slip $s = 0$ (synchronous speed).

$$P_{ph} = \frac{V_{ph}^{\,2}}{R_0}, \quad Q_{ph} = \sqrt{(V_{ph}I)^2 - P_{ph}^{\,2}} = \frac{V_{ph}^{\,2}}{X_m}$$

- Locked-rotor test: let slip $s = 1$ (stationary transformer).

$$P_{ph} = I_{in}^{\,2}\left(R_1 + \frac{R_2{}'}{s}\right), \quad Q_{ph} = \sqrt{(V_{ph}I)^2 - P_{ph}^{\,2}} = I_{in}^{\,2}\left(X_1 + X_2{}'\right)$$

Power, Torque and Efficiency: Electromagnetic torque: $T_{EM} = \dfrac{3\left(I_2{}'\right)^2 R_2{}'}{s\,\omega_S}$.

To find $I_2{}'$, use a Thevenin circuit equivalent and take $I_2{}' = V_{TH}\left|Z_{TH} + \dfrac{R_2{}'}{s}\right|^{-1}$.

$P = T\omega$, $P_{loss} = T_{loss}\omega_R$, $P_{out} = T_{out}\omega_R$ and $T_{out} = T_{EM} - T_{loss}$ → efficiency: $\eta = \dfrac{P_{out}}{3\,V_{ph}\,I\cos\varphi_{in}}$.

- Maximum torque: use Thevenin and max power transfer theorems: $\dfrac{R_2{}'}{s} = |Z_{TH}|$.

- Maximum output power: split as $\dfrac{R_2'}{s} = \underbrace{R_2}_{\text{wasted}} + \underbrace{\left(\frac{1}{s} - 1\right)R_2}_{\text{power out}}$, maximise similarly.

- Maximum starting torque:
$\omega_R = 0$ so let $s = 1$ and add the remaining (referred) rotor resistance to make $R_2{}'' = Z_{TH}$.

8.4.7. Separately Excited DC Motor Equivalent Circuit
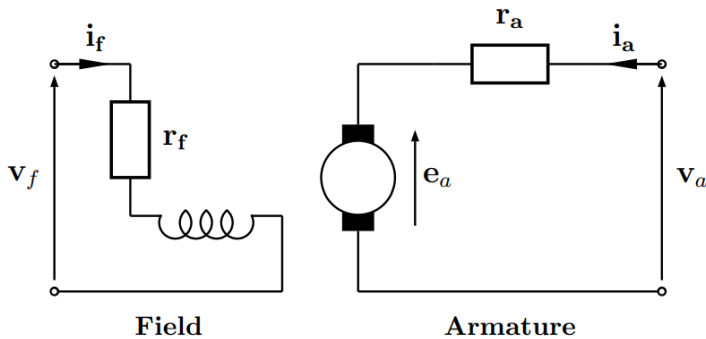
Armature back emf, $e_a = K\phi\omega$; torque, $T = K\phi i_a$
(K: emf constant, ϕ: flux per pole, ω: rotor speed, i_a: armature current)

The field winding circuit represents the **stator** and the armature circuit is the **rotor**. Dynamics: (θ: rotor/shaft angular position, J: shaft polar moment of inertia, λ: rotor damping constant, $\{R_a, L_a\}$: armature resistance/inductance)

$$J\ddot{\theta} + \lambda\dot{\theta} = K\phi\, i_a, \qquad L_a\frac{\mathrm{d}i_a}{\mathrm{d}t} + R_a i_a = V_a - K\phi\dot{\theta}$$

8.4.8. Electrical Grid Transmission System and Per-Unit Calculations

Typical distribution system: Example per-phase, per-unit representation to a single load:
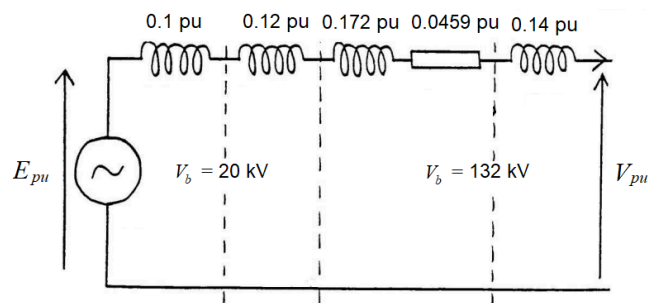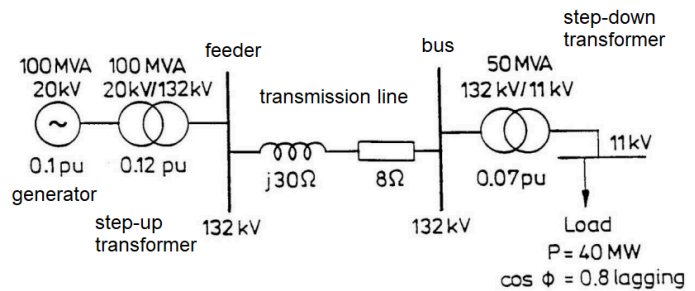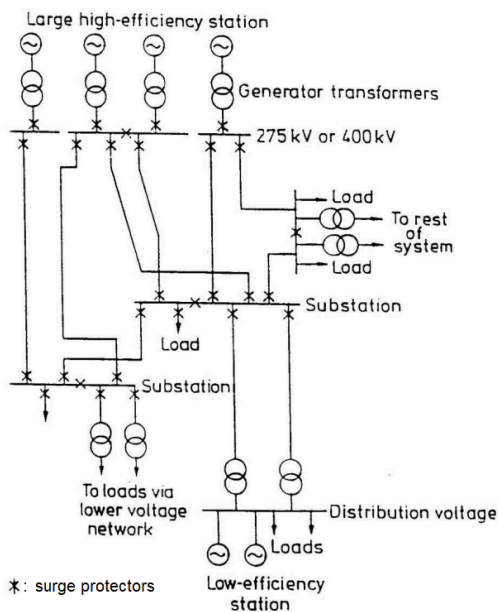
Per-unit calculations: VA_b: base VA (three-phase), V_b: base line voltage, with

$$S_{pu} = V_{pu}I_{pu}, \quad Z_b = \frac{V_b^2}{VA_b} \text{ and } I_b = \frac{VA_b}{\sqrt{3}\,V_b}. \qquad \text{Change of base: } Z_{pu}' = \frac{VA_b'}{VA_b}Z_{pu}.$$

Per-unit reactances are often expressed as percentages e.g. 15% pu = 0.15 pu.
For a transformer, the rated voltage and reactance always refer to the primary coil.

Fault analysis: assume a three-phase symmetrical fault to earth (worst-case: max surge current) Model all generators as $E_{pu} = 1 \angle 0°$ pu emfs with their synchronous reactances so that all generators output to a common node. Neglect resistances and loads. Determine fault current and required VA rating of the circuit breaker.

8.5. Optics, Electromagnetic Waves and Plasma Physics

8.5.1. Reflection and Refraction
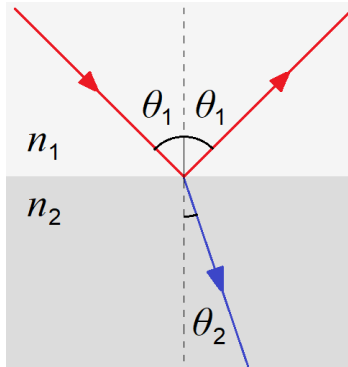
At a perfectly flat interface, an incoming ray can undergo reflection and/or refraction such that:

$$n_1 \sin \theta_1 = n_2 \sin \theta_2 \qquad \text{(Snell's law of refraction)}$$

For any reflected component, angle of incidence = reflection.

Critical angle: $\quad \sin \theta_c = \dfrac{n_2}{n_1} \qquad (\theta_2 = 90°)$

For total internal reflection: $n_1 > n_2$ and $\theta_1 > \theta_c$.

The refractive index depends on medium material, wavelength and temperature.

8.5.2. Angle of Dispersion in a Prism
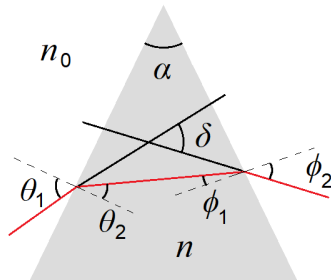
Geometry: $\theta_2 + \phi_1 = \alpha$ and $\delta = \theta_1 - \theta_2 + \phi_2 - \phi_1$

Refraction: $n_0 \sin \theta_1 = n \sin \theta_2$ and $n \sin \phi_1 = n_0 \sin \phi_2$

Angle of dispersion: $\dfrac{n}{n_0} = \dfrac{\sin \frac{1}{2}(\alpha + \delta)}{\sin \frac{1}{2}\alpha} \rightarrow \delta = 2 \sin^{-1}\left(\dfrac{n}{n_0} \sin \dfrac{\alpha}{2}\right) - \alpha$

8.5.3. Thin Convex (Converging) Lenses
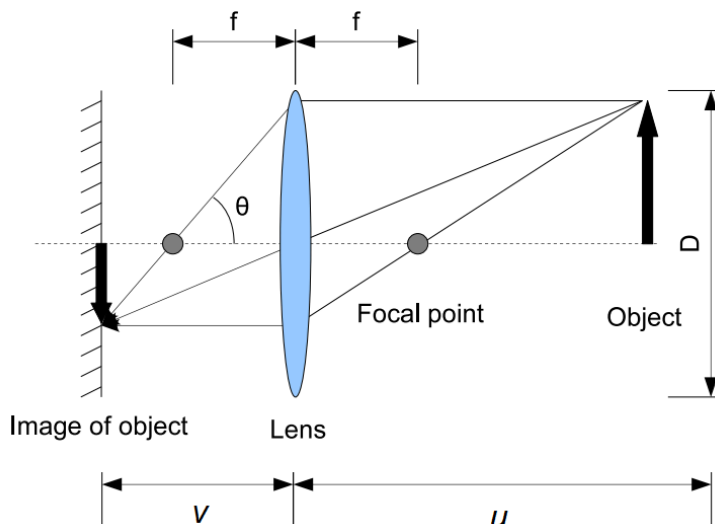
Distances u and v relate to the focal length f by

$$\frac{1}{f} = \frac{1}{u} + \frac{1}{v}$$

Magnification: $m = \dfrac{v}{u}$

Numerical aperture: $NA = n \sin \theta$

f-number ($f/\#$): $N = \dfrac{f}{D}$; $\quad NA \approx \dfrac{n}{2N}$

8.5.4. Fibre Optics

For a single straight fibre of total length L, acceptance half-angle α, core index n_1 and cladding index n_2 (such that $n_1 > n_2$):
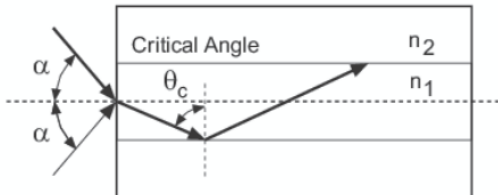
- Numerical aperture: $\mathrm{NA} = \sin \alpha = \sqrt{n_1^2 - n_2^2}$

- Propagation time range: $\dfrac{Ln_1}{c} < T < \dfrac{Ln_1^2}{cn_2}$

- Chromatic dispersion: shorter wavelengths travel faster than longer wavelengths.

Fibre optic cables have a characteristic attenuation spectrum (due to Rayleigh scattering, impurity metal ions, absorption peaks, glass absorption), with varying losses (measured in signal power drop per length of cable, dB/km).

An impurity of 1 ppm of metal ions (e.g. Fe^{2+}, Cu^{2+}) causes ~1 dB/km loss.

The coating should be impermeable to hydrogen (produced from e.g. steel cable corrosion, bacterial presence) as H_2 and its OH^- byproducts also have absorption peaks.

Fibre optic cables that are bent sharply risk attenuation due to light incident below the critical angle at the bend. Sharp bends can also induce stresses and micro-scale flaws in the core interface, contributing to the dB/km losses. A common standard is to ensure no bends with radius of curvature $r < 15d$ exist (d: diameter of cable).

8.5.5. Polarisation and Malus' Law

EM waves can be plane-polarised i.e. all electric/magnetic field oscillations are in the same plane. The direction of polarisation refers to the plane of the electric field.

Radiation can be polarised by passing through a polariser. For polarisation by reflection, see Section 8.5.5.

Malus' law: for a perfect polariser, $\frac{I_t}{I_i} = \cos^2 \Delta\theta$

(I_t: transmitted intensity, I_i: incident intensity, $\Delta\theta$: difference between angle of initial and final polarisation.)

For initially unpolarised (uniformly distributed) radiation, transmission coefficient $\frac{I_t}{I_i} = \frac{1}{2}$.

Losses in a Polaroid filter result in actual $\frac{I_t}{I_i} \sim 0.38$.

Plane Polarised Light and Circularly Polarised Light as Superpositions of Coherent Waves

- Superposition of two perpendicularly plane-polarised waves with different amplitudes and/or phases produces **elliptically polarised light**. If the phase difference is 90°, then the axes of the ellipse align with the polarisation directions. If additionally the amplitudes are equal then the result is **circularly polarised light.**

- Superposition of coherent in-phase left- and right-circularly polarised light produces **plane polarised light**, with the polarisation direction being the coincident vectors of the waves.

Circularly polarised light can be created using a birefringent quarter-wave plate whose 'fast' (lower index) and 'slow' (higher index) axes are at 45° to the plane of polarisation. The thickness of the plate is chosen such that the component in the slow axis lags the component in the fast axis by 90° at their exit, creating circular polarisation.
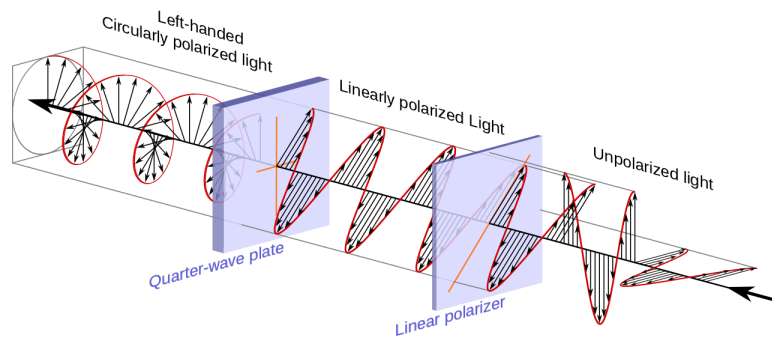
Required quarter-wave plate thickness: $d = \frac{\lambda_0}{4\,|\Delta n|}$ (Δn: difference in refractive index in axes)

For values of Δn for different crystals see Section 8.5.12.

8.5.6. Waves at Interfaces: The Fresnel Equations and Polarisation by Reflection

Snell's law using impedances: $n_1 \sin \theta_i = n_2 \sin \theta_t$ so $\eta_2 \sin \theta_i = \eta_1 \sin \theta_t$ where $H = E / \eta$.
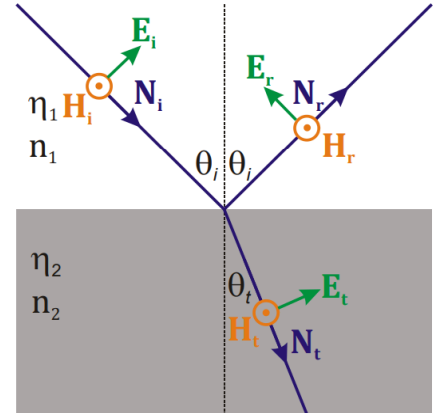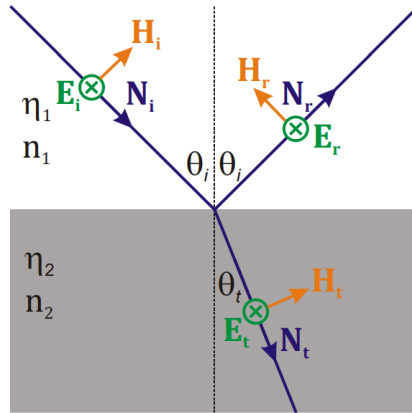
Electric field perpendicular to plane	Magnetic field perpendicular to plane
$(E_i + E_r = E_t)$	$(H_i + H_r = H_t)$

Transmission:

$$\left(\frac{E_t}{E_i}\right)_\perp = \frac{2\eta_2 \cos\theta_i}{\eta_2 \cos\theta_i + \eta_1 \cos\theta_t} \qquad \left(\frac{E_t}{E_i}\right)_{||} = \frac{2\eta_2 \cos\theta_i}{\eta_1 \cos\theta_i + \eta_2 \cos\theta_t}$$

Reflection:

$$\left(\frac{E_r}{E_i}\right)_\perp = \frac{\eta_2 \cos\theta_i - \eta_1 \cos\theta_t}{\eta_2 \cos\theta_i + \eta_1 \cos\theta_t} \qquad \left(\frac{E_r}{E_i}\right)_{||} = \frac{\eta_1 \cos\theta_i - \eta_2 \cos\theta_t}{\eta_2 \cos\theta_i + \eta_1 \cos\theta_t}$$

At normal incidence ($\theta_i = 0°$), we have $\left(\dfrac{E_t}{E_i}\right) = \dfrac{2\eta_2}{\eta_1 + \eta_2}$, $\left(\dfrac{E_r}{E_i}\right)_\perp = \dfrac{\eta_2 - \eta_1}{\eta_1 + \eta_2}$, $\left(\dfrac{E_r}{E_i}\right)_{||} = \dfrac{\eta_1 - \eta_2}{\eta_1 + \eta_2}$.

Polarisation by Reflection: if $\tan \theta_i = \dfrac{\eta_1}{\eta_2}$ (**Brewster angle**) then $\left(\dfrac{E_r}{E_i}\right)_{||} = 0$ (**plane polarised**).

In this case the reflected wave is **plane-polarised** with the electric field perpendicular to the plane of incidence i.e. electric field oscillates in the plane of the **interface** surface.

Anti-Reflection Coatings: inserting a layer of material with $\eta = \sqrt{\eta_1 \eta_2}$ allows for quarter-wave matching (layer thickness is equal to ¼ of the wavelength within the layer).

However, this is only tuned to the one wavelength. An alternative is to use nanostructured materials with size much less than λ (metamaterials: see Section 8.5.15). In this case the electromagnetic wave does not interact with individual structures but sees a spatial average of the structure so the nanostructure can appear to modulate the characteristic impedance smoothly as a function of depth into the layer: reflections are minimised across a broad range of wavelengths.

8.5.7. Scattering of Light by Particles in a Medium

Rayleigh Scattering (particles with size $x \ll \lambda$): $I(r, \theta) = I_0 \dfrac{8\pi^4 \alpha^2}{\lambda^4 r^2} \left(1 + \cos^2 \theta\right)$

Mie Scattering (particles with size $x \sim \lambda$): more intense forward lobe, much less dependent on λ.

Molecular polarisability, $\alpha = \dfrac{3}{4\pi N} \left(\dfrac{\varepsilon_r - 1}{\varepsilon_r + 2} \right)$ (Clausius-Mossotti relation)

where $\varepsilon_r = n^2$ for nonmagnetic media.

(N: number of scatterers per unit volume)

Rayleigh Scattering   Mie Scattering

Direction of incident light
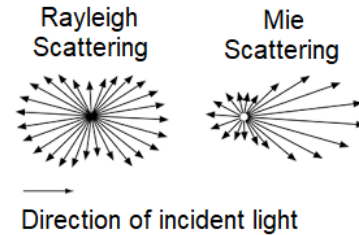
8.5.8. Maxwell's Equations and the Electromagnetic Wave Equations (Differential Form)

For the integral forms, see Section 8.1.4-6.

$$\nabla \cdot \mathbf{D} = \rho$$

Gauss' law for electricity: charge produces an electric field

$$\nabla \cdot \mathbf{B} = 0$$

Gauss' law for magnetism: magnetic monopoles do not exist

$$\nabla \times \mathbf{E} = -\frac{\partial \mathbf{B}}{\partial t}$$

Faraday's law: changing magnetic flux induces an electric field

$$\nabla \times \mathbf{H} = \mathbf{J} + \frac{\partial \mathbf{D}}{\partial t}$$

Ampere-Maxwell law: moving charge or changing electric flux both induces a magnetic field

To derive the electromagnetic wave equations in free space, set $\rho = 0$ and $\mathbf{J} = 0$ (no charge, no current). Take the curl of both sides of Faraday's law, use the vector product identity in Section 3.5.12 and substitute $\nabla \cdot \mathbf{E} = 0$ (from Gauss' law). The wave PDEs are then

$$\nabla^2 \mathbf{E} = \frac{1}{c^2} \frac{\partial^2 \mathbf{E}}{\partial t^2} \quad \text{and} \quad \nabla^2 \mathbf{H} = \frac{1}{c^2} \frac{\partial^2 \mathbf{H}}{\partial t^2} \quad \text{where} \quad c = \frac{1}{\sqrt{\varepsilon_0 \varepsilon_r \mu_0 \mu_r}}.$$

8.5.9. Telegrapher's Wave Equations and the Loss Transmission Line Model

If the wavelength is of similar order to the physical length of the system we are looking at, then we can no longer consider the current to be behaving as an 'incompressible fluid' i.e. conventional circuit analysis. This is the case in e.g. transmission lines.

Let C and L be the capacitance and inductance **per unit length** of transmission line.

For a **lossless** transmission line (no series resistance, no shunt conductance):
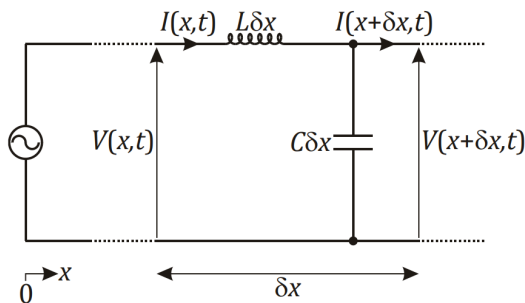
Telegrapher's equations:

$$\frac{\partial V}{\partial x} = -L\frac{\partial I}{\partial t} \quad \text{and} \quad \frac{\partial I}{\partial x} = -C\frac{\partial V}{\partial t}$$

Wave equations:

$$\frac{\partial^2 V}{\partial x^2} = \frac{1}{c^2}\frac{\partial^2 V}{\partial t^2} \quad \text{and} \quad \frac{\partial^2 I}{\partial x^2} = \frac{1}{c^2}\frac{\partial^2 I}{\partial t^2} \quad \text{where} \quad c = \frac{1}{\sqrt{LC}}.$$

- General solution: $\quad V = \bar{V}_F e^{j(\omega t - \beta x)} + \bar{V}_B e^{j(\omega t + \beta x)} \quad$ and $\quad I = \bar{I}_F e^{j(\omega t - \beta x)} + \bar{I}_B e^{j(\omega t + \beta x)}$
- Amplitudes: $\quad V_F = I_F Z_0 \text{ and } V_B = -I_B Z_0$

(Wavelength: $\lambda = \frac{2\pi c}{\omega}$. Characteristic impedance: $Z_0 = \sqrt{\frac{L}{C}}$. Propagation constant $= j\beta$.

Phase constant (wavenumber): $\beta = k = \frac{2\pi}{\lambda} = \frac{\omega}{v}$. Speed of light in media: $v = c/n$).

Connection to a Load: at $x = 0$, with load Z_L, voltage reflection ρ_L / transmission τ_L coefficients are ($\tau_L - \rho_L = 1$):
$$\rho_L = \frac{V_B}{V_F} = \frac{Z_L - Z_0}{Z_L + Z_0}, \quad \tau_L = \frac{2Z_L}{Z_L + Z_0}.$$

- For any value of x, $\rho(x) = \rho_L e^{j2\beta x}$.

- Input impedance: $Z_{in} = Z_0 \dfrac{Z_L + Z_0 j \tan \beta l}{Z_0 + Z_L j \tan \beta l}$.

- Voltage standing wave ratio (VSWR): $\dfrac{|V_F| + |V_B|}{|V_F| - |V_B|} = \dfrac{1 + |\rho_L|}{1 - |\rho_L|}$.

- Incident reflected power is proportional to $|\rho_L|^2$.
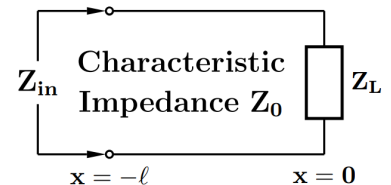
- Open circuit: $Z_L = \infty$ so $\rho_L = 1$ (0 shift). Perfect reflection with an antinode at the terminal.
- Closed circuit: $Z_L = 0$ so $\rho_L = -1$ (π shift). Perfect reflection with a node at the terminal.
- Load impedance matched: $Z_L = Z_0$ so $\rho_L = 0$. No reflection; perfect transmission.

8.5.10. Lossy Transmission Lines

There are incremental series resistances $R\,\delta x$ and shunt conductances $G\,\delta x$:
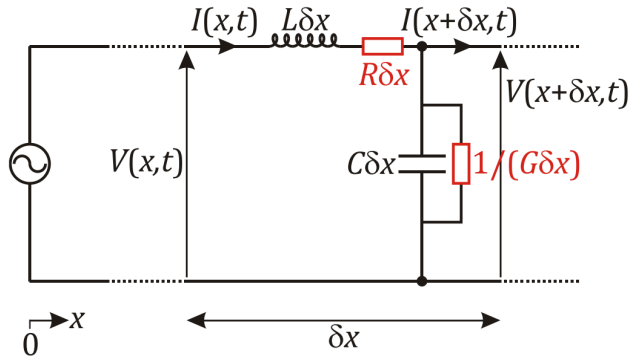
General wave solution is now

$$
\begin{aligned}
V(x,t) &= (V_F e^{-\gamma x} + V_B e^{\gamma x})e^{j\omega t} \\
I(x,t) &= (I_F e^{-\gamma x} + I_B e^{\gamma x})e^{j\omega t}
\end{aligned}
$$

Propagation constant:
$$\gamma = \alpha + j\beta = \sqrt{(R + j\omega L)(G + j\omega C)}$$

Characteristic impedance: $Z_0 = \sqrt{\dfrac{R + j\omega L}{G + j\omega C}}$

For any value of x,
$$\rho(x) = \rho_L\, e^{j2\gamma x}.$$

Input impedance: $Z_{in} = Z_0 \dfrac{Z_L + Z_0\, j\,\tanh \gamma l}{Z_0 + Z_L\, j\,\tanh \gamma l}.$

8.5.11. Propagation of Waves in Insulating Media

Electric and magnetic field wave solutions (1D):

$$
E_x = \mathrm{Re}\left\{\mathbf{E}_{xF}e^{j(\omega t - \beta z)} + \mathbf{E}_{xB}e^{j(\omega t + \beta z)}\right\}
\qquad
H_y = \mathrm{Re}\left\{\mathbf{H}_{yF}e^{j(\omega t - \beta z)} + \mathbf{H}_{yB}e^{j(\omega t + \beta z)}\right\}
$$

Refractive index: $n = \sqrt{\varepsilon_r \mu_r}$. Intrinsic impedance: $\eta = \sqrt{\mu/\varepsilon}$. Wave speed: $v = \dfrac{1}{\sqrt{\varepsilon\mu}}$.

For air or vacuum, $\eta = 377\ \Omega$, $n = 1$, $\varepsilon_r = 1$, $\mu_r = 1$, $v = c = 299{,}792{,}458\ \mathrm{ms^{-1}} \approx 3 \times 10^8\ \mathrm{ms^{-1}}$.

Intensity of an EM wave (complex Poynting vector): $I = \dfrac{1}{2}\mathrm{Re}\,(\mathbf{E} \times \mathbf{H}^*)$

For the reflection and transmission coefficients, see Section 8.5.5.

8.5.12. Propagation of Waves in Conducting Media

Electric and magnetic field wave solutions (1D):

$$
E_x = \mathrm{Re}\left\{\mathbf{E}_{xF}e^{-\gamma z} + \mathbf{E}_{xB}e^{\gamma z}\right\}e^{j\omega t}
\qquad
H_y = \mathrm{Re}\left\{\mathbf{H}_{yF}e^{-\gamma z} + \mathbf{H}_{yB}e^{\gamma z}\right\}e^{j\omega t}
$$

When conductivity $\sigma \neq 0$, the propagation constant is $\gamma = \alpha + j\beta = \sqrt{j\omega\mu(\sigma + j\omega\varepsilon)}$.

Intrinsic impedance: $\eta = \sqrt{\dfrac{j\omega\mu}{\sigma + j\omega\varepsilon}}$. Reflection coefficient: $\rho_L = \dfrac{\eta_2 - \eta_1}{\eta_1 + \eta_2}$. Skin depth: $\delta = \dfrac{1}{\alpha}$.

8.5.13. Skin Effect

AC signals (like all electromagnetic waves in conducting media) have maximum current density **J** at the surfaces of any conductor, and minimum in the centre.

The skin depth is the reciprocal of the real part of the propagation constant γ (Section 8.5.10). The skin depth decreases with frequency, which increases the effective impedance.

For low frequencies $\omega \ll \sigma/\varepsilon$, this simplifies to $\delta \approx \sqrt{\frac{2}{\sigma\omega\mu}}$.

For high frequencies $\omega \ll \sigma/\varepsilon$, the asymptotic limit is $\delta \approx \frac{2}{\sigma}\sqrt{\frac{\varepsilon}{\mu}}$.

Variation of current density **J** with depth d from surface: $\mathbf{J}(d) = \mathbf{J}_{\mathrm{S}}\, e^{-(1+j)\frac{d}{\delta}}$.

When $\delta \sim R$ (wire radius), the current density is (for circular sections):

$$\mathbf{J}(r) = \mathbf{I}\,\frac{k}{2\pi R}\frac{J_0(kr)}{J_1(kR)} = \mathbf{J}(R)\,\frac{J_0(kr)}{J_0(kR)}$$

(J_n: Bessel function (Section 1.7.10), $k = \sqrt{-j\omega\mu\sigma}$: wavenumber, **I**: total current phasor)

In both cases, both the magnitude and phase (represented by the complex current density) vary with depth.

8.5.14. Antenna Design

Poynting vector: $\mathbf{N} = \mathbf{E} \times \mathbf{H}$ ($\mathbf{N}$ is parallel to the direction of propagation / energy transfer)

Instantaneous intensity (power density, W m^{-2}): $|\mathbf{N}(t)| = |\mathbf{E}(t)||\mathbf{H}(t)|$.

Mean intensity: $\frac{1}{2}|\mathbf{N}| = E_{rms} H_{rms}$

Half-wave dipole (grand plane) antenna: conductor of length $\frac{\lambda}{4}$ extending from a grounded plane (common for e.g. radio antenna). AC signal in the conductor produces circulating $\mathbf{H}$-field with $\mathbf{E}$-field parallel to the dipole so propagation is in all surrounding perpendicular directions.

Current variation is a standing wave: $i = i_0 \cos \omega t \cos kx$ ($k = \frac{2\pi}{\lambda}$, for $|x| \leq \frac{\lambda}{4}$)

Anisotropic far-field electric field: $E_\theta = \dfrac{I_0 Z_0}{2\pi r} \dfrac{\cos\left(\frac{\pi}{2}\cos\theta\right)}{\sin\theta} \sin(\omega t - kr)$
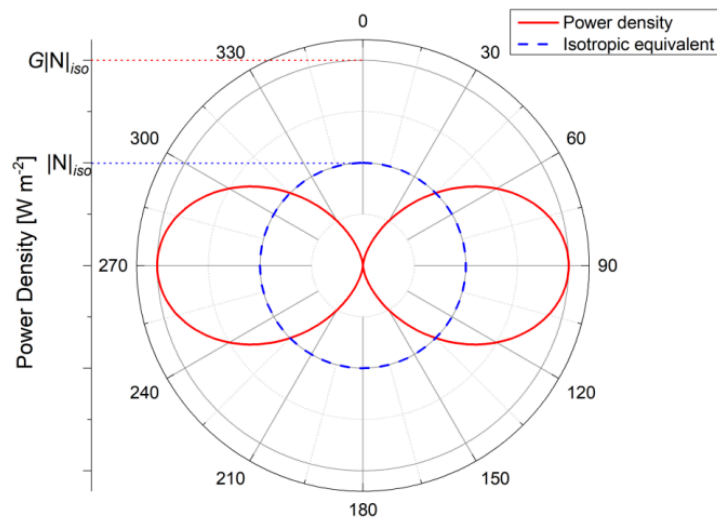
Antenna gain: $G = \dfrac{maximum\ power\ density}{isotropic\ power\ density}$ such that $I_{max} = \dfrac{G\,P}{4\pi r^2}$. For a $\frac{\lambda}{4}$-dipole, $G = 1.64$.

The total power can be computed by integrating $\dfrac{|E_\theta|^2}{2\,Z_0}$ over all space.

Radiation resistance: $R_a = \dfrac{P}{I_{rms}^2}$.   ($P$: total power emitted by antenna)

8.5.15. Smith Chart for Impedance Matching of Complex Reflection Coefficients

RADIALLY SCALED PARAMETERS
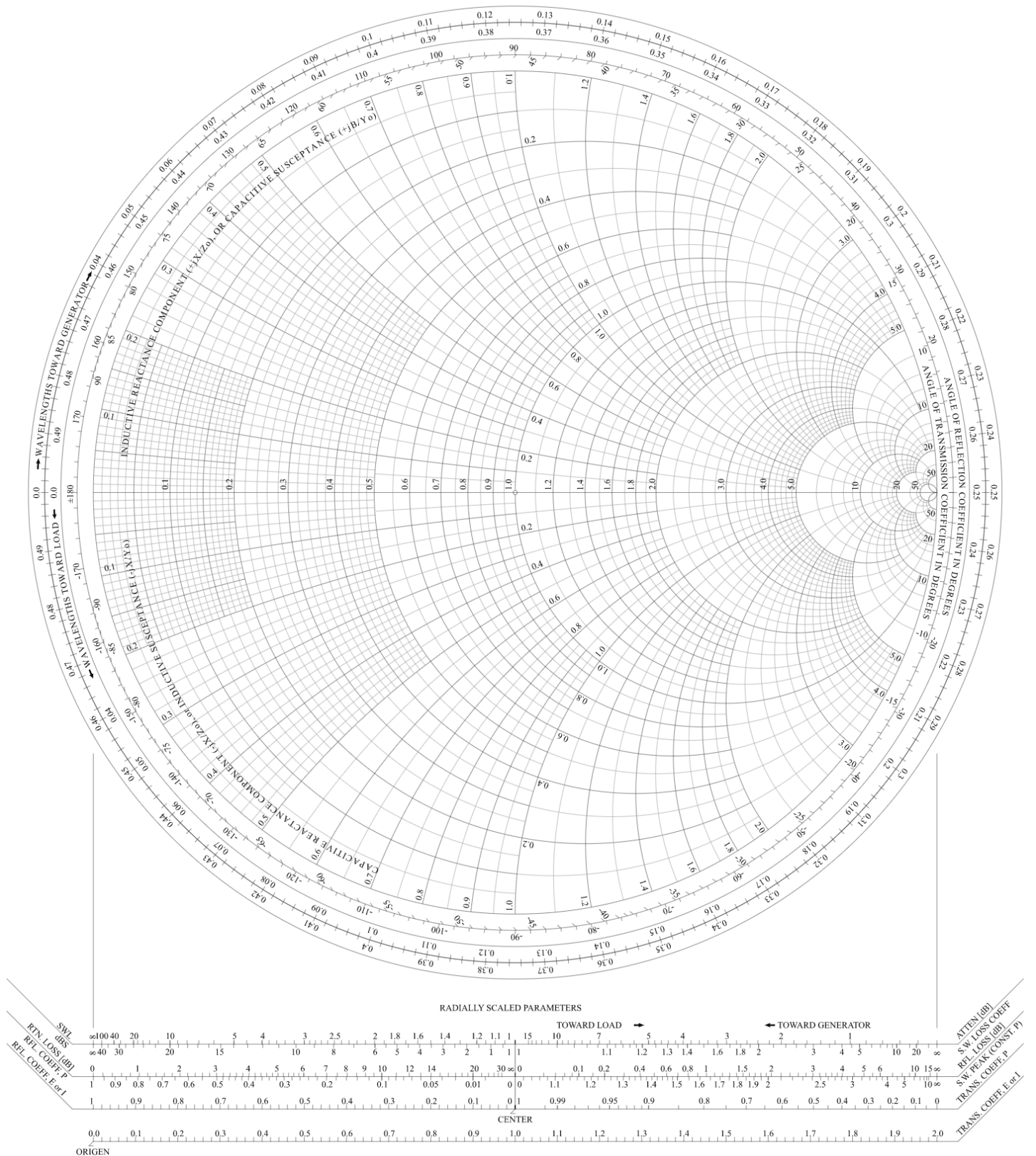
8.5.16. Magnetohydrodynamics (MHD)

Electrically conductive fluids (liquid metals, electrolytes, plasmas) respond to changing magnetic fields by developing an internal electric current (Faraday's law), which exert Lorentz forces on the fluid, which can produce fluid flow, unlike in solid conductors.

- Current density: $\mathbf{J} = \sum_i n_i q_i \mathbf{u}_i$ (n: number density, q: charge, $\mathbf{u}$: mean velocity, i: species)
- Fluid COM velocity: $\rho \mathbf{v} = \sum_i n_i m_i \mathbf{u}_i$ (ρ: fluid density, m: particle mass)
- Ampere's law: $\mu_0 \mathbf{J} = \nabla \times \mathbf{B}$ (**B**: magnetic flux density)
- Faraday's law: $\partial \mathbf{B} / \partial t = -\nabla \times \mathbf{E}$ (**E**: electric field strength)
- Ohm's law: $\mathbf{E} + \mathbf{v} \times \mathbf{B} = \rho_e \mathbf{J}$ ($\rho_e = 1/\sigma$: electrical resistivity, σ: electrical conductivity)
- Cauchy momentum: $\rho\, D\mathbf{v} / Dt = \mathbf{J} \times \mathbf{B} - \nabla p$ ($D/Dt = d/dt + \mathbf{v} \cdot \nabla$: material derivative operator)
- Force per unit volume: $d\mathbf{F} = \mathbf{J} \times \mathbf{B}\, dV$ ($\mathbf{F} = \iiint_V \mathbf{J} \times \mathbf{B}\, dV$: body force on fluid control volume)
- **Induction equation:** $\partial \mathbf{B} / \partial t = \nabla \times (\mathbf{v} \times \mathbf{B}) + \eta \nabla^2 \mathbf{B}$ ($\eta = 1/(\mu_0 \sigma)$: magnetic diffusivity)
  In 'ideal MHD', it is assumed that $\eta \to 0$, while in 'resistive MHD', η is finite.

Dimensionless numbers in MHD:

- Magnetic Reynolds number: $Re_m = \frac{vL}{\eta}$ (v: velocity scale, L: length scale)

Alfvén's theorem: conducting fluid streamlines and magnetic flux lines are identical when $Re_m \to \infty$.

8.6. Functional Materials and Solid State Physics

8.6.1. Band Theory of Network Solids

Overlap of atomic orbitals in close proximity causes energy level splitting. For a large network of atoms, the resulting orbitals (bonding is valence; $E \leq$ HOMO and antibonding is conduction; $E \geq$ LUMO) approximate continuous bands of energies. The HOMO-LUMO gap (band gap) is zero in metals (due to overlap), small in semiconductors (< 2eV) and large in insulators (> 2 eV). Thermal excitation can promote valence electrons to the conduction band.

Tight Binding Model: analogous the LCAO model from MO theory (Section 13.1.10)
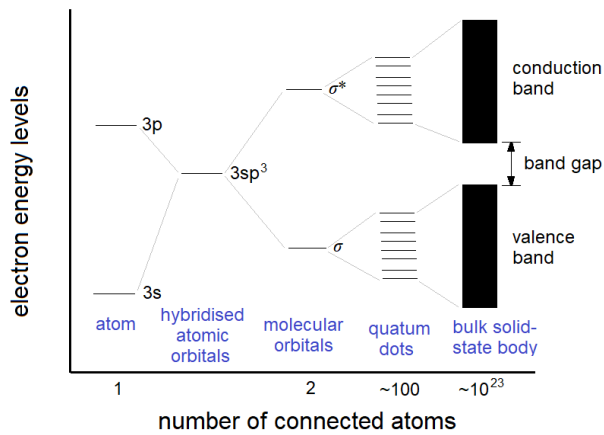
Number of splits increases with atom count
Hybridisation of AOs for covalent bond formation
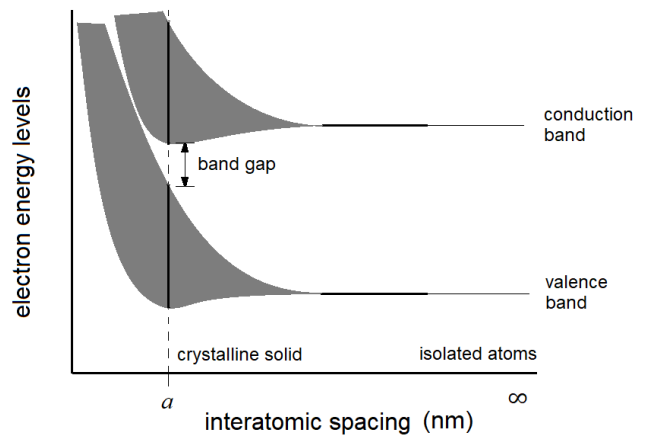
Magnitude of splitting energy increases
with proximity to other atoms

Nearly-Free Electron Model: periodic lattice perturbations to free electron wavefunction
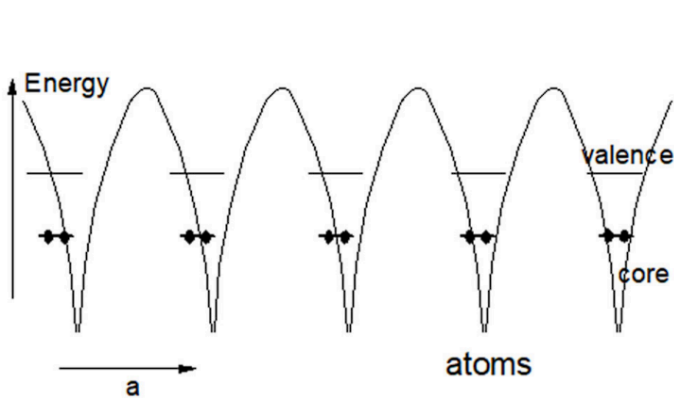
Lattice potential function, $V(x)$
Superposition of Coulomb potentials at lattice points
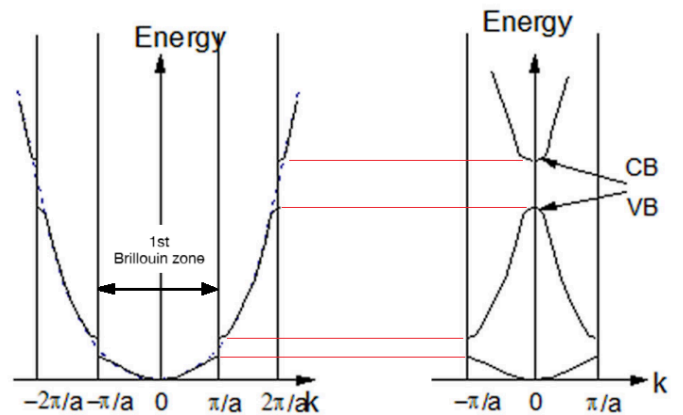
Repeated zone scheme
Band-stopped free electron

Folded zone scheme
Reflected: band gaps

8.6.2. Quantum Physics of Crystalline Semiconductors

- **Wavevector** $\mathbf{k}$ is the quantum of momentum $\mathbf{p}$: $\mathbf{p} = \hbar\mathbf{k}$ ($\hbar = \frac{h}{2\pi} = 1.055 \times 10^{-34}$ J s)

  A 3D Fourier transform maps position $\mathbf{x}$ into spatial frequency $\mathbf{k}$ (spatial frequency); if the domain of $\mathbf{x}$ is a unit cell then the domain of $\mathbf{k}$ is the union of all nth-order Brillouin zones (Section 13.2.7). The components of $\mathbf{k}$ represent the frequency of the wavefunction for a state in each lattice direction, and the vector $\mathbf{k}$ indicates the direction of its stationary oscillation in real space.

- **De Broglie wavelength** λ: $|\mathbf{k}| = k = \frac{2\pi}{\lambda}$

- **Kinetic energy**, by free electron model (Section 11.1.11): $E = \frac{p^2}{2m} = \frac{\hbar^2 k^2}{2m}$

- Lattice symmetry (size a) imposes **constraints on wavelength**:

  $\lambda_n = 2a / n \rightarrow k_n = \frac{2\pi}{\lambda_n} = \frac{2\pi}{a} n \rightarrow E_n = \frac{2\pi^2 \hbar^2 n^2}{ma^2}$ (particle in a box model)

- **Bloch's theorem of periodicity**, $u(\mathbf{r})$ is a unit cell wavefunction: $\psi(\mathbf{r}) = \exp(i\,\mathbf{k}\cdot\mathbf{r})\,u(\mathbf{r})$

- **Effective mass** (electrons: $m^* > 0$, holes: $m^* < 0$): $m^* = \hbar^2\,(d^2E / dk^2)^{-1}$
  m^* is typically quoted in multiples of the free electron mass, $m_e = 9.1 \times 10^{-31}$ kg.

- **Hydrogenic model of dopant levels**: $E_n = -\frac{R_0'}{n^2}, \quad R_0' = \frac{Z^2 m^*}{\varepsilon_r^2} R_0, \quad R_0 = 13.6$ eV.

  (R_0': modified Rydberg constant (dopant binding energy).
  Z: dopant valency relative to host, m^* [m_e]: dopant effective mass, ε_r: host relative permittivity.)

- **Deep impurities / trap levels:** dopant binding energy R_0' is large for **wide band gap** semiconductors, due to heavier carriers (high m^*) and poorer screening (low ε_r).

- **Linear dispersion**: $m^* = 0$ (zero second derivative). Charge carriers behave like bosons or zero rest mass fermions i.e. light, giving very **high mobility**.
- **Quadratic dispersion**: $m^* \neq 0$ (parabolic band edge).

- **Light carriers**: $|m^*|$ is small, band dispersion is **narrow** and mobility is higher.
- **Heavy carriers**: $|m^*|$ is large, band dispersion is **wide** and mobility is lower.

- **Doubly degenerate levels**: multiple bands coinciding at the same band edge.

- **Fermi level** E_f: HOMO energy at $T = 0$ K (minimum entropy, no lattice vibrations). At other temperatures, E_f is the energy at which the Fermi-Dirac distribution of electron energies,

  $f(E) = \dfrac{1}{1 + \exp(\frac{E - E_f}{kT})} = \dfrac{1}{2}.$

8.6.3. Transport Properties of Crystalline Semiconductors

- **Ohm's law:** $\mathbf{J} = \sigma\mathbf{E}$ ($\mathbf{J}$ [A m^{-2}]: current density, σ [S m^{-1}]: conductivity, $\mathbf{E}$ [V m^{-1}]: electric field)

- **Fermi energy:** $E_F = \frac{3h^2}{8m}\left(\frac{N}{V}\right)$,   **Wavenumber**: $k_F = \left(\frac{2m^*E_F}{\hbar^2}\right)^{1/2}$ (m^*: effective carrier mass)

- **Density of states for nearly free electrons:** $g(E) = \frac{\sqrt{2(m^*)^3 E}}{\pi^2\hbar^3}$ (E: relative to bottom band)

- **Conduction band density:** if $E_c - E_f > 3kT$ then $n = N_C\,exp\left(-\frac{E_c - E_f}{kT}\right)$ where $N_C = \frac{2(2\pi m^* kT)^{3/2}}{h^3}$.
  (E_c: energy of conduction band min, N_C [m^{-3}]: effective density of states)

- **Mobility** kinetics: $\mu = \frac{v}{E} = \frac{e\tau}{m^*}$ (τ: mean time between collisions)

- Continuity equation for excess minority electrons: $\frac{\partial n}{\partial t} = -\frac{n}{\tau} + D\,\nabla^2 n + \mu\,\nabla\cdot(n\mathbf{E})$

- **Diffusion and mobility:** $D = \frac{kT}{e}\mu$ (Einstein's relation. μ: mobility, D: diffusion coefficient)

- **Thermal voltage:** $\frac{kT}{e} = \frac{D}{\mu}$.   (thermal energy: kT)

- **Conductivity:** $\sigma = \sum\limits_{carriers} n\mu|q| = e(n\mu_e + p\mu_h)$

Data for Some Crystalline Semiconductors:

Semiconductor		Crystal Struct.	Lattice Const. at 300 K (Å)	Bandgap (eV)		Band	Mobility at 300 K (cm²/V-s)		Effective Mass		$\varepsilon_s/\varepsilon_0$
				300 K	0 K		μ_n	μ_p	m_n^*/m_0	m_p^*/m_0	
C	Carbon (diamond)	D	3.56683	5.47	5.48	I	1,800	1,200	0.2	0.25	5.7
Ge	Germanium	D	5.64613	0.66	0.74	I	3,900	1,900	1.64^l,0.082^t	0.04^{lh},0.28^{hh}	16.0
Si	Silicon	D	5.43102	1.12	1.17	I	1,450	500	0.98^l,0.19^t	0.16^{lh},0.49^{hh}	11.9
IV-IV SiC	Silicon carbide	W	a=3.086,c=15.117	2.996	3.03	I	400	50	0.60	1.00	9.66
III-V AlAs	Aluminum arsenide	Z	5.6605	2.36	2.23	I	180		0.11	0.22	10.1
AlP	Aluminum phosphide	Z	5.4635	2.42	2.51	I	60	450	0.212	0.145	9.8
AlSb	Aluminum antimonide	Z	6.1355	1.58	1.68	I	200	420	0.12	0.98	14.4
BN	Boron nitride	Z	3.6157	6.4		I	200	500	0.26	0.36	7.1
"	"	W	a=2.55,c=4.17	5.8		D			0.24	0.88	6.85
BP	Boron phosphide	Z	4.5383	2.0		I	40	500	0.67	0.042	11
GaAs	Gallium arsenide	Z	5.6533	1.42	1.52	D	8,000	400	0.063	0.076^{lh},0.5^{hh}	12.9
GaN	Gallium nitride	W	a=3.189,c=5.182	3.44	3.50	D	400	10	0.27	0.8	10.4
GaP	Gallium phosphide	Z	5.4512	2.26	2.34	I	110	75	0.82	0.60	11.1
GaSb	Gallium antimonide	Z	6.0959	0.72	0.81	D	5,000	850	0.042	0.40	15.7
InAs	Indium arsenide	Z	6.0584	0.36	0.42	D	33,000	460	0.023	0.40	15.1
InP	Indium phosphide	Z	5.8686	1.35	1.42	D	4,600	150	0.077	0.64	12.6
InSb	Indium antimonide	Z	6.4794	0.17	0.23	D	80,000	1,250	0.0145	0.40	16.8
II-VI CdS	Cadmium sulfide	Z	5.825	2.5		D			0.14	0.51	5.4
"	"	W	a=4.136,c=6.714	2.49		D	350	40	0.20	0.7	9.1
CdSe	Cadmium selenide	Z	6.050	1.70	1.85	D	800		0.13	0.45	10.0
CdTe	Cadmium telluride	Z	6.482	1.56		D	1,050	100			10.2
ZnO	Zinc oxide	R	4.580	3.35	3.42	D	200	180	0.27		9.0
ZnS	Zinc sulfide	Z	5.410	3.66	3.84	D	600		0.39	0.23	8.4
"	"	W	a=3.822,c=6.26	3.78		D	280	800	0.287	0.49	9.6
IV-VI PbS	Lead sulfide	R	5.9362	0.41	0.286	I	600	700	0.25	0.25	17.0
PbTe	Lead telluride	R	6.4620	0.31	0.19	I	6,000	4,000	0.17	0.20	30.0

D = diamond, W = wurtzite, Z = zincblende, R = rock salt (simple cubic). I/D = indirect/direct band gap.

l / t / lh / hh = longitudinal, transverse, light-hole, heavy-hole effective mass.

8.6.4. Optical and Transport Properties from Band Structure

For a **direct** band gap transition (carrier $\mathbf{k}$ constant), energy E is conserved via photon exchange: (e^-: electron, h^+: hole, γ: photon. Alternative notation - $e^{/}$: electron, $h^{\bullet}$: hole)

- **Photon Absorption:** e^- (low E) $+ \gamma \rightarrow e^-$ (high E) or equivalently $\gamma \rightarrow e^- + h^+$
- **Radiative Recombination:** e^- (high E) $\rightarrow e^-$ (low E) $+ \gamma$ or equivalently $e^- + h^+ \rightarrow \gamma$

For an **indirect** band gap transition, momentum $\mathbf{p} = \hbar\mathbf{k}$ is conserved via phonon exchange from thermal lattice vibrations, which significantly lowers the rate (efficiency) of the photon exchange.

Extrinsic semiconductors can be formed by substitutional doping with impurities:

n-type Doping: insertion of e^- **p-type Doping:** insertion of h^+
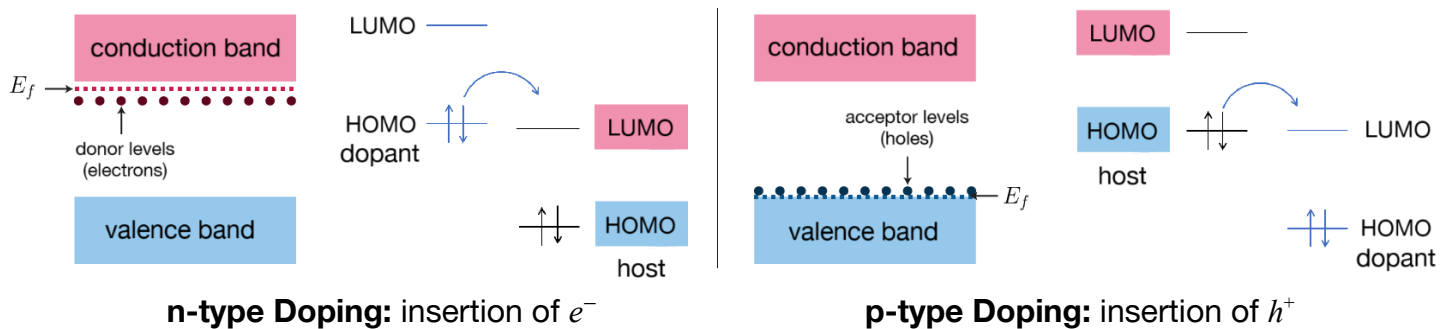
Transparent Extrinsic Semiconductors: needs band gap >3 eV and **shallow dopant levels**
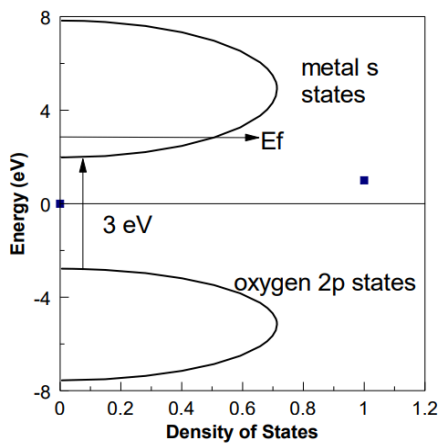
More ionic lattices and smaller lattice constants have **larger band gaps** (s-block oxides, or III-V semiconductors) since molecular orbital splitting is decreased (less covalent).

Left: density of states (DoS) for n-doped metal oxide e.g. In_2O_3 with In^{3+} substituted by Sn^{4+}. E_f rises to the conduction band. The band gap remains >3 eV, so the resulting semiconductor (indium tin oxide, ITO) is transparent. Other transparent oxides include SnO_2, ZnO.

Indirect band gap semiconductors e.g. GaP, can be n-doped to insert localised (small Δx) donor levels below the conduction min. Due to Heisenberg's uncertainty principle, $\Delta\mathbf{k}$ is large so the band gap becomes **'quasi-direct'**, in which light emission does not require a phonon (**more efficient light emission**).

Intrinsic Defects: imperfections in crystalline lattices can degrade transparency

- **Lattice vacancies** forms a **dangling bond** (DB, unpaired / free radical), which falls in the middle of the band gap since there is no MO splitting. This also occurs at surfaces.

- DBs are recombination centres, trapping electrons and holes formed by light excitation (Schottky-Read-Hall model). **Passivation** with gas (e.g. O_2 or H_2) forms oxide or hydride bonds which remove the trap levels.

The radiative recombination of electrons and holes in current-carrying semiconductors is generally known as **electroluminescence**. Electroluminescent materials include ZnS_2:Cu/Ag/Mn, natural diamond with trace boron, InP, GaAs, GaN (used in LEDs), $[Ru(bpy)_3]^{2+}(PF_6^-)_2$, $[Ir(ppy)_3]$ and Tb_2O_3.

Other mechanisms of light emission include:

- **Incandescence:** all solids and liquids emit thermal radiation due to their temperature, with good emitters following the black-body spectrum. At around 798 K (the Draper point), hot objects begin to glow a dull red, moving towards brighter red, orange-yellow, white and blue at the hottest temperatures.

- **Photoluminescence:** excitation by UV photons and relaxation of electrons in atoms.
  - **Fluorescence:** fast relaxation from a singlet state.
  - **Phosphorescence:** slow relaxation from a triplet state after intersystem crossing.

- **Chemiluminescence:** a chemical reaction forms an excited species which then undergoes relaxation. In biological systems, this is known as **bioluminescence**, occuring in e.g. fireflies, anglerfish and the sea pansy (soft coral). In an electrochemical reaction, this is known as **electrochemiluminescence** (ECL), used in an ECL assay: e.g. an antibody linked with the complex $[Ru(bpy)_3]^{2+}$, which undergoes a reaction with an oxidised radical species $(CH_3CH_2CH_2)_3N^{+\bullet}$ to form an excited complex which releases light.

- **Mechanoluminescence:** nanosecond-order radiation emission due to mechanical stress
  - **Sonoluminescence:** microbubbles in liquids rapidly collapse in high-intensity ultrasound, releasing light. The mechanism of light emission is not well understood.
  - **Triboluminescence:** triboelectric charging at sliding interfaces generates strong local electric fields that cause breakdowns at the microscopic level, releasing radiation. This can also occur during fast fracture (fractoluminescence).
  - **Crystalloluminescence:** emission of light on rapid crystallisation of some salts.

- **Radioluminescence:** light emission on absorption of ionising radiation (alpha/beta/gamma rays), usually using a phosphor material (scintillation). This also includes Cherenkov radiation (braking radiation of relativistic electrons in a dielectric).

8.6.5. Heterojunctions (p-n Junctions)

A p-n junction is formed between the interfaces of oppositely-doped semiconductors.

The Fermi level (electrochemical potential: indicates direction of electron flow) jumps at the interface of two oppositely doped semiconductors because the carrier levels are different. For a good heterojunction, dopants should insert localised energy levels inside or just below/above the host conduction/valence band.

Diode operation: applied electric field (p.d.) reroutes n-type electrons around an external circuit.
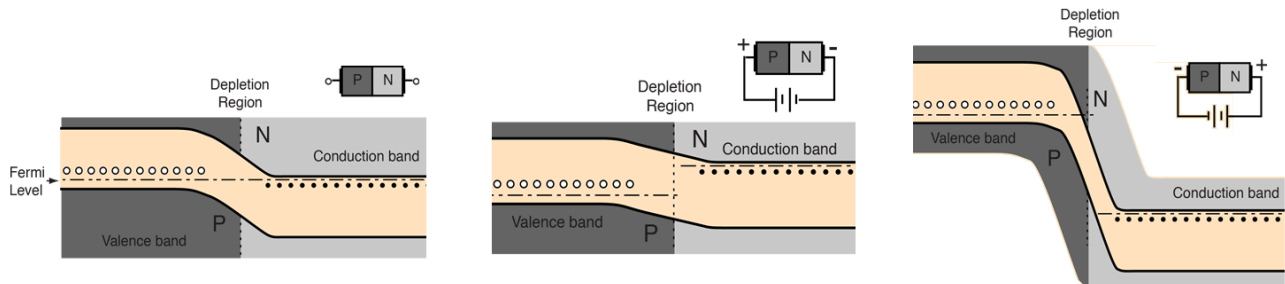
Equilibrium: depleting
Fermi level constant across junction

Forward Bias: conducting

Reverse Bias: insulating
Electrons cannot flow

Carrier energy from p-n recombination is released as photons which heat the material unless the system is designed to allow emission (e.g. as a light-emitting diode (LED)).

Photovoltaic operation: excitation of n-type electrons and rerouting around an external circuit

- Silicon solar cell: uses a Si-based pn-junction
- **Perovskite solar cell**: uses an organic halide perovskite ABX_3 e.g. $CH_3NH_3PbI_3$ ($MAPbI_3$) crystal structure between an electron (ETL) and hole (HTL) transport layer (e.g. organic semiconductors, Section 8.6.8). Transparent electrodes are used (e.g. ITO).
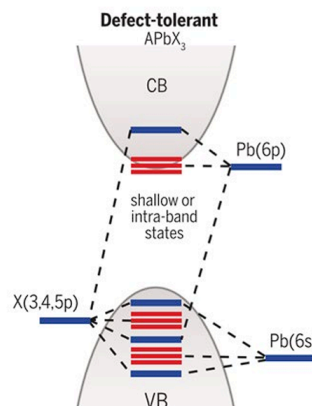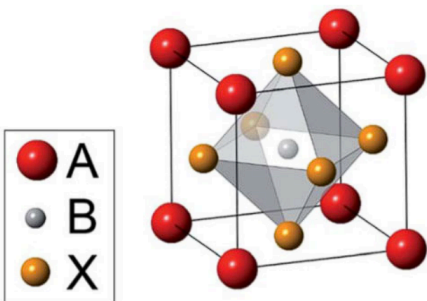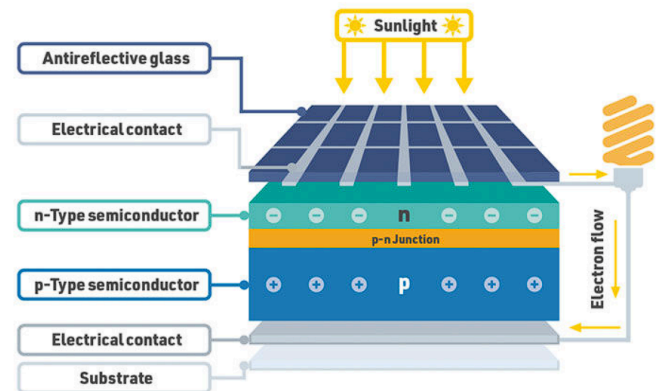
The PbX_6 octahedra primarily sets the band gap (valence band: I ($5p$), conduction band: Pb ($6p$).)

Differently sized A-sites (e.g. MA, FA) allow for tuning of lattice constant and band gap.

Perovskites are defect tolerant as the defect energy levels are shallow.

239

8.6.6. Amorphous Semiconductors

In non-crystalline semiconductors, the concept of $\mathbf{k}$ and direct/indirect band gaps are invalid as there is no symmetry element/unit cell. The band structure remains.

Amorphous silicon (a-Si): has no long-range order, but all atoms remain sp^3 hybridised (approximately tetrahedral) and bonded to 4 other atoms. There are a large number of dangling bonds, which produce a **continuous band structure**:
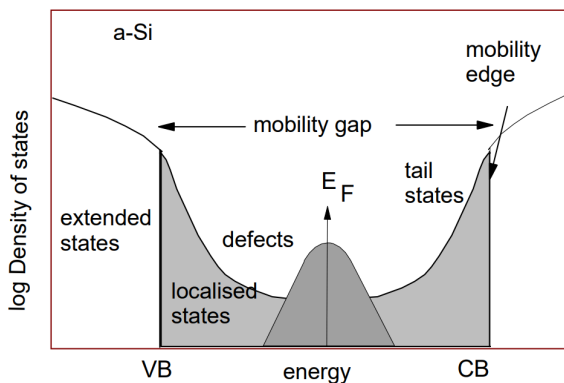
Defects produce a band in the middle. Bond distortion 'smears' the bands into **localised states**. Neither of these states conduct, so the material is still a semiconductor. The **mobility gap is larger** than the crystalline band gap. The efficiency of doping is decreased, as the dopants bond with defects rather than substitution, but is still practical for large area applications (e.g. thin film transistors (TFTs), solar cells).

a-Si:H is made by plasma deposition with SiH_4. It is much cheaper, easier to make at large areas and lower temperatures, than c-Si.

Thin-Film Transistors: improved FETs which can use a-Si:H as the channel

The 'bottom gate, inverted staggered' architecture of an a-Si:H TFT is:
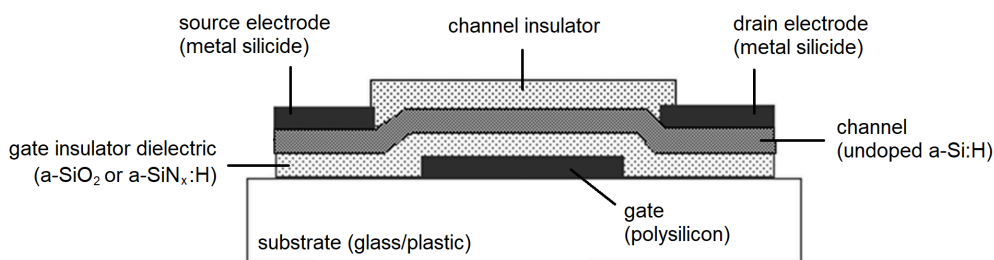
Polysilicon (polycrystalline silicon) has properties intermediate between a-Si and c-Si. The TFT is in enhancement mode, with the $\mathbf{E}$-field pulling electrons into the channel to be conducted.

Other Amorphous Semiconductors: a-Si:H has low mobility and is unstable under constant E-field (gate threshold voltage drift). Oxides such as $InZnGaO_4$ (IGZO) have higher mobilities and are more stable.

Glass: amorphous SiO_2, very wide (**insulating**, ~9 eV) band gap. Doping with various substances (e.g. Na for soda glass) can insert trap levels throughout, giving specific colours of glass.

8.6.7. Organic Semiconductors

Organic materials such as polymers and small molecules open up new manufacturing pathways (spin-coating, inkjetting) which can be done at lower temperatures than a-Si:H. They typically have **low screening** (low ε_r).

- **Band gap decreases as 1 / N** (N: chain length) due to splitting of π-π* orbitals in conjugated polymer (electron in a box quantum model). Subject to Peierls instability. There is then a valence (π) band and a conduction (π*) band.

- **Exciton:** short-range electron-hole pair quasiparticles, formed in light. Excitons dominate charge transfer phenomena in organic semiconductors, as their binding energy E_b (can be estimated with dopant hydrogenic model, Section 8.6.2) is large.

  Exciton binding energy = HOMO-LUMO gap − Optical gap (singlet)
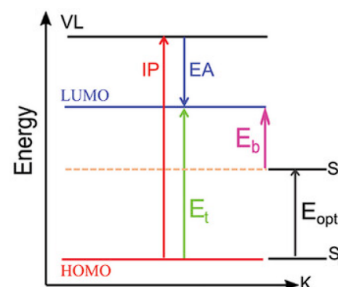
- **Exciton decay** is the mechanism of the photovoltaic effect (light → exciton) and light emission (exciton → light) in organic semiconductors (Section 8.6.8).

- **Doping:** oxidation (with I_2, Br_2, AsF_5) or reduction (with Na, Li) to give radical polycations (hole carriers) or polyanions (electron carriers), both known as **polarons** (another quasiparticle). Doping further increases the conductivity of these polymers.

Examples of conjugated semiconductive polymers:

| polyacetylene (PA, all *trans*) | polyaniline (PANI) | polypyrrole (PPy) | polyfluorene (PF) | poly(3,4-ethylenedi-oxythiophene) polystyrene sulfonate (PEDOT:PSS) |
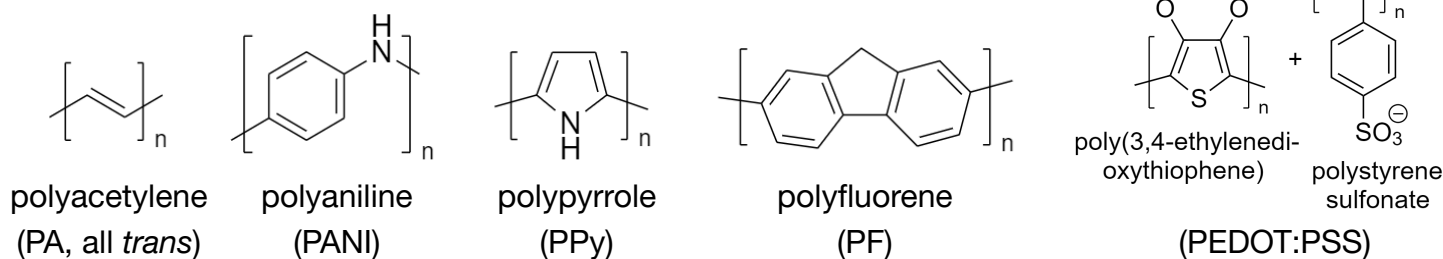
Small-Molecule Organic Semiconductors: fully conjugated monomer molecules with small HOMO-LUMO gaps e.g. anthracene, coronene, copper phthalocyanine (CuPc), tris(2-phenylpyridine)iridium(III) [Ir(ppy)$_3$] (a phosphorescent complex), buckminsterfullerene (C_{60}, 'buckyballs').

The optoelectronic properties of such small-molecule organic semiconductors are dependent on the crystallinity, crystal orientation, and size. Again, the exciton state dominates their optoelectronic behaviour. The complex charge transport mechanisms taking place in such weakly van-der-Waals bonded molecular crystals remains a subject of research and has implications for e.g. studying photosynthesis by chlorophyll molecules (conjugated porphyrin ring).

8.6.8. Organic Electronics

The excitons generated in organic semiconductors can dissociate at a heterojunction (photovoltaic effect: light → current). Excitons can also decay by recombination to produce light (current → light).

Organic Light-Emitting Diodes (OLEDs): exciton recombination at the heterojunction.
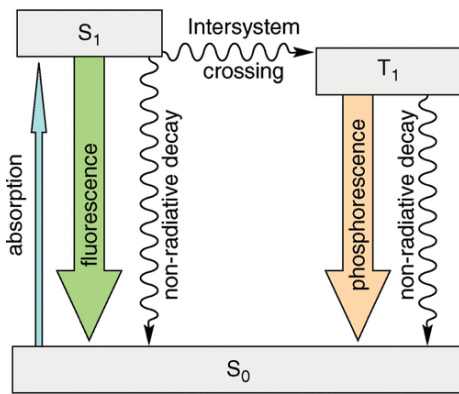
Conducting polymers comprise the emitter layer. Spin-orbit coupling in polymer compounds combines conduction band singlet (S_1) and triplet (T_1) states even more than in pure hydrocarbons, allowing phosphorescence ($T_1 \rightarrow S_0 + h\nu$) to become a permitted transfer by intersystem crossing in addition to fluorescence ($S_1 \rightarrow S_0 + h\nu$). Non-radiative decay emits a phonon without emitting a photon.
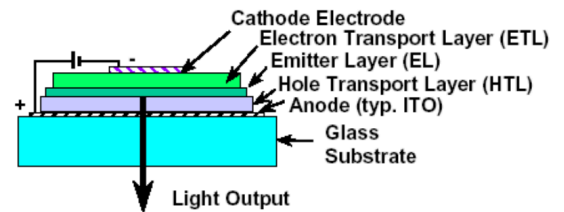
Organic Field-Effect Transistors (OTFTs / OFETs): organic semiconductor channel.
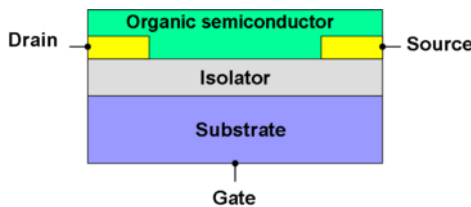
Polymers for p-type OFETs have HOMO energy between 5.0-5.5 eV and LUMO > 3.5 eV. Polymers for n-type OFETs may be fluorinated to reduce HOMO and LUMO. OFETs adopt the TFT (thin-film transistor, Section 8.6.6) architecture (as opposed to e.g. MOSFET, MeSFET).

OLED Displays: uses (O)TFTs to power OLEDs for each pixel (active matrix display architecture)
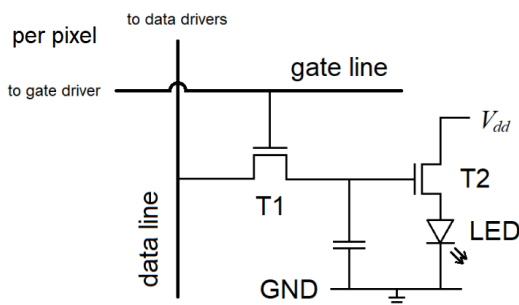
When TFTs are used in OLED displays (two (O)TFTs and one OLED per pixel), mobility translates to frame rate, so there are demands for higher performance.

T1 acts as a switch and is in linear bias.

T2 drives the current through the light modulator (LED) and is in saturation mode (current source depending only on gate voltage).

White light emission can be achieved by either 1) RGB tuned OLEDs, 2) down-conversion from blue LEDs using phosphorescent materials (excitons recombine from multiple triplet states) or 3) colour filters with white organic EML (protects against differential degradation).

8.6.9. Quantum Dots (0D Nanomaterials)

Quantum dots (QDs) are semiconducting nanoparticles. Quantum dot optoelectronic properties are easily tunable by their size D.

Common photoluminescent QDs include CdSe, ZnS, CdTe.

- **Exciton (*e-h*) Bohr radius:** $a_{Bx} = \dfrac{4\pi\varepsilon\hbar^2}{m_0 e^2}\left(\dfrac{1}{m_e^*} + \dfrac{1}{m_h^*}\right) \sim D$

- **Idealised energy levels** (3D cubic well): $E_n = \dfrac{3\hbar^2\pi^2 n^2}{2m_e^* D^2}$ (D: quantum dot diameter)

- **Quantum dot band gap**: $\Delta E_{QD} = \Delta E_{bulk} + \Delta E_{well}(e^-) + \Delta E_{well}(h^+) + \Delta E_{Coulomb}$

  where $\Delta E_{Coulomb} \approx \dfrac{-3.6 \times e^2}{4\pi\varepsilon_0 \varepsilon_r D}$ and confinement energy $\Delta E_{well}(e^-) + \Delta E_{well}(h^+)$ scales with D^{-2}.

- **QD Emission Energy:** $\Delta E_{QD} \approx \Delta E_{bulk} + \dfrac{2\hbar^2\pi^2}{D^2}\left(\dfrac{1}{m_e^*} + \dfrac{1}{m_h^*}\right)$ (Brus equation)

AMQLED Displays (Active Matrix QDs Light Emitting Diode)
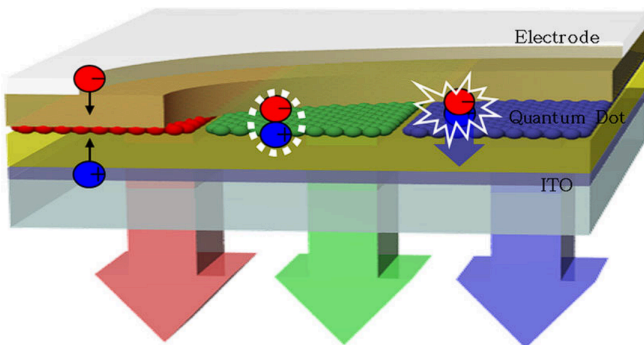
An electroluminescent QD nanoparticle film is used as the emitter layer (EML). QDs are superior to organic luminescent materials due to their inherent luminescent properties, including narrow spectral emission bandwidths, high photoluminescence quantum efficiency, good photostability and controllable bandgap.

QDs naturally produce monochromatic light, so they are more efficient than white light sources when colour filtered and allow more saturated colours.

QDs often exhibit localised surface plasmon resonance, altering their reflectivity.

8.6.10. Nanotubes and Nanoribbons (1D Nanomaterials)

Nanotubes are 1D nanostructures, geometrically equivalent to a rolled-up cylindrical monolayer of conducting or semiconducting thin-film material.

Carbon Nanotubes (CNTs): cylindrical sp^2 carbons.

The orientation of a nanotube has two degrees of freedom (size and pitch). These are enumerated with a chiral vector (n, m), for positive integers $m \leq n$ as defined in terms of a unit cell of graphene as shown.
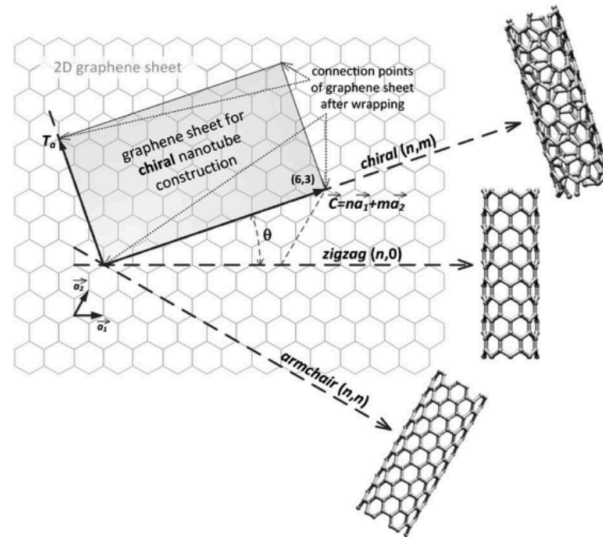
Chiral vector: $\mathbf{c} = n\mathbf{a_1} + m\mathbf{a_2}$ $(\mathbf{a_1} = \frac{a}{2}(\sqrt{3}\mathbf{i} + \mathbf{j})$ and $\mathbf{a_2} = \frac{a}{2}(\sqrt{3}\mathbf{i} - \mathbf{j})$, $a = 0.2461$ nm$)$

Tube diameter: $d = c/\pi = \frac{a\sqrt{n^2 + m^2 + mn}}{\pi}$ $(c = |\mathbf{c}|$: circumference of nanotube$)$

Chiral angle: $\tan\theta = \frac{\sqrt{3}m}{2n + m}$ $(0 \leq \theta \leq 30°)$

Translational vector: $\mathbf{T_a} = \frac{2m + n}{d_R}\mathbf{a_1} - \frac{2n + m}{d_R}\mathbf{a_2}$ $(d_R = \gcf\{2m + n, 2n + m\}$, greatest common factor$)$

Length of unit cell: $|\mathbf{T_a}| = \frac{\sqrt{3}c}{d_R}$ (surface area of unit cell: $A = |\mathbf{c}||\mathbf{T_a}| = \frac{\sqrt{3}a^2(n^2 + m^2 + mn)}{d_R})$

Number of atoms per unit cell: $N = \frac{4(n^2 + m^2 + mn)}{d_R}$ (number of hexagons per unit cell is $\frac{N}{2}$)

Types of nanotube based on geometry:

- **Metallic CNTs:** when $n = m$ (armchair). The 0 eV band gap is at the *K* point.
- **Semi-metallic CNTs:** when $n - m \equiv 0$ (mod 3). Band gap is on the order of $k_B T$ (< 0.1 eV).
- **Semiconductor CNTs:** when $n - m \not\equiv 0$ (mod 3). Larger band gap, inversely proportional to the nanotube diameter: E [eV] $\approx 0.85/d$ [nm]. (1, 0) and (2, 0) are insulators.

When grown, carbon nanotubes can naturally form multi-walled structures, consisting of concentric CNTs. These are typically metallic due to statistical probability of at least one layer being metallic. Other materials can also form nanotubes such as h-BN and MoS_2. Heterostructures (analogous to multi-layer materials) can also be made from these materials.

Graphene Nanoribbons: narrow graphene; open nanotube. Semiconductive with **finite band gap**.

8.6.11. Thin-Film Materials (2D Nanomaterials)

Graphene: a 2D monolayer. Comprises the layers of graphite (stable carbon allotrope)

Graphene is a single layer hexagonal lattice of carbon, and is a fully conjugated system. It is a **zero band gap** semiconductor (0 eV, semi-metal) with **linear dispersion** around the K point giving **very high mobility.**

(a) Bravais lattice   (b) Reciprocal lattice

Doping of graphene involves charge transfer, filling up or depleting the π-π^* bands.
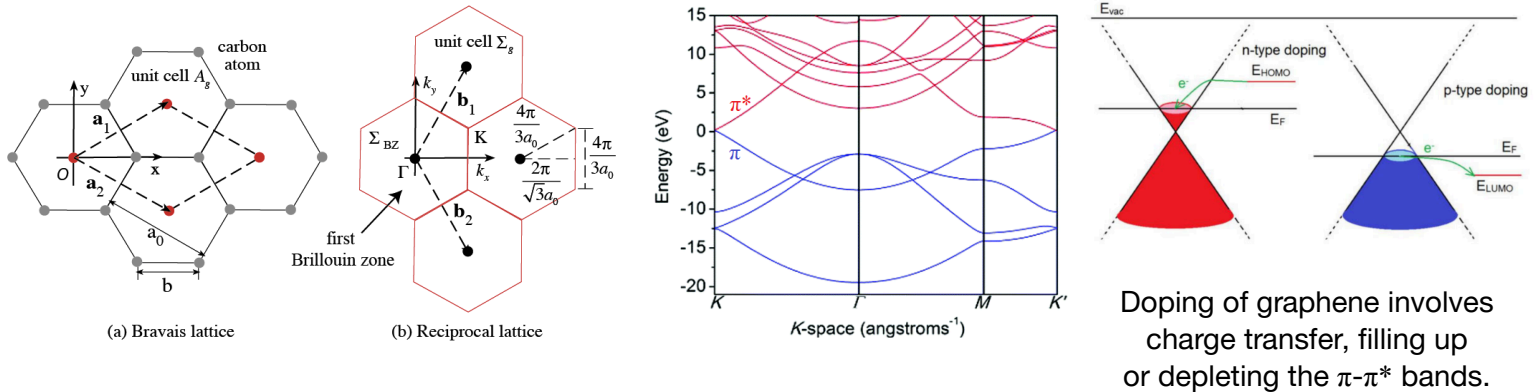
Graphene can be stacked into bilayers. The most stable conformation is the Bernal arrangement (AB: half of the sites are above/below hexagon centres). The layers can also be positioned at a small angle of deviation, forming a Moiré superlattice. These structures have **tunable bandgaps** (twistronics).

Hexagonal Boron Nitride (h-BN): isomorphic to graphene with alternating B and N

Due to the partial ionic character (III-V), h-BN has a **large band gap** (~6 eV, insulator). Due to its exceptional environmental, thermal, and chemical stability, atom thin h-BN is emerging as dielectric, support and barrier layer for nanoelectronics, and also as host material for quantum emitters. 3D amorphous oxides that work well in silicon technology have ill-defined interfaces with 2D materials and numerous defects. Currently, crystalline dielectrics like h-BN layers show most promise for 2D nanoelectronics despite having only moderate dielectric constants ($\varepsilon \approx 3$). Specialised integrated processes are required for manufacture of these integrated heterogeneous monolayers.

Amorphous Monolayers: can be used to test for tolerance of defects in monolayers

Monolayer sp^2-bonded amorphous carbon films have been demonstrated, highlighting the possibility of stable amorphous material in the 2D monolayer limit. The amorphous structure consists of small crystallites embedded in a continuous random network, analogous to spherulites in semi-crystalline polymers (Section 16.5.3). Similar to 3D materials, **localised states** emerge. 2D silica glass has also been demonstrated. Amorphous BN does not form a planar layer, instead forming a 3D thin structure.

Phosphorene (Black Phosphorus): hexagonal structure like graphene, but not in-plane

Forms a puckered structure (fused chair conformations) and is a **direct bandgap** semiconductor (2.3 eV). Band gap decreases with more layers with **high mobility**.

245

Transition Metal Dichalcogenides (TMDs, MS$_2$):
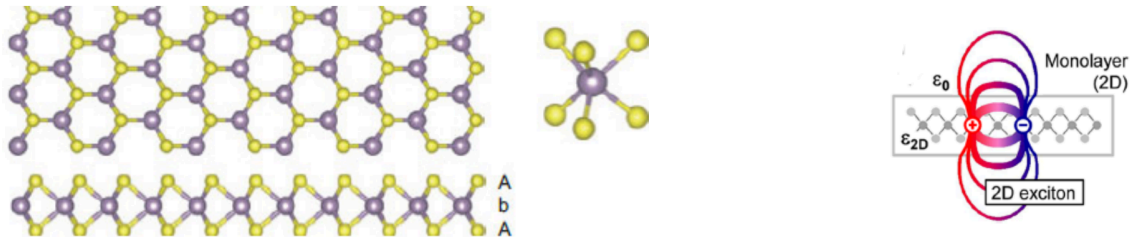
MS$_2$ forms three-atom-thick layers with D_{3h} symmetry (trigonal prismatic).

Weak dielectric screening enhances the *e-h* Coulomb interaction, making excitons more strongly bound.

Monolayer MS$_2$ is a **direct bandgap** semiconductor (MoS$_2$: 1.9 eV) at the *K* point, while multiple layers gives an indirect and smaller bandgap from valence $\Gamma \rightarrow$ conduction near *K*. The strongly-bound Frenkel excitons dominate optical and charge-transport properties. Others include WS$_2$, WSe$_2$, MoTe$_2$.

MXenes: transition metal carbide, nitrides and borides of the form M$_{n+1}$X$_n$, with terminal groups.

MXenes are multi-layer (ML) or few-layer (FL) 2D materials. Monolayers are conductors while FL-MXenes are small band gap semiconductors. Intercalation is possible in between the layers, and have been used to replace graphite as electrodes in Li-ion batteries.

Band gaps of other layered materials:
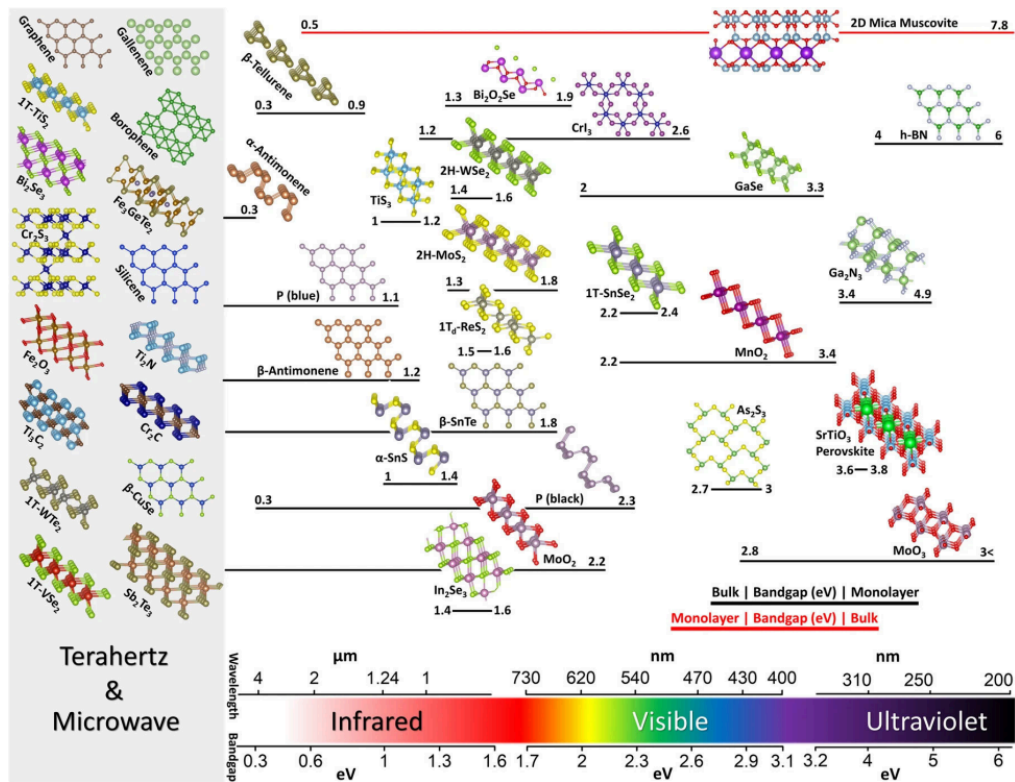
8.6.12. Band Structure Engineering

Interfaces between semiconductors allow for tuning of band gaps. This can be very useful to guide electrons or holes into the desired layers, either for recombination, or to separate them.

- **Electrons sink down** the conduction band surface (like water in a landscape).
- **Holes rise up** the valence band surface (like bubbles in water).
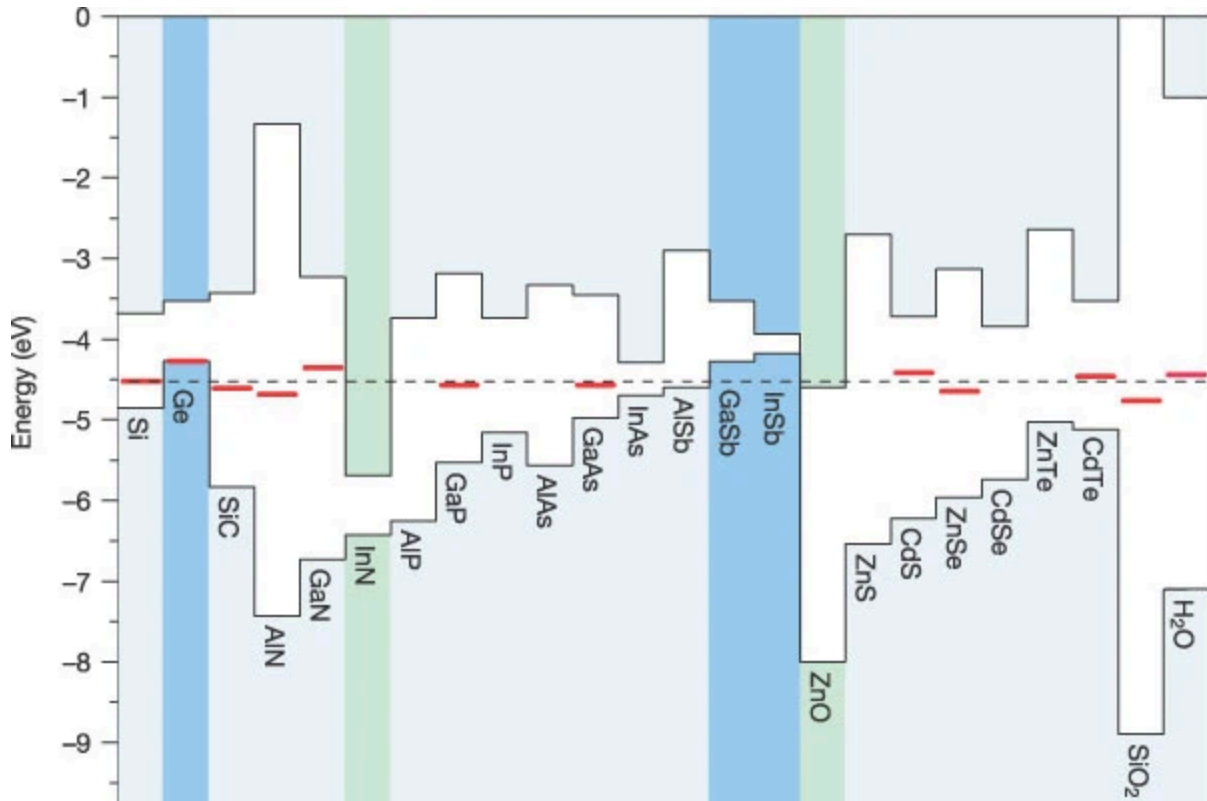
Band edge landscape for various semiconductors
red: hydrogen levels, green: H acts only as donor, blue: H acts only as acceptor
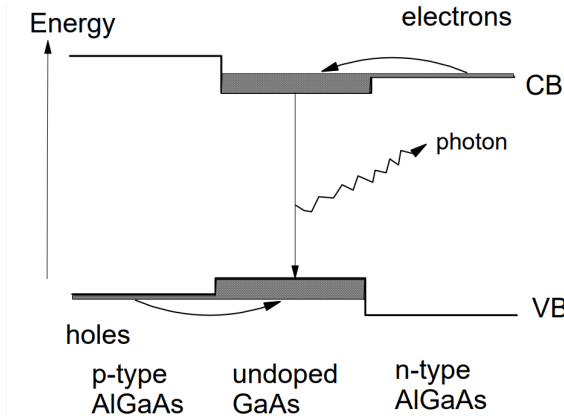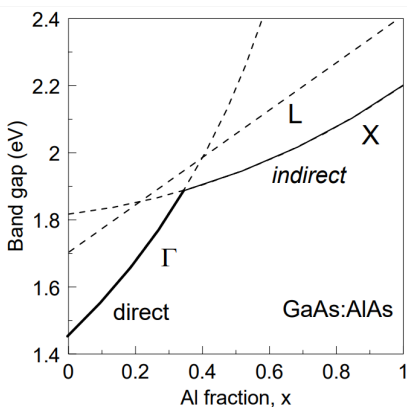
Transfer doping is used to exploit this flow of electrons and holes, e.g. in the GaAs diode laser.

8.6.12. Very Large Scale Integration (VLSI) Semiconductor Technologies

Oxides such as SiO_2 and Al_2O_3 are **defect tolerant**, remaining insulating (~9 eV band gap) even when doped or impure. Conduction occurs only at high electric fields. Impurities in metal oxides create trap levels where carriers can more easily enter the conduction band.

Non-breakdown (reversible) conduction mechanisms in defect-dense metal oxides:

- **Poole-Frenkel conduction:** thermal excitation over the potential barrier at a defect.
- **Quantum tunnelling:** probabilistic bypassing through the potential barrier.
- **Hot carrier injection:** acceleration of carrier by applied electric field over the barrier.

Non-volatile flash memory (programmable ROM, a type of EEPROM) consists of FETs with an additional floating gate and tunneling oxide in between the channel and gate oxide (to which the control gate is attached). In a high field, electrons are drawn into the floating gate, which shifts the gate threshold voltage to more positive values, so the charge can be stored for as long as needed (up to ~10 years).

- Use of **high K (high dielectric constant) oxides** (e.g. ZrO_2, HfO_2, $ZrSiO_4$) allows for scaling of FETs to **prevent tunneling through nanometre-scale gates** (thicker oxide, same capacitance per unit area). These oxides can be manufactured using atomic layer deposition (ALD), where localised surface chemical reactions with adsorbed reagents occur (e.g. $HfCl_4 + 2\,H_2O \rightarrow HfO_2 + 4\,HCl$).

- **High-speed FETs** require inter-layer dielectrics with **low K materials**, such as fluorinated SiO_2 or organo-silicon polymers. In high-power-density chips, high thermal conductivity is also required to dissipate heat quickly, with covalent organic frameworks and amorphous BN (Section 8.6.8) as suitable materials.

- **Strained Si or Ge**, in which the mechanical stress field **splits the degenerate (symmetric) conduction band valleys** (analogous to the Jahn-Teller effect, Section 15.5.15) to **reduce scattering**, can be used as a **high-mobility** channel material.

- III-V semiconductors (based on e.g. InSb, $InGaAs_2$) have also been used in complex stacked architectures: in III-V semiconductors, Si can act as either p or n type dopant depending on whether it substitutes the group III or V atom (amphoteric dopant).

- In **ultra-short channel FETs** (< 5 nm), drain-induced barrier lowering (DIBL) means that leakage becomes a significant problem, requiring semiconducting TMDs (Section 8.6.11) e.g. MoS_2 for the channel.

8.6.13. Linear Magnetic Materials (Diamagnetism and Paramagnetism)

Linear magnetic materials possess reversible spin alignment, magnetising in the presence of an externally applied magnetic field, and demagnetising when the field is removed.

- **Magnetic constitutive relation:** $\mathbf{B} = \mu_0(\mathbf{H} + \mathbf{M})$.
  ($\mathbf{B}$ [T]: magnetic flux density, $\mathbf{H}$: magnetic field intensity [A m^{-1}], $\mathbf{M}$ [A m^{-1}]: magnetisation, μ_0 $= 4\pi \times 10^{-7}$ N A^{-2}: vacuum permeability.)

- Outside of a magnetic material: $\mathbf{M} = 0$ and $\mathbf{B} = \mu_0 \mathbf{H}$ (non-magnetic: $\chi_m = 0$)

- **Inside a linear magnetic material:** $\mathbf{M} = \chi_v \mathbf{H}$ and $\mathbf{B} = \mu \mathbf{H}$.
  ($\chi_v = \mu_r - 1$: volume magnetic susceptibility, $\mu = \mu_0 \mu_r$: permeability)

- **Mass and molar magnetic susceptibility:** mass: $\chi_\rho = \chi_v / \rho$, molar: $\chi_m = M_r \chi_\rho$

- **Bulk saturation magnetisation, $\mathbf{M}_{sat}$** [A m^{-1}] $= \dfrac{total\ dipole\ moment}{V} = \dfrac{n_{atoms/unit\ cell}}{V_{unit\ cell}} \times \boldsymbol{\mu} = \dfrac{\rho N_A}{M_r} \boldsymbol{\mu}$

- **Magnetic moment µ** (per atom) is the sum of spin-only (intrinsic, unpaired electrons) and angular momentum (unbalanced p / d / f orbitals) contributions (Section 15.5.10).

Magnetic Susceptibility of Weakly Magnetic Materials (diamagnetic or weakly paramagnetic):

- **Diamagnetic** materials produce weakly **repulsive** magnetisations ($-1 \leq \chi_v < 0$).
- **Paramagnetic** materials produce **attractive** magnetisations ($\chi_m > 0$) (Section 13.1.2).

Material	χ_v [-]	Material	χ_v [-]
mercury	-2.84 × 10^{-5}	air	+2.6 × 10^{-7}
silver	-2.38 × 10^{-5}	oxygen	+1.908 × 10^{-6}
lead	-1.7 × 10^{-5}	aluminium	+2.11 × 10^{-5}
copper	-9.63 × 10^{-6}	neodymium	+0.00336
hydrogen	-2.23 × 10^{-9}	terbium	+0.112
fused silica glass	-1.13 × 10^{-5}	titanium	+1.81 × 10^{-4}
graphite (parallel)	-6.14 × 10^{-4}	uranium	+4.11 × 10^{-4}
graphite (perpendicular)	-1.4 × 10^{-5}	BMIM-FeCl$_4$	+0.21
diamond	-2.2 × 10^{-5}		
water	-9.04 × 10^{-6}		
polyvinyl chloride	-1.07 × 10^{-5}		

Iron, cobalt and nickel are nonlinear ferromagnets with initial $\chi_v \sim 10^3$ - 10^5.

8.6.14. Nonlinear Magnetic Materials (Ferromagnetism)

Ferromagnetism occurs when a paramagnetic metal experiences quantum exchange interactions between neighbouring spins (which depends on crystal structure). Elevated temperatures can impede this alignment but below the Curie temperature T_c, the material remains ferromagnetic. The ferromagnetic elements at room temperature are BCC iron, FCC nickel, HCP cobalt and body-centred tetragonal ruthenium. Austenitic steels (contain FCC γ-Fe) are not ferromagnetic.

Neutron diffraction shows increased neutron scattering in ferromagnetic materials near the Curie point, as magnetic domains have larger fluctuations. Above T_c, the domains are fully randomised and the materials are paramagnetic with $\chi_m = \frac{C}{T - T_c}$ (Curie-Weiss law).

(C: Curie constant, theoretically given by $C = \frac{\mu_0 \, (N/V) \, \mu^2}{k_B}$ (N/V: dipole number density).)

Spin Exchange Interactions in Spontaneously Aligned Dipoles

- **Soft Ferromagnetic:** spontaneous magnetic dipoles in domains (nonlinear B-H curve, no hysteresis).
- **Hard Ferromagnetic:** irreversible once magnetised into a single domain (hysteresis) (Section 8.6.15).
- **Antiferromagnetic:** all adjacent dipoles cancel, resulting in no net magnetisation
- **Ferrimagnetic:** antiferromagnetism with two opposing magnitudes (net ferromagnetism)

Field lines for a permanent bar ferromagnet (N: North-seeking pole, S: South-seeking pole)

| **B** field (outside: N → S) | **H** field (N → S) | **M** field (S → N) |
| continuous in space | demagnetising (stray) field | internal magnetisation |
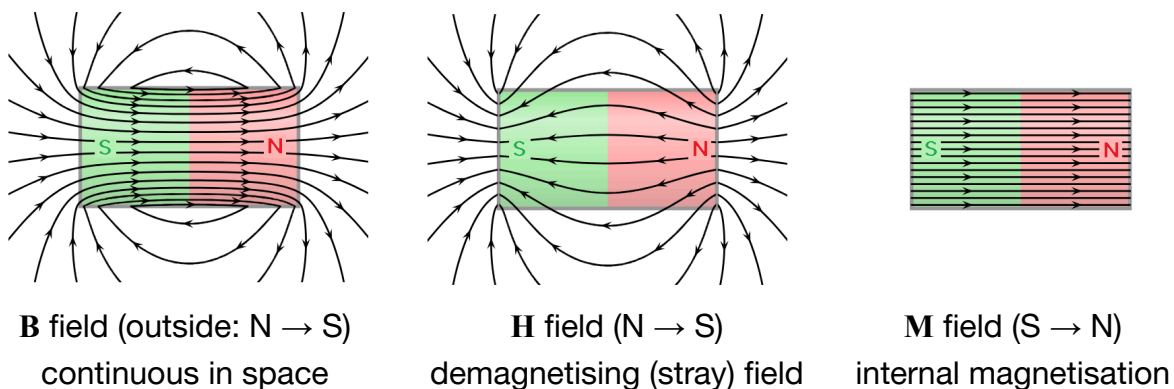
Smelted (solidified from molten) iron forms magnetic 'domains' of locally saturated (fully aligned) magnetisations. The size of the domains are usually smaller than the grains in polycrystalline ferromagnets. When exposed to an external magnetic field for the first time, the domains align, reaching a net large saturation magnetisation M_S.

8.6.15. Hysteresis in Hard Ferromagnets
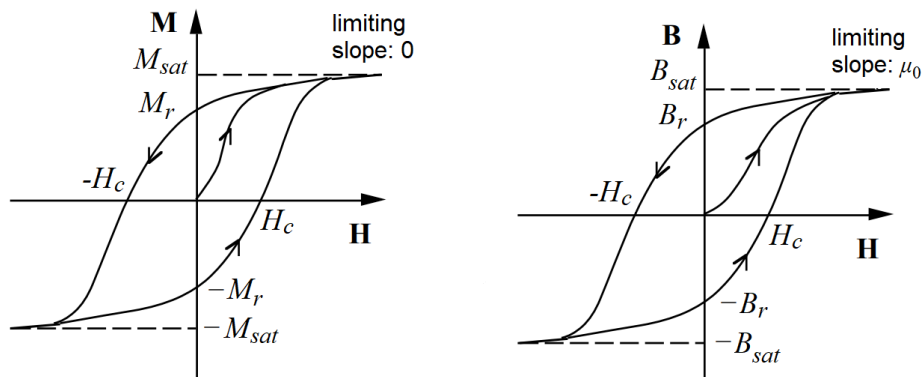
The fields are sometimes shown in CGS units: 1 Gauss = 100 μT and 1 Oersted = $\frac{1000}{4\pi}$ A m^{-1}.
The energy loss per unit volume per cycle is the area of the B-H loop.

Initial Magnetisation

- Spins begin spontaneously aligned within domains. Each domain is randomised.
- As H increases, **domains aligned in the lattice 'easy' direction grow**; others shrink.
- For small H, this domain growth is reversible (no hysteresis).
- Growing domains can be **pinned on defects**, which snap off as H grows (Barkhausen effect).
- When the material is all one domain, further increases in H slowly **rotate the alignment towards the field**, up to its saturation magnetisation M_{sat}.

Demagnetisation

- As H is removed, the alignment relaxes back to the lattice 'easy' direction, retaining a 'remanence' M_r.
- The average **stray (demagnetising) self-field** (at $H = 0$) can be written as $\mathbf{H}_d = -N\,\mathbf{M}$.
  ($0 < N < 1$: shape factor, e.g. flat plate: $N = 1$, infinite parallel cylinder: $N = 0$.)
  Plotting this as a **'load line'** gives the **operating point** (intersection with B-H curve).
- The $(BH)_{max}$ point contains the most magnetic energy **(optimal operating point)**.

  For a linear B-H line, $(BH)_{max} = \mu_0 \left(\frac{M_{sat}}{2}\right)^2$, optimal for $N = \frac{1}{2}$, since $\frac{B}{H} = -\mu_0 \frac{1-N}{N}$.

- If a reversed H is applied, the magnetisation will remain aligned until exceeding the 'coercivity' $H < -H_c$. The process of reverse saturation and relaxation repeats, completing the magnetic cycle. If the operating H_d is close to H_c, the magnet is prone to spontaneous demagnetisation in operation.

Magnetostriction in Hard Ferromagnets: mechanical strain due to domain rotation in applied H

Material	Maximum magnetostrictive strain λ (microstrain ppm, $\times 10^{-6}$)	Saturation field H_c / kA m^{-1}
Terfenol-D ($Tb_xDy_{1-x}Fe_2$)	-2000	160
Alperm (Fe_xAl_{1-x})	-300	16
Metglas 2605SC ($Fe_{81}Si_{3.5}B_{13.5}C_2$)	-20	1
Cobalt ferrite ($CoFe_2O_4$)	-200	0.25

The **magnetoelastic effect** (Villari effect) is the inverse of magnetostriction
(applied mechanical stress → change in magnetic susceptibility → change in M in applied H).

8.6.16. Properties of Soft Ferromagnetic Materials

Soft ferromagnetic materials are highly paramagnetic, with potentially large μ_r. They magnetise reversibly in the presence of an external field (very little hysteresis, small remanence/coercivity).

Soft ferromagnets are manufactured with **large grains** e.g. by annealing, to allow large domains.

B-H **Magnetisation Curves of Group I and Group II Alloys** (Soft Ferromagnetic Materials): grain-oriented silicon steel (GOSS), Fe-4% Si, cast steel, mumetal, radiometal, rhometal.
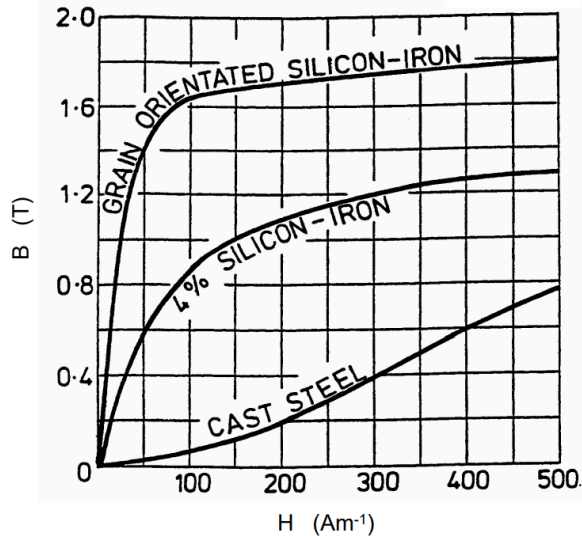
Group I	Group II
Materials used in the electrical power industry	The nickel-iron alloys
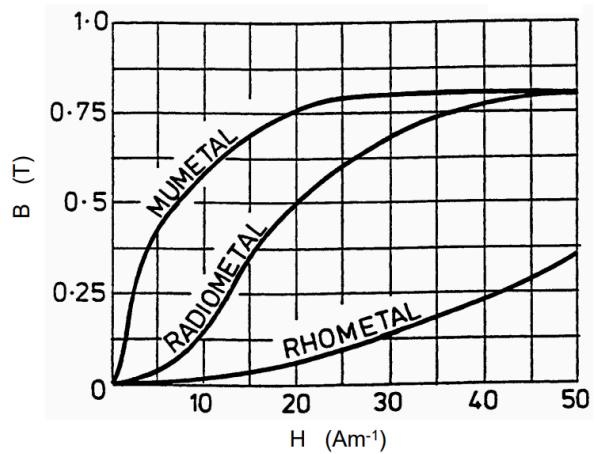
Properties of Silicon Steels (Electrical Steel): Group I, little hysteresis, high electrical resistivity

Fe-Si alloys are used as iron cores in AC power transformers as they have high resistivity (low eddy current loss), large grains (low magnetostriction, low stress sensitivity and transformer hum) and low magnetocrystalline anisotropy (high permeability). The Fe-Si phase diagram (Section 6.7.13) is such that the BCC phase is always stable for >2.5% Si. Thermo-mechanical treatment to form a Goss texture (fixed grain orientation) increases permeability further. Fe-Al is also used (e.g. Sendust, Fe-5.4% Al-9.6% Si), competitive with Mo-doped permalloy.

Properties of Nickel-Iron Alloys (Permalloys): Group II, very high μ_r

wt% Ni	Name	Initial μ_r	Maximum flux density [T]	Resistivity [Ω m]
70-90	Mumetal (Permalloy C)	10000-30000	0.8	6.0×10^{-7}
45-50	Radiometal (Permalloy B)	1800-2400	1.6	5.5×10^{-7}
35-45	Rhometal (Permalloy D)	1500-2000	1.3	9.0×10^{-7}

Mumetal is used in magnetic shielding as it channels the magnetic flux efficiently.

Properties of Ferrites: Group IV spinels with general formula $MO \cdot Fe_2O_3$.

Ferrite Alloy	Initial μ_r	AC frequency range []	Maximum flux density [T]	Resistivity [Ω m]
Mn-Zn	850 - 1500	1 k - 20 M	0.34 - 0.40	0.5 - 1.0
Ni-Zn	20 - 650	1 k - 200 M	0.19 - 0.32	1000
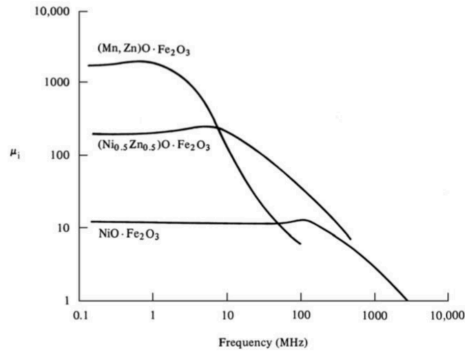
AC operation requires constant permeability over a frequency range: ferrites act as low pass filters. They are useful for switch-mode electronics (SMPS) and EM interference suppression as ferrite bead core inductors.

Gigahertz (>1000 M) applications (sub-millimetre, microwave radar, radio antennas) use specialised silicates and garnets (e.g. $Y_3Fe_5O_{12}$).

8.6.17. Properties of Hard Ferromagnetic Materials (Permanent Magnets)

Hard ferromagnets are manufactured with **small grains**, e.g. by sintering, to form many pinning sites.

Normal Demagnetisation Curves of Group III Alloys (Hard Ferromagnetic Materials, Permanent Magnets): neodymium, samarium-cobalt, ferrites, alcomax (alnico), columax, hynico, 35% Co-Fe.
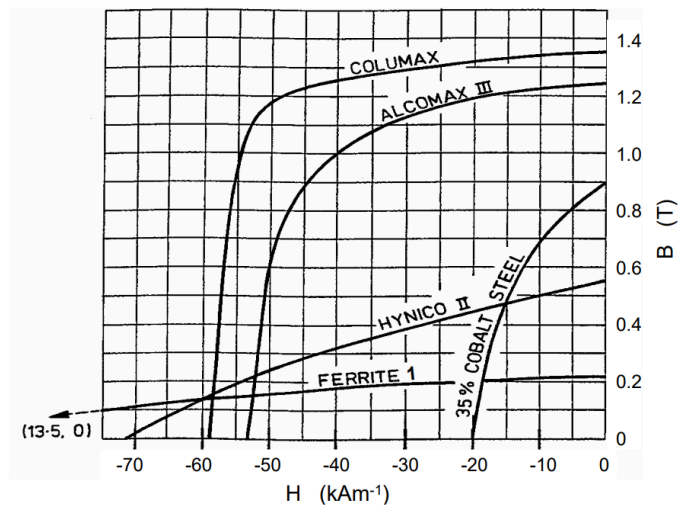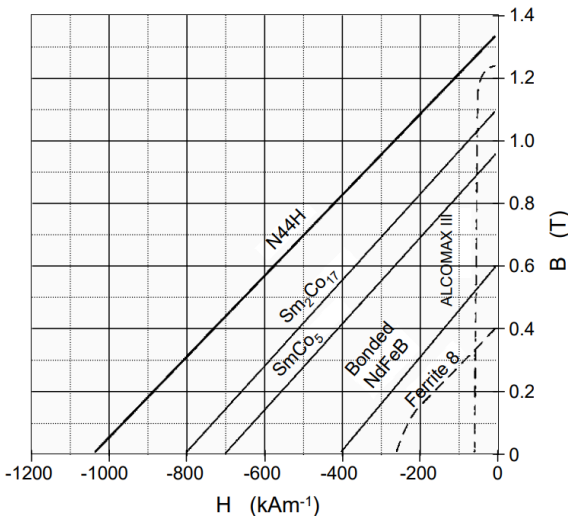
N44H is a high grade of sintered NdFeB. Samarium-cobalt alloy is available in two forms and is machinable:

Sm-Co alloys	B_r, Remanent flux density / T	H_c, Coercive force / A m^{-1}
Sintered metal	0.87	1.280×10^6
Moulded powder in epoxy	0.435	6.40×10^5

Barium ferrites are permanent magnets with $B_r = 0.36$ T and $H_c = 1.1 \times 10^5$ A m^{-1}.

8.6.18. Superconductivity

Superconductors exhibit zero electrical resistivity below a critical temperature T_c, critical current density J_c and applied magnetic field H_c.

- Superconducting order parameter (wavefunction), ψ: complex amplitude of electron density.
- **London penetration depth**, λ: length scale for the **magnetic field**, decaying from the surface inwards
- **Coherence length**, ξ: length scale for **electron density** ψ, rising from zero at the surface into the bulk.
- Ginzburg-Landau parameter, $\kappa = \lambda / \xi$: If $\kappa < 1 / \sqrt{2} \rightarrow$ type I. If $\kappa > 1 / \sqrt{2} \rightarrow$ type II.
- Bohr radius of Cooper pairs: $a_{CP} = \xi / \sqrt{2}$. If $a_{CP} >$ grain boundary gap, then good superconductor.

Type I Superconductivity: superdiamagnetism up to a critical field H_c. Most common in metals.

The quantum mechanical model of type I superconductivity is given by Bardeen-Cooper-Schrieffer theory (BCS theory). Conduction band electrons of opposite spin form **Cooper pairs**, which have lower energy than the Fermi level. The Cooper pairs act as bosons so **cannot be scattered by phonons** and propagate freely in a single degenerate quantum state. The electron spins can be realigned by an external magnetic field (Zeeman energy), giving a maximum field H_c and current capacity $I_c = 2\pi r H_c$ (Silsbee effect, r: radius of superconducting wire).

In the presence of an external magnetic field, a persistent **screening current** is set up at the surface which expels the field from the interior (for $x > \lambda$). Type I superconductors have low critical field and temperature ($T_c \sim 10$ K). Examples include Hg, Al, Pb, TaSi$_2$, SiC:B.

Type II Superconductivity: intermediate phase of flux penetration. Most common in ceramics.

Type II superconductivity currently lacks a complete theoretical model, but a starting point is the Ginzburg-Landau theory. If $\xi \ll \lambda$, then **magnetic fields and electron density can overlap significantly**. For intermediate fields ($H_{c1} < H < H_{c2}$), a **mixed (Shubnikov) state** forms instead, where local points of normal phase material form to channel incoming magnetic flux through flux tubes / **flux vortices** / fluxoids, with persistent screening **supercurrents** surrounding them (like a solenoid). In a current-carrying superconductor, the current will flow through the superconducting region as usual, but may move the flux vortices if they are not pinned strongly enough, which leads to dissipation (flux creep).

- **Magnetic flux per flux tube**: one quanta, $\Phi_0 = h / 2e = 2.07 \times 10^{-15}$ Wb
- Flux tube radius: approximately ξ (length scale over which surrounding current density can decay)
- Number of flux tubes per unit area: proportional to applied field, B / Φ_0
- Upper breakdown field H_{c2}: when the flux tubes become numerous enough to touch each other.
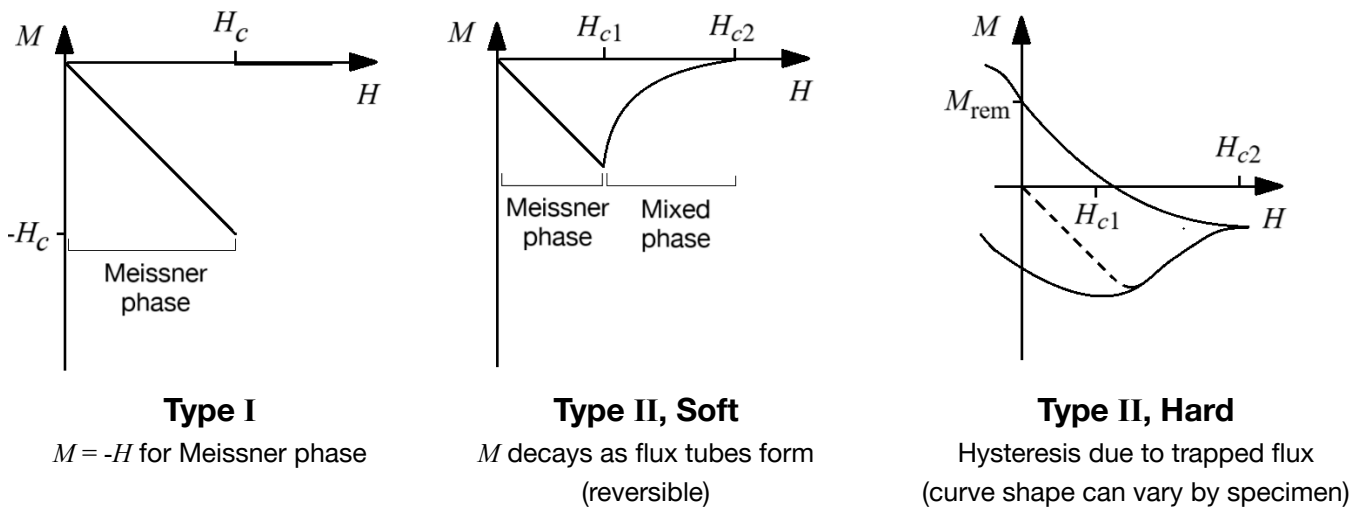
Type II superconductors may have a **hysteresis effect** when an external magnetic field is removed (**'hard'** superconductor). This occurs when the flux tubes are **pinned on hard obstacles** such as precipitate inclusions (other material phases). The flux vortices remain when the external field is removed (like a hard ferromagnet), while for soft superconductors the material returns to its Meissner phase (reversible magnetisation). The hysteresis effect in hard type II superconductors can be described by the **Bean critical state model**.

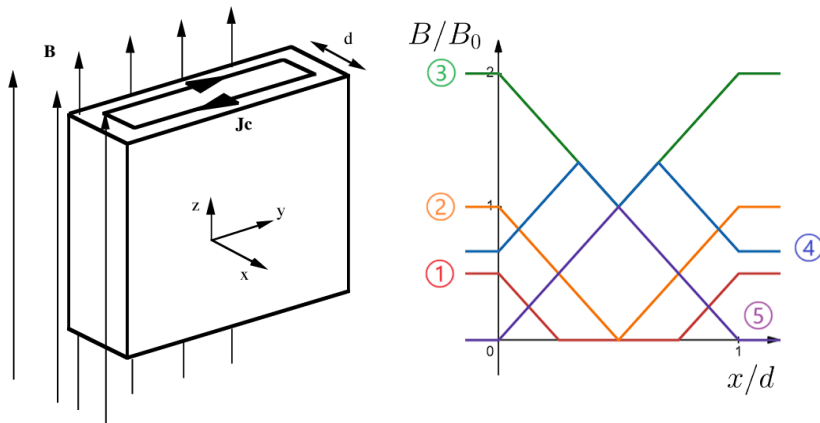## Temperature Dependence of Critical Field and Superconducting State
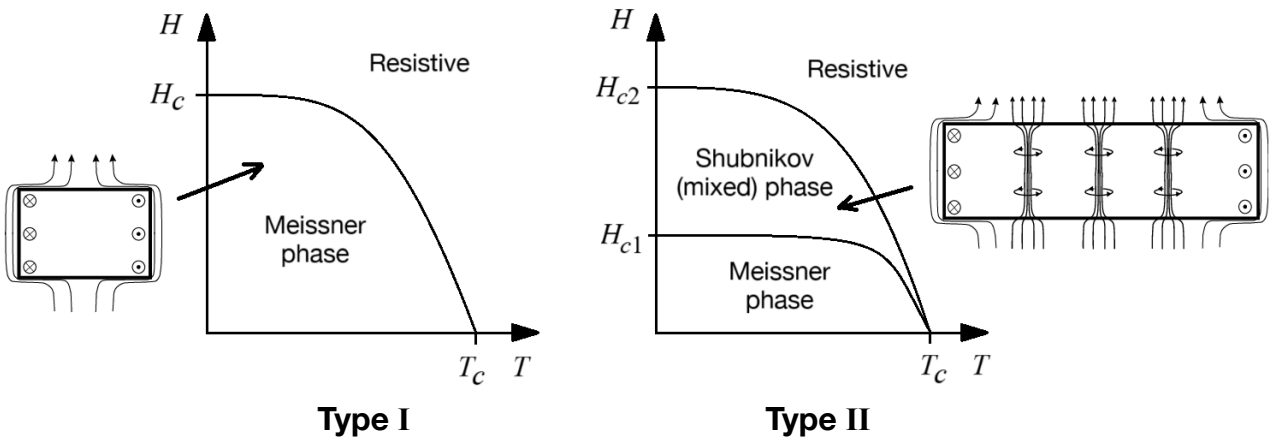
Type I

Type II

Empirical relation for critical field:

$$H_c(T) = H_c(0) \times \left[1 - \left(\frac{T}{T_c} \right)^2 \right]$$

M-H Curves for Superconductors: external **H**-field cycled from 0 to H_{c2} and back

Type I

$M = -H$ for Meissner phase

Type II, Soft

M decays as flux tubes form
(reversible)

Type II, Hard

Hysteresis due to trapped flux
(curve shape can vary by specimen)

Bean's Critical State Model: for a thin slab of hard type II superconducting material

Field slope: $\frac{dB}{dx} = \mu_0 J$ (from 1D Ampere's law)

Assume that J is either $\pm J_c$ or 0.
In the 'critical state', $J = \pm J_c$ for all x.

By varying the external field up to $2B_0$
and back down (①→⑤), a maximum
field of B_0 can be trapped within the material.

8.6.19. Bulk Superconductors and Applications

Typically only **hard type II superconductors** are practically useful, and are used in their **mixed phase**. Transition metal and rare-earth (RE) cuprates are practical ceramic bulk superconductors with high critical temperatures (>90 K). Large-grain YBCO ($YBa_2Cu_3O_{7-x}$) is produced by peritectic cooling, with Y-211 (Y_2BaCuO_5) inclusions acting as the flux pinning centres. Practical lower T_c (~10 K) superconductors include NbTi, with α-Ti precipitates in Nb-βTi acting as pinning centres. Nb_3Sn and Nb_3Al (A15 materials) are also used, as is MgB_2 (39 K). As a rule of thumb, mechanical/material fabrication properties and superconducting performance are a trade-off.
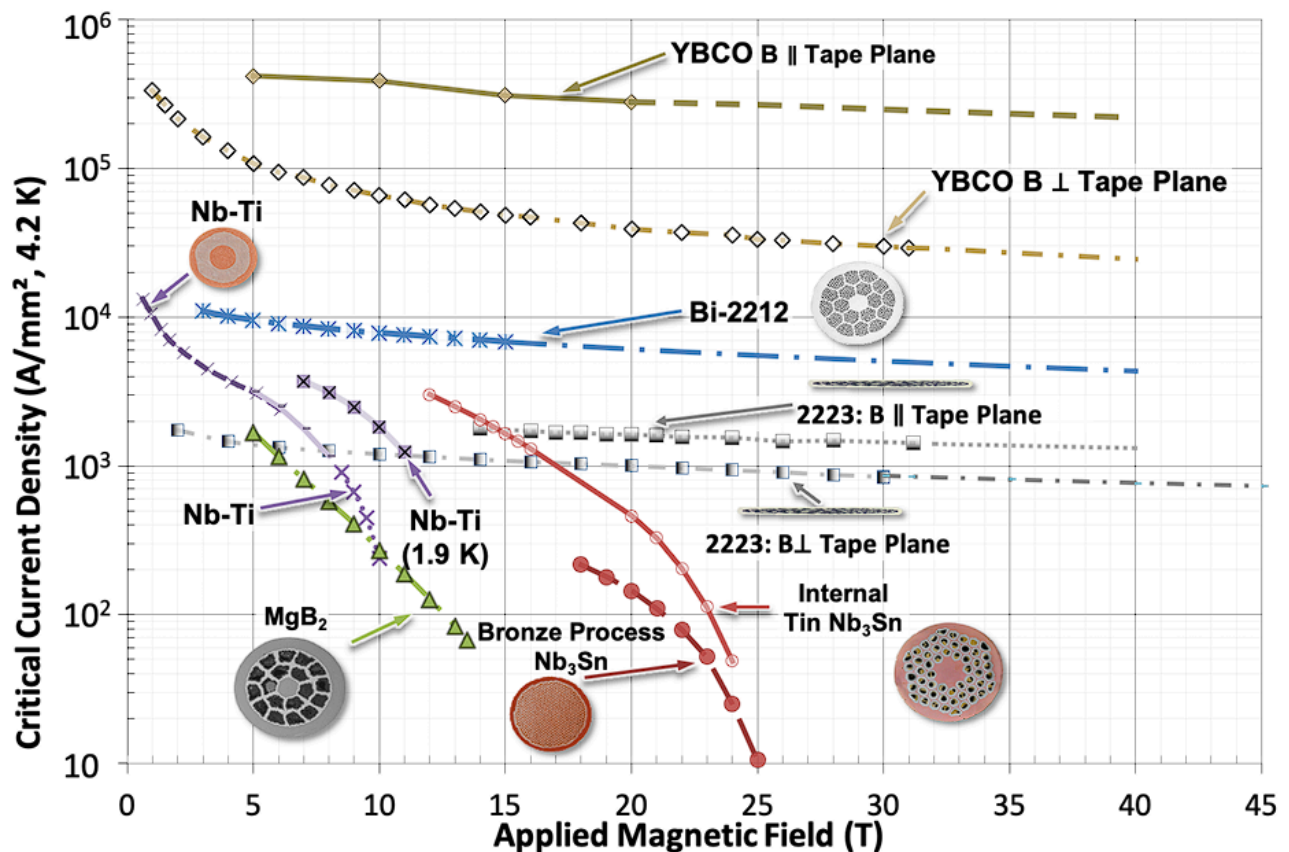
Superconducting wires must be manufactured carefully to maintain **thermal stability** (prevent thermal runaway due to local breakdown with fluctuation in operating conditions). They are made as multifilamentary **bundles of superconductors with copper conductor cores and shell** (shunt layer), for high thermal and electrical conductivity paths to divert excess heat and current generation. For AC applications, these fibres are also twisted to minimise coupling losses. Cryocoolers are used to achieve the low temperatures required. Low temperatures can be maintained by using superinsulating materials (e.g. multi-layer insulation (MLI): Kapton polyimide + aluminised mylar foil).

Applications: current and emerging, but somewhat limited by engineering constraints.

- **Magnetic bearings:** frictionless for high efficiency, used in high-performance flywheels and vibration isolators.
- **Magnetic resonance imaging (MRI):** generates high magnetic fields for imaging the body.
- **Maglev trains:** on-board superconductors and a track with ferromagnets to levitate the train for frictionless propulsion to high speeds.
- **Superconducting quantum interference devices (SQUIDs):** highly sensitive measuring device for tiny magnetic fields, through the use of Josephson junctions (superconductor-insulator-superconductor junctions). Used in magnetoencephalopathy (MEG, brain imaging based on magnetic activity, detecting fields ~100 fT).
- **Nuclear fusion:** strong magnetic fields are used to guide plasma in magnetic confinement fusion (MCF) tokamaks and stellarators.
- **Underwater DC transmission connectors:** AC currents experience impedance in superconductors, so is more suitable for DC submarine cables (no reactive dissipation).

Data for Superconductors

Critical current density is very variable:

- NbSn will carry 109 A/m^2 in a field of 5 T at 4.2 K in wire form.
- YBaCuO will carry 1010 A/m^2 in zero magnetic field at 77 K in thin film form.

Flux quantum $\dfrac{h}{2e} = 2.07 \times 10^{-15}$ V s. Energy gap $\approx 3500\ T_c$.

	T_c K	B_c or B_{c2} at 0 K tesla (T)
Al	1.2	0.01
Pb	7.2	0.08
Nb	9.2	0.08
NbSn	18.4	24
YBaCuO	93	~ 100
TlBaCaCuO	125	~ 120

8.6.20. Properties of Electrical Conductors and Insulators

Electrically Conductive Materials:

	Resistivity at 20 °C Ω m	Temp. Coeff. of Resistance K^{-1} at 20°C	Temp. Coeff of Expansion K^{-1}	Specific Heat-Capacity J/kg K	Thermal Conducti-vity W/m K	Melting Point °C
Copper	1.72×10^{-8}	39×10^{-4}	25.5×10^{-6}	380	385	1083
Aluminium	2.8×10^{-8}	40×10^{-4}	16.7×10^{-6}	880	200	660
Tungsten	5.5×10^{-8}	45×10^{-4}	4.4×10^{-6}	140	160	3370
Manganin	44.5×10^{-8}	0.1×10^{-4}	18×10^{-6}		26	910
Nichrome	103×10^{-8}	1.5×10^{-4}	17×10^{-6}	450	13	1350
Carbon	4500×10^{-8}	-5×10^{-4}	5.4×10^{-6}	840	1.7	3500
Iron	100×10^{-8}	54×10^{-4}	11.6×10^{-6}	250	67	1537
Stainless steel	72×10^{-8}	-	9×10^{-6}	500	16	1427

Dielectric Materials:

	Relative Permit-tivity	Dielectric Strength MV/m	tanδ at 50Hz	tanδ at 1MHz	tanδ at 1GHz	Resistivity Ω m
Mica	6	200	25×10^{-4}	3×10^{-4}	3×10^{-4}	$10^{11} - 10^{15}$
Glass	5	20	6×10^{-4}	8×10^{-4}	12×10^{-4}	$10^{9} - 10^{12}$
Porcelain	6	30	220×10^{-4}	75×10^{-4}	100×10^{-4}	-
Polystyrene	2.5	20	0.5×10^{-4}	0.7×10^{-4}	3.3×10^{-4}	-
P.T.F.E	2.1	20	5×10^{-4}	2×10^{-4}	2×10^{-4}	$10^{15} - 10^{19}$
Transfr. Oil	2.2	15	4×10^{-4}	5×10^{-4}	30×10^{-4}	-
Alumina	8.5	-	20×10^{-4}	-	-	-
Quartz	3.8	20	10×10^{-4}	-	-	10^{16}
Polythene	2.3	20	2×10^{-4}	-	-	$10^{8} - 10^{14}$
Polycarbonates	3.1	-	50×10^{-4}	-	-	$10^{11} - 10^{14}$

8.6.21. Piezoelectric Materials

Electric properties of crystalline materials are intrinsically linked to their crystal structures. For the 32 point groups, see Section 13.2.9.

Piezoelectric point group: a lattice lacking an inversion symmetry i (exception: cubic group O). There are 20 such point groups.

Piezoelectric materials attain an induced polarisation (lattice dipole) in response to an electric field as the charges are displaced in different directions.

Crystal system	Point groups	Piezoelectric tensor	Surface representation
Cubic	$\begin{matrix}23 & (T)\\ \bar{4}3m & (T_d)\end{matrix}$	$\begin{pmatrix} 0 & 0 & 0 & e_{14} & 0 & 0 \\ 0 & 0 & 0 & 0 & e_{14} & 0 \\ 0 & 0 & 0 & 0 & 0 & e_{14} \end{pmatrix}$	
Hexagonal, Tetragonal	$\begin{matrix}6mm & (C_{6v})\\ 4mm & (C_{4v})\end{matrix}$	$\begin{pmatrix} 0 & 0 & 0 & 0 & e_{15} & 0 \\ 0 & 0 & 0 & e_{15} & 0 & 0 \\ e_{31} & e_{31} & e_{33} & 0 & 0 & 0 \end{pmatrix}$	
Hexagonal, Tetragonal	$\begin{matrix}6 & (C_6)\\ 4 & (C_4)\end{matrix}$	$\begin{pmatrix} 0 & 0 & 0 & e_{14} & e_{15} & 0 \\ 0 & 0 & 0 & e_{15} & -e_{14} & 0 \\ e_{31} & e_{31} & e_{33} & 0 & 0 & 0 \end{pmatrix}$	

Applications of piezoelectricity include microphones (direct) and buzzers / loudspeakers (converse). Piezoelectric materials in the form of structural frames can be used as energy harvesting devices, as vibrations on the frame generate internal stresses which produce current in a complete circuit.

Piezoelectric tensor $\mathbf{d}$ is a rank 3 tensor typically written as a 3 × 6 matrix.

- Electric and mechanical tensors: $\mathbf{D} = \varepsilon_0\mathbf{E} + \mathbf{P}$ (ε: permittivity) and $\mathbf{S} = \mathbf{C}\boldsymbol{\sigma}$ (C: elastic compliance)
- Piezoelectric effect: $\Delta\mathbf{P} = \mathbf{d}\boldsymbol{\sigma}$ (i.e. $\Delta P_i = d_{ij}\,\sigma_j$) (passive) and $\Delta\mathbf{S} = \mathbf{d}^\mathsf{T}\mathbf{E}$ (active)
- **Piezoelectric equations:** $\mathbf{P} = \varepsilon_0\chi_e\mathbf{E} + \mathbf{d}\boldsymbol{\sigma}$ (direct effect) and $\mathbf{S} = \mathbf{C}\boldsymbol{\sigma} + \mathbf{d}^\mathsf{T}\mathbf{E}$ (converse effect)

($\mathbf{P} = [P_1, P_2, P_3]^\mathsf{T}$: polarisation field (bound charge density) [C m^{-2}], $\boldsymbol{\sigma} = [\sigma_1, \sigma_2, \sigma_3, \tau_{23}, \tau_{13}, \tau_{12}]^\mathsf{T}$: stress, $\mathbf{d} = \{d\}_{ij}$: piezoelectric tensor, $\mathbf{S} = [\varepsilon_1, \varepsilon_2, \varepsilon_3, \gamma_{23}, \gamma_{13}, \gamma_{23}]^\mathsf{T}$: strain)

Piezoelectric tensor in another dimension: $d_{ijk}{}^* = M_{il}M_{jm}M_{kn}d_{lmn}$ (**M**: transformation matrix from crystal frame)

Piezoelectric Modes of Operation: constraints reduce complexity of response.

Practical piezoelectric materials are usually made as thin slabs, where the only major electric field/strain is developed through the thickness direction. Using ferroelectrics (Section 8.6.22) allows poling control.

Thickness mode (d_{33})	**Longitudinal mode** (d_{31})	**Shear mode** (d_{15})
$P_3 = d_{33}\sigma_3 \;\rightarrow\; Q = d_{33}F_3$	$P_3 = d_{31}\sigma_1 \;\rightarrow\; Q = \frac{A}{a}d_{31}F_1$	$P_1 = d_{15}\sigma_5 \;\rightarrow\; Q = \frac{A}{a}d_{15}F_5$

(A: electrode area, a: stressed area, Q: charge on electrodes, F: applied force, P: polarisation)
Applying a tensile stress instead of compressive stresses reverses the charge polarity.

8.6.22. Pyroelectric and Ferroelectric Materials

Pyroelectric point group: a piezoelectric point group with an **intrinsic dipole**. There are 10 such groups.

When temperature changes, the lattice becomes more or less disordered, changing the alignment of the dipoles and hence the polarisation changes.

Pyroelectric effect: $\Delta \mathbf{P} = \mathbf{p}\, \Delta T$ (**p**: pyroelectric coefficient. Typically, $\mathbf{p} < 0$).

Measured coefficient: $\mathbf{D} = \mathbf{p_g}\, \Delta T = Q/A$ ($\mathbf{p_g} = \mathbf{p} + \frac{\partial \varepsilon}{\partial T}\mathbf{E}$. **E**: applied field, **D**: measured charge density)

Ferroelectric crystal (electret): a pyroelectric crystal where poling with an applied **E** gives **hysteresis** due to spontaneous formation of **domains** of polarisation.

Common application: Passive Infrared (PIR) motion sensor, detecting changes in IR radiation.

IR-transparent windows
element with matte black coating
element with gold coating
protective can
shield
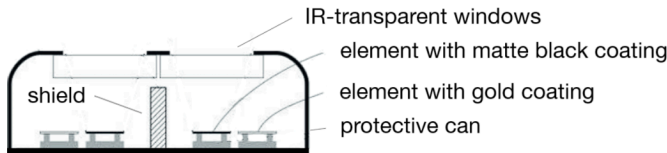
The detector unit is placed behind a multi-segment Fresnel lens which focuses IR radiation into the two detection zones. The **gold-coated** pyroelectric element ensures that the differential signal corrects for overall temperature changes (all IR radiation is reflected away). The two **zones** are positioned to receive IR radiation from different sides of the scene FOV, so that motion from IR-emitting objects (e.g. people, warm-blooded animals) across the scene produces a signal. High input impedance FET-based differential amplifiers are used to contrast the signals. The contact area of the pyroelectric element with the protective can is minimised to increase the thermal time constant of the sensor.
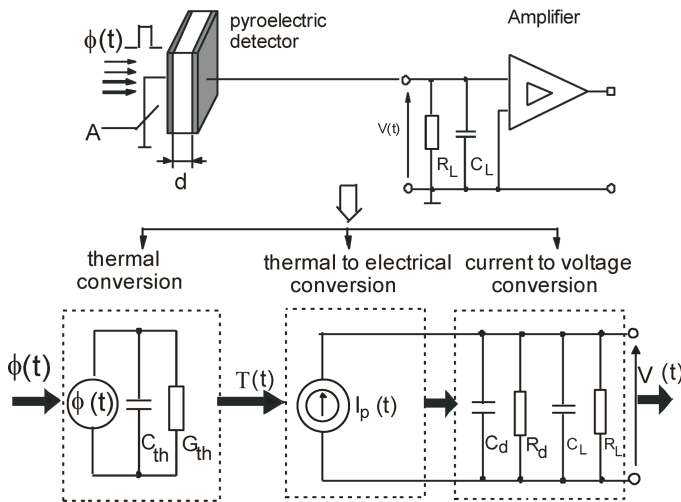
Thermal conversion ($C_{th} = cAd$: thermal capacitance, G_{th}: thermal conductance, c: vol. heat capacity, η: emissivity, $\Phi(t) = \Phi_0\, e^{j\omega t}$: incident thermal power, $\tau_{th} = C_{th} / G_{th}$: thermal time constant)

$$C_{th}\,\frac{dT}{dt} + G_{th}\, T(t) = \eta\, \Phi(t) \iff T(t) = \frac{\eta\, \Phi_0}{G_{th}(1 + j\omega\tau_{th})}\, e^{j\omega t}$$

Thermal to electrical conversion ($i_p(t)$: pyroelectric current)

$$i_p(t) = pA\,\frac{dT}{dt} \iff i_p(t) = \frac{j\omega pA\eta\, \Phi_0}{G_{th}(1 + j\omega\tau_{th})}\, e^{j\omega t}$$

Current to voltage conversion ((R_d, C_d): leakage, (R_L, C_L): amplifier input), $R = R_d \| R_L$, $C = C_d + C_L$, $\tau_e = RC$: electrical time constant, $Y = R^{-1} + j\omega C = i_p / v$: input admittance)

$$C\,\frac{dv}{dt} + \frac{1}{R}v(t) = i_p(t) \iff v(t) = \frac{j\omega pAR\eta\, \Phi_0}{G_{th}(1 + j\omega\tau_{th})(1 + j\omega\tau_e)}\, e^{j\omega t}$$

Current responsivity (current mode): $\left|\dfrac{i_p}{\Phi_0}\right| = \dfrac{pA\eta\omega}{G_{th}\sqrt{1 + \omega^2\tau_{th}^2}} \approx \dfrac{pA\eta}{G_{th}\tau_{th}} = \dfrac{p\eta}{cd}$ for $\omega \gg \tau_{th}^{-1}$.

Voltage responsivity (voltage mode): $\left|\dfrac{v}{\Phi_0}\right| = \dfrac{pAR\eta\omega}{G_{th}\sqrt{(1 + \omega^2\tau_{th}^2)(1 + \omega^2\tau_e^2)}} \approx \dfrac{pAR\eta}{G_{th}\tau_{th}\tau_e\omega} = \dfrac{p\eta}{cdC\omega}$ for $\omega \gg \tau_{th}^{-1}, \tau_e^{-1}$.

Data for Practical Pyroelectric Materials: data at 25 °C. All listed materials are **also** ferroelectric.

Material	p [μC m^{-2} K^{-1}]	Material	p [μC m^{-2} K^{-1}]
PMN-PT (lead magnesium niobate-lead titanate)	-1300	PZT (lead zirconium titanate)	-30
BST (barium strontium titanate)	-7570	triglycine sulfate	-550
LiTaO$_3$ (lithium tantalate)	-230	PVDF (polyvinylidene fluoride)	-27
Ca$_{10}$(PO$_4$)$_6$(OH)$_2$ (hydroxyapatite)	-1 to -400	HfO$_2$ (hafnium oxide)	-46
tourmaline	-6		

Pyroelectrics/ferroelectrics often have a perovskite structure. In ideal cubic perovskite ABO$_3$, the B-site ion is shifted away from its body centre position, forming lower energy covalent bonds with O atoms.

Electrostriction in Hard Ferroelectrics: mechanical strain due to dipole rotation

Electrostrictive strain: $S_{ij} = Q_{ijkl} P_k P_l$ (strain is proportional to P^2, Q: 4th order electrostriction tensor)

Strains generated by electrostriction are typically smaller than by the piezoelectric effect.

Electrostriction is responsible for the 'equivalent series resistance' (ESR) in AC capacitor dielectrics.

Multiferroic Materials: both ferroelectric and ferromagnetic. The mechanism of ferroelectricity is typically different for multiferroics.

8.6.23. Thermoelectric Materials

The thermoelectric effect is the formation of a potential difference between two points on a material at different temperatures. The converse is applying a potential difference to two points on the material, which results in heat transfer in the material.

Seebeck effect electric field: $\mathbf{E} = -\nabla V - S\,\nabla T$ where $\mathbf{J} = \sigma\mathbf{E}$

Full steady-state heat transfer model (combined Joule heating, Seebeck, Peltier/Thompson effects):

$$-\dot{q}_{\text{ext}} = \underbrace{\nabla\cdot(\kappa\nabla T)}_{\text{heat conduction}} + \underbrace{\mathbf{J}\cdot(\sigma^{-1}\mathbf{J})}_{\text{Joule heating}} - \underbrace{T\mathbf{J}\cdot\nabla S}_{\text{Thompson effect}}$$

(q_{ext}': external heat transfer rate per unit volume, κ: thermal conductivity, σ: electrical conductivity, S: Seebeck coefficient)

Seebeck coefficients are typically on the order of $S \sim 100$ μV K^{-1}. These materials can be doped to create spatial variations (∇S).

A thermoelectric generator uses a thermopile design to produce a current from heat.

- Power factor performance index: σS^2 (units: W m^{-1} K^{-2})

- Thermoelectric material performance index: $z = \dfrac{\sigma S^2}{\kappa}$ (figure of merit: zT)

- Compatibility factor: $s = \dfrac{\sqrt{1+zT}-1}{ST}$

- Maximum 1st law efficiency: $\eta_{th} = \dfrac{electrical\ power\ generated}{heat\ absorbed\ at\ hot\ side} \leq \dfrac{T_H - T_C}{T_H}\dfrac{\sqrt{1+z\overline{T}}-1}{\sqrt{1+z\overline{T}}+\frac{T_C}{T_H}}$ (where $\overline{T} = \dfrac{T_C + T_H}{2}$)

- Maximum 2nd law efficiency (exergy): $\eta_{ex} = \dfrac{maximum\ electrical\ power\ generated}{power\ generated\ by\ Carnot\ engine} \leq \dfrac{\sqrt{1+z\overline{T}}-1}{\sqrt{1+z\overline{T}}+\frac{T_C}{T_H}}$

In terms of exergy efficiency, thermoelectric generators are only competitive with heat engines for large T_H - $T_C \sim 1000$ K, in materials having $zT \sim 3$, for which $\eta_{ex} \sim 0.4$ - 0.5. Around room temperatures, $zT \sim 1$. They are suitable only for low power applications at near-ambient conditions.

Thermoelectric Materials and their typical Figure of Merits

Material	zT	at T [K]	Material	zT	at T
Bi_2Te_3	0.8 - 1.0	298	PbTe:Tl	1.0	600
Bi_2Se_3	0.8 - 1.0	298	Sb_2Te_3	1.5	700
SnSe	2.6 (**b** axis)	923	PEDOT:PSS	0.42	298
$Mg_2Si_{0.55-x}Sn_{0.4}Ge_{0.05}Bi_x$	1.4	800			

8.6.24. Birefringence and the Permittivity / Refractive Index Tensors

Tensor constitutive relationship: $\mathbf{D} = \varepsilon\mathbf{E}$ (ε: 3 × 3 permittivity tensor: $\varepsilon = \varepsilon_0 \begin{bmatrix} n_a^2 & 0 & 0 \\ 0 & n_b^2 & 0 \\ 0 & 0 & n_c^2 \end{bmatrix}$.)

The index ellipsoid (optical indicatrix) for a birefringent crystal represents the refractive indices for different orientations of wavefronts. The principal axes are the principal refractive indices n_a, n_b, n_c. (Uniaxial: two different, Biaxial: three different)

When this ellipsoid is cut through its centre by a plane parallel to the wavefront, the resulting intersection (central / diametral section) is an ellipse whose major and minor semiaxes have lengths equal to the two refractive indices for that orientation of the wavefront, and have the directions of the respective polarizations as expressed by the electric displacement vector $\mathbf{D}$.

Index ellipsoid equation: $\dfrac{\cos^2 \xi}{n_a^2} + \dfrac{\cos^2 \eta}{n_b^2} + \dfrac{\cos^2 \zeta}{n_c^2} = \dfrac{1}{n^2}$

Speed: $\nu^2 = a^2 \cos^2 \xi + b^2 \cos^2 \eta + c^2 \cos^2 \zeta$

(cos ξ, cos η and cos ζ are the direction cosines (Section 2.4.1) with the principal axes. The principal refractive indices can also be replaced with the relative permittivities $\sqrt{\varepsilon_{ra}}$, $\sqrt{\varepsilon_{rb}}$, $\sqrt{\varepsilon_{rc}}$.)

Sources of birefringence, other than natural anisotropy:

● Stress-induced birefringence: transparent isotropic (linear photoelastic) materials with stress fields have refractive indices as a function of the stress state.

● Circular birefringence: chiral substances (in the chemical sense) rotate plane-polarised light in opposite directions (circular dichroism).

● Magneto-optic Faraday effect: in the presence of an external static magnetic field directed parallel to the direction of propagation, and in a permeable material medium, plane-polarised light is rotated in one direction.

8.6.25. Principal Refractive Indices for Uniaxial and Biaxial Crystal Systems

Uniaxial crystals, at 590 nm

Material	Crystal system	n_o	n_e	Δn
barium borate BaB_2O_4	trigonal	1.6776	1.5534	-0.1242
beryl $Be_3Al_2(SiO_3)_6$	hexagonal	1.602	1.557	-0.045
calcite $CaCO_3$	trigonal	1.658	1.486	-0.172
ice H_2O (ice I_h)	hexagonal	1.3090	1.3104	+0.0014
lithium niobate $LiNbO_3$	trigonal	2.272	2.187	-0.085
magnesium fluoride MgF_2	tetragonal	1.380	1.385	+0.006
quartz SiO_2	trigonal	1.544	1.553	+0.009
ruby Al_2O_3	trigonal	1.770	1.762	-0.008
rutile TiO_2	tetragonal	2.616	2.903	+0.287
sapphire Al_2O_3	trigonal	1.768	1.760	-0.008
silicon carbide SiC	hexagonal	2.647	2.693	+0.046
tourmaline (complex silicate)	trigonal	1.669	1.638	-0.031
zircon, high $ZrSiO_4$	tetragonal	1.960	2.015	+0.055

Biaxial crystals, at 590 nm

Material	Crystal system	n_α	n_β	n_γ
borax $Na_2(B_4O_5)(OH)_4 . 8H_2O$	mono-clinic	1.447	1.469	1.472
epsom salt $MgSO_4 . 7H_2O$	mono-clinic	1.433	1.455	1.461
mica, biotite $K(Mg,Fe)_3(AlSi_3O_{10})(F,OH)_2$	mono-clinic	1.595	1.640	1.640
mica, muscovite $KAl_2(AlSi_3O_{10})(F,OH)_2$	mono-clinic	1.563	1.596	1.601
olivine $(Mg,Fe)_2SiO_4$	ortho-rhombic	1.640	1.660	1.680
perovskite $CaTiO_3$	ortho-rhombic	2.300	2.340	2.380
topaz $Al_2SiO_4(F,OH)_2$	ortho-rhombic	1.618	1.620	1.627
ulexite $NaCaB_5O_6(OH)_6 . 5H_2O$	triclinic	1.490	1.510	1.520

8.6.26. Metamaterials

Metamaterials are manufactured as periodic arrays of *LC* circuit resonators.

Ray diagram for a typical medium into a negative-index metamaterial (NIM):
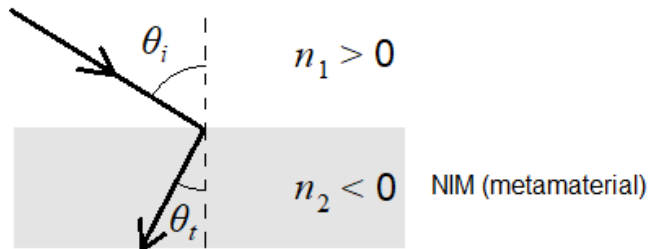
$n_2 < 0$ so $n_1 \sin \theta_i = |n_2| \sin \theta_t$

For the metamaterial, $n_2 = -\sqrt{\varepsilon_r \mu_r}$

where effective $\varepsilon < 0$ and $\mu < 0$.

Frequency of radiation remains constant.

Transmission Line Model of Metamaterials: metamaterials are left-handed ($\mathbf{E} \times \mathbf{H}$ is antiparallel to the Poynting vector) and use opposite-signed reactances in their transmission line models i.e. they have series *capacitances* and shunt *inductances* (reverse to normal materials: see Section 8.5.7).

Metamaterials constructed from arrays of split-ring resonators and conducting wires exhibit negative-index behaviour only for wavelengths of similar order to the cell size. Microwave radiation can be used with cells of ~1 cm. Metamaterial antennas are used for radio waves. Nanomaterials are required for visible wavelengths. Broadband metamaterials are currently under research development.

Reverse Cherenkov Radiation: when charged particles (e.g. electrons) pass through a metamaterial at speed $v > c/|n_2|$, the particle emits radiation directed *behind* it.

8.6.27. Liquid Crystals

A liquid crystal is a fluid of rod shaped molecules in which the molecules align locally along a direction vector field $\mathbf{n}(\mathbf{x})$. Examples of materials forming LCs include cholesteryl benzoate and *N*-(4-methoxybenzylidene)-4-butylaniline. Some biomolecules such as proteins and cell membranes act as LCs.

LCs may be thermotropic, lyotropic or metallotropic.

Distorsion free energy (Frank elastic energy) density for a non-chiral nematic liquid crystal:

$$\mathcal{F}_d = \frac{1}{2}K_1(\nabla \cdot \hat{\mathbf{n}})^2 + \frac{1}{2}K_2(\hat{\mathbf{n}} \cdot \nabla \times \hat{\mathbf{n}})^2 + \frac{1}{2}K_3(\hat{\mathbf{n}} \times \nabla \times \hat{\mathbf{n}})^2$$

($K_{1,2,3}$: Frank constants)

8.6.27. Summary of the Classes of Self-Powered and Functional Materials

Responsive / Functional Materials: conversion between forms of energy

Effect	Applied stimulus	Resulting effect
Piezoelectric	Mechanical stress	Potential difference
	Potential difference	Mechanical strain
Pyroelectric	Temperature gradient (in **time**)	Potential difference
Thermoelectric	Temperature gradient (in **space**)	
Triboelectric	Friction	
Magnetoresistance	Magnetic field	Resistivity change
Photoelectric	Light	Electron radiation
Electro-optic	Electric field	Refractive index change (birefringence)
Magneto-optic	Magnetic field	
Photoelastic	Mechanical stress	
Magnetoelastic	Mechanical stress	Magnetic susceptibility change
Electrostriction	Electric field	Mechanical strain
Magnetostriction	Magnetic field	

Interactions with Electric and Magnetic Fields:

		Characteristics
Electrically conducting materials	Conductor	Carries a **current proportional to the applied potential difference**. Low resistivity, increases with temperature (Joule heating).
	Semiconductor	**Conducts electricity above a threshold voltage**. Resistivity decreases with temperature (thermal excitation of carriers into conduction band).
	Superconductor	Carries constant current when potential difference is applied once, below a critical temperature. **Zero resistivity and zero magnetic permeability** (fully diamagnetic).
Electrically insulating materials	Insulator	Ideally **infinite resistivity, below a breakdown voltage.**
	Linear polar dielectric	Has an **electric polarisation proportional to the applied electric field**. Constant permittivity.
	Paraelectric	Electric polarisation is **nonlinearly** dependent on the applied electric field with **no hysteresis**.
	Ferroelectric	Permanent electric polarisation **with hysteresis** depending on the applied electric field.
Magnetic materials	Diamagnetic	Has a magnetisation **proportional** to the applied magnetic field, in the **same** direction. Constant permeability.
	Paramagnetic	Has a magnetisation **proportional** to the applied magnetic field, in the **opposite** direction. Constant permeability.
	Ferromagnetic	Permanent magnetisation **with hysteresis** depending on the applied magnetic field.

8.7. Semiconductor Devices and Transistor Circuits

8.7.1. p-n Junction Representation of a Diode
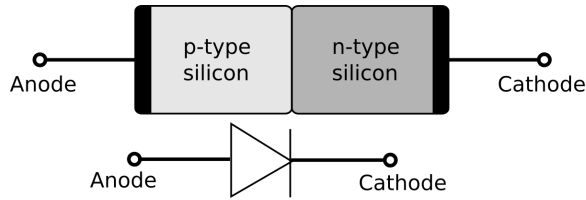
(Measurements at 25 °C.)

Semiconductor		Threshold voltage / V	Band gap / eV	Electron mobility / m^2 V^{-1} s^{-1}	Hole mobility / m^2 V^{-1} s^{-1}	Relative permittivity
Silicon	Si	0.7	1.12	0.16	0.05	12
Germanium	Ge	0.3	0.67	0.39	0.19	16
Gallium arsenide	GaAs	1.2	1.40	0.9	0.04	12.5
Indium antimonide	InSb	-	0.16	7.0	0.07	17

Values of the mobilities vary with temperature proportional to $T^{5/2}$ (in Kelvins).

8.7.2. p-n Junction Representation of a Bipolar Junction Transistor (BJT)
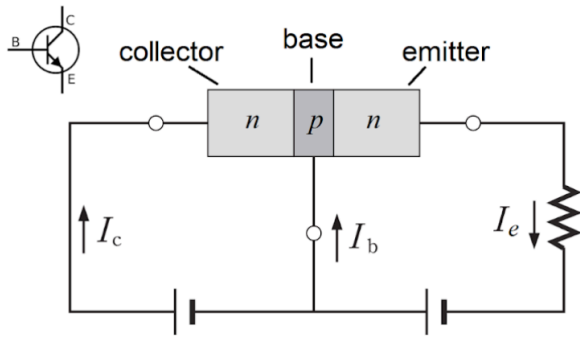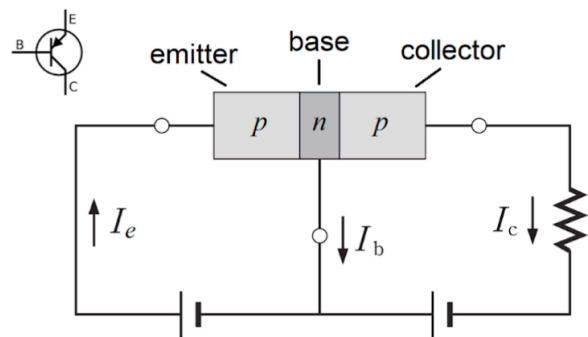
npn-type BJT   **pnp-type BJT**

8.7.3. Modes of Operation for Insulated Gate Field-Effect Transistors (MOSFETs)

In enhancement mode, the transistor is 'off' (non-conducting) by default ($V_{GS} = 0 \rightarrow I_{DS} = 0$).
In depletion mode, the transistor is 'on' (conducting) by default ($V_{GS} = 0 \rightarrow I_{DS} \neq 0$).

In a p-channel, holes (current) flow from source to drain when on ($V_{GS} < V_{th}$)
In an n-channel, electrons flow from source to drain when on ($V_{GS} > V_{th}$).
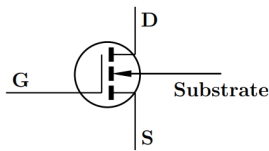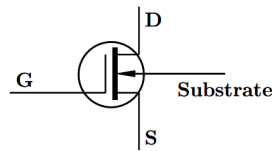
n channel enhancement mode	**n channel depletion mode**	**p channel enhancement mode**	**p channel depletion mode**
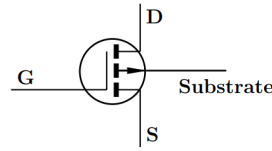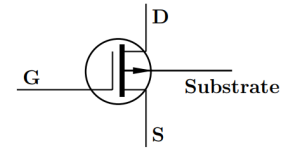
The circuit model is equivalent to that of the BJT (Section 8.7.2.) with

G: gate ↔ B: base;   S: source ↔ E: emitter,   D: drain ↔ C: collector

In many cases, the substrate is internally connected to the source electrode and is shown on the circuit symbol as such.

For the detailed structure (materials and solid state physics) of p-n junctions and related semiconductor fundamentals, see Section 8.6.5.

8.7.4. Discrete Semiconductor Devices and Characteristic Datasheets

BS170 (n-Channel Enhancement Mode MOSFET): Input-Output Characteristics
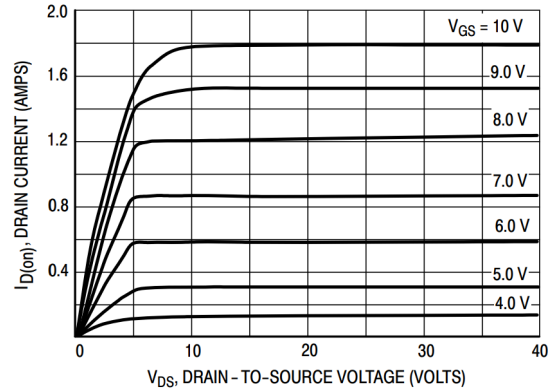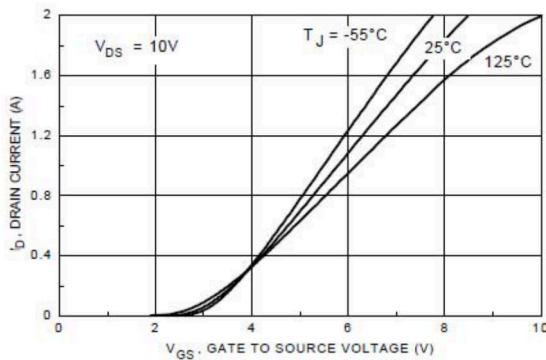
Representative parameters (at 25 °C):

- Gate-source threshold voltage (pinch-off), V_{th}:   2.1 V
- Zero Gate Voltage Drain Current, I_{DSS}:   500 nA
- Mutual conductance, g_m: 370 mS
- Drain resistance, r_d: 350 Ω
- Gate-drain parasitic capacitance, C_{DG}:   30 pF
- Dissipative thermal resistance, R_{TH}:   150 K W^{-1}

BC182L (npn-Type BJT): Input-Output Characteristics
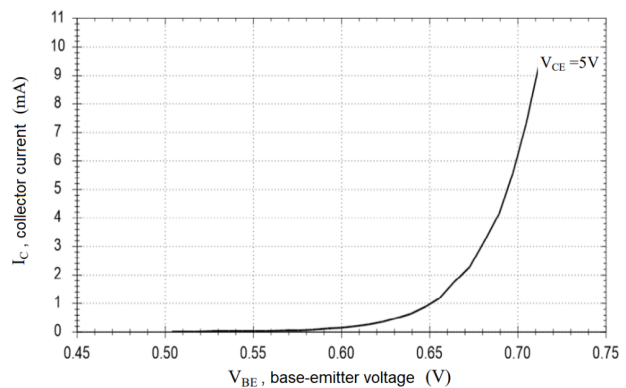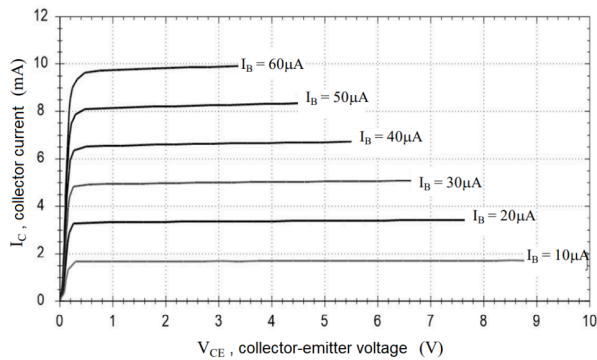
Representative parameters (25 °C, a.c. characteristics at 1 k, $I_C = 2$ mA, $V_{CE} = 5$ V):

- Base-emitter threshold voltage (forward-bias voltage), V_{th}:   0.7 V
- Current gain, h_{FE} (DC) and h_{fe} (AC small signal): $h_{FE} = 170$, $h_{fe} = 250$
- Input impedance, h_{ie} (AC):   5 kΩ
- Output conductance, h_{oe} (AC):   50 µS
- Base-collector parasitic capacitance, C_{CB}:   8 pF

1N4001 (Silicon Diode): Voltage-Current Characteristic
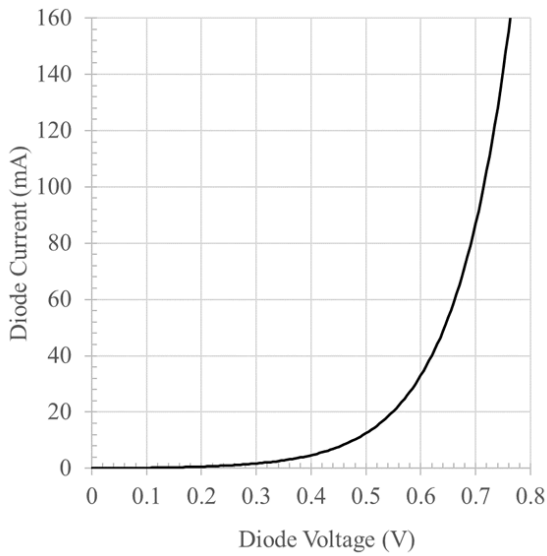
The forward-bias behaviour of a diode is modelled by the Shockley equation:

$$I = I_S \left(\exp \left(\frac{V_D}{nV_T} \right) - 1 \right)$$

(I_S: reverse bias saturation current, V_D: diode voltage; n: emission coefficient $V_T = \dfrac{k_B T}{|e|}$: thermal voltage)

BZX55 (Zener Diode): Voltage-Current Characteristic
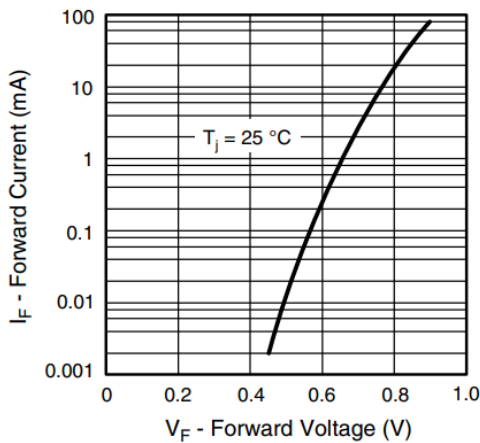
Forward bias mode
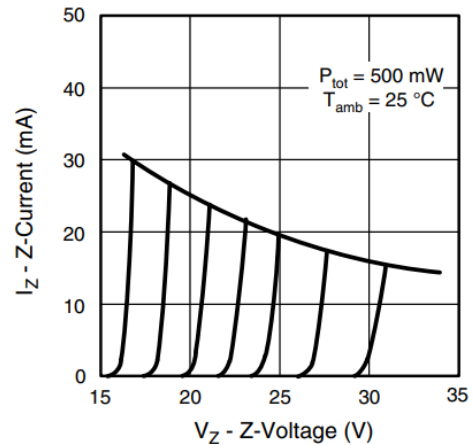
Zener (reverse bias) mode
(rated voltages at $I_Z = 5$ mA)

BPX65 (Photodiode): Light-Current Characteristic
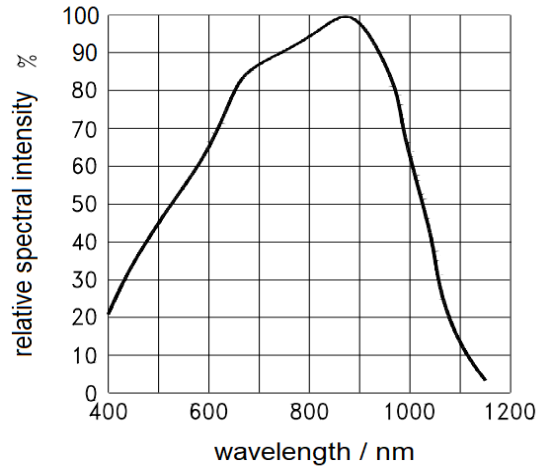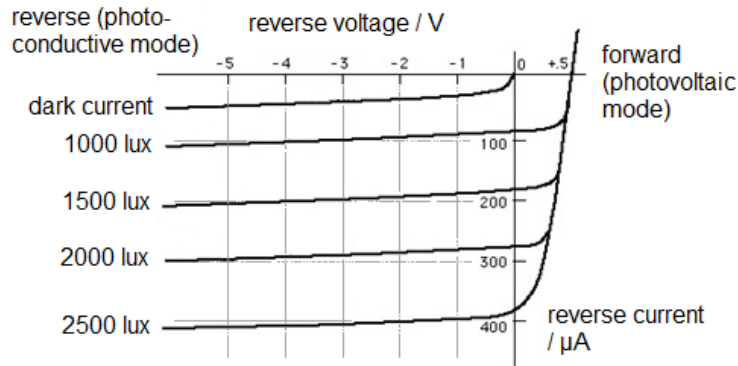
(1 lux = 1 cd sr m^{-2} = 7.9 mW m^{-2} for sunlight)

Peak spectral sensitivity: 550 µA mW^{-1}, at 850 nm.

SS490 (Hall Effect Sensor): Field-Voltage Characteristic
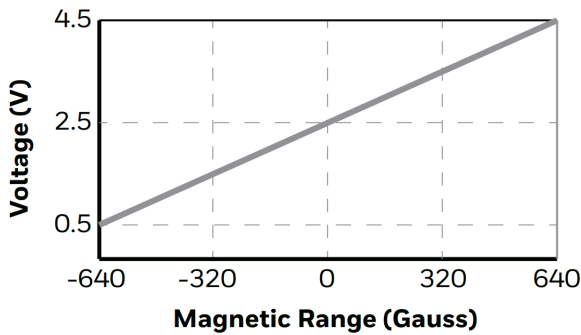
Gradient:

    3.125 mV / Gauss = 31.25 mV / mT

(1 Gauss = 100 microteslas (µT))

NORP12 (LDR): Light-Resistance Characteristic
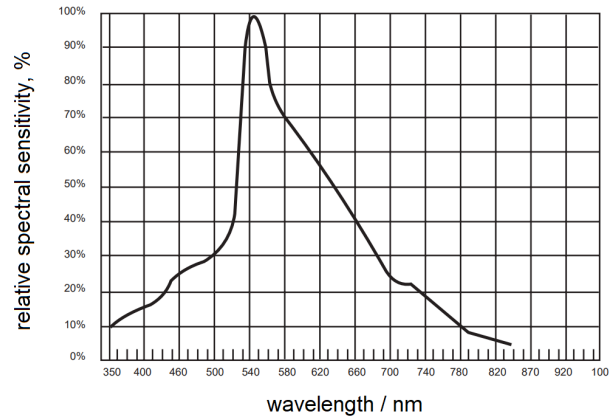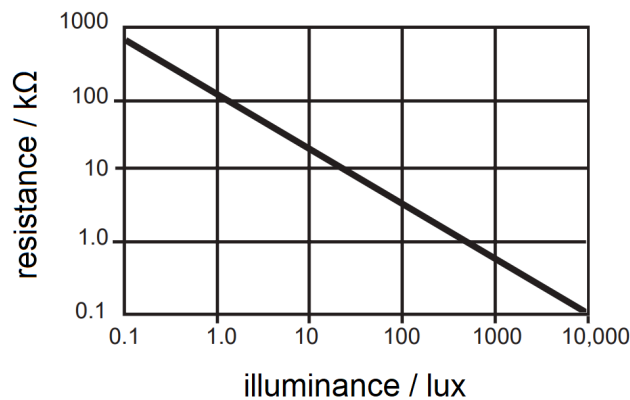
Power-law curve: $R\,[k\Omega] = 104.7\,e^{-0.755\,E_v\,[lux]}$

Peak sensitivity: 550 nm.

B57164K (10 kΩ NTC Thermistor): Temperature-Resistance Characteristic
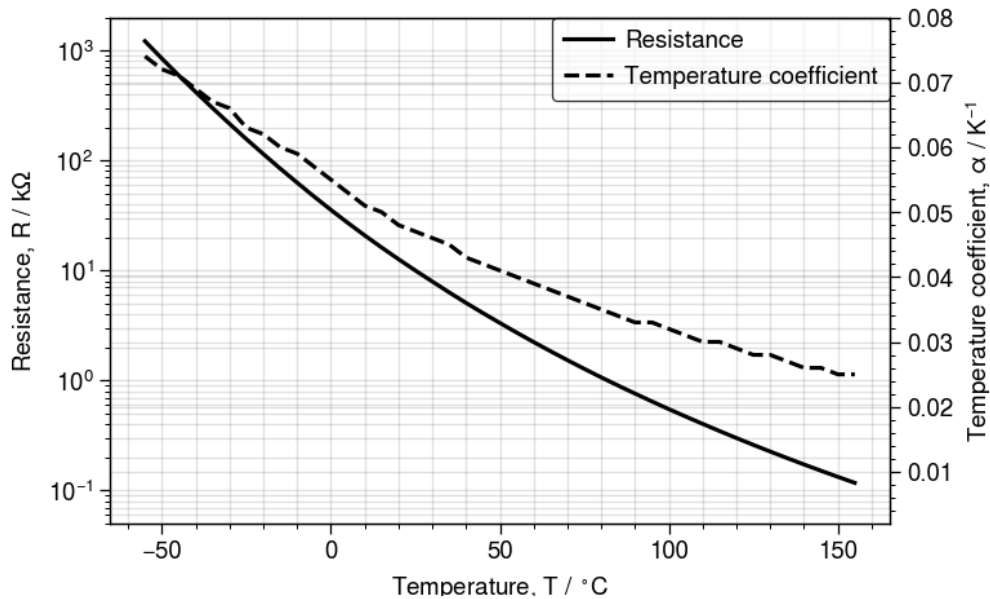
$$R = R_0 \exp\left(\frac{B}{T} - \frac{B}{T_0}\right) \quad \text{where } (R_0, T_0) = (10 \text{ k}\Omega, 298 \text{ K}) \qquad \text{(Steinhart-Hart equation)}$$

At 25 °C: $R = 10$ kΩ, $\alpha = 0.047$ K^{-1}, $B = 4300$ K ($\pm$ 3%) (B can be considered constant.

The temperature coefficient is defined as $\alpha = -\dfrac{1}{R}\dfrac{dR}{dT}$ (locally, $R = R_0(1 + \alpha \Delta T)$.)

8.7.5. AC Small-Signal Model for JFETs and MOSFETs (Hybrid-Pi Model)

Gate   Drain

i_d

v_{gs} $g_m v_{gs}$ r_d v_{ds}

Source   Source
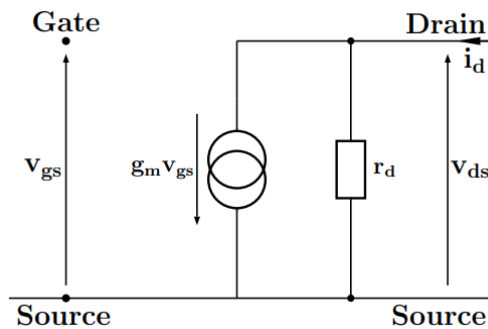
The small-signal drain current is $i_d = g_m v_{gs} + \dfrac{v_{ds}}{r_d}$ i.e. $g_m = \dfrac{\partial i_d}{\partial v_{gs}}$ and $\dfrac{1}{r_d} = \dfrac{\partial i_d}{\partial v_{ds}}$.

(g_m: mutual conductance/transconductance, r_d: drain resistance)

- To find the **input** impedance, short the **output** and find $\dfrac{v_x}{i_x}$ for a test **input** v_x & i_x.

- To find the **output** impedance, short the **input** and find $\dfrac{v_x}{i_x}$ for a test **output** v_x & i_x.

- To find the **gain**, find $\dfrac{v_{out}}{v_{in}}$.

It is commonly assumed that $r_d \to \infty$ (no current through it) to simplify the circuit analysis.

8.7.6. AC Small-Signal Model for BJTs (h-parameter Model)

Base   Collector

i_b i_c

h_{ie}
(Ω)

v_{be} $i_b h_{fe}$ h_{oe} v_{ce}
                                        (S)

$v_{ce} h_{re}$

Emitter   Emitter
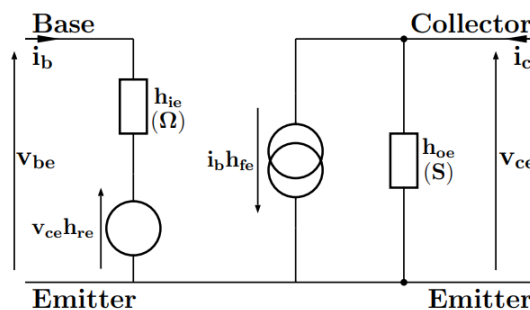
The small-signal voltages and currents are $v_{be} = h_{ie} i_b + h_{re} v_{ce}$ and $i_c = h_{fe} i_b + h_{oe} v_{ce}$

i.e. $h_{ie} = \dfrac{\partial v_{be}}{\partial i_b}$, $h_{re} = \dfrac{\partial v_{be}}{\partial v_{ce}}$, $h_{fe} = \dfrac{\partial i_c}{\partial i_b}$, $h_{oe} = \dfrac{\partial i_c}{\partial v_{ce}}$.

(h_{ie}: input resistance, h_{re}: reverse voltage transfer ratio, $h_{fe} = \beta$: forward current gain, h_{oe}: output conductance)

It is commonly assumed that $h_{re} \to 0$ and $h_{oe} \to 0$ to simplify the circuit analysis.

8.7.7. FET-Based Differential Amplifier and Current Mirror
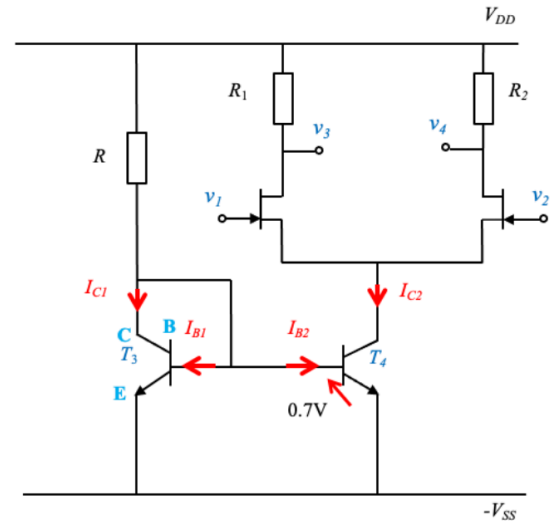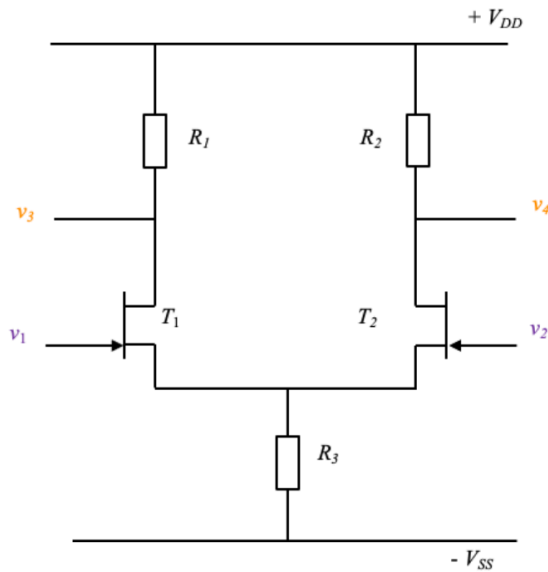
<table>
<tr><td align="center">Long-tailed pair:</td><td align="center">R_3 replaced by current mirror:</td></tr>
</table>

$$v_3 - v_4 = A(v_1 - v_2) \qquad I_C = h_{FE}I_{B1} = h_{FE}I_{B2} \text{ and } I_{C1} = I_{C2} = \frac{V_{DD} - V_{SS} - 0.7}{R}$$

Common Mode Rejection Ratio, $\text{CMRR} = \dfrac{differential\ mode\ gain}{common\ mode\ gain} = \dfrac{1 + 2g_m R_3 + \dfrac{2R_3}{r_d} + \dfrac{R_1}{r_d}}{1 + \dfrac{R_3}{r_d}}$

which is approximately $CMRR \approx 2g_m R_3$ if $r_d \gg R_1$ and R_3.

- In common mode, $v_1 = v_2$ and R_3 can be split into $2R_3 \parallel 2R_3$ by symmetry.

- In differential mode, $v_1 = -v_2$ and the FET sources are small-signal grounded.

8.7.8. Operational Amplifier (Op-Amp) Circuits
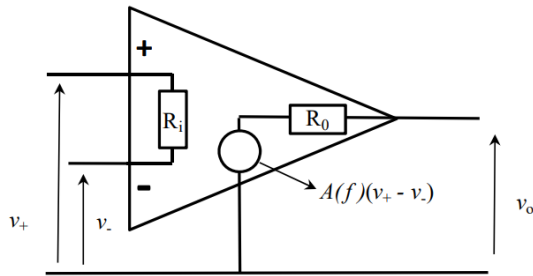
Input resistance: R_i Output resistance: R_o

Open-loop gain: A (ideally infinite)

Ideal Comparator (without hysteresis):

$$V_{out} = \begin{cases} V_{--}, & \text{if } V_+ > V_- \\ V_{++}, & \text{if } V_+ < V_- \end{cases}.$$
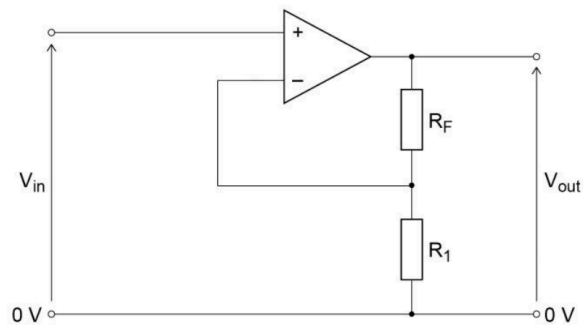
(The power supply rails, V_- and V_{++} are omitted.)
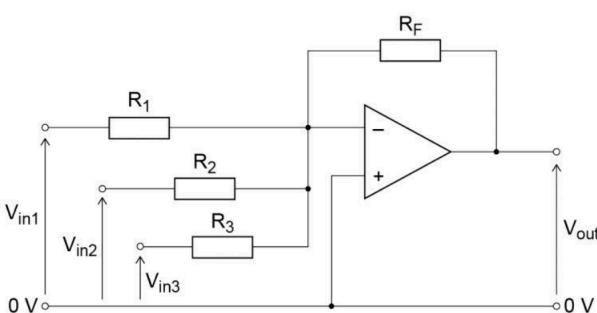
Some common op-amp circuits with resistive feedback are:
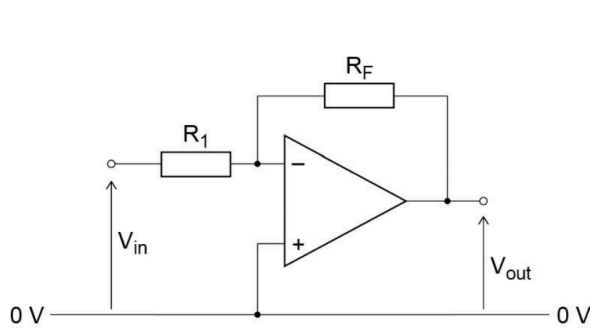
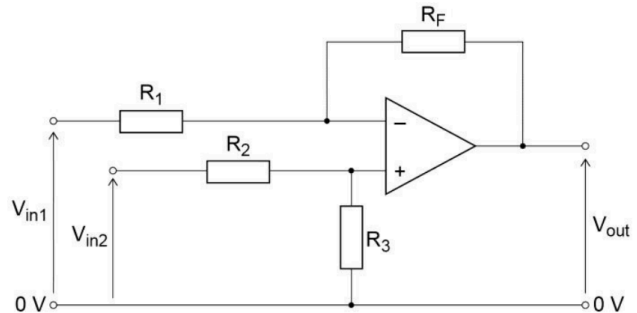**Inverting Amplifier**

$$\frac{V_{out}}{V_{in}} = -\frac{R_F}{R_1}$$

Non-Inverting Amplifier

$$\frac{V_{out}}{V_{in}} = 1 + \frac{R_F}{R_1}$$
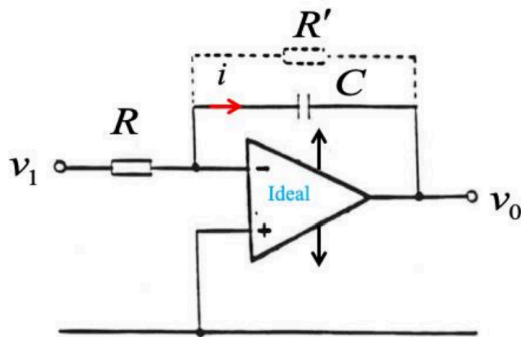
Summing Amplifier

$$V_{out} = -R_F\left(\frac{V_{in1}}{R_1} + \frac{V_{in2}}{R_2} + \frac{V_{in3}}{R_3}\right)$$
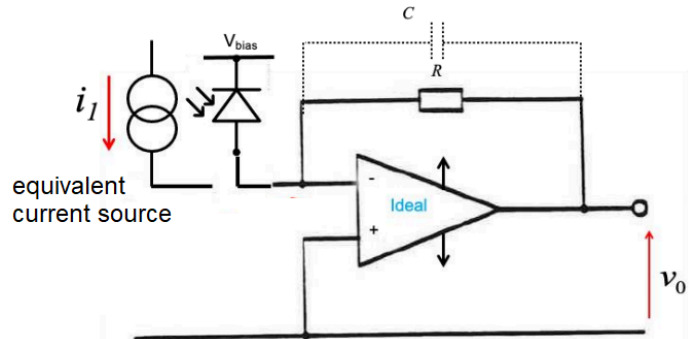
Difference Amplifier

$$V_{out} = \frac{R_3}{R_2}V_{in2} - \frac{R_F}{R_1}V_{in1}$$

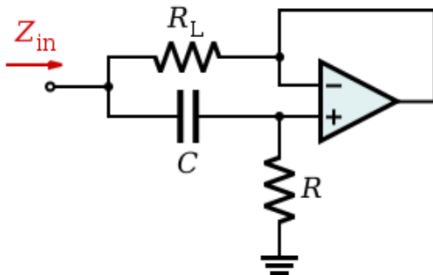Some common op-amp circuits with more complex feedback are:
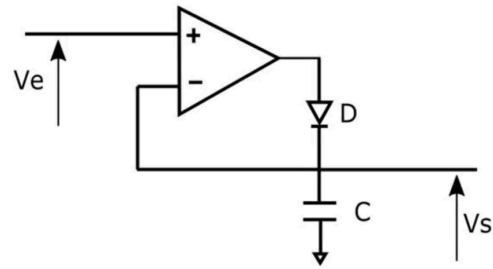

Integrator

$$v_o = \frac{-1}{RC} \int_0^t v_{in}\, dt$$

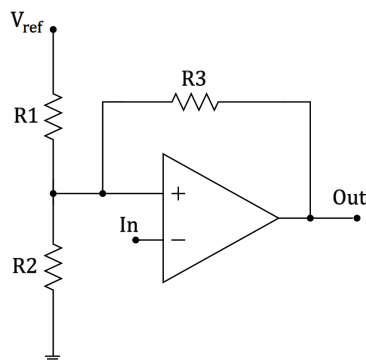**Transimpedance Amplifier**

$$\frac{v_0}{i_1} = -R$$

Gyrator

$$Z_{in} = R_L \,||\, j\omega R R_L C$$

Peak Detector

$$V_s = max\,\{V_e\}$$

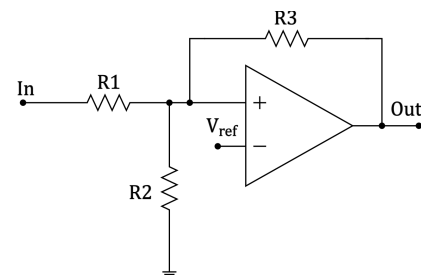**Schmitt Trigger** (inverting)

Inverting comparator with hysteresis

$$V_{thresh}^{(high)} = \frac{R_2(R_3 V_{ref} + R_1 V_{out}^{(high)})}{R_2 R_3 + R_1 R_2 + R_1 R_3},$$

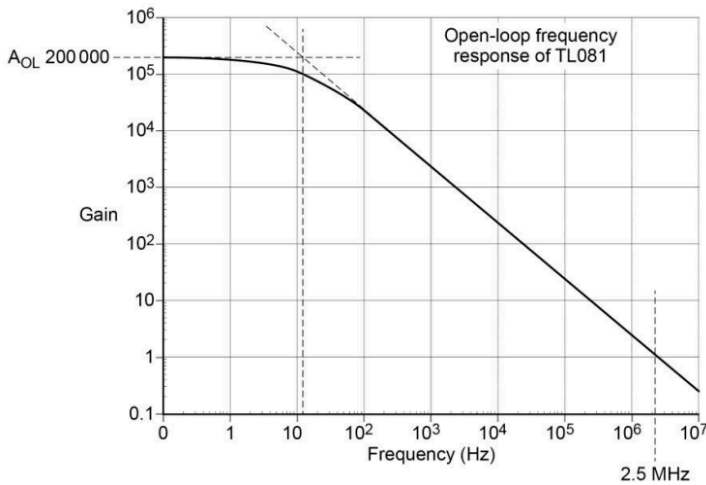$$V_{thresh}^{(low)} = \frac{R_2(R_3 V_{ref} + R_1 V_{out}^{(low)})}{R_2 R_3 + R_1 R_2 + R_1 R_3}$$

Schmitt Trigger (non-inverting)

Comparator with hysteresis

$$V_{thresh}^{(high)} = V_{ref} + R_1\left(\frac{V_{ref} - V_{out}^{(low)}}{R_3} + \frac{V_{ref}}{R_2}\right)$$

$$V_{thresh}^{(low)} = V_{ref} - R_1\left(\frac{V_{out}^{(high)} - V_{ref}}{R_3} - \frac{V_{ref}}{R_2}\right)$$

TL081 (Op-Amp) Open-Loop Frequency Response

For finite gain amplifiers, $V_{out} = A(V_+ - V_-)$

Gain-Bandwidth product: $A(f) \times f_2 = constant$

$A(f) = ($low freq. cut off, f_1 $)$ x A_o x $($high freq. cut off, f_2 $)$

$$A(f) = \left(\frac{1}{1 + \dfrac{f_1}{jf}} \right) A_0 \left(\frac{1}{1 + \dfrac{jf}{f_2}} \right)$$

Component-Level Diagram of 741 Op-Amp (LM741) Integrated Circuit
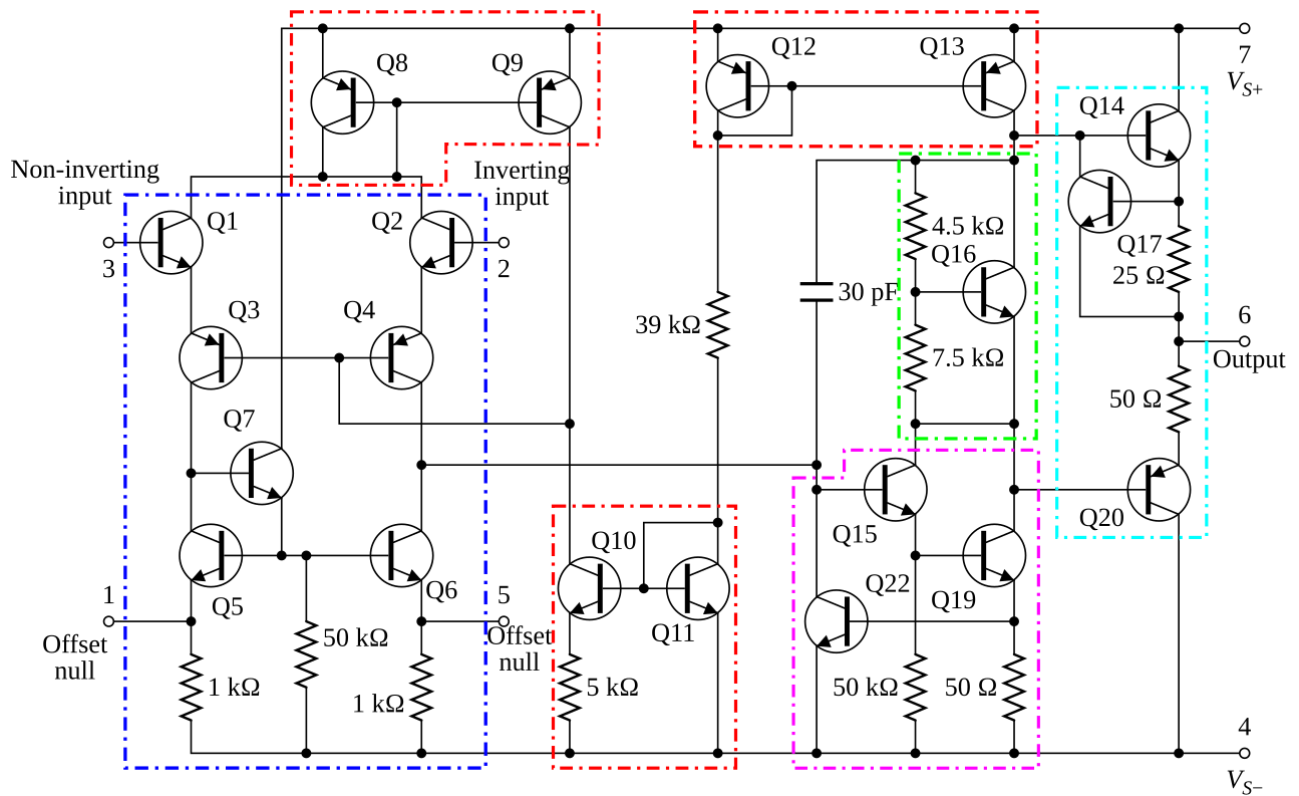
current mirrors   differential amplifier   class A gain stage
voltage level shifter   output level stage

8.7.9. Power Amplifiers and CMOS Logic
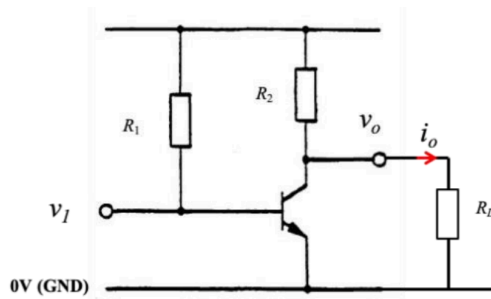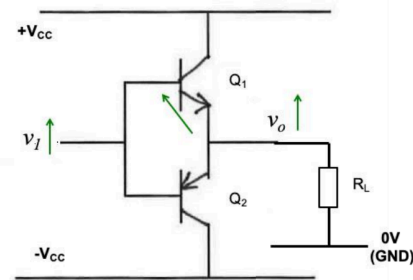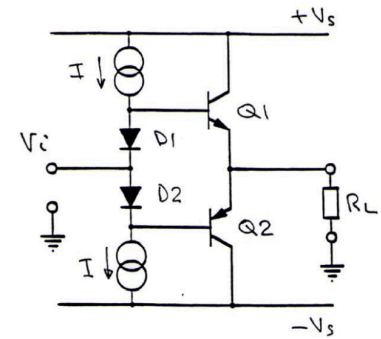
Class A	**Class B**	**Class AB**
Common Source	Complementary	Biassed Complementary
Amplifier	Emitter Follower	Emitter Follower

For the logic applications of complementary metal-oxide semiconductors (CMOS), see Section 9.1.1.

P9. DIGITAL ELECTRONICS, INSTRUMENTATION AND CONTROL

9.1. Digital Electronics

9.1.1. CMOS Circuits for Logic Gates
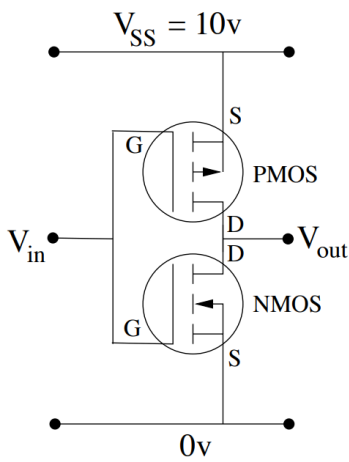
CMOS NOT Gate
(Inverter)
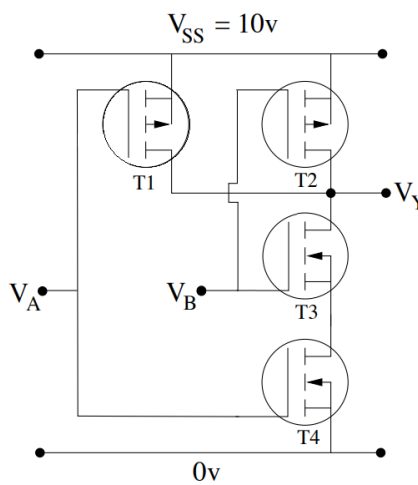
CMOS NAND Gate
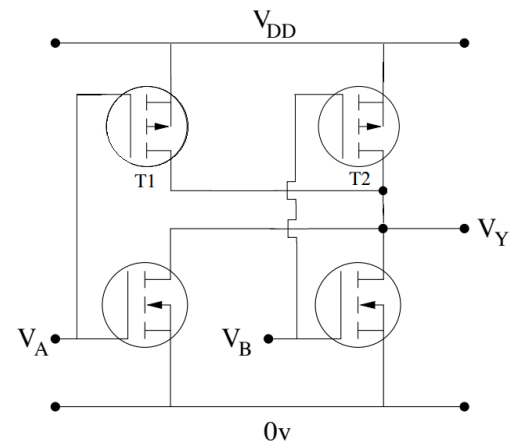
CMOS NOR Gate

9.1.2. Logic Gate Notation

Logic gates:
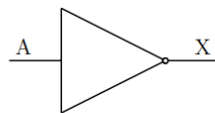
NOT: $X = \overline{A}$
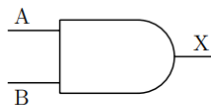
AND: $X = A \cdot B$
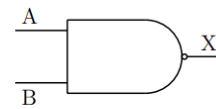
NAND: $X = \overline{A \cdot B}$
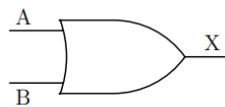
OR: $X = A + B$
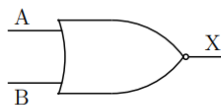
NOR: $X = \overline{A + B}$
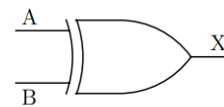
EXCLUSIVE OR: $X = A\overline{B} + \overline{A}B$

9.1.3. Boolean Algebra Identities and Combinational Logic Design

Simple identities: $\quad A \cdot \overline{A} = 0, \qquad A \cdot A = A, \qquad A \cdot 0 = 0, \qquad A \cdot 1 = A$

$\qquad\qquad\qquad\quad A + \overline{A} = 1, \qquad A + A = A, \qquad A + 0 = A, \qquad A + 1 = 1$

De Morgan's theorems: $\qquad\qquad \overline{A + B} = \overline{A} \cdot \overline{B} \qquad\qquad\qquad \overline{A \cdot B} = \overline{A} + \overline{B}$

Inversion from NAND / NOR: $\qquad \overline{A} = \overline{A \cdot A} = \overline{A + A}$

XOR: $\qquad\qquad\qquad\qquad\qquad A \oplus B = A \cdot \overline{B} + \overline{A} \cdot B$

XNOR: $\qquad\qquad\qquad\qquad\qquad A \odot B = \overline{A \oplus B} = A \cdot B + \overline{A + B}$

Karnaugh maps (K-maps): enumerated input states form a Gray code
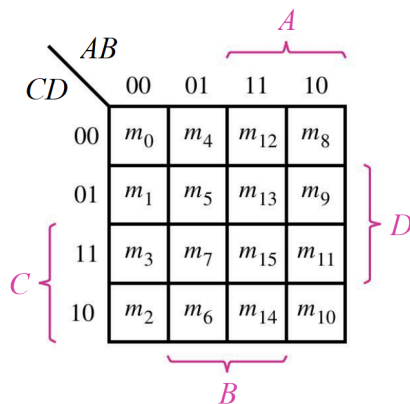
$\leftarrow$ Typical 4-variable Karnaugh map for $m = f(A, B, C, D)$

For a NAND circuit, find a sum-of-products expression for the output (covering all **1**'s in the map), then apply De Morgan's theorem. Use $\overline{A} = \overline{A \cdot A}$ for inverters.

For a NOR circuit, find a sum-of-products expression for the **inverse** of the output (covering all **0**'s in the map), then apply De Morgan's theorem. Use $\overline{A} = \overline{A + A}$ for inverters.

Hazards:

- **Static 1-hazard:** a momentary single erroneous $1 \to 0 \to 1$ transition, occurring when sum-of-products terms for the **output** (1) do not overlap.

- **Static 0-hazard:** a momentary single erroneous $0 \to 1 \to 0$ transition, occurring when sum-of-products terms for the **inverse** (0) of the output do not overlap.

- **Dynamic hazard:** twice-repeated static hazards within the same transition period, resulting in an incorrect final state.

- Propagation delay: equal to the delay of a single gate times the maximum number of nested logic gate operations.

- Static hazards can be removed by ensuring all sum-of-products overlap on the Karnaugh map.

- If there are no static hazards, then there can be no dynamic hazards.

9.1.4. Bistable Circuits

Set-Reset Bistable (SR Flip-Flop): S turns Q_1 on (and Q_2 off); R turns Q_1 off (and Q_2 on).
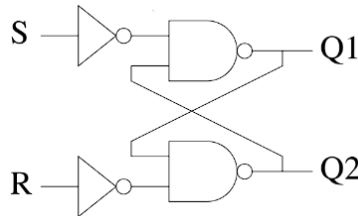
The outputs remain even when inputs return to $S = 0$ and/or $R = 0$. State $S = R = 1$ is not allowed (race condition).

Outputs: $Q_1 = \overline{\overline{S} \cdot Q_2} = S + \overline{Q_2}$ and $Q_2 = \overline{\overline{R} \cdot Q_1} = R + \overline{Q_1}$.

The SR-bistable can be used to mitigate contact debouncing from mechanical switches.

The **gated SR bistable** has inputs $\overline{S} = \overline{S \cdot G}$ and $\overline{R} = \overline{R \cdot G}$ where G is a clock (CLK), where the output can only change when the CLK is high (synchronous circuit).

Master-Slave Bistable: two clock-gated SR bistables in series with manual override
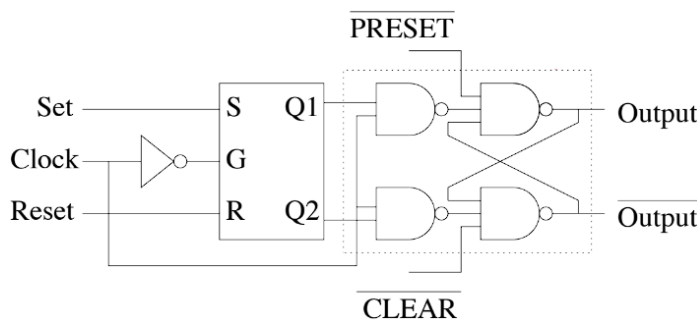
The 'master' (first) bistable is synchronous and controls the 'slave' (second) bistable.

Preset and clear inputs in the slave SR bistable allow for asynchronous override. These are 'active low' signals.

D-type Latch (Data Latch; Delay Latch): output Q follows D, synchronised to a clock
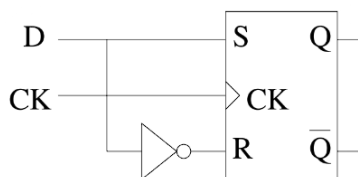
Single-input clocked SR bistable, $Q = D$ when the clock rises.

JK-Bistable (JK Flip Flop): same function as SR, but now $J = K = 1$ swaps the outputs.
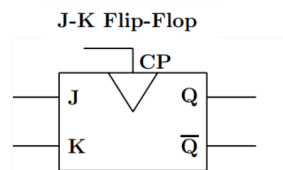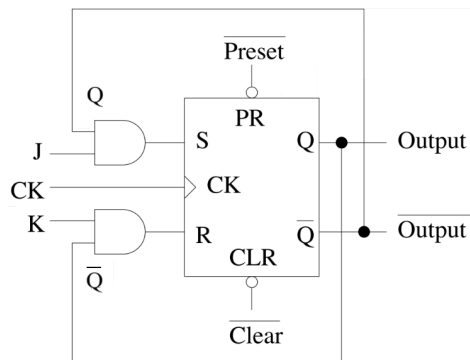
Constructed using a master-slave SR bistable with output feedback.

(J: 'set' input, K: 'reset' input, CP: clock pulse, Q_n: current state, Q_{n+1}: next state, X: 'don't care' state)

Excitation table					Truth table		
Q_n	Q_{n+1}	J	K		J_n	K_n	Q_{n+1}
0	0	0	X		0	0	Q_n
0	1	1	X		0	1	0
1	1	X	0		1	0	1
1	0	X	1		1	1	$\overline{Q}_n$

9.1.5. Sequential Logic Design using JK Bistables

General procedure for synchronous logic design using J-K flip-flops (bistables) and logic gates:

($J/K_i^{(n)}$: ith bistable input J/K at time step n, $Q_i^{(n)}$: ith bistable output at time step n,
A_i: input variable i, P_i: output variable i.)

1. Draw the **State Transition Diagram**, for each state identifying the output variables, input variables, and transitions.

2. Enumerate the states and allocate JK bistables to each state.

3. Draw the **State Transition Table**, consisting of the current bistable outputs $Q_i^{(n)}$, the current input variables A_i and the resulting next state $Q_i^{(n+1)}$. Use the excitation table to find the required bistable inputs, $J_i^{(n+1)}$ and $K_i^{(n+1)}$ to change $Q_i^{(n)}$ into $Q_i^{(n+1)}$.

4. Determine the input circuit logic for each input J_i and K_i as functions of the bistable outputs $Q_i^{(n)}$ and the inputs A_i, using **Karnaugh maps**.

5. Determine the output circuit logic to convert bistable outputs $Q_i^{(n)}$ to the outputs P_i.

9.1.6. Counting Circuits Using D-Type Latches
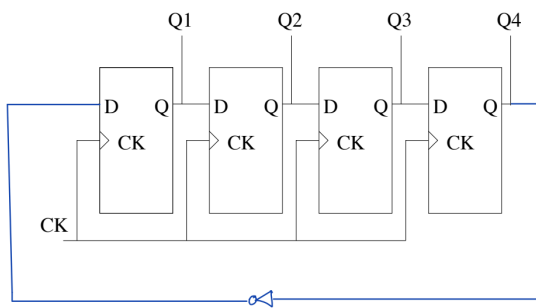
Johnson Counter
The number $Q_4Q_3Q_2Q_1$ increments
in binary at every clock cycle.
Can also be made with
JK bistables (**ripple counter**).
Additional logic can result
in modulo n counters.
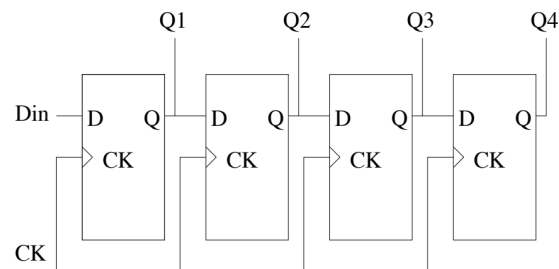
Shift Register
Each output is sequentially
retimed and delayed.
Used for parallel loading to a
serial data stream (serial data link).

9.1.7. Tri-State Buffer

Symbol: CMOS circuitry implementation of tri-state buffer:
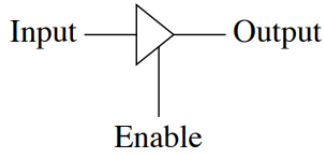
Truth Table:

Enable	Input	Output
0	0	floating
0	1	floating
1	0	0
1	1	1
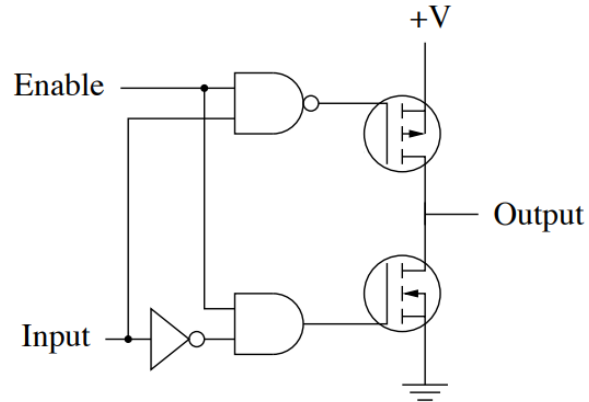
Note that some tri-state buffers may be 'active low' on the enable pin, which are indicated with a small circle.

9.1.8. Full Adder

If S is the result bit and C_{in} is the input carry bit (initialised to 0), then the sum $A + B$ and output carry bit are computed by

$$S = A \oplus B \oplus C_{in} \qquad\qquad C_{out} = A \cdot B + (A \oplus B) \cdot C_{in}$$

If the remaining (most significant) carry bit is ignored, then these expressions are also valid for two's complement representations of negative numbers (Section 8.8.2.), which can compute effective subtraction.

Binary numbers can be added in n-bit registers in a single clock cycle by connecting n full adders together (one per bit) (the 'ripple carry adder circuit').

9.1.9. Digital and Analogue Conversion

Digital to Analog (DAC):
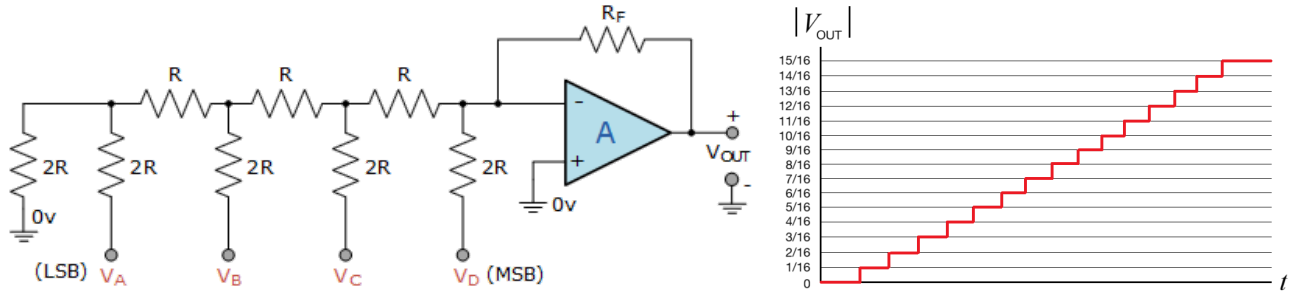
4-bit R-$2R$ Ladder DAC

$$V_{OUT} = -\frac{R_F}{R} \cdot \frac{1}{2^n} \sum_{i=0}^{n-1} 2^i V_i$$

Analog to Digital (ADC):

Inputs								Outputs		
D_7	D_6	D_5	D_4	D_3	D_2	D_1	D_0	Q_2	Q_1	Q_0
0	0	0	0	0	0	0	1	0	0	0
0	0	0	0	0	0	1	x	0	0	1
0	0	0	0	0	1	x	x	0	1	0
0	0	0	0	1	x	x	x	0	1	1
0	0	0	1	x	x	x	x	1	0	0
0	0	1	x	x	x	x	x	1	0	1
0	1	x	x	x	x	x	x	1	1	0
1	x	x	x	x	x	x	x	1	1	1

X = dont care
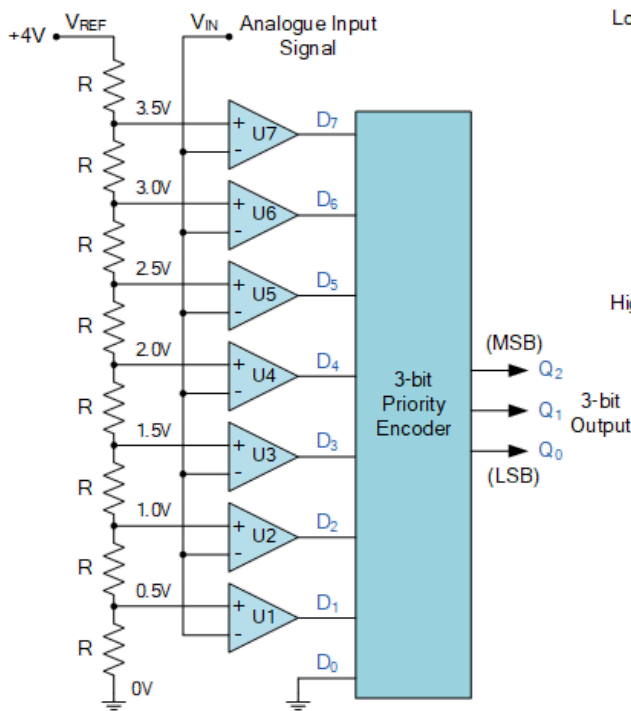
3-bit Flash ADC
Input: $0 \leq V_{IN} \leq V_{REF}$
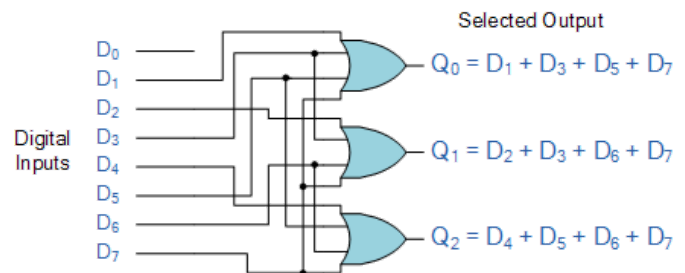
OR gate implementation of 3-bit priority encoder

The flash ADC requires large numbers of comparators and resistors for high-bit resolution. An alternative is the 'stair-step ADC', which uses a divide by 2^n counter, DAC and Schmitt trigger, but is slower.

9.2. Computer Engineering and Communications

9.2.1. Decimal - Hexadecimal - ASCII Character Conversion

DEC	HEX	ASCII	DEC	HEX	ASCII	DEC	HEX	ASCII	DEC	HEX	ASCII
0	00	^@	32	20	SPACE	64	40	@	96	60	`
1	01	^A	33	21	!	65	41	A	97	61	a
2	02	^B	34	22	"	66	42	B	98	62	b
3	03	^C	35	23	#	67	43	C	99	63	c
4	04	^D	36	24	$	68	44	D	100	64	d
5	05	^E	37	25	%	69	45	E	101	65	e
6	06	^F	38	26	&	70	46	F	102	66	f
7	07	^G	39	27	'	71	47	G	103	67	g
8	08	^H	40	28	(	72	48	H	104	68	h
9	09	^I	41	29	)	73	49	I	105	69	i
10	0A	^J	42	2A	*	74	4A	J	106	6A	j
11	0B	^K	43	2B	+	75	4B	K	107	6B	k
12	0C	^L	44	2C	,	76	4C	L	108	6C	l
13	0D	^M	45	2D	–	77	4D	M	109	6D	m
14	0E	^N	46	2E	.	78	4E	N	110	6E	n
15	0F	^O	47	2F	/	79	4F	O	111	6F	o
16	10	^P	48	30	0	80	50	P	112	70	p
17	11	^Q	49	31	1	81	51	Q	113	71	q
18	12	^R	50	32	2	82	52	R	114	72	r
19	13	^S	51	33	3	83	53	S	115	73	s
20	14	^T	52	34	4	84	54	T	116	74	t
21	15	^U	53	35	5	85	55	U	117	75	u
22	16	^V	54	36	6	86	56	V	118	76	v
23	17	^W	55	37	7	87	57	W	119	77	w
24	18	^X	56	38	8	88	58	X	120	78	x
25	19	^Y	57	39	9	89	59	Y	121	79	y
26	1A	^Z	58	3A	:	90	5A	Z	122	7A	z
27	1B	^[	59	3B	;	91	5B	[	123	7B	{
28	1C	^\	60	3C	<	92	5C	\	124	7C	|
29	1D	^]	61	3D	=	93	5D	]	125	7D	}
30	1E	^^	62	3E	>	94	5E	^	126	7E	~
31	1F	^_	63	3F	?	95	5F	_	127	7F	DEL

9.2.2. Binary Representation of Negative Numbers - Two's Complement

0 0 0 0 0 0 1 1	3
0 0 0 0 0 0 1 0	2
0 0 0 0 0 0 0 1	1
0 0 0 0 0 0 0 0	0
1 1 1 1 1 1 1 1	−1
1 1 1 1 1 1 1 0	−2
1 1 1 1 1 1 0 1	−3

To obtain a negative number:

| 0 0 0 1 0 1 0 0 | 20 |

invert each bit

| 1 1 1 0 1 0 1 1 |

add 1

| 1 1 1 0 1 1 0 0 | −20 |
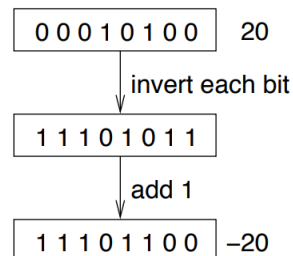
9.2.3. Schematic of PIC Microprocessor

The PIC microprocessor is based on a Harvard architecture.

Special registers:

GPIO Register (register location 0x05, bank 0)

U-0	U-0	R/W-x	R/W-x	R/W-x	R/W-x	R/W-x	R/W-x
—	—	GPIO5	GPIO4	GPIO3	GPIO2	GPIO1	GPIO0
bit 7							bit 0

Bits 0-5   General purpose input or outputs
(NB GPIO3 can only be an input)
Bit 6-7   Unimplemented (read as 0)

TRISIO Register (register location 0x85, bank 1)

U-0	U-0	R/W-x	R/W-x	R-1	R/W-x	R/W-x	R/W-x
—	—	TRISIO5	TRISIO4	TRISIO3	TRISIO2	TRISIO1	TRISIO0
bit 7							bit 0

Bits 0-5   Set (=1) means equivalent GPIO pin is input
Clear (=0) means equivalent GPIO pin is output
NB TRISIO3 is always 1
Bit 6-7   Unimplemented (read as 0)

STATUS Register (register location 0x03, bank 0)

IRP	RP1	RP0	TO	PD	Z	DC	C
bit 7							bit 0

C   Carry Flag
DC   Digital Carry Flag
Z   Zero Flag
PD   Power Down
TO   Time Out
RP0   Register Bank (0 sets bank 0, 1 sets bank 1)
RP1   Not Used
IRP   Not Used

Other Registers

W   Working register
PC   Programme Counter (13 bits, using PCL, 0x02, for lower 8 bits and PCLATH, 0x0A, for upper 5 bits)
FSR   File select register (0x04, bank 0)
INDF   Indirect file register (used for indirect addressing)
   - doesn't have a physical address

9.2.4. PIC Microprocessor Instruction Set

File Register Instructions that operate with whole bytes:

mnemonic	args	Description	Cycles			Opcode	
addwf	F,d	Add W and F and store the result in d	1	00	0111	dfff	ffff
andwf	F,d	AND W and F and store the result in d	1	00	0101	dfff	ffff
clrf	F	Clear F	1	00	0001	1fff	ffff
comf	F,d	Complement F and store the result in d	1	00	1001	dfff	ffff
decf	F,d	Decrement F and store the result in d	1	00	0011	dfff	ffff
decfsz	F,d	Decrement F and store the result in d,	1(2)	00	1011	dfff	ffff
		if the result is zero then skip the next instruction					
incf	F,d	Increment F and store the result in d	1	00	1010	dfff	ffff
incfsz	F,d	Increment F and store the result in d,	1(2)	00	1111	dfff	ffff
		if the result is zero then skip the next instruction					
iorwf	F,d	Inclusive OR W with F and store the result in d	1	00	0100	dfff	ffff
movf	F,d	Copy F to d (d = F)	1	00	1000	dfff	ffff
movwf	F	Copy W to F (F = W)	1	00	0000	1fff	ffff
rlf	F,d	Rotate F left through Carry and store the result in d	1	00	1101	dfff	ffff
rrf	F,d	Rotate F right through Carry and store the result in d	1	00	1100	dfff	ffff
subwf	F,d	Subtract W from F and store the result in d	1	00	0010	dfff	ffff
swapf	F,d	Swap low and high 4 bits of F and store the result in d	1	00	1110	dfff	ffff
xorwf	F,d	Exclusive OR W with F and store the result in d	1	00	0110	dfff	ffff

File Register Instructions that operate with bits:

addlw	Q	Add Q to W and store the result in W	1	11	111x	qqqq	qqqq
andlw	Q	AND Q with W and store the result in W	1	11	1001	qqqq	qqqq
iorlw	Q	Inclusive OR Q with W and store the result in W	1	11	1000	qqqq	qqqq
movlw	Q	Copy Q to W (W=Q)	1	11	00xx	qqqq	qqqq
retlw	Q	Return from Subroutine (Pull program counter from stack)	2	11	01xx	qqqq	qqqq
		and Copy Q to W (W=Q)					
sublw	Q	Subtract W from Q and store the result in W	1	11	110x	qqqq	qqqq
xorlw	Q	Exclusive OR Q with W and store the result in W	1	11	1010	qqqq	qqqq

Call and Goto:

call	P	Push program counter onto the stack and Jump to program location P	2	10	0ppp	pppp	pppp
goto	P	Jump to program location P	2	10	1ppp	pppp	pppp

Instructions with no arguments:

clrw		Clear W (W=0)	1	00	0001	0xxx	xxxx
clrwdt		Clear Watchdog timer	1	00	0000	0110	0100
		(if the watchdog timer overflows, the PIC is reset)					
nop		No operation	1	00	0000	0xx0	0000
retfie		Return from interrupt	2	00	0000	0000	1001
		(Pull program counter from stack and enable interrupts)					
return		Return from subroutine	2	00	0000	0000	1000
		(Pull program counter from stack)					
sleep		Go into standby mode	1	00	0000	0110	0011

9.2.5. Von Neumann Architecture
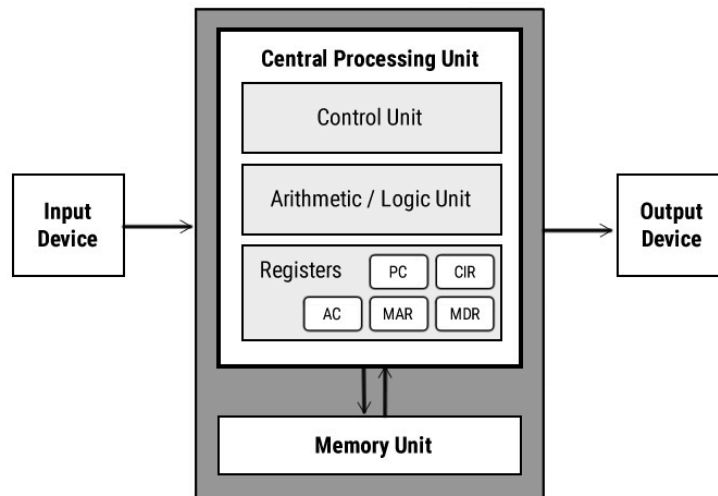
Components of the CPU (Central Processing Unit):

- CU (Control Unit): receives input from the CIR, flags and clock, and sends appropriate control signals to the control bus.

- ALU (Arithmetic and Logic Unit): performs binary mathematical and bitwise logical operations.

- Registers: high-speed storage for recording temporary data.

Registers in the CPU:

- MAR (Memory Address Register): points to the address of data that needs to be accessed
- MDR (Memory Data Register): holds data that is being transferred to or from memory
- AC (Accumulator): where intermediate arithmetic and logic results are stored
- PC (Program Counter): points to the address of the next instruction to be executed
- CIR (Current Instruction Register): contains the current instruction code during processing

Buses:

- Address bus: carries the **addresses** of data from the processor to the memory
- Data bus: carries data between the processor, the memory unit and the I/O devices
- Control bus: carries control signals/commands from the CPU (and status signals from other devices) in order to control and coordinate all the activities within the computer

9.2.6. Fetch-Decode-Execute Cycle

Every instruction cycle, the following sequence of microinstructions are executed:

1. The address in the PC is copied to the MAR.
2. The PC is incremented, to point at the next instruction.
3. The MAR address is read and the instruction is copied to the MDR.
4. The instruction is copied to the CIR.
5. The instruction in the CIR is decoded by the CU.
6. The CU sends signals to relevant components e.g. ALU.

9.2.7. OSI Model for Network Communication Protocols

A general protocol can operate at one or more of a series of layers:

(Lowest layer, most hardware-dependent)

1. Physical layer: transmits the raw bitstream over a medium (channel)
2. Data link layer: defines the format of the data. In computers, the OS drivers and NIC (Network Interface Card) operate here.
3. Network layer: decides which physical path the data will take (in a given topology)
4. Transport layer: decides on settings such as 'language' and size of packets
5. Session layer: maintains connections and controls ports and sessions
6. Presentation layer: ensures usability of data and applies encryption/decryption
7. Application layer: the human-computer interaction, where apps access the network

(Highest layer, most software-dependent)

Ethernet: a family of wired communication protocols at the physical and data link layers.

The access method is CSMA/CD (Carrier Sense Multiple Access with Collision Detection).

Coaxial cables are slower with ~10 Mbps. Twisted pair and fibre cables are used for Fast Ethernet and Gigabit Ethernet (~100-1000 Mbps).

Bluetooth: a family of IEEE 802.15 wireless communication protocols at the data link layer.

Bluetooth networks (piconets) use a controller/peripheral (master/slave) model to control which devices can send and receive data. Creating a Bluetooth connection requires inquiry (acquiring the address of the target) and paging (establishing a connection).

The carrier frequency is 2.4 GHz. Bluetooth uses AFH (Adaptive Frequency Hopping) to identify specific carrier frequencies (channels) not in use to minimise interference.

The bit rate is lower than Wi-Fi (<1 Mbps) and the range is lower but also has low latency. BLE (Bluetooth 4.0 Low Energy) is a variation using less power. It is best suited for replacing short-cable interactions.

Wi-Fi: a family of IEEE 802.11 wireless communication protocols at the data link layer.

This is the most common protocol in a WLAN (Wireless Local Access Network).

The carrier frequency is either 2.4 G or 5 G and the modulation method is QAM (using either 64-bit, 256-bit, or 1024-bit constellations; see Section 9.2.11.)

TCP/IP (Transmission Control Protocol / Internet Protocol):

A broad set of protocols spanning the application layer, transport layer (TCP), internet layer (IP), and data link layer.

UDP (User Datagram Protocol):

UDP packets are called 'datagrams'. Unlike TCP, there is no 'handshake' process before data transmission begins. The response is sent as soon as the request is received.

UDP can encapsulate IPv4 or IPv6. In IPv6, a checksum with error correction bits are included in the header.

The UDP is used by many internet applications including DNS (Domain Name Service) and DHCP (Dynamic Host Configuration Protocol).

HTTPS (Hypertext Transfer Protocol Secure): an encrypted extension of HTTP

The communication is encrypted with either TLS (Transport Layer Security) or SSL (Secure Sockets Layer).

A URL (Uniform Resource Locator) starting with `https://www.` denotes a HTTPS-secured website using the WWW (World Wide Web) domain name.

Web browsers trust HTTPS websites based on certificates.

FTP (File Transport Protocol): Client-server interaction for downloading/uploading files.

SMTP (Simple Mail Transfer Protocol): Transfers text-only (ASCII) emails.

IMAP (Internet Message Access Protocol): Transfers emails containing MIME (multimedia: images, videos, sound, files, typical attachments).

9.2.8. Distributed Systems

In a distributed system, computing resources are spread across wide distances, typically connected via the internet, and may be accessed from any connected device. Resource allocation techniques (concurrency, synchronisation / asynchronous programming, threading, multiprocessing, scheduling, load balancing) are essential to ensure reliability of service.

Cloud Computing: delivery of computing resources (storage, processing power, and services) over the internet instead of owning and maintaining physical hardware and software. Users use resources on-demand from remote data centres. Service models include:

- Infrastructure as a Service (IaaS): Provides virtualized computing resources e.g. virtual machines, storage, and networking. Users have control over the operating systems and applications they run.

- Platform as a Service (PaaS): Offers a platform that includes the infrastructure and tools for building, deploying, and managing applications. Developers can focus on coding without worrying about underlying infrastructure.

- Software as a Service (SaaS): Delivers fully developed software applications over the internet. Users access these applications through a web browser without the need for installation or maintenance.

Serverless and Edge Computing: cloud providers automatically manage the infrastructure, scaling, and provisioning of resources. Developers write code in the form of functions that are executed on-demand. Serverless architectures are event-driven, and developers are billed based on the actual compute resources used, rather than pre-provisioned instances.

Edge computing involves processing data closer to its source, reducing latency and improving response times. Instead of sending all data to centralised cloud servers, edge devices (like IoT devices) process data locally or in nearby edge servers (beneficial for applications that require real-time processing or work in environments with limited connectivity).

Blockchain: a decentralised digital ledger technology that records transactions across multiple computers in a secure and immutable manner. It enables secure and transparent data storage and transfer without the need for intermediaries. Most well-known is its application to cryptocurrencies, although the future of these instruments is uncertain.

9.2.9. Analogue Communications

Analogue communications: used by radios, television video (AM) and audio (FM).

Amplitude Modulation (AM): the modulated signal $s(t)$ is related to the source signal $x(t)$ by

$$s(t) = \left(a_0 + x(t)\right) \cos 2\pi f_c t$$

The modulation index is $m_A = \dfrac{max\{\,x(t)\,\}}{a_0}$ and f_c is the carrier frequency.

AM signal power $= \dfrac{1}{2}a_0^2 + \dfrac{1}{2}P_x$.

If $a_0 = 0$ then this is Double Sideband Suppressed Carrier (DSB-SC). Receiver (RX) uses a product modulator (multiply with $\cos 2\pi f_c t$) and low-pass filter.

The frequency spectrum of the AM signal is:
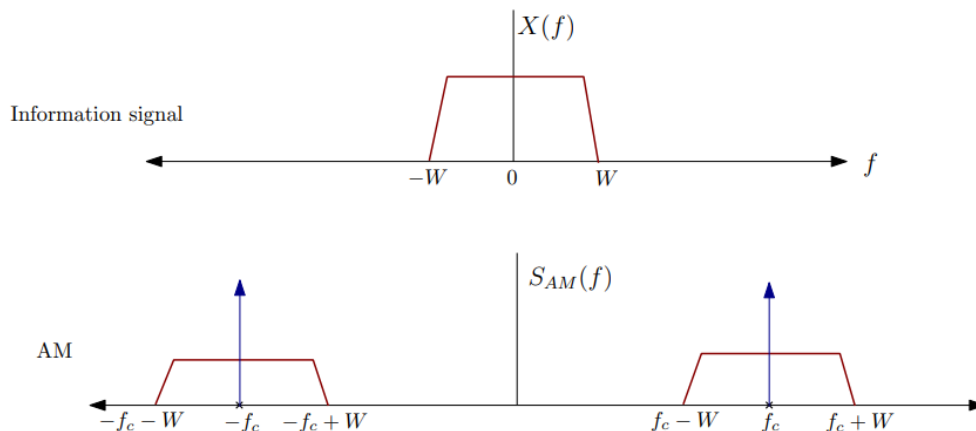
Frequency Modulation (FM): the modulated signal $s(t)$ is related to the information signal $x(t)$ by

$$s(t) = a_0 \cos \left(2\pi f_c t + 2\pi k_F \int_0^t x(\tau)\, d\tau\right)$$

The frequency deviation is $\Delta f = k_F \max\{\,x(t)\,\}$.

If the information signal is $x(t) = a_x \cos 2\pi f_x t$, then the modulation index is $m_F = \dfrac{\Delta f}{f_x} = \dfrac{k_F a_x}{f_x}$.

Carson's rule for FM signals: If the information signal has bandwidth W and the frequency deviation is Δf, then the modulated signal bandwidth is approximately $2W + 2\,\Delta f$.

9.2.10. Digital Communications

- Quantisation noise: if quantisation step size is $\Delta = \frac{2V}{2^n}$ then the noise is assumed to be uniformly distributed on $[\frac{-\Delta}{2}, \frac{\Delta}{2})$. The noise power is $\frac{\Delta^2}{12}$ (RMS power $= \frac{\Delta}{2\sqrt{3}}$).

- If a sinusoidal signal is quantised with an n-bit quantiser, the signal-to-quantisation noise ratio is $\text{SNR} = 1.76 + 6.02n$ dB.

- Non-uniform quantisation (companding) can reduce data rate.

- In baseband Pulse Amplitude Modulation (PAM: digital carrier, analogue data), the modulated signal is

$$x(t) = \sum_k X_k \, p(t - kT)$$

  where X_k are information symbols drawn from a real-valued constellation, $p(t)$ is a unit-energy baseband pulse waveform, and T is the symbol period.

- In a constellation with M symbols, each symbol represents $\log_2 M$ bits. The transmission rate is $\frac{1}{T}$ symbols per second or $\frac{\log_2 M}{T}$ bits per second (bps).

  1 byte (B) = 8 bits (b); 1 kilobyte = 1000 bytes etc. "-ibi" prefix indicates powers of 1024 instead of 1000 e.g. 1 kibibyte (KiB) = 1024 bytes, 1 mibibit (Mib) = 1048576 bits.

- In Quadrature Amplitude Modulation (QAM: analogue carrier, digital data), the modulated signal is

$$\begin{aligned}
x(t) &= \sum_k \text{Re}\left[X_k e^{j2\pi f_c t}\right] p(t - kT) \\
&= \sum_k \left[\text{Re}[X_k]\cos(2\pi f_c t) - \text{Im}[X_k]\sin(2\pi f_c t)\right] p(t - kT) \\
&= \sum_k |X_k| \cos(2\pi f_c t + \arg(X_k)) p(t - kT).
\end{aligned}$$

  where X_k are information symbols drawn from a constellation (that can be complex valued), $p(t)$ is a unit-energy baseband pulse waveform, and T is the symbol period.

9.2.11. Constellations for Common Digital Modulation Schemes

Constellation: shows the set of symbols on a phasor plot. Each symbol is mapped to a unit of data e.g. $\{-A, A\} \rightarrow \{0, 1\}$ in BPSK. In a constellation with M symbols, each symbol represents $\log_2 M$ bits.

Phase Shift Keying (PSK): Quadrature Amplitude Modulation (QAM):

BPSK QPSK 8-PSK
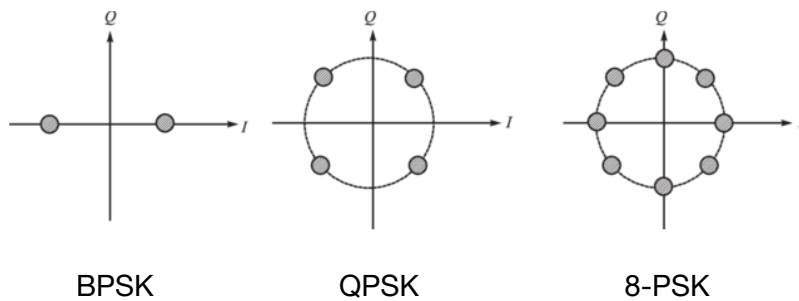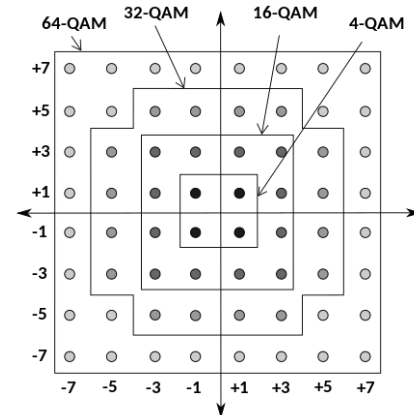
The most modern WiFi standard (WiFi 6: 802.11ax) uses 1024-QAM. Mobile data uses 16-QAM (3G) up to 1024-QAM (5G).

9.2.12. Channel Model for Wireless Communications

- Complex Gaussians: $h \sim \mathrm{CN}(0, \sigma^2)$ means that h is a complex random variable whose real and imaginary parts are independent Gaussian random variables, each distributed as $\mathrm{N}(0, \frac{1}{2}\sigma^2)$.

- If $h \sim \mathrm{CN}(0, \sigma^2)$, then the squared-magnitude $|h|^2$ is exponentially distributed, i.e., if $X = |h|^2$, the pdf of X is $f_X(x) = \dfrac{1}{\sigma^2} \exp\left(-\dfrac{x}{\sigma^2}\right)$ (see Section 5.2.2. for details)

- The Delay Spread T_d of a multipath fading channel is the maximum difference between delays of the paths from transmitter to receiver. The number of channel taps is ceil($2WT_d$), where W is the one-sided baseband bandwidth of the signal.

- If $T_d << \frac{1}{2W}$, the channel is said to have flat fading (no inter-symbol interference).

   If $T_d > \frac{1}{2W}$, the fading channel has multiple taps (frequency selective).

- The coherence bandwidth of the channel is $\frac{1}{2T_d}$. If the one-sided baseband bandwidth of the transmitted signal is less than the coherence bandwidth, there will be only one channel tap, i.e., flat fading.

9.2.13. Multiplexing and Cellular Networks

Techniques for Multiple Access:

- **TDMA** (Time Division Multiple Access): each of K users gets one slot in a frame of duration $T_f = KT_u$, where T_u is the individual transmission window. Used by 2G.

- **FDMA** (Frequency Division Multiple Access): each of K users gets a non-overlapping frequency band of the total bandwidth $B > KB_u$, where B_u is the individual bandwidth allocation. Orthogonal FDMA (OFDM) is a combination of TDMA and FDMA, and is used by 4G LTE and 5G.

- **CDMA** (Code Division Multiple Access): each of K users gets a unique signature function (spreading code) $c_i(t)$, all of which are orthogonal ($\int c_i(t) \, c_j(t) \, dt = 1$ if $i = j$ else 0) over the symbol period T, so that each user transmits the signal $\sum c_i(t) x_i(t)$ (before upconversion by multiplying with $\cos(2\pi f_c t)$. At the RX, after downconverting (product modulator $\to$ low pass filter), correlating the signal with each signature produces the data for that signature. Used by 3G.

Cellular Networks:

A network is divided into cells, with one base station per cell with users within each cell using a multiple access scheme to communicate simultaneously. Different telecommunications companies (cellular providers) typically place their antennas on the same tower in a given cellular region as they are assigned different frequency bands. Hand-off occurs when users move between cells, as the mobile automatically seeks the strongest signal. Adjacent cells must use different frequency bands to prevent interference.

The cell tower receives the sum of the modulated signals from its users. After demodulation, decorrelation and denoising, the data signals are recovered. The tower then forwards the data to the telecomms company's core network, and is then routed through the carrier's network to its destination.

For antenna design, see Section 8.5.13.

9.2.14. Hamming(7, 4) Code for Error Correction

The code generator matrix $\mathbf{G}$ and the parity-check matrix $\mathbf{H}$ for the (7, 4) Hamming code:

$$\mathbf{G^T} := \begin{pmatrix} 1 & 1 & 0 & 1 \\ 1 & 0 & 1 & 1 \\ 1 & 0 & 0 & 0 \\ 0 & 1 & 1 & 1 \\ 0 & 1 & 0 & 0 \\ 0 & 0 & 1 & 0 \\ 0 & 0 & 0 & 1 \end{pmatrix}, \qquad \mathbf{H} := \begin{pmatrix} 1 & 0 & 1 & 0 & 1 & 0 & 1 \\ 0 & 1 & 1 & 0 & 0 & 1 & 1 \\ 0 & 0 & 0 & 1 & 1 & 1 & 1 \end{pmatrix}.$$
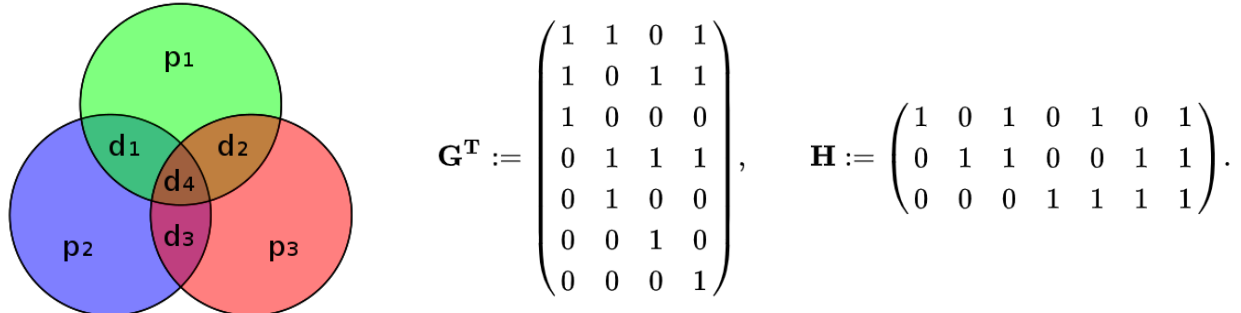
The data bits are $\{d_1, d_2, d_3, d_4\}$ and the parity bits are $\{p_1, p_2, p_3\}$, which are set to

$$p_1 = d_1 \oplus d_2 \oplus d_3; \qquad p_2 = d_2 \oplus d_3 \oplus d_4; \qquad p_3 = d_1 \oplus d_3 \oplus d_4$$

so that the transmitted codeword is $\{d_1, d_2, d_3, d_4, p_1, p_2, p_3\}$. The parity of each circle in the figure above must be even. ($\oplus$: bitwise addition)

9.2.15. General Linear Block Codes

- A k-dimensional linear block code of codeword length n (an (n, k) linear code) has encoder matrices of size $k \times n$, parity-check matrices of size $(n - k) \times n$, and rate $R = k / n$.

- An (n, k) linear block code has a systematic encoder matrix of the form $\mathbf{G} = [\mathbf{I}_k, \mathbf{P}]$, to which corresponds to a parity-check matrix of the form $\mathbf{H} = [-\mathbf{P^T}, \mathbf{I}_{n-k}]$.

- Singleton Bound: The minimum distance of any (n, k) block code satisfies $d_{min} \leq n - k + 1$, with equality for Maximum Distance Separable (MDS) codes.

- A block code with minimum distance d_{min} is guaranteed to correct any pattern of up to ceil$((d_{min} - 1) / 2)$ errors. It can recover up to $d_{min} - 1$ erasures.

- The minimum distance d_{min} of a linear block code is the minimum Hamming weight of any nonzero codeword. For binary codes, it is also the minimum number of columns of $\mathbf{H}$ that add up to the all-zero vector.

9.2.16. Binary LDPC Codes and Message Passing Algorithms

- Degree polynomials from a node perspective: $L(x) = \sum_{i=1}^{d_v^{\max}} L_i x^i, \quad R(x) = \sum_{i=1}^{d_c^{\max}} R_i x^i.$

- Degree polynomials from an edge perspective: $\lambda(x) = \sum_{i=1}^{d_v^{\max}} \lambda_i x^{i-1}, \quad \rho(x) = \sum_{i=1}^{d_c^{\max}} \rho_i x^{i-1}.$

- Average degrees: $\bar{d}_v = L'(1) = \left(\int_0^1 \lambda(x) dx \right)^{-1}$ and $\bar{d}_c = R'(1) = \left(\int_0^1 \rho(x) dx \right)^{-1}.$

- Design rate of an LDPC code is

$$R = 1 - \frac{\bar{d}_v}{\bar{d}_c} = 1 - \frac{L'(1)}{R'(1)} = 1 - \frac{\int_0^1 \rho(x) dx}{\int_0^1 \lambda(x) dx}.$$

- Density evolution for binary erasure channels with erasure probability ε: The probability p_t of a variable-to-check message along a (randomly picked) edge remaining erased after $t \geq 1$ steps of message passing is (Initialise with $p_0 = \varepsilon$.)

$$p_t = \varepsilon \lambda (1 - \rho(1 - p_{t-1})).$$

- Log-likelihood ratios for $j = 1, \ldots, n$ are $L(y_j) = \ln \frac{P(y_j|c_j=0)}{P(y_j|c_j=1)}.$

- Log-likelihood ratio for a binary-input AWGN channel with inputs $\{+1, -1\}$ and noise variance σ^2, for an output value y is $L(y) = \frac{2}{\sigma^2} y.$

- Log-likelihood ratio based decoding rules (for sum-product/belief propagation algorithm), with a check node denoted by i and a variable node by j:

The variable-to check messages are

$$L_{ji} = L(y_j) + \sum_{i' \backslash i} L_{i'j}.$$

and the check-to-variable messages are

$$L_{ij} = 2 \tanh^{-1} \left[\prod_{j' \backslash j} \tanh \left(\frac{L_{j'i}}{2} \right) \right].$$

where $i' \backslash i$ denotes all the check nodes i' connected to j except i, and conversely for $j' \backslash j$.

- Min-sum simplified decoding rule for a check node:

$$\text{sign}(L_{ij}) = \prod_{j' \backslash j} \text{sign}(L_{j'i}) \text{ and } |L_{ij}| = \min_{j' \backslash j}(|L_{j'i}|).$$

9.2.17. Finite Fields for Cryptography and Reed-Solomon Codes

- A Galois Field $\mathrm{GF}(q)$ for $q = p^m$ where p is any prime number consists of a multiplicative group of order $q - 1$ and an additive group of order q.

- The order of an element α in a group is the smallest power l such that $\alpha^l = 1$, where 1 is the neutral element of the group.

- Lagrange Theorem: The order of a subgroup (and thus the order of any element in a group) divides the order of the group.

- The Discrete Fourier Transform (DFT) of a vector $\mathbf{x} = [x_0, ..., x_{n-1}]$ with elements over a finite field F is defined by $X_k = \sum\limits_{m=0}^{n-1} x_m \alpha^{mk}$ for $k = 0, ..., (n-1)$. Here α must be an element of multiplicative order n in F.

- The inverse DFT is $x_m = \dfrac{1}{n^*} \sum\limits_{k=0}^{n-1} X_k \alpha^{-mk}$ for $m = 0, ..., (n-1)$. Here $n^* = \sum\limits_{j=1}^{n} 1$, where the sum is taken in F.

- Blahut's theorem: The linear complexity of the DFT of a sequence of length n equals the Hamming weight of the sequence, provided the Hamming weight is less than $n/2$.

- Reed-Solomon code: An (n, k) linear code over $\mathrm{GF}(q)$ with a parity-check matrix $\mathbf{H} = [\alpha^{ij}]$ for $i = 0, ..., (n - k - 1)$, and $j = 0, ..., (n-1)$, where α is an element of multiplicative order n in $\mathrm{GF}(q)$.

- A Reed-Solomon code has rate $R = k/n$, has minimum distance $d_{\min} = n - k + 1$ and hence satisfies the singleton bound with equality, i.e., it is Maximum Distance Separable (MDS).

9.3. Data Structures, Algorithms and Programming

9.3.1. Algorithm Flowchart Notation

Start / Stop   Process   Decision   Input / Output
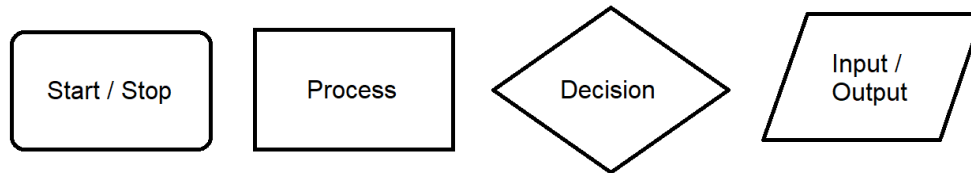
9.3.2. Algorithmic Complexity

The time (number of operations T) complexity or space (amount of memory S) complexity of an algorithm can be represented as a function of the input size n, as n approaches infinity. Proportionality constants are omitted.

Big-O notation: $O(f(n))$ indicates that $T(n) \leq k f(n)$ for all n above some finite value, for **some** positive constant k (an upper bound).

Little-o notation: $o(f(n))$ indicates that $T(n) \leq k f(n)$ for all n above some finite value, for **all** positive values of k (a weak upper bound).

Omega notation: $\Omega(f(n))$ indicates that $T(n) \geq k f(n)$ for all n above some finite value, for **some** positive constant k (a lower bound).

Theta notation: $\Theta(f(n))$ indicates both $O(f(n))$ and $\Omega(f(n))$ simultaneously.

Growth rates follow $n^n \gg n! \gg a^n \gg P(n) \gg n \log n \gg n \gg P(\log n) \gg \log^* n \gg 1$.

(red: non-polynomial time complexity class (NP), green: polynomial time complexity class (P), $\log^* n = \text{ceil}(1 + \log(1 + \log(1 + \dots (n \text{ times}) n)))$ the iterated logarithm (inverse tetration: $n = {}^T T$)).

Master Theorem: typically used for evaluating complexities of recursive algorithms.

If $T(n) = a T\left(\frac{n}{b}\right) + g(n)$ for any $a \geq 1$ and $b > 1$ and function $g(n)$, then:

- If $g(n) = O(n^{\log_b a - \varepsilon})$ for some positive ε, then $T(n) = \Theta(n^{\log_b a})$.
- If $g(n) = \Theta(n^{\log_b a})$, then $T(n) = \Theta(n^{\log_b a} \log n)$.
- If $g(n) = \Omega(n^{\log_b a + \varepsilon})$ for some positive ε, and if $a\, g\left(\frac{n}{b}\right) \leq c\, g(n)$ for some $c < 1$ and all sufficiently large n, then $T(n) = \Theta(g(n))$.

9.3.3. Data Types

Many programming languages provide default implementations of common data types.

- **Integer:** a whole number, typically in base 10.

- **Floating-point Number:** a number with a decimal part, typically in base 10.

- **Character string:** one or more characters (letters, numbers, etc).

- **Boolean:** a value representing 'True' or 'False', typically as a single bit '1' or '0'.

- **Array:** an ordered sequence of elements.

- **Linked list:** a type of array in which each element has associated data and a pointer to the next (and previous in a doubly-linked list) element in the list.

- **Set:** an unordered collection of elements. The implementation is optimised for membership access in O(1) time by hashing the elements.

- **Hashmap:** an associative array in which keys are mapped to values. The implementation is optimised for membership access in O(1) time by hashing the elements.

- **Queue:** a sequence of elements in which operations are performed FIFO (first in first out).

- **Tree:** each node element has associated data and pointers to 'child' nodes.
    - Binary search tree: at each node: all left values < node value < all right values.
    - Heap: at each node: left child node value ≤ node value ≤ right child node value.
    - Trie (prefix tree): node values are strings. Each child value starts with the parent value, with one additional character appended.
    - k-D tree: a decision tree to partition k-dimensional search space into subspaces. The nodes represent subspaces and the decisions represent hyperplane cuts, so that the child nodes are the spaces on the 'left' and 'right' of the cut.

- **Graph:** each node element has pointers to other data and connection elements ('branches') which may have associated data ('weights').

- **Function:** in first-class programming languages, functions are objects like any other, which input and output other data types.

9.3.9. Algorithms on Arrays (Lists)

Binary Search: finds the index of an item in an array in O(log n) time.

Recursive algorithm:

```python
def binary_search(arr: list, x, low: int = 0, high: int = float('inf')) -> int:
    high = len(arr) - 1 if high == float('inf') else high  # default: last index
    if high >= low:
        mid = (high + low) // 2
        if arr[mid] == x:  # found: return index
            return mid
        elif arr[mid] > x:  # x is in left half, reject right half
            return binary_search(arr, x, low, mid - 1)
        else:  # x is in right half, reject left half
            return binary_search(arr, x, mid + 1, high)
    else:  # not found
        return None
```

Iterative algorithm:

```python
def binary_search(arr: list, x) -> int:
    low = 0; high = len(arr) - 1; mid = 0
    while low <= high:
        mid = (high + low) // 2
        if arr[mid] < x:  # x is in right half, reject left half
            low = mid + 1
        elif arr[mid] > x:  # x is in left half, reject right half
            high = mid - 1
        else:  # found: return index
            return mid
    return None  # not found
```

Examples:

```python
print(binary_search([1, 2, 6, 7, 10], 6))  # returns 2
print(binary_search([1, 2, 6, 7, 10], 5))  # returns None
```

Two Pointer Algorithm: a general technique to iterate through an array in a single pass.

Example: given an array of stock value data, find the maximum profit that can be achieved by buying then selling. *(LeetCode #121: Best Time to Buy and Sell Stock)*

```python
def maxProfit(prices: list[float]) -> float:
    left = 0; right = 1  # main idea: left < right, always
    max_profit = 0  # track the variable of interest so far
    while right < len(prices):  # loop until the right pointer reaches the end
        if prices[left] < prices[right]:  # if there is potential profit here...
            profit = prices[right] - prices[left]
            max_profit = max(max_profit, profit)  # update with observed profit
        else:
            left = right  # no profit here - skip this whole window and start over
        right += 1  # keep the buy point, shift the sell point over by 1 to iterate
    return max_profit

maxProfit([7, 1, 5, 3, 6, 4])  # returns 5: buy at 1, sell at 6
```

Hashmaps: can be used to cache values, reducing O(n) lookups to O(1).

Example: given an array of distinct numbers, find the indices of the two numbers in the array which add up to a given target value. *(LeetCode #1: Two Sum)*

```python
def twoSum(nums: list[int], target: int) -> tuple[int]:
    mapping = {}  # maps required remainders to indices where they were seen
    for i in range(len(nums)):
        remainder = target - nums[i]
        if nums[i] in mapping:  # we have seen the required remainder before
            return (mapping[nums[i]], i)
        else:
            mapping[remainder] = i   # store the required remainder and its index

twoSum([2, -1, 8, 15, 10], 7)  # returns (1, 2) because -1 + 8 = 7
```

9.3.10. Algorithms on Undirected Graphs

Dijkstra's Shortest Path Algorithm

It is a greedy algorithm. Each stage the visited set contains nodes closest to the destination and all the shortest paths. The set of shortest paths form a tree.

- Mark all nodes unvisited, and assign to every node a tentative distance value: zero for the destination node and infinity for all nodes.
- Set the destination node to the current node.
- While the current node is not the initial node:
  - Consider all unvisited neighbours of the current node and calculate their distances to the destination node through the current node. Compare this distance to the current assigned tentative distance for that node and assign the smaller one as the new tentative distance.
  - Mark the current node as visited.
  - Set the new current node to be the unvisited node with the smallest tentative distance.

A* Shortest Path Algorithm

Dijkstra's algorithm plus heuristic $h(x)$: distance from initial node to x is at least $h(x)$.

Last step: Set the new current node to be the unvisited node x with the smallest sum of tentative distance and heuristic $h(x)$.

Prim's Algorithm for Minimum Spanning Tree Generation

Bellman-Ford Algorithm for Shortest Path

9.3.11. Algorithms on Singly-Linked Lists (Directed Graphs)

A linked list contains `Node` objects, starting with a `head` node each of which have a `value` attribute and a `next` attribute, which points at the next node in the list, ending with a null pointer.

Implementation of a Linked List:

```python
from __future__ import annotations  # allows type hinting before type definition
class ListNode:
    def __init__(self, x, next: ListNode = None):
        self.val = x
        self.next = next
```

Reversing a Linked List

- Initialise the 'current' node at the head, the 'previous' node is null, the 'next' node is `head.next`.
- While the 'current' node is not null:
    - Set the `current.next` pointer to the 'previous' node.
    - Set the 'previous' node to the 'current' node.
    - Set the 'current' node to the 'next' node.
    - Set the 'next' node to the node pointed to by `current.next`.

Cycle Detection

To detect whether a linked list contains a cycle or not, and if so where it starts, use Floyd's tortoise-and-hare algorithm:

- Initialise a 'fast' pointer (the 'hare') and a 'slow' pointer (the 'tortoise') at the head.
- Do while the fast/slow pointers are different (and not at the start):
  - Move the fast pointer by two nodes and the slow pointer by one node.
  - If the fast pointer reaches the end at any point, there is **no** cycle.
- If the pointers have met, there **is** a cycle. Now initialise a second 'slow' pointer at the head.
- While the two slow pointers are different:
  - Move the slow pointers each by one node.
- The two slow pointers are now both at the start of a cycle.

Example: given the head of a linked list, determine whether or not it contains a cycle, and if so, return the value of its starting node. *(LeetCode #141: Linked List Cycle)*

```python
def hasCycle(head: ListNode):
    i_slow = head; i_fast = head
    while True:
        if i_fast is not None and i_fast.next is not None:
            i_slow = i_slow.next
            i_fast = i_fast.next.next
        else:
            return False  # pointer reached the end: there is no cycle
        if i_slow == i_fast:
            i_slow_2 = head
            while i_slow_2 != i_slow:
                i_slow_2 = i_slow_2.next
                i_slow = i_slow.next
            return i_slow.val
```

Example: given an array of $N + 1$ integers such that each and every integer in $[1, N]$ is in the array, find the duplicate integer in O(1) space without modifying the array. *(LeetCode #287: Find Duplicate Number)*

By the pigeonhole principle, there is exactly one such integer. Consider forming a linked list from the array such that the head is the first item in the array, and the next item of any node is the value at this index of the array. Then there will be a cycle at the repeated integer.

```python
def findDuplicate(nums: list[int]) -> int:
    slow_i = nums[0]
    fast_i = nums[0]
    while True:
        slow_i = nums[slow_i]
        fast_i = nums[nums[fast_i]]
        if slow_i == fast_i:
            break
    slow_i_2 = nums[0]
    while slow_i != slow_i_2:
        slow_i = nums[slow_i]
        slow_i_2 = nums[slow_i_2]
    return slow_i
```

9.3.12. Algorithms on Binary Search Trees (BSTs)

Implementation of a BST

```
from __future__ import annotations  # allows type hinting before type definition
class TreeNode:
    def __init__(self, val, left: TreeNode = None, right: TreeNode = None):
        self.val = val
        self.left = left
        self.right = right
```

Traversal of a BST: can be done depth-first (in-/pre-/post-order) or breadth-first (level-order).
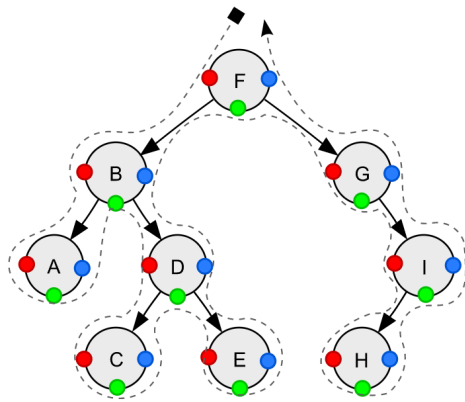
In-order traversal: starting with the root,

- If this node is the root:
    - Recursively traverse the left node.
    - Visit the root.
    - Recursively traverse the right node.

For **pre-order** traversal or **post-order** traversal, visit the root before or after both traversals respectively.

Depth-First Search (DFS):

In-order traversal: A → B → C → D → E → F → G…

```
def traverseInOrder(root):
    if root:
        traverseInOrder(root.left)
        print(root.val)  # visit the node
        traverseInOrder(root.right)
```

Pre-order traversal: F → B → A → D → C → E → G…

```
def traversePreOrder(root):
    if root:
        print(root.val)  # visit the node
        traversePreOrder(root.left)
        traversePreOrder(root.right)
```

Post-order traversal: A → C → E → D → B → H → I…

```
def traversePostOrder(root):
    if root:
        traversePostOrder(root.left)
        traversePostOrder(root.right)
        print(root.val)  # visit the node
```

Breadth-First Search (BFS):

Level-order traversal: F → B → G → A → D → I → C…

```
def traverseLevelOrder(root):
    h = height(root)
    for i in range(1, h + 1):
        traverseCurrentLevel(root, i)

def traverseCurrentLevel(root, level):
    if root is None:
        return None
    if level == 1:
        print(root.val)  # visit the node
    elif level > 1:
        traverseCurrentLevel(root.left, level - 1)
        traverseCurrentLevel(root.right, level - 1)

def height(node):
    if node is None:
        return 0
    else:
        lheight = height(node.left)
        rheight = height(node.right)
        return lheight + 1 if lheight > rheight else rheight + 1
```

9.3.12. Dynamic Programming

Dynamic programming (DP) involves recognising that a problem can be written in terms of the answer to the same problem on subdivisions of the input, forming a decision tree.

The solution to a dynamic programming problem can be written in terms of the solution to the same problem (subproblems) of a smaller input.

Fibonacci-like Recurrence Relations: common in combinatorics questions ("how many ways…")

Simple Fibonacci: $f(n) = f(n-1) + f(n-2)$

Generalised Fibonacci: $f(n) = \sum\limits_{k=1}^{N} a_k f(n-k)$

2D Fibonacci: $f(m, n) = a_1 f(m-1, n) + a_2 f(m, n-1)$

All Fibonacci relations have a closed form (O(1) evaluation time) by solving the corresponding difference equation (Section 3.4.15)

- Top-down traversal by DFS (backtracking: recursion with memoisation), or
- Bottom-up solution (tabulation).

Example: Given an array of reusable positive integer coin values $\mathbf{c}$ and a total amount value v to be made, find the minimum number of coins needed to make up the amount. *(LeetCode #322: Coin Change)*

Let $f(v)$ be the number of ways to make a value of v from the available selection of coins.

Observe that
$$\underbrace{f(v)}_{\substack{\text{ways to make} \\ \text{value } v}} = \min_{c_i \in \mathbf{c}} \left\{ \underbrace{1}_{\substack{\text{chosen} \\ \text{coin}}} + \underbrace{f(v - c_i)}_{\substack{\text{ways to make} \\ \text{remaining amount}}} \right\}.$$

Using a top-down approach:

```python
def coinChange(coins, amount, memo={}) -> int:
    if amount < 0:  # amount cannot be made - set to negative to fail check
        return -1
    if amount == 0:  # base case
        return 0
    if amount in memo:
        return memo[amount]
    min_count = float('inf')
    for c in coins:
        if 0 <= (f := coinChange(coins, amount - c, memo)) < min_count:
            min_count = 1 + f
    memo[amount] = min_count if min_count != float('inf') else -1
    return memo[amount]
```

Using a bottom-up approach:

```python
def coinChange(coins: list[int], amount: int) -> int:
    dp = {0: 0}  # Base case. dp maps amounts to number of ways {v: f(v)}
    for v in range(1, amount + 1):  # starting from v = 1, build upwards
        # float('inf') is used to ignore all cases where v - c cannot be made
        dp[v] = min(1 + dp.get(v - c, float('inf')) for c in coins)
    return dp[amount] if dp[amount] != float('inf') else -1
```

Example: Given an integer array nums, return the length of the longest strictly increasing subsequence. *(LeetCode #300: Longest Increasing Subsequence)*

Let $f(i)$ be the maximum length of a subsequence ending at position i.

Observe that
$$\underbrace{f(i)}_{\substack{\text{longest subsequence} \\ \text{ending at } i}} = \max_{0 \leq j < i:\ x_i > x_j} \left\{ \underbrace{1}_{\text{including } x_i} + \underbrace{f(j)}_{\substack{\text{longest subsequence} \\ \text{ending at } j < i}} \right\}.$$

```python
def lengthOfLIS(nums: list[int]) -> int:
    dp = {0: 1}  # base case: {end index: longest increasing subsequence}
    for i in range(1, len(nums)):
        dp[i] = max((1 + dp[j]) if nums[i] > nums[j] else 1 for j in range(i))
    return max(dp.values())
```

Example: Given an array of houses each containing value x_i, find the maximum value that can be robbed from the houses if no two neighbouring houses can be robbed. *(LeetCode #198: House Robber)*

Let $f(i)$ be the amount that can be robbed from the houses up to index i (i.e. $x[0 : i + 1]$).

Observe that
$$\underbrace{f(i)}_{\substack{\text{amount that can be robbed} \\ \text{from houses up to index } i}} = \max \left\{ \underbrace{x_i + f(i-2)}_{\substack{\text{choose to rob} \\ \text{house } i}}, \quad \underbrace{f(i-1)}_{\substack{\text{choose to not rob} \\ \text{house } i}} \right\}$$

```python
def rob(self, nums: List[int]) -> int:
    dp = {0: nums[0]}  # base case: {end index -> max amount robbable}
    for i in range(1, len(nums)):
        dp[i] = max(nums[i] + dp.get(i - 2, 0), dp.get(i - 1, 0))
    return dp[len(nums) - 1]
```

9.3.13. Python Cheat Sheet

Keywords

Keyword	Description	Code Examples
False, True	Boolean data type	`False == (1 > 2)` 👎👍 `True == (2 > 1)`

and, or, not	Logical operators
	→ Both are true
	→ Either is true
	→ Flips Boolean
		`True and True    # True`
		`True or False    # True`
		`not False    # True`

break	Ends loop prematurely	`while True:` `    break # finite loop`

continue	Finishes current loop iteration	`while True:`
		`    continue`
		`    print("42") # dead code`

class	Defines new class	`class Coffee:` `    # Define your class`
def	Defines a new function or class method.	`def say_hi():` `    print('hi')`

if, elif, else	Conditional execution:
	- "if" condition == True?
	- "elif" condition == True?
	- Fallback: else branch
		`x = int(input("ur val:"))`
		`if   x > 3:  print("Big")`
		`elif x == 3: print("3")`
		`else:        print("Small")`

for, while	# For loop
	for i in [0,1,2]:
	    print(i)
		# While loop does same
		`j = 0`
		`while j < 3:`
		`    print(j); j = j + 1`

in	Sequence membership	`42 in [2, 39, 42] # True`

is	Same object memory location	`y = x = 3`
		`x is y        # True`
		`[3] is [3]    # False`

None	Empty value constant	`print() is None # True`
lambda	Anonymous function	`(lambda x: x+3)(3) # 6`

return	Terminates function. Optional return value defines function result.	`def increment(x):`
		`    return x + 1`
		`increment(4) # returns 5`

Basic Data Structures

Type	Description	Code Examples

Boolean	The Boolean data type is either True or False. Boolean operators are ordered by priority:
	not → and → or
	{ } → 👎
	{1, 2, 3} → 👍
		`## Evaluates to True:`
		`1<2 and 0<=1 and 3>2 and 2>=2 and 1==1`
		`and 1!=0`
		
		`## Evaluates to False:`
		`bool(None or 0 or 0.0 or '' or [] or`
		`{} or set())`
		
		Rule: *None, 0, 0.0, empty strings, or empty container types evaluate to False*

Integer, Float	An **integer** is a positive or negative number without decimal point such as 3.
	
	A **float** is a positive or negative number with floating point precision such as 3.1415926.
	
	Integer division rounds toward the smaller integer (example: 3//2==1).
		`## Arithmetic Operations`
		`x, y = 3, 2`
		`print(x + y)      # = 5`
		`print(x - y)      # = 1`
		`print(x * y)      # = 6`
		`print(x / y)      # = 1.5`
		`print(x // y)     # = 1`
		`print(x % y)      # = 1`
		`print(-x)         # = -3`
		`print(abs(-x))    # = 3`
		`print(int(3.9))   # = 3`
		`print(float(3))   # = 3.0`
		`print(x ** y)     # = 9`

String	Python Strings are sequences of characters.
	
	String Creation Methods:
	1. Single quotes
	`>>> 'Yes'`
	2. Double quotes
	`>>> "Yes"`
	3. Triple quotes (multi-line)
	`>>> """Yes`
	`    We Can"""`
	4. String method
	`>>> str(5) -- '5'`
	`True`
	5. Concatenation
	`>>> "Ma" + "hatma"`
	`'Mahatma'`
	
	Whitespace chars:
	Newline \n,
	Space \s,
	Tab \t
		`## Indexing and Slicing`
		`s = "The youngest pope was 11 years"`
		`s[0] # 'T'`
		`s[1:3] # 'he'` Slice [::2]
		`s[-3:-1] # 'ar'`
		`s[-3:] # 'ars'` | 1 | 2 | 3 | 4 |
		`x = s.split()` 0 1 2 3
		`x[-2] + " " + x[2] + "s" # '11 popes'`
		
		`## String Methods`
		`y = "   Hello world\t\n   "`
		`y.strip() # Remove Whitespace`
		`"HI".lower() # Lowercase: 'hi'`
		`"hi".upper() # Uppercase: 'HI'`
		`"hello".startswith("he") # True`
		`"hello".endswith("lo") # True`
		`"hello".find("ll") # Match at 2`
		`"cheat".replace("ch", "m") # 'meat'`
		`''.join(["F", "B", "I"]) # 'FBI'`
		`len("hello world") # Length: 15`
		`"ear" in "earth" # True`

Complex Data Structures

Type	Description	Example	Type	Description	Example
List	Stores a sequence of elements. Unlike strings, you can modify list objects (they're *mutable*).	`l = [1, 2, 2]` `print(len(l)) # 3`	Dictionary	Useful data structure for storing (key, value) pairs	`cal = {'apple' : 52, 'banana' : 89,` `       'choco' : 546} # calories`

Adding elements	Add elements to a list with (i) append, (ii) insert, or (iii) list concatenation.	`[1, 2].append(4) # [1, 2, 4]`
		`[1, 4].insert(1,9) # [1, 9, 4]`
		`[1, 2] + [4] # [1, 2, 4]`
			Reading and writing elements	Read and write elements by specifying the key within the brackets. Use the **keys()** and **values()** functions to access all keys and values of the dictionary	`print(cal['apple'] < cal['choco'])`
					`# True`
					`cal['cappu'] = 74`
					`print(cal['banana'] < cal['cappu'])`
					`# False`
					`print('apple' in cal.keys()) # True`
					`print(52 in cal.values())    # True`

Removal	Slow for lists	`[1, 2, 2, 4].remove(1) # [2, 2, 4]`			

Reversing	Reverses list order	`[1, 2, 3].reverse() # [3, 2, 1]`	Dictionary Iteration	You can access the (key, value) pairs of a dictionary with the **items()** method.	`for k, v in cal.items():`
					`    print(k) if v > 500 else ''`
					`# 'choco'`

Sorting	Sorts list using fast Timsort	`[2, 4, 2].sort() # [2, 2, 4]`			

Indexing	Finds the first occurrence of an element & returns index. Slow worst case for whole list traversal.	`[2, 2, 4].index(2)`
		`# index of item 2 is 0`
		`[2, 2, 4].index(2,1)`
		`# index of item 2 after pos 1 is 1`
			Membership operator	Check with the **in** keyword if set, list, or dictionary contains an element. Set membership is faster than list membership.	`basket = {'apple', 'eggs',`
					`          'banana', 'orange'}`
					`print('eggs' in basket)      # True`
					`print('mushroom' in basket) # False`

Stack	Use Python lists via the list operations append() and pop()	`stack = [3]`
		`stack.append(42) # [3, 42]`
		`stack.pop() # 42 (stack: [3])`
		`stack.pop() # 3 (stack: [])`
			List & set comprehension	List comprehension is the concise Python way to create lists. Use brackets plus an expression, followed by a for clause. Close with zero or more for or if clauses. Set comprehension works similar to list comprehension.	`l = ['hi ' + x for x in ['Alice',`
					`'Bob', 'Pete']]`
					`# ['Hi Alice', 'Hi Bob', 'Hi Pete']`
					
					`l2 = [x * y for x in range(3) for y`
					`in range(3) if x>y] # [0, 0, 2]`
					
					`squares = { x**2 for x in [0,2,4]`
					`if x < 4 } # {0, 4}`

Set	An unordered collection of unique elements (*at-most-once*) → fast membership O(1)	`basket = {'apple', 'eggs',`
		`          'banana', 'orange'}`
		`same = set(['apple', 'eggs',`
		`            'banana', 'orange'])`			

312

9.3.14. C/C++ Cheat Sheet

Include Headers
#include <headerfile>

Common Headers
iostream, fstream, math, cctype, string

Namespace
using namespace std;

Data Types
int, char, float, double, void, bool

Comments
// Comment text
/ Multi-line comment text */*

Arithmetic Operators
*+ (Addition), - (Subtraction), * (Multiplication), / (Division), % (Modulus)*

Relational Operators
< (Less Than), <= (Less Than or Equal To),> (Greater Than),
>= (Greather Than or Equal To),== (Equal To),!= (Not Equal To)

Logical Operators
|| (logical OR), && (logical AND), ! (logical NOT)

Pointers
*int *ptr;   //Define pointer*
ptr = &var //ptr set to address of var
*var2 = *ptr //Set var2, to value of var1*

If Else
if(<condition>)
*   { <statement 1>; }*
else
*   { <statement 2>; }*

For Loop
for(<initialize>;<condition>;<update>)
{ <statement>; }

While Loop
while (<condition>)
{ <statement>; }

Do-While Loop
do { <statement>; }
while (<condition>);

Switch Statement
switch(<expression>)
{
case <constant1>:
* <statement sequence 1>;*
* break;*
case <constant2>:
* <statement sequence 2>;*
* break;*

case <constantn+1>:
* <statement sequence n+1>;*
* break;*
[default:
* <statement sequence n>;*
* break;]*
}

Arrays
//New 5 element array
int myArray[5];
//Array index starts at 0
//Access 3rd Element
myArray[2]=var;

I/O Operators
>> //Input Operator
<< //Output Operator
cin >> var1, var2, var3;
cout << "TEXT: " << var1 << endl;
cin.get(char buffer, streamsize num, char delim);*

File I/O
fstream file;
file.open("filename",<file mode constant>);
*   //Reads and Writes like cin and cout*
*   file >> var;*
*   file << "Text: "<< var << endl;*
*   // Read Entire Line*
*   getline (file,line);*
*   //Reading Writing Binary Data*
*   file.read(memory_block, size);*
*   file.write(memory_block, size);*
file.close();

File Mode Constants
ios::in //Opens file for reading
ios::out //Opens file for writing
ios::ate //Seeks the EOF.I/O operations can occur anywhere
ios::app //Causes output to be appended at EOF
ios::trunc //Destroys the previous contents
ios::nocreate //Causes open() to fail if file doesnt already exist
ios::noreplace //Causes open() to fail if file already exists

Function Prototype
<return_data_type> <function_name> (parameter list)
{ body of the function }

Class Prototype
class <class_name>
{
public:
*   //method_prototypes*
protected:
*   //method_prototypes*
private:
*   //method_prototypes*
*   //data_attributes*
};

Structure Prototype
struct <structure_name> {
member_type1 member_name1;
member_type2 member_name2;
} <object_name>;

Accessing Data Structures
//Access member variable from Struct/Class
myStruct.membervar1 = var;
//Call Class Method
myClass.method1(args);
//Pointer to Struct/Class
*myStructType *ptr;*
ptr = &myStruct;
ptr->membervar1 = var;

9.3.15. Classes and Object-Oriented Programming (OOP)

Instantiation: objects are instances of classes, which are created at runtime.
Inheritance: a class (child) may derive its methods and attributes from another (parent).
Polymorphism: a class or function which can inherit or take objects of multiple types.
Method: a function associated with an object.
Attribute: a variable associated with an object.
Encapsulation: restriction of the scope of attributes to e.g. within the class or method.
Metaclass: a class whose instances are classes.
Abstract class: a class whose methods and attributes can be overwritten by its children.

Python example: Note: true private attributes are not available in Python. A more accurate term is 'protected'.

```python
class Animal: pass                              # parent class not implemented

class Dog(Animal):                              # Dog inherits from Animal
    known_owners = ['Ross', 'James']            # class attribute
    def __init__(self, age, **kwargs):          # initialisation and parameters
        self.age = age                          # setting an attribute
    def human_years(self):                      # method
        return self.age * 7                     # referencing an attribute
    @staticmethod                               # static decorator
    def is_hungry(time, last_fed):              # utility method with no self
        return (time.hour - last_fed.hour) > 5
    @classmethod                                # class decorator passes the class
    def create_puppy(cls, age=0):
        return cls(age, puppy=True)             # instantiating with keywords
    @property                                   # property decorator
    def owner(self):
        return self._owner                      # replace with private attribute
    @owner.setter                               # encapsulation of attribute owner
    def owner(self, name):
        if name not in Dog.known_owners:        # referencing a class attribute
            raise ValueError                    # entry validation
        self._owner = name                      # update private (internal) attribute

my_dog = Dog(5)                                 # instantiation, creating an object
print(my_dog.human_years())                     # calling a method

my_puppy = my_dog.create_puppy()                # create a new Dog using the classmethod
while not hasattr(my_dog, 'owner'):             # check if object has an attribute
    try:
        owner_name = input('Who owns this dog? ')   # take input from STDIN
        my_dog.owner = owner_name                   # attempt to set attribute
    except ValueError:                              # blocked due to encapsulation
        print(f'{owner_name} cannot own a dog.')    # simple error to STDOUT
print(f'{my_dog.owner} now owns this dog.')         # print attr once allowed
```

9.3.16. Memory and File Access

9.3.17. Version Control

9.3.18. Unit Testing

9.4. Control Theory

9.4.1. Principles of Classical Control Theory for a Negative Feedback Loop

Laplace Domain: classical control theory performs analysis in the complex frequency domain via the Laplace transform of all time-dependent signals (Section 3.4.12).

For digital control (discrete time), use the Z-transform.

Block Diagram: controllers, systems and observers represented as transfer functions
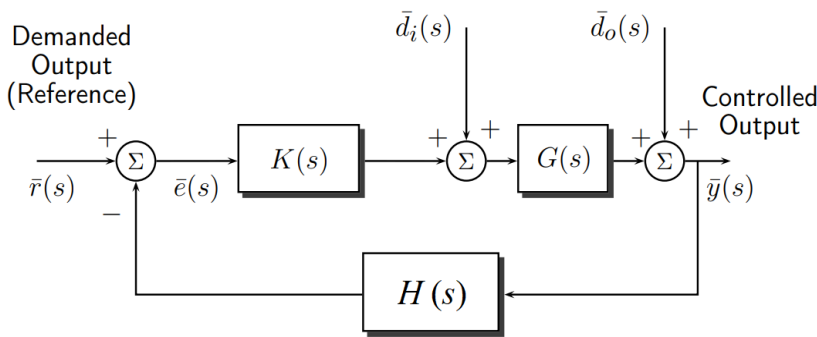
y: output
u: controlled input (computed as $u = K\bar{e}$)
d_i: input disturbance
d_o: output disturbance
e: output error
r: demanded steady-state (set-point) for y
$K(s)$: controller (compensator)
$G(s)$: plant (process dynamics)
$H(s)$: observer (sensors, filters)

- Error signal: $\bar{e}(s) = \bar{r}(s) - \bar{z}(s)$.
- Control signal: $\bar{u}(s) = K(s)\,\bar{e}(s)$
- Feedback signal: $\bar{z}(s) = H(s)\,\bar{y}(s) = H(s)\,G(s)\,K(s)\,\bar{e}(s) = L(s)\,\bar{e}(s)$.

- Open loop transfer function (OLTF, return ratio): $\dfrac{H(s)\,\bar{y}}{\bar{e}} = L(s) = H(s)\,G(s)\,K(s)$.

- Sensitivity function: $\dfrac{\bar{y}}{\bar{d}_o} = S(s) = \dfrac{1}{1+L(s)}$ for $r = d_i = 0$

- Complementary sensitivity function: $T(s) = 1 - S(s) = \dfrac{L(s)}{1+L(s)}$

- Closed-loop transfer function (CLTF): $\dfrac{\bar{y}}{\bar{r}} = \dfrac{G(s)\,K(s)}{1+L(s)}$ for $d_i = d_o = 0$ (same as $T(s)$ if $H = 1$)

Mason's Gain Rule: technique for quickly calculating transfer functions from block diagrams

To find the transfer function G mapping y_{in} to y_{out}, find $G(s) = \dfrac{y_{out}}{y_{in}} = \dfrac{\sum_{paths\,i} G_i \Delta_i}{\Delta}$ where

G_i is the product of TFs along forward paths i from y_{in} to y_{out}, Δ is the 'graph determinant' given by

$\Delta = 1 - \underset{(1)}{\sum L(s)} + \underset{(2)}{\sum L_i(s)\,L_j(s)} - \underset{(3)}{\sum L_i(s)\,L_j(s)\,L_k(s)}$... and Δ_i is Δ for the graph excluding path i.

The summation over '(2)' is the sum over all (i, j) loop gain pairs $L_i L_j$ of non-touching loops, and similarly triples for '(3)' etc.

9.4.2. Analysis of Transfer Functions

In MATLAB, proper rational TFs such as $L(s) = k \dfrac{As^2 + Bs + C}{Ds^3 + Es^2 + Fs + G}$ can be represented using

`sys = tf([A, B, C], [D, E, F, G]);`   where k is a free parameter.

Stability: the 'poles' of the transfer function must be in the left half plane

For single input single output (SISO) systems, the closed-loop system, is stable if the roots of the characteristic equation, $1 + L(s) = 0$, have negative real parts ($\mathrm{Re}(s) < 0$).

From the Routh-Hurwitz stability criteria (see also Section 6.2.11.), the roots of the polynomial equation $a_n s^n + a_{n-1} s^{n-1} + a_{n-2} s^{n-2} + \ldots + a_1 s + a_0 = 0$, with $a_0 > 0$, must all have $\mathrm{Re}(s) < 0$ if:

- for $n = 2$, if and only if all $a_i > 0$;
- for $n = 3$, if and only if all $a_i > 0$ and $a_1 a_2 > a_0 a_3$;
- for $n = 4$, if and only if all $a_i > 0$ and $a_1 a_2 a_3 > a_0 a_3^2 + a_4 a_1^2$.

Frequency Response:

Considering a feedback control system with unit-gain feedback ($H(s) = 1$), then $L(s) = K(s)\, G(s)$. If $e(t) = -\cos \omega t$ then the open-loop response at steady state is $y_{ss}(t) = \overline{A} \cos(\omega t - \varphi)$, where gain $\overline{A} = |L(j\omega)|$, phase $\varphi = \arg L(j\omega)$. In the Laplace domain, $\overline{y}(s) = L(s)\, \overline{e}(s)$.

A pole at $s = \sigma + \omega j$ represents a transfer function factor of $\dfrac{\omega}{(s - \sigma)^2 + \omega^2}$ with ILT $\exp(\sigma t) \sin(\omega t)$. Therefore when $\sigma < 0$, the signal decays and does not contribute to the steady-state signal.

The frequency response from $e(t)$ to $y(t)$ can be represented graphically in terms of $L(s)$:

Bode Plot: two plots, of $|L(s)|$ (gain) and $\arg L(s) = \angle L(s)$ (phase) against real ω where $s = j\omega$.

The Bode plot represents the gain $|L(j\omega)|$ in decibels (dB) as $20 \log_{10} |L(j\omega)|$. The phase $\angle L(j\omega)$ is typically given in degrees. Frequency ω is plotted logarithmically in 'decades'. For rational TFs, the Bode plot can be estimated by hand by adding together the plots for each factor, given in Section 5.4.5. MATLAB command: `bode(sys);`

- **Gain margin:** measures how much the gain of the return ratio can be increased before the closed-loop system becomes unstable.
  The **gain margin** is the value of $|L(j\omega)|$ in dB for the ω at which $\angle L(s) = -180°$.

- **Phase margin:** measures how much phase shift lag can be added to the return ratio before the closed-loop system becomes unstable.
  The **phase margin** is the value of $\angle L(j\omega) - (-180°)$ for the ω at which $20 \log_{10} |L(j\omega)| = 0$.

Nyquist Plot: plot $L(s)$ in the complex plane parameterised by real ω where $s = j\omega$

It is often useful to let $L(s) = k\,g(s)$, where k is the gain and $g(s)$ is the normalised return ratio, and then make a Nyquist plot of $g(s)$ instead. MATLAB command: `nyquist(sys);`

Nyquist stability criterion: for a stable closed-loop system, the full Nyquist plot of $g(s)$, for $s = j\omega$ and $-\infty < \omega < \infty$, should encircle the $(-1\,/\,k,\ 0j)$ point as many times as there are poles of $g(s)$ (i.e. open-loop poles) in the right half of the s-plane. The encirclements, for the path traced by increasing ω, are counted positive in an anticlockwise direction.

Bode's sensitivity integral: $\dfrac{1}{\pi}\displaystyle\int_0^\infty \ln|S(j\omega)|\ d\omega = \dfrac{1}{\pi}\displaystyle\int_0^\infty \ln\left|\dfrac{1}{1 + L(j\omega)}\right|\ d\omega = \sum_k \mathrm{Re}\{p_k\} - \dfrac{1}{2}\lim_{s\to\infty} s\,L(s)$

(sum over the **unstable** poles of $L(s)$: all p_k with $\mathrm{Re}\{p_k\} > 0$)

The integral places constraints on the designer's ability to modify the control system loop-shape by simply re-tuning the parameters in the controller transfer function or by changing its basic form.

- The **gain margin** is the value of $\dfrac{1}{\alpha}$ where $L(j\omega)$ crosses the negative real axis at $s = -\alpha$.
- The **phase margin** is the value of $\angle L(j\omega) - (\text{-}180°)$ for the ω at which $L(j\omega)$ intersects the unit circle.

Nichols Plot: plot $|L(s)|$ in dB against $\angle L(s)$ parameterised by real ω where $s = j\omega$.

The Nichols chart is used in robust control for quantitative feedback theory to assist with loop-shaping. MATLAB: `nichols(sys);`

Root-Locus Plot: trace the poles in the complex plane as components of $L(s)$ are varied

For rational L, let $L(s) = k\,g(s) = k\,\dfrac{(s - z_1)...(s - z_Z)}{(s - p_1)...(s - p_P)}$ (k: controller gain, $g(s)$: normalised CLTF)

The roots of $1 + k\,g(s) = 0$, the closed loop poles, trace loci as k varies from 0 to ∞, starting at the open-loop poles ($k \to 0$) and ending at the open-loop zeros ($k \to \infty$) or at infinite distances. All sections of the real axis with an odd number of poles and zeros to their right are sections of the root locus (even number of poles and zeros to their right if $k < 0$). MATLAB: `rlocus(sys);`

- $P > Z \to$ TF is strictly proper; $P = Z \to$ TF is bi-proper; $P \geq Z \to$ TF is proper; $P < Z \to$ TF is improper.
- At the breakaway points (coincident roots): $\dfrac{dg}{ds} = 0$.
- Angle condition: $\angle g(s) = (2m + 1)\pi$ if $k > 0$; $\angle g(s) = 2m\pi$ if $k < 0$, for integers m.
- Magnitude condition: $|g(s)| = \dfrac{1}{k}$.
- Asymptotes: If $g(s)$ has P poles and Z zeros, the asymptotes of the loci as $k \to \infty$ are straight lines at angles $\dfrac{(2m + 1)\pi}{P - Z}$ to the real axis if $k > 0$ and angles $\dfrac{2m\pi}{P - Z}$ if $k < 0$.

  Their point of intersection σ with the real axis is given by: $\sigma = \dfrac{\sum(\text{poles of } g(s)) - \sum(\text{zeros of } g(s))}{P - Z}$

9.4.3. Bode Diagrams for Common Factors in Rational Transfer Functions

Bode plot for K: (constant gain factor)

- gain is $20 \log_{10} |K|$ for all ω.
- Phase is 0° if $K > 0$; -180° if $K < 0$, for all ω.

Bode plot for s^n: ($n > 0 \rightarrow$ origin zero, differentiator; $n < 0 \rightarrow$ origin pole, integrator)

- gain is a straight line with slope $+20n$ dB/decade, passing 0 dB at $\omega = 1$ rad s^{-1}.
- phase is $90n°$ for all ω.

Bode plots for $1 + Ts$:   Phase reflected if $T < 0$. Gradient of phase at $1/T = 66°$ per decade
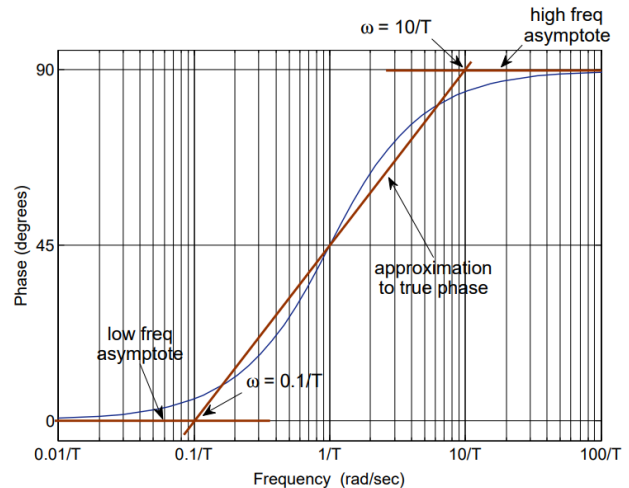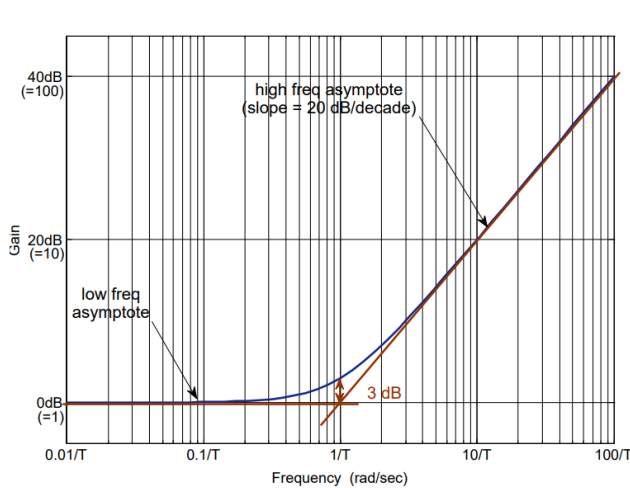
Bode plots for $\dfrac{1}{1 + 2\zeta T s + T^2 s^2}$:
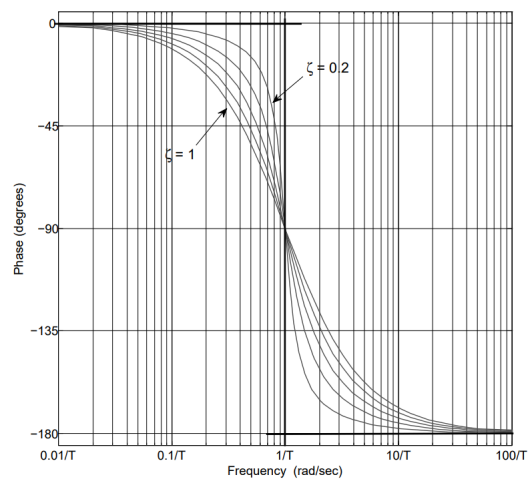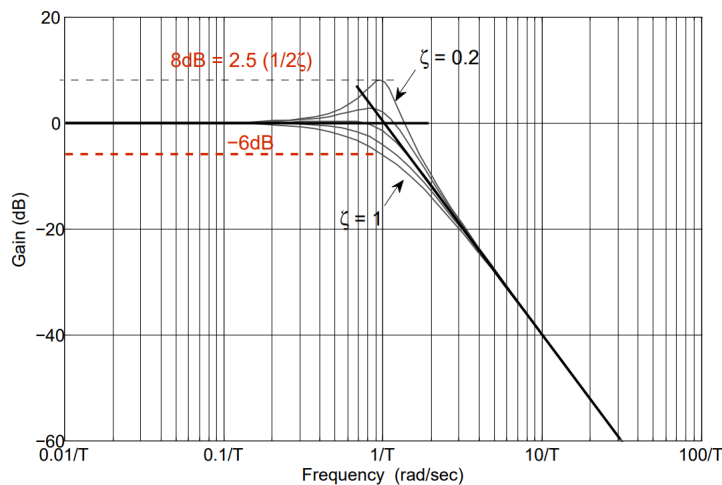
More information on the step response, impulse response and harmonic response of first-order and second-order systems can be found in Section 6.2.

9.4.4. Model Linearisation, Reduction and System Identification

Model Linearisation: approximate a system as linear in the vicinity of an operating point

For a general nonlinear state space model of the form $\dot{\mathbf{x}} = \mathbf{f}(\mathbf{x}, \mathbf{u}, \mathbf{w})$, $\mathbf{y} = \mathbf{g}(\mathbf{x}, \mathbf{v})$, the model can be linearised by substituting $\tilde{\mathbf{x}} = \mathbf{x} - \mathbf{x}_0$, $\tilde{\mathbf{u}} = \mathbf{u} - \mathbf{u}_0$, $\tilde{\mathbf{y}} = \mathbf{y} - \mathbf{y}_0$, ..., $\dot{\tilde{\mathbf{x}}} = \dot{\mathbf{x}}$.
The linearised model is then $\dot{\tilde{\mathbf{x}}} = \mathbf{A}\tilde{\mathbf{x}} + \mathbf{B}\tilde{\mathbf{u}} + \mathbf{B}_{\mathbf{w}}\tilde{\mathbf{w}}$, $\tilde{\mathbf{y}} = \mathbf{C}\tilde{\mathbf{x}} + \mathbf{B}_{\mathbf{v}}\tilde{\mathbf{v}}$
where the state matrices are $\mathbf{A} = \mathbf{J}_{\mathbf{f,x}}$, $\mathbf{B} = \mathbf{J}_{\mathbf{f,u}}$, $\mathbf{B}_{\mathbf{w}} = \mathbf{J}_{\mathbf{f,w}}$, $\mathbf{C} = \mathbf{J}_{\mathbf{g,x}}$, $\mathbf{B}_{\mathbf{v}} = \mathbf{J}_{\mathbf{g,v}}$
(all Jacobians $\mathbf{J}$ evaluated at the operating point to be linearised about, $(\mathbf{x}_0, \mathbf{u}_0, \mathbf{y}_0, \mathbf{w}_0, \mathbf{v}_0)$. It is common to choose $\mathbf{y}_0$ as the set point $\mathbf{r}$, let $\mathbf{w}_0 = \mathbf{v}_0 = \mathbf{0}$, solve $\mathbf{r} = \mathbf{g}(\mathbf{x}_0, \mathbf{v}_0)$ for $\mathbf{x}_0$, then solve $\mathbf{0} = \mathbf{f}(\mathbf{x}_0, \mathbf{u}_0, \mathbf{w}_0)$ for $\mathbf{u}_0$. If $\mathbf{y}$ has lower dimension than $\mathbf{x}$, then optimisation approach is necessary to solve for $\mathbf{x}_0 = \mathbf{x}_0^*$.)
For transfer functions, using $e^{-Ts} \approx 1 - Ts \approx (1 + Ts)^{-1}$, small poles can exchanged with delays.

Model Order Reduction and System Identification: simplify models with high-order derivatives

To approximate a high-order system as an n order system with a time delay (NOPDT), apply Skogestad's Half Rule: for a numerator of the form $K\, e^{-\theta s}$ and a denominator of the form $(1 + T_1 s)(1 + T_2 s)(1 + T_3 s)...$ where $T_1 > T_2 > T_3 > ...$, the new model transfer function is

$$G(s) \approx \frac{K\, e^{-(\theta + \frac{1}{2}T_{n+1})}}{(1 + T_1 s)(1 + T_2 s)...(1 + T_{n-1}s)(1 + (T_n + \frac{1}{2}T_{n+1})s)}$$

i.e. only the n most dominant time constants are retained, with the next most dominant being absorbed half-and-half into the delay and least dominant retained constant. Common process models are

- P1D (first-order plus dead time, FOPDT): $n = 1$ $\quad G(s) = \dfrac{K\, exp(-\theta s)}{1 + T_{p1}s}$

- P2D (second-order plus dead time, SOPDT): $n = 2$ $\quad G(s) = \dfrac{K\, exp(-\theta s)}{(1 + T_{p1}s)(1 + T_{p2}s)}$

- P2DU (2nd-order underdamped plus time delay): $\quad G(s) = \dfrac{K\, exp(-\theta s)}{1 + 2\zeta T_w s + T_w^2 s^2}$

The MATLAB System Identification Toolbox can be used to fit the unknown parameters to given input and output data arrays. For an overdamped response, the following reference curves fit to first-order step responses (r: set point for y)
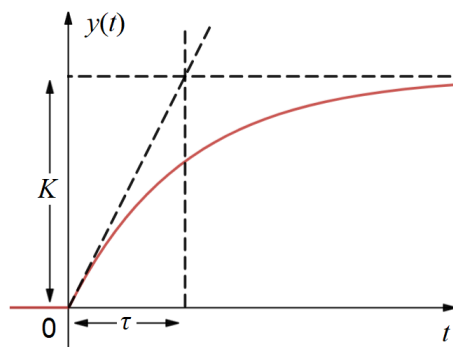
First Order:

$$\frac{y}{r} = \frac{K}{1 + \tau s} \quad \leftrightarrow \quad y = K(1 - e^{-t/\tau})$$
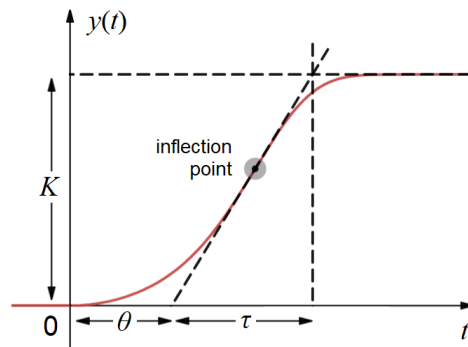
FOPDT (inflection point on t-axis if exact)

$$\frac{y}{r} = \frac{K\, e^{-\theta s}}{1 + \tau s} \quad \leftrightarrow \quad y = K\, H(t - \theta)(1 - e^{-t/\tau})$$

320

9.4.5. Direct Synthesis and Internal Model Methods for Controller Specification

Direct Synthesis: a target (controlled) transfer function is pre-specified and the required controller terms are solved for algebraically. For an open-loop system, let

$\widehat{G}$: return ratio (OLTF) **without** controller, $\dfrac{Y}{Y_{sp}}$: desired CLTF; $\widehat{L} = \dfrac{Y/Y_{sp}}{1 - Y/Y_{sp}}$: desired OLTF

Then the desired controller is given by $G_c = \widehat{L}/\widehat{G}$. Equate the found G_c with the coefficients of a known controller type e.g. PI. Taylor approximation is needed if desired CLTF has a delay (let $e^{-\theta s} = 1 - \theta s$).

Internal Model Control (IMC) Tuning:

(a) Conventional feedback control

Let the internal model $\overline{G}$ be an approximation of the process G, and factor as $\overline{G} = \overline{G}_- \overline{G}_+$ where $\overline{G}_+$ contains all time delays and right-half plane zeros and has unit steady-state gain. Then:

$$ f = \frac{1}{1 + \tau_c s}; \qquad G_c^* = \frac{1}{\overline{G}_-} f; \qquad G_c = \frac{G_c^*}{1 - G_c^* \overline{G}}; \qquad \frac{Y}{Y_{sp}} = \overline{G}_+ f $$

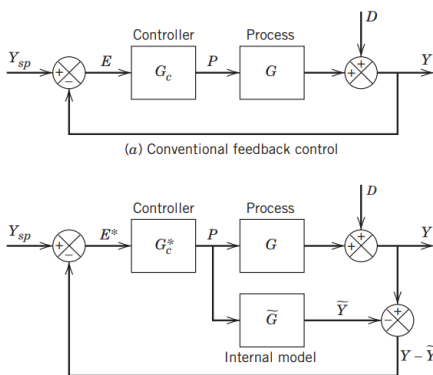(τ_c: desired closed loop time constant, f: unit-gain low-pass filter)
For a given model $\overline{G}$, the table gives the corresponding controller G_c expanded to fit a PI or PID controller $G_c \approx K_c(1 + (\tau_I s)^{-1} + (\tau_D s))$.

Model	$K_c K$	τ_I	τ_D
$\dfrac{K}{\tau s + 1}$	$\dfrac{\tau}{\tau_c}$	τ	—
$\dfrac{K}{(\tau_1 s + 1)(\tau_2 s + 1)}$	$\dfrac{\tau_1 + \tau_2}{\tau_c}$	$\tau_1 + \tau_2$	$\dfrac{\tau_1 \tau_2}{\tau_1 + \tau_2}$
$\dfrac{K}{\tau^2 s^2 + 2\zeta\tau s + 1}$	$\dfrac{2\zeta\tau}{\tau_c}$	$2\zeta\tau$	$\dfrac{\tau}{2\zeta}$
$\dfrac{K(-\beta s + 1)}{\tau^2 s^2 + 2\zeta\tau s + 1}, \ \beta > 0$	$\dfrac{2\zeta\tau}{\tau_c + \beta}$	$2\zeta\tau$	$\dfrac{\tau}{2\zeta}$
$\dfrac{K}{s}$	$\dfrac{2}{\tau_c}$	$2\tau_c$	—
$\dfrac{K}{s(\tau s + 1)}$	$\dfrac{2\tau_c + \tau}{\tau_c^2}$	$2\tau_c + \tau$	$\dfrac{2\tau_c \tau}{2\tau_c + \tau}$
$\dfrac{Ke^{-\theta s}}{\tau s + 1}$	$\dfrac{\tau}{\tau_c + \theta}$	τ	—
$\dfrac{Ke^{-\theta s}}{\tau s + 1}$	$\dfrac{\tau + \dfrac{\theta}{2}}{\tau_c + \dfrac{\theta}{2}}$	$\tau + \dfrac{\theta}{2}$	$\dfrac{\tau\theta}{2\tau + \theta}$
$\dfrac{K(\tau_3 s + 1)e^{-\theta s}}{(\tau_1 s + 1)(\tau_2 s + 1)}$	$\dfrac{\tau_1 + \tau_2 - \tau_3}{\tau_c + \theta}$	$\tau_1 + \tau_2 - \tau_3$	$\dfrac{\tau_1 \tau_2 - (\tau_1 + \tau_2 - \tau_3)\tau_3}{\tau_1 + \tau_2 - \tau_3}$
$\dfrac{K(\tau_3 s + 1)e^{-\theta s}}{\tau^2 s^2 + 2\zeta\tau s + 1}$	$\dfrac{2\zeta\tau - \tau_3}{\tau_c + \theta}$	$2\zeta\tau - \tau_3$	$\dfrac{\tau^2 - (2\zeta\tau - \tau_3)\tau_3}{2\zeta\tau - \tau_3}$
$\dfrac{K(-\tau_3 s + 1)e^{-\theta s}}{(\tau_1 s + 1)(\tau_2 s + 1)}$	$\dfrac{\tau_1 + \tau_2 + \dfrac{\tau_3 \theta}{\tau_c + \tau_3 + \theta}}{\tau_c + \tau_3 + \theta}$	$\tau_1 + \tau_2 + \dfrac{\tau_3 \theta}{\tau_c + \tau_3 + \theta}$	$\dfrac{\tau_3 \theta}{\tau_c + \tau_3 + \theta} + \dfrac{\tau_1 \tau_2}{\tau_1 + \tau_2 + \dfrac{\tau_3 \theta}{\tau_c + \tau_3 + \theta}}$
$\dfrac{K(-\tau_3 s + 1)e^{-\theta s}}{\tau^2 s^2 + 2\zeta\tau s + 1}$	$\dfrac{2\zeta\tau + \dfrac{\tau_3 \theta}{\tau_c + \tau_3 + \theta}}{\tau_c + \tau_3 + \theta}$	$2\zeta\tau + \dfrac{\tau_3 \theta}{\tau_c + \tau_3 + \theta}$	$\dfrac{\tau_3 \theta}{\tau_c + \tau_3 + \theta} + \dfrac{\tau^2}{2\zeta\tau + \dfrac{\tau_3 \theta}{\tau_c + \tau_3 + \theta}}$
$\dfrac{Ke^{-\theta s}}{s}$	$\dfrac{2\tau_c + \theta}{(\tau_c + \theta)^2}$	$2\tau_c + \theta$	—
$\dfrac{Ke^{-\theta s}}{s}$	$\dfrac{2\tau_c + \theta}{\left(\tau_c + \dfrac{\theta}{2}\right)^2}$	$2\tau_c + \theta$	$\dfrac{\tau_c \theta + \dfrac{\theta^2}{4}}{2\tau_c + \theta}$
$\dfrac{Ke^{-\theta s}}{s(\tau s + 1)}$	$\dfrac{2\tau_c + \tau + \theta}{(\tau_c + \theta)^2}$	$2\tau_c + \tau + \theta$	$\dfrac{(2\tau_c + \theta)\tau}{2\tau_c + \tau + \theta}$

Note that for models with integrated elements, the following alternative expression for f is used:

$$ f = \frac{(2\tau_c - C)s + 1}{(\tau_c s + 1)^2} $$

where $\ C = \left.\dfrac{d\widetilde{G}_+}{ds}\right|_{s=0}$

9.4.6. PID Controller Tuning for FOPDT Processes

Controller tuning aims to optimise closed-loop responses by minimising an error criterion:

Absolute error   Squared error   Time-weighted IAE   Error

$$IAE = \int_0^\infty |e(t)|\, dt; \quad ISE = \int_0^\infty e(t)^2\, dt; \quad ITAE = \int_0^\infty t\,|e(t)|\, dt; \quad IE = \int_0^\infty e(t)\, dt.$$

where $e(t) = y(t) - y_{sp}(t)$. Controller: $G_c(s) = K_c\left(1 + \frac{1}{T_i s} + T_d s\right)$. Process: $G(s) = \frac{K\,e^{-\theta s}}{1 + \tau s}$.

The controller terms can be found using the expression $\kappa = A\,(\theta / \tau)^B$, where $\kappa = KK_c$ for P, $\kappa = \tau/T_i$ for I, and $\kappa = \tau/T_d$ for D (θ: pure delay time, τ: first-order time constant).

Controller	Criterion	Term	A	B
PI	IAE	P	0.758	-0.861
		I	1.02	-0.323
	ITAE	P	0.586	-0.916
		I	1.03*	-0.165*
PID	IAE	P	1.086	-0.869
		I	0.740	-0.130
		D	0.348	0.914
	ITAE	P	0.965	-0.855
		I	0.796*	-0.1465*
		D	0.308	0.929

Alternative tuning methods are: *: for ITAE integrators on **set-point** changes, use $Y = A + B(\theta / \tau)$.)

Controller	Ziegler-Nichols (ZN)	Cohen-Coon (CC)
P	$KK_c = (\theta / \tau)^{-1}$	$KK_c = (\theta / \tau)^{-1} + 0.333$
PI	$KK_c = 0.9\,(\theta / \tau)^{-1}$	$KK_c = 0.9\,(\theta / \tau)^{-1} + 0.082$
	$\dfrac{T_i}{\tau} = 3.33\,(\theta / \tau)$	$\dfrac{T_i}{\tau} = \dfrac{3.33\,(\theta / \tau)\left[1 + \frac{1}{11}(\theta / \tau)\right]}{1 + 2.2\,(\theta / \tau)}$
PID	$KK_c = 1.2\,(\theta / \tau)^{-1}$	$KK_c = (\theta / \tau)^{-1} + 0.27$
	$\dfrac{T_i}{\tau} = 2\,(\theta / \tau)$	$\dfrac{T_i}{\tau} = \dfrac{2.5\,(\theta / \tau)\left[1 + \frac{1}{5}(\theta / \tau)\right]}{1 + 0.6\,(\theta / \tau)}$
	$\dfrac{T_d}{\tau} = 0.5\,(\theta / \tau)$	$\dfrac{T_d}{\tau} = \dfrac{0.37\,(\theta / \tau)}{1 + 0.2\,(\theta / \tau)}$

9.4.7. Practical Control Implementations

Feedforward Control: often used to compensate for a known measurable output disturbance.
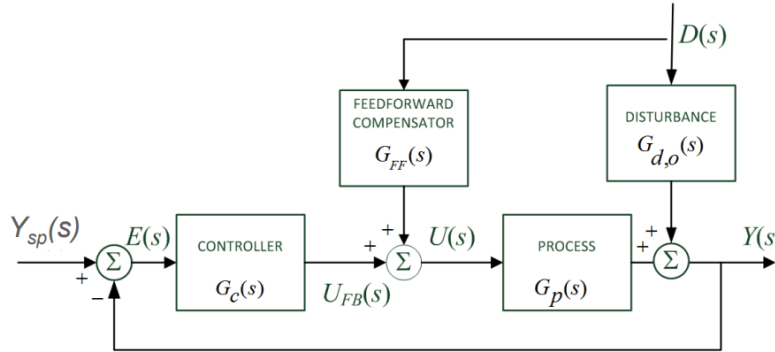
Ideal compensator: $\quad\quad\quad\quad G_{FF} = -\dfrac{G_{d,o}}{G_p}$ $\quad\quad\quad$ (if delays present, requires $\theta_d \geq \theta_p$)

Transfer function: $\quad\quad\quad Y = \dfrac{G_{d,o} + G_p G_{FF}}{1 + G_p G_c}D + \dfrac{G_p G_c}{1 + G_p G_c}Y_{sp}$

If $\theta_d < \theta_p$ then the ideal compensator will not be realisable, and a reduced model in which time delays are neglected (a lead-lag unit) is used, or alternatively ignore all dynamic terms (static compensation).

Loop Shaping and the Lead/Lag Compensator: a generalised PID controller

The loop shaping strategy involves choosing the controller $G_c(s)$ to shape $L(s) = G_c(s)\,G_p(s)$ such that

- $|G_c(j\omega)G_p(j\omega)| \gg 1$ for all $\omega < \omega_c$ i.e. get the benefits of feedback for low frequencies $\rightarrow |S(j\omega)| \ll 1$.
- $|G_c(j\omega)G_p(j\omega)| \ll 1$ for all $\omega > \omega_c$ i.e. suppress high frequency noise $\rightarrow |T(j\omega)| \ll 1$.
- $G_c(j\omega)G_p(j\omega)$ satisfies the Nyquist stability criterion, with adequate gain and phase margins. (ensuring that neither $S(j\omega)$ or $T(j\omega)$ have a large peak in the crossover region in between)

Choose the poles β and zeros α (all are negative) to shape the loop using compensators:

- Phase **lead** compensator: $G_c(s) = \dfrac{s - \alpha_1}{s - \beta_1}$ for $|\alpha_1| < \omega_c < |\beta_1|$, generalised PD controller

The lead compensator has zero gain for $\omega < |\alpha_1|$ and rises to unit gain for $\omega > |\beta_1|$ (bad), but introduces a phase lead for $|\alpha_1| < \omega < |\beta_1|$ (good - but only beneficial if $|\alpha_1| < \omega_c < |\beta_1|$).

- Phase **lag** compensator: $G_c(s) = \dfrac{s - \alpha_2}{s - \beta_2}$ for $|\beta_2| < |\alpha_2| < \omega_c$, reduces to a PI controller if $\beta_2 = 0$.

The lag compensator has unit gain for $\omega < |\beta_2|$ and drops to zero gain for $\omega > |\alpha_2|$ (good), but introduces a phase lag for $|\beta_2| < \omega < |\alpha_2|$ (bad - but ok if $\omega_c \gg |\alpha_2|$).

- Lead-lag compensator: $G_c(s) = \dfrac{(s - \alpha_1)(s - \alpha_2)}{(s - \beta_1)(s - \beta_2)}$ for $|\beta_2| < |\alpha_2| < |\alpha_1| < \omega_c < |\beta_1|$.

Cascade Control: often used to control a secondary variable whose disturbances lead to noise in the main controlled variable.
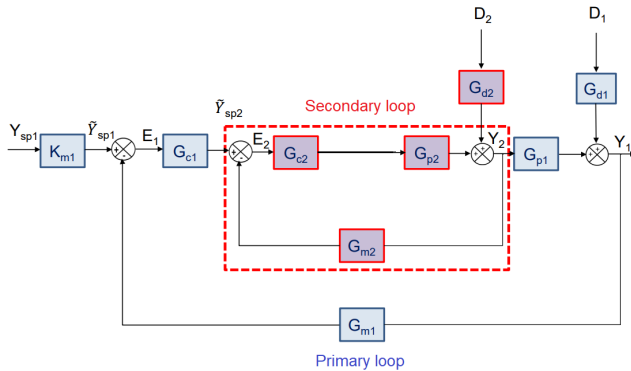
Transfer function (the secondary loop gain is $\dfrac{Y_2}{\bar{Y}_{sp2}} = \dfrac{G_{c2}G_{p2}}{1 + G_{c2}G_{p2}G_{m2}}$):

$$Y_1 = \frac{G_{c1}G_{c2}G_{p1}G_{p2}K_{m1}}{1 + G_{c2}G_{p2}G_{m2} + G_{c1}G_{c2}G_{p1}G_{p2}G_{m1}}Y_{sp}$$
$$+ \frac{G_{d1}\left(1 + G_{c2}G_{p2}G_{m2}\right)}{1 + G_{c2}G_{p2}G_{m2} + G_{c1}G_{c2}G_{p1}G_{p2}G_{m1}}D_1$$
$$+ \frac{G_{p1}G_{d2}}{1 + G_{c2}G_{p2}G_{m2} + G_{c1}G_{c2}G_{p1}G_{p2}G_{m1}}D_2$$

Centralised and Decentralised Control: for MIMO systems, it is the designer's choice whether to make several independent SISO controllers from each output variable to each control input, or to use a single MIMO controller, or to group some of the variables together.

Input and Output Constraints: all physical systems have some limits on the control inputs, reference, state and measured variables, either due to physical constraints (e.g. actuator limits), safety constraints (e.g. temperature/pressure limits) or performance constraints (e.g. overshooting a reference). Optimal operating points (e.g. for optimal profit) are often near or at the limits of one constraint. Most control methods address constraints either a posteriori (e.g. anti-windup methods) or by including constraints in the cost (e.g. H_∞, H_2, L_1).

Computer Control Hardware
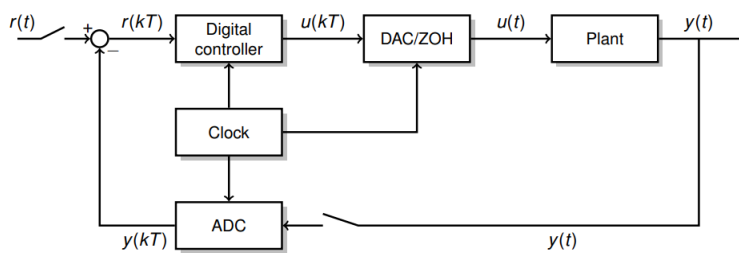
(DAC: digital-to-analog converter, ZOH: zero-order hold, ADC: analog-to-digital converter.

T: sample period, k: sample index $x(kT) = x_k = $ "$x(k)$": discrete signal.)

Full-State Feedback (Pole Placement)

For a controllable state-space model $\{\dot{\mathbf{x}} = \mathbf{Ax} + \mathbf{Bu}, \mathbf{y} = \mathbf{Cx} + \mathbf{Du}\}$, where the control inputs $\mathbf{u}$, state $\mathbf{x}$ and measured output $\mathbf{y}$ may be multivariable (vectors):

- Transfer function from $u \to y$: $\mathbf{G}(s) = \mathbf{C}(s\mathbf{I} - \mathbf{A})^{-1} + \mathbf{D}$
- Full state feedback: controller $\mathbf{u}(s) = -\mathbf{K}(s)\,\mathbf{x}(s)$ $(\mathbf{x}_{SP} = 0) \to \{\dot{\mathbf{x}} = (\mathbf{A} - \mathbf{BK})\mathbf{x},\ \mathbf{y} = (\mathbf{C} - \mathbf{DK})\mathbf{x}\}$
- Closed-loop poles s: $\det[s\mathbf{I} - (\mathbf{A} - \mathbf{BK})] = 0$

If the desired closed-loop poles are at known $s_1, s_2 \dots s_n$, form the desired characteristic equation $P(s) = (s - s_1)(s - s_2)...(s - s_n)$. By writing $\mathbf{K}$ as a matrix of unknowns, the above determinant can be expanded algebraically to match coefficients of the characteristic equations, solving for the required entries in $\mathbf{K}$ to give the desired pole placement.

9.4.10. Practical Examples of MATLAB and Simulink for Control System Design

Using the System Identification Toolbox

```
% import data into arrays from Excel file
data = xlsread('StepTestingData.xlsx');
t = data(:,1);  % first column
u = data(:,2);  % second column
y = data(:,3);  % third column
% subtract initial values of u and y
u = u - u(1);
y = y - y(1);
```
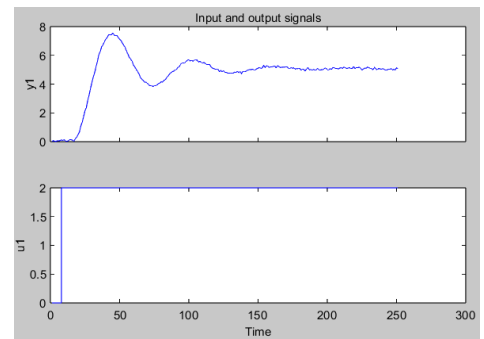

With these variables in the workspace, open Apps > System Identification.

Import time domain data > input u, output y, start time 1, sample time 1. Then:

- View important plots: time plot, data spectra, frequency function (Bode plot)
- Estimate transfer function models: choose # poles, # zeros, delay and estimate. Right-click on tf1 and export to MATLAB to make the `tf1` object in the workspace.
- Estimate state space model: choose delay in u by inspection, model order. Right click on ss1 and export to MATLAB and make the `ss1` object in the workspace.
- Estimate process model: best-fit for a transfer function with given structure.
- Frequency domain analysis: drag a model to the LTI Viewer, right-click in the plot and click Plot types to choose Step response, Impulse response, Linear simulation (another input signal), Bode/Nyquist/Nichols/pole-zero plots.

Tuning a PID controller

Open Apps > PID Tuner and import a plant or transfer function from the workspace.

Choose type PID, add Time domain plot (for a step change) and view the tuned controller responses. When ready, show the parameters and export to a `zpk` object in the workspace.

9.4.11. Optimal Discrete-Time MIMO State Feedback Control

Denote the n states of a system $\mathbf{x}_k \in \mathrm{R}^n$ and m control inputs $\mathbf{u}_k \in \mathrm{R}^m$ at integer time steps $k \in \mathrm{N}$.
For a given initial state $\mathbf{x}_0$ and a set of control inputs $\mathbf{u}_k \in \mathrm{R}^m$, a trajectory $\mathbf{x}_k$ is generated:

● State-space dynamic model: $\mathbf{x}_{k+1} = \mathbf{f}(\mathbf{x}_k, \mathbf{u}_k)$, for $0 \le k \le h$ (h: finite horizon time)

In an optimal control problem, $\mathbf{u}_k$ is to be chosen such that a cost function J is minimised:

● Finite horizon cost function: $J(\mathbf{x}, \mathbf{u}) = \sum_{k=0}^{h-1} c(\mathbf{x}_k, \mathbf{u}_k) + J_h(\mathbf{x}_h)$ (c: stage cost, J_h: terminal cost)

● Objective: find sequence $\mathbf{u}_k{}^*$ such that J is minimised over all $\mathbf{u}_k$.

Discrete-Time Dynamic Programming: allows for a recursive approach to find the optimal $\mathbf{u}_k{}^*$

● Bellman's Principle of Optimality: the optimal $\mathbf{u}^*$ also minimises $\sum_{i=k}^{h-1} c(\mathbf{x}_i, \mathbf{u}_i) + J_h(\mathbf{x}_h)$.

● Value function (cost to go): $V(\mathbf{x}, k) = \min\limits_{\mathbf{u}_k,\ldots,\mathbf{u}_{h-1}} \left(\sum_{i=k}^{h-1} c(\mathbf{x}_i, \mathbf{u}_i) + J_h(\mathbf{x}_h) \right)$, $V(\mathbf{x}, h) = J_h(\mathbf{x})$, $V(\mathbf{x}, 0) = J(\mathbf{x}, \mathbf{u}_k{}^*)$

● Dynamic programming solution: $V(\mathbf{x}, k) = \min\limits_{\mathbf{u}_k} \left(c(\mathbf{x}, \mathbf{u}_k) + V(\mathbf{x}_{k+1}, k+1) \right)$
   (backwards recursion from $k = h$ to $k = 0$) $\mathbf{u}_k^* = \arg\min\limits_{\mathbf{u}} \left(c(\mathbf{x}_k, \mathbf{u}) + V(\mathbf{f}(\mathbf{x}_k, \mathbf{u}), k+1) \right)$

Discrete-Time Finite Horizon Linear Quadratic Regulator (LQR): quadratic cost and $\mathbf{x}_{k+1} = \mathbf{A}\mathbf{x}_k + \mathbf{B}\mathbf{u}_k$

● LQR cost function: $J(\mathbf{x}, \mathbf{u}) = \sum_{k=0}^{h-1} (\mathbf{x}_k{}^\mathsf{T}\mathbf{Q}\mathbf{x}_k + \mathbf{u}_k{}^\mathsf{T}\mathbf{R}\mathbf{u}_k) + \mathbf{x}_h{}^\mathsf{T}\mathbf{X}_h\mathbf{x}_h$ for $\mathbf{Q} \ge 0$, $\mathbf{R} > 0$, $\mathbf{X}_h \ge 0$

   Diagonal entries in $\mathbf{Q}$ and $\mathbf{R}$ represent multipliers on the signal energy $\|\mathbf{x}\|_2^2$ and $\|\mathbf{u}\|_2^2$.

● Minimisation of quadratic forms lemma: $\min\limits_{\mathbf{u}\in\mathbb{R}^m} \begin{bmatrix} \mathbf{x}^\top & \mathbf{u}^\top \end{bmatrix} \begin{bmatrix} \mathbf{Q} & \mathbf{S}^\top \\ \mathbf{S} & \mathbf{R} \end{bmatrix} \begin{bmatrix} \mathbf{x} \\ \mathbf{u} \end{bmatrix} = \mathbf{x}^\mathsf{T}(\mathbf{Q} - \mathbf{S}^\mathsf{T}\mathbf{R}^{-1}\mathbf{S})\mathbf{x},$

   achieved when $\mathbf{u}^* = -\mathbf{R}^{-1}\mathbf{S}\mathbf{x}$. The LHS expands to $\mathbf{x}^\mathsf{T}\mathbf{Q}\mathbf{x} + \mathbf{u}^\mathsf{T}\mathbf{S}\mathbf{x} + \mathbf{x}^\mathsf{T}\mathbf{S}^\mathsf{T}\mathbf{u} + \mathbf{u}^\mathsf{T}\mathbf{R}\mathbf{u}$.

● DP solution: $\mathbf{X}_{k-1} = \mathbf{Q} + \mathbf{A}^\mathsf{T}\mathbf{X}_k\mathbf{A} - \mathbf{A}^\mathsf{T}\mathbf{X}_k\mathbf{B}(\mathbf{R} + \mathbf{B}^\mathsf{T}\mathbf{X}_k\mathbf{B})^{-1} \mathbf{B}^\mathsf{T}\mathbf{X}_k\mathbf{A}$ where $V(\mathbf{x}, k) = \mathbf{x}^\mathsf{T}\mathbf{X}_k\,\mathbf{x}$ for any $0 \le k \le h$.
● Optimal cost: $\mathbf{x}_0{}^\mathsf{T}\mathbf{X}_0\,\mathbf{x}_0$; Optimal controls: $\mathbf{u}_k{}^* = \mathbf{K}\mathbf{x}_k$ where $\mathbf{K} = -(\mathbf{R} + \mathbf{B}^\mathsf{T}\mathbf{X}_{k+1}\mathbf{B})^{-1}\mathbf{B}^\mathsf{T}\mathbf{X}_{k+1}\mathbf{A}$.
● Stability: controller $\mathbf{u}_k{}^* = \mathbf{K}\mathbf{x}_k$ is stabilising if $\rho(\mathbf{A} + \mathbf{B}\mathbf{K}) < 1$. ($\rho$: spectral radius, Section 4.1.7)

Discrete-Time Infinite Horizon LQR: solving $\mathbf{x}_{k+1} = \mathbf{A}\mathbf{x}_k + \mathbf{B}\mathbf{u}_k$ with horizon as $h \to \infty$

● Infinite horizon LQR cost function: $J(\mathbf{x}, \mathbf{u}) = \sum_{k=0}^{\infty} (\mathbf{x}_k{}^\mathsf{T}\mathbf{Q}\mathbf{x}_k + \mathbf{u}_k{}^\mathsf{T}\mathbf{R}\mathbf{u}_k)$

● Optimal cost: $\mathbf{x}_0{}^\mathsf{T}\mathbf{X}_0\,\mathbf{x}_0$; Optimal controls: $\mathbf{u}_k{}^* = -(\mathbf{R} + \mathbf{B}^\mathsf{T}\mathbf{X}\mathbf{B})^{-1}\mathbf{B}^\mathsf{T}\mathbf{X}\mathbf{A}\mathbf{x}_k$
   where $\mathbf{X} = \mathbf{X}^\mathsf{T} > 0$ is the solution to the discrete algebraic Riccati equation (DARE):

$$\mathbf{X} = \mathbf{Q} + \mathbf{A}^\mathsf{T}\mathbf{X}\mathbf{A} - \mathbf{A}^\mathsf{T}\mathbf{X}\mathbf{B}(\mathbf{R} + \mathbf{B}^\mathsf{T}\mathbf{X}\mathbf{B})^{-1}\mathbf{B}^\mathsf{T}\mathbf{X}\mathbf{A}.$$

● To solve the DARE numerically:
  ○ Python: X = scipy.linalg.solve_discrete_are(A, B, Q, R)
  ○ MATLAB: [X, K, L, info] = idare(A, B, Q, R, [], [])

9.4.12. Optimal Continuous-Time MIMO State Feedback Control

Denote the n states of a system $\mathbf{x} \in \mathrm{R}^n$ and m control inputs $\mathbf{u} \in \mathrm{R}^m$ at real time $t \in \mathrm{R}$.
For a given initial state $\mathbf{x}_0 = \mathbf{x}(0)$ and a control input $\mathbf{u} \in \mathrm{R}^m$, a trajectory $\mathbf{x}(t)$ is generated:

- State-space dynamic model: $\dot{\mathbf{x}} = \mathbf{f}(\mathbf{x}, \mathbf{u})$, for $0 \le t \le T$ (T: finite horizon time)

In an optimal control problem, $\mathbf{u}(t)$ is chosen such that a cost function J_h is minimised:

- Finite horizon cost function: $J(\mathbf{x}, \mathbf{u}) = \int\limits_0^T c(\mathbf{x}, \mathbf{u}) \, dt + J_T(\mathbf{x}_T)$ (c: stage cost, J_T: terminal cost)

- Objective: find function $\mathbf{u}^*(t)$ such that J is minimised over all $\mathbf{u}(t)$.

Continuous-Time Dynamic Programming

- Bellman's Principle of Optimality: the optimal $\mathbf{u}^*$ also minimises $\int\limits_t^T c(\mathbf{x}_i, \mathbf{u}_i) \, dt + J_T(\mathbf{x}_T)$.

- Value function (cost to go): $V(\mathbf{x}, t) = \min\limits_{\mathbf{u}} \int_t^T c(\mathbf{x}, \mathbf{u}) \, d\tau + J_T(\mathbf{x}_T)$, $V(\mathbf{x}, T) = J_T(\mathbf{x}), V(\mathbf{x}, 0) = J(\mathbf{x}, \mathbf{u}_k^*)$

- Discretised model: $\mathbf{x}(t + h) = \mathbf{x}(t) + \mathbf{f}(\mathbf{x}(t), \mathbf{u}(t)) \, h + O(h^2)$ and $\int\limits_t^{t+h} c(\mathbf{x}, \mathbf{u}) \, d\tau = c(\mathbf{x}, \mathbf{u}) \, h$

- Solution: $-\dfrac{\partial V}{\partial t} = \min\limits_{\mathbf{u}} \left(c(\mathbf{x}, \mathbf{u}) + \dfrac{\partial V}{\partial \mathbf{x}} \mathbf{f}(\mathbf{x}, \mathbf{u}) \right)$ (boundary condition: $(V(\mathbf{x}, T) = J_T(\mathbf{x}))$

  (the Hamilton-Jacobi-Bellman partial differential equation, HJB PDE).
  The quantity being minimised is the system Hamiltonian H and can also be written as

  $$-\frac{\partial V}{\partial t} = \min\limits_{\mathbf{u}} \ H(\mathbf{x}, \mathbf{u}, \nabla V(\mathbf{x})) \ \text{where} \ H(\mathbf{x}, \mathbf{u}, \lambda) = c(\mathbf{x}, \mathbf{u}) + \lambda^\mathsf{T} \mathbf{f}(\mathbf{x}, \mathbf{u}) \qquad \text{(Pontryagin's principle)}.$$

  λ is the Lagrange multiplier (costate vector for Lagrangian c) for the optimisation problem.

- Optimal cost: $V(\mathbf{x}_0, 0)$; Optimal controls: $\mathbf{u}^*(t) = \arg\min\limits_{\mathbf{u}} \left(c(\mathbf{x}, \mathbf{u}) + \dfrac{\partial V}{\partial \mathbf{x}} \mathbf{f}(\mathbf{x}, \mathbf{u}) \right)$

Continuous-Time Linear Quadratic Regulator (LQR): for a linearised system, $\dot{\mathbf{x}} = \mathbf{A}\mathbf{x} + \mathbf{B}\mathbf{u}$:

- LQR cost function: $J(\mathbf{x}, \mathbf{u}) = \int\limits_0^{t_1} (\mathbf{x}^\mathsf{T}\mathbf{Q}\mathbf{x} + \mathbf{u}^\mathsf{T}\mathbf{R}\mathbf{u}) \, dt + \mathbf{x}^\mathsf{T}\mathbf{X}_{t_1}\mathbf{x}$ for $\mathbf{Q} \ge 0$, $\mathbf{R} > 0$, $\mathbf{X}_{t_1} \ge 0$

- Derivatives of value function: $V(\mathbf{x}, t) = \mathbf{x}^\mathsf{T} \mathbf{X}(t) \mathbf{x} \rightarrow \ \dfrac{\partial V}{\partial \mathbf{x}} = \nabla V = 2\mathbf{x}^\mathsf{T}\mathbf{X}(t); \ \dfrac{\partial V}{\partial t} = \mathbf{x}^\mathsf{T}\dot{\mathbf{X}}(t)\mathbf{x}$

- DP solution: $-\dot{\mathbf{X}}(t) = \mathbf{Q} + \mathbf{X}\mathbf{A} + \mathbf{A}^\mathsf{T}\mathbf{X} - \mathbf{X}\mathbf{B}\mathbf{R}^{-1}\mathbf{B}^\mathsf{T}\mathbf{X}$

- Optimal cost: $\mathbf{x}_0^\mathsf{T}\mathbf{X}(0)\,\mathbf{x}_0$; Optimal controls: $\mathbf{u}^*(t) = -\mathbf{R}^{-1}\mathbf{B}^\mathsf{T}\mathbf{X}(t)\mathbf{x}(t)$.

Continuous-Time Infinite Horizon LQR: solving $\dot{\mathbf{x}} = \mathbf{A}\mathbf{x} + \mathbf{B}\mathbf{u}$ with horizon as $T \to \infty$

- A convenient formulation is to use $\mathbf{z} = \begin{bmatrix} \mathbf{C}\mathbf{x} \\ \mathbf{u} \end{bmatrix}$ (solution $\mathbf{X}$ is constant so 1 less dof)

- Infinite horizon LQR cost function: $J(\mathbf{x}, \mathbf{u}) = \|\mathbf{z}(t)\|_2^2 = \int\limits_0^\infty \mathbf{z}^\mathsf{T}\mathbf{z} \, dt = \int\limits_0^\infty (\mathbf{x}^\mathsf{T}\mathbf{C}^\mathsf{T}\mathbf{C}\mathbf{x} + \mathbf{u}^\mathsf{T}\mathbf{u}) \, dt$ for $\mathbf{C} \ge 0$

- Optimal cost: $\mathbf{x}_0^\mathsf{T}\mathbf{X}(0)\,\mathbf{x}_0$; Optimal controls: $\mathbf{u}^*(t) = -\mathbf{B}^\mathsf{T}\mathbf{X}\mathbf{x}(t)$, where $\mathbf{X}$ is the stabilising solution
  ($\dot{\mathbf{X}}(t) = 0$ as $t \to \infty$, $(\mathbf{A}, \mathbf{B})$ controllable and $(\mathbf{A}, \mathbf{C})$ observable): $\mathbf{X} > 0$ to the control algebraic Riccati
  equation (CARE): $\mathbf{C}^\mathsf{T}\mathbf{C} + \mathbf{X}\mathbf{A} + \mathbf{A}^\mathsf{T}\mathbf{X} - \mathbf{X}\mathbf{B}\mathbf{B}^\mathsf{T}\mathbf{X} = 0$. To solve the CARE numerically:
  - Python: `X = scipy.linalg.solve_continuous_are(A, B, C.T @ C, np.eye(1))`
  - MATLAB: `[X, K, L] = icare(A, [], C'*C, [], [], [], -B*B')`

9.4.13. Multivariable Observable Systems

For a system with internal states $\mathbf{x} \in \mathrm{R}^n$, control inputs $\mathbf{u} \in \mathrm{R}^p$ and measured output $\mathbf{y} \in \mathrm{R}^q$:

- State space dynamic model: $\dot{\mathbf{x}} = \mathbf{A}\mathbf{x} + \mathbf{B}\mathbf{u}$ and $\mathbf{y} = \mathbf{C}\mathbf{x}$ (continuous time)
  ($\mathbf{A} \in \mathrm{R}^{n \times n}$: state transition matrix, $\mathbf{B} \in \mathrm{R}^{n \times p}$: control input matrix,
  $\mathbf{C} \in \mathrm{R}^{q \times n}$: output matrix describing observation)

- Time-domain solution: $\mathbf{x}(t) = \exp(\mathbf{A}(t - t_0))\, \mathbf{x}(t_0) + \int_{t_0}^{t} \exp(\mathbf{A}(t - \tau))\, \mathbf{B}\, \mathbf{u}(\tau)\, \mathrm{d}\tau$

- Transfer function: $\hat{\mathbf{Y}}(s) = \mathbf{G}\,\hat{\mathbf{u}}(s)$ where $\mathbf{G}(s) = \mathbf{C}(s\mathbf{I} - \mathbf{A})^{-1}\mathbf{B}$ (from state space realisation)
- Impulse responses: if $u_j(t) = \delta(t)$ then $y_i(t) = g_{ij}(t)$, where $\mathbf{g}(t) = L^{-1}\{\mathbf{G}(s)\} = \mathbf{C}\exp(\mathbf{A}t)\,\mathbf{B}$
- Open loop stability: all eigenvalues of $\mathbf{A}$ have negative real part, so $\exp(\mathbf{A}t) \to 0$ as $t \to \infty$.
- Closed loop stability: if $\mathbf{u}(t) = \mathbf{K}\mathbf{x}(t)$ then all eigenvalues of $\mathbf{A} + \mathbf{B}\mathbf{K}$ have negative real part.

- Observability: the ability to recover the unique $\mathbf{x}$ from a given $\mathbf{y}$.
  It is said that $(\mathbf{A}, \mathbf{C})$ is 'observable' if: (these two conditions are equivalent)
  ○ the $nq \times n$ observability matrix $[\mathbf{C}, \mathbf{CA}, \mathbf{CA}^2, \mathbf{CA}^3, \dots \mathbf{CA}^{n-1}]^\mathsf{T}$ has rank n
  ○ the observability Gramian $\mathbf{W}_o = \int_0^t \exp(\mathbf{A}^\mathsf{T}\tau)\, \mathbf{C}^\mathsf{T}\mathbf{C}\, \exp(\mathbf{A}\tau)\, \mathrm{d}\tau$, which solves the Lyapunov equation
    $\mathbf{A}^\mathsf{T}\mathbf{W}_o + \mathbf{W}_o\mathbf{A} + \mathbf{C}^\mathsf{T}\mathbf{C} = 0$, is nonsingular for all $t > 0$. To solve this numerically,

  Python: `W_o = scipy.linalg.solve_continuous_lyapunov(A.T, -C.T @ C)`
  MATLAB: `W_o = lyap(A', -C'*C)`

- Controllability: the ability to choose some $\mathbf{u}(t)$ such that $\mathbf{x}$ moves **from** any given initial state $\mathbf{x}_0$
  to all final states $\mathbf{x}(T)$ within a finite time period T.
  It is said that $(\mathbf{A}, \mathbf{B})$ is 'controllable' if: (these two conditions are equivalent)
  ○ the $n \times np$ controllability matrix $[\mathbf{B}, \mathbf{AB}, \mathbf{A}^2\mathbf{B}, \mathbf{A}^3\mathbf{B}, \dots \mathbf{A}^{n-1}\mathbf{B}]$ has rank n
  ○ the controllability Gramian $\mathbf{W}_c = \int_0^t \exp(\mathbf{A}\tau)\, \mathbf{B}\mathbf{B}^\mathsf{T} \exp(\mathbf{A}^\mathsf{T}\tau)\, \mathrm{d}\tau$, which solves the Lyapunov
    equation $\mathbf{A}\mathbf{W}_c + \mathbf{W}_c\mathbf{A}^\mathsf{T} + \mathbf{B}\mathbf{B}^\mathsf{T} = 0$, is nonsingular for all $t > 0$.

- Balanced realisation: a state space model such that the Gramians $\mathbf{W}_o$ and $\mathbf{W}_c$ are equal and
  diagonal matrices. The entries of the diagonal are the Hankel singular values σ_i ordered descending.
  Can be used for model order reduction (retain only top σ).
  Maximum reduction error for order k: $\sigma_{k+1} \leq \|\mathbf{G}(s) - \mathbf{G}_k(s)\|_\infty \leq 2 \sum_{i=k+1}^{n} \sigma_i$

- State transformation: if $\mathbf{x} = \mathbf{T}\mathbf{z}$ then the system $\{\dot{\mathbf{z}} = \mathbf{A'}\mathbf{z} + \mathbf{B'}\mathbf{u}, \mathbf{y} = \mathbf{C'}\mathbf{z}\}$ has $\mathbf{A'} = \mathbf{T}^{-1}\mathbf{A}\mathbf{T}$, $\mathbf{B'} = \mathbf{T}^{-1}\mathbf{B}$,
  $\mathbf{C'} = \mathbf{C}\mathbf{T}$ ($\mathbf{D}$ is unchanged if present). Controllability and observability are conserved under $\mathbf{T}$.
  In modal coordinates, $\mathbf{A'}$ is a block-diagonal matrix.

- Reachability: the ability to choose some $\mathbf{u}(t)$ such that $\mathbf{x}$ moves **to** any given final state $\mathbf{x}(T)$ from all
  initial states $\mathbf{x}_0$ within a finite time period T. Equivalent to controllability for continuous LTI systems,
  but is not always preserved when a system is discretised.

- Stabilisability: a weaker form of reachability.
  It is said that $(\mathbf{A}, \mathbf{B})$ is 'stabilisable' if there exists $\mathbf{K}$ such that $\mathbf{A} + \mathbf{B}\mathbf{K}$ is stable.

- Detectability: a weaker form of observability.
  It is said that $(\mathbf{C}, \mathbf{A})$ is 'detectable' if there exists $\mathbf{L}$ such that $\mathbf{A} + \mathbf{L}\mathbf{C}$ is stable.

9.4.14. Kalman Filter: Linear Quadratic Estimator

For an **observable** system with disturbances realised by a discrete state space model

$$\mathbf{x}_{k+1} = \mathbf{A}\mathbf{x}_k + \mathbf{B}\mathbf{u}_k + \mathbf{w}_k; \qquad \mathbf{y}_k = \mathbf{C}\mathbf{x}_k + \mathbf{v}_k$$

where the noise signals are assumed to be Gaussian with $\mathbf{w}_k \sim \mathrm{N}(\mathbf{0}, \mathbf{Q})$ and with $\mathbf{v}_k \sim \mathrm{N}(\mathbf{0}, \mathbf{R})$, the optimal observer when state feedback is unavailable is achieved with the Kalman filter. ($\mathbf{Q}$: covariance matrix of the process noise, $\mathbf{R}$: covariance matrix of the measurement noise)

The Kalman filter is the optimal Wiener filter (Section 5.4.13), making it highly robust to noise. To compute an optimal estimate $\hat{\mathbf{x}}_{k|k}$ of the state $\mathbf{x}$ at time k using measured $\mathbf{y}_k$:

($\hat{\mathbf{x}}_{k|k-1}$: *a priori* estimate of state $\mathbf{x}_k$, $\mathbf{P}_{k|k-1}$: *a priori* covariance matrix of $\mathbf{x}_k$;
$\hat{\mathbf{x}}_{k|k}$: *a posteriori* estimate of state $\mathbf{x}_k$, $\mathbf{P}_{k|k}$: *a posteriori* covariance matrix of $\mathbf{x}_k$)

- Prediction: $\qquad\qquad\qquad\quad \hat{\mathbf{x}}_{k|k-1} = \mathbf{A}\hat{\mathbf{x}}_{k-1|k-1} + \mathbf{B}\mathbf{u}_{k-1}$ and $\mathbf{P}_{k|k-1} = \mathbf{A}\mathbf{P}_{k-1|k-1}\mathbf{A}^\mathsf{T} + \mathbf{Q}$
- Optimal Kalman Gain: $\qquad \mathbf{K}_k = \mathbf{P}_{k|k-1}\mathbf{C}^\mathsf{T}(\mathbf{C}\mathbf{P}_{k|k-1}\mathbf{C}^\mathsf{T} + \mathbf{R})^{-1}$, then take measurement $\mathbf{y}_k$
- State/uncertainty update: $\hat{\mathbf{x}}_{k|k} = \hat{\mathbf{x}}_{k|k-1} + \mathbf{K}_k(\mathbf{y}_k - \mathbf{C}\hat{\mathbf{x}}_{k|k-1})$ and $\mathbf{P}_{k|k} = (\mathbf{I} - \mathbf{K}_k\mathbf{C})\mathbf{P}_{k|k-1}$

Note that the matrices $\mathbf{A}$, $\mathbf{B}$, $\mathbf{C}$, $\mathbf{Q}$, $\mathbf{R}$ do not need to be constant in time, and should be evaluated at time step k. A model-free version of the Kalman filter is the 'alpha-beta(-gamma) filter', however it is typically less precise and suboptimal.

A common application of the Kalman filter is for filtering kinematics data, where the state space is [position, velocity, acceleration]. The filter is used to combine multiple sensor readings (e.g. attitude, accelerometer, rotary encoder) to produce a reliable state estimate (sensor fusion).

Linear Quadratic Gaussian (LQG) Control: LQR controller with Kalman filter observer

LQG is the optimal control policy for an LQR cost function (Section 9.4.12) when the input and output disturbances are assumed to be Gaussian. This is equivalent to static H_2 optimal control (Section 9.4.16).

9.4.15. Nonlinear Kalman Filters

Extended Kalman Filter (EKF): can use a nonlinear model $\mathbf{x}_{k+1} = \mathbf{f}(\mathbf{x}_k, \mathbf{u}_k) + \mathbf{w}_k$; $\mathbf{y}_k = \mathbf{h}(\mathbf{x}_k) + \mathbf{v}_k$

The Jacobians $\mathbf{J_f}(\hat{\mathbf{x}}_{k-1|k-1}, \mathbf{u}_k) = \partial\mathbf{f}/\partial\mathbf{x}$ and $\mathbf{J_h}(\hat{\mathbf{x}}_{k|k-1}) = \partial\mathbf{h}/\partial\mathbf{x}$ computed to linearise the model about the current state.

- Prediction: $\hat{\mathbf{x}}_{k|k-1} = \mathbf{f}(\hat{\mathbf{x}}_{k-1|k-1}, \mathbf{u}_{k-1})$ and $\mathbf{P}_{k|k-1} = \mathbf{J_f}\mathbf{P}_{k-1|k-1}\mathbf{J_f}^\mathsf{T} + \mathbf{Q}$
- Optimal Kalman Gain: $\mathbf{K}_k = \mathbf{P}_{k|k-1}\mathbf{J_h}^\mathsf{T}(\mathbf{J_h}\mathbf{P}_{k|k-1}\mathbf{J_h}^\mathsf{T} + \mathbf{R})^{-1}$
- State/uncertainty update: $\hat{\mathbf{x}}_{k|k} = \hat{\mathbf{x}}_{k|k-1} + \mathbf{K}_k(\mathbf{y}_k - \mathbf{h}(\hat{\mathbf{x}}_{k|k-1}))$ and $\mathbf{P}_{k|k} = (\mathbf{I} - \mathbf{K}_k\mathbf{J_h})\mathbf{P}_{k|k-1}$

Unscented Kalman Filter (UKF): uses deterministic sampling to estimate covariances

Using an 'unscented transformation', the covariance is propagated correctly, accounting for the nonlinear model. The UKF performs significantly better than the EKF for nonlinear models.

Unscented Transformation: produces a minimal set of sigma points $\mathbf{s}$ that represent $\mathbf{x}$

Using preset parameters (α, β, κ): α is typically set to a small positive number (e.g. $\alpha = 10^{-3}$). $\beta = 2$ is optimal when the distribution of $\mathbf{x}$ is known to be Gaussian. κ is an additional scaling degree of freedom but often $\kappa = 0$ is used. For a given $\hat{\mathbf{x}}$ and $\mathbf{P}$:

- First sigma point and weights: $\mathbf{s}_0 = \hat{\mathbf{x}}$, $W_0^{(a)} = \dfrac{\alpha^2\kappa - L}{\alpha^2\kappa}$, $W_0^{(c)} = W_0^{(a)} + 1 - \alpha^2 + \beta$
- For j in range $[1, ..., L]$: $\mathbf{s}_j = \hat{\mathbf{x}} + \alpha\kappa^{1/2}\mathbf{A}_j$, $\mathbf{s}_{L+j} = \hat{\mathbf{x}} - \alpha\kappa^{1/2}\mathbf{A}_j$
- For j in range $[1, ..., 2L]$: $W_j^{(c)} = W_j^{(a)} = \dfrac{1}{2\alpha^2\kappa}$

The weights are constrained to satisfy $E[x_i] = \sum\limits_{j=0}^{N} W_j^{(a)}s_{j,i}$ and $E[x_i x_l] = \sum\limits_{j=0}^{N} W_j^{(c)}s_{j,i}s_{j,l}$.

(L: dimension of state vector $\mathbf{x}$, $N = 2L + 1$: number of sigma points, $\mathbf{A}_j$: jth column of $\mathbf{A}$, where $\mathbf{P} = \mathbf{A}\mathbf{A}^\mathsf{T}$ is the Cholesky decomposition (Section 4.3.4) of the covariance matrix.)

Unscented Kalman Filter Algorithm:

- Generate a set of sigma points $\mathbf{s}$ and weights ($\mathbf{W}^{(a)}$, $\mathbf{W}^{(c)}$) using $\hat{\mathbf{x}}_{k-1|k-1}$ and $\mathbf{P}_{k-1|k-1}$.
- Propagate: $\mathbf{x}_j = \mathbf{f}(\mathbf{s}_j, \mathbf{u}_{k-1})$ for $0 \leq j \leq 2L$
- Predict: $\hat{\mathbf{x}}_{k|k-1} = \sum\limits_{j=0}^{2L} W_j^{(a)}\mathbf{x}_j$ and $\mathbf{P}_{k|k-1} = \sum\limits_{j=0}^{2L} W_j^{(c)}(\mathbf{x}_j - \hat{\mathbf{x}}_{k|k-1})(\mathbf{x}_j - \hat{\mathbf{x}}_{k|k-1})^\mathsf{T} + \mathbf{Q}$
- Generate a **new** set of sigma points $\mathbf{s}$ and weights ($\mathbf{W}^{(a)}$, $\mathbf{W}^{(c)}$) using $\hat{\mathbf{x}}_{k|k-1}$ and $\mathbf{P}_{k|k-1}$.
- Propagate: $\mathbf{y}_j = \mathbf{h}(\mathbf{s}_j)$ for $0 \leq j \leq 2L$
- Compute $\hat{y} = \sum\limits_{j=0}^{2L} W_j^{(a)}\mathbf{y}_j$, $\hat{\mathbf{S}}_k = \sum\limits_{j=0}^{2L} W_j^{(c)}(\mathbf{y}_j - \hat{y})(\mathbf{y}_j - \hat{y})^\mathsf{T} + \mathbf{R}$, $\mathbf{C_{xy}} = \sum\limits_{j=0}^{2L} W_j^{(c)}(\mathbf{x}_j - \hat{\mathbf{x}}_{k|k-1})(\mathbf{y}_j - \hat{y})^\mathsf{T}$
- Optimal Kalman gain: $\mathbf{K}_k = \mathbf{C_{xz}}\hat{\mathbf{S}}_k^{-1}$ ($\hat{y}$: mean, $\hat{\mathbf{S}}$: covariance, $\mathbf{C_{xy}}$: cross-covariance)
- State/uncertainty update: $\hat{\mathbf{x}}_{k|k} = \hat{\mathbf{x}}_{k|k-1} + \mathbf{K}_k(\mathbf{y}_k - \hat{y})$ and $\mathbf{P}_{k|k} = \mathbf{P}_{k|k-1} - \mathbf{K}_k\hat{\mathbf{S}}_k\mathbf{K}_k^\mathsf{T}$

9.4.16. H_2 Optimal Control

Linear Fractional Transformations (LFTs): useful formulation of noisy MIMO system
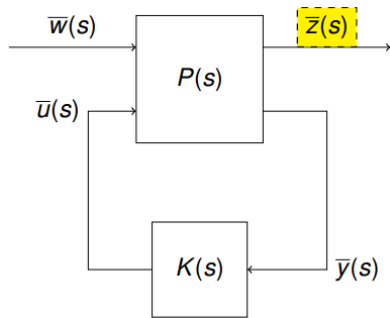
(**w**: input disturbance, **x**: state, **y**: measured output, **z**: performance output, **u**: control input, **P**: generalised plant, **K**: controller)

Lower LFT: TF from **w** to **z**: $\mathcal{F}_l(\mathbf{P}(s), \mathbf{K}(s)) = T_{\widehat{w}(s) \to \widehat{z}(s)}$

From generalised plant: $\mathbf{z} = \mathcal{F}_l(\mathbf{P}(s), \mathbf{K}(s)) \, \mathbf{w} = (\mathbf{P}_{11} + \mathbf{P}_{12}(\mathbf{I} - \mathbf{KP}_{22})^{-1}\mathbf{KP}_{21})\mathbf{w}$

$$\begin{bmatrix} \overline{z}(s) \\ \overline{y}(s) \end{bmatrix} = \underbrace{\begin{bmatrix} P_{11}(s) & P_{12}(s) \\ P_{21}(s) & P_{22}(s) \end{bmatrix}}_{P(s)} \begin{bmatrix} \overline{w}(s) \\ \overline{u}(s) \end{bmatrix}$$

$\overline{z}(s) = P_{11}(s)\overline{w}(s) + P_{12}(s)\overline{u}(s)$
$\overline{y}(s) = P_{21}(s)\overline{w}(s) + P_{22}(s)\overline{u}(s)$
$\overline{u}(s) = K(s)\overline{y}(s).$

For a stable system $\{\dot{\mathbf{x}} = \mathbf{Ax} + \mathbf{Bu}; \mathbf{y} = \mathbf{Cx}\}$ with transfer function $\hat{\mathbf{y}}(s) = \mathbf{G}\hat{\mathbf{u}}(s)$ $(\mathbf{G}(s) = \mathbf{C}(s\mathbf{I} - \mathbf{A})^{-1}\mathbf{B})$:

- System $\mathcal{H}_2$ norm: $\|\mathbf{G}\|_2^2 = \int_{-\infty}^{\infty} \text{trace}\{\mathbf{G}(j\omega)^* \, \mathbf{G}(j\omega)\} \, d\omega = \sum_{i,j} \|G_{ij}\|_2^2 \quad \hat{y}_i(s) = G_{ij}(s)\hat{u}_j(s) \, (\ )$

- Lemma: $\|\mathbf{y}\|_\infty \leq \frac{1}{\sqrt{2\pi}}\|\mathbf{G}\|_2\|\mathbf{u}\|_2$ where $\|\mathbf{y}\|_\infty = \sup\{\mathbf{y}^\mathsf{T}(t)\,\mathbf{y}(t)\}^{1/2}$ and $\|\mathbf{u}\|_2^2 = \int_{-\infty}^{\infty} \mathbf{u}^\mathsf{T}(t)\,\mathbf{u}(t)\,dt$

  Using Parseval's theorem, $\|\mathbf{g}(t)\|_2 = \frac{1}{\sqrt{2\pi}}\|\mathbf{G}(s)\|_2 = (\text{trace}\{\mathbf{B}^\mathsf{T}\mathbf{W}_o\mathbf{B}\})^{1/2}$

  $(\mathbf{g}(t) = L^{-1}\{\mathbf{G}(s)\} = \mathbf{C}\,e^{\mathbf{A}t}\,\mathbf{B}$: impulse response matrix, $\mathbf{W}_o$: observability Gramian)

- The objective of $\mathcal{H}_2$ optimal control is to achieve $\min\limits_{K(s) \text{ stabilising}} \|\mathcal{F}_l(P(s), K(s))\|_2^2$.
- Generalised state space model:

$$\begin{bmatrix} \dot{x} \\ \hline z \\ y \end{bmatrix} = \left[\begin{array}{c|cc} A & [B_1 \ 0] & B_2 \\ \hline \begin{bmatrix} C_1 \\ 0 \end{bmatrix} & \begin{bmatrix} 0 & 0 \\ 0 & 0 \end{bmatrix} & \begin{bmatrix} 0 \\ I \end{bmatrix} \\ C_2 & [0 \ I] & 0 \end{array} \right] \begin{bmatrix} x \\ \hline w \\ u \end{bmatrix} \quad \text{where} \quad \begin{cases} (A, B_2) & \text{controllable} \\ (A, C_1) & \text{observable} \\ (A, B_1) & \text{controllable} \\ (A, C_2) & \text{observable} \end{cases}$$

$\mathcal{H}_2$ Optimal Control with State Feedback: case when $C_2 = \mathbf{I}$

- Optimal $\mathcal{H}_2$ controller: $\mathbf{u} = \mathbf{Fx}$ where $\mathbf{F} = \mathbf{B}_2{}^\mathsf{T}\mathbf{X}$, and $\mathbf{X} > 0$
  is the stabilising solution to the CARE, $\mathbf{0} = \mathbf{XA} + \mathbf{A}^\mathsf{T}\mathbf{X} + \mathbf{C}_1{}^\mathsf{T}\mathbf{C}_1 - \mathbf{XB}_2\mathbf{B}_2{}^\mathsf{T}\mathbf{X}$.
- Optimal H_2 norm: $\min \|\mathcal{F}_l(\mathbf{P}, \mathbf{K})\|_2^2 = 2\pi \times \text{trace}\{\mathbf{B}_1{}^\mathsf{T}\mathbf{XB}_1\}$ (note: MATLAB omits the 2π factor)

H_2 Optimal Control with Output Feedback: assume optimal estimate $\hat{\mathbf{x}} = \mathbf{x}_k$ (Kalman $\to$ LQG problem)

- Optimal $\mathcal{H}_2$ controller: $\left[\begin{array}{c} \dot{x}_k \\ \hline u \end{array} \right] = \left[\begin{array}{c|c} A - B_2F - HC_2 & -H \\ \hline F & 0 \end{array} \right] \left[\begin{array}{c} x_k \\ \hline y \end{array} \right]$

  where $\mathbf{F} = \mathbf{B}_2{}^\mathsf{T}\mathbf{X}$, $\mathbf{H} = \mathbf{YC}_2{}^\mathsf{T}$, and $\mathbf{X} > 0$, $\mathbf{Y} > 0$ are the stabilising solutions to
  $\mathbf{0} = \mathbf{XA} + \mathbf{A}^\mathsf{T}\mathbf{X} + \mathbf{C}_1{}^\mathsf{T}\mathbf{C}_1 - \mathbf{XB}_2\mathbf{B}_2{}^\mathsf{T}\mathbf{X}$ (CARE) and $\mathbf{0} = \mathbf{YA}^\mathsf{T} + \mathbf{AY} + \mathbf{B}_1\mathbf{B}_1{}^\mathsf{T} - \mathbf{YC}_2{}^\mathsf{T}\mathbf{C}_2\mathbf{Y}$ (FARE)
- Optimal $\mathcal{H}_2$ norm: $\min \|\mathcal{F}_l(\mathbf{P}, \mathbf{K})\|_2^2 = 2\pi \times (\text{trace}\{\mathbf{B}_1{}^\mathsf{T}\mathbf{XB}_1\} + \text{trace}\{\mathbf{FYF}^\mathsf{T}\})$

MATLAB: `[K, CL, gamma] = h2syn(P, nmeas, ncont)`

9.4.17. H_∞ Optimal Control

For a stable system $\{\dot{\mathbf{x}} = \mathbf{A}\mathbf{x} + \mathbf{B}\mathbf{u};\ \mathbf{y} = \mathbf{C}\mathbf{x};\ \mathbf{x}(0) = 0\}$ with transfer function $\mathbf{G}(s) = \mathbf{C}(s\mathbf{I} - \mathbf{A})^{-1}\mathbf{B}$:

- System $\mathcal{H}_\infty$ norm: $\|\mathbf{G}\|_\infty = \sup_\omega\{$largest singular value of $\mathbf{G}(j\omega)\} = \sup\{\dfrac{\|y\|_2}{\|u\|_2}\}$

- Boundedness: iff $\mathbf{A}^\mathsf{T}\mathbf{X} + \mathbf{X}\mathbf{A} + \mathbf{C}^\mathsf{T}\mathbf{C} + \gamma^{-2}\mathbf{X}\mathbf{B}\mathbf{B}^\mathsf{T}\mathbf{X} = 0$ (CARE) has a solution $\mathbf{X} > 0$ then $\|\mathbf{G}\|_\infty \leq \gamma$.

With noise, so that $\dot{\mathbf{x}} = \mathbf{A}\mathbf{x} + \mathbf{B}_1\mathbf{w}_1 + \mathbf{B}_2\mathbf{u},\ \ \mathbf{z} = [\mathbf{C}_1\mathbf{x};\ \mathbf{u}]$ and $\mathbf{y} = \mathbf{C}_2\mathbf{x} + \mathbf{w}_2$,

- Objective: find stabilising $\mathbf{K}$ such that $\|\mathcal{F}_l(\mathbf{P}(s), \mathbf{K}(s))\|_\infty \leq \gamma$ ($\mathcal{F}_l$: lower LFT, Section 9.4.12)

- Let the value function be $V = \mathbf{x}^\mathsf{T}\mathbf{X}\mathbf{x}$ for some $\mathbf{X} = \mathbf{X}^\mathsf{T}$. For suitable $\mathbf{X}$,
  - the Riccati equation $\mathbf{A}^\mathsf{T}\mathbf{X} + \mathbf{X}\mathbf{A} + \mathbf{C}_1^\mathsf{T}\mathbf{C}_1 - \mathbf{X}(\mathbf{B}_2\mathbf{B}_2^\mathsf{T} - \gamma^{-2}\mathbf{B}_1\mathbf{B}_1^\mathsf{T})\mathbf{X} = 0$, and
  - $\mathbf{A} - \mathbf{B}_2\mathbf{B}_2^\mathsf{T}\mathbf{X}$ is stable when $\mathbf{u} = -\mathbf{B}_2^\mathsf{T}\mathbf{X}\mathbf{x}$ and $\mathbf{w} = 0$ (**best** disturbance), and
  - $\mathbf{A} - \mathbf{B}_2\mathbf{B}_2^\mathsf{T}\mathbf{X} - \gamma^{-2}\mathbf{B}_1\mathbf{B}_1^\mathsf{T}\mathbf{X}$ is stable when $\mathbf{u} = -\mathbf{B}_2^\mathsf{T}\mathbf{X}\mathbf{x}$ and $\mathbf{w} = \gamma^{-2}[\mathbf{B}_1^\mathsf{T};\ 0]\mathbf{X}\mathbf{x}$ (**worst** disturbance),
  then with state feedback $\mathbf{u} = -\mathbf{B}_2^\mathsf{T}\mathbf{X}\mathbf{x}$, we have $\|\mathbf{z}\|_2^2 \leq \gamma^2\|\mathbf{w}\|_2^2$ so $\|T_{w\to z}\|_\infty \leq \gamma$.
  The smallest γ for which the above Riccati equation has a solution can be found by bisection.

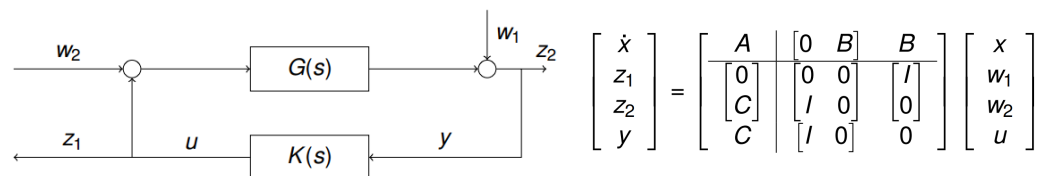### $\mathcal{H}_\infty$ Optimal Control with State Feedback

- Optimal $\mathcal{H}_\infty$ controller: $\mathbf{u} = -\mathbf{F}\mathbf{x}$ where $\mathbf{F} = \mathbf{B}_2^\mathsf{T}\mathbf{X}$, and $\mathbf{X} > 0$ is the stabilising solution to the CARE
  $0 = \mathbf{A}^\mathsf{T}\mathbf{X} + \mathbf{X}\mathbf{A} + \mathbf{C}_1^\mathsf{T}\mathbf{C}_1 - \mathbf{X}(\mathbf{B}_2\mathbf{B}_2^\mathsf{T} - \gamma^{-2}\mathbf{B}_1\mathbf{B}_1^\mathsf{T})\mathbf{X}$

$\mathcal{H}_\infty$ Optimal Control with Output Feedback

- Optimal $\mathcal{H}_\infty$ controller: $\begin{bmatrix} \dot{x}_k \\ \hline u \end{bmatrix} = \left[\begin{array}{c|c} \hat{A} - B_2F - HC_2 & -H \\ \hline F & 0 \end{array} \right] \begin{bmatrix} x_k \\ \hline y \end{bmatrix}$

  where $\mathbf{F} = \mathbf{B}_2^\mathsf{T}\mathbf{X}$, $\mathbf{H} = \mathbf{Y}\mathbf{C}_2^\mathsf{T}$, $\hat{\mathbf{A}} = \mathbf{A} + \gamma^{-2}\mathbf{B}_1\mathbf{B}_1^\mathsf{T}\mathbf{X}$, and $\mathbf{X} > 0$, $\mathbf{Y} > 0$ are the stabilising solutions to
  $0 = \mathbf{X}\mathbf{A} + \mathbf{A}^\mathsf{T}\mathbf{X} + \mathbf{C}_1^\mathsf{T}\mathbf{C}_1 - \mathbf{X}(\mathbf{B}_2\mathbf{B}_2^\mathsf{T} - \gamma^{-2}\mathbf{B}_1\mathbf{B}_1^\mathsf{T})\mathbf{X}$ (CARE) and
  $0 = \mathbf{Y}\hat{\mathbf{A}}^\mathsf{T} + \hat{\mathbf{A}}\mathbf{Y} + \mathbf{B}_1\mathbf{B}_1^\mathsf{T} - \mathbf{Y}(\mathbf{C}_2^\mathsf{T}\mathbf{C}_2 - \gamma^{-2}\mathbf{F}^\mathsf{T}\mathbf{F})\mathbf{Y}$ (FARE)

$\mathcal{H}_\infty$ Loop-Shaping:

$$\begin{bmatrix} \dot{x} \\ z_1 \\ z_2 \\ y \end{bmatrix} = \left[\begin{array}{c|cc|c} A & 0 & B & B \\ \hline 0 & 0 & 0 & I \\ C & I & 0 & 0 \\ \hline C & I & 0 & 0 \end{array} \right] \begin{bmatrix} x \\ w_1 \\ w_2 \\ u \end{bmatrix}$$

- **Loop-Shifting Transformation:** let
  Then $\|\mathcal{F}_l(\mathbf{P}, \mathbf{K})\|_\infty < \gamma \Leftrightarrow \|\mathcal{F}_l(\tilde{\mathbf{P}}, \tilde{\mathbf{K}})\|_\infty < \gamma$ for $\tilde{\mathbf{K}} = \frac{1}{\beta}\mathbf{K}$.

  $$\tilde{P} \triangleq \left[\begin{array}{c|cc|c} A & 0 & \frac{1}{\beta}B & \frac{1}{\beta}B \\ \hline 0 & 0 & I \\ C & & 0 \\ \hline C & I & 0 & 0 \end{array} \right]$$ where $\beta^2 = 1 - \gamma^{-2}$.

- Solution: $\mathbf{X}$ and $\mathbf{Y}$ solve their CARE and FARE above for the transformed system iff
  - $\mathbf{X} = \mathbf{X}^\mathsf{T}$ solves the CARE $\mathbf{X}\mathbf{A} + \mathbf{A}^\mathsf{T}\mathbf{X} + \mathbf{C}^\mathsf{T}\mathbf{C} - \mathbf{X}\mathbf{B}\mathbf{B}^\mathsf{T}\mathbf{X} = 0$ $\to$ $\mathbf{F} = \mathbf{B}_2^\mathsf{T}\mathbf{X}$,
  - $\mathbf{Z} = \mathbf{Z}^\mathsf{T}$ ($\mathbf{A} - \mathbf{Z}\mathbf{C}^\mathsf{T}\mathbf{C}$ stable) solves the FARE $\mathbf{Z}\mathbf{A}^\mathsf{T} + \mathbf{A}\mathbf{Z} + \mathbf{B}\mathbf{B}^\mathsf{T} - \mathbf{Z}\mathbf{C}^\mathsf{T}\mathbf{C}\mathbf{Z} = 0$, and
  - $\gamma^2 - 1 > \max\{\text{eig}\{\mathbf{X}\mathbf{Z}\}\}$.

MATLAB: `K, CL, gamma = hinfsyn(P, nmeas, ncont, gam)`

Mixed-sensitivity H_∞ loop shaping can be achieved by introducing weighting transfer functions at the performance outputs to form an augmented plant $\mathbf{P}$ to be used in synthesis.

Augmented Plant P
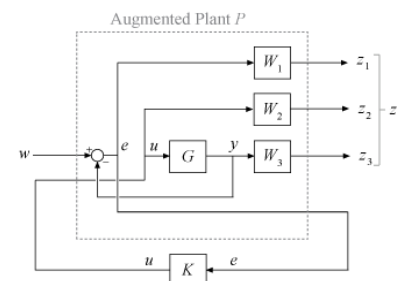
9.4.18. Convex Optimisation and Linear Matrix Inequalities for Control Design

For a stable linear system $\{\dot{\mathbf{x}} = \mathbf{A}\mathbf{x} + \mathbf{B}\mathbf{u}; \mathbf{y} = \mathbf{C}\mathbf{x}\}$ with transfer function $\mathbf{G}(s)$:

- Stability occurs if there exists $\mathbf{X} = \mathbf{X}^\mathsf{T} > 0$ such that $\dot{V} < 0$ for $\mathbf{u} = 0$ (where $V = \mathbf{x}^\mathsf{T}\mathbf{X}\mathbf{x}$)
- Solving $\dot{V} = \mathbf{x}^\mathsf{T}(\mathbf{A}^\mathsf{T}\mathbf{X} + \mathbf{X}\mathbf{A})\mathbf{x} < 0$ is equivalent to finding $\mathbf{X} = \mathbf{X}^\mathsf{T} > 0$ such that $\mathbf{A}^\mathsf{T}\mathbf{X} + \mathbf{X}\mathbf{A} < 0$, which is an LMI in $\mathbf{X}$.

Useful identities:

- **Positive semi-definiteness:** iff $\mathbf{Q} \geq 0$ then $\mathbf{R}^\mathsf{T}\mathbf{Q}\mathbf{R} \geq 0$ for any invertible $\mathbf{R}$.

- **Schur complement:** given $\mathbf{Q} = \mathbf{Q}^\mathsf{T}$ and $\mathbf{R} = \mathbf{R}^\mathsf{T}$ is invertible,

$$\text{iff} \quad \begin{bmatrix} Q & S \\ S^T & R \end{bmatrix} \geq 0 \quad \text{then} \ \ \mathbf{R} \geq 0 \ \ \text{and} \ \ \mathbf{Q} - \mathbf{S}\mathbf{R}^{-1}\mathbf{S}^\mathsf{T} \geq 0$$

- **Kalman-Yakubovich-Popov (KYP) lemma:** given $\gamma > 0$, $(\mathbf{A}, \mathbf{B})$ controllable, $\mathrm{Re}\{\mathrm{eig}(\mathbf{A})\} < 0$,

  iff $\mathbf{P} = \mathbf{P}^\mathsf{T}$ and $\mathbf{Q}$ satisfying $\{\mathbf{A}^\mathsf{T}\mathbf{P} + \mathbf{P}\mathbf{A} + \mathbf{Q}\mathbf{Q}^\mathsf{T}; \mathbf{P}\mathbf{B} - \mathbf{C} = \gamma^{1/2}\mathbf{Q}\}$ exist

  then $\gamma + 2\,\mathrm{Re}\{\mathbf{C}^\mathsf{T}(\mathrm{j}\omega\mathbf{I} - \mathbf{A})^{-1}\mathbf{B}\} \geq 0$

  and $\{\mathbf{x}: \mathbf{x}^\mathsf{T}\mathbf{P}\mathbf{x} = 0\}$ is the unobservable subspace for $(\mathbf{C}, \mathbf{A})$.

For a stabilising feedback controller $\mathbf{u} = \mathbf{K}\mathbf{x}$, let $\mathbf{Y} = \mathbf{X}^{-1}$ and $\mathbf{Z} = \mathbf{K}\mathbf{Y}$ so that the LMI is $\mathbf{Y}\mathbf{A}^\mathsf{T} + \mathbf{Z}^\mathsf{T}\mathbf{B}^\mathsf{T} + \mathbf{A}\mathbf{Y} + \mathbf{B}\mathbf{Z} \leq 0$, which can be solved for $\mathbf{Y}$ and $\mathbf{Z}$; then $\mathbf{X} = \mathbf{Y}^{-1}$ and $\mathbf{K} = \mathbf{Z}\mathbf{X}$.

The **state feedback** $\mathcal{H}_\infty$ **control problem** can also be written in terms of an LMI using the KYP lemma: for $\{\dot{\mathbf{x}} = \mathbf{A}\mathbf{x} + \mathbf{B}\mathbf{u} + \mathbf{B}_\mathbf{w}\mathbf{w}; \mathbf{z} = \mathbf{C}\mathbf{x} + \mathbf{D}\mathbf{u}\}$, find stabilising $\mathbf{u} = \mathbf{K}\mathbf{x}$ to minimise $\|T_{w \to z}\|_\infty \leq \gamma$.

With $\mathbf{Z} = \mathbf{K}\mathbf{Y}$, this translates to solving $\mathrm{d}V/\mathrm{d}t \leq -\mathbf{z}^\mathsf{T}\mathbf{z} + \gamma^2\,\mathbf{w}^\mathsf{T}\mathbf{w}$, represented as an LMI with:

$$\begin{bmatrix} \mathbf{Y}\mathbf{A}^\top + \mathbf{Z}^\top\mathbf{B}^\top + \mathbf{A}\mathbf{Y} + \mathbf{B}\mathbf{Z} & \mathbf{Y}\mathbf{C}^\top + \mathbf{Z}^\top\mathbf{D}^\top & \mathbf{B}_\mathbf{w} \\ \mathbf{C}\mathbf{Y} + \mathbf{D}\mathbf{Z} & -\mathbf{I} & 0 \\ \mathbf{B}_\mathbf{w}{}^\top & 0 & -\gamma^2\mathbf{I} \end{bmatrix} \leq 0$$

Solve for $\mathbf{Y}$ and $\mathbf{Z}$, minimising γ; then $\mathbf{X} := \mathbf{Y}^{-1}$ and $\mathbf{K} = \mathbf{Z}\mathbf{X}$.

The library CVX can be used to solve LMIs, available in Python (`cvxpy`) and MATLAB (`cvx`).

9.4.19. Robust Control

Robust controllers are designed to accommodate uncertainties in plant models, due to e.g. neglecting complex higher order dynamics, manufacturing variations between systems, uncertain driving forces, stochastic noise inputs or drift of the system properties.

Disk Margin: generalised combined gain and phase margin

Enforcing gain/phase margins (Section 9.4.2) allows the inputs to vary in magnitude or phase at critical frequencies without losing closed-loop stability. However, this does **not** guarantee stability against simultaneous variation in gain and phase (even within their respective margins). It also does not guarantee performance across ranges of frequencies.

Gain and phase variation are encapsulated in a complex number $f = |f| \exp(\mathrm{j}\theta)$ ($|f|$: gain multiplier, θ: phase shift). f can be plotted in the complex plane. $f = 1$ represents the original system. The modified loop gain $f L(s)$ is stable if it satisfies the Nyquist stability criterion (Section 9.4.2).

- Stability map: locus of all $f \in \mathbb{C}$ such that $f L(s)$ is stable.
- Disk margin: the radius of the largest circle in the stability map that encloses $z = 1$.

Disk Margin for MIMO Systems:

The 'multi-loop I/O disk margin' is the radius of the largest circle in the stability map

MATLAB: for transfer functions of the plant `K` and controller `C`:

- Disk margins for input variations: `[dmi, mmi] = diskmargin(C*G);`
- Disk margins for output variations: `[dmo, mmo] = diskmargin(G*C);`
- Disk margin for input and output variations: `mmio = diskmargin(G, C);`

Parameter Uncertainty: represent physical parameters as ranges of possible values

MATLAB: uncertain parameters can be defined by e.g. `p = ureal('p', 5, 'percent', 20)`, which defines a variable p having nominal (mean) value 5 and varying by up to $\pm 20\%$.

Robust analysis is then performed with `[stabilityMargin, wcu] = robstab(G_cl, …)`

Robust $\mathcal{H}_\infty$ Control (Mu Synthesis): accounts for uncertainty in model parameters

For imperfect models, the entries of $\mathbf{P}$ are subject to some unknown variation. By minimising $\|\mathcal{F}_l(\mathbf{P}, \mathbf{K})\|_\infty$ (Section 9.4.17) over all possible uncertainties in a given range of models, robust performance is guaranteed. This can be done algorithmically by mu synthesis, in which a D-K iteration scheme runs $\mathcal{H}_\infty$ control design, checks robustness, scales the $\mathcal{H}_\infty$ norm appropriately and recomputes the $\mathcal{H}_\infty$ controller until convergence (μ: structured singular value).

MATLAB: `[K, CLperf] = musyn(P, nmeas, ncont)`

9.4.20. Predictive Control

Predictive control is an alternative approach to optimal control that performs the optimisation on-line (in the loop, at each time step) as opposed to off-line (during setup of the controller).
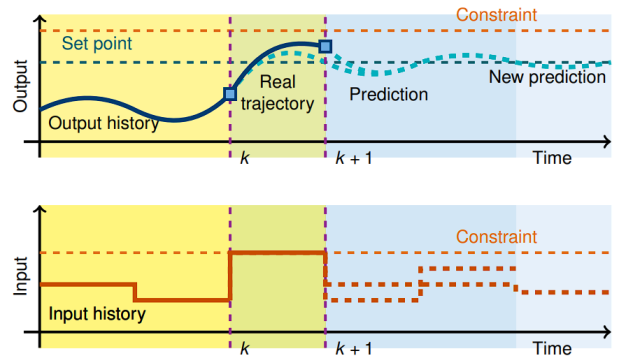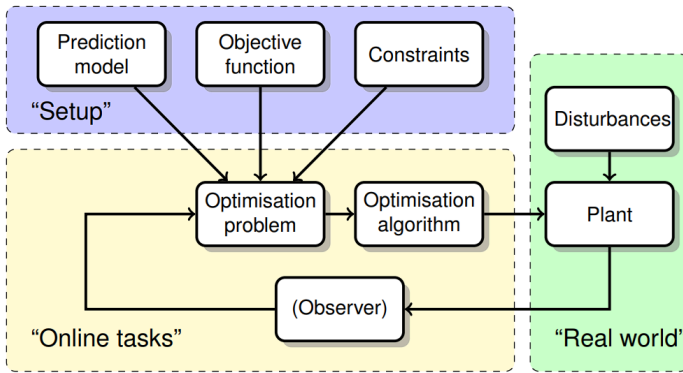
Loop diagram: control input **u** determined by optimisation algorithm

Receding Horizon:
Compute optimal trajectory and take only the **first** control input

Notation: x_i is the **prediction** of $x(k + i)$ (i time steps into the future), given the current state $x_0 = x(k)$, computed optimal controls $u(k + i) = u_i$ for $i \in \{0, 1, ..., N - 1\}$ and state space model $\{x_{i+1} = Ax_i + Bu_i, y_i = Cx_i\}$ (N: finite time horizon for receding horizon control (RHC)).

At a given time step k, starting with a given (or estimated) current state $x_0 = x(k)$, compute a sequence $u = \{u_0, u_1, ..., u_{N-1}\}$ such that:

- the value function $V(x, u) = x_N^T P x_N + \sum\limits_{i=0}^{N-1} (x_i^T Q x_i + u_i^T R u_i)$ is minimised

- subject to the sets of linear constraints $M_i x_i + E_i u_i \leq b_i$ for $i \in \{0, 1, ..., N - 1\}$ and $M_N x_N \leq b_N$.

  If all $M_i = 0$ the constraints are on the admissible inputs **u**.
  If all $E_i = 0$ the constraints are on the admissible states **x**.
  Time-independent constraints (very common simplification) have all $M_i = M$ and all $E_i = E$.

  If no constraints are applied, the controller is linear. Otherwise, the controller is nonlinear.

Once the optimisation problem has been solved for an optimal sequence $u = \{u_0, u_1, ..., u_{N-1}\}$, the controller selects only the first input: $\kappa_{RHC} = u_0 = [I, 0, 0, ... 0]^T [u_0, u_1, ..., u_{N-1}]$.

The closed loop dynamics are then given by $x(k + 1) = Ax(k) + B\kappa_{RHC}(x)$.
The feasible region in state space will often be partitioned into subregions, within which the control law is linear, but is overall piecewise due to differences across subregion boundaries.

9.4.21. Matrix Formulation of the Predictive Control Problem

Define the horizon state vector $\boldsymbol{\theta} = [\mathbf{u}_0; \mathbf{x}_1; \mathbf{u}_1; \mathbf{x}_2; \mathbf{u}_2; \ldots \mathbf{x}_{N-1}; \mathbf{u}_{N-1}; \mathbf{x}_N]$. The optimal control problem can be stated compactly as

$$\text{Find } \boldsymbol{\theta} \text{ to minimise } V(\mathbf{x}, \mathbf{u}) = \mathbf{x}_0^\mathsf{T}\mathbf{Q}\mathbf{x}_0 + \boldsymbol{\theta}^\mathsf{T}\boldsymbol{\Omega}\boldsymbol{\theta} \text{ subject to } \mathbf{G}\boldsymbol{\theta} \le \mathbf{h} \text{ and } \boldsymbol{\Lambda}\boldsymbol{\theta} = \mathbf{b}.$$

where $V(\mathbf{x}, \mathbf{u})$ contains the value function, $\mathbf{G}\boldsymbol{\theta} \le \mathbf{h}$ contains the constraints and $\boldsymbol{\Lambda}\boldsymbol{\theta} = \mathbf{b}$ acts as another constraint containing the prediction model.

Value function: **Prediction** (using state space model):

$$V(\mathbf{x}, \mathbf{u}) = \mathbf{x}_0^\top \mathbf{Q}\mathbf{x}_0 + \underbrace{\begin{bmatrix} u_0 \\ x_1 \\ u_1 \\ x_2 \\ \vdots \\ u_{N-1} \\ x_N \end{bmatrix}}_{\theta}^{T} \underbrace{\begin{bmatrix} R & 0 & 0 & 0 & \cdots & 0 & 0 \\ 0 & Q & 0 & 0 & \cdots & 0 & 0 \\ 0 & 0 & R & 0 & \cdots & 0 & 0 \\ 0 & 0 & 0 & Q & \cdots & 0 & 0 \\ \vdots & \vdots & \vdots & \vdots & \ddots & \vdots & \vdots \\ 0 & 0 & 0 & 0 & \cdots & R & 0 \\ 0 & 0 & 0 & 0 & \cdots & 0 & P \end{bmatrix}}_{\Omega} \underbrace{\begin{bmatrix} u_0 \\ x_1 \\ u_1 \\ x_2 \\ \vdots \\ u_{N-1} \\ x_N \end{bmatrix}}_{\theta}$$

$$\underbrace{\begin{bmatrix} B & -I & 0 & 0 & \cdots & 0 & 0 \\ 0 & A & B & -I & \cdots & 0 & 0 \\ 0 & 0 & 0 & A & \cdots & 0 & 0 \\ \vdots & \vdots & \vdots & \vdots & \ddots & \vdots & \vdots \\ 0 & 0 & 0 & 0 & \cdots & B & -I \end{bmatrix}}_{\Lambda} \underbrace{\begin{bmatrix} u_0 \\ x_1 \\ u_1 \\ x_2 \\ \vdots \\ u_{N-1} \\ x_N \end{bmatrix}}_{\theta} = \underbrace{\begin{bmatrix} -A\,x_0 \\ 0 \\ 0 \\ \vdots \\ 0 \end{bmatrix}}_{b}$$

Constraints: for example, for saturation constraints i.e. $\mathbf{u}_{\text{low}} \le \mathbf{u} \le \mathbf{u}_{\text{high}}$, $\mathbf{y}_{\text{low}} \le \mathbf{y} \le \mathbf{y}_{\text{high}}$, the optimisation problem constraints can be written as $\mathbf{G}\boldsymbol{\theta} \le \mathbf{h}$, where $\boldsymbol{\theta}$ contains $\mathbf{x}$ and $\mathbf{u}$ over the horizon period:

$$M_i \triangleq \begin{bmatrix} 0 \\ 0 \\ -C \\ +C \end{bmatrix}, \quad E_i \triangleq \begin{bmatrix} -I \\ +I \\ 0 \\ 0 \end{bmatrix}, \quad b_i \triangleq \begin{bmatrix} -u_{\text{low}} \\ +u_{\text{high}} \\ -y_{\text{low}} \\ +y_{\text{high}} \end{bmatrix}$$

$$M_N \triangleq \begin{bmatrix} -C \\ +C \end{bmatrix}, \quad b_N \triangleq \begin{bmatrix} -y_{\text{low}} \\ +y_{\text{high}} \end{bmatrix}.$$

$$\underbrace{\begin{bmatrix} E_0 & 0 & 0 & 0 & \cdots & 0 & 0 \\ 0 & M_1 & E_1 & 0 & \cdots & 0 & 0 \\ 0 & 0 & 0 & M_2 & \cdots & 0 & 0 \\ \vdots & \vdots & \vdots & \vdots & \ddots & \vdots & \vdots \\ 0 & 0 & 0 & 0 & \cdots & E_{N-1} & 0 \\ 0 & 0 & 0 & 0 & \cdots & 0 & M_N \end{bmatrix}}_{G} \underbrace{\begin{bmatrix} u_0 \\ x_1 \\ u_1 \\ x_2 \\ \vdots \\ u_{N-1} \\ x_N \end{bmatrix}}_{\theta} \le \underbrace{\begin{bmatrix} -M_0 x_0 + b_0 \\ b_1 \\ b_2 \\ \vdots \\ b_{N-1} \\ b_N \end{bmatrix}}_{b}$$

Quadratic Programming: value function of the form $V(\mathbf{x}, \mathbf{u}) = \frac{1}{2}\boldsymbol{\theta}^\mathsf{T}\mathbf{Q}\boldsymbol{\theta} + \mathbf{c}^\mathsf{T}\boldsymbol{\theta}$ (s.t. $\mathbf{G}\boldsymbol{\theta} \le \mathbf{h}$, $\boldsymbol{\Lambda}\boldsymbol{\theta} = \mathbf{b}$)

If $\mathbf{Q} > 0$ then the optimisation problem is convex, and a unique global minima exists.

QPs such as the above can be solved using the OSQP library, which is available in Python, MATLAB, C/C++, R and Julia. The sparsity of the matrices involved can be exploited (e.g. in Python, use the `scipy.sparse.csc_matrix` class) to improve computation speed. If nonzero set points and disturbances are used, the value function to be used is

$$V(\mathbf{x}, \mathbf{u}) = \sum_{i=0}^{N-1} [(\mathbf{y}_i - \mathbf{y}_s)^\mathsf{T}\mathbf{Q}(\mathbf{y}_i - \mathbf{y}_s) + \Delta\mathbf{u}_i^\mathsf{T}\mathbf{R}\,\Delta\mathbf{u}_i + (\mathbf{x}_N - \mathbf{x}_s)^\mathsf{T}\mathbf{P}(\mathbf{x}_N - \mathbf{x}_s)]$$

$$= \sum_{i=0}^{N-1} [(\mathbf{x}_i - \mathbf{x}_s)^\mathsf{T}(\mathbf{C}^\mathsf{T}\mathbf{Q}\mathbf{C})(\mathbf{x}_i - \mathbf{x}_s) + \Delta\mathbf{u}_i^\mathsf{T}\mathbf{R}\,\Delta\mathbf{u}_i + (\mathbf{x}_N - \mathbf{x}_s)^\mathsf{T}\mathbf{P}(\mathbf{x}_N - \mathbf{x}_s)]$$

where $\Delta\mathbf{u}_i = \mathbf{u}_i - \mathbf{u}_{i-1}$ and $\mathbf{y}_s = \mathbf{C}\mathbf{x}_s$. Let $\mathbf{y}(k) = \mathbf{y}_0 + \mathbf{d}_0$ and $\mathbf{d}_i = \mathbf{d}_0$ (constant disturbance). See the OSQP documentation for an example of the above predictive control QP. Other problems can be cast as QPs:

Piecewise linear constraint: $\min V$ subject to $\max\{\mathbf{e}^\mathsf{T}\boldsymbol{\theta}, \mathbf{f}^\mathsf{T}\boldsymbol{\theta}\} \le \mathbf{b} \to \min V$ subject to $\mathbf{e}^\mathsf{T}\boldsymbol{\theta} \le \mathbf{b}$, $\mathbf{f}^\mathsf{T}\boldsymbol{\theta} \le \mathbf{b}$.

Piecewise linear cost: $\min |\mathbf{c}^\mathsf{T}\boldsymbol{\theta}|$ subject to $\mathbf{G}\boldsymbol{\theta} \le \mathbf{h} \to \min \delta$ subject to $\mathbf{G}\boldsymbol{\theta} \le \mathbf{h}$, $\mathbf{c}^\mathsf{T}\boldsymbol{\theta} - \delta \le 0$, $-\mathbf{c}^\mathsf{T}\boldsymbol{\theta} - \delta \le 0$.

9.4.22. Stability of Constrained Predictive Control

Definitions:

- Set S is **'invariant'** if, for a given system $\mathbf{x}(k+1) = \mathbf{f}(\mathbf{x}(k))$, starting at any $\mathbf{x}(0) \in S$ implies $\mathbf{x}(k) \in S$ for all subsequent k.

- Set S is **'constraint admissible'** if, for a given control law $\mathbf{u} = \boldsymbol{\kappa}(\mathbf{x})$, $(\mathbf{x}, \boldsymbol{\kappa}(\mathbf{x})) \in \{(\mathbf{x}, \mathbf{u}) : \mathbf{Mx} + \mathbf{Eu} \leq \mathbf{b}\}$ for all $\mathbf{x} \in S$.

- The origin is a **'stable'** equilibrium point if, for any $\varepsilon > 0$ there exists $\delta > 0$ such that $\|\mathbf{x}(0)\| < \delta \Rightarrow \|\mathbf{x}(k)\| < \varepsilon$ for all $k > 0$. The origin is 'asymptotically stable' if $\lim_{k \to \infty} \|\mathbf{x}(k)\| = 0$.

- $V : S \to \mathrm{R}$ is a **'Lyapunov function'** if 1) $V(\mathbf{0}) = 0$, 2) $V(\mathbf{x}) > 0$ for all $\mathbf{x} \in S \setminus \mathbf{0}$ and 3) $V(\mathbf{f}(\mathbf{x})) \leq V(\mathbf{x})$ for all $\mathbf{x} \in S$ (in continuous time, condition (3) is instead $dV/dt \leq 0$.)

Conditions for Stability:

Consider the system $\mathbf{x}(k+1) = \mathbf{Ax}(k) + \mathbf{Bu}(k)$ with state and input constraints $\mathbf{Mx} + \mathbf{Eu} \leq \mathbf{b}$. Let $\mathbf{P} > 0$ and $\mathbf{K}$ satisfy $\rho(\mathbf{A} + \mathbf{BK}) < 1$ and $(\mathbf{A} + \mathbf{BK})^{\mathsf{T}}\mathbf{P}(\mathbf{A} + \mathbf{BK}) - \mathbf{P} \leq -\mathbf{Q} - \mathbf{K}^{\mathsf{T}}\mathbf{RK}$. If the terminal constraint $\mathbf{M}_N\mathbf{x}_N \leq \mathbf{b}_N$ is chosen to be a constraint admissible invariant set for the closed loop system $\mathbf{x}(k+1) = (\mathbf{A} + \mathbf{BK})\mathbf{x}(k)$ for some $\mathbf{K}$ and the constrained finite horizon control problem is feasible at time $k = 0$, then it is feasible for all $k \geq 1$ if the control input is given by the receding horizon control law $\mathbf{u}(k) = \mathbf{u}_0^*(\mathbf{x}(k))$, and **the resulting closed loop system is asymptotically stable.**

If there exists a Lyapunov function such that $V(\mathbf{f}(\mathbf{x})) < V(\mathbf{x})$ for all $\mathbf{x} \in S \setminus \mathbf{0}$ then the origin is an asymptotically stable equilibrium point for $\mathbf{x}(k+1) = \mathbf{f}(\mathbf{x}(k))$ with region of attraction S. If S is the whole space and $V(\mathbf{x}) \to \infty$ as $\|\mathbf{x}\| \to \infty$ then it is **globally asymptotically stable**.

For the constrained **infinite horizon** predictive control problem, the value function

$$V(\mathbf{x}, \mathbf{u}) = \sum_{k=0}^{\infty} (\mathbf{x}(k)^{\mathsf{T}}\mathbf{Qx}(k) + \mathbf{u}(k)^{\mathsf{T}}\mathbf{Ru}(k))$$

is to be minimised while obeying constraints for all times k. Let $\mathbf{P} \geq 0$ be the solution to the DARE $\mathbf{P} = \mathbf{Q} + \mathbf{A}^{\mathsf{T}}\mathbf{PA} - \mathbf{A}^{\mathsf{T}}\mathbf{PB}(\mathbf{R} + \mathbf{B}^{\mathsf{T}}\mathbf{PB})^{-1}\mathbf{B}^{\mathsf{T}}\mathbf{PA}$ and let $\mathbf{K} = -(\mathbf{R} + \mathbf{B}^{\mathsf{T}}\mathbf{PB})^{-1}\mathbf{B}^{\mathsf{T}}\mathbf{PA}$. At each time step k, let $\mathbf{x} = \mathbf{x}(k)$ and compute a finite horizon input sequence that minimises the finite horizon cost function

$$V(\mathbf{x}, \mathbf{u}) = \mathbf{x}_N^{\mathsf{T}}\mathbf{Px}_N + \sum_{i=0}^{N-1} (\mathbf{x}_i^{\mathsf{T}}\mathbf{Qx}_i + \mathbf{u}_i^{\mathsf{T}}\mathbf{Ru}_i)$$

where $\mathbf{x}_0 = \mathbf{x}$, $\mathbf{x}_{i+1} = \mathbf{Ax}_i + \mathbf{Bu}_i$, subject to $\mathbf{Mx}_i + \mathbf{Eu}_i \leq \mathbf{b}_i$ and $\mathbf{M}_N\mathbf{x}_N \leq \mathbf{b}_N$ for $i \in \{0, 1, \ldots, N - 1\}$, where the set $\{\mathbf{x} : \mathbf{M}_N\mathbf{x} \leq \mathbf{b}_N\}$ is constraint admissible and invariant for the closed loop system with control law $\mathbf{u}(k) = \mathbf{Kx}(k)$, and apply the control $\mathbf{u}(k) = \mathbf{u}_0^*$. This controller is stable.

9.4.23. Model-Based Reinforcement Learning (RL)

Reinforcement learning is a model-free approach to optimal control i.e. the 'plant' is unknowable. It is most practically useful when the sets of states and control inputs are discrete and **finite**.

At each time step $t \in \{0, 1, 2, ...\}$, the **agent (controller)** takes **actions (inputs)** $a \in \mathcal{A}(s)$ which cause the **environment (plant)** to feed back to the agent with a new **state** $s \in \mathcal{S}$ and a **reward** $r \in \mathcal{R} \subset \mathbb{R}$.

Setup: the random variables $\{S, A, R\}$ are sampled at each iteration (finite Markov decision process, MDP).

- State transition model: $p(s', r \mid s, a) = P(S_{t+1} = s', r_{t+1} = r \mid S_t = s, A_t = a)$.
- Agent policy: $p(a \mid s) = \pi(a \mid s)$, or if deterministic then can be written as $a = \pi(s)$

- Return (discounted reward): $G_t = \sum\limits_{k=t+1}^{T} \gamma^{k-t-1} R_k = R_{t+1} + \gamma R_{t+2} + \gamma^2 R_{t+3} + \ldots + \gamma^{T-t+1} R_T$ $\qquad (0 \le \gamma \le 1)$

  If $\gamma = 1$ then this is an 'episodic' (non-continuing) case, eventually entering a terminal state $s \in \mathcal{S}^+ \subset \mathcal{S}$ at time $t = T$. This indicates the end of an 'episode'.

- Objective: find policy $\pi = \pi^*$ that maximises $E_{\pi^*}[G_t]$ (under policy π^*).
  Optimal policy π^* satisfies $v_{\pi^*}(s) \ge v_\pi(s)$ and $q_{\pi^*}(s, a) \ge q_\pi(s, a)$.

Useful constructs in solving this problem are:

- **Action-value function**: $q_\pi(s, a) = E_\pi[G_t \mid S_t = s, A_t = a]$ $\qquad$ (expected return given current state/action)

- **State-value function**: $v_\pi(s) = E_\pi[G_t \mid S_t = s] = \sum\limits_{a \in A} \pi(a \mid s)\, q_\pi(s, a)$ $\qquad$ (policy weighted average q)

If a model is available (full access to $p(s', r \mid s, a)$), then a DP solution gives the optimal policy, using the Bellman equation (Section 9.4.8).

Since $v_\pi(s) = \sum\limits_{a \in A} \pi(a \mid s)\, q_\pi(s, a)$ and $G_t = R_{t+1} + \gamma G_{t+1} \rightarrow q_\pi(s, a) = \sum\limits_{r \in R} \sum\limits_{s' \in S} p(s', r \mid s, a)\, (r + \gamma v_\pi(s'))$.

Policy Evaluation: iterate the Bellman equations to find the value function of the current policy π

- $v_\pi(s) = \sum\limits_{a \in A} \pi(a \mid s) \sum\limits_{r \in R} \sum\limits_{s' \in S} p(s', r \mid s, a)\, (r + \gamma v_\pi(s'))$ $\qquad$ (Bellman Equation for v)

- $q_\pi(s, a) = \sum\limits_{r \in R} \sum\limits_{s' \in S} p(s', r \mid s, a)\, (r + \gamma \sum\limits_{a \in A} \pi(a \mid s)\, q_\pi(s, a))$ $\qquad$ (Bellman Equation for q)

Policy Improvement: converges to the optimal policy $v_{\pi^*}(s) = \max q_{\pi^*}(s, a)$ over all a

- Using deterministic $a = \pi(s)$, choose the new policy as $\pi'(s) = \arg\max q_\pi(s, a)$ over all a (greedy wrt $v_\pi(s)$).
  By the policy improvement theorem, $v_{\pi'}(s) \ge v_\pi(s)$. $q_\pi(s, a)$ is found from its Bellman Equation.

Policy Iteration: to find $\pi^*(s)$ and $v_{\pi^*}(s)$: compute $\{\pi_0, v_{\pi 0}, \pi_1, v_{\pi 1}, \pi_2, v_{\pi 2}, \ldots \pi^*, v_{\pi^*}\}$.

- Start from an initial policy $\pi_0(s)$, then iterate ... until optimal $\pi^*(s)$ and $v_{\pi^*}(s)$.
  - Use **Policy Evaluation (to convergence)** to find its value $v_{\pi 0}(s)$.
  - Use **Policy Improvement** to find a new policy $\pi_1(s)$.

Value Iteration: same as policy iteration but only using **one step** during the policy evaluation part.

9.4.24 Model-Free Reinforcement Learning (RL)

In model-free RL, the environment model $p(s', r \mid s, a)$ is unavailable, so policy iteration / value iteration cannot be used. Instead, only a finite sample of trajectories $\{S_0, A_0, R_1, S_1, A_1, R_2, S_2, A_2, \ldots, R_T, A_T\}$ is available, found by running a policy through the MDP.

Monte-Carlo Evaluation: given M samples under π, estimate q_π, updating once per episode

Expand the new set of states to include actions as $S_t^{\text{new}} = \{S_t, A_t\}$, so that $v_\pi(s^{\text{new}}) = q_\pi(s, a)$, and the new 'Markov reward process' (MRP) is the trajectory $\{S_0, R_1, S_1, R_2, S_2, \ldots, R_T, S_T\}^{(m)}$ (trajectories $m = 1, 2, \ldots, M$).

The Monte-Carlo estimate is then $V(s) = \mathrm{E}_\pi[G_t \mid S_t = s] \approx \frac{1}{C(s)} \sum_{m=1}^{M} \sum_{\tau=0}^{T_m-1} \mathbf{I}\{s_\tau^{(m)} = s\} \, g_\tau^{(m)}$, or as an update rule:

$$V(s_t^{(m)}) \leftarrow V(s_t^{(m)}) + \alpha(g_t^{(m)} - V(s_t^{(m)}))$$

($g_\tau^{(m)}$: evaluated return, $\mathbf{I} \in \{0, 1\}$: indicator, $C(s)$: number of times state s visited overall, α: step size hyperparameter replacing $1/C(s_t^{(m)})$ in constant-MC)

Monte-Carlo Control: allow for some exploration instead of greedily optimising q_π

- ε-greedy policy: with probability ε, act randomly; else, choose a to optimise q_π.

Off-Policy Method:

Monte-Carlo Exploring Starts:

Simulating an Episode

Initialisation: at $t = 0$, let $\pi(a \mid s)$ be uniform across all $a \in \mathcal{A}(s)$ (random action) and let $p_0(s)$ be uniform across all $s \in \mathcal{S}$ (random starting state).

Iteration:
- Draw from $p_0(s)$ to find the starting state s.
- Draw from $\pi(a \mid s)$ to find the action a.
- Draw from $p(s', r \mid s, a)$ to find the next state s' and reward r.

This generates a trajectory of $\{s_0, a_0, r_1, s_1, a_1, r_2, s_2, a_2, r_3, s_3, a_3, \ldots r_{T-1}, s_{T-1}, a_{T-1}, r_T, s_T\}^{(m)}$

The objective is to use a policy that maximises $g_0 = r_1 + \gamma r_2 + \gamma^2 r_3 + \ldots \gamma^{T-1} r_T$.

9.4.30. Practical Examples of Control System Implementations

Example 1: LSTM-based MPC for a corn-to-sugar process

Chemical engineering applications operate on 'slower' time scales than mechanical systems so the computational complexity of using neural network models is less important.

Reference: Meng *et al*. RNN-LSTM-Based Model Predictive Control for a Corn-to-Sugar Process. Processes 2023, 11, 1080.

Example 2: 3D Kinematics Data Fusion with a Mahony Filter

A magnetic and inertial measurement unit (MIMU) consists of a 3-axis MEMS gyroscope, accelerometer and magnetometer. MIMUs are widely used in many applications of attitude determination (e.g. human motion tracking, unmanned aerial vehicles (UAV), mobile navigation).

An embedded MEMS chip contains an on-board 3-axis accelerometer, gyroscope and magnetometer to measure acceleration, attitude (orientation) and magnetic field strength

Example 3: Optimal Control of an Insulin Pump with a Glucose Biosensor

Robust H_∞ Glucose Control in Diabetes Using a Physiological Model

Example 4: Optimal Control of VTOL Drone

State variables: $\mathbf{x} = [x_1, x_2, x_3, x_4, x_5, x_6]$ (x_1: yaw angle, x_2: yaw rate, x_3: pitch angle, x_4: pitch rate, x_5: roll angle, x_6: roll rate)

Control variables: $\mathbf{u} = [u_1, u_2, u_3]$ (u_1: yawing torque, u_2: pitching torque, u_3: rolling torque)

Output variables: $\mathbf{y} = [y_1, y_2, y_3]$ (y_1: yaw angle, y_2: pitch angle, y_3: roll angle)

P10. ASTROPHYSICS AND COSMOLOGY

10.1. Aerospace Engineering and Orbital Mechanics

10.1.1. Ideal (Tsiolkovsky) Rocket Equation and Specific Impulse

The maximum possible delta-v with no drag is given by

$$\Delta v = v_{\mathrm{e}} \ln \frac{m_0}{m_f} = I_{\mathrm{sp}} g_0 \ln \frac{m_0}{m_f},$$

($v_e = I_{sp} g_0$: effective exhaust velocity (assumed constant), I_{sp}: specific impulse (dimensions of time), g_0: standard surface gravity = 9.81 ms^{-2}, m_0: wet mass (initial), m_f: dry mass.)

Typical values of I_{sp} are given below:

Propulsion Performance
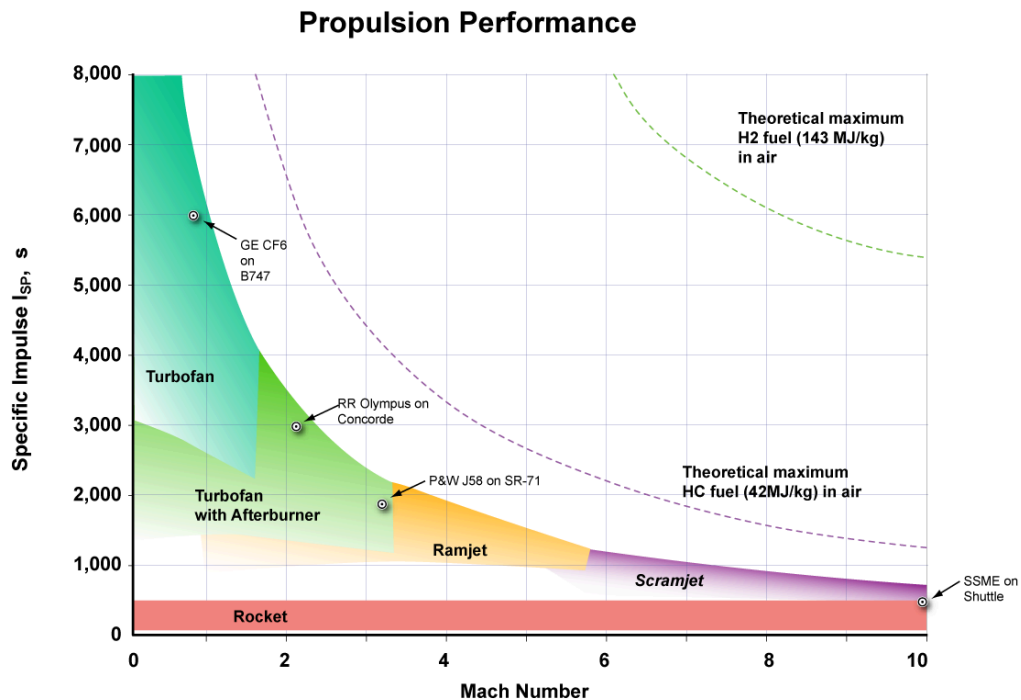
10.1.2. Breguet Range Equation for Aeronautical Vehicles

10.1.3. Kinematics and Geometry of Elliptical Orbits

Satellites in a central gravitational potential follow trajectories of conic sections
(circle: $e = 0$, ellipse: $0 < e < 1$, parabola: $e = 1$, hyperbola, $e > 1$), with the central body (e.g. a planet's COM) as one of its foci. Long-range, zero-drag projectile motion also follows this type of trajectory.

Circular Orbits: satellite maintains a constant distance above the primary.

Centripetal-gravitational force balance: $v = \sqrt{\mu/r}$ (v: satellite speed, r: radius)

Geosynchronous orbit: $r^3 = \dfrac{\mu P^2}{4\pi^2}$ (P: rotational period of primary)

Elliptical Orbits: satellite follows an ellipse with one focus at the primary's COM.
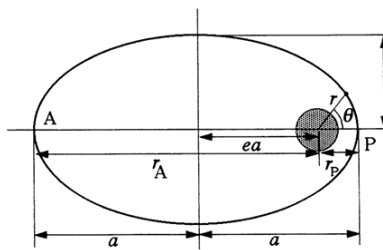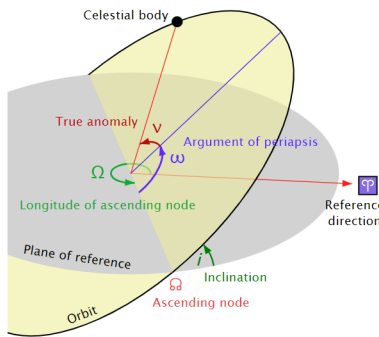
Polar equation: $\dfrac{l}{r} = 1 + e \cos \theta$

where $\dfrac{1}{l} = \dfrac{a}{b^2} = \dfrac{GM}{h^2}$ and $e^2 = 1 - \left(\dfrac{b}{a}\right)^2$.

Periapsis: $\theta = 0 \rightarrow r_P = (1 - e)a$
Apoapsis: $\theta = \pi \rightarrow r_P = (1 + e)a$

(a: semi-major axis, e: eccentricity, i: inclination, ω: argument of periapsis, T: time of periapsis passage, Ω: celestial longitude of ascending node, v: true anomaly, P: orbital period, N_1: ascending node, N_2: descending node, $\mu = GM$: gravitational parameter, γ: zenith angle (between $\mathbf{r}$ and $\mathbf{v}$), $h = rv \sin \gamma$: specific angular momentum)

Kepler's third law: P^2 is proportional to a^3; specifically, $P^2 = \dfrac{4\pi^2}{G(M + m)}a^3$.

Launch of a Space Vehicle: given a vehicle entering free-fall after burnout at state $\{r_0, v_0, \gamma_0\}$:

Apoapsis and Periapsis: $\dfrac{r_{A,P}}{r_0} = \dfrac{-C \pm \sqrt{C^2 + 4(1 - C) \sin^2 \gamma_0}}{2(1 - C)}$ where $C = \dfrac{2\mu}{hv_0} = \dfrac{2GM}{r_0 v_0^2}$.

Eccentricity: $e^2 = \left(\dfrac{hv_0}{\mu} - 1\right)^2 \cos^2 \phi + \sin^2 \phi$ where $\phi = \dfrac{\pi}{2} - \gamma$ (flight path angle).

True anomaly: $\tan v = \dfrac{\sin \gamma_0 \cos \gamma_0}{\sin^2 \gamma_0 - \dfrac{\mu}{hv_0}}$.   Semi-major axis: $\dfrac{1}{a} = \dfrac{2}{r} - \dfrac{v^2}{\mu}$ (vis-viva equation)

Termination launch at apogee/perigee ($\gamma = 90°$) results in minimum propellant consumption.

Given β, δ and λ_2: $\tan l = \dfrac{\tan \delta}{\cos \beta}$;
$\cos i = \cos \delta \sin \beta$; $\omega = l - v$;
$\tan \Delta\lambda = \sin \delta \tan \beta$; $\lambda_1 = \lambda_2 - \Delta\lambda$
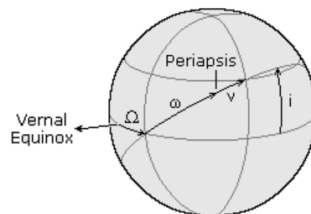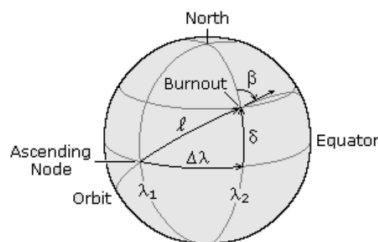
(β: azimuth heading, δ: geocentric latitude / declination, $\Delta\lambda$: angular distance between ascending node and burnout point in equatorial plane, λ_1: geographic longitude of ascending node, λ_2: geographic longitude of burnout)

10.1.4. Time Evolution of an Orbit

Given an initial state $\mathbf{r}_0 = (r_0, \theta_0)$ and $\mathbf{v}_0 = (v_{r0}, v_{t0})$ (in 2D polar coordinates), the state at a time Δt later can be found using the methods below.

$$r = \frac{h^2}{\mu} \frac{1}{1 + \left(\frac{h^2}{\mu r_0} - 1\right)\cos\Delta\theta - \frac{h v_{r0}}{\mu}\sin\Delta\theta}.$$
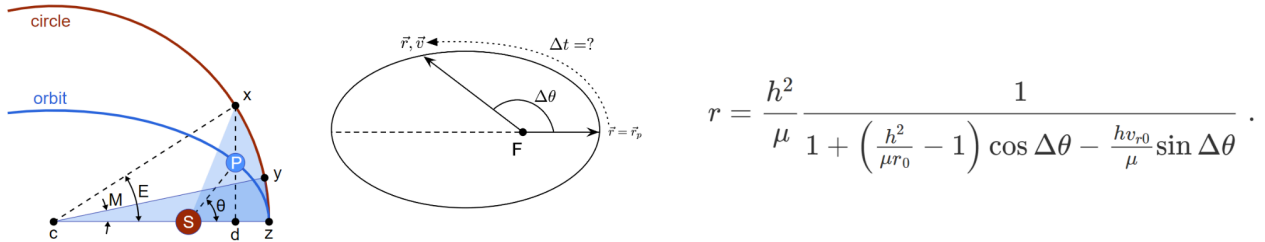
Lagrange coefficients: defined such that $\vec{r} = f\vec{r}_0 + g\vec{v}_0$ and $\vec{v} = \dot{f}\vec{r}_0 + \dot{g}\vec{v}_0$:

$$f = 1 - \frac{\mu r}{h^2}(1 - \cos\Delta\theta)$$

$$\dot{f} = \frac{\mu}{h}\frac{1 - \cos\Delta\theta}{\sin\Delta\theta}\left[\frac{\mu}{h^2}(1 - \cos\Delta\theta) - \frac{1}{r_0} - \frac{1}{r}\right]$$

$$g = \frac{r r_0}{h}\sin\Delta\theta$$

$$\dot{g} = 1 - \frac{\mu r_0}{h^2}(1 - \cos\Delta\theta) , \qquad f\dot{g} - g\dot{f} = 1$$

Kepler problems: given change in true anomaly $\Delta\theta$, find flight time Δt.
(M_e: mean anomaly, E: eccentric anomaly)

$$\int_{\theta_0 = 0}^{\theta = \Delta\theta} \left(\frac{1}{1 + e\cos\theta}\right)^2 d\theta = \int_0^t \frac{\mu^2}{h^3} dt$$

$$\frac{2\pi}{T} t = M_e = E - e\sin E$$

$$\tan\frac{E}{2} = \sqrt{\frac{1 - e}{1 + e}}\tan\frac{\Delta\theta}{2} ,$$

Inverse Kepler problems: given travel time Δt, find the change in true anomaly $\Delta\theta$.

The equation above has no closed form in E (it is transcendental) so must be solved numerically. To help with numerical stability in this calculation, the Universal variable method is used:

Universal anomaly: $\dot{\chi} \equiv \dfrac{\sqrt{\mu}}{r}$ (the Sundman transformation; χ_0: initial guess (Chobotov approximation))

Kepler's equation:
$$\sqrt{\mu}\Delta t = \frac{r_0 v_{r0}}{\sqrt{\mu}}\chi^2 C\left(\alpha\chi^2\right) + (1 - \alpha r_0)\chi^3 S\left(\alpha\chi^2\right) + r_0\chi ,$$
$$\alpha = \frac{1}{a} = \frac{2}{r_0} - \frac{v_0^2}{\mu} , \qquad z = \alpha\chi^2 . \qquad \chi_0 = \frac{\sqrt{\mu}}{|a|}\Delta t .$$

Stumpff functions:
$$S(x) = \begin{cases} (\sqrt{x} - \sin(\sqrt{x}))/\sqrt{x^3} & \text{if } x > 0 \\ 1/6 & \text{if } x = 0 , \\ (\sinh(\sqrt{-x}) - \sqrt{-x})/\sqrt{(-x)^3} & \text{if } x < 0 \end{cases} \quad C(x) = \begin{cases} (1 - \cos\sqrt{x})/x & \text{if } x > 0 \\ 1/2 & \text{if } x = 0 , \\ (1 - \cosh\sqrt{-x})/x & \text{if } x < 0 \end{cases} \quad \begin{array}{l} S'(z) = \frac{1}{2z}(C - 3S) \\ C'(z) = \frac{1}{2z}(1 - 2C - zS) \end{array}$$

Lagrange coefficients:
$$f = 1 - \frac{\chi^2}{r_0}C\left(\alpha\chi^2\right)$$
$$g = \Delta t - \frac{1}{\sqrt{\mu}}\chi^3 S\left(\alpha\chi^2\right)$$
$$\dot{f} = \frac{\sqrt{\mu}}{r r_0}\left[\alpha\chi^3 S\left(\alpha\chi^2\right) - \chi\right]$$
$$\dot{g} = 1 - \frac{\chi^2}{r}C\left(\alpha\chi^2\right)$$
$$\vec{r} = f\vec{r}_0 + g\vec{v}_0.$$
$$\vec{v} = \dot{f}\vec{r}_0 + \dot{g}\vec{v}_0.$$

343

10.1.5. Ballistic Kinematics

Ballistic motion is a generalisation of projectile motion (Section 6.1.2) to include the spherical curvature of the Earth and its physical properties. In a radial gravitational field, ballistic objects follow elliptical trajectories, with identical properties to elliptical orbits (Section 10.1.3).

Atmosphere Modelling: relevant physical properties vary with height

$$T = 288.19 - 0.00649h \qquad\qquad T = 216.69 \qquad\qquad T = 141.94 + 0.00299h$$

$$p = 101.29\left(\frac{T}{288.08}\right)^{5.256} \qquad p = 22.65\, e^{1.73 - 0.000157h} \qquad p = 2.488\left(\frac{T}{216.6}\right)^{-11.388}$$

Troposphere	Lower Stratosphere	Upper Stratosphere
$h < 11$ km	11 km $< h < 25$ km	$h > 25$ km

(p [kPa]: pressure, T [K]: temperature, $\frac{dT}{dh}$: lapse rate).

With the atmosphere as an ideal gas, the density is ρ [kg m^{-3}] $= \frac{p}{0.2869\,T}$.

Gravitational Modelling: surface gravity varies with latitude due to Earth being an ellipsoid

- WGS80-refined Somigliana equation (gravity at sea level): $g_0(\varphi) = g_e \dfrac{1 + k\, sin^2\varphi}{\sqrt{1 - e^2\, sin^2\varphi}}$

  where $g_e = 9.7803253359\, ms^{-2}$, $k = 0.00193185265241$, $e = 0.08181919084$.

- Variation with height above sea level: $g(h_0,\, \varphi) = g_0(\varphi)\left(1 - (k_1 - k_2\, sin^2\varphi)h_0 + k_2 h_0^{\ 2}\right)$

  where $k_1 = 3.15704 \times 10^{-7}\, m^{-1}$, $k_2 = 2.10269 \times 10^{-9}\, m^{-1}$, $k_3 = 7.37452 \times 10^{-14}\, m^{-2}$.

(g [ms^{-2}]: gravitational acceleration at ground level, h_0 [m]: height above sea level, φ: latitude)

Keplerian Trajectories: elliptical arc ballistic trajectories with gravity as the only force

- Spherical arc range (launch to impact): $d = \dfrac{u^2\, sin\, 2\alpha}{g\,\sqrt{1 - (2 - \hat{u}^2)\,\hat{u}^2\, cos^2\alpha}}$ $\qquad\qquad \left(\hat{u} = \dfrac{u}{\sqrt{gR}} < 1\right)$

- Maximum range: $d^* = \dfrac{u^2}{g\left(1 - \frac{1}{2}\hat{u}^2\right)}$ achieved when $\alpha^* = \dfrac{1}{2}\, cos^{-1}\dfrac{\hat{u}^2}{2 - \hat{u}^2}$

- Maximum height above surface: $h = \dfrac{u^2\, sin^2\theta}{g\left(1 - \hat{u}^2 + \sqrt{1 - (2 - \hat{u}^2)\,\hat{u}^2\, cos^2\alpha}\right)}$ $\quad$ (for $\theta = \frac{\pi}{2}$, $h = \dfrac{u^2}{2g\left(1 - \frac{1}{2}\hat{u}^2\right)}$)

- Time of flight: $t = \dfrac{2u\, sin\,\alpha}{g\,(2 - \hat{u}^2)}\left(1 + \dfrac{1}{\hat{u}\sqrt{2 - \hat{u}^2}\, sin\,\alpha}\, sin^{-1}\dfrac{\hat{u}\sqrt{2 - \hat{u}^2}\, sin\,\alpha}{\sqrt{1 - (2 - \hat{u}^2)\,\hat{u}^2\, cos^2\alpha}}\right)$

Equation of Motion: often implemented in ECEF (Earth-centred, Earth-fixed Cartesian) coordinates and converted to/from geodetic (spheroidal (ϕ, λ, h)) coords. If **r** is in the Earth's rotating frame, then:

$$\underbrace{\dot{m}\mathbf{v}_{P/R}}_{\text{thrust}} - \underbrace{\frac{GMm}{r^2}\hat{\mathbf{r}}}_{\text{gravity}} - \underbrace{\frac{1}{2}C_D\rho A v^2\hat{\mathbf{r}}}_{\substack{\text{atmospheric} \\ \text{drag}}} + \underbrace{\frac{1}{2}C_L\rho A v^2\hat{\mathbf{e}}_L}_{\substack{\text{atmospheric} \\ \text{lift}}} + \underbrace{\mathbf{F}_{ext}}_{\substack{\text{external} \\ \text{forces}}} = m(\ddot{\mathbf{r}} + \underbrace{\mathbf{\Omega} \times \mathbf{\Omega} \times \mathbf{r}}_{\substack{\text{centrifugal} \\ \text{acceleration}}} + \underbrace{2\mathbf{\Omega} \times \dot{\mathbf{r}}}_{\substack{\text{Coriolis} \\ \text{acceleration}}})$$

This equation does not constrain the orientation of the body (requires torque/angular momentum). If orientation and velocity are aligned and not rotating, the lift force has direction $\mathbf{e}_L = \mathbf{r} - (\mathbf{r} \cdot \hat{\mathbf{r}})\hat{\mathbf{r}}$

10.1.5. The Hohmann Transfer

The ideal Hohmann transfer orbit is elliptical, initiated by a short-burst impulse tangent to the starting circular orbit (A) and ending with a second impulse on the opposite side (B) to fall into a second circular orbit.
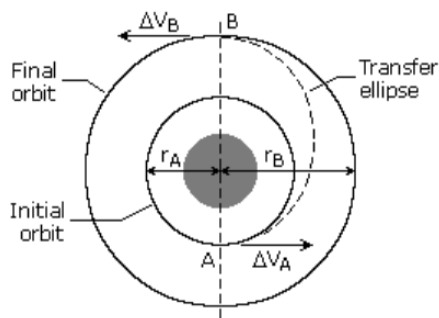
- Impulse at A and B: $\qquad J_A = m\,\Delta V_A \qquad J_B = m\,\Delta V_B$

- Velocity on transfer orbit at A and B: $\qquad V_t = \sqrt{\mu\left(\dfrac{2}{r} - \dfrac{1}{a}\right)} \quad \left(a = \dfrac{r_A + r_B}{2}\right)$

- Eccentricity of transfer ellipse: $\qquad e = 1 - \dfrac{r_A}{a}$

10.1.6. Radiation Pressure

Solar radiation pressure is exerted on an object in space due to the change in momentum of incident photons.

- Radiation pressure by reflection: $\quad\quad\quad\quad\quad p = (1 + \rho)\,\dfrac{I}{c}\cos^2\theta$

- Radiation force (parallel component): $\quad\quad\quad F = (1 + \rho)\,\dfrac{P}{c} \quad\quad (P = IA,\ F = pA)$

- Radiation pressure by absorption / emission: $\quad p = \varepsilon\,\dfrac{I}{c}\cos^2\theta$

(ρ: surface reflectivity, ε: surface emissivity, θ: angle of incidence, I: irradiant intensity, P: radiant power, c: speed of light, A: projected area normal to incident radiation)

The irradiant intensity due to a star follows an inverse-square law with distance:

$$I \sim d^{-2} \quad\Rightarrow\quad I = I_0\left(\frac{d_0}{d}\right)^2 \quad\quad\quad (I_0\text{: intensity measured at distance } d_0)$$

For the Sun, the irradiance at a distance of 1 A.U. is $I_0 = 1.361$ kW m^{-2}.

To satisfy conservation of momentum, the photons get slightly redshifted after a reflection.

Solar Sails: a solar sail is a spacecraft with a large planar reflector (up to 1 km in size) which is pushed (propelled) by radiation pressure. The point at which the radiation pressure balances the gravitational pull is the heliocentric equilibrium point. Diffraction-based solar sails have also been developed, which use metamaterial gratings to diffract incoming radiation, allowing photons to be reused in e.g. solar panels.

10.1.7. Hydrostatic Equilibrium of Rotating Spheres

10.1.7. Potential Futures of Space Travel and Space Civilisations

Kardashev Scale: classification of civilisations by magnitude of energy consumption

Assuming that all potential civilisations are expansionist and require resources, like humanity:

- **Type 0:** incomplete utilisation of the available energy in its home planet.
- **Type 1:** fully utilise the available energy in its home planet ($\sim 10^{16}$ W); start interplanetary travel.
- **Type 2:** fully utilise the available energy in its star ($\sim 10^{26}$ W); start interstellar travel.
- **Type 3:** fully utilise the available energy in its galaxy ($\sim 10^{36}$ W); start intergalactic travel.
- **Type 4:** fully utilise the available energy in the whole universe.

Humanity is a Type 0 civilisation, and is $\sim 75\%$ the way to becoming a Type 1 civilisation, which may occur at some point in the next ~ 200 years.

Dyson Sphere: extracts energy from a star, feasible for a type 2 civilisation
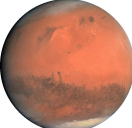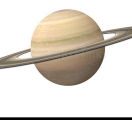
An orbiting swarm of satellites carrying reflective mirrors or solar panels. Acquiring the materials for constructing these satellites would require planet-scale mining.

Penrose Sphere: extracts energy from a rotating black hole, feasible for a type 3 civilisation

Frame dragging around the 'ringularity' of a rapidly rotating black hole leads to the formation of an ergosphere outside the event horizon. With a giant spherical mirror surrounding the black hole, radiation can be beamed into the black hole to be partially absorbed in the event horizon while the remainder is amplified in energy by superradiant scattering in the ergosphere (the Penrose process), extracting some of the black hole's angular momentum.

10.2. Astronomy

10.2.1. Planets in the Solar System

(not to scale)	Planet	Mass / kg	Mean Radius / km	Semi-major Axis / AU	Orbital Eccentricity	Orbital Period (Sidereal, Earth years)	Rotational Period (Sidereal, Earth days)	Structure
	Mercury	3.285×10^{23}	2439.7	0.387	0.205	0.241	58.6462	Solid rock; no atmosphere
	Venus	4.867×10^{24}	6051.8	0.723	0.007	0.615	-243.02 (retrograde)	Semi-solid Fe/Ni core; supercritical CO_2 + H_2SO_4 atmosphere
	Earth	5.972×10^{24} $(M_\oplus)$	6371.0	1.000	0.0167	1.000	0.99727	Fe/Ni core; N_2 + O_2 atmosphere (See Section 14.2 for more)
	Mars	6.390×10^{23}	3389.5	1.52	0.093	1.881	1.0259	Liquid Fe core; thin CO_2 atmosphere
	Jupiter	1.898×10^{27}	69911	5.20	0.0488	11.86	0.41354	Solid core; metallic hydrogen mantle; H_2 + He atmosphere
	Saturn	5.683×10^{26}	58232	9.58	0.0565	29.46	0.44002	
	Uranus	8.681×10^{25}	25362	19.2	0.0472	84.01	-0.71833 (retrograde)	Solid rock core; water + ammonia + methane ice mantle; H_2 + He + methane atmos.
	Neptune	1.024×10^{26}	24622	30.1	0.0086	164.8	0.67125	

10.2.2. Telescopes and Stellar Luminosity

Angular magnification in normal adjustment: $M = \dfrac{angle\ subtended\ by\ image\ at\ an\ eye}{angle\ subtended\ by\ object\ at\ a\ naked\ eye}$

Reflecting telescopes can be made using a Cassegrain arrangement of a parabolic concave primary mirror and convex secondary mirror.

Hipparcos scale: ranked from 1-6 (brightest to dimmest).

Apparent magnitude m: A difference of 1 on the magnitude scale is equal to an intensity ratio of 2.51.

Minimum angular resolution of telescope (Rayleigh criterion): $\theta = 1.22 \times \frac{\lambda}{D}$.
Collecting power is proportional to diameter squared.

Absolute magnitude M: equal to the apparent magnitude at a distance of 10 parsecs.
Conversion: $m - M = 5 \log_{10} \dfrac{d\ [pc]}{10}$. Neglects extinction due to interstellar or cosmic dust.

10.2.3. Stellar Evolution
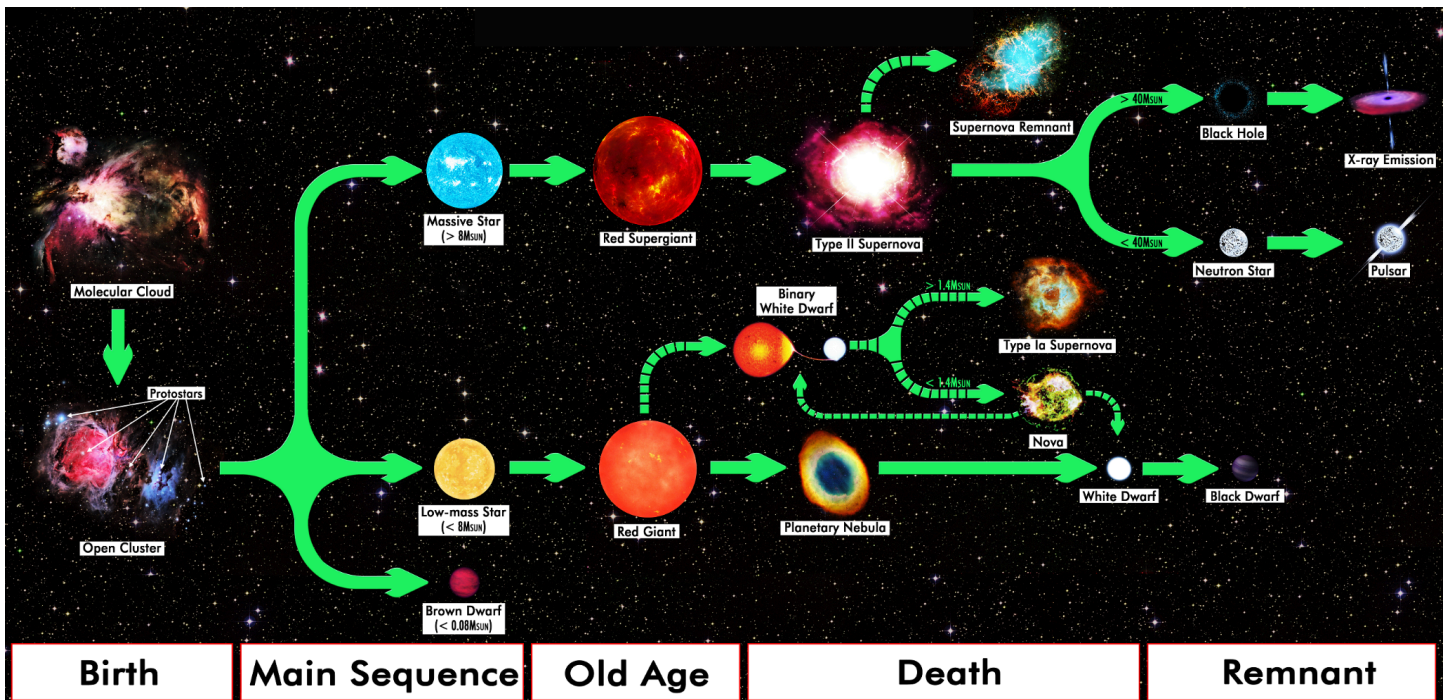
10.2.4. Stellar Spectral Classes and the Hertzsprung-Russell Diagram
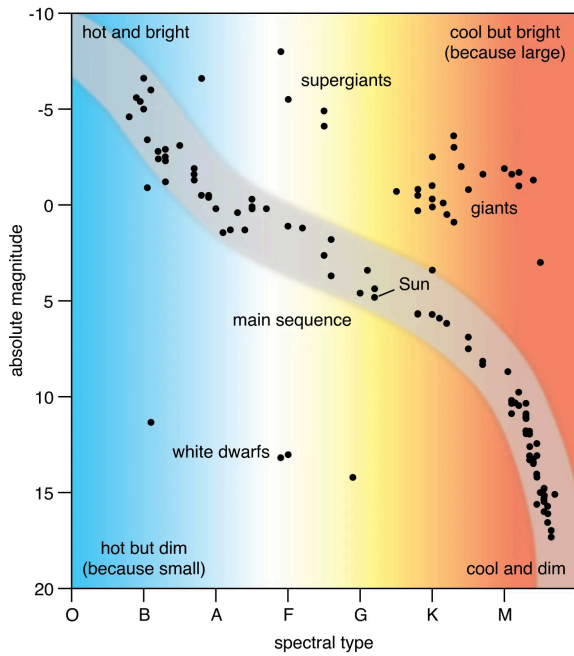
Spectral Class	Intrinsic Colour	Temperature / K	Prominent Absorption Lines
O	blue	25000 - 50000	He$^+$, He, H
B	blue	11000 - 25000	He, H
A	blue-white	7500 - 11000	H (strongest), ionised metals
F	white	6000 - 7500	Ionised metals
G	yellow-white	5000 - 6000	Ionised and neutral metals
K	orange	3500 - 5000	Neutral metals
M	red	< 3500	Neutral atoms, TiO

Stellar evolution of Sun-like stars:
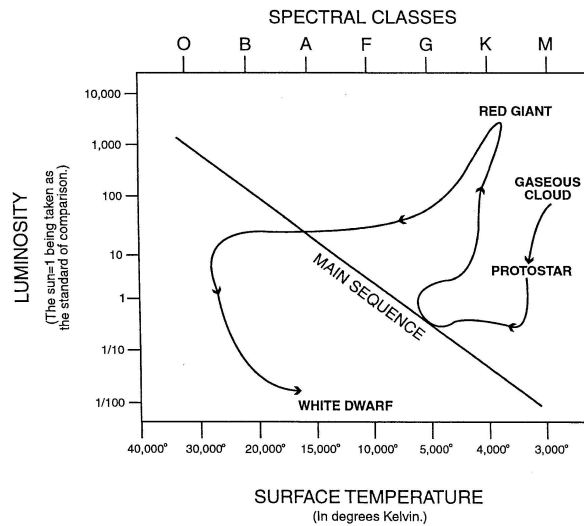
10.2.5. Degenerate Matter

Electron degeneracy pressure: repulsive force arising from the Pauli exclusion principle of electrons. It supports the white dwarf state against further gravitational collapse in low-mass stars (below the Chandrasekhar limit: $M < 1.44\ M_\odot$). Stars exceeding this mass will collapse to a neutron star.

Neutron degeneracy pressure: repulsive force arising from the Pauli exclusion principle of neutrons. It supports the neutron star state against further gravitational collapse in medium and high-mass stars (below the Tolman-Oppenheimer-Volkoff limit (TOV limit): $M \lesssim 2.1\ M_\odot$). Stars exceeding this mass will collapse to a black hole (or, hypothetically, a quark star).

10.2.6. Formation of Stellar Remnants

Brown dwarf: a 'failed star', too light to sustain ^{1}H-fusion. They still produce a little light due to a small amount of deuterium fusion.

White dwarf: at the end of a red dwarf's life, the lighter outer layers of the star are ejected as a planetary nebula (nova) due to heat from core fusion, leaving behind a dense carbon-oxygen rich core (the white dwarf). It is hypothesised that the white dwarf will burn out to become a black dwarf (cold and inert) over an extremely long period of time.

Neutron star: at the end of a red supergiant's life, the iron core formed from fusion cannot fuse any further and cannot support the gravitational pull of the star. Once a critical mass of iron is attained, the core is rapidly compressed into neutron degenerate matter while the remainder of the star is ejected as a supernova. Their formation is accompanied by a gamma ray burst (GRB).

Pulsar: a rapidly rotating neutron star which expels electromagnetic radiation (typically radio waves) from its poles which sweep across observable space.

Magnetar: a neutron star with extremely strong magnetic fields at their poles, emitting energetic X-rays and gamma rays.

10.2.7. Supernovas

Classification:

Type I - When a star accumulates matter from its companion star in a binary system and explodes after reaching a critical mass. Emission spectra has no hydrogen Balmer lines.

Type Ia - a Type I supernova with a white dwarf. When the companion star in the binary system runs out of hydrogen, it expands, allowing the white dwarf to begin accumulating some of its mass. When the white dwarf star reaches a critical mass, fusion begins and becomes unstoppable as the mass continues to increase, eventually causing the white dwarf to explode in a supernova.

Type II - The death of a high-mass star after it runs out of fuel.

Light Curves:

All types of supernovae occur at the same critical mass, meaning they all have a very similar peak absolute magnitude (about -19.3) and produce very consistent light curves, allowing astronomers to use them as standard candles to calculate distances to far-off galaxies (they can be seen up to 1000Mpc away).
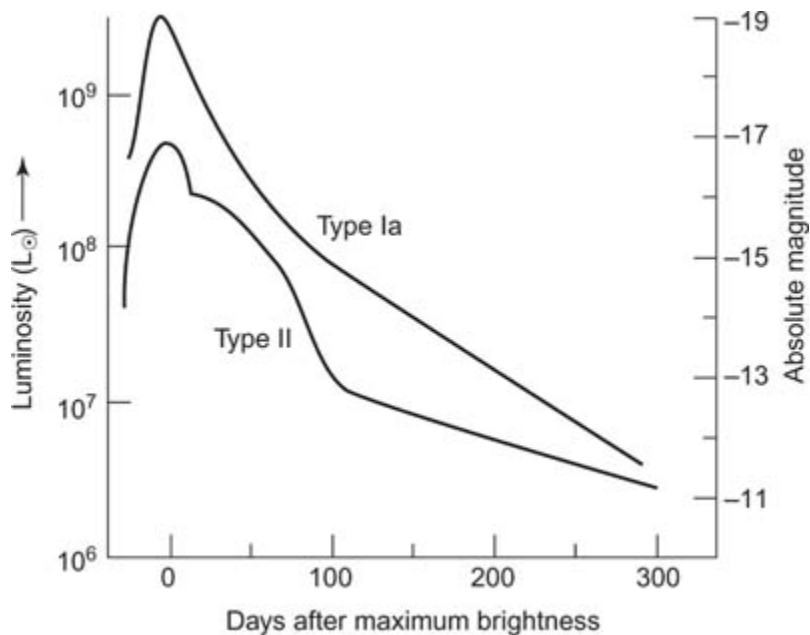
Other important sources for standard candles are the Cepheid Variable stars, whose apparent magnitude fluctuates with a time period proportional to its absolute magnitude (Leavitt's law).

10.3. Cosmology and Relativity

10.3.1. Doppler Effect for Electromagnetic Waves

10.3.2. Hubble's Law and Redshift

10.3.3. Quasars and Galactic Structures

Quasars are extremely distant, luminous active galactic nuclei (AGN) that contain a rapidly accreting supermassive black hole at their core.

Quasars are observed with cosmological redshift, indicative of extreme distances. The most distant quasars formed only a few hundred million years after the Big Bang.

Large quasar groups (LQGs) are collections of quasars.

Galaxies consist of millions of stars in an elliptical, spiral or irregular shape. Most (but not all) galaxies have a large black hole in the centre.

Galaxies located together form a galaxy cluster (e.g. the Local Group).
Galaxy clusters located together form a galaxy supercluster (e.g. Virgo supercluster).
Galaxy superclusters located together form a galactic filament (e.g. Sloan Great Wall).
Galactic filaments surround sparse regions of space known as voids (e.g. Boötes Void).

Our galaxy, the Milky Way, may have been a 'Seyfert galaxy' in the past, in which the supermassive black hole Sagittarius A* emitted polar jets, at a lower intensity than a typical quasar.

A 'blazar' is a quasar whose polar jet is directed at observers on Earth, in which the jet energy is amplified by relativistic beaming (length contraction to higher intensity).

The Blandford–Znajek process provides the power for quasar extragalactic jets.

10.3.4. Michelson-Morley Interferometer

10.3.5. Special Relativity

Profound consequences:

- The speed of light c is constant in all inertial reference frames.
- The passage of time, including simultaneity, depends on the reference frame.
- It is impossible to distinguish between absolute and relative motion.

A relativistic body moving relative to an inertial observer frame will experience both time dilation (the body experiences time passing slower) and length contraction (the frame coordinates are compressed parallel to its motion).

The following are valid for motion in a straight line at constant speed with non-zero rest mass:

- Lorentz factor: $\gamma = \dfrac{1}{\sqrt{1 - v^2/c^2}} = \dfrac{\Delta t'}{\Delta t_0} = \dfrac{\Delta x_0}{\Delta x'}$ $\qquad$ ($\gamma \geq 1, \quad 0 \leq v < c$)

- Length contraction: $\Delta x' = \dfrac{\Delta x_0}{\gamma} = \Delta x_0 \sqrt{1 - v^2/c^2}$ $\qquad$ (Δx_0: proper length)

- Time dilation: $\Delta t' = \gamma \, \Delta t_0 = \dfrac{\Delta t_0}{\sqrt{1 - v^2/c^2}}$ $\qquad$ (Δt_0: proper time)

- Speed: $v = \dfrac{\Delta x'}{\Delta t_0}$ (in object frame) $= \dfrac{\Delta x_0}{\Delta t'}$ (in observer frame)

- Relative speed: in 1D: $v_{B/A} = \dfrac{v_B - v_A}{1 - \frac{v_A v_B}{c^2}}$

  $\qquad$ in 2D: $v_{B/A} = \sqrt{1 - \eta^2} \times c$ where $\eta^2 = \dfrac{(c^2 - v_A^2)(c^2 - v_B^2)}{\left(c^2 - \overline{v_A} \cdot \overline{v_B}\right)^2}$ $\quad$ ($\overline{v_A}$, $\overline{v_B}$: velocity vectors)

- Effective mass: $m' = \gamma \, m_0 = \dfrac{m_0}{\sqrt{1 - v^2/c^2}}$ $\qquad$ (m_0: rest mass)

- Linear momentum: $p = m'v = \gamma m_0 v$

- Kinetic energy: $T = (\gamma - 1) \, m_0 c^2$

- Rest energy: $E_0 = m_0 c^2$

- Total energy: $E = E_0 + T = \gamma \, m_0 c^2$ where $E^2 = m_0^2 c^4 + p^2 c^2$.

Special relativity is a particular case of general relativity in the Minkowski metric tensor (flat spacetime). Accelerations and forces are more complicated in SR. In the rest frame:

- Acceleration: $a = \dfrac{\Delta v}{\Delta t_0}$

- Force (1D motion): $F = m_0 \dfrac{d}{dt_0}(\gamma v) = \gamma^3 m_0 a$ $\qquad$ (linear force: $\mathbf{a} \parallel \mathbf{v}$)

- Force (circular motion): $F = \gamma m_0 \dfrac{dv}{dt_0} = \gamma m_0 a$ $\qquad$ (centripetal force: $\mathbf{a} \perp \mathbf{v}$)

- Newton's second law: $F = m_0 a \dfrac{c^3}{\left(c^2 - v^2\right)^{3/2}}$

Applications of Special Relativity

Terrestrial Muon Flux: muons are generated from primary cosmic rays in the upper atmosphere of Earth, at 15 km, travelling at near-light speeds ($v \sim 0.998c$). At rest, muons have a half-life of 2.2 μs, so by classical predictions, muons should only be able to travel ~2 km before decaying. A higher muon flux is observed at the ground in reality, due to special relativity: there is time dilation (in the Earth's frame) or length contraction (in the muon's frame).

10.3.7. General Relativity

A particle in 3D space, observed with coordinate time t, moving with three-velocity $\mathbf{v} = \frac{dx}{dt}\mathbf{i} + \frac{dy}{dt}\mathbf{j} + \frac{dz}{dt}\mathbf{k}$, constitutes a world line in 4D space time, in which it experiences proper time τ. The dilation factor is $\gamma = \frac{d\tau}{dt} = \frac{1}{\sqrt{1-v^2}} \geq 1$ where v is normalised such that $c = 1$.
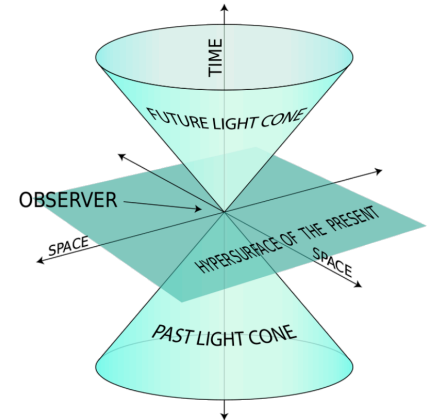
Einstein notation: $v^\alpha u_\alpha = \sum_i v^i u_i$, a summation over variables.

The Christoffel symbols Γ_{ij} denote the rate of change of basis vector $\mathbf{e}_i$ along a coordinate x^j, and depend only on the choice of coordinate system.

Geodesic equation: $\frac{dv}{d\tau} = 0 \iff \frac{dv^\alpha}{d\tau} = -\Gamma^\alpha_{\mu\nu} v^\mu v^\nu$ Metric tensor: $|v|^2 = (ds)^2 = g_{\mu\nu} dx^\mu dx^\nu = c^2$

In general, $\Gamma^\gamma_{\alpha\beta} = \frac{g^{\gamma\sigma}}{2}\left(\frac{dg_{\sigma\alpha}}{dx^\beta} + \frac{dg_{\sigma\beta}}{dx^\alpha} - \frac{dg_{\alpha\beta}}{dx^\sigma}\right)$, but in orthogonal coordinates, $\Gamma^\gamma_{\alpha\beta} = \frac{1}{2g_{\gamma\gamma}}\left(\frac{dg_{\gamma\alpha}}{dx^\beta} + \frac{dg_{\gamma\beta}}{dx^\alpha} - \frac{dg_{\alpha\beta}}{dx^\sigma}\right)$

($g^{\gamma\sigma}$: inverse of $g_{\gamma\sigma}$)

Minkowski metric tensor (pseudo-Riemannian metric, (-, +, +, +) signature): $\eta = \begin{pmatrix} -1 & 0 & 0 & 0 \\ 0 & 1 & 0 & 0 \\ 0 & 0 & 1 & 0 \\ 0 & 0 & 0 & 1 \end{pmatrix}$

This metric tensor has zero curvature (flat spacetime).

Riemann curvature tensor of spacetime: $R^\alpha_{\beta\mu\nu} = \frac{d\Gamma^\alpha_{\beta\nu}}{dx^\mu} + \Gamma^\lambda_{\beta\nu}\Gamma^\alpha_{\lambda\mu} - \frac{d\Gamma^\alpha_{\beta\mu}}{dx^\nu} - \Gamma^\lambda_{\beta\mu}\Gamma^\alpha_{\lambda\nu}$. Ricci tensor: $R_{\mu\nu} = R^\lambda_{\mu\lambda\nu}$

Ricci scalar: for orthogonal coordinates, $R = g^{\mu\nu} R_{\mu\nu}$ (average curvature in all directions)

If $R > 0$, parallel lines converge. If $R < 0$, parallel lines diverge.

Energy-momentum tensor: T_{tt} (energy density), $T_{xt} = T_{tx}$ (momentum density), T_{xx} (pressure).

In 4D spacetime, cross-terms in space arise, which are the viscosities.

Einstein field equation: $R_{\mu\nu} - \frac{1}{2}Rg_{\mu\nu} + \Lambda g_{\mu\nu} = \frac{8\pi G}{c^4} T_{\mu\nu}$ ($\Lambda \approx 1.1 \times 10^{-52}$ m²: cosmological constant)

For a 1-body (mass M) problem in spherical coordinates (t, r, θ, φ),

(the Schwarzschild metric). Schwarzschild radius: $r = \frac{2GM}{c^2}$

(temporal term becomes zero → black hole horizon radius:).

$$g_{\mu\nu} = \begin{bmatrix} c^2 - \frac{2GM}{r} & 0 & 0 & 0 \\ 0 & \frac{1}{\frac{2GM}{rc^2}-1} & 0 & 0 \\ 0 & 0 & -r^2 & 0 \\ 0 & 0 & 0 & -r^2\sin^2\theta \end{bmatrix}$$

10.3.8. Hawking Model of Black Holes

Hawking radiation

- Hawking radiation temperature: $\qquad T_H = \frac{\hbar c^3}{8\pi GMk_B}$ (typically $T_H \sim 10^{-9}$ K)

- Luminosity (radiant power): $\qquad P = \frac{\hbar c^6}{15360\pi G^2 M^2}$ (black body, photons only)

- Evaporation time: $\qquad t = \frac{5120\pi G^2 M^3}{\hbar c^4}$ (in the absence of absorption)

- Entropy: $\qquad S = \frac{k_B c^3 A}{4G\hbar}$ (A: surface area of black hole)

As black holes emit Hawking radiation, their temperature increases and size decreases.

Black holes continually absorb CMB photons. Since $T_{CMB} \gg T_H$, black holes tend to grow, not shrink. Black holes also increase in size when absorbing infalling matter.

Relativistic Models

The Kerr metric describes the geometry around a rotating mass.

The Morris-Thorne metric describes the geometry of non-gravitating wormholes.

10.3.9. The Big Bang Theory and the ΛCDM Model (Dark Matter and Dark Energy)

ΛCDM (lambda-cold dark matter) is the standard model of Big Bang cosmology. Based on general relativity, it explains the anisotropy of the cosmic microwave background (CMB) radiation, the large-scale structure of galaxy clusters, the observed abundances of H, He and Li, and the accelerating expansion of the universe from distant starlight. The observed mass-energy density balance is made up of ~68% dark energy, ~27% dark matter and ~5% ordinary matter.
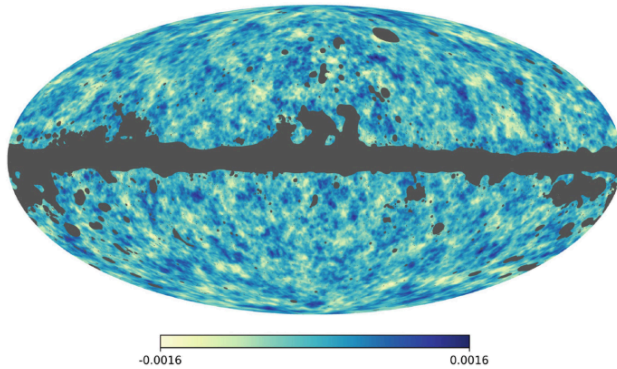
Temperature Fluctuations in the Cosmic Microwave Background Radiation
Nearly isotropic, black body spectrum
with radiation temperature T_{CMB} = 2.7255 K.
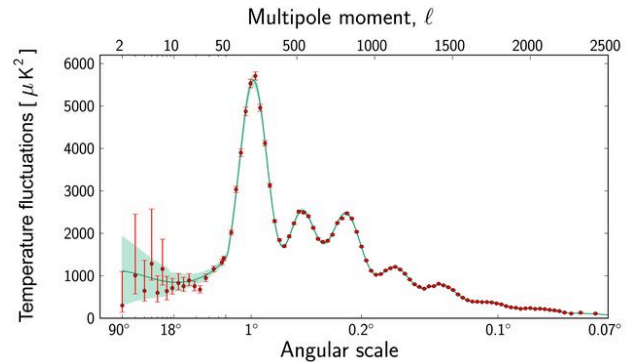
Power Spectrum of Spherical Harmonic Transform
The predicted spatial frequency
distribution matches observation.

Evidence for the Accelerating Expansion of the Universe

- Spectral lines from distant galaxies are redshifted.
- Supernova luminosity curves decay with distance in accordance with time dilation.

Properties of Dark Matter: in ΛCDM, dark matter:

- cannot not consist of any matter made from protons, neutrons, electrons or neutrinos
- has a velocity far less than the speed of light (cold)
- does not cool by radiative emission of photons
- interacts with itself and ordinary matter only by gravity (and possibly by the weak force)

Properties of Dark Energy: in ΛCDM, dark energy:

- is responsible for the accelerating expansion of the universe

There are some alternative models that attempt to explain the accelerating expansion without invoking dark energy (e.g. MOND: modified Newtonian dynamics), although they have been criticised, with many instances of experimental falsification.

Recent evidence (baryon acoustic oscillation measurements by DESI) suggests that mass-energy consumed by black holes is converted to dark energy.

Friedmann Equations: ΛCDM uses the Friedmann-Lemaître-Robertson-Walker (FLRW) metric to describe the observable universe from approximately 0.1 ms after the Big Bang to the present.

10.3.10. Mechanisms of Redshift

Sunyaev-Zel'dovich Effect: CMB photons are shifted to higher frequency due to an inverse Compton effect interaction with relativistic electrons in the corona of a black hole.

Integrated Sachs-Wolfe Effect: photons lose less energy when emerging from a potential well than the energy gained when entering due to the presence of **dark energy** causing the expansion of spacetime, flattening the potential well.

P11. NUCLEAR, QUANTUM AND MEDICAL PHYSICS

11.1. Quantum Physics and The Standard Model

11.1.1. Standard Model of Elementary Particles

Quarks   Leptons   Gauge (Vector) Bosons   Scalar Bosons

Generations of matter (fermions)			Force carriers / interactions (bosons)	
I	II	III		
Up quark (u) m = 2.2 MeV/c^2 q = ⅔, spin = ½	Charm quark (c) m = 1.28 GeV/c^2 q = ⅔, spin = ½	Top quark (t) m = 173.1 GeV/c^2 q = ⅔, spin = ½	Gluon (g) strong nuclear force m = 0 q = 0, spin = 1	Higgs boson (H) m = 124.97 GeV/c^2 q = 0, spin = 0
Down quark (d) m = 4.7 MeV/c^2 q = -⅓, spin = -½	Strange quark (s) m = 96 MeV/c^2 q = -⅓, spin = -½	Bottom quark (b) m = 4.18 GeV/c^2 q = -⅓, spin = -½	Photon (γ) electromagnetic force m = 0 q = 0, spin = 1	
Electron (e) m = 0.511 MeV/c^2 q = -1, spin = ½	Muon (μ) m = 105.66 MeV/c^2 q = -1, spin = ½	Tauon (τ) m = 1.7768 GeV/c^2 q = -1, spin = ½	Z boson (Z) weak nuclear force m = 91.19 GeV/c^2 q = 0, spin = 1	
Electron neutrino (ν_e) m = 0.07 eV/c^2 q = 0, spin = ½	Muon neutrino (ν_μ) m < 0.17 MeV/c^2 q = 0, spin = ½	Tauon neutrino (ν_τ) m < 18.2 MeV/c^2 q = 0, spin = ½	W boson (W) weak nuclear force m = 80.433 GeV/c^2 q = ±1, spin = 1	

Mass m conversion: 1 MeV/c^2 = 1.7827 × 10^{-30} kg

Charge q is given as a multiple of the elementary charge e = 1.602 × 10^{-19} C.

- The W boson exists as either W^+ or W^-, with the corresponding charge.
- Gluons have colour charge and anticolour charge (red / green / blue), with 8 different types.
- Gravitons (G) are hypothetical tensor bosons (spin = 2), predicted by theories in quantum gravity. If they exist, they are difficult to detect due to being extremely low energy (m < 10^{-22} eV/c^2, q = 0). They may be the quanta of the gravitational field comprising gravitational waves (which have been detected).
- Anti-electrons are commonly called positrons (e^+).

11.1.2. Composite Particles (Hadrons)

Baryons (composed of three quarks):

Proton (p): uud Antiproton ($\bar{p}$): $\overline{uud}$ Delta baryons (Δ): uuu / uud / udd / ddd

Neutron (n): udd Antineutron ($\bar{n}$): $\overline{udd}$ Lambda baryons (Λ): uds / udc / udb

Tetraquarks and pentaquarks are exotic baryons with 4 and 5 quarks respectively.

Mesons (composed of one quark and one antiquark):

Pion (π): $u\bar{d}$ / $u\bar{u}$ / $d\bar{d}$ / $\bar{u}d$ Kaon (K): $u\bar{s}$ / $d\bar{s}$ / $s\bar{u}$ Rho meson (ρ): $u\bar{d}$

11.1.3. Heisenberg Uncertainty Principles

Strictly, these uncertainties are standard deviations, but can also be interpreted qualitatively with less rigorous bounds.

Uncertainties in position and momentum: $\Delta x\, \Delta p_x \geq \frac{\hbar}{2}$

Uncertainties in time and energy: $\Delta t\, \Delta E \geq \frac{\hbar}{2}$

11.1.5. Wave-Particle Duality

De Broglie wavelength: $\lambda = \frac{h}{p}$

Quantisation: $E = n\hbar\omega$ $p = n\hbar k$ ($\omega = 2\pi f,\ k = \frac{2\pi}{\lambda}$) n: integer

Dispersion relation: $\omega = \frac{\hbar k^2}{2m}$

11.1.6. Single-Slit Diffraction

Collinear and coherent quantum particles incident on a single slit undergo diffraction in a plane spanned by the momentum vector of the particle and the direction of the slit whose dimension a is similar to the (De Broglie) wavelength λ of the particle.
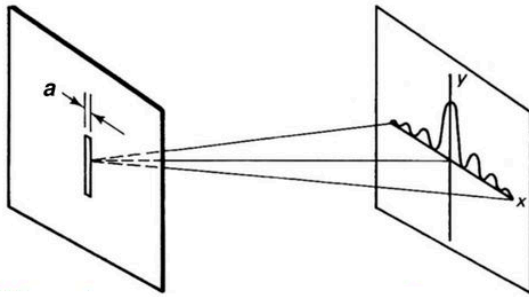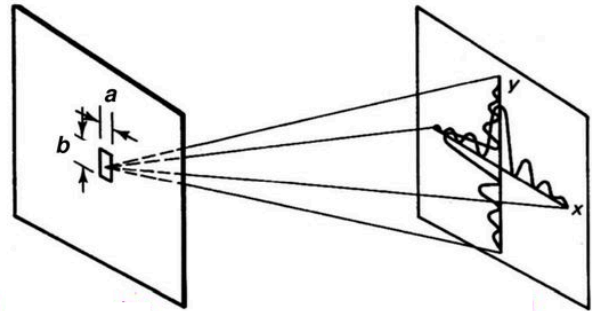
1D diffraction: $a \sim \lambda$ 2D diffraction: $a \sim b \sim \lambda$

Angles of diffraction for **minima**: $\sin \theta_n = \frac{n\lambda}{a}$

$\qquad$ (n = 1, 2, ...: order of diffraction, $x_n \approx D \sin \theta_n$ for flat screen)

At $\theta = 0$, there is the zero-order **maxima**, of intensity I_0.

Angles of diffraction for **maxima:** solutions to $\tan u_n = u_n$ where $u_n = \frac{a\pi}{\lambda} \sin \theta_n$ (n = 0, 1, 2...)
(u_n = 0, 4.493, 7.725, 10.904, 14.066, 17.221, 20.371...)

Fraunhofer diffraction intensity:

$$I(\theta) = I_0 \, sinc^2\left(\frac{a\pi}{\lambda} \sin \theta\right) = I_0 \frac{\lambda^2 \sin^2\left(\frac{a\pi}{\lambda} \sin \theta\right)}{\pi^2 a^2 \sin^2 \theta} \quad \text{or} \quad I(x) = I_0 \, sinc^2 \frac{\pi a x}{\lambda D} = I_0 \frac{\lambda^2 D^2 \sin^2 \frac{\pi a x}{\lambda D}}{\pi^2 a^2 x^2}$$

Diffraction of X-rays or electrons on polycrystalline graphite leads to a radially-symmetric circular diffraction pattern due to the random orientation of the splitting direction.

11.1.7. Double-Slit Diffraction and Interference

11.1.8. Quantum Mechanical Operators

Dirac's 'bra-ket' notation:

- 'Bra' operator: $\langle \Psi | = \int d\mathbf{x}\ \Psi^*(\mathbf{x})$ and   'Ket' operator: $|\Phi\rangle = \Phi(\mathbf{x})$

- Bra-ket inner product: $\langle \Psi | \hat{C} | \Phi \rangle = \int \Psi^*(\mathbf{x})\ \hat{C}\Phi(\mathbf{x})\ d\mathbf{x}$ (in a Hilbert space)

($\{\Psi, \Phi\}$: wavefunctions, $\mathbf{x}$: position vector, $\hat{C}$: operator, integrals taken over all space ($\mathbf{x} \in \mathrm{R}^3$))

- Quantum superposition: $|\psi\rangle = \alpha|\psi_1\rangle + \beta|\psi_2\rangle$ ($\{\alpha, \beta\} \in \mathrm{C}$: state coefficients)

- Expectation of an observable: $\langle C \rangle = \langle \psi | \hat{C} | \psi \rangle$

- Hermitian adjoint: $\langle \phi | \hat{C}\psi \rangle = \langle \hat{C}^\dagger \phi | \psi \rangle$ ($\hat{C}^\dagger$ exists for any linear $\hat{C}$)

- Hermitian operator $\hat{C}$ (self-adjoint): $\langle \phi | \hat{C} | \psi \rangle = \langle \psi | \hat{C} | \phi \rangle^*$ (ψ^*: complex conjugate)

- Eigenstates of an operator: $\hat{C}f_i = \lambda_i f_i$ (f_i: eigenfunctions, λ_i: eigenvalues)
  All Hermitian operators have real eigenvalues.

- Probability density function: $p(\mathbf{x}) = \psi(\mathbf{x})^*\ \psi(\mathbf{x}) = |\psi(\mathbf{x})|^2$

Operators representing physical observables (energy, momentum) are Hermitian as they have real expected values. Their eigenfunctions form an orthonormal basis.

- Position operator: $\hat{\mathbf{x}} = \mathbf{x}$

- Energy operator: $\hat{E} = -i\hbar\dfrac{\partial}{\partial t}$

- Momentum operator: $\hat{\mathbf{p}} = -i\hbar\nabla$

- Kinetic energy operator: $\hat{T} = -\dfrac{\hbar^2}{2m}\nabla^2$

- Potential energy operator: $\hat{V} = V(\mathbf{x})$

- Hamiltonian operator: $\hat{H} = \hat{T} + \hat{V}$

- Time evolution operator: $\hat{U} = \exp(-i\hat{H}t/\hbar)$

Schrödinger's equation (general time-dependent): $\hat{H}\Psi = \hat{E}\Psi$

Schrödinger's equation (time-independent): $\hat{H}\Psi = E\Psi$ (E: energy eigenvalues)

Probability current: $\mathbf{j} = \dfrac{1}{2m}\left(\Psi^*\hat{\mathbf{p}}\Psi - \Psi\hat{\mathbf{p}}\Psi^*\right) = -\dfrac{i\hbar}{2m}(\psi^*\nabla\psi - \psi\nabla\psi^*) = \dfrac{\hbar}{m}\,\mathrm{Im}(\psi^*\nabla\psi)$

Probability conservation law: for any control volume V and control surface S,

$$\int_V \left(\frac{\partial p}{\partial t} + \nabla\cdot\mathbf{j}\right)\,dV = 0 \quad\Leftrightarrow\quad \frac{\partial}{\partial t}\int_V p\,dV + \oiint_S \mathbf{j}\cdot d\mathbf{S} = 0$$

$\qquad\qquad$ (divergence form) $\qquad\qquad\qquad\qquad$ (flux form)

The 3D plane wave solution $\psi(\mathbf{x}) = A\exp(i(\mathbf{k}\cdot\mathbf{x} - \omega t))$ ($\mathbf{k}$: wavevector, ω: angular frequency) has a probability density $p(\mathbf{x}) = |A|^2$ and probability current $\mathbf{j}(\mathbf{x}) = |A|^2\,\dfrac{\hbar}{m}\,\mathbf{k} = p\mathbf{v}$ (since $\mathbf{p} = \hbar\mathbf{k}$).

Stationary states (e.g. standing waves) have $\mathbf{j} = \mathbf{0}$ everywhere.

Transmission and reflection coefficients: $T + R = 1$ where $\quad T = \left|\dfrac{\mathbf{j}_{\text{trans}}\cdot\mathbf{n}}{\mathbf{j}_{\text{inc}}\cdot\mathbf{n}}\right|, \qquad R = \left|\dfrac{\mathbf{j}_{\text{ref}}\cdot\mathbf{n}}{\mathbf{j}_{\text{inc}}\cdot\mathbf{n}}\right|$
($\mathbf{n}$: normal vector to barrier, $\mathbf{j}_{\text{trans}}$: transmission current, $\mathbf{j}_{\text{inc}}$: incident current, $\mathbf{j}_{\text{ref}}$: reflected current)

In an external electromagnetic field, $\quad \mathbf{j} = \dfrac{1}{2m}\left[\left(\Psi^*\hat{\mathbf{p}}\Psi - \Psi\hat{\mathbf{p}}\Psi^*\right) - 2q\mathbf{A}|\Psi|^2\right]$
($\mathbf{A}$: magnetic vector potential)

For a spin-s particle without internal structure (e.g. electron),

$$\mathbf{j} = \mathbf{j}_e/q = \frac{1}{2m}\left[\left(\Psi^*\hat{\mathbf{p}}\Psi - \Psi\hat{\mathbf{p}}\Psi^*\right) - 2q\mathbf{A}|\Psi|^2\right] + \frac{\mu_S}{qs\hbar}\nabla\times(\Psi^*\mathbf{S}\Psi)$$

($\mathbf{j}_e$: electric current density, q: charge, μ_S: spin magnetic moment, $\mathbf{S}$: spin vector)

Ladder Operators (Dirac Creation-Annihilation Operators)

$$\hat{J}_\pm \equiv \hat{J}_x \pm i\hat{J}_y; \qquad \hat{J}_\pm|J,M\rangle = \sqrt{J(J+1) - M(M\pm 1)}\,|J,M\pm 1\rangle$$

where $|\,.\,\rangle$ is bra-ket notation for a quantum superposition of states.

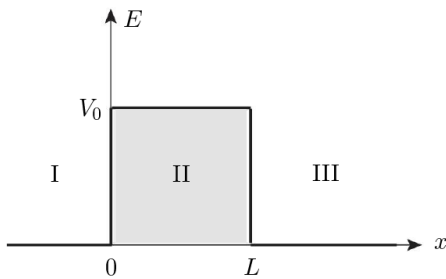### 11.1.9. 1D Infinite Potential Well (Particle in a Box)
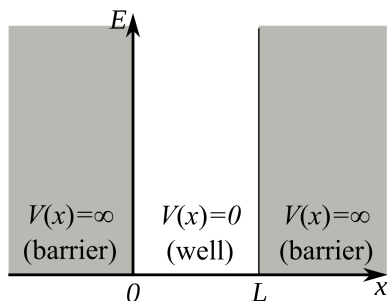
Potential: $V(x) = 0$ if $0 < x < L$ else ∞

Eigenfunctions: $\psi_n = \sqrt{\dfrac{2}{L}} \sin k_n x$ where $k_n = \dfrac{n\pi}{L}$

Eigenenergies: $E_n = \dfrac{h^2 n^2}{8mL^2}$

$V(x)=\infty$ (barrier) $V(x)=0$ (well) $V(x)=\infty$ (barrier)

Momentum: $\langle \psi | \hat{p} | \psi \rangle = 0$ Kinetic energy: $\langle \psi | \hat{T} | \psi \rangle = \dfrac{h^2 n^2}{8mL^2}$

11.1.10. 1D Finite Barrier Potential

Potential: $V(x) = V_0$ if $0 < x < L$ else 0

Eigenfunctions: $\begin{cases} \psi_{\mathrm{I}} = A_r e^{ik_0 x} + A_l e^{-ik_0 x} & x < 0 \\ \psi_{\mathrm{II}} = B_r e^{ik_1 x} + B_l e^{-ik_1 x} & 0 \leq x \leq L \\ \psi_{\mathrm{III}} = C_r e^{ik_0 x} + C_l e^{-ik_0 x} & x > L \end{cases}$

Wavenumbers: $k_0 = \sqrt{\dfrac{2mE}{\hbar^2}}, \quad k_1 = \sqrt{\dfrac{2m(E - V_0)}{\hbar^2}}$

Coefficients are constrained by:
$$A_r + A_l = B_r + B_l$$
$$ik_0(A_r - A_l) = ik_1(B_r - B_l)$$
$$B_r e^{ik_1 L} + B_l e^{-ik_1 L} = C_r e^{ik_0 L} + C_l e^{-ik_0 L}$$
$$ik_1\left(B_r e^{ik_1 L} - B_l e^{-ik_1 L}\right) = ik_0\left(C_r e^{ik_0 L} - C_l e^{-ik_0 L}\right)$$

Transmission coefficient: Reflection coefficient:

$$t = \dfrac{4k_0 k_1 e^{-iL(k_0 - k_1)}}{(k_0 + k_1)^2 - e^{2iLk_1}(k_0 - k_1)^2} \qquad r = \dfrac{(k_0 - k_1)^2 \sin k_1 L}{2ik_0 k_1 \cos k_1 L + (k_0^2 + k_1^2)\sin k_1 L}$$

Transmission probability (quantum tunnelling from I to III):

If $E < V_0$: $T = |t|^2 = \left(1 + \dfrac{V_0^2 \sinh^2 k_1 L}{4E(V_0 - E)}\right)^{-1}$

If $E > V_0$: $T = |t|^2 = \left(1 + \dfrac{V_0^2 \sin^2 k_1 L}{4E(E - V_0)}\right)^{-1}$

If $E = V_0$: $T = \left(1 + \dfrac{2mL^2 V_0}{\hbar^2}\right)^{-1}$

11.1.11. 1D Quadratic Potential (Quantum Harmonic Oscillator)
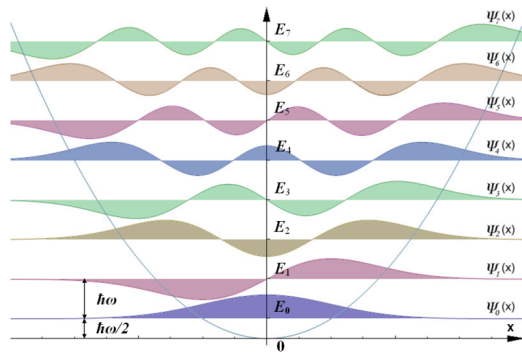
Potential: $V(x) = \dfrac{1}{2}kx^2$

Eigenfunctions:

$$\psi_n = \frac{1}{\sqrt{2^n n!}} \left(\frac{m\omega}{\pi\hbar}\right)^{1/4} \exp\left(-\frac{m\omega x^2}{2\hbar}\right) H_n\left(\sqrt{\frac{m\omega}{\hbar}}x\right)$$

(H_n: Hermite polynomials (Section 1.7.12), $\omega = \sqrt{\dfrac{k}{m}}$)

Eigenenergies: $E_n = (2n+1)\dfrac{\hbar\omega}{2}$

The zero point (ground state) energy is non-zero and is given by $E_0 = \dfrac{h}{4\pi}\sqrt{\dfrac{m}{k}}$.

11.1.12. 3D Quadratic Potential (Spherically Symmetric Quantum Harmonic Oscillator)

Potential: $V(r) = \dfrac{1}{2}kr^2$ (μ: particle mass; $\omega = \sqrt{\dfrac{k}{\mu}}$)

Wavefunctions (in spherical coordinates):

$$\psi_{klm} = \sqrt{\left(\frac{2}{\pi}\right)^{1/2}\left(\frac{\mu\omega}{2\hbar}\right)^{l+3/2}\frac{2^{k+2l+3}\,k!}{(2k+2l+1)!!}} \times r^l \exp\left(-\frac{\mu\omega}{2\hbar}r^2\right) L_k^{(l+1/2)}\left(\frac{\mu\omega}{\hbar}r^2\right) Y_{lm}(\theta,\phi)$$

($L^n{}_k$: generalised Laguerre polynomials, Y_{lm}: spherical harmonics, Section 1.7.13-14.)

Eigenenergies: $E_n = \hbar\omega\left(2k + l + \dfrac{3}{2}\right)$ where $n = 2k + l$.

For the **inverse** square potential, see the quantum model of hydrogenic atoms (Section 13.1.2).

11.1.13. Casimir Forces due to Vacuum Fluctuations

For two parallel, perfectly conducting plates separated by a submicron distance d, long-wave virtual bosons (primarily photons) are excluded from the region between them, exerting a Casimir pressure (force per unit area) pushing the plates together given by

$$\frac{F}{A} = \frac{\pi^2}{240}\frac{\hbar c}{d^4} = \frac{1.302 \times 10^{-27}}{d^4}$$

The Casimir force can also be interpreted as a generalisation of the Van der Waals' force.

11.1.14. Quantum Electrodynamics (Special Relativistic Quantum Mechanics)

Klein-Gordon Equation: describes bosons (e.g. Higgs boson) (Ψ: $\mathrm{R}^{1,3} \to \mathrm{C}$).

$$\left(\frac{1}{c^2} \frac{\partial^2}{\partial t^2} - \nabla^2 + \frac{m^2 c^2}{\hbar^2} \right) \Psi(t, \mathbf{x}) = 0 \qquad \text{or with the wave operator } \Box^2 = \frac{1}{c^2} \frac{\partial^2}{\partial t^2} - \nabla^2$$

Dirac Equation: describes fermions (e.g. electrons) (Φ: $\mathrm{R}^{1,3} \to \mathrm{C}^4$ (spinor)).

$$\left(i\hbar\, \gamma^\mu \partial_\mu - mc \right) \Phi(t, \mathbf{x}) = 0 \qquad \text{where the contravariant Dirac matrices are}$$

$$\gamma^0 = \begin{pmatrix} 1 & 0 & 0 & 0 \\ 0 & 1 & 0 & 0 \\ 0 & 0 & -1 & 0 \\ 0 & 0 & 0 & -1 \end{pmatrix}, \qquad \gamma^1 = \begin{pmatrix} 0 & 0 & 0 & 1 \\ 0 & 0 & 1 & 0 \\ 0 & -1 & 0 & 0 \\ -1 & 0 & 0 & 0 \end{pmatrix},$$

$$\gamma^2 = \begin{pmatrix} 0 & 0 & 0 & -i \\ 0 & 0 & i & 0 \\ 0 & i & 0 & 0 \\ -i & 0 & 0 & 0 \end{pmatrix}, \qquad \gamma^3 = \begin{pmatrix} 0 & 0 & 1 & 0 \\ 0 & 0 & 0 & -1 \\ -1 & 0 & 0 & 0 \\ 0 & 1 & 0 & 0 \end{pmatrix}.$$

11.2. Radioactivity and Nuclear Power Engineering

11.2.1. Radioactive Decay

Modes of Radioactive Decay

- **Alpha decay:** an alpha particle (^{4}He nucleus) escapes from the nucleus. $\quad ^A_Z X \to ^{A-4}_{Z-2} Y + ^4_2 \alpha$

- **Beta-minus decay:** a neutron becomes a proton. $\quad ^A_Z X \to ^A_{Z+1} Y + ^{\ 0}_{-1}\beta^- + ^0_0\bar{\nu}_e$

- **Beta-plus decay:** a proton becomes a neutron. $\quad ^A_Z X \to ^A_{Z-1} Y + ^0_1\beta^+ + ^0_0\nu_e$

- **Gamma decay:** an excited nucleus reduces in energy: $\quad ^A_Z X^* \to ^A_Z X + ^0_0\gamma$

- **Electron capture:** a proton becomes a neutron: $\quad ^A_Z X + ^{\ 0}_{-1} e \to ^A_{Z-1} Y + ^0_0\gamma + ^0_0\nu_e$

- **Internal Conversion:** orbital electron ejected: $\quad ^A_Z X^* \to ^A_Z X + ^{\ 0}_{-1} e$

- **Cluster decay:** nucleus releases small nucleus e.g. ^{14}C: $\quad ^A_Z X \to ^{A-N}_{Z-M} Y + ^N_M C$

- **Spontaneous fission:** nucleus breaks into smaller nuclei: $\quad ^A_Z X \to ^{A-N-k}_{Z-M} Y + ^N_M C + k^1_0 n$

Radius of nucleon: $\quad r \approx r_0 A^{1/3} \qquad$ ($r_0 \sim$ 1.2 fm, A: mass number)   (sphere packing model)

Liquid Drop Model: estimates the binding energy of a nucleus

- Nuclear mass: $m_X = Zm_p + (A - Z)m_n - E_b/c^2 \qquad$ (E_b: binding energy, E_b/c^2: mass defect)

- Semi-empirical mass formula:
$$E_b = \underbrace{a_V A}_{\text{volume}} - \underbrace{a_S A^{2/3}}_{\text{surface}} - \underbrace{a_C Z(Z-1)A^{-1/3}}_{\text{Coulomb}} - \underbrace{a_A(A-2Z)^2 A^{-1}}_{\text{asymmetry}} \pm \underbrace{a_P A^{k_P}}_{\text{pairing}}$$
($a_V \approx$ 15.75 MeV, $a_S \approx$ 17.8 MeV, $a_C \approx$ 0.711 MeV, $a_A \approx$ 23.7 MeV, $a_P \approx$ 11.18 MeV, $k_P \approx$ -0.5. Pairing term is **zero** if A is odd; else, pairing term sign is $+$ if Z is even and $-$ if Z is odd.)

- Most stable neutron-proton ratio: $\max E_b(A) \to N/Z \approx 1 + \frac{a_C}{2a_A} A^{2/3}$.

    In this model, binding energy per nucleon $\frac{E_b(A)}{A}$ is achieved at $A = 63$ (Cu).
    This neglects the nuclear shells - magic nucleon numbers.

The nucleus with the true highest binding energy per nucleon is ^{62}Ni. It does **not** have the lowest mass per nucleon (most efficient binding), which is ^{56}Fe. Nuclei below ^{56}Fe release nuclear energy by fusion. Nuclei above ^{56}Fe release nuclear energy by fission.

The magic nucleon numbers are 2, 8, 20, 28, 50, 82, 126, which correspond to filled nuclear shells. Nuclei with proton or neutron counts equal to these magic numbers are especially stable. ^{4}He and ^{16}O are exceptionally stable (higher than usual binding energy per nucleon) due to being 'doubly magic' - both their protons and neutrons fill their nuclear shells.

Decay Rates and Activity: a random process following an exponential distribution

- Activity (decays per second): $A = \lambda N = A_0 e^{-\lambda t}$ (λ: decay constant, units: s^{-1})
- Mean lifetime: $\tau = 1/\lambda$.
- Median lifetime (half-life): $t_{1/2} = \frac{ln\,2}{\lambda} = \tau\,ln\,2$

Units of A: Becquerels (Bq), Curies (Ci) where 1 Bq = 1 disintegration per second; 1 Ci = 37 GBq.

Conservation of Energy and Momentum

Considering a general nuclear reaction, $A \rightarrow M + m + \gamma$ (speed of M: V, speed of m: v)

- Kinetic energy: $KE_{products}\,[MeV] = \frac{1}{2}mv^2 + \frac{1}{2}MV^2 = 931.37 \times (A - M - m)\,[amu] - E_\gamma - KE_{A,\,0}$
  Q-value (disintegration energy released): $931.37\,MeV \times (m_r - m_p)$ [amu]

- Momentum: since $p_\gamma \approx 0$ and $M >> m$ then $MV = mv \rightarrow \frac{1}{2}mv^2 \approx KE_{products}$, $\frac{1}{2}MV^2 = \frac{KE_{products}}{1 + \frac{M}{m}}$.

(A: mass number, Z: charge number, neutron count = A - Z, in units of amu)
(1 amu = 1 u = 1/12 of ^{12}C atom mass = 1.6605 × 10^{-27} kg = 931.37 MeV via $\Delta E = \Delta m\,c^2$.
Proton mass: 1.007277 u. Neutron mass: 1.008665 u. ^{1}H mass: 1.007825 u.
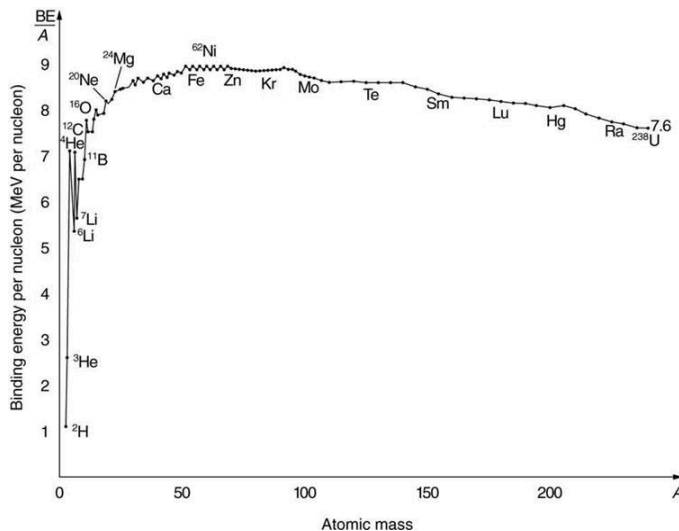
Binding Energy per Nucleon
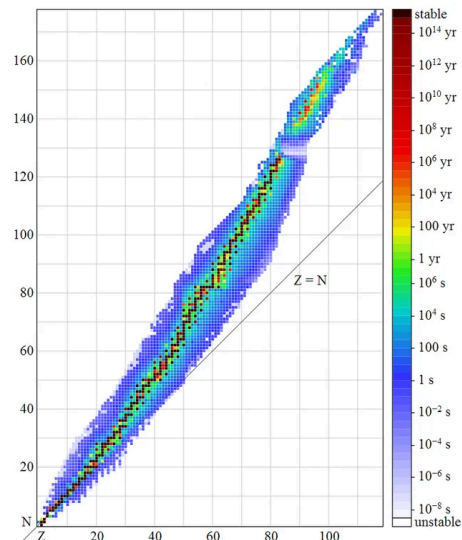
Chart of Nuclides (half-lives)

11.2.2. Alpha Decay

Alpha decay releases an α-particle from a neutron-deficient nucleus: $^A_Z X \rightarrow ^{A-4}_{Z-2} Y + ^4_2 \alpha$

Energy balance: $\qquad m_X c^2 = m_Y c^2 + \frac{1}{2} m_Y v_Y^2 + m_\alpha c^2 + \frac{1}{2} m_\alpha v_\alpha^2 \qquad$ (parent X at rest)

Momentum balance: $\qquad m_Y v_Y = m_\alpha v_\alpha$

Geiger-Nutall Law: short-lived isotopes emit more energetic alpha particles

Geiger-Nuttall law: $\log_{10} t_{1/2} = a\, E^{-1/2} + b$ ($t_{1/2}$: half life, E: α-particle energy, a, b: depend on Z)

Gamow Theory: alpha particles can quantum tunnel out of a strong nuclear force potential well

This model can derive the semi-empirical Geiger-Nutall law.

- Potential energy: $V(r) = \left\{ r < r_1: U; \; r \geq r_1: \frac{2Ze^2}{4\pi\varepsilon_0 r} \right\}$
  (r_1: radius of X, U: strong potential energy)

- Alpha particle mean lifetime: $\frac{1}{\lambda} = \frac{2r_1}{V} e^{2\gamma}$

  ($e^{2\gamma}$ ~ transmission coefficient, V: alpha velocity,

  $\gamma = \frac{\sqrt{2mE}}{\hbar} \int_{r_1}^{r_2} \sqrt{\frac{r_2}{r} - 1}\, dr$, r_2: position such that $V(r_2) = E$)

Coulomb barrier / free alpha — Energy (MeV) vs Separation of centers (fermis)

- If $r_2 \gg r_1$, then $\gamma = \frac{K_1 Z}{\sqrt{E}} - K_2\sqrt{Z r_1}$ (K_1 = 1.980 MeV$^{1/2}$, K_2 = 1.85 fm$^{-1/2}$)

- Gamow factor: $P(E) = e^{-\sqrt{E_G/E}} \qquad (E_G = 2\mu_{12}\left(\pi\alpha c Z_1 Z_2\right)^2, \; \mu_{12} = \frac{m_1 m_2}{m_1 + m_2}, \; \alpha = \frac{e^2}{4\pi\varepsilon_0 \hbar c})$
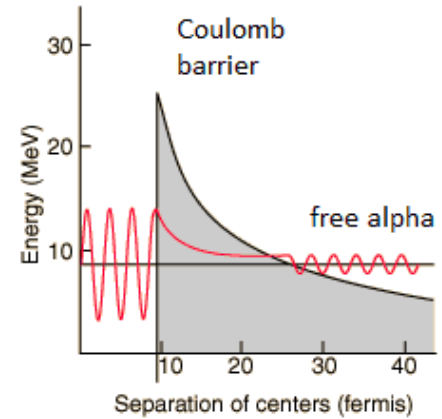
11.2.3. Beta Decay, Electron Capture, Gamma Decay and Internal Conversion

Beta Decay: change in one nucleon by releasing leptons

The W-boson mediates the weak nuclear force, changing the flavour of one quark in a nucleon (neutron: udd, proton: udu).

- β^- decay: $d \to u + W^-$ $(n \to p + W^-)$ and $W^- \to e^- + \bar{\nu}_e$
- β^+ decay: $u \to d + W^+$ $(p \to n + W^+)$ and $W^+ \to e^+ + \nu_e$

The Feynman diagram for β^- decay is shown on the right.

β^- decay is favoured in neutron-rich nuclei. β^+ decay is favoured in neutron-poor nuclei. β^+ decay can only occur when the daughter binding energy is higher than the parent.
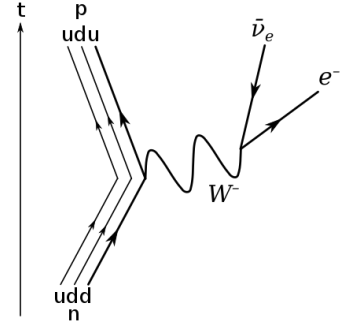
The released energy is distributed among the lepton and the neutrino on a spectrum. The interaction breaks chiral symmetry (alignment of spin and momentum). All observed ν_e have left-handed chirality; all observed $\bar{\nu}_e$ have right-handed chirality. The beta particle is released with the opposite chirality.

Bound state decay: for highly ionised radioisotopes, the emitted electron may be released at an energy lower than the ion's ionisation energy, allowing it to enter an atomic orbital. This can result in a faster rate of beta decay, though this is only significant for total ionisation (bare nuclei: e$^-$ into 1s).

Electron Capture: absorption of shell electron to mediate the weak interaction

If the wavefunction of an electron orbital is found to be within the nucleus, it can interact with the weak nuclear force. It is similar to β^+ decay in effect:

- EC decay: $u \to d + W^+$ $(p \to n + W^+)$ and $e^- + W^+ \to \nu_e$,   or
  $u + W^- \to d$ $(p + W^- \to n)$ and $e^- \to \nu_e + W^-$

EC may occur whenever β^+ decay is possible. The electron may be sourced from any shell (K: $n = 1$, L: $n = 2$, M: $n = 3$…) but K-electron capture is most common. Radioisotopes that are fully ionised (no electrons) will not undergo electron capture.

Gamma Decay: emission of a photon from an excited state (isomeric transition)

Beta decays may result in an excited daughter nucleus, which then decay by gamma decay. Multiple gamma emissions may be required to fall down the nuclear energy levels to reach the ground state.

The energy of the nucleus decreases by hf, where f is the frequency of the photon. The photon is typically in the gamma ray region of the EM spectrum.

Internal Conversion: shell electron interacts with an excited nucleus and is ejected

IC is possible whenever gamma decay is possible. The inner shell electron is ejected, forming a hole, from which a cascade of higher shell electrons can fall, releasing characteristic X-rays. These X-rays can hit other electrons in the same atom, releasing them as Auger electrons.

11.2.3. Radiometric Dating

Carbon Dating: used on organic material and bones. Half-life of ^{14}C = 5740 years.
Living organisms take in carbon from the atmosphere at a constant ^{14}C : ^{12}C isotopic ratio during their lifetime. After death, the ^{14}C within them decays and the resulting ratio can be used to determine the time since death.

**Uranium-Lead Dating:** used on rocks and minerals. Half-life of ^{235}U = 704 million years.
When rocks crystallise, they incorporate uranium which decays into lead. The ratio of lead to uranium indicates the time since crystallisation. With multiple samples, this can be done with the isochron method (plotting a 'concordia' curve).

11.2.4. Nuclear Weapons

History of Nuclear Weapons:

- Before World War 2 (1930s), scientists understood the potential of nuclear weapons, and Allied forces feared that Axis (Nazi) powers would develop weapons of mass destruction.
- Trinity test (June 1945): the first test of an atomic bomb, using plutonium fission.
- Hiroshima (Little Boy, Uranium) and Nagasaki (Fat Man, Plutonium) bombings (August 1945) forced the surrender of Imperial Japan and decisively ended WW2.
- Ivy Mike (1952): the first test of a thermonuclear bomb (hydrogen bomb), using plutonium for fission and deuterium for fusion. Start of the nuclear arms race between the USSR and USA.
- Tsar Bomba (1961): the most powerful bomb ever made, developed by the Soviets.
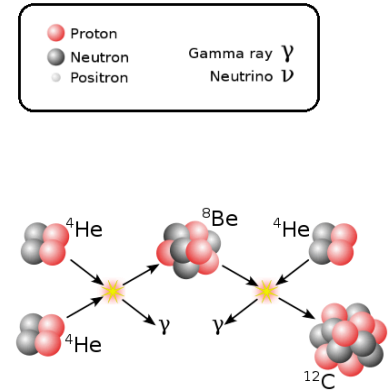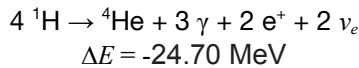
11.2.4. Stellar Nucleosynthesis
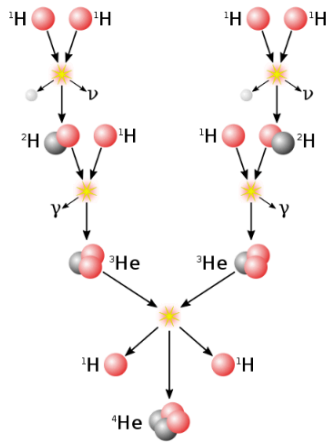
PP Chain:

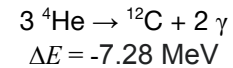Hydrogen is fused to helium.
Low-mass stars (incl. the Sun).

$$4\ {}^1H \rightarrow {}^4He + 2\ e^+ + 2\ \nu_e + 2\ \gamma$$
$$\Delta E = \text{-26.73 MeV}$$
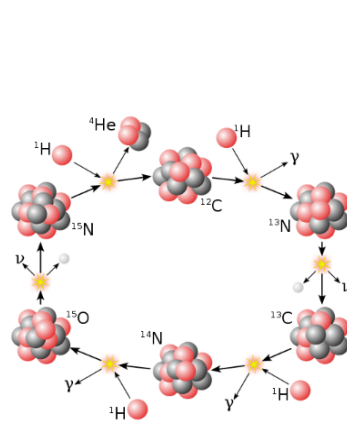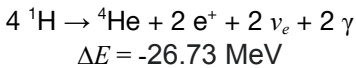
CNO Cycle (CNO-I)**:**

Catalytic formation of helium.
High-mass stars.

$$4\ {}^1H \rightarrow {}^4He + 3\ \gamma + 2\ e^+ + 2\ \nu_e$$
$$\Delta E = \text{-24.70 MeV}$$

Triple Alpha Process:

Helium is fused to carbon.
Late-stage stellar evolution.

$$3\ {}^4He \rightarrow {}^{12}C + 2\ \gamma$$
$$\Delta E = \text{-7.28 MeV}$$

The emitted positrons from these processes annihilate 1:1 with electrons in the environment, releasing two photons and an additional $2 m_e c^2 = 1.02$ MeV per positron emitted.
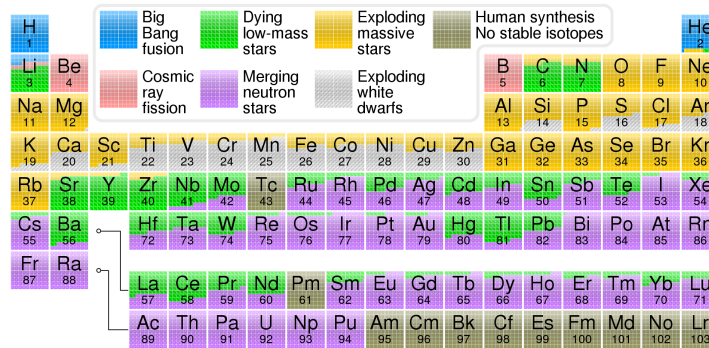
Heavier elements (up to Fe/Ni) are synthesised towards the end of a star's life, after nuclei like C, O, Ne, Si have been burned.

For elements heavier than iron, two processes dominate, which occur during and after supernova:

- *r*-process: rapid multiple neutron capture by ${}^{56}Fe$ (up to the neutron 'drip line': size for which the nuclear strong force can retain the neutron), followed by β-decay to form elements with higher proton numbers and also typically large neutron numbers.
- *s*-process: slow (one by one) neutron capture by ${}^{56}Fe$, the products of which may undergo either α or β decay at each stage depending on stability, producing a wider range of products.

The *r*-process also occurs inside thermonuclear warheads to a limited extent, which produce synthetic transuranic elements (e.g. ${}^{252}Es$, ${}^{257}Fm$) in nuclear fallout.

11.2.5. Cosmic Ray Spallation (The *x*-process)

Cosmic Rays (Astroparticles): near-light speed massive particles travelling across space

Primary cosmic rays consist of stable fully ionised atomic nuclei (85% protons, 14% alpha particles, 1% heavier (HZE) nuclei: C, O, Mg, Si, Fe), as well as high-energy electrons and trace positrons and antiprotons.

On Earth, they can originate from the Sun's solar wind, or from deep space (supernovas and active galactic nuclei/blazars).

When these particles interact with atoms such as in the upper atmosphere of Earth, they form **secondary cosmic rays**, consisting of pions (π^0, $\pi^\pm$), muons ($\pi^\pm \to \mu^\pm$), neutrons and muon neutrinos. The muons produced by the weak interaction are spin-polarised, do not interact strongly with matter, and persist down to Earth's surface due to relativistic time dilation before decaying to Michel electrons: $\mu^\pm \to e^\pm$.

Cosmic Ray Spallation:

Cosmic rays form the majority of ^{7}Li, ^{9}Be and ^{10}B, as well as some of the ^{3}He.

Typical reactions:
$$^{14}N + {}^1n \to {}^{10}Be + {}^4\alpha + {}^1p$$
$$^{14}N + {}^1n \to {}^{14}C + {}^1p$$
$$^{16}O + {}^1p \to {}^{10}Be + {}^4\alpha + 2\,{}^1p + {}^1n$$

11.2.5. Principles of Nuclear Fusion Power

Important nuclides for synthetic nuclear fusion:

| Nuclide	Natural abundance on Earth	Decay and Half-life	Sources
Deuterium (D = ^{2}H)	156 ppm	(stable)	Can be extracted readily from seawater.
Tritium (T = ^{3}H)	trace	β^-: T $\to$ ^{3}He$^+$ $t_{1/2}$ = 12.32 years ΔE = -18.6 keV	Must be produced from neutron bombardment of lithium: ^{6}Li + n $\to$ T + ^{4}He + 4.8 MeV ^{7}Li + n $\to$ T + ^{4}He + n - 2.5 MeV
Helium-3 (^{3}He)	1.37 ppm	(stable)	Helium is rare on Earth but known to be present (especially ^{3}He) on the Moon (suitable for lunar mining).

Popular fusion reactions include:

- 2 D $\to$ T + ^{1}H + 4.02 MeV   and   2 D $\to$ ^{3}He + n + 3.25 MeV
- ^{11}B + ^{1}H $\to$ 3 ^{4}He + 8.7 MeV
- D + T $\to$ ^{4}He + n + 17.6 MeV
- D + ^{3}He $\to$ ^{4}He + ^{1}H + 18.3 MeV

The source of tritium is a concern since it is non-existent on Earth. Its production from lithium is also a concern since lithium is also somewhat rare and is already a critical material (used for e.g. batteries).

11.2.6. Nuclear Fusion Reactor Physics

Reaction rate as a function of temperature for important fusion reactions:
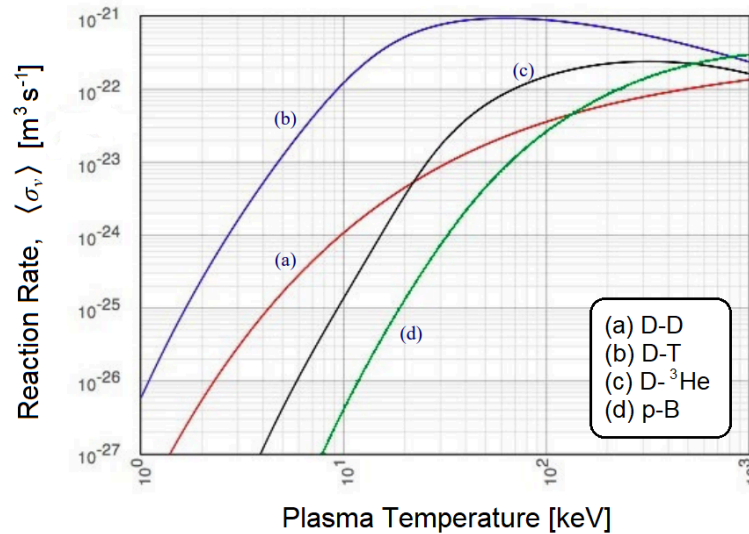

Plasma parameters and correlations:

- Beta: $\beta = \dfrac{plasma\ pressure:\ \langle P \rangle = nk_B T}{magnetic\ pressure:\ p_{mag} = B^2/(2\mu_0)} = \dfrac{2nk_B\mu_0 T}{B^2}$ $\beta \gtrsim 5\%$ for viable reactor

- Normalised beta: $\overline{\beta} = \dfrac{aB_T}{I_P} \times \beta$ (I_P [MA]: plasma current, a [m]: radius)

- Greenwald density limit: $n_G = \dfrac{I_P}{\pi a^2}$ [10^{20} m^3 s^{-1}]

- Plasma parameter $\Lambda_D = \dfrac{4\pi\varepsilon_0 T_e^{3/2}}{3e^3 n_e^{1/2}} >> 1$

- Confinement time scaling law: $\tau_e = H \times 0.145\, I^{0.93} R_0^{1.39} a^{0.58} \kappa^{0.78} n_{20}^{0.41} B_0^{0.15} A^{0.19} P^{-0.69}$

  (R_0 [m]: major radius, n_{20} [10^{23} m^{-3}]: density, B_0 [T]: magnetic flux density, P [MW]: power)
  (Tokamak ELMy H-mode correlation, IPB98(y,2))

- Lawson criteria: $n_e \tau_E \geq \dfrac{12k_B T}{E\langle\sigma_v\rangle}$ ($\approx 1.5 \times 10^{20}$ s m^{-3} for D-T)

  Triple product: $n_e \tau_E T_e \geq \dfrac{12k_B T^2}{E\langle\sigma_v\rangle}$ ($\approx 10^{21}$ keV s m^{-3} for D-T)

- Bremsstrahlung radiation: $P_{brem} = 0.85\, Pr^2\, \dfrac{Z_{eff}^2}{T_{10keV}^{3/2}}$ [MW m^{-3}]

- Effective plasma ion charge: $Z_{eff} = \dfrac{\Sigma Z_i^2 n_i}{\Sigma Z_i n_i}$

- Larmor gyromagnetic radius: $\rho_L = \dfrac{v_{th}}{\omega_{cy}} = \dfrac{(2mT)^{1/2}}{ZeB}$
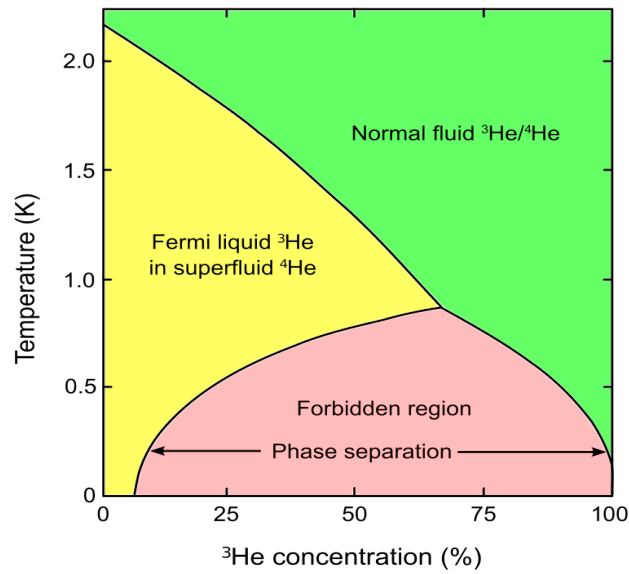
11.2.7. Phase Diagrams of Hydrogen and Helium

Hydrogen, high p and T
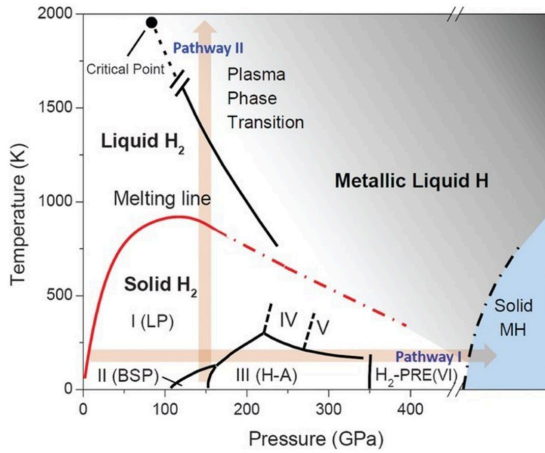
Helium (^{4}He), low T
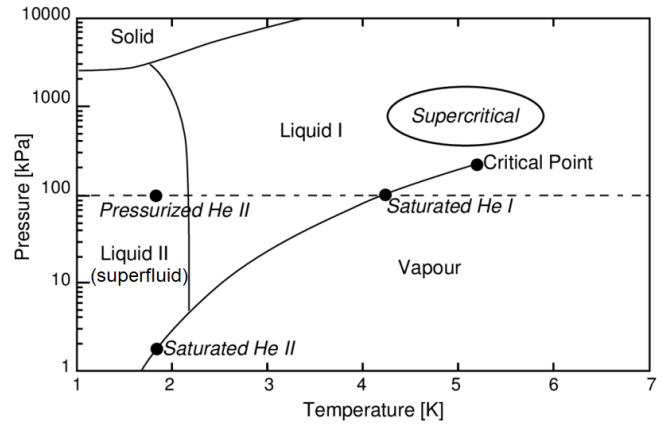
^{4}He-^{3}He mixture (low T, 1 bar, no magnetic field)

11.3. Acoustics and Medical Imaging

11.3.1. Acoustic Waves, the Doppler Effect and Beats

Sound is a longitudinal wave of pressure P and displacement s in a medium of density ρ.
Amplitude of pressure and displacement variations are related by $\Delta P_{max} = \rho c \omega \, \Delta s_{max}$ $(\omega = 2\pi f)$.

Intensity: $I = \dfrac{sound\ power}{area} = \dfrac{1}{2}\rho c \omega^2 (\Delta s_{max})^2$; dB $= 10 \log_{10} \dfrac{I}{I_{ref}}$ where $I_{ref} = 10^{-12}$ W m^{-2} = 1 pW m^{-2}.

General Equation of Travelling Waves and Stationary Waves:

Travelling right: $y_R(x,\ t) = A \cos(kx - \omega t + \phi_1)$;　　　Travelling left: $y_L(x,\ t) = A \cos(kx + \omega t + \phi_2)$

Standing wave: $y_S(x,\ t) = y_L + y_R = 2A \cos\left(kx + \dfrac{\phi_1 + \phi_2}{2}\right) \cos\left(\omega t - \dfrac{\phi_1 - \phi_2}{2}\right)$

Wave PDE: $\dfrac{\partial^2 y}{\partial t^2} = c^2 \dfrac{\partial^2 y}{\partial x^2}$;　Wave speed $c = \dfrac{\omega}{k}$;　　　$y(x, t)$: pressure P or displacement s
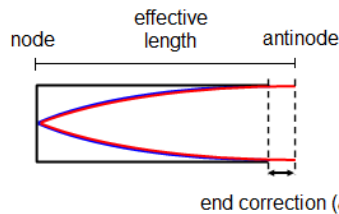
Resonance tube: for a tube of length L, mode shapes of the displacement
waves are $(n$: nth harmonic$)$

$$L = \frac{2n-1}{4}\lambda = \frac{\lambda}{4},\ \frac{3\lambda}{4},\ \frac{5\lambda}{4},\ \text{... (one end open)}$$

$$L = \frac{n}{2}\lambda = \frac{\lambda}{2},\ \lambda,\ \frac{3\lambda}{2},\ \text{... (both ends closed \textbf{or} both ends open)}$$

Closed end: node, reflection has no phase shift. Open end: antinode, reflection has 180° shift
Standing wave representation of the particle displacement:

node　effective length　antinode

end correction (e)

End effect correction: e is independent of mode number.
For each open end, $e \approx 0.31\, d$ $(d$: tube diameter$)$
Fundamental frequency: $f_0 = \dfrac{c}{\lambda_0} = \dfrac{c}{4(L + e)}$ (decreases due to e)

Pressure variation has a 90° phase lead relative to the displacement variation. Pressure wave has a node at **both** the closed and open end.

**Doppler reflection:** 　$\dfrac{f'}{f_0} = \dfrac{c + v_{obs}}{c + v_{src}}$

(f': observed frequency, f_0: source frequency, c: wave speed, v_{obs}, v_{src}: observer and source speed)

Sign conventions: observed frequency increases when the source is moving away from the observer, and vice versa for moving towards.

Oblique incidence of pulses (e.g. on a bloodstream):　　　$\dfrac{\Delta f}{f_0} = \dfrac{2v}{c} \cos \theta$　　　　(θ: angle of incidence)

Beats: when two acoustic waves of frequency f_1 and f_2 are superposed such that $f_1 \approx f_2$, the resultant sound contains beats of frequency $|f_1 - f_2|$.

11.3.3. Ultrasound
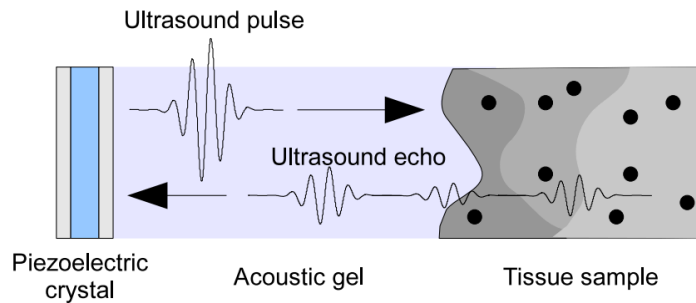
A broadband (high bandwidth) acoustic wave is generated by applying a short duration voltage to a piezoelectric crystal, causing it to vibrate. The pulse travels into the tissue, reflects at boundaries and is scattered by very small objects in the tissue. The ultrasound echo from the tissue in turn causes the piezoelectric crystal to vibrate, which generates an electrical signal.

- Acoustic impedance: $\quad\quad\quad\quad Z = \rho c \quad\quad\quad$ (ρ: medium mass density, c: speed of ultrasound)

- Reflection coefficient: $\quad\quad\quad \dfrac{I_r}{I_0} = \left(\dfrac{Z_2 - Z_1}{Z_1 + Z_2}\right)^2$

- Attenuation within matter: $I(x) = I_0\, e^{-\mu x} \quad\quad$ (μ: attenuation coefficient)

The acoustic gel is used for impedance matching, minimising reflections away from the interface.

Medium	Density ρ (kg m^{-3})	Speed of ultrasound c (ms^{-1})	Acoustic impedance Z (kg m^{-2} s^{-1})
air	1.3	330	429
water	1000	1500	1.5×10^6
fat	925	1450	1.34×10^6
muscle	1075	1590	1.70×10^6
bone	1400 - 1900	4080	$5.7 - 7.8 \times 10^6$

Ultrasound A-Scan (Amplitude Scan): short-pulse ultrasound waves are transmitted into the body, and the electron beam on a cathode ray oscilloscope (CRO) begins to move across the screen. The piezo transducer generates a pd on reflection and is displayed on the CRO. This type of scan is used to measure distances in the eye and the bi-parietal diameter of a foetus to measure its development.

Ultrasound B-Scan (Brightness Scan): forms an image by moving the ultrasound beam across the patient, this is done because reflected signals can only be received if the transducer is normal to the reflected beam. A 2D image of a section of the body can be formed. This type of scan is used to find the midline structure of the brain in a foetus in order to know in which region an A-scan can be used to measure bi-parietal diameter, it is also used to determine the position of the placenta so that it can be determined whether a baby will have a safe delivery or if it will need to be delivered by C-section. It is also used in order to perform genetic testing on a foetus by imaging the position of the placenta and foetus accurately.

11.3.4. Mechanisms of Interactions of High-Energy Photons with Matter

The main four mechanisms of high energy (above UV) photon-matter interactions:

- **Simple (Rayleigh, elastic) scattering:** photon interacts with electron, scattered with same energy. Most common in ~keV range (high energy UV / low energy X-ray). Does not contribute to attenuation. Higher energy radiation is scattered more.

- **Photoelectric effect:** photon absorbed completely by electron, electron is ejected. Dominates in ~keV range (high energy UV and X-rays). The fastest photoelectrons have energy E_k, where $E_k = hf - \phi$, where ϕ is the work function of the material. For X-ray photons, these electrons can reach relativistic speeds.

- **Compton (inelastic) scattering:** electron in an atom ejected by photon (ionisation); photon is then scattered to lower energy. Dominates in ~100 keV range (low energy gamma rays).

- **Pair production:** photon spontaneously splits into electron and positron in the strong E-field near the nucleus of an atom. The positron rapidly annihilates with an electron, releasing a photon at half energy. Dominates in ~MeV range (energy $> 2m_ec^2 = 1.022$ MeV, high energy gamma rays).

High-energy radiation (typically X-rays) are easily produced as *bremsstrahlung* (braking radiation) by 'boiling' electrons from a hot cathode, accelerated into an anode. About 1% of the electron energy is converted to X-rays on a spectrum (with characteristic peaks due to ionisation of shell electrons). The rest of the collisions heat the anode.
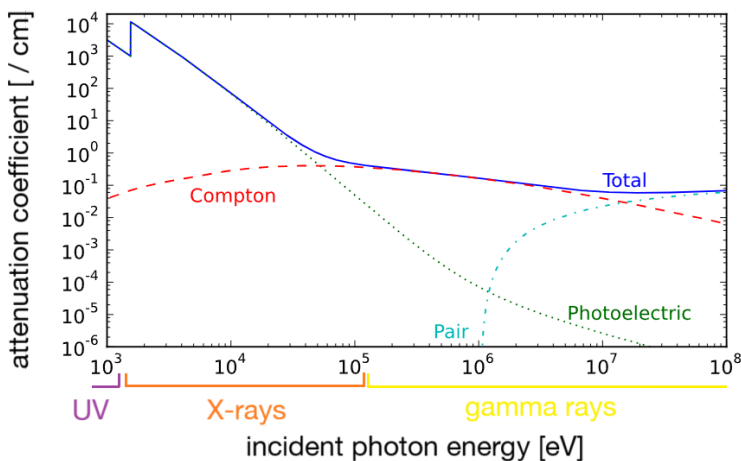
Total attenuation coefficient: the value of μ for aluminium, by contribution from each mechanism of dissipative interaction. K-absorption edge at 1.566 keV.

Attenuated intensity: $I(x) = I_0 e^{-\mu x}$
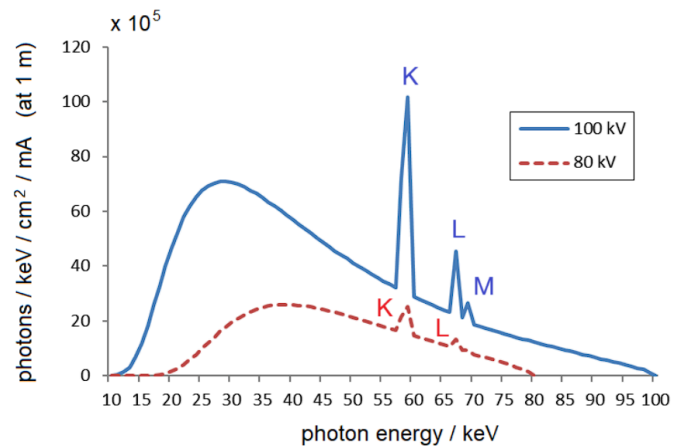
X-ray Tube Spectrum: the bremsstrahlung photon intensity for a tungsten anode, for tube voltages of 100 kV and 80 kV. K, L, M characteristic peaks shown.

11.3.5. X-Ray Imaging

An X-ray tube emits photons of a range of different energies, with maximum energy $E \leq eV$ (V: X-ray tube pd). This results in a variation in penetrating power into body tissue.

X-Ray Filters: lower-energy X-rays can damage tissue as they are absorbed, so X-ray filters are applied to the beam to reduce low-energy X-ray photon intensity ('beam hardening'). X-ray filters are made of metals to selectively absorb low-energy radiation by photoelectric effect (copper for therapy, aluminium for radiography).

The **sharpness and contrast** of an X-ray image is dependent on competing factors:

- For geometric sharpness, the distance between the focal spot and the film should be large (~1 m), while the distance of the film from the object should be small.

- A smaller focal spot can improve sharpness, but too small a spot can cause a concentration of energy in the target, which can lead to harmful heating effects.

- The exposure time determines the density/blackening of the film, so should be relatively long, however it is often determined by the amount of movement of the body part being imaged.

- Ideally, voltage and exposure would be set, and then the tube current would be chosen to produce the desired density, however this current level is often too high for the tube's rating and so the focal spot size would have to increase.

- Poor-contrast regions can be enhanced using contrast media e.g. barium sulfate for the GI tract and organic iodine compounds for the bloodstream.

The **beam size** must be controlled to minimise the radiation that the patient receives:

- A diaphragm consisting of two perpendicular pairs of metal sheets is used.
- Beam size is determined by the diaphragm aperture and its distances to the film & target.
- The diaphragm is close to the target, so the edge of the beam is less sharp.
- In therapeutic work a sharp edge is required so collimators are used.

An **X-ray film** is irradiated by primary photons (passing directly through the body, producing the image) and secondary photons (scattering, irradiating the whole film almost evenly). To reduce the amount of secondary photons reaching the film, a grid of fine strips of lead is used. However, this grid also absorbs small amounts of primary photons and so to counteract this, a longer exposure is used. This helps to maintain a suitable film density.

Intensifying screens can be used to increase the resulting exposure of the film. This allows a shorter X-ray exposure time to be used, whilst achieving the same density. They consist of a stiff ~1 mm thick cardboard sheet, a fluorescent layer of crystals e.g. $CaWO_4$, a white material e.g. MgO sandwiched between them (redirects visible light towards film), and a tough waterproof material. Intensifying screens are placed either side of the film in a cassette. A pair of screens positioned like this, can result in an intensification factor of around 30 times. A metal cassette back is added behind the back screen to reduce radiation scattering back, which would result in a reduction of the film contrast.

Image Intensifiers are another method to intensify X-ray images, which increases the light output while maintaining a low X-ray dose. The X-ray pattern is directed onto a fluorescent screen and a corresponding pattern of light is emitted from this screen. The light pattern is incident on a photocathode emitting electrons, which are accelerated by a pd of around 25kV towards another fluorescent screen, which produce a much brighter image due to their higher energy. The brightness is increased by an order of around 5000 times, although the electron lens decreases the size of the pattern in the process. The viewing screen is viewed through a lead glass window. The image can also be photographed.

Indirect Flat Panel Detectors are a faster and more sensitive method of producing an X-ray image, than using a traditional film method. A scintillator converts X-ray photons into visible light photons which are directed at a low-noise photodiode (CCD) array. Each diode acts as a pixel. The stored charge is read by electronic scanning, producing digital signals used to form a digital image. The high sensitivity level means that a lower dose of radiation is required to achieve a given image quality. The digital image that is produced is also more transportable.

11.3.7. MRI Scan (Magnetic Resonance Imaging)

An MRI scanner consists of a circular superconducting magnet, enclosing a gradient coil and an RF (radio frequency) coil. The RF coil emits a radio pulse, causing proton spins to precess about the magnetic field, re-emitting during relaxation, which is received and measured using Fourier transform spectroscopy. Relaxation rates are tissue-dependent, which leads to a contrast in the signal received, represented as image voxel brightness.

Mechanism of Nuclear Magnetic Resonance

When exposed to strong external magnetic fields, nuclei with spin (primarily ^{1}H protons) have their spin vectors $\mathbf{s}$ precess about the external field vector $\mathbf{B}$ at a certain frequency ω.

Larmor equation: $\quad \boldsymbol{\omega} = \gamma \mathbf{B} \qquad$ (ω: precession angular velocity, γ: gyromagnetic ratio)

Bloch equation: $\quad \dot{\mathbf{M}} = \gamma \left(\mathbf{M} \times \mathbf{B} \right)$

^{1}H proton gyromagnetic ratio: $\quad \gamma = 2.675 \times 10^8$ rad T^{-1} s^{-1} = 42.58 M T^{-1}

Detected signal: $\quad S = \dfrac{N\gamma^3 \hbar^2 B_0^2}{4kT} \quad$ (at thermal equilibrium) $\qquad$ Spin polarisation: $\quad P = \dfrac{\gamma \hbar B_0}{2kT}$

Signal at measurement: $\quad S = \underbrace{M_0 \left(1 - e^{-\mathrm{TR}/T_1} \right)}_{\substack{\text{longitudinal} \\ \text{magnetisation}}} \underbrace{e^{-\mathrm{TE}/T_2}}_{\substack{\text{transverse} \\ \text{magnetisation}}}$

Boltzmann magnetisation: $\quad \mathbf{M}_0 = \chi_0 \, \mathbf{B}_0 \quad$ (Curie's law) $\left(\chi_0 = \dfrac{N\gamma^2 \hbar^2}{16\pi^2 kT} \right.$: static nuclear susceptibility)

(N: total number of nuclei, T_1 and T_2 are tissue-dependent time constants representing rates of spin realignment (relaxation) and proton spin decoherence (dephasing) respectively.)

Time constants for tissues:

Tissue (at B_0 = 1 T)	T_1 (ms)	T_2 (ms)
water	2500	2500
fat	240	90
spleen	460	80
white matter	680	90
grey matter	810	100
CSF	2500	1400
liver	490	40
blood	800	180
muscle	730	40
bone	210	5.6

Types of scan by contrasting time constants:

	TR $\sim T_1$ (short TR)	TR $\gg T_1$ (long TR)
TE $\sim T_2$ (short TE)	not used	T_2 weighted image
TE $\gg T_2$ (long TE)	T_1 weighted image	M_0 weighted image

Some nuclei (^{3}He, ^{13}C, ^{129}Xe) may be hyperpolarised up to $P \sim 0.5$, allowing for inhalation of e.g. xenon-129 gas to image the lungs.

11.3.8. CAT Scan (CT Scan, Computed Axial Tomography)

CT scans are used to produce cross-sectional images of the body by taking a **continuous X-ray rotated** around the region being scanned. The X-ray beam is collimated and monochromatic. A circular ring of detectors records the intensity transmitted over the required cross-section. A computer algorithm (inverse Radon transform) reconstructs the 2D attenuation image, and these can be stacked across multiple cross-sections to develop a 3D model.

It can produce good images of bone fractures, organ calcification, the brain and abdominal organs, and it has high resolution. However, it is highly ionising, produces low contrast between similar-density tissues and requires the patient to hold their breath.

11.3.9. PET Scan (Positron Emission Tomography)

PET scanning produces 3D and cross-sectional images of the body.

- Patient is injected with a radionuclide e.g. FDG-18 (fluorodeoxyglucose, using ^{18}F)
- The patient lies on an examination table which is moved into the scanning machine. Throughout the scanning process, the patient must remain as stationary as possible.
- The radionuclide is metabolised in the imaged body part.
- ^{18}F atoms emit positrons due to β^+ decay. These positrons annihilate with electrons in the tissue to release gamma photons.
- Gamma cameras detect the gamma photons to produce 3D images.

Gamma cameras: used to detect the gamma radiation emitted by the radiopharmaceutical

- Gamma photons from the patient pass through a lead collimator
- They travel through to a large diameter crystal of sodium iodide
- Due to the collimator, each photon reaching the crystal has come from a position in the body that is directly below where it is incident on the crystal
- Scintillation occurs in the crystal and light photons are produced
- The light photons then pass into photomultiplier tubes for amplification.

The output pulses from these tubes are used to form an image. The pulses are produced by:

- Light is incident on a photocathode resulting in electrons being emitted
- The electrons are accelerated to a series of electrodes known as dynodes
- Each dynode is more positive than the previous, until the electrons reach the anode
- The electron beam reaching the anode outputs an electrical pulse

SPECT (Single Photon Emission Computed Tomography): positron-free 3D imaging

In SPECT, a radioactive tracer (e.g. ^{99m}Tc as $NaTcO_4$ or organic chelating agents) is injected into the patient, with its pharmacokinetics designed to accumulate in a specific organ (e.g. bone, heart, brain). ^{99m}Tc undergoes gamma decay with half life ~6 hours into ^{99}Tc (half life 211,000 years), emitting photons in all directions from the targeted organ, detected with rotating gamma cameras, and the image is reconstructed by tomography techniques. The remaining ^{99}Tc in the body is eliminated through the kidneys.

11.3.14. Optical Coherence Tomography (OCT) for Ophthalmological Retinal Imaging

Setup: the fibre optic coupler acts as a Michelson-Morley interferometer.

Alternative detector
for spectral OCT
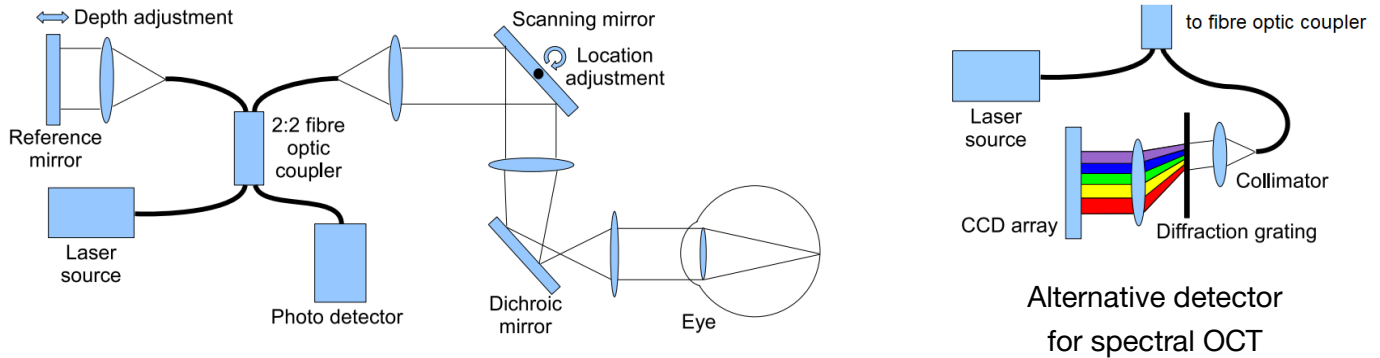
Interferometer Signal

In an ideal OCT system with no dispersion, the intensity I at the output of the interferometer, as a function of frequency ω, is given by:

$$\underbrace{I(\omega)}_{\text{detected}} = \underbrace{S(\omega)}_{\text{input pulse}} + \underbrace{S(\omega)\left|\int_{-\infty}^{\infty} r_s(l_s)e^{j\frac{\omega}{c}l_s}\,\mathrm{d}l_s\right|^2}_{\text{scattered}} + \underbrace{2\Re\left\{S(\omega)\int_{-\infty}^{\infty} r_s(l_s)e^{j\frac{\omega}{c}(l_r-l_s)}\,\mathrm{d}l_s\right\}}_{\text{interference}}$$

(S: laser pulse power spectrum, r_s: tissue reflectivity density function, l_r: round-trip distance from the laser source to the reference mirror and back to the photodetector, l_s: round-trip distance from the laser source to a scatterer at a particular depth and back to the photodetector, c: average speed of light through the media in its path.)

The quantity $\dfrac{l_r - l_s}{c}$ represents time t. In time-domain OCT, the singular photodiode detects $I = \int_{-\infty}^{\infty} I(\omega)\,d\omega$. In spectral OCT, $I(\omega)$ is detected directly due to the diffraction grating and CCD array.

~ LN, 2024